ASTRONOMICAL INSTITUTE
SLOVAK ACADEMY OF SCIENCES

PROCEEDINGS OF THE WORKSHOP

OBSERVING TECHNIQUES, INSTRUMENTATION AND SCIENCE FOR METRE-CLASS TELESCOPES II

September 24 – 28, 2018, Tatranská Lomnica, Slovakia

CONTRIBUTIONS OF THE ASTRONOMICAL OBSERVATORY SKALNATÉ PLESO

• VOLUME XLIX •

Number 2

May 2019

ISSN: 1336–0337 (on-line version)

CODEN: CAOPF8

Editorial Office: Astronomical Institute of the Slovak Academy of Sciences
SK - 059 60 Tatranská Lomnica, The Slovak Republic

CONTENTS

Session B: SCIENCE WITH SMALL TELESCOPES

The Contributions of the Astronomical Observatory Skalnaté Pleso
are available in a full version
in the frame of ADS Abstract Service
and can be downloaded in a usual way from the URL address:

‘’http://adsabs.harvard.edu/article_service.html‘’

as well as from the web-site of
the Astronomical Institute of the Slovak Academy of Sciences
on the URL address:

‘’http://www.astro.sk/caosp/‘’

The journal is covered/indexed by:

Thomson Reuters services (ISI)
Science Citation Index Expanded (also known as SciSearch®)
Journal Citation Reports/Science Edition

SCOPUS

PROCEEDINGS OF THE WORKSHOP

Edited by

Ján Budaj, Richard Komžík,
Theodor Pribulla, Augustín Skopal

OBSERVING TECHNIQUES, INSTRUMENTATION AND SCIENCE FOR METRE-CLASS TELESCOPES II

September 24 – 28, 2018, Tatranská Lomnica, Slovakia

The Astronomical Institute of the Slovak Academy of Sciences

https://www.ta3.sk/conferences/75AI2018/

LIST OF PARTICIPANTS

Baklanov, Aleksey	Crimean Astrophysical Observatory, Russian Federation
Barsunova, Olga Y.	Central Astronomical Observatory of RAS, Russian Federation
Bauer, Thilo	Bornheim Observatory, Germany
Bayliss, Daniel	University of Warwick, United Kingdom
Bikulova, Dinara A.	Pulkovo Observatory of RAS, Russian Federation
Brunsden, Emily J.	University of York, United Kingdom
Budaj, Ján	Astronomical Institute, Slovak Academy of Sciences, Tatranská Lomnica, Slovakia
Cabezas, Mauricio E.	Astronomical Institute of the Academy of Sciences of the Czech Republic, Czech Republic
Chochol, Drahomír	Astronomical Institute, Slovak Academy of Sciences, Tatranská Lomnica, Slovakia
Dębski, Bartłomiej	Astronomical Observatory of the Jagiellonian University, Poland
Dubovský, Pavol A.	Vihorlat Observatory Humenné, Slovakia
Duffard, Rene	Instituto de Astrofísica de Andalucia - CSIC, Spain
Fedurco, Miroslav	Institute of Physics, Faculty of Science, P.J. Šafárik University, Košice, Slovakia
Gajdoš, Pavol	Institute of Physics, Faculty of Science, P.J. Šafárik University, Košice, Slovakia
Gális, Rudolf	Institute of Physics, Faculty of Science, P.J. Šafárik University, Košice, Slovakia
Garai, Zoltán	Astronomical Institute, Slovak Academy of Sciences, Tatranská Lomnica, Slovakia
Garcés, Juan	Department of Astronomy. Universidad de Concepción, Chile
Godunova, Vira	ICAMER Observatory of NASU, Ukraine
Golysheva, Polina Y.	Sternberg Astronomical Institute, Lomonosov Moscow State University, Russian Federation
Hambálek, Ľubomír	Astronomical Institute Slovak Academy of Sciences, Tatranská Lomnica, Slovakia
Harris, Robert James	Zentrum für Astronomie der Universität Heidelberg, Landessternwarte, Germany
Holdsworth, Daniel	North-West University, South Africa; UCLan, United Kingdom
Isogai, Keisuke	Department of Astronomy, Kyoto University, Japan
Kabáth, Petr	Astronomical Institute of Czech Academy of Sciences, Czech Republic

Kartashova, Anna	Institute of Astronomy, Russian Academy of Sciences, Russian Federation
Katysheva, Nataly A.	Sternberg State Astronomical Institute, Lomonosov Moscow State University, Russian Federation
Kılıçoğlu, Tolgahan	Ankara University, Faculty of Science, Department of Astronomy and Space Sciences, Turkey
Knežević, Sladjana	Astronomical Observatory Belgrade, Republic of Serbia
Kornoš, Leonard	Faculty of Mathematics, Physics and Informatics, Comenius University, Bratislava, Slovakia
Kostić, Petar	Astronomical Observatory of Belgrade, Astronomical Station Vidojevica, Republic of Serbia
Krushevska, Viktoriia	Main astronomical observatory of National academy of sciences of Ukraine, Ukraine
Kudak, Viktor	Institute of Physics, Faculty of Science, P.J. Šafárik University, Košice, Slovakia
Kundra, Emil	Astronomical Institute, Slovak Academy of Sciences, Tatranská Lomnica, Slovakia
Kurtenkov, Alexander	Institute of Astronomy and National Astronomical Observatory, Bulgarian Academy of Sciences, Bulgaria
Kuznyetsova, Yuliana	Main astronomical observatory of National academy of sciences of Ukraine, Ukraine
Kvernadze, Teimuraz	Abastumani Astrophysical Observatory, Ilia State University, Georgia
Lee, Chung-Uk	Korea Astronomy and Space Science Institute, Republic of Korea
Lee, Dong-Joo	Korea Astronomy and Space Science Institute 776, Daedeokdae-ro, Yuseong-gu, Daejeon, Republic of Korea
Lendl, Monika	Space Research Institute, Austrian Academy of Sciences, Austria
Maciejewski, Gracjan	Nicolaus Copernicus University, Poland
Mallonn, Matthias	Leibniz Institute for Astrophysics Potsdam (AIP), Germany
Mennickent, Ronald	Department of Astronomy, University of Concepción, Chile
Merc, Jaroslav	Institute of Physics, P.J. Šafárik University, Košice, Slovakia; Astronomical Institute of Charles University, Prague, Czech Republic
Mugrauer, Markus	Astrophysical Institute and University Observatory Jena, Germany
Munari, Ulisse	National Institute of Astrophysics INAF, Astronomical Observatory of Padova, Italy

Ogłoza, Waldemar	Pedagogical University of Cracow, Poland
Özavcı, İbrahim	Ankara University Department of Astronomy and Space Sciences, Turkey
Pakštienė, Erika	Institute of Theoretical Physics and Astronomy, Physics Department, Vilnius University, Lithuania
Panko, Elena	I.I. Mechnikov Odessa National University, Odessa, Ukraine
Parimucha, Štefan	Institute of Physics, University of P.J. Šafárik in Košice, Slovakia
Paunzen, Ernst	Department of Theoretical Physics & Astrophysics, Masaryk University, Czech Republic
Pavlenko, Elena P.	Crimean Astrophysical Observatory, Russian Federation
Pawlak, Michal	Institute of Theoretical Physics, Faculty of Mathematics and Physics, Charles University in Prague, Czech Republic
Polińska, Magdalena	Institute Astronomical Observatory, Adam Mickiewicz University in Poznań, Poland
Pollmann, Ernst	51375 Leverkusen, Emil-Nolde-Str. 12, Germany
Pravec, Petr	Astronomical Institute AS CR, Ondřejov, Czech Republic
Pribulla, Theodor E.	Astronomical Institute, Slovak Academy of Sciences, Tatranská Lomnica, Slovakia
Ratajczak, Milena	University of Wrocław, Poland
Roettenbacher, Rachael	Yale University, United States
Schroefl, Thomas	WAA Wiener Arbeitsgemeinschaft für Astronomie, Austria
Sekeráš, Matej	Astronomical Institute, Slovak Academy of Sciences, Tatranská Lomnica, Slovakia
Seli, Bálint A.	Konkoly Observatory, MTA CSFK, Budapest, Hungary
Shagatova, Natalia	Astronomical Institute, Slovak Academy of Sciences, Tatranská Lomnica, Slovakia
Shchurova, Alisa	Astronomical Institute, Slovak Academy of Sciences, Tatranská Lomnica, Slovakia
Shporer, Avi	MIT, United States
Shugarov, Andrey	Institute of Astronomy, Russian Academy of Sciences (INASAN), Russian Federation
Shugarov, Sergey Y.	Astronomical Institute, Slovak Academy of Sciences, Tatranská Lomnica, Slovakia; Sternberg Astronomical Institute of Moscow University, Russian Federation
Simon, Andrii	Taras Shevchenko National University of Kyiv, Ukraine

Skarka, Marek	Department of Theoretical Physics and Astrophysics, Masaryk University, Czech Republic
Skopal, Augustin	Astronomical Institute, Slovak Academy of Sciences, Tatranská Lomnica, Slovakia
Stanik, Kristina	Astronomical Observatory of Belgrade, Republic of Serbia
Szabados, László	Konkoly Observatory of the Hungarian Academy of Sciences, Hungary
Šilha, Jiří	Faculty of Mathematics, Physics and Informatics, Comenius University, Bratislava, Slovakia
Taşpinar, Özlem	Akdeniz University - Department of Space Science & Technologies, Turkey
Teyssier, François	ARAS, France
Tóth, Juraj	Faculty of Mathematics, Physics and Informatics, Comenius University in Bratislava, Slovakia
Tsvetkov, Dmitry	Sternberg Astronomical Institute, Russian Federation
Tunç, Efecan	Akdeniz University - Department of Space Science & Technologies, Turkey
Volkov, Igor M.	Institute of Astronomy of Academy of Sciences, Moscow; Sternberg State Astronomical Institute, Moscow, Russian Federation
Vos, Joris	Institut für Physik und Astronomie, University of Potsdam, Germany
Vrašťák, Martin	Czech astronomical society, Variable Star and Exoplanet section, Slovakia
Vudragović, Ana	Astronomical Observatory Belgrade, Republic of Serbia
Vukotić, Branislav	Astronomical Observatory, Republic of Serbia
Yilmaz, Mesut	Ankara University, Turkey
Yücel, Gökhan	Department of Space Science and Technology, Akdeniz University, Turkey
Zampieri, Luca	INAF-Astronomical Observatory of Padova, Italy
Zasche, Petr	Astronomical Institute, Faculty of Mathematics and Physics, Charles University, Czech Republic
Zejda, Miloslav	Dept. of Theoretical Physics and Astrophysics, Masaryk University, Brno, Czech Republic
Zhou, George	Harvard-Smithsonian Center for Astrophysics, United States
Zieliński, Paweł	Warsaw University Astronomical Observatory, Poland
Zoła, Stanisław	Astronomical Observatory, Jagiellonian University, Poland
Zwitter, Tomaž	University of Ljubljana, Faculty of Mathematics and Physics, Slovenia

PREFACE

The metre-class telescopes are still vital for current astrophysics. Although large telescopes excel in the studies of faint objects at the edge of the observable Universe and provide high-angular and spectral resolution of astrophysically important objects, small telescopes (diameter < 2 m) are valuable in long-term monitoring, continuous observations or large-scale surveys. A large flotilla of small telescopes can often provide observations which would be cost-prohibitive for large telescopes. Most of astrophysically crucial objects/events are still being discovered through extensive all-sky surveys run by robotic telescopes, or by very small telescopes of well-organized amateur astronomers. Also, small telescopes continue to play a vital role in recruiting and training the next generation of astronomers and instrumentalists, and serve as test beds for developments of novel instruments and experimental methods for larger telescopes. Moreover, a metre-class telescope is available at almost any historical observatory and, after some effort, can be turned into a powerful instrument. This requires better focal instrumentation and modern telescope control.

This book contains proceedings of the 2$^{\rm nd}$ international conference on the role of small telescopes in astrophysics. *Observing techniques, instrumentation and science for metre-class telescopes II.* It took place in the Congress Center Academia near a village called Tatranská Lomnica at the foothill of the scenic High Tatra mountains in the northern Slovakia from September 24 to September 28, 2018. Its program was divided into three sessions: *A: Observing techniques and instrumentation for metre-class telescopes, B: Science with small telescopes, and C: Ground-based support of cosmic missions and telescope networks.* The first conference of this series was held at the same place in 2013. The conference commemorates the 75$^{\rm th}$ anniversary of the very first observation performed at the Skalnaté Pleso Observatory. Currently, thanks to the European Regional Development Fund (ITMS No. 26220120029), a new 1.3 m telescope, equipped with several advanced focal instruments, was inaugurated.

The SOC thanks all the participants for their high-level contributions. Ninety participants from 22 countries took part in the meeting. The organizers are indebted to the Astronomical Institute of the Slovak Academy of Sciences for general support and also to the Congress Center Academia for smooth cooperation during the conference. We thank the members of the LOC: Ľubomír Hambálek (chair), Richard Komžík, Emil Kundra, Matej Sekeráš, Natalia Shagatova, and Alisa Shchurova for their help in preparing and running this workshop. Finally, we also thank all the referees and language correctors for their hard work in peer-reviewing all contributions.

J. Budaj, T. Pribulla & A. Skopal
the editors

Contrib. Astron. Obs. Skalnaté Pleso **49**, 85 – 96, (2019)

(Very) Fast astronomical photometry for meter-class telescopes

L. Zampieri[1], G. Naletto[2], C. Barbieri[1,2], A. Burtovoi[1,2], M. Fiori[2], A. Spolon[2], P. Ochner[2], L. Lessio[1], G. Umbriaco[2] and M. Barbieri[3]

[1] *INAF-Astronomical Observatory of Padova, Italy*
(E-mail: luca.zampieri@inaf.it)
[2] *University of Padova, Italy*
[3] *University of Atacama, Chile*

Received: December 2, 2018; Accepted: January 30, 2019

Abstract. Our team at the INAF-Astronomical Observatory of Padova and the University of Padova is engaged in the design, construction and operations of instruments with very high time accuracy in the optical band for applications to High Time Resolution Astrophysics and Quantum Astronomy. Two instruments were built to perform photon counting with sub-nanosecond temporal accuracy, Aqueye+ and Iqueye. Aqueye+ is regularly mounted at the 1.8m Copernicus telescope in Asiago, while Iqueye was mounted at several 4m class telescopes around the world and is now attached through the Iqueye Fiber Interface to the 1.2m Galileo telescope in Asiago. They are used to perform coordinated high time resolution optical observations and, for the first time ever, experiments of optical intensity interferometry on a baseline of a few kilometers. We report on recent technological developments and scientific results obtained within the framework of this project.

Key words: Astronomical instrumentation, methods and techniques – Instrumentation: photometers – Techniques: interferometric – Occultations – pulsars: general – pulsars: individual: PSR J0534+2200 – X-rays: binaries – X-rays: individual: MAXI J1820+070

1. Introduction

The origin of the AQUEYE+IQUEYE project[1] dates back to September 2005, when we completed an instrument design study (QuantEYE, the ESO Quantum Eye; Dravins et al. 2005) within the framework of the proposal for new instrumentation for the 100 m diameter Overwhelmingly Large (OWL) telescope. The main objective of the study was to demonstrate the possibility to reach picosecond time resolution in the optical band, needed to bring Quantum Optics concepts into the astronomical domain. We had two main scientific goals in mind: measuring the entropy of light through the statistics of the photon arrival times and performing optical High Time Resolution Astrophysics with sub-ms time resolution.

[1] https://web.oapd.inaf.it/zampieri/aqueye-iqueye/index.html

Starting from the QuantEYE design, we realized two similar instruments, Aqueye+ and Iqueye. They are non-imaging photon-counting instruments dedicated to performing very fast optical photometry, with a field of view of few arcsec and the capability of time tagging the detected photons with sub-ns time accuracy. This instrumentation is extremely versatile because the photon event lists are stored in a mass memory and the data analysis is entirely done in post-processing with a selection of time bins (from nanoseconds to minutes). In addition, simultaneous observations with distant telescopes can be made, because a suitable synchronization of the signals is implemented. This fact allows us to correlate the simultaneous acquisitions from the two instruments.

The first instrument that was realized is Aqueye, the Asiago Quantum Eye, mounted on the AFOSC instrument at the Copernicus telescope in Asiago (Barbieri et al., 2009). The second step was Iqueye, the Italian Quantum Eye, designed for applications to 4 m class telescopes (Naletto et al., 2009). It was mounted on the ESO 3.5 m New Technology Telescope in La Silla, and the Telescopio Nazionale Galileo and the William Herschel Telescope in La Palma.

In 2014 Aqueye become an independent instrument, called Aqueye+ and no longer attached to AFOSC (Naletto et al., 2013). It is now remotely controlled and regularly mounted at the 1.8 m Copernicus telescope in Asiago (Zampieri et al., 2015). The acquisition electronics was moved to a dedicated room and is kept under stable temperature and humidity conditions. In 2015 Iqueye returned to Asiago for a general refurbishment and was mounted at the 1.2 m Galileo telescope to perform experiments of intensity interferometry (Zampieri et al., 2016). A direct mount at the Cassegrain focus was soon discarded because of potential mechanical problems. We opted for a soft-mount solution, installing a dedicated optical bench at the Nasmyth focus of the Galileo telescope and connecting Iqueye to it through an optical fiber.

Since 2015 the two instruments have been used to perform coordinated high time resolution optical observations and, for the first time ever, exploratory experiments of stellar intensity interferometry on a baseline of a few kilometers. Some of the results obtained within the framework of these programs are reported here.

2. Instrumentation

Both instruments, Aqueye+ and Iqueye, adopt a very convenient optical design (Barbieri et al. 2009; Naletto et al. 2009). The detectors are Single Photon Avalanche Photodiodes (SPADs), photon counting detectors with high quantum effciency ($\sim 50\%$) and very high time resolution (30-50 ps), but rather small effective area. To better couple the small detectors effective area to the telescope pupil and to increase the maximum sustainable count rate, Aqueye+ and Iqueye implement the same concept of splitting the telescope entrance pupil proposed

for QuantEYE. The pupil is divided in four parts, each of them focused on a single detector.

The core of the instrumentation is its very accurate acquisition and timing system. The instruments time tag and store the arrival time of each detected photon with a $\simeq$ 100 ps relative time accuracy and $<$ 500 ps absolute time accuracy (compared to UTC; Naletto et al. 2009). All recorded times are stored in event lists that can be analyzed in post-processing (Zampieri et al. 2015). At present the most important limitation is the maximum data rate, of the order of few MHz (in the linear regime).

3. Interfacing the instruments with optical fibers

In order to connect Iqueye to the 1.2 m Galileo telescope, we were forced to opt for a soft-mount solution. To avoid potential problems related to the mechanics of the telescope, we installed a dedicated optical bench at the telescope lateral focus and connected Iqueye to it by means of an optical fiber (Zampieri et al., 2016). Besides facilitating the mounting of the instrument, this solution has also the advantage of maintaining Iqueye in a separate room under controlled temperature and humidity conditions (reducing potential systematics related to varying ambient conditions). At the same time, it mitigates scheduling requirements related to the time needed to mount and dismount the instrument.

Since 2015, the bench has been modified and upgraded, becoming an indepedent instrument, the Iqueye Fiber Interface (IFI; Figure 1). The alignment, focusing and overall optical efficiency of IFI (including the optical fiber) have been tested in the laboratory. Taking into account the loss on the beam splitter (that re-directs 8% of the light to the field camera) the total transmittance efficiency is $\sim$ 80%. At present, IFI can be mounted and used independently for fiber-coupling also other instruments and/or performing imaging and photometry with the field camera.

Building on the experience gained with IFI, a parallel work for the implementation of an optical fiber interface is under way also for Aqueye+. In this case, the main purpose is to trigger a prompt use of Aqueye+ in the ToO mode for targeting transient or short duration events. As for Iqueye, this solution has also the advantage of maintaining Aqueye+ in a dedicated, thermally controlled room in the telescope dome. The final solution adopted for fiber-coupling Aqueye+ is different from that of Iqueye, because the Nasmyth focus of the Copernicus telescope is not available. After considering other possibilities (Zampieri et al., 2016), eventually we opted for positioning an optical fiber directly at the telescope focal plane, exploiting the mechanical support provided by AFOSC and the telescope field camera for pointing and guiding. This activity is still ongoing.

For both instruments, a major concern is the efficiency of the optical coupling. In this respect, a crucial problem to face is to minimize the losses when

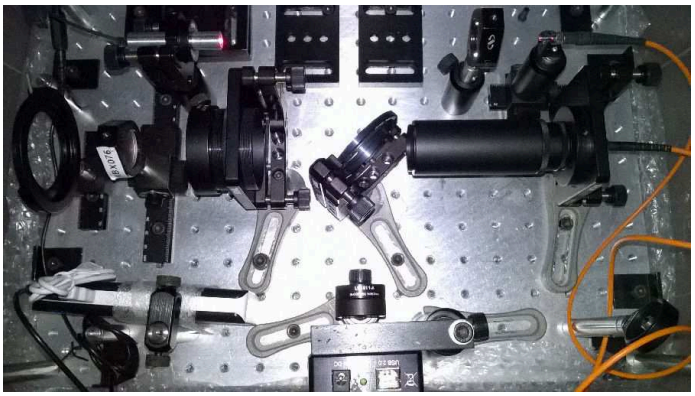

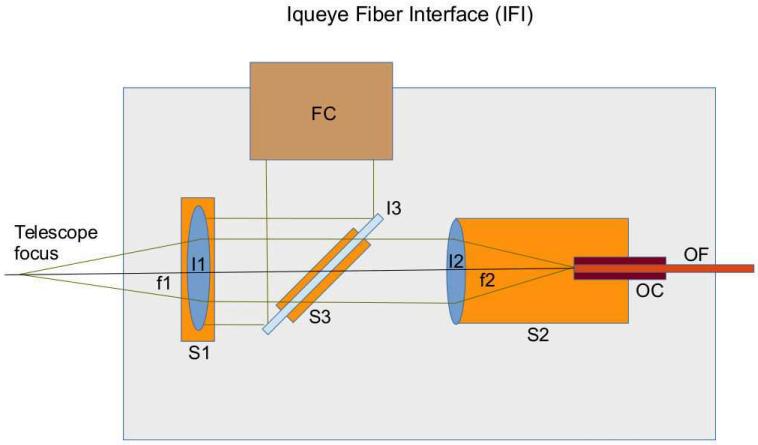

Figure 1. *Top*: Iqueye Fiber Interface (IFI). Opto-mechanical interface for coupling Iqueye with the 1.2 m Galileo telescope, attached at the Nasmyth focus. *Bottom*: Optical design and main opto-mechanical components of IFI. After the telescope focus the incoming beam is collimated through an achromatic lens doublet (I1) and then focused on the optical fiber (OF) with a second achromatic doublet (I2). A beam splitter (I3) is inserted in the collimated portion of the beam. S1, S2 and S3 are the corresponding opto-mechanical supports, and OC is the fiber connector. I3 reflects 8% of the incoming light towards a field camera (FC), and transmits the remaining 92% to the optical fiber. The focal lengths of the two doublets are $f_1 = 200$ mm and $f_2 = 100$ mm, leading to an overall demagnification of 1:2. The core of the (multimode) optical fiber has a diameter of 365 micrometers, that corresponds to 12.5 arcsec. The image of the field camera has a plate scale of 62.3 arcsec/mm and a field of view of 11.8 x 7.4 arcmin^2. Filters can be inserted in the collimated beam between I1 and I3.

injecting light into the instruments. To this end, one needs to carefully select the properties of the optical fiber and to insert additional optical elements. The light injection from the fiber into each instrument is realized by means of a dedicated opto-mechanical module (module Z), that acts as a focal multiplier. A module is placed in front of each instrument, and is properly centered and focussed. For Iqueye the magnification of this module is 2.5, while for Aqueye+ it is 2.

4. Scientific goals, experiments and projects

As mentioned above, one of the main goals of the AQUEYE+IQUEYE project is achieving tens of ps time resolution, needed to bring Quantum Optics concepts into the astronomical domain. We are pursuing it in exploratory experiments, in particular the measurement of the second order correlation of star light through a modern version of the Hanbury Brown and Twiss Intensity Interferometry experiment (Hanbury Brown et al. 1974 and references therein). In 2016 we started *an experiment of stellar intensity interferometry on* a km baseline using the Asiago telescopes and our instrumentation (Zampieri et al., 2016; Naletto et al., 2016). Nowadays, there is renewed interest for this technique because of the possibility of exploiting multiple and very long (km) baselines *to image and resolve stellar environments* on sub-milli-arcsec angular scales.

The other main goal of the project is performing optical High Time Resolution Astrophysics with ms or sub-ms time resolution to study rapidly varying phenomena in different types of astrophysical sources. We are pursuing it in a number of regular observing programs tailored to:

- Optical pulsars (in synergy with facilities operating at other wavelengths), to study with unprecedented accuracy their timing behaviour and pulse shape.

- Timing of optical transients and counterparts of binary systems with compact objects, to search for rapid optical variability.

- Lunar occultations (in synergy with other telescopes in Europe), to measure stellar radii/asymmetries with milli-arcsec angular resolution and determine the binary nature and separation of tight binary systems.

- Transits/occultations of Trans-Neptunian Objects, to determine their orbit and physical properties.

In the following we will report on recent results obtained from the first two programs.

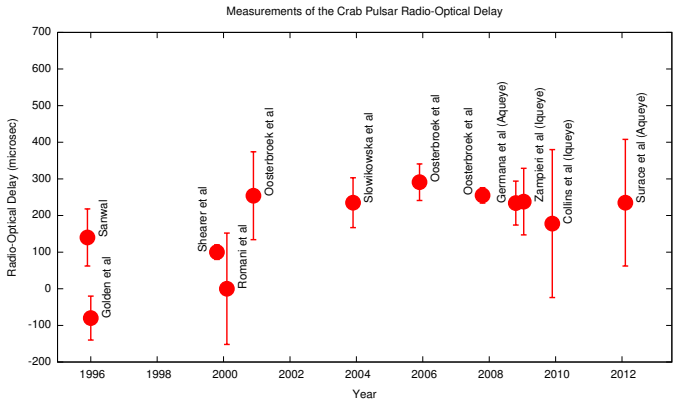

Figure 2. Delay between the time of arrival of the main pulse of the Crab pulsar in the radio band and that in the optical band. Different points refer to measurements taken by different authors (as indicated) with different instruments since 1996. Results before year 2000 may be affected by significant systematic errors. We have been regularly monitoring this delay since 2008.

5. Scientific results

5.1. Very fast photometry (timing) of optical pulsars

Within this program we perform a regular monitoring of the Crab pulsar with both Aqueye+@Copernicus (e.g. Germanà et al. 2012) and IFI+Iqueye@Galileo. At present, this is the only regular optical monitoring program of the Crab pulsar and represents the optical analogue of the Jodrell Bank radio monitoring program[2]. Observations of the Crab pulsar were taken also with Iqueye@NTT in two runs (Jan, Dec) in 2009 (Zampieri et al., 2014), when very fast photometry (timing) of a number of optical pulsars including PSRB 0540-69 (Fermi LAT Collaboration et al., 2015) and the Vela pulsar (Spolon et al., 2019), was carried out.

One of the main goals of this program is to study the evolution of the delay between the time of arrival of the main pulse in the radio band and that in the optical band. It is quite well established that, since at least the beginning of 2000, the pulse in the optical leads that in the radio by 150–250 μs (e.g. Oosterbroek et al. 2008 and references therein). Our most recent measurements, taken since 2008, confirm these findings (Figure 2; see Germanà et al. 2012; Zampieri et al. 2014). The optical and radio beams are probably misaligned (1.5–3 deg) because at the position where electrons emit optical photons the magnetic field has a slightly different orientation. Regular monitoring observations are carried out to

[2]http://www.jb.man.ac.uk/ pulsar/crab.html

search for a possible evolution of this delay, that may be induced by a significant reconfiguration of the magnetic field of the pulsar or by a change in the geometry of the emission region.

Besides a delay, the optical timing solution calculated on a timescale of a few days shows a significant drift from the radio ephemeris. This difference may be related to the optical measurements tracking the intrinsic daily/weekly pulsar noise (Čadež et al., 2016) and/or to dispersion measure variations not completely removed from radio data (while optical data do not depend on them). In this respect, optical data provide a robust and independent confirmation of the radio timing solution and a means to study the "typical" Crab pulsar frequency noise on a daily timescale. Another reason to monitor the timing history of the Crab pulsar in the optical band is to study its short term evolution after the occurrence of glitches and/or flares in the Crab nebula (e.g. Čadež et al. 2016).

5.2. Very fast photometric monitoring of optical transients

MAXI 1820+070 is a bright and uncatalogued X-ray transient source discovered on Mar 11, 2018 by Kawamuro et al. (2018), later identified with the optical transient ASASSN-18ey. The source was proposed to be a candidate black hole X-ray binary by Baglio et al. (2018). It shows pronounced and fast variability/flaring activity in both the X-ray and optical bands (Tucker et al., 2018).

After the discovery of the source, in April 2018 we promptly started a fast-photometry monitoring campaign with IFI+Iqueye and Aqueye+ (Zampieri et al., 2018a,b; Fiori et al., 2018). This effort was carried out in synergy with the SMARTNet multiwavelength network[3]. A joint photometric and spectroscopic campaign was simultaneously undertaken with the Asiago and ANS Collaboration telescopes (Munari et al., 2018a,b). We found that, compared to a nearby reference star, in Apr and Jun 2018 the power spectrum of MAXI J1820+070 shows significant red noise and quasi periodic oscillations (QPOs).

The power spectrum of 3600s of data taken on Apr 18-19, 2018 is shown in Figure 3. We detect a significant quasi-periodic oscillation (QPO) on the top of three broad-band noise components (in part induced by the sky background; Zampieri et al. 2018a). The QPO has a centroid frequency of 128±2 mHz, a full-width-half-maximum of 24±5 mHz, and a fractional root-mean-square (rms) variability of 3.1±0.3%. Another QPO-like feature at a lower frequency and with lower significance is present in the power spectrum with a centroid frequency of 71±4 mHz, a full-width-half-maximum of 36±16 mHz, and a fractional rms variability of 3.2±0.6%. The properties (frequency and width) of the 128 mHz optical QPO are also consistent with those of the QPO at ∼0.12 Hz detected in the power spectrum of quasi-simultaneous Swift observations of MAXI J1820+070 taken between Apr 16 and 20, 2018. Furthermore, the 128 mHz QPO has a

[3]https://www.isdc.unige.ch/SMARTNet/

width consistent with that of the optical QPO reported in Yu et al. (2018). The frequency difference between the two measurements, that are approximately 3.7 days apart, is 29 mHz. The fractional increment of the centroid frequency is consistent with that calculated for a similar QPO detected in the X-rays with *NuSTAR* and reported in Buisson et al. (2018).

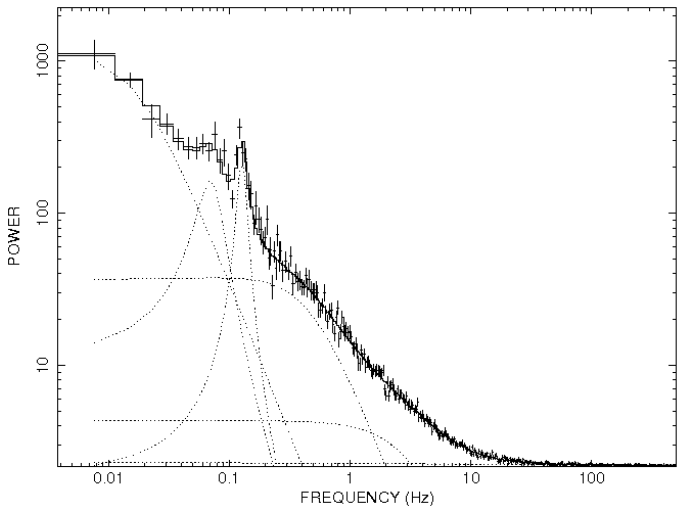

Figure 3. Power density spectrum (Lehay normalized) of MAXI 1820+070 taken with IFI+Iqueye on Apr 18-19, 2018 (Zampieri et al., 2018a). Four observations for a total duration of 3600s were considered. Power spectra were computed from the non-background subtracted light curves with a time bin of 1 ms and were then averaged over intervals of 130s duration.

On June 9-10, 2018, we detected other two QPO-like features (Fiori et al., 2018). The power spectra of 4500s of data, calculated with a time bin of 1 ms and then averaged over intervals of 65s duration, show two broad peaks on the top of a broad-band noise component. The higher frequency QPO-like feature has a centroid frequency of 268±12 mHz, a full-width-half-maximum of 150±39 mHz, and a fractional rms variability of 1.9±0.2%. The lower frequency QPO is less significant and has a centroid frequency of 151±6 mHz, a full-width-half-maximum of 33±16 mHz, and a fractional rms variability of 1.2±0.3%. We obtained acceptable fits of the power spectrum also with two harmonically-related QPOs, that have width and significance similar to those reported above. Acceptable fits are obtained for 1:2, 2:3, or 3:5 centroid frequency ratios. A fit with harmomically-related QPOs performed on the April IFI+Iqueye observations gives similar results for the same harmonic ratios (1:2, 2:3 or 3:5).

The origin of the low frequency X-ray QPOs detected in black hole X-ray binaries has been matter of intense debate. They are thought to originate from the LenseThirring (LT) precession of the hot inner part of the accretion disc, tilted from the equatorial plane of the central rotating black hole (Ingram et al., 2009). The recent detection of QPOS in the optical and infrared band, in addition to the X-ray band, provides precious additional information to understand this phenomenon. Optical and infrared QPOs may be produced directly from the inner disc through synchrotron emission, modulated at the LT precession frequency (Veledina et al., 2015). Or, the inner disc undergoes LT precession and illuminates varying outer regions of the accretion disc, generating a reprocessed optical QPO (Veledina & Poutanen, 2015). If the optical/infrared emission comes from a jet launched from the accretion disc, jet precession/modulation may be driven by LT precession of the disc (Malzac et al., 2018).

6. Conclusions

Aqueye+ and IFI+Iqueye are two very fast photon counters operating in Asiago. They are used for performing very fast photometry of astrophysical sources and modern implementation experiments of the Hanbury Brown and Twiss Intensity Interferometer. Iqueye is fiber-fed through an independent instrument (IFI).

As part of our very-fast photometry observing programs, we have been regularly monitoring the Crab pulsar radio-optical delay since 2008. No significant variation of the delay has occurred, indicating that the relative position and geometry of the radio and optical emission regions have not changed. We carried out also a monitoring campaign of the X-ray transient MAXI J1820+070, detecting a number of QPOs in the power spectrum that will provide precious additional information on this phenomenon. We plan to continue the presently active experiments and observing programs, and to make Aqueye+@Copernicus fiber-fed and permanently available in the ToO mode. We may in principle export this technique for coupling instruments at other meter-class facilities.

Very fast optical multicolor photometry allows a variety of prime interest scientific questions to be addressed in the domain of High Time Resolution Astrophysics even with meter-class telescopes. Coordinated multi-wavelength campaigns most often benefit from the support of small telescopes world-wide to guarantee adequate temporal coverage. At the same time, forefront instrumentation allows for unique observations to be made. Highly experimental programs, technological development activities, and training of young astronomers can be run almost exclusively on such facilities.

Acknowledgements. We are grateful to all the staff of the Asiago observing station (Venerio Chiomento, Giancarlo Farisato, Aldo Frigo, Giorgio Martorana, Luciano Traverso, Robertino Bau', Giovanni Costa, Alessandro Siviero) for their work and support. We also thank Marco Fiaschi, Tommaso Occhipinti, Enrico Verroi and Paolo Zoccarato for their external support to the project. This wok is based on observations

collected at the Copernicus telescope (Asiago, Italy) of the INAF-Osservatorio Astronomico di Padova and at the Galileo telescope (Asiago, Italy) of the University of Padova. This project is partly supported by the University of Padova under the Quantum Future Strategic Project, by the Italian Ministry of University MIUR through the programme PRIN 2006, by the Project of Excellence 2006 Fondazione CARIPARO, by INAF-Astronomical Observatory of Padova under the grant "Osservazioni con strumentazione astronomica ad elevata risoluzione temporale e modellizzazione di emissione ottica variabile", and by Fondazione Banca Popolare di Marostica-Volksbank.

References

Baglio, M. C., Russell, D. M., & Lewis, F., Optical observations of MAXI J1820+070 suggest it is a black hole X-ray binary. 2018, *The Astronomer's Telegram*, **11418**

Barbieri, C., Naletto, G., Occhipinti, T., et al., AquEYE, a single photon counting photometer for astronomy. 2009, *Journal of Modern Optics*, **56**, 261, DOI: 10.1080/09500340802450565

Buisson, D., Fabian, A., Alston, W., et al., Exponential increase in X-ray QPO frequency with time in MAXI J1820+070. 2018, *The Astronomer's Telegram*, **11578**

Dravins, D., Barbieri, C., Fosbury, R. A. E., et al., QuantEYE: The Quantum Optics Instrument for OWL. 2005, *ArXiv Astrophysics e-prints, astro-ph/0511027*

Fermi LAT Collaboration, Ackermann, M., Albert, A., et al., An extremely bright gamma-ray pulsar in the Large Magellanic Cloud. 2015, *Science*, **350**, 801, DOI: 10.1126/science.aac7400

Fiori, M., Zampieri, L., Burtovoi, A., et al., Other low-frequency optical QPO-like features in MAXI J1820+070 detected with IFI+IQUEYE@Galileo. 2018, *The Astronomer's Telegram*, **11824**

Germanà, C., Zampieri, L., Barbieri, C., et al., Aqueye optical observations of the Crab Nebula pulsar. 2012, *Astron. Astrophys.*, **548**, A47, DOI: 10.1051/0004-6361/201118754

Hanbury Brown, R., Davis, J., & Allen, L. R., The Angular Diameters of 32 Stars. 1974, *Mon. Not. R. Astron. Soc.*, **167**, 121, DOI: 10.1093/mnras/167.1.121

Ingram, A., Done, C., & Fragile, P. C., Low-frequency quasi-periodic oscillations spectra and Lense-Thirring precession. 2009, *Mon. Not. R. Astron. Soc.*, **397**, L101, DOI: 10.1111/j.1745-3933.2009.00693.x

Kawamuro, T., Negoro, H., Yoneyama, T., et al., MAXI/GSC detection of a probable new X-ray transient MAXI J1820+070. 2018, *The Astronomer's Telegram*, **11399**

Malzac, J., Kalamkar, M., Vincentelli, F., et al., A jet model for the fast IR variability of the black hole X-ray binary GX 339-4. 2018, *Mon. Not. R. Astron. Soc.*, **480**, 2054, DOI: 10.1093/mnras/sty2006

Munari, U., Zampieri, L., Ochner, P., & Manzini, F., MAXI 1820+070 has completed the decline from the recent optical re-brightening following the soft to hard transition. 2018a, *The Astronomer's Telegram*, **12157**

Munari, U., Zampieri, L., Ochner, P., & Manzini, F., Short-lived episodes of emission line splitting in the candidate black hole X-ray binary MAXI 1820+070. 2018b, *The Astronomer's Telegram*, **11899**

Naletto, G., Barbieri, C., Occhipinti, T., et al., Iqueye, a single photon-counting photometer applied to the ESO new technology telescope. 2009, *Astron. Astrophys.*, **508**, 531, DOI: 10.1051/0004-6361/200912862

Naletto, G., Barbieri, C., Verroi, E., et al., Aqueye Plus: a very fast single photon counter for astronomical photometry to quantum limits equipped with an Optical Vortex coronagraph. 2013, in Proc. SPIE, Vol. **8875**, *Quantum Communications and Quantum Imaging XI*, 88750D

Naletto, G., Zampieri, L., Barbieri, C., et al., A 3.9 km baseline intensity interferometry photon counting experiment. 2016, in Proc. SPIE, Vol. **9980**, *Quantum Communications and Quantum Imaging XIV*, 99800G

Oosterbroek, T., Cognard, I., Golden, A., et al., Simultaneous absolute timing of the Crab pulsar at radio and optical wavelengths. 2008, *Astron. Astrophys.*, **488**, 271, DOI: 10.1051/0004-6361:200809751

Spolon, A., Zampieri, L., Burtovoi, A., et al., Timing analysis and pulse profile of the Vela pulsar in the optical band from Iqueye observations. 2019, *Mon. Not. R. Astron. Soc.*, **482**, 175, DOI: 10.1093/mnras/sty2605

Tucker, M. A., Shappee, B. J., Holoien, T. W.-S., et al., ASASSN-18ey: The Rise of a New Black Hole X-Ray Binary. 2018, *Astrophys. J., Lett.*, **867**, L9, DOI: 10.3847/2041-8213/aae88a

Čadež, A., Zampieri, L., Barbieri, C., et al., What brakes the Crab pulsar? 2016, *Astron. Astrophys.*, **587**, A99, DOI: 10.1051/0004-6361/201526490

Veledina, A. & Poutanen, J., Reprocessing model for the optical quasi-periodic oscillations in black hole binaries. 2015, *Mon. Not. R. Astron. Soc.*, **448**, 939, DOI: 10.1093/mnras/stu2737

Veledina, A., Revnivtsev, M. G., Durant, M., Gandhi, P., & Poutanen, J., Discovery of correlated optical/X-ray quasi-periodic oscillations in black hole binary SWIFT J1753.5-0127. 2015, *Mon. Not. R. Astron. Soc.*, **454**, 2855, DOI: 10.1093/mnras/stv2201

Yu, W., Lin, J., Mao, D., et al., Further detection of the optical low frequency QPO in the black hole transient MAXI J1820+070. 2018, *The Astronomer's Telegram*, **11591**

Zampieri, L., Fiori, M., Burtovoi, A., et al., Low-frequency optical QPO in MAXI J1820+070 detected with IFI+IQUEYE@Galileo. 2018a, *The Astronomer's Telegram*, **11723**

Zampieri, L., Fiori, M., Burtovoi, A., et al., Optical timing observations of MAXI J1820+070 with IFI+IQUEYE and AQUEYE+ soon after state transition. 2018b, *The Astronomer's Telegram*, **11936**

Zampieri, L., Naletto, G., Barbieri, C., et al., Intensity interferometry with Aqueye+ and Iqueye in Asiago. 2016, in Proc. SPIE, Vol. **9907**, *Optical and Infrared Interferometry and Imaging V*, 99070N

Zampieri, L., Naletto, G., Barbieri, C., et al., Aqueye+: a new ultrafast single photon counter for optical high time resolution astrophysics. 2015, in Proc. SPIE, Vol. **9504**, *Photon Counting Applications 2015*, 95040C

Zampieri, L., Čadež, A., Barbieri, C., et al., Optical phase coherent timing of the Crab nebula pulsar with Iqueye at the ESO New Technology Telescope. 2014, *Mon. Not. R. Astron. Soc.*, **439**, 2813, DOI: 10.1093/mnras/stu136

Contrib. Astron. Obs. Skalnaté Pleso **49**, 97 – 106, (2019)

Interferometry with Meter-Class Telescopes

R.M. Roettenbacher

Yale Center for Astronomy & Astrophysics
Yale University, (E-mail: rachael.roettenbacher@yale.edu)

Received: November 1, 2018; Accepted: January 23, 2019

Abstract. Small telescopes have the potential to be connected into an interferometric array to effectively make a significantly larger telescope. Interferometric arrays utilizing small telescopes, particularly the Center for High-Angular Resolution Astronomy (CHARA) Array, are at the forefront of optical interferometry with observations leading to accurate stellar radii and even images of stellar surfaces. Here, the challenges and advantages of small-telescope, long-baseline optical interferometry will be discussed, alongside the current status and recent results from small-telescope interferometric arrays.

Key words: Instrumentation: interferometers – Techniques: interferometric – Stars: imaging

1. Introduction

Long-baseline optical interferometry (LBOI) is a technique that allows for a number of small telescopes to be connected to effectively make a much larger telescope. While individual telescopes are limited in angular resolution, θ, by the diffraction limit $\theta \approx \lambda/D$, where λ is wavelength and D is telescope diameter, the angular resolution of an interferometer is $\theta \approx \lambda/B$, where B is the distance between two telescopes (the baseline). This allows for smaller telescopes to be used together in order to obtain the resolution of a prohibitively large telescope with a single or segmented mirror.

Light emitted from a star at one point in time will hit the telescopes in an array at different times, traveling a different distance to each telescope. In order to make use of interference between the light collected at the different telescopes, the light emitted from the star at one point in time must be recombined at the same time. Unlike sub-millimeter and radio interferometry, LBOI, which operates in visible and infrared wavelengths, requires the light be combined at the interferometer. In order to account for the difference in path length that the light travels, there are movable delay lines that lengthen the distance that the light travels.

Each pair of telescopes used to make an observation is a projected baseline that uniquely maps to a point on the stellar surface (or one point in the uv plane, the projection of each baseline onto the plane of the sky). As the Earth rotates, the projected baseline of each pair of telescopes changes and different points on

the stellar surface are mapped to. By observing a target for many hours or even nights, the surface can be mapped by the interferometric observations.

For more detailed explanations of optical interferometry, see Lawson (2000) and Labeyrie et al. (2006).

2. Long-baseline Optical Interferometers

Today, there are three routinely-functioning long-baseline optical interferometers. The interferometers are all different, and included here are the major characteristics of each. Also included is an interferometer currently being constructed and another being discussed as the next-generation interferometer.

2.1. Very Large Telescope Interferometer

The Very Large Telescope Interferometer (VLTI) is located at the European Southern Observatory (ESO; Paranal, Chile). The interferometer is capable of combining light from either the four 8.2-m Unit Telescopes (UTs) or four 1.8-m Auxiliary Telescopes (ATs). The baselines accessible to VLTI span lengths up to 130 m. While the locations of the UTs are fixed, the ATs are movable. The configurations of the ATs change several times each observing semester and are designed such that no two baselines are the same in a single configuration. Up to four telescopes can be combined at once at VLTI, allowing for 6 baselines for each configuration (Glindemann et al., 2000). Recently, the New Adaptive Optics Module for Interferometry (NAOMI) has been added to the ATs to improve performance (Le Bouquin et al., 2018).

Currently, three instruments are available at VLTI that each combine four telescopes and can be used on either the UTs or ATs. The Precision Integrated-Optics Near-infrared Imaging ExpeRiment (PIONIER) combines light in H-band (Le Bouquin et al., 2011). GRAVITY is combines light in K-band and can reach resolutions of 2 milliarcseconds (mas) with the longest baseline of the ATs (Gravity Collaboration et al., 2017). The Multi-AperTure mid-Infrared SpectrScopic Experiment (MATISSE) can be used in L, M, or N band, with $R \sim 1000$ in L-band (Lopez et al., 2014).

Up-to-date, detailed information can be found at `https://www.eso.org/sci/facilities/paranal/telescopes/vlti.html`.

2.2. Navy Precision Optical Interferometer

The Navy Precision Optical Interferometer (NPOI) is located at the Anderson Mesa Station of Lowell Observatory (Arizona, USA) and is jointly run by the U.S. Naval Observatory, the Naval Research Laboratory, and Lowell Observatory. Currently, NPOI consists of six siderostats that are located at fixed positions. However, three new movable 1-m telescopes are being obtained and installed. NPOI will have baselines spanning 8–432 m (van Belle et al., 2018).

There are three instruments available at NPOI. NPOI Classic combines light from two telescopes in visible wavelengths. New Classic is similar, but uses light from three telescopes (Sun et al., 2014). The Visible Imaging System for Interferometric Observations at NPOI (VISION) combines light from six telescopes in the visible wavelengths (Garcia et al., 2016, based off of the MIRC instrument at CHARA, see below) for a maximum resolution of ~ 0.2 mas.

Information on NPOI can be found at `http://www2.lowell.edu/rsch/npoi/index.php`.

2.3. Center for High-Angular Resolution Astronomy Array

The Center for High-Angular Resolution Astronomy (CHARA) Array is owned and operated by Georgia State University. The CHARA Array is located at Mount Wilson Observatory (California, USA). The CHARA Array consists of six 1-m telescopes at fix locations. The baselines span 34–331 m (ten Brummelaar et al., 2005). When using all six telescopes, 15 different baselines are possible. Currently, adaptive optics are being installed at each telescope to improve seeing and magnitude limits (ten Brummelaar et al., 2018).

The CHARA Array has six beam combiners available. The CLASSIC and the CLassic Interferometry with Multiple Baselines (CLIMB) beam combiners at the CHARA Array make use of two or three telescopes, respectively, and operate in H- or K-band (ten Brummelaar et al., 2013). The Jouvence of the Fiber-Linked Unit for optical recombination (JouFLU) beam combiner uses two telescopes and operates in the K-band (Scott et al., 2013). The two-beam Precision Astronomical Visible Observations (PAVO) instrument operates in visible wavelengths (Ireland et al., 2008). The Visible spEctroGraph and polArimeter (VEGA) beam combiner uses visible light from four telescopes and can operate with a resolution of to $R \sim 30000$. The Michigan InfraRed Combiner (MIRC) instrument was the first interferometric instrument able to combine light from six telescopes (Monnier et al., 2004). MIRC originally worked in H-band, but recent upgrades to MIRC-X allow for observations in H- and J-bands (Kraus et al., 2018), with maximum resolutions of 0.5 and 0.4 mas, respectively.

Current information can be found at `http://www.chara.gsu.edu/`.

2.4. Magdalena Ridge Observatory Interferometer

The Magdalena Ridge Observatory Interferometer (MROI) is currently under construction by the New Mexico Institute of Mining and Technology. It is located at Magdalena Ridge Observatory (New Mexico, US). When complete, MROI will consist of 10 1.4-m telescopes. There will be a total of 28 positions for the telescopes with baselines possible from 7.8–347 m.

The first telescope had first light in 2016 (Creech-Eakman et al., 2018). With the second telescope arriving by the end of 2019, first fringes are expected

in 2020. Up-to-date information can be found at `http://www.mro.nmt.edu/about-mro/interferometer-mroi/`.

2.5. Planet Formation Imager

The Planet Formation Imager (PFI) is a concept for the next generation of interferometers. PFI will consist of twelve 3-m telescopes and have a maximum baseline of 1.2 km, a significant increase over current baseline sizes. This increase will allow for an angular resolution ($\sim$ 0.2 mas) capable of imaging planets in their protoplanetary disks (Monnier et al., 2018). Many of the current interferometric technologies need to be advanced to adapt to this significantly bigger and more complicated array.

For more information on PFI, see `http://www.planetformationimager.org/`.

3. Science Results

Using stellar interferometers to measure the angular diameter of stars were first theorized and attempted in the mid-nineteenth century, but it was nearly fifty years before the diameter of a star was first directly measured. The interferometers and instruments listed above are only the most recent and most impressive iterations capable of doing far more then measuring angular diameters, θ. With these tools, LBOI has been used to produce a wide range of results in astronomy, many of which have been fundamental to the field.

3.1. Stellar Radii

The first and most common results from interferometry are angular diameters (e.g., Michelson & Pease, 1921). Along with parallax estimates, this is a straight-forward measurement of the radius of a star. These observations have been collected for hundreds of stars in order to establish a well-constrained relationships between temperatures and radii across the Hertzsprung-Russell (H-R) diagram (e.g., Boyajian et al., 2015). Radii measurements of low-mass stars, in particular, have been used to improve theoretical interior and atmosphere models (e.g., Ségransan et al., 2003; Berger et al., 2006).

Using detailed measurements of stellar diameters, the ages of co-evolving stars can be constrained (e.g., Jones et al., 2015, for the Ursa Major moving group). Changes in angular diameter can be measured for pulsating stars, such as Cepheid variables (e.g., Mérand et al., 2005).

3.2. Binary Orbits and Stellar Multiplicity

Interferometry has been able to constrain the orbits of a number and large variety of binary systems using visual detections (e.g., Anderson, 1920). Combining

interferometric and radial velocity observations allows for a detailed understanding of the system, resulting in the ability to determine stellar masses and place the system components on the H-R diagram (e.g., Roettenbacher et al., 2015b). Interferometry also makes it possible to detect the secondary components of single-lined spectroscopic orbits with the ability to detect secondary stars up to nearly 400 times fainter than the primary (the highest confirmed H-band flux ratio between primary and secondary components is 370:1 with MIRC at the CHARA Array; Roettenbacher et al., 2015a). The VLTI interferometric detection of nearby companions have been instrumental in showing that nearly all O-stars ($91 \pm 3\%$; Sana et al., 2014) are gravitationally bound to at least one other star.

Very recently, the orbits of stars at the center of the galaxy have been measured interferometrically (Gravity Collaboration et al., 2018) with the GRAVITY instrument and the UTs at VLTI. These remarkable observations serve as tests to general relativity.

3.3. Parametric Model Fitting and Aperture Synthesis Imaging

When combining observations from many baselines, parametric model fitting and aperture synthesis imaging become possible. Parametric model fitting uses regularization to obtain the best-fit model based on the information on the object's size, shape, orientation, etc. that is extracted from interferometric data. The aperture synthesis technique allows for the stars to be directly imaged as they appear on the sky. A distinct advantage of aperture synthesis is that imaging techniques using other types of observations (e.g., Doppler imaging with high-resolution spectroscopy) have degeneracies in the location of features on the stellar surface and are unable to determine the position angle on the sky.

Parametric model fitting has been used, in particular, to investigate the structure of disks around stars. For example, this includes young stellar objects, Herbig Ae/Be stars (e.g., Lazareff et al., 2017, with PIONIER at VLTI), disks around post-asymptotic giant branch binary systems (e.g., Hillen et al., 2017, with the decommissioned MID-infrared Interferometric (MIDI) combiner at VLTI), and Be star disks (e.g., ζ Tauri, Tycner et al., 2004, with NPOI).

The first image of a main-sequence star other the Sun was imaged using the MIRC beam combiner at the CHARA Array. With this technique, Altair was shown to definitively be an oblate spheroid from its rapid rotation (Monnier et al., 2007). Altair was just one of several rapidly rotating stars to be used to constrain gravity darkening in stars with radiative outer envelopes (e.g., Che et al., 2011; Zhao et al., 2011). The distorted shape of interacting binary systems has also been imaged (e.g., Zhao et al., 2008; Baron et al., 2012).

The disk of ejected material around the Be star δ Scorpii has been imaged throughout the star's orbit (Che et al., 2012). Another system with a disk, ϵ Aurigae was observed throughout the eclipse of the supergiant primary star by a companion with a disk. A series of interferometric images clearly show

the disk passing in front of the supergiant star (Kloppenborg et al., 2010). The eject of Nova Delphini 2013 was observed interferometrically as it expanded. On three nights of observation, the expanding shell was imaged and showed signs of asymmetry (Schaefer et al., 2014).

Features on the surfaces of stars are also resolved. The temperature differences across convective cells of asymptotic giant branch stars have been resolved (Paladini et al., 2018). Snapshot images of cool stars with starspots have also been obtained (Hummel et al., 2017). The entire surface of the spotted stars ζ Andromedae and σ Geminorum have been imaged by observing with the MIRC instrument at the CHARA Array throughout a stellar rotation (Roettenbacher et al., 2016, 2017).

4. Summary

LBOI is a unique and powerful tool that allows us to obtain fundamental measurements and direct images of the stars. Current interferometers are used for a wide variety of science, from measuring stellar angular diameters to determining the orbit of stars at the galactic center to detecting spots on the stellar surface. The references for the science cases included here merely scratch the surface of the literature available on each topic. The upcoming advancements in interferometric instrumentation and technology will allow for studies across astronomy, particularly probes into stellar astrophysics and the formation of stellar and protoplanetary systems to detect the beginnings of planet formation.

The slides for the talk associated with these conference proceedings can be found at `https://www.astro.sk/conferences/75AI2018/talks/A02.pdf`.

Acknowledgements. R.M.R. acknowledges support from the YCAA Prize Postdoctoral Fellowship and is grateful to M. Creech-Eakman, J.D. Monnier, G.H. Schaefer, and G.T. van Belle for additional information on the interferometric resources. Additional thanks are given to A. Mérand for thoughtful suggestions that improved these proceedings.

References

Anderson, J. A., Application of Michelson's interferometer method to the measurement of close double stars. 1920, *Astrophys. J.*, **51**, DOI: 10.1086/142551

Baron, F., Monnier, J. D., Pedretti, E., et al., Imaging the Algol Triple System in the H Band with the CHARA Interferometer. 2012, *Astrophys. J.*, **752**, 20, DOI: 10.1088/0004-637X/752/1/20

Berger, D. H., Gies, D. R., McAlister, H. A., et al., First Results from the CHARA Array. IV. The Interferometric Radii of Low-Mass Stars. 2006, *Astrophys. J.*, **644**, 475, DOI: 10.1086/503318

Boyajian, T., von Braun, K., Feiden, G. A., et al., Stellar diameters and temperatures - VI. High angular resolution measurements of the transiting exoplanet host stars HD 189733 and HD 209458 and implications for models of cool dwarfs. 2015, *Mon. Not. R. Astron. Soc.*, **447**, 846, DOI: 10.1093/mnras/stu2502

Che, X., Monnier, J. D., Tycner, C., et al., Imaging Disk Distortion of Be Binary System δ Scorpii near Periastron. 2012, *Astrophys. J.*, **757**, 29, DOI: 10.1088/0004-637X/757/1/29

Che, X., Monnier, J. D., Zhao, M., et al., Colder and Hotter: Interferometric Imaging of β Cassiopeiae and α Leonis. 2011, *Astrophys. J.*, **732**, 68, DOI: 10.1088/0004-637X/732/2/68

Creech-Eakman, M. J., Romero, V. D., Payne, I., et al., The Magdalena Ridge Observatory interferometer: first light and deployment of the first telescope on the array. 2018, in Society of Photo-Optical Instrumentation Engineers (SPIE) Conference Series, Vol. **10701**, *Society of Photo-Optical Instrumentation Engineers (SPIE) Conference Series*, 1070106

Garcia, E. V., Muterspaugh, M. W., van Belle, G., et al., Vision: A Six-telescope Fiber-fed Visible Light Beam Combiner for the Navy Precision Optical Interferometer. 2016, *Publ. Astron. Soc. Pac.*, **128**, 055004, DOI: 10.1088/1538-3873/128/963/055004

Glindemann, A., Abuter, R., Carbognani, F., et al., The VLT Interferometer: a unique instrument for high-resolution astronomy. 2000, in Proc. SPIE, Vol. **4006**, *Interferometry in Optical Astronomy*, ed. P. Léna & A. Quirrenbach, 2–12

Gravity Collaboration, Abuter, R., Accardo, M., et al., First light for GRAVITY: Phase referencing optical interferometry for the Very Large Telescope Interferometer. 2017, *Astron. Astrophys.*, **602**, A94, DOI: 10.1051/0004-6361/201730838

Gravity Collaboration, Abuter, R., Amorim, A., et al., Detection of the gravitational redshift in the orbit of the star S2 near the Galactic centre massive black hole. 2018, *Astron. Astrophys.*, **615**, L15, DOI: 10.1051/0004-6361/201833718

Hillen, M., Van Winckel, H., Menu, J., et al., A mid-IR interferometric survey with MIDI/VLTI: resolving the second-generation protoplanetary disks around post-AGB binaries. 2017, *Astron. Astrophys.*, **599**, A41, DOI: 10.1051/0004-6361/201629161

Hummel, C. A., Monnier, J. D., Roettenbacher, R. M., et al., Orbital Elements and Stellar Parameters of the Active Binary UX Arietis. 2017, *Astrophys. J.*, **844**, 115, DOI: 10.3847/1538-4357/aa7b87

Ireland, M. J., Mérand, A., ten Brummelaar, T. A., et al., Sensitive visible interferometry with PAVO. 2008, in Proc. SPIE, Vol. **7013**, *Optical and Infrared Interferometry*, 701324

Jones, J., White, R. J., Boyajian, T., et al., The Ages of A-Stars. I. Interferometric Observations and Age Estimates for Stars in the Ursa Major Moving Group. 2015, *Astrophys. J.*, **813**, 58, DOI: 10.1088/0004-637X/813/1/58

Kloppenborg, B., Stencel, R., Monnier, J. D., et al., Infrared images of the transiting disk in the ϵ Aurigae system. 2010, *Nature*, **464**, 870, DOI: 10.1038/nature08968

Kraus, S., Monnier, J. D., Anugu, N., et al., The MIRC-X 6-telescope imager: key science drivers, instrument design and operation. 2018, in Society of Photo-Optical Instrumentation Engineers (SPIE) Conference Series, Vol. **10701**, *Society of Photo-Optical Instrumentation Engineers (SPIE) Conference Series*, 1070123

Labeyrie, A., Lipson, S. G., & Nisenson, P. 2006, *An Introduction to Optical Stellar Interferometry* (Cambridge, UK: Cambridge University Press), 360

Lawson, P. R., ed. 2000, *Principles of Long Baseline Stellar Interferometry*

Lazareff, B., Berger, J.-P., Kluska, J., et al., Structure of Herbig AeBe disks at the milliarcsecond scale . A statistical survey in the H band using PIONIER-VLTI. 2017, *Astron. Astrophys.*, **599**, A85, DOI: 10.1051/0004-6361/201629305

Le Bouquin, J.-B., Berger, J.-P., Beuzit, J.-L., et al., Characterization of ALPAO deformable mirrors for the NAOMI VLTI Auxiliary Telescopes adaptive optics. 2018, in Society of Photo-Optical Instrumentation Engineers (SPIE) Conference Series, Vol. **10703**, *Society of Photo-Optical Instrumentation Engineers (SPIE) Conference Series*, 1070371

Le Bouquin, J.-B., Berger, J.-P., Lazareff, B., et al., PIONIER: a 4-telescope visitor instrument at VLTI. 2011, *Astron. Astrophys.*, **535**, A67, DOI: 10.1051/0004-6361/201117586

Lopez, B., Lagarde, S., Jaffe, W., et al., An Overview of the MATISSE Instrument—Science, Concept and Current Status. 2014, *The Messenger*, **157**, 5

Mérand, A., Kervella, P., Coudé du Foresto, V., et al., The projection factor of δ Cephei. A calibration of the Baade-Wesselink method using the CHARA Array. 2005, *Astron. Astrophys.*, **438**, L9, DOI: 10.1051/0004-6361:200500139

Michelson, A. A. & Pease, F. G., No. 203. Measurement of the diameter of alpha Orionis with the interferometer. 1921, *Contributions from the Mount Wilson Observatory / Carnegie Institution of Washington*, **203**, 1

Monnier, J. D., Berger, J.-P., Millan-Gabet, R., & ten Brummelaar, T. A., The Michigan Infrared Combiner (MIRC): IR imaging with the CHARA Array. 2004, in Proc. SPIE, Vol. **5491**, *New Frontiers in Stellar Interferometry*, ed. W. A. Traub, 1370

Monnier, J. D., Ireland, M., Kraus, S., et al., Planet formation imager: project update. 2018, in Society of Photo-Optical Instrumentation Engineers (SPIE) Conference Series, Vol. **10701**, *Society of Photo-Optical Instrumentation Engineers (SPIE) Conference Series*, 1070118

Monnier, J. D., Zhao, M., Pedretti, E., et al., Imaging the Surface of Altair. 2007, *Science*, **317**, 342, DOI: 10.1126/science.1143205

Paladini, C., Baron, F., Jorissen, A., et al., Large granulation cells on the surface of the giant star π^1 Gruis. 2018, *Nature*, **553**, 310, DOI: 10.1038/nature25001

Roettenbacher, R. M., Monnier, J. D., Fekel, F. C., et al., Detecting the Companions and Ellipsoidal Variations of RS CVn Primaries. II. o Draconis, a Candidate for Recent Low-mass Companion Ingestion. 2015a, *Astrophys. J.*, **809**, 159, DOI: 10.1088/0004-637X/809/2/159

Roettenbacher, R. M., Monnier, J. D., Henry, G. W., et al., Detecting the Companions and Ellipsoidal Variations of RS CVn Primaries. I. σ Geminorum. 2015b, *Astrophys. J.*, **807**, 23, DOI: 10.1088/0004-637X/807/1/23

Roettenbacher, R. M., Monnier, J. D., Korhonen, H., et al., No Sun-like dynamo on the active star ζ Andromedae from starspot asymmetry. 2016, *Nature*, **533**, 217, DOI: 10.1038/nature17444

Roettenbacher, R. M., Monnier, J. D., Korhonen, H., et al., Contemporaneous Imaging Comparisons of the Spotted Giant σ Geminorum Using Interferometric, Spectroscopic, and Photometric Data. 2017, *Astrophys. J.*, **849**, 120, DOI: 10.3847/1538-4357/aa8ef7

Sana, H., Le Bouquin, J.-B., Lacour, S., et al., Southern Massive Stars at High Angular Resolution: Observational Campaign and Companion Detection. 2014, *Astrophys. J., Suppl.*, **215**, 15, DOI: 10.1088/0067-0049/215/1/15

Schaefer, G. H., Brummelaar, T. T., Gies, D. R., et al., The expanding fireball of Nova Delphini 2013. 2014, *Nature*, **515**, 234, DOI: 10.1038/nature13834

Scott, N. J., Millan-Gabet, R., Lhomé, E., et al., Jouvence of Fluor: Upgrades of a Fiber Beam Combiner at the CHARA Array. 2013, *Journal of Astronomical Instrumentation*, **2**, 1340005, DOI: 10.1142/S2251171713400059

Ségransan, D., Kervella, P., Forveille, T., & Queloz, D., First radius measurements of very low mass stars with the VLTI. 2003, *Astron. Astrophys.*, **397**, L5, DOI: 10.1051/0004-6361:20021714

Sun, B., Jorgensen, A. M., Landavazo, M., et al., The new classic data acquisition system for NPOI. 2014, in Proc. SPIE, Vol. **9146**, *Optical and Infrared Interferometry IV*, 914620

ten Brummelaar, T. A., McAlister, H. A., Ridgway, S. T., et al., First Results from the CHARA Array. II. A Description of the Instrument. 2005, *Astrophys. J.*, **628**, 453, DOI: 10.1086/430729

ten Brummelaar, T. A., Sturmann, J., Ridgway, S. T., et al., The Classic/climb Beam Combiner at the CHARA Array. 2013, *Journal of Astronomical Instrumentation*, **2**, 1340004, DOI: 10.1142/S2251171713400047

ten Brummelaar, T. A., Sturmann, J., Sturmann, L., et al., The CHARA array adaptive optics program. 2018, in Society of Photo-Optical Instrumentation Engineers (SPIE) Conference Series, Vol. **10703**, *Society of Photo-Optical Instrumentation Engineers (SPIE) Conference Series*, 1070304

Tycner, C., Hajian, A. R., Armstrong, J. T., et al., The Circumstellar Envelope of ζ Tauri through Optical Interferometry. 2004, *Astron. J.*, **127**, 1194, DOI: 10.1086/381068

van Belle, G. T., Armstrong, J. T., Benson, J. A., et al., Many interesting things are afoot at the Navy Precision Optical Interferometer. 2018, in Society of Photo-Optical Instrumentation Engineers (SPIE) Conference Series, Vol. **10701**, *Society of Photo-Optical Instrumentation Engineers (SPIE) Conference Series*, 1070105

Zhao, M., Gies, D., Monnier, J. D., et al., First Resolved Images of the Eclipsing and Interacting Binary β Lyrae. 2008, *Astrophys. J., Lett.*, **684**, L95, DOI: 10.1086/592146

Zhao, M., Monnier, J. D., & Che, X., Interferometric studies of rapid rotators. 2011, in IAU Symposium, Vol. **272**, *Active OB Stars: Structure, Evolution, Mass Loss, and Critical Limits*, ed. C. Neiner, G. Wade, G. Meynet, & G. Peters, 44–55

Contrib. Astron. Obs. Skalnaté Pleso **49**, 107 – 118, (2019)

High precision ground-based photometry with 1-m class telescopes

M. Lendl

Space Research Institute, Austrian Academy of Sciences, (E-mail: monika.lendl@oeaw.ac.at)

Received: December 20, 2018; Accepted: January 24, 2019

Abstract. Recent years have seen an improvement of photometric precision with ground-based observatories routinely achieving a relative precision at the sub-mmag level. With optimized instrumentation and observing strategies, as well as ample time resources, ground-based 1m-class facilities are important players in a wide range of fields. I here summarize the main instrumental and observational strategies conductive to obtaining high-precision ground-based photometry, and review data analysis methods to account for instrumental correlated noise. Finally, I review the main applications of high-precision photometry related to the search for, and characterization of, extrasolar planets.

Key words: photometry – exoplanets – observing techniques

1. Introduction

The technique of monitoring the brightness of stars, photometry, is one of the fundamental pillars of observational astronomy. Thanks to major advances in technology (in particular the rise of CDD detectors, which have enabled digitized data processing), the attainable precision has improved by several orders of magnitude over the last few decades. While measurements at the part-per-million level remain reserved for space mission such as Kepler (Borucki et al., 2010), TESS (Ricker et al., 2014) and soon CHEOPS (Broeg et al., 2013), small ground-based observatories have shown to routinely achieve precisions at the sub-mmag level. Operating at this level of precision, small ground-based telescopes have become key players in a wide variety of fields, ranging from Solar System research to extragalactic astronomy. Ground-based photometry with 1m-class telescopes benefits from ample time resources, cost-efficient facilities and high operational flexibility.

In the following, I summarize the main aspects of instrumentation related to high-precision ground-based telescopes and detail the most common observational and data analysis strategies. I further review recent results of high-precision photometry in the framework of exoplanet research.

2. Instrumentation, observing techniques and data analysis

2.1. Optimizing instrument and setup

Most current set-ups for photometric instruments at 1-m class telescopes consist of a CCD camera paired with a set of photometric filters designed to match – as closely as possible – the requirements imposed on the system by its scientific purpose. The wavelength range often presents a prime constraint, as some observations might target specific emission or absorption lines, obtain precise measurements across different wavelength ranges, or simply maximize the overall photometric precision. To this end, back-illuminated CCDs have found widespread use as these offer improved quantum efficiencies compared to traditional front-illuminated designs. Further enhancements in terms of S/N can be reached by using deep-depletion chips, which allow for better efficiency towards the near-IR.

While improved quantum efficiency and broad filters serve to optimize the signal photon noise, detector readout noise and thermal noise (*dark current*) can remain an issue. The former may be limited by choosing optimal exposure times that both, maximize the duty cycle and limit the number of readouts necessary. The latter can be efficiently controlled by actively cooling the instrument. While temperatures below -100 C previously necessitated the use of coolants such as liquid Nitrogen, low temperatures can now be obtained through multi-stage Peltier elements.

Finally, uneven CCD sensitivity and system throughput manifest in flat field variations across the detector frame. While occasional cleaning of detector entrance window and filters can help reduce some flat field inhomogeneities, defects located at the CCD itself cannot be easily eliminated. In practice, the best way for the user to avoid these is to map their location on the CCD and optimize pointing such that no imperfections coincide with any target of interest.

2.2. Observing techniques

Any observation using relative photometry is naturally limited by the quality and number of the available reference sources. The first and most basic step for successful high-precision photometry thus consists in optimizing the pointing direction such that the field of view contains a maximum number of stable reference sources with magnitudes similar to that of the target. As the on-sky density of stars of a given magnitude decreases drastically for bright stars, the need to fit at least two objects onto the detector usually places a natural limit on the typical magnitudes accessible by any given instrument. Small telescopes here benefit from large fields of view that allow them to often outperform large facilities on bright stars.

Two approaches are commonly used (often in concert) to minimize the effects of detector sensitivity variations in high precision photometry:

– **Improved guiding:** Ideally, if the targets' location on the detector is invariant, the flat-field remains constant throughout the observations. Precise guiding is employed to approach as much as possible to this ideal case. However, many 1-m class telescopes do not possess their own guiding camera. This situation can be remedied by employing a self-guiding mechanism using the science frames to measure guiding drifts. If absolute positional information is required, this can be done matching the frames against a catalog (as done e.g. with EulerCam, Lendl et al., 2012). Alternatively, frames can also be matched directly against each other using e.g. the DONUTS algorithm (McCormac et al., 2013).

– **Widening the PSF:** The second approach to limit flat-field effects consists in artificially widening the stellar PSFs on the detector. Most commonly, this is done by slightly defocusing the telescope and thereby spreading the starlight over many pixels and averaging out sensitivity variations. An added advantage of this technique is that exposure times can be increased without saturating the detector, which in turn leads to improved duty cycles and observation efficiency. Defocusing has been used widely, and Figure 1 shows a typical PSF of a defocused observation (Southworth et al., 2009) dedicated to exoplanet science. Recently, also diffusers have been used to this end, leading to encouraging results (Stefansson et al., 2017, 2018). Limits of this technique are naturally imposed by the observed field. Well-suited to low-density star fields or bright stars, defocusing will decrease the overall precision when crowded fields, e.g. stellar clusters, are observed and defocusing leads to a high degree of blended sources.

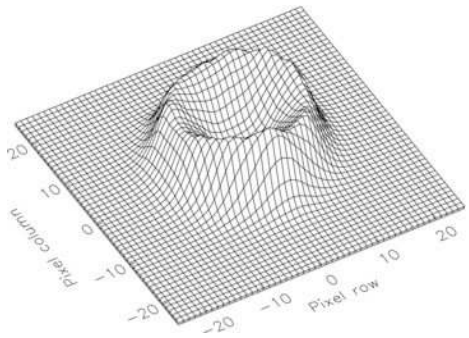

Figure 1. Example of a heavily defocused PSF by Southworth et al. (2009).

2.3. Data analysis techniques

Once photometry has been obtained and extracted, relative photometry is usually obtained by constructing a reference source by co-adding several stable field stars and dividing the target by this reference flux. At this point, the most prominent signatures of the Earth's atmosphere, such as variable transparency and absorption due to changing air mass, are removed. Usually however, at this point, a light curve is not entirely free of systematic effects. These are often smooth trends caused by differential extinction and sky background variations, or effects due to variable seeing or pointing jitter. As this *red noise* is usually related to external parameters, we can attempt to model its behavior and eventually account for it when making astrophysical inferences. To do so, two methods are currently widely used.

– **Parametric baseline models:** In this approach, one assumes that the red noise can be approximated by parametric functions of a set of state variables ($\bar{\xi}$) describing the observations. Typical state variables are time (t), the stellar FWHM, coordinate offsets ($\Delta x, \Delta y$), or the sky background (see e.g. Gillon et al., 2010, 2012). One then assumes that the observed signal can be modeled by an equation of the form

$$F(t) = M(t)\, B(\bar{\xi})\,, \tag{1}$$

where $F(t)$ is the observed flux, $M(t)$ is the astrophysical effect and $B(\bar{\xi})$ is the photometric baseline function. In principle, $B(\bar{\xi})$ may take any analytic form deemed adequate, however, it is most commonly assumed to be relatively simple, such as combinations of low-order polynomials. As an example $B(\bar{\xi})$ may be a second-order polynomial in time combined with a linear drift in coordinate shifts:

$$B(t, \Delta x, \Delta y) = A_0 + A_1 t + A_2 t^2 + A_3 \Delta x + A_4 \Delta y\,, \tag{2}$$

where A_i are coefficients. To correctly propagate errors, baseline coefficients are best fitted at the same time as the astrophysical model. Further, care should be taken at selecting the most appropriate baseline model and avoid over-fitting. A common approach for model selection is via the Bayesian Information Criterion (e.g. Schwarz, 1978). When several models show similar evidence, it is advantageous to combine results obtained from a range of models to avoid biasing the results (Gibson, 2014).

– **Gaussian processes:** Often correlations are too complex to be easily described with parametric models, or their dependence on external parameters does not follow a simple analytic form. In this case, Gaussian Processes offer a remedy to account for red noise in the data analysis while at the same time correctly accounting for uncertainties (see e.g. Rasmussen & Williams, 2006 for a detailed introduction to GPs). In short, within the GP framework, a

time-series is interpreted as a multivariate Gaussian distribution around a mean function defined by the astrophysical model and having a covariance matrix C. The elements of the covariance matrix take a functional form (the *kernel*). An example of a widely used kernel is the square exponential kernel,

$$C_{i,j} = \xi \exp\left(-\frac{1}{2}\frac{(t_i - t_j)^2}{l}\right), \tag{3}$$

where ξ denotes the maximum covariance and l is the length scale parameter. In this example, time is the only state variable included, however kernels incorporating one or several other state variables are easily devised. If desired, an additional term $\delta_{i,j}\sigma^2$ can be added to account for extra white noise. As with parametric models, the kernel parameters *"hyperparameters"* are usually fit at the same time as the parameters of the mean function. Since the introduction of GPs to high precision photometry (Gibson et al., 2012), several open-source software packages (Aigrain et al., 2016; Foreman-Mackey et al., 2017) have become available simplifying the use of GPs in the framework of light curve analysis.

3. High-precision photometry for exoplanet science

Transiting exoplanets have been one of the key fields pushing ground-based photometric observations to their optimum: for the detection of transiting sub-Joivan planets, relative precisions at the sub-mmag level have to be obtained throughout several hours. Furthermore, photometric observations open up a range of charcterization avenues. I will briefly outline a set of projects and results related to exoplanets that have been obtained with 1-m class telescopes.

3.1. Transit searches and follow-up

Until the advent of the TESS space mission (Ricker et al., 2014), ground based surveys were the only means of discovering transiting planets across the entire sky. While monitoring mostly relied on very small aperture facilities (e.g. Bakos et al., 2004; Pollacco et al., 2006), 1-m-class facilities have been instrumental in the follow-up efforts, eliminating false positives such as blended eclipsing binaries, and obtaining high-precision transit light curves. Figure 2 shows an example of a follow-up transit light curve of the hot Jupiter WASP-164b observed with the 1.2m Euler telescope. Some surveys have been making use of 1-m-class instrumentation (e.g. OGLE (Konacki et al., 2003), NGTS (Wheatley et al., 2018) and TRAPPIST-UCDTS/SPECULOOS (Gillon et al., 2016; Delrez et al., 2018a)) to search for the signatures of transiting planets. In these cases, the choice for larger instruments has mostly been driven by needs of observing faint sources (see e.g. the discovery of a planetary system around an ultra-cool dwarf, Gillon et al. 2016), or the need for high photometric precision (see e.g. the detection of a sub-Neptune, West et al. 2018).

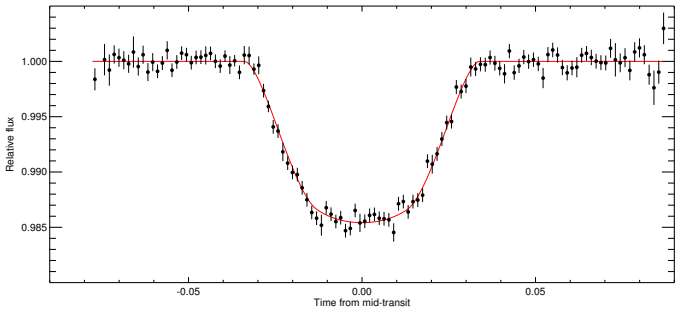

Figure 2. Follow-up photometry for the hot Jupiter WASP-164 obtained with EulerCam at the 1.2m Euler telescope, Lendl et al. (2019).

3.2. Atmospheric characterization: occultations and transmission spectra

Going beyond the mere detection of exoplanets, 1-m class ground-based facilities have also provided ample opportunities to study these planets in detail. For hot Jupiters (close-in gas giants), thermal emission from the planetary dayside produces occultation depths of several hundreds of ppm in the red optical or near-IR (I or z' band). By combining several individual occultation light curves, 1-m class facilities have secured a number of detections (Abe et al., 2013; Lendl et al., 2013; Mancini et al., 2013; Delrez et al., 2016, 2018b). The example of the hot Jupiter WASP-103b (Delrez et al., 2018b), a detection for which 13 individual light curves were combined, is shown in Figure 3.

Similarly, precise measurements of transit light curves at different wavelengths allow to obtain a planetary transmission spectrum at low resolution. While the most prominent features of Na and K (Seager & Sasselov, 2000; Charbonneau et al., 2002) are too narrow-band to be accessible with small facilities, broad spectral features, such as slopes due to high-altitude hazes can be detected (Pont et al., 2008). A wide range of facilities and observing programs (e.g. de Mooij et al., 2012; Mancini et al., 2013; Mallonn et al., 2015; Southworth et al., 2017) have been dedicated to this science case. As an example, the detection of increased atmospheric absorption towards the blue (as expected from high-altitude hazes), in the hot Jupiter WASP-36b is shown in Figure 4. Since stellar spots (occulted or unoculted during transit) can bias the observed transit depth, this technique is most ideally pursued with simultaneous multi-band observations.

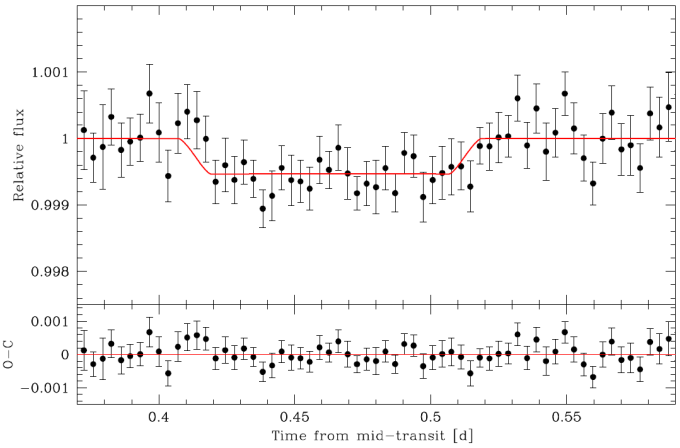

Figure 3. Occultation light curve of the hot Jupiter WASP-103b (Delrez et al., 2018b) using EulerCam and TRAPPIST.

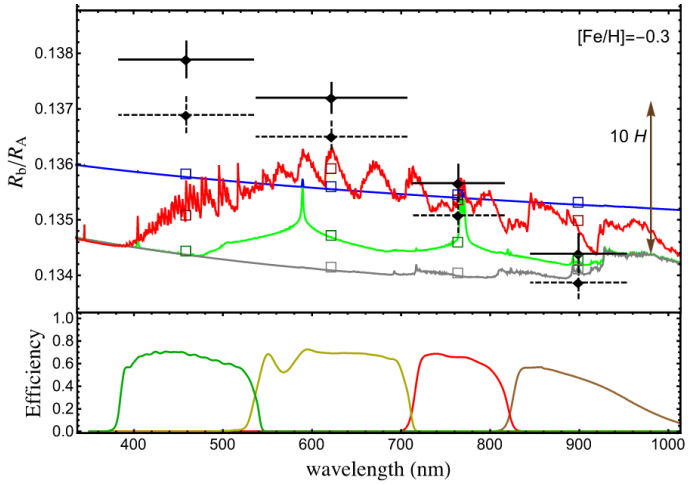

Figure 4. Low-resolution transmission spectrum of WASP-36 by Mancini et al. (2016) using the MPG 2.2m telescope.

3.3. Transit timing variations

While in single-planet systems, transits are expected to occur in equally-spaced intervals, the observed transit periods can vary in multi-planet systems, owing to the dynamical interactions between the host and its several planets. If detected, these *transit timing variations (TTVs)* (Agol et al., 2005; Holman & Murray, 2005) can reveal additional planets and serve to measure planet masses. For extremely close-in planets, TTVs can even occur due to tidal interactions between the planet and the host: planets are losing angular momentum and slowly spiraling into inwards. Measuring the decay rate of the planetary orbit can thus reveal the dissipation of tidal energy in the host star, constraining the tidal quality parameter Q'_* (see e.g. Collier Cameron & Jardine, 2018, and references therein). A range of surveys have targeted hot Jupiters with 1m-class facilities, searching for TTVs (e.g. Holman et al., 2006; Lendl et al., 2010; Maciejewski et al., 2010). While TTVs can be substantial for planets in multiplanet systems (e.g. Holman et al., 2010), tentative evidence for a period decay has only been found in one hot Jupiter to date (Maciejewski et al., 2018). The same technique can be used to determine the nature of planet candidates identified by the Kepler satellite (von Essen et al., 2018), in cases where the radial-velocity method cannot be used (e.g. faint objects).

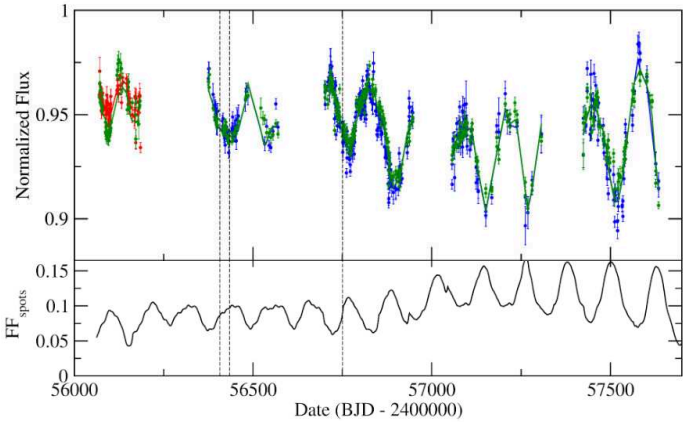

Figure 5. The long-term variability (top) and spot filling factors (bottom) of the planet host star GJ 1214 by Mallonn et al. (2018).

3.4. Stellar hosts

Next to the planets themselves, information on the activity and rotation of stellar hosts can be gathered with high-precision photometry. This is either done

through long-term monitoring (e.g. Mallonn et al., 2018, see Fig, 5), capturing the stellar variability induced as star spots move in- and out-of view. In transit light curves observed at very high precision, short-term brightenings have been observed (Tregloan-Reed et al., 2013; Juvan et al., 2018). These can be attributed to the planet crossing over a star spot, and consequently blocking light from a less emissive stellar region. As similar short-term variations can easily be due to correlated noise rather than a physical effect, simultaneous observations from several facilities have shown to help to distinguish real star spot crossings from instrumental systematics (e.g. Lendl et al., 2013; Mancini et al., 2017; Juvan et al., 2018). When observed in several subsequent transits, spot crossings can reveal the stellar rotation rate and constrain the planetary orbital obliquity.

Acknowledgements. M.L. acknowledges support from the Austrian Research Promotion Agency (FFG) under project 859724 "GRAPPA".

References

Abe, L., Gonçalves, I., Agabi, A., et al., The secondary eclipses of WASP-19b as seen by the ASTEP 400 telescope from Antarctica. 2013, *Astron. Astrophys.*, **553**, A49, DOI: 10.1051/0004-6361/201220351

Agol, E., Steffen, J., Sari, R., & Clarkson, W., On detecting terrestrial planets with timing of giant planet transits. 2005, *Mon. Not. R. Astron. Soc.*, **359**, 567, DOI: 10.1111/j.1365-2966.2005.08922.x

Aigrain, S., Parviainen, H., & Pope, B. J. S., K2SC: flexible systematics correction and detrending of K2 light curves using Gaussian process regression. 2016, *Mon. Not. R. Astron. Soc.*, **459**, 2408, DOI: 10.1093/mnras/stw706

Bakos, G., Noyes, R. W., Kovács, G., et al., Wide-Field Millimagnitude Photometry with the HAT: A Tool for Extrasolar Planet Detection. 2004, *Publ. Astron. Soc. Pac.*, **116**, 266, DOI: 10.1086/382735

Borucki, W. J., Koch, D., Basri, G., et al., Kepler Planet-Detection Mission: Introduction and First Results. 2010, *Science*, **327**, 977, DOI: 10.1126/science.1185402

Broeg, C., Fortier, A., Ehrenreich, D., et al., CHEOPS: A transit photometry mission for ESA's small mission programme. 2013, in European Physical Journal Web of Conferences, Vol. **47**, *European Physical Journal Web of Conferences*, 03005

Charbonneau, D., Brown, T. M., Noyes, R. W., & Gilliland, R. L., Detection of an Extrasolar Planet Atmosphere. 2002, *Astrophys. J.*, **568**, 377, DOI: 10.1086/338770

Collier Cameron, A. & Jardine, M., Hierarchical Bayesian calibration of tidal orbit decay rates among hot Jupiters. 2018, *ArXiv e-prints* [[arXiv]1801.10561]

de Mooij, E. J. W., Brogi, M., de Kok, R. J., et al., Optical to near-infrared transit observations of super-Earth GJ 1214b: water-world or mini-Neptune? 2012, *Astron. Astrophys.*, **538**, A46, DOI: 10.1051/0004-6361/201117205

Delrez, L., Gillon, M., Queloz, D., et al., SPECULOOS: a network of robotic telescopes to hunt for terrestrial planets around the nearest ultracool dwarfs. 2018a, in Society of Photo-Optical Instrumentation Engineers (SPIE) Conference Series, Vol. **10700**, *Ground-based and Airborne Telescopes VII*, 107001I

Delrez, L., Madhusudhan, N., Lendl, M., et al., High-precision multiwavelength eclipse photometry of the ultra-hot gas giant exoplanet WASP-103 b. 2018b, *Mon. Not. R. Astron. Soc.*, **474**, 2334, DOI: 10.1093/mnras/stx2896

Delrez, L., Santerne, A., Almenara, J.-M., et al., WASP-121 b: a hot Jupiter close to tidal disruption transiting an active F star. 2016, *Mon. Not. R. Astron. Soc.*, **458**, 4025, DOI: 10.1093/mnras/stw522

Foreman-Mackey, D., Agol, E., Ambikasaran, S., & Angus, R., Fast and Scalable Gaussian Process Modeling with Applications to Astronomical Time Series. 2017, *Astron. J.*, **154**, 220, DOI: 10.3847/1538-3881/aa9332

Gibson, N. P., Reliable inference of exoplanet light-curve parameters using deterministic and stochastic systematics models. 2014, *Mon. Not. R. Astron. Soc.*, **445**, 3401, DOI: 10.1093/mnras/stu1975

Gibson, N. P., Aigrain, S., Roberts, S., et al., A Gaussian process framework for modelling instrumental systematics: application to transmission spectroscopy. 2012, *Mon. Not. R. Astron. Soc.*, **419**, 2683, DOI: 10.1111/j.1365-2966.2011.19915.x

Gillon, M., Jehin, E., Lederer, S. M., et al., Temperate Earth-sized planets transiting a nearby ultracool dwarf star. 2016, *Nature*, **533**, 221, DOI: 10.1038/nature17448

Gillon, M., Lanotte, A. A., Barman, T., et al., The thermal emission of the young and massive planet CoRoT-2b at 4.5 and 8 μm. 2010, *Astron. Astrophys.*, **511**, A3, DOI: 10.1051/0004-6361/200913507

Gillon, M., Triaud, A. H. M. J., Fortney, J. J., et al., The TRAPPIST survey of southern transiting planets. I. Thirty eclipses of the ultra-short period planet WASP-43 b. 2012, *Astron. Astrophys.*, **542**, A4, DOI: 10.1051/0004-6361/201218817

Holman, M. J., Fabrycky, D. C., Ragozzine, D., et al., Kepler-9: A System of Multiple Planets Transiting a Sun-Like Star, Confirmed by Timing Variations. 2010, *Science*, **330**, 51, DOI: 10.1126/science.1195778

Holman, M. J. & Murray, N. W., The Use of Transit Timing to Detect Terrestrial-Mass Extrasolar Planets. 2005, *Science*, **307**, 1288, DOI: 10.1126/science.1107822

Holman, M. J., Winn, J. N., Latham, D. W., et al., The Transit Light Curve Project. I. Four Consecutive Transits of the Exoplanet XO-1b. 2006, *Astrophys. J.*, **652**, 1715, DOI: 10.1086/508155

Juvan, I. G., Lendl, M., Cubillos, P. E., et al., PyTranSpot: A tool for multiband light curve modeling of planetary transits and stellar spots. 2018, *Astron. Astrophys.*, **610**, A15, DOI: 10.1051/0004-6361/201731345

Konacki, M., Torres, G., Jha, S., & Sasselov, D. D., An extrasolar planet that transits the disk of its parent star. 2003, *Nature*, **421**, 507, DOI: 10.1038/nature01379

Lendl, M., Afonso, C., Koppenhoefer, J., et al., New parameters and transit timing studies for OGLE2-TR-L9 b. 2010, *Astron. Astrophys.*, **522**, A29, DOI: 10.1051/0004-6361/201014940

Lendl, M., Anderson, D. R., Bonfanti, A., et al., WASP-147b, 160Bb, 164b, and 165b: two hot Saturns and two Jupiters, including two planets with metal-rich hosts. 2019, *Mon. Not. R. Astron. Soc.*, **482**, 301, DOI: 10.1093/mnras/sty2667

Lendl, M., Anderson, D. R., Collier-Cameron, A., et al., WASP-42 b and WASP-49 b: two new transiting sub-Jupiters. 2012, *Astron. Astrophys.*, **544**, A72, DOI: 10.1051/0004-6361/201219585

Lendl, M., Gillon, M., Queloz, D., et al., A photometric study of the hot exoplanet WASP-19b. 2013, *Astron. Astrophys.*, **552**, A2, DOI: 10.1051/0004-6361/201220924

Maciejewski, G., Dimitrov, D., Neuhäuser, R., et al., Transit timing variation in exoplanet WASP-3b. 2010, *Mon. Not. R. Astron. Soc.*, **407**, 2625, DOI: 10.1111/j.1365-2966.2010.17099.x

Maciejewski, G., Fernández, M., Aceituno, F., et al., Planet-star interactions with precise transit timing. I. The refined orbital decay rate for WASP-12 b and initial constraints for HAT-P-23 b, KELT-1 b, KELT-16 b, WASP-33 b, and WASP-103 b. 2018, *arXiv e-prints* [[arXiv]1812.02438]

Mallonn, M., Herrero, E., Juvan, I. G., et al., GJ 1214: Rotation period, starspots, and uncertainty on the optical slope of the transmission spectrum. 2018, *Astron. Astrophys.*, **614**, A35, DOI: 10.1051/0004-6361/201732300

Mallonn, M., Nascimbeni, V., Weingrill, J., et al., Broad-band spectrophotometry of the hot Jupiter HAT-P-12b from the near-UV to the near-IR. 2015, *Astron. Astrophys.*, **583**, A138, DOI: 10.1051/0004-6361/201425395

Mancini, L., Ciceri, S., Chen, G., et al., Physical properties, transmission and emission spectra of the WASP-19 planetary system from multi-colour photometry. 2013, *Mon. Not. R. Astron. Soc.* [[arXiv]1306.6384], DOI: 10.1093/mnras/stt1394

Mancini, L., Kemmer, J., Southworth, J., et al., An optical transmission spectrum of the giant planet WASP-36 b. 2016, *Mon. Not. R. Astron. Soc.*, **459**, 1393, DOI: 10.1093/mnras/stw659

Mancini, L., Southworth, J., Raia, G., et al., Orbital alignment and star-spot properties in the WASP-52 planetary system. 2017, *Mon. Not. R. Astron. Soc.*, **465**, 843, DOI: 10.1093/mnras/stw1987

McCormac, J., Pollacco, D., Skillen, I., et al., DONUTS: A Science Frame Autoguiding Algorithm with Sub-Pixel Precision, Capable of Guiding on Defocused Stars. 2013, *Publ. Astron. Soc. Pac.*, **125**, 548, DOI: 10.1086/670940

Pollacco, D. L., Skillen, I., Collier Cameron, A., et al., The WASP Project and the SuperWASP Cameras. 2006, *Publ. Astron. Soc. Pac.*, **118**, 1407, DOI: 10.1086/508556

Pont, F., Knutson, H., Gilliland, R. L., Moutou, C., & Charbonneau, D., Detection of atmospheric haze on an extrasolar planet: the 0.55-1.05 μm transmission spectrum of HD 189733b with the HubbleSpaceTelescope. 2008, *Mon. Not. R. Astron. Soc.*, **385**, 109, DOI: 10.1111/j.1365-2966.2008.12852.x

Rasmussen, S. & Williams, C. 2006, *Gaussian Processes for Machine Learning* (The MIT Press)

Ricker, G. R., Winn, J. N., Vanderspek, R., et al., Transiting Exoplanet Survey Satellite (TESS). 2014, in Proc. SPIE, Vol. **9143**, *Space Telescopes and Instrumentation 2014: Optical, Infrared, and Millimeter Wave*, 914320

Schwarz, Estimating the Dimension of a Model. 1978, *Annals of Statistics*, **6**, 461

Seager, S. & Sasselov, D. D., Theoretical Transmission Spectra during Extrasolar Giant Planet Transits. 2000, *Astrophys. J.*, **537**, 916, DOI: 10.1086/309088

Southworth, J., Hinse, T. C., Jørgensen, U. G., et al., High-precision photometry by telescope defocusing - I. The transiting planetary system WASP-5. 2009, *Mon. Not. R. Astron. Soc.*, **396**, 1023, DOI: 10.1111/j.1365-2966.2009.14767.x

Southworth, J., Mancini, L., Madhusudhan, N., et al., Detection of the Atmosphere of the 1.6 M Exoplanet GJ 1132 b. 2017, *Astron. J.*, **153**, 191, DOI: 10.3847/1538-3881/aa6477

Stefansson, G., Li, Y., Mahadevan, S., et al., Diffuser-assisted Photometric Follow-up Observations of the Neptune-sized Planets K2-28b and K2-100b. 2018, *Astron. J.*, **156**, 266, DOI: 10.3847/1538-3881/aae6ca

Stefansson, G., Mahadevan, S., Hebb, L., et al., Toward Space-like Photometric Precision from the Ground with Beam-shaping Diffusers. 2017, *Astrophys. J.*, **848**, 9, DOI: 10.3847/1538-4357/aa88aa

Tregloan-Reed, J., Southworth, J., & Tappert, C., Transits and starspots in the WASP-19 planetary system. 2013, *Mon. Not. R. Astron. Soc.*, **428**, 3671, DOI: 10.1093/mnras/sts306

von Essen, C., Ofir, A., Dreizler, S., et al., Kepler Object of Interest Network. I. First results combining ground- and space-based observations of Kepler systems with transit timing variations. 2018, *Astron. Astrophys.*, **615**, A79, DOI: 10.1051/0004-6361/201732483

West, R. G., Gillen, E., Bayliss, D., et al., NGTS-4b: A sub-Neptune Transiting in the Desert. 2018, *ArXiv e-prints* [[arXiv]1809.00678]

Wheatley, P. J., West, R. G., Goad, M. R., et al., The Next Generation Transit Survey (NGTS). 2018, *Mon. Not. R. Astron. Soc.*, **475**, 4476, DOI: 10.1093/mnras/stx2836

Contrib. Astron. Obs. Skalnaté Pleso **49**, 119 – 124, (2019)

Astrophotonic technologies for small telescopes

R.J. Harris, Th. Anagnos and P. Hottinger

Zentrum für Astronomie der Universität Heidelberg, Landessternwarte, Königstuhl 12, 69117 Heidelberg, (E-mail: rharris@lsw.uni-heidelberg.de)

Received: November 1, 2018; Accepted: January 24, 2019

Abstract. Astrophotonics is a field combining astronomical instrumentation and photonics, with the aim of making instruments cheaper, smaller or increasing their functionality. Small telescopes are perfectly placed to take advantage of these technologies, as their size reduces the complexity of instruments. In our group at the Landessternwarte we are working on two experimental technologies that could greatly benefit spectrographs behind small telescopes. The first is photonic reformatting, akin to image slicing, but using a photonic lantern to sample the telescope point spread function. The second technology is a sensor at the focal plane of the telescope, allowing increased coupling efficiency. This sensor is composed of a 3D printed microlens array coupled to a fibre bundle. We summarise both of these devices and their potential in future small telescope instruments.

Key words: astronomy – photonics – astrophotonics – instrumentation – photonic lantern – spectroscopy – wavefront sensing

1. Introduction

The field of astrophotonics combines astronomical instrumentation and photonics, with the aim of making instruments cheaper, smaller or increasing their functionality (e.g. Bland-Hawthorn & Kern, 2009). Examples of devices developed in the field include integrated spectrographs known as arrayed waveguide gratings (e.g. Cvetojevic et al., 2009)) and wavelength filters such as fibre bragg gratings (e.g. Trinh et al., 2013). Over the last decade the challenge has been adapting these technologies to compete with conventional instrumental technologies and prove the added functionalities are useful. However, many challenges have come from the fact that most astrophotonics technologies were designed for the telecommunications industry. They generally work in the single-mode (SM) (diffraction limited) or few-mode (close to diffraction limited) regime covering wavelengths of tens of nanometers. By contrast in astronomy sources are usually multi-mode (MM) (seeing limited) and the filters used operate over wavelength ranges of hundreds of nanometers. This has required the development of new devices to allow the transition between the two. The best example of this is the photonic lantern (PL) (Leon-Saval et al., 2005), a device that allows a MM PSF to be 'split up' into many single modes. In order to retain throughput (or conserve etendue), an equal number of SMs is required to those contained in the telescope PSF.

In order to reduce the complexity of these challenges, it is necessary to close the gap on the two regimes, this requires a reduction in the number of modes. The equation governing the number of modes (e.g. Harris & Allington-Smith, 2012; Spaleniak et al., 2013) is

$$M = \left(\frac{\pi \chi D_{\mathrm{T}}}{4\lambda} \right)^2 . \tag{1}$$

Here, χ represents the seeing, or the angular point spread function (PSF) size to couple to the fibre, D_{T} is the telescope diameter and λ is the wavelength.

This shows that instruments on large telescopes in visible wavelengths require many thousands of modes. For example, we can use equation 1 to calculate the number of modes for ELT HIRES. Assuming a seeing limited mode, with a seeing of 0.6 arcseconds, at a wavelength of 400 nm and a 39.5 m telescope, we require $\approx$ 60,000 modes to efficiently sample the telescope PSF. To use SM technologies would require a more complex instrument than the current plan of using fibre bundles containing roughly 100 MM fibres. The fibres would need to operate reasonably uniformly across the seeing disc, then need to be put into a spectrograph or multiple spectrographs. Assuming an SM slit would lead to the slit being 30 cm long, which would be difficult to accurately re-image in an Echelle configuration and require very large detectors. Whilst these problems can be overcome, they are not trivial. In addition, due to the conservative nature of instrument builders, the first demonstration of the technology on these scales is unlikely. This means it is much better to start with simpler, more manageable instruments.

These simpler instruments can be for small telescopes, or large telescopes with adaptive optics (AO) systems where the PSF is SM, or contains few modes. Whilst both options have their advantages, small telescopes are normally more amenable to new technology demonstrations, with more time available. In our group at the Landessternwarte we are working on two experimental technologies that could greatly benefit small telescopes.

2. Work being undertaken at the Landessternwarte

The working group at the Landessternware consists of Robert Harris, Theodoros Anagnos and Philipp Hottinger and is mostly funded through the DFG NAIR grant. Below we detail the two main projects that benefit small telescopes.

2.1. Photonic Reformatting

Photonic reformatting is akin to image slicing, but fully integrated within the fibre. At the focal plane the tapered end of a PL acts like a conventional MM fibre, to efficiently sample the whole seeing limited PSF. This is then split up into individual SMs, or single waveguides, each of which carries a fraction of the light.

These can then be reformatted into a slit, straight line, or other shapes to be fed into a spectrograph e.g. Bland-Hawthorn et al. (2010); Spaleniak et al. (2013). Due to the nature of the reformatting, spatial information is not preserved, helping scramble the image.

As the number of modes is related to the length of the slit, fewer modes are preferable as the slit is simpler to re-image (Harris et al., 2016). This means smaller telescopes are ideally placed to test reformatting technologies.

Previous practical work (e.g. Thomson et al. (2012); Jovanovic et al. (2012); Harris et al. (2015)) and theory work (Anagnos et al., 2018) have shown the technology is viable and we are currently working on the next generation, for use with the Minerva-red spectrograph (see Figure 1).

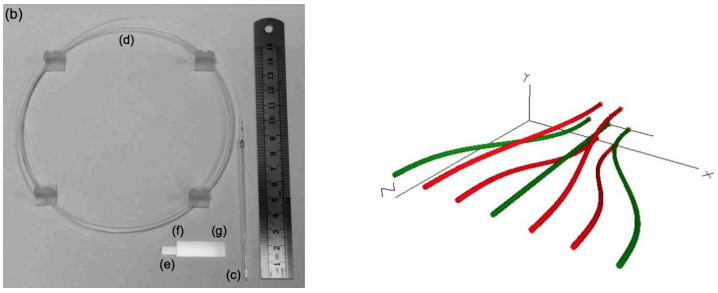

Figure 1. Example images of reformatters : **Left)** The Hybrid reformatter, modified from MacLachlan et al. (2016). (c) contains the multimode end of the photonic lantern, which is placed at the telescope focal plane. This gradually expands into a multicore fibre, containing many single mode cores (d). (e) is is the interface to the reformatter and (f-g) show the ultrafast laser inscribed (ULI) reformatter chip which takes the arrangement of fibre cores and repositions them into a slit. **Right)** The preliminary design of the Minerva-red ULI reformatter, showing the re-arrangement of cores that also takes place in the Hybrid reformatter. Once this model has been optimised, the full device will be built and packaged.

2.2. Tip-tilt sensing

Fibre fed astronomical instruments tend to use larger MM fibres, due to ease of coupling. However, to efficiently use these requires larger spectrographs (e.g. Lee & Allington-Smith, 2000), which are more difficult and costly to build and are less stable. In order to reduce the size of instruments, it helps to use smaller fibres, equivalent to smaller slits. This makes the instrument smaller, but is more difficult to efficiently couple to the telescope.

Firstly, the PSF must be diffraction limited, or close to diffraction limited in order to couple light efficiently. With small telescopes or complex AO systems

this is possible; however these still suffer from residual tip-tilt motion, reducing the coupling efficiency. With such small system it is essential to solve this problem and remove this tip-tilt motion.

Our solution, a focal plane tip-tilt sensor, allows increased coupling efficiency. This sensor is composed of a 3D printed microlens array coupled to a fibre bundle. In the centre, an SM fibre is fed to the spectrograph and surrounding this fibre are six MM fibres. In order to increase the fill fraction these surrounding fibres have a freeform microlens array printed on top (see Figure 2). The outer fibres are coupled to a fast detector, which feeds the signal to a tip-tilt mirror, stabilising the beam and reducing coupling error. It is currently under development for testing with the near diffraction limited extreme AO system at the Large Binocular Telescope (LBT), which makes it easily modifiable to allow it to work with much smaller telescopes. For more information, see Hottinger et al. (2018).

Figure 2. Example images of the tip-tilt sensor system : **Left)** The camera image of the fibre bundle. The end on the left hand side contains seven fibres, a single mode central core and six larger sensing cores. These are split off into two bundles (terminating on the right), one with a sole single mode core and the other with six larger cores for sensing. **Right)** The preliminary microlens design, adapted from Hottinger et al. (2018).

3. Conclusions and future

As astrophotonics matures it is showing that it can provide useful instrumentation for both smaller and larger scale telescopes. However, due to the complexity

and practical difficulties of building these instruments lots of technologies are ideally suited for smaller telescopes or larger telescopes with extreme adaptive optics (AO) systems. This means the more practical solution is commonly using smaller telescopes for technology development. Our research at the Landesternwarte focusses on two devices with few modes that could be of particular use to smaller telescopes.

The first is a photonic reformatter, a device akin to an image slicer for use with a high resolution spectrograph. At the focal plane of the telescope it is a large multi-mode (MM) fibre, which splits off into lots of single modes (SMs) using a photonic lantern. These SM waveguides can then be reformatted into a long slit, or other formation, to increase spectral resolving power and stability. The device is created by drawing a fibre down at one end and reformatted using ultrafast laser inscription. This device is similar in concept to an image slicer, but with a gaussian point spread function (PSF) and fully integrated, reducing alignment constraints.

The second is a tip-tilt sensor to increase coupling efficiency into SM instrumentation. Both small and large telescopes with extreme AO systems tend to suffer from tip-tilt variations, either due to the atmosphere or structural vibrations. The conventional system can compensate, though usually with an element of light loss or incomplete correction. Our solution aims to maximise the light into the SM fibre. We do this by creating a fibre bundle, with the SM fibre in the centre and six surrounding MM fibres. The inner fibre is used to transmit the science light, while the larger outer fibres are used for sensing.

We envision both technologies will help increase the coupling efficiency into few or single mode fed instruments on small telescopes and enable the new generation of astrophotonic instrumentation on telescopes.

Acknowledgements. Robert J. Harris is supported by the Deutsche Forschungsgemeinschaft (DFG) through project 326946494, 'Novel Astronomical Instrumentation through photonic Reformatting'.

References

Anagnos, T., Harris, R. J., Corrigan, M. K., et al., Simulation and optimisation of an astrophotonic reformatter. 2018, *Monthly Notices of the Royal Astronomical Society*, **478**, 4881, DOI: 10.1093/mnras/sty1396

Bland-Hawthorn, J. & Kern, P., Astrophotonics: a new era for astronomical instruments. 2009, *Optics Express*, **17**, 1880

Bland-Hawthorn, J., Lawrence, J., Robertson, G., et al., PIMMS: photonic integrated multimode microspectrograph. 2010, in Society of Photo-Optical Instrumentation Engineers (SPIE) Conference Series, Vol. **7735**, *Society of Photo-Optical Instrumentation Engineers (SPIE) Conference Series*

Cvetojevic, N., Lawrence, J. S., Ellis, S. C., et al., Characterization and on-sky demonstration of an integrated photonic spectrograph for astronomy. 2009, *Optics Express*, **17**, 18643

Harris, R. J. & Allington-Smith, J., Applications of integrated photonic spectrographs in astronomy. 2012, *Monthly Notices of the Royal Astronomical Society*, **428**, 3139

Harris, R. J., Labadie, L., Lemke, U., et al., Performance estimates for spectrographs using photonic reformatters. 2016, in *Performance estimates for spectrographs using photonic reformatters*, 9912 – 9912 – 8

Harris, R. J., MacLachlan, D. G., Choudhury, D., et al., Photonic spatial reformatting of stellar light for diffraction-limited spectroscopy. 2015, *MNRAS*, **450**, 428, DOI: 10.1093/mnras/stv410

Hottinger, P., Harris, R. J., Dietrich, P.-I., et al., Micro-lens arrays as tip-tilt sensor for single mode fiber coupling. 2018, in *Micro-lens arrays as tip-tilt sensor for single mode fiber coupling*, 10706 – 10706 – 15

Jovanovic, N., Spaleniak, I., Gross, S., et al., Integrated photonic building blocks for next-generation astronomical instrumentation I: the multimode waveguide. 2012, *Optics Express*, **20**, 17029

Lee, D. & Allington-Smith, J. R., An experimental investigation of immersed gratings. 2000, *Monthly Notices of the Royal Astronomical Society*, **312**, 57, DOI: 10.1046/j.1365-8711.2000.03151.x

Leon-Saval, S. G., Birks, T. A., Bland-Hawthorn, J., & Englund, M., Multimode fiber devices with single-mode performance. 2005, *Optics letters*, **30**, 2545

MacLachlan, D. G., Harris, R. J., Gris-Sánchez, I., et al., Efficient photonic reformatting of celestial light for diffraction-limited spectroscopy. 2016, *Monthly Notices of the Royal Astronomical Society*, **464**, 4950

Spaleniak, I., Jovanovic, N., Gross, S., et al., Integrated photonic building blocks for next-generation astronomical instrumentation II: the multimode to single mode transition. 2013, *Optics Express*, **21**, 27197, DOI: 10.1364/OE.21.027197

Thomson, R., Harris, R., Birks, T., et al., Ultrafast laser inscription of a 121-waveguide fan-out for astrophotonics. 2012, *Optics Letters*, **37**, 2331

Trinh, C. Q., Ellis, S. C., Bland-Hawthorn, J., et al., GNOSIS: the first instrument to use fiber Bragg gratings for OH suppression. 2013, *The Astronomical Journal*, **145**, 51

Contrib. Astron. Obs. Skalnaté Pleso **49**, 125 – 131, (2019)

CPCS 2.0 – new automatic tool for time-domain astronomy

P. Zieliński[1], Ł. Wyrzykowski[1], K. Rybicki[1], Z. Kołaczkowski[2,3] †, P. Bruś[3] and P. Mikołajczyk[3]

[1] *Warsaw University Astronomical Observatory, Al. Ujazdowskie 4, 00-478 Warsaw, Poland, (E-mail: pzielinski@astrouw.edu.pl)*

[2] *Nicolaus Copernicus Astronomical Centre, Polish Academy of Sciences, ul. Bartycka 18, 00-716 Warsaw, Poland*

[3] *Astronomical Institute, University of Wrocław, ul. Kopernika 11, 51-622 Wrocław, Poland*

Received: November 15, 2018; Accepted: February 25

Abstract. The Cambridge Photometric Calibration Server (CPCS) has been designed to respond to the need of automated rapid photometric data calibration and dissemination for transient events, primarily from *Gaia* space mission. The Calibration Server has been in operation since 2013 and has been used to calibrate around 50 000 observations of hundreds of transients. We present the status of the tool and demonstrate improvements made in the newest version, which is enhanced with build-in profile photometric measurement. After tests and implementation on the dedicated website, the new Server will be able to combine imaging data from multiple telescopes and is intended to provide science-ready photometric data within minutes from observations. We also present the OPTICON-supported network of telescopes for *Gaia* alerts follow-up.

Key words: time-domain astronomy – photometry – automatic data reduction and calibration – *Gaia* Science Alerts

1. Introduction

Time-Domain Astronomy (TDA) is a rapidly developing field of observational astronomy, which includes studies of both continuously variable (periodic and non-periodic) sources as well as temporally appearing or changing objects. Transient astrophysical events, e.g., supernovae, gravitational wave optical counterparts, microlenses or tidal disruption events, often require immediate follow-up observations soon after their discovery. In the era of large photometric surveys, for example *Gaia* [1], PTF [2], ASAS-SN [3], OGLE [4] and recently initiated ZTF[5],

[1] http://sci.esa.int/gaia

[2] https://www.ptf.caltech.edu/iptf

[3] http://www.astronomy.ohio-state.edu/ assassin/index.shtml

[4] http://ogle.astrouw.edu.pl

[5] https://www.ztf.caltech.edu

there are thousands of transient phenomena reported every year (about 1000 by *Gaia* alone, currently about 4 per day). Therefore, a careful selection of those which are of the highest scientific interest, or are rare examples of events, play a crucial role. It is essential to observe as many of them as possible in detail from the ground while they are still on-going, in order to understand their nature and discover new types of objects. Early multi-band photometry informs us on how an event develops in brightness and colour, allowing for early characterisation and helping decide on further follow-up observations, both photometric and spectroscopic.

2. OPTICON follow-up network

Coordination of the operation of a network of observatories collecting time-domain data over days-to-years is the main goal of the OPTICON TDA Work Package 13 (H2020 Network Activity 4)[6]. This includes technical support, training, help with the observations and data processing and workshops. Our main product, however, is the automatic software dedicated for TDA, which is a necessity in this field (see Sec. 3.)

Within the OPTICON TDA Work Package we have been coordinating the operation of multiple small- and medium-sized telescopes scattered around Europe and beyond. Many of these telescopes were build in the previous century and now have almost become obsolete due to poor weather conditions in Europe, compared to the best sites, like Chile or Hawaii. However, such telescopes, when gathered into a network, can still provide very useful scientific data, as well as serve as great training facilities for young generations of astronomers. Involvement in a coordinated network is also an opportunity for developing countries to take part in a world-class research.

We have been cooperating with a network of nearly 100 telescopes from around the globe. It is worth noticing that members of the OPTICON follow-up network are volunteers – they are both professional astronomers and amateurs. Some of them were contributing hundreds of observations, while others contributed only a few. Fig. 1 presents the geographical distribution of our partners.

3. Cambridge Photometric Calibration Server

In order to facilitate the homogenous data processing and coordinate the storage of the data, we have been developing and maintaining a unique tool, the Cambridge Photometric Calibration Server. This online tool provides the service to the astronomical community of observers, who are willing to contribute with their observations of objects for which the time-domain aspect is important,

[6]http://astro-opticon.org

Figure 1. The follow-up network of volunteering observers supported by the OPTICON program within TDA Work Package 13.

e.g., variable stars or various transient phenomena (supernovae, microlensing, etc.).

3.1. Current version of CPCS

The CPCS in its current version[7] has been in operation since 2013 and was developed in by Ł. Wyrzykowski and S. Koposov at the Institute of Astronomy, University of Cambridge (UK).

The service is used as a central point of where the data are being stored and calibrated in a homogenous way, so that they can be used in future scientific research. It allows us to combine data collected by different setups and instruments to be standardized in order to provide science-ready photometric light curves. More than 50 000 data points were collected already through our system and several scientific publications have used the data from the CPCS.

The examples of intensive follow-up observations of different types of objects are shown in Fig 2.

[7] http://gsaweb.ast.cam.ac.uk/followup

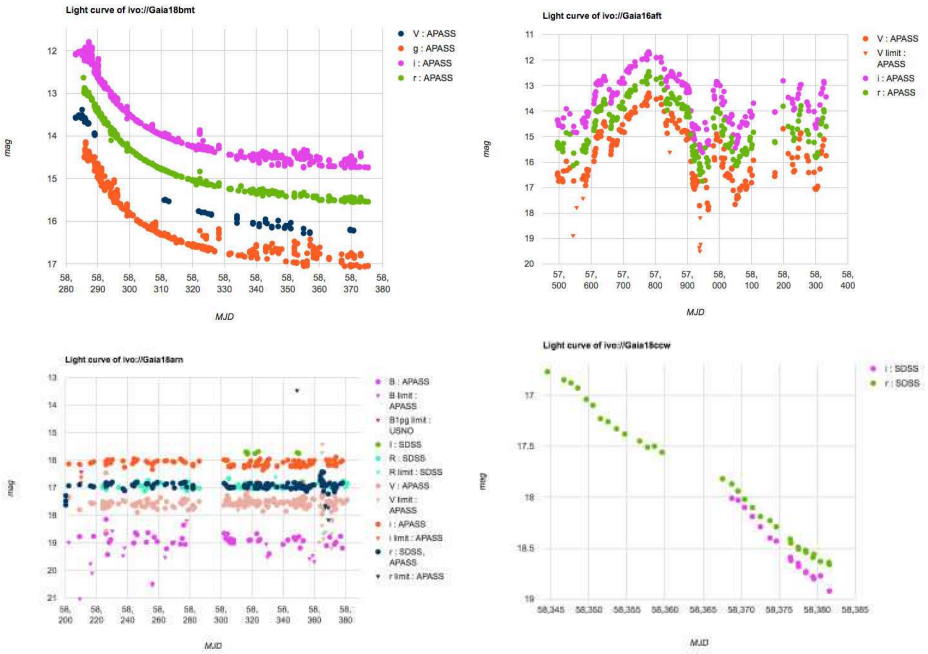

Figure 2. The example light curves of *Gaia* Science Alerts constructed by CPCS. *Top left:* Gaia18bmt – a microlensing event. *Top right:* Gaia16aft – an eruptive star. *Bottom left:* Gaia18arn – unknown nature of the object. *Bottom right:* Gaia18ccw – a supernova of Type Ia.

3.2. Towards CPCS 2.0

Over recent years we have been working on the new version of the automated data processing pipeline, the Calibration Server 2.0 (CPCS 2.0). Fig. 3 presents a schematic diagram of CPCS 2.0. Its main feature is that it accepts images from the observers and performs the measurements of stars' brightness and positions. The input CCD files must be calibrated (bias-, dark-subtracted and normalized by flat-field). This approach allows less experienced observers, including amateurs and even school pupils, to collect scientifically important observations without the need of tedious and difficult data processing.

The new version is currently under tests on data from various observatories, including instruments from LCOGT, REM (Chile), Moletai (Lithuania), Loiano (Italy), OHP (France), Ostrowik, Białków, Borówiec (Poland), SMARTS (Chile), Terskol (Ukraine), Aristarchos (Greece), etc. After appropriate software examination and old website rebuilt, the CPCS 2.0 will be publicly available online for everyone.

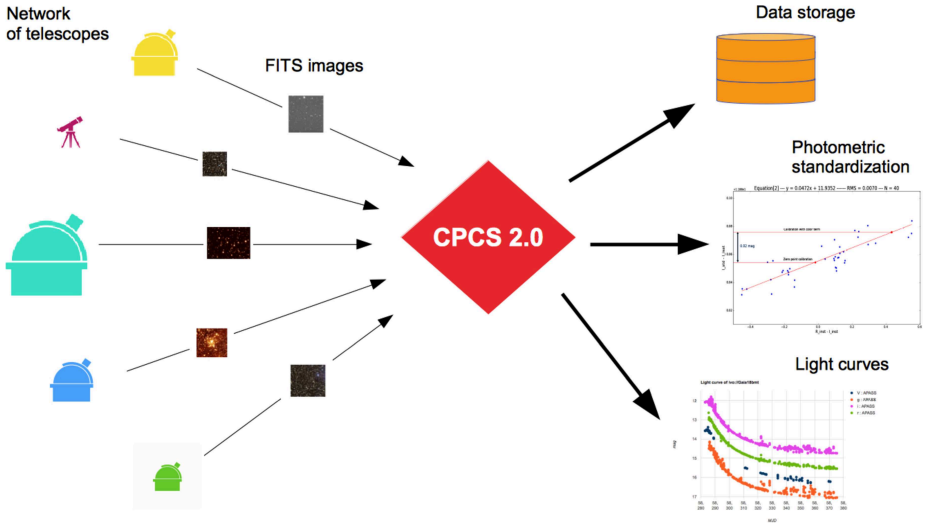

Figure 3. The schematic diagram of the Cambridge Photometric Calibration Server 2.0. On the left hand side, the input data are shown – calibrated FITS files, while on the right hand side are the CPCS 2.0 outputs.

The main improvements comparing to the current version of CPCS include the following issues:

– automatic photometric and astrometric reduction of CCD images by using CCDphot software as a kernel of the new Calibration Server. CCDphot is based on bash shell and Python tasks and scripts and uses several well-known packages and programs such as IRAF/PyRAF[8], SExtractor (Bertin & Arnouts, 1996), SCAMP (Bertin, 2006), DAOphot[9] and WCStools[10],

– transition from ASCI data files to CCD FITS images as input data for the Calibration Server,

– the selection of reference astrometric and photometric catalogues for a specific field-of-view includes (at this moment): URAT-1 (Zacharias et al., 2015), UCAC-4 (Zacharias et al., 2013), USNOB1 (Monet et al., 2003) and *Gaia*-DR2 (Gaia Collaboration et al., 2016, 2018) for astrometric solutions, as

[8]IRAF is written and supported by the National Optical Astronomy Observatories (NOAO) in Tucson, Arizona. NOAO is operated by the Association of Universities for Research in Astronomy (AURA), Inc. under cooperative agreement with the National Science Foundation. PyRAF is a product of the Space Telescope Science Institute, which is operated by AURA for NASA.

[9]http://www.star.bris.ac.uk/ mbt/daophot

[10]http://tdc-www.harvard.edu/wcstools

well as ASAS (Pojmanski, 1997), SDSS (Gunn et al., 1998), PS1 (Chambers et al., 2016), DES (Abbott et al., 2018) and 2MASS (Skrutskie et al., 2006) catalogues for photometric references,

- standardization of CCD file headers originating from different observatories (telescopes, instruments) according to the FITS[11] standard,
- automatic procedure for selection of stars to construct the Point Spread Function (PSF) model of the whole CCD image,
- both aperture and PSF photometry based on DAOphot calculation procedure obtained with precision ∼0.01 mag,
- final astrometric solution based on *Gaia*-DR2 coordinates and proper motions obtained with precision ∼0.01 arcsec,
- transformation of instrumental magnitudes to the standard ones by zero-point calibration and colour term application.

In addition, an important feature available in both versions of CPCS is the possibility of uploading or deleting the data in an automatic manner (e.g. by using shell scripting).

4. Summary

Our ultimate goal is to facilitate the data flow from an astrophysical trigger (alert) to a science-ready observational data point. This will allow us to gather time-domain data produced by a network of heterogenous instruments and telescopes. By inclusion of robotic telescopes and homogeneous protocols, it will become possible to avoid (or at least minimize) human intervention in generating science-ready data.

We demonstrate here the status and recent work on the Calibration Server which helps in the automatisation process of data reduction and constitutes a step forward towards the above mentioned goal. The current version of CPCS has been publicly available since 2013. The work under the second version is in progress now, but it should be available via the dedicated website soon. Finally, we emphasize that everyone can use this tool for own research independently. Everyone interested please contact Ł. Wyrzykowski via e-mail: `lw@astrouw.edu.pl`.

Please feel invited to cooperate within the OPTICON follow-up network and use the Calibration Server!

Acknowledgements. We are grateful for the support of a number of observers involved in collecting follow-up data and *Gaia* Science Alerts Team, Cambridge, UK.

[11] Flexible Image Transport System, https://fits.gsfc.nasa.gov

We acknowledge the Polish National Science Center grant HARMONIA, No. 2015/18/M/ST9/00544, as well as OPTICON H2020 EC grant No. 730890.

This work has made use of data from the European Space Agency (ESA) mission *Gaia*, processed by the *Gaia* Data Processing and Analysis Consortium (DPAC). Funding for the DPAC has been provided by national institutions, in particular the institutions participating in the *Gaia* Multilateral Agreement.

References

Abbott, T. M. C., Abdalla, F. B., Allam, S., et al., The Dark Energy Survey Data Release 1. 2018, *ArXiv e-prints*, arXiv:1801.03181

Bertin, E., Automatic Astrometric and Photometric Calibration with SCAMP. 2006, in Astronomical Society of the Pacific Conference Series, Vol. **351**, *Astronomical Data Analysis Software and Systems XV*, ed. C. Gabriel, C. Arviset, D. Ponz, & S. Enrique, 112

Bertin, E. & Arnouts, S., SExtractor: Software for source extraction. 1996, *Astron. Astrophys., Suppl.*, **117**, 393, DOI: 10.1051/aas:1996164

Chambers, K. C., Magnier, E. A., Metcalfe, N., et al., The Pan-STARRS1 Surveys. 2016, *ArXiv e-prints*, arXiv:1612.05560

Gaia Collaboration, Brown, A. G. A., Vallenari, A., et al., Gaia Data Release 2. Summary of the contents and survey properties. 2018, *Astron. Astrophys.*, **616**, A1, DOI: 10.1051/0004-6361/201833051

Gaia Collaboration, Prusti, T., de Bruijne, J. H. J., et al., The Gaia mission. 2016, *Astron. Astrophys.*, **595**, A1, DOI: 10.1051/0004-6361/201629272

Gunn, J. E., Carr, M., Rockosi, C., et al., The Sloan Digital Sky Survey Photometric Camera. 1998, *Astron. J.*, **116**, 3040, DOI: 10.1086/300645

Monet, D. G., Levine, S. E., Canzian, B., et al., The USNO-B Catalog. 2003, *Astron. J.*, **125**, 984, DOI: 10.1086/345888

Pojmanski, G., The All Sky Automated Survey. 1997, *Acta Astron.*, **47**, 467

Skrutskie, M. F., Cutri, R. M., Stiening, R., et al., The Two Micron All Sky Survey (2MASS). 2006, *Astron. J.*, **131**, 1163, DOI: 10.1086/498708

Zacharias, N., Finch, C., Subasavage, J., et al., The First U.S. Naval Observatory Robotic Astrometric Telescope Catalog. 2015, *Astron. J.*, **150**, 101, DOI: 10.1088/0004-6256/150/4/101

Zacharias, N., Finch, C. T., Girard, T. M., et al., The Fourth US Naval Observatory CCD Astrograph Catalog (UCAC4). 2013, *Astron. J.*, **145**, 44, DOI: 10.1088/0004-6256/145/2/44

Contrib. Astron. Obs. Skalnaté Pleso **49**, 132 – 136, (2019)

Photometric data around us

M. Zejda[1], O. Skýba[1], M. Krajčovič[2], P. Gajdoš[3] and M. Fedurco[3]

[1] *Department of Theoretical Physics and Astrophysics, Masaryk University, Kotlářská 2, CZ 611 37 Brno, Czech Republic*

[2] *Faculty of Informatics, Masaryk University, Botanická 554/68a, CZ 602 00 Brno, Czech Republic*

[3] *Institute of Physics, Faculty of Science, P. J. Šafárik University, Park Angelinum 9, 040 01 Košice, Slovakia*

Received: October 31, 2018; Accepted: February 15, 2019

Abstract. A researcher of variable stars needs photometric data. Their sources could be very varied, from our own observations to different photometric surveys or previously published papers. In this paper, we present the tool PDR for retrieving photometric data from selected surveys and the system AMPER for archiving photometric data for periodic variable stars.

Key words: photometry – surveys – data

1. Introduction

From the beginning, astronomy is a science based on observational data, their analyses and interpretations. Even though we are flooded with big data nowadays, to obtain time series of selected target(s) in suitable time-resolutions and several photometric bands is often a very difficult and time-consuming task. However, data search is only one part of the task. The competence of the correct processing of the found data is also very important.

Furthermore, one has to be careful reading old texts, because common styles of the given timings, magnitudes, errors, and filters are changing over time. Sometimes the heliocentric correction and the way of its computation and application, are wrong.

The lack of photometric data can be solved by our own observations if possible. We can also ask for assistance from amateur observers, who are often able to provide high quality data. Photometric observations made by amateurs are not appreciated duly even though amateurs, or small observatories, produce huge amount of data. Unfortunately, their data are hidden somewhere or even deleted. CCD cameras have been widely used for several decades. Let's imagine one observer with one telescope and a CCD camera, who has been active for 10 years. Each year he observes for, let say, 50 nights. Each night he obtains 100 frames with 100 stars in them. In total, we obtain 5 millions photometric points with this pessimistic estimate. However, some observers have more telescopes, observe more nights with more frames per night and have more stars in frames. Adjusting our estimate to 10 years, 100 nights/year, 500 frames/night, 10 000

stars/frame, we obtain five billion photometric points! And this is only an estimate for one observer, or a small observatory. In total, all data from this source are comparable with data from a huge survey.

2. Photometric surveys

Very valuable pieces of information are included in historical surveys made on photographic plates. However, only part of them is digitalized and available to the public. Let us mention, as a very nice example, the project DASCH (http://dasch.rc.fas.harvard.edu/).

Nowadays, we can use data from many ground based surveys as for example:

- *ASAS - http://www.astrouw.edu.pl/asas/,
- *OGLE - http://ogle.astrouw.edu.pl/,
- *MACHO - http://wwwmacho.anu.edu.au/Data/MachoData.html,
- EROS - http://eros.in2p3.fr/,
- *ROTSE (NSVS) - http://www.rotse.net/,http://skydot.lanl.gov/nsvs/nsvs.php,
- *SuperWASP - http://wasp.cerit-sc.cz/form,
- *APASS - http://www.aavso.org/apass,
- SDSS - http://www.sdss3.org,
- *Catalina (CRTS) - http://crts.caltech.edu/,
- 2MASS - http://www.ipac.caltech.edu/2mass/,
- *LINEAR - https://astroweb.lanl.gov/lineardb/,
- TASS - http://www.tass-survey.org/,
- Stardial - http://stardial.astro.illinois.edu/,
- HATNet - http://www.hatnet.org/,
- *Pi of the sky - http://grb.fuw.edu.pl/,
- Pan-STARRS ??? http://pan-starrs.ifa.hawaii.edu/,
- *ASAS-SN http://www.astronomy.ohio-state.edu/~assassin/index.shtml,
- MASCARA https://home.strw.leidenuniv.nl/~burggraaff/MASCARA_variables/.
- *PTF - https://www.ptf.caltech.edu/,
- *KWS - http://kws.cetus-net.org/~maehara/VSdata.py

Great collections of data are available from space projects such as

- *Hipparcos - https://www.cosmos.esa.int/web/hipparcos/catalogues,
- *OMC Integral - https://sdc.cab.inta-csic.es/omc/index.jsp,
- MOST - http://www.cadc-ccda.hia-iha.nrc-cnrc.gc.ca/en/most/,
- COROT - http://idoc-corot.ias.u-psud.fr/,
- *KEPLER,K2 - http://kepler.nasa.gov, http://keplerscience.arc.nasa.gov,
- Chandra - http://cxc.harvard.edu/vguide/index.php,
- GAIA - http://sci.esa.int/science-e/www/area/index.cfm?fareaid=26,
- BRITE - http://www.brite-constellation.at/,
- WISE - http://wise.ssl.berkeley.edu/,
- TESS - https://tess.gsfc.nasa.gov/.

Data from photometric surveys are usually available on their webpages or mirrors or on specialised data servers such as CDS (Centre de Données astronomiques de Strasbourg) http://cdsportal.u-strasbg.fr/, MAST (Barbara A. Mikulski Archive for Space Telescopes) http://mast.stsci.edu/

`portal/Mashup/Clients/Mast/Portal.html`, IPAC, IRSA (Infrared Processing and Analysis Center, Infrared Science Archive) `http://www.ipac.caltech.edu/`, `http://irsa.ipac.caltech.edu/frontpage/`, Canadian Astronomy Data Centre `http://www.cadc-ccda.hia-iha.nrc-cnrc.gc.ca/en/` or can be found using virtual observatories.

The general problem of photometric surveys is that practically each survey or project has its own format of data. Researchers spend a lot of time not only searching the data for selected target(s), but also transforming them into a simple useable format in which they can compare measurements. The time stamps of measurements are, for example, given in somewhat modified Julian Date, numbers of seconds from the beginning of the project measurements and brightness of objects are given in (relative) magnitudes, fluxes or counts.

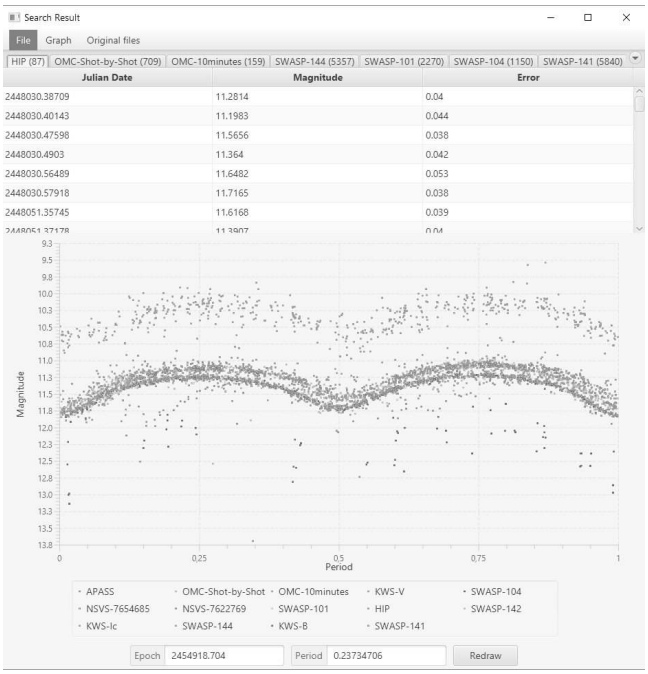

Figure 1. The example of visualisation of the result of data search for RW Com.

To increase efficiency of obtaining data, we developed a tool PDR (Photometric Data Retriever) which searches data in selected surveys and if any data are found, then transform them. Right now 15 surveys are bundled with PDR[1],

[1]The surveys included in a PDR search are noted by asterisks in the above given list. PDR also searches in the data archive of the Danish 1.54m telescope at La Silla `http://vos2.asu.cas.cz/extract_dec17/q/web/form`.

but it is possible for the user to write a plugin for a new survey and add it to the list. It is possible to search for a star by its name or coordinates and radius. The application gathers data from services such as SESAME and VSX to get as many aliases as possible, as well as other information about the object. After that it uses survey plugins to search for photometric data on the surveys APIs and websites. Data from surveys are transformed into a uniform format and shown to the user in a list with graph (of a phase curve for periodic variable stars).

A user obtains data in a uniform Julian Date format, magnitude, and error. No additional correction is applied to the time stamps, thus if original data are with heliocentric/barycentric correction, PDR gives heliocentric/barycentric Julian dates. PDR calculates magnitudes from given fluxes or takes them as they are published in the survey. Original data downloaded from the survey is stored as well and can be easily accessed through the application. All the data found can be exported in multiple ways.

To run PDR you will have to have Java 8+ installed on your computer. The application itself is platform independent, but as of right now there is only the Windows installation package available. It is possible to run the app on Linux or MacOS, it's just not that simple. The application is still under development. The latest version is always available on `https://github.com/m-krajcovic/photometric-data-retriever/releases`. The application will automatically update when a new update is available. The only known problem in some searching of data is matching the requested object with objects in surveys, because an astrometry from different surveys is slightly shifted in some cases and also coordinates given in SESAME differ from those at SIMBAD or VSX. The system is still in development. Any assistance, notes or recommendation are welcome.

3. Combine own measurements with found data

Obtaining data is only part of the common task. The other one is how to save and handle the data. We develop the Archiv of Measurements of PERiodic variable stars (AMPER), which is available for free at `http://amper.physics.muni.cz/`. AMPER can serve as a personal observational diary or a database for teams that need to share data hidden from non-members. It is possible to save one's own measurements, data from surveys or publications. AMPER offers visualisation of data in phase light curves as well as several tools, such as tools to show object visibility or to determine the timings of minima for eclipsing binaries. The database is still under development and it is upgraded regularly. The new users are welcome.

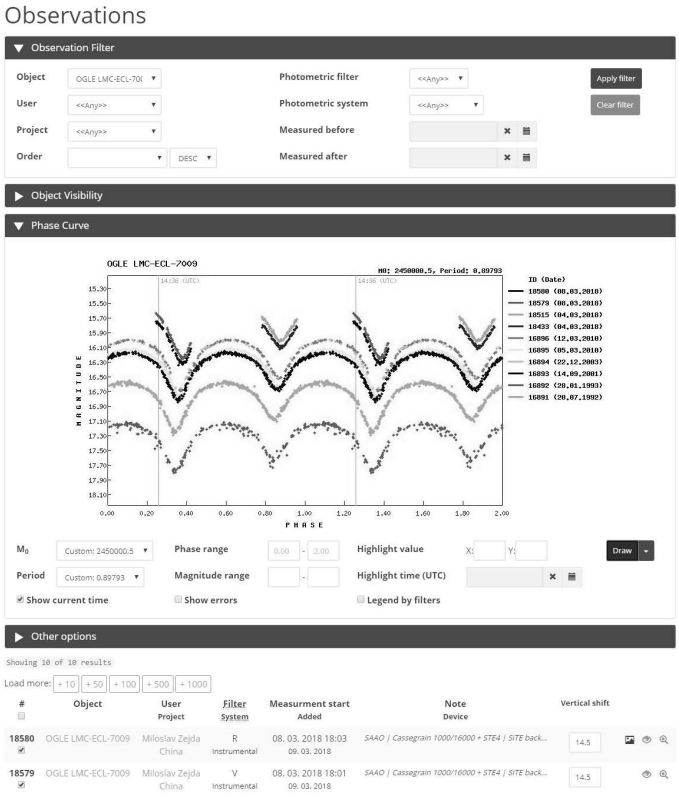

Figure 2. An example of the dataset for a star in the AMPER database.

4. Conclusion

We introduced tools for variable star researchers such as PDR – a tool for data search in a selected survey and their conversion into the uniform style and website service AMPER for saving photometric data. Both applications are still under development and any recommendations and notes are welcome.

Acknowledgements. The authors are thankful to present and future users of PDR and AMPER for their constructive comments. P.G. would like to thank the projects APVV-15-0458 and VVGS-PF-2017-724.

Contrib. Astron. Obs. Skalnaté Pleso **49**, 137 – 141, (2019)

Synergy between professional and amateur astronomers

M. Skarka[1,2] **and P. Kabáth**[2]

[1] *Department of Theoretical Physics and Astrophysics, Masaryk University, Kotlářská 2, CZ-611 37 Brno, Czech Republic (E-mail: maska@physics.muni.cz)*

[2] *Astronomical Institue, Czech Academy of Sciences, Fričova 298, 251 65 Ondřejov, Czech Republic*

Received: November 5, 2018; Accepted: February 1, 2019

Abstract. Since the CCD technique became financially reachable for amateur astronomers, they can cover topics of professional science. Mainly in the time-domain astronomy, such as variable star research, their help is invaluable. We focus on a cooperation between amateur and professional astronomers in the Czech Republic, give some examples of successful projects and propose new programs that can benefit from such cooperation and bring high-quality results.
Key words: methods: observational – techniques: photometric – techniques: spectroscopic – planetary systems – stars: variables: RR Lyrae – TESS

1. Introduction

Even in the time of large sky surveys the new multicolour photometric and mainly spectroscopic data are desirable. Without the ground-based follow-up observations, the space missions such as *Kepler* (Borucki et al., 2010) cannot provide us with the full spectrum of information. Because getting the data for many objects is very time demanding and observing time at professional observatories is often very restricted, the incorporation of amateur astronomers (AMs) to the professional projects could be very helpful.

Mainly in time-domain astronomy (for example, multicolour photometry of variable stars), AMs under the coordination of professional astronomers (PROs) can contribute significantly. By using telescopes with 20-30cm in diameter, which are common among AMs, with proper equipment the AMs can get single-point precision down to several mmag. Because of the technical and data-processing demands, spectroscopy is not common among AMs, although some exceptions exist.

2. Variable star research in the Czech Republic

Observation of variable stars has a long tradition in the Czech Republic and the relation between AMs and PROs is very tight. The AMs are united in

the Variable Stars and Exoplanet Section (VSES) of the Czech Astronomical Society, which was founded in 1924 (Skarka et al., 2015). For a long time, the main topic was the observation of minima of eclipsing binary stars. However, the AMs currently observe also exoplanetary transits, eruptive and pulsating stars.

The VSES maintains two important databases: the Exoplanet Transit Database (ETD, Poddaný et al., 2010) and the O-C gate (Paschke & Brat, 2006a), which are used by astronomers around the world. The VSES also provides a possibility to publish the results of AMs observations – the Open European Journal on Variable stars (OEJV, Paschke & Brat, 2006b).

The Czech AMs participated in very nice projects and discovered interesting binaries. For example, Cagaš & Pejcha (2012) studied the double eclipsing binary with periods near 3:2 ratio, AMs contributed to the study of multiple stellar systems (Zasche et al., 2017) and eruptive stars (Šmelcer et al., 2017), an amateur observer allowed for the precise description of modulation properties of Z CVn (Skarka et al., 2018).

3. Possible projects with AMs in the era of TESS

The Transiting Exoplanet Survey Satellite (TESS) was launched on April 18, 2018. This mission is designed to scan the whole sky and search for exoplanetary transits (Ricker et al., 2015). However, the satellite will be extremely useful in discovering and monitoring variable stars. Due to the observing strategy, most of the sky will be observed only for 27 days with 30-min cadence[1] in one broadband filter (spatial resolution 21 arcsec/px). This opens a great opportunity for the multicolour photometric and spectroscopic follow-up observations. Again, mainly in photometric observations, the AMs can contribute significantly.

3.1. RR Lyrae and Cepheid observations

In the investigation of long-term phenomena in RR Lyrae and Cepheid type stars, it is extremely important to have a regular sampling and the longest possible time base of the data. We demonstrate this need on the artificially generated data of a sample RR Lyrae light curve with modulation known as the Blazhko effect (Blažko, 1907).

We simulated the 27-days TESS observations with 30-minutes cadence (see the top right-hand panel of Fig. 1) by using the mathematical description of a modulated RR Lyrae star by adding the white noise of 0.001 mag, which roughly corresponds to the expected accuracy for a 12.5-mag star (Ricker et al., 2015).

The ground-based observations were simulated similarly, but by adding 0.01-0.05-mag white noise to the observations (top left panel of Fig. 1), which is typical of 20-30 cm telescopes with CCD in various filters. We considered three

[1] About 200 000 stars will be monitored also in a 2-min mode.

locations (0, +8 hours, −6 hours) and cadence 4 minutes to simulate three ground-based observatories. The data cover 3 seasons in a random range up to 120 days, with the random start of the observations (within the local nights, of course) and the random length of the night to simulate the weather conditions (the bottom panels of Fig. 1).

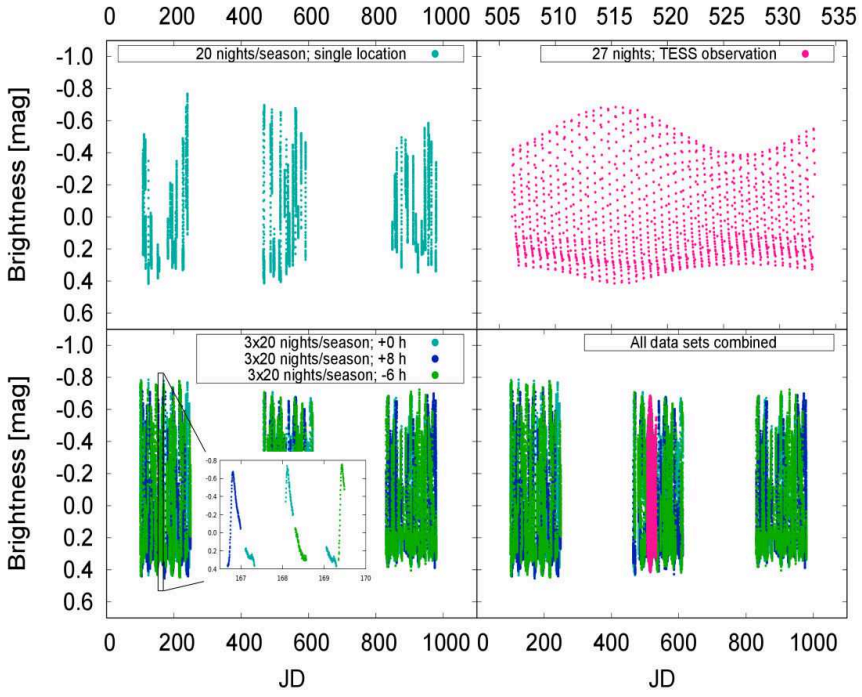

Figure 1. The simulated data. See the text for the description.

The resulting frequency spectra of the TESS and combined data are shown in Fig. 2. The spectrum of TESS data with a 27-days long time base has very broad peaks and show no apparent aliases. On the other hand, the spectrum of the ground-based data from one observing base suffers from strong daily aliases. The aliases are significantly reduced in the data from three observing sites and almost disappear in the combined dataset shown by the black line. The longer the database, the better the frequency resolution. For the 3-year combined data set the resolution is $1/(3 \times 365) \approx 0.001\,\mathrm{cd}^{-1}$, which is 40 times better than for the TESS observations. This clearly shows the advantages of a multi-site observing campaign and the time demands of such campaign. Therefore, the cooperation with AMs is considered in the research of RR Lyrae and Cepheid stars observed by TESS.

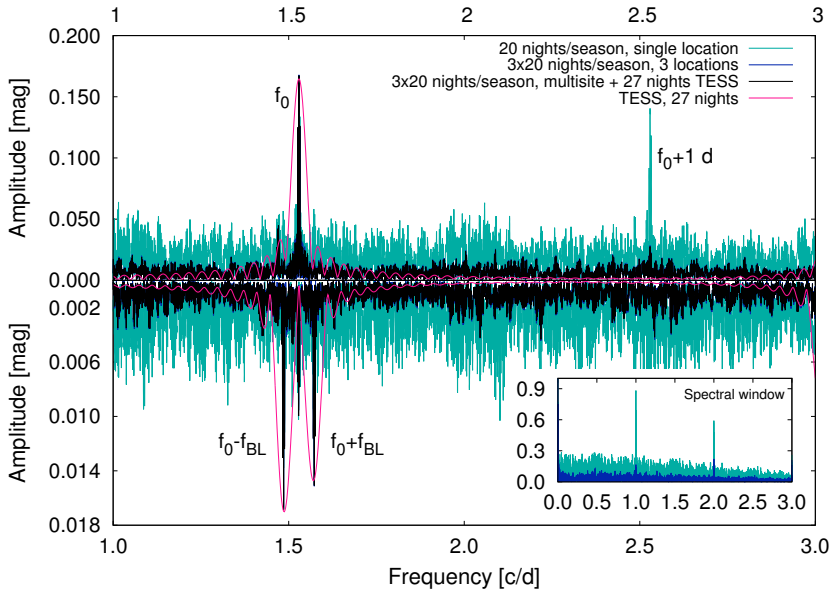

Figure 2. Frequency spectra of the artificially generated data (top panel) and the residuals after removal of the basic pulsation frequency f_0 (bottom panel). On the bottom panel, the peaks $f_0 \pm f_{\rm BL}$ are generated by the Blazhko effect. In the detail the spectral window is shown.

3.2. Follow-up of exoplanets

Amateur observers can also significantly contribute to the follow-up observations of exoplanetary candidates. Due to short observing runs of TESS, the transits detected from the ground will help to better estimate the orbital parameters. The observations will also help to detect peculiarities in the transits and identify blends that were unresolved by TESS. Detection of secondary transits (eclipse minima) will help to identify binaries that were misclassified as exoplanets. This clearly shows the need for a large amount of observing time that would be impossible to get on professional observatories. In addition, the multi-site observations will increase the amount of gathered data.

To unambiguously constrain the real planetary nature of the candidate, spectroscopic radial velocity observations will be necessary. For that, 2-m Perek telescope in Ondrejov, Czech Republic can be used (see Kabáth et al. 2019, these proceedings for more details).

4. Conclusions

We discussed the possible involvement of amateurs in professional projects. Their help can be especially important in the TESS follow-up observations.

We propose two projects, one focused on RR Lyrae and Cepheid stars, the second on exoplanetary candidates, which will be organized in the near future in collaboration with the home institutes and in combination with the instruments available there (the 2-m telescope in Ondřejov (spectroscopy) and a 0.6-m telescope (photometry) in Brno).

Acknowledgements. MS acknowledges financial support of Postdoc@MUNI project CZ.02.2.69/0.0/0.0/16 027/0008360. PK acknowledges GACR international grant 17-01752J.

References

Blažko, S., Mitteilung über veränderliche Sterne. 1907, *Astronomische Nachrichten*, **175**, 325, DOI: 10.1002/asna.19071752002

Borucki, W. J., Koch, D., Basri, G., et al., Kepler Planet-Detection Mission: Introduction and First Results. 2010, *Science*, **327**, 977, DOI: 10.1126/science.1185402

Cagaš, P. & Pejcha, O., Discovery of a double eclipsing binary with periods near a 3:2 ratio. 2012, *Astron. Astrophys.*, **544**, L3, DOI: 10.1051/0004-6361/201219815

Paschke, A. & Brat, L., O-C Gateway, a Collection of Minima Timings. 2006a, *Open European Journal on Variable Stars*, **23**, 13

Paschke, A. & Brat, L., Open European Journal on Variable Stars. 2006b, *Open European Journal on Variable Stars*, **23**, 15

Poddaný, S., Brát, L., & Pejcha, O., Exoplanet Transit Database. Reduction and processing of the photometric data of exoplanet transits. 2010, *New Astronomy*, **15**, 297, DOI: 10.1016/j.newast.2009.09.001

Ricker, G. R., Winn, J. N., Vanderspek, R., et al., Transiting Exoplanet Survey Satellite (TESS). 2015, *Journal of Astronomical Telescopes, Instruments, and Systems*, **1**, 014003, DOI: 10.1117/1.JATIS.1.1.014003

Skarka, M., Liška, J., Dřevěný, R., et al., A cautionary tale of interpreting O-C diagrams: period instability in a classical RR Lyr star Z CVn mimicking as a distant companion. 2018, *Mon. Not. R. Astron. Soc.*, **474**, 824, DOI: 10.1093/mnras/stx2737

Skarka, M., Liška, J., Šmelcer, L., & Brát, L., Variable Star and Exoplanet Section of the Czech Astronomical Society. 2015, in Astronomical Society of the Pacific Conference Series, Vol. **496**, *Living Together: Planets, Host Stars and Binaries*, ed. S. M. Rucinski, G. Torres, & M. Zejda, 307

Šmelcer, L., Wolf, M., Kučáková, H., et al., Flare activity on low-mass eclipsing binary GJ 3236. 2017, *Mon. Not. R. Astron. Soc.*, **466**, 2542, DOI: 10.1093/mnras/stw3179

Zasche, P., Juryšek, J., Nemravová, J., et al., V773 Cas, QS Aql, and BR Ind: Eclipsing Binaries as Parts of Multiple Systems. 2017, *Astron. J.*, **153**, 36, DOI: 10.3847/1538-3881/153/1/36

Contrib. Astron. Obs. Skalnaté Pleso **49**, 142 – 144, (2019)

Spectroscopic instrumentation of 1-m class telescopes for ground support of the space mission WSO-UV

M. Sachkov[1], V. Panchuk[2], V. Klochkova[2], S. Sichevsky[1], E. Kanev[1] and A. Kartashova[1]

[1] *Institute of Astronomy RAS, Russia, (E-mail: msachkov@inasan.ru)*
[2] *Special Astrophysical Observatory RAS, Russia*

Received: November 6, 2018; Accepted: January 30, 2019

Abstract. The World Space Observatory Ultraviolet (WSO - UV), an international mission with Russia and Spain as the main contributors, consists of a 1.7 m telescope with an imaging camera, two spectrographs in the range of 115–176 and 174–310 nm with a resolution of R = 50,000 for high resolution spectral observations and a long-slit-spectrograph for R=1,000 observations. Some of astrophysical studies require both Ultraviolet orbital observations with the WSO-UV as well as observations with ground based instrumentations in visual wavelengths. In this paper we will discuss spectroscopic instrumentations of 1-m class telescopes to be used as project ground support. We also discuss astrophysical studies that require both ground base and orbital observations.
Key words: ultraviolet – space mission – ground support

1. Introduction

The WSO-UV observatory (Shustov et al. (2018)) includes a 170 cm aperture telescope with WUVS (WSO-UV Spectrographs) and FCU (Field Camera Unit) instruments. The launch date is 2025. Many astrophysical tasks of the mission Core program require high resolution spectroscopic observations (R = 50000) in UV wavelengths (115 – 300 nm) as well as in the visual range (300–700 nm) (Boyarchuk et al. (2016)). This means that observations with space based instrumentation should be complemented with ground support spectroscopic observations in the spectral domain of 300-1000 nm. For these purposes we plan to install new spectrographs on 1–m telescopes of SAO RAS and Simeiz Observatory of INASAN and to a 2–m telescope of the Terscol observatory. Here we present detailed information on such instrumentation and our recent achievements.

2. WSO-UV spectrographs

The WUVS instrument consists of a set of three spectrographs (Sachkov et al. (2014)): the far UV high resolution spectrograph (VUVES) that will permit to

carry out echelle spectroscopy with the resolution of about 50000 in the 115–176 nm range; the near UV high resolution spectrograph (UVES) to carry out echelle spectroscopy with the resolution of about 50 000 in the 174–310 nm range; the Long Slit Spectrograph (LSS) that will provide the low resolution (R=1000), long slit spectroscopy in the 115–305 nm range. The spatial resolution will be 0.5 arcsec. All spectrographs will be equipped with a CCD cooled to minus $100^o\,C$ (Shugarov et al. (2014)).

3. Ground based spectrographs

For monitoring programs we plan to use 1–m telescopes of SAO RAS and INASAN. The INASAN 1–m telescope will be fully occupied with ground support observations of WSO–UV during its operation on orbit. The 1–m SAO RAS telescope will be equipped with CAES (Panchuk et al. (2018)). The 1–m INASAN telescope will be equipped with a similar spectrograph that is under construction now. Connection of a high resolution spectrograph and a telescope with the help of a fiber fed allows to reach high positioning accuracy with light loose in the fiber and with stabilisation of the spectrograph housing.

Many astronomical tasks require such approach with a classical slit. They are: radial velocity of gas movement in atomic and ion lines in different parts of planetary nebulae; absorbtion cell radial velocity measurements; observation of faint objects to take into account sky background; visual binary star Doppler measurements when one needs to register both component spectra (see Gorynya et al. (1996)); in survey observations of magnetic stars where one does not need precise Zeeman measurements.

For ground base ultraviolet observations (300 – 400 nm) light loose in a fiber is very significant hence the design of the spectrograph should exclude the fiber. For this spectral range we will install a spectrograph to the 2–m Terscol telescope. The optical scheme of this spectrograph will be similar to WUVS high resolution spectrographs (see Fig. 1, Panchuk et al. (2014)).

4. Conclusions

The WSO–UV project is an efficient multipurpose orbital observatory for high and low resolution spectroscopy, high sensitivity imaging and slitless spectroscopy in the ultraviolet. The imaging instrument FCU onboard WSO–UV will be the first UV camera to be flown to a geosynchronous orbit. The WUVS spectrographs will deliver spectroscopic performance on a range of astronomical sources, combining high sensitivity, low background and high resolution at FUV and NUV wavelengths. According to the current Roscosmos plans, WSO–UV will be launched in 2025. Up to date information on the WSO–UV mission can be found on the web site of the Joint Centre of Ultraviolet Astronomy: http://jcuva.space.

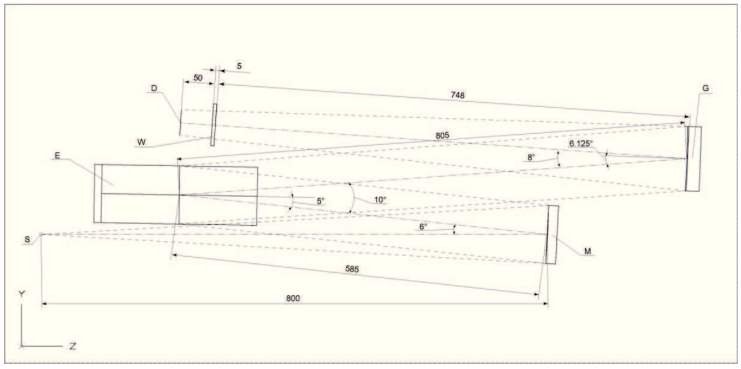

Figure 1. The UVES spectrograph optical layout. S - a slit, M1 - a collimator, E - an echelle grating, G - a cross disperser and camera mirror, W - a detector window, D - a detector.

Acknowledgements. This work has been supported by a RF government Grant N 14.W03.31.0017.

References

Boyarchuk, A. A., Shustov, B. M., Savanov, I. S., et al., Scientific problems addressed by the Spektr-UV space project (world space Observatory Ultraviolet). 2016, *Astronomy Reports*, **60**, 1, DOI: 10.1134/S1063772916010017

Gorynya, N. A., Samus', N. N., Rastorguev, A. S., & Sachkov, M. E., A catalog of Cepheid radial velocities measured in 1992-1995 with a correlation spectrometer. 1996, *Astronomy Letters*, **22**, 175

Panchuk, V., Sachkov, M., & Klochkova, V., Spectral and polarimetric facilities for ground support of the WSO-UV Space mission. 2018, in Society of Photo-Optical Instrumentation Engineers (SPIE) Conference Series, Vol. **10702**, *Society of Photo-Optical Instrumentation Engineers (SPIE) Conference Series*, 107022R

Panchuk, V., Yushkin, M., Fatkhullin, T., & Sachkov, M., Optical layouts of the WSO-UV spectrographs. 2014, *Astrophys. Space Sci.*, **354**, 163, DOI: 10.1007/s10509-014-2087-4

Sachkov, M., Shustov, B., & Gómez de Castro, A. I., Instrumentation of the WSO-UV project. 2014, in Proc. SPIE, Vol. **9144**, *Space Telescopes and Instrumentation 2014: Ultraviolet to Gamma Ray*, 914402

Shugarov, A., Savanov, I., Sachkov, M., et al., UV detectors for spectrographs of WSO-UV project. 2014, *Astrophys. Space Sci.*, **354**, 169, DOI: 10.1007/s10509-014-1911-1

Shustov, B., Gómez de Castro, A. I., Sachkov, M., et al., The World Space Observatory Ultraviolet (WSO-UV), as a bridge to future UV astronomy. 2018, *Astrophys. Space Sci.*, **363**, 62, DOI: 10.1007/s10509-018-3280-7

Contrib. Astron. Obs. Skalnaté Pleso **49**, 145 – 147, (2019)

WSO-UV Field Camera Unit: science case and ground support with 1-m class telescopes

M. Sachkov, S. Sichevsky, E. Kanev and A. Kartashova

Institute of Astronomy RAS, Russia, (E-mail: msachkov@inasan.ru)

Received: November 6, 2018; Accepted: January 30, 2019

Abstract. We present here the new imaging instrument onboard the WSO–UV (World Space Observatory - Ultraviolet) project for observations in the UV (115–310 nm) spectral range. We describe the key scientific drivers of the instrument and Ground based instrumentation of the 1–m class telescopes to support space UV observations. The World Space Observatory–Ultraviolet is a Russian-Spanish space mission born as a response to the growing up demand for UV facilities by the astronomical community. It is the only 2-meter class on–orbit telescope in the after HST epoch fully devoted to UV observations.

Key words: ultraviolet – space mission – ground support

1. Introduction

World Space Observatory UltraViolet (WSO–UV) is a new generation space mission dedicated to astronomical observations in the UV spectral range(Shustov et al. (2018)). The observatory includes a 170 cm aperture telescope capable of high-resolution spectroscopy and long slit low-resolution spectroscopy with the WUVS (WSO-UV Spectrographs) instrument; moreover UV imaging will be available with the Field Camera Unit (FCU) instrument. WSO will work as a space observatory with a core program, guaranteed time for the project partners and time open to the world-wide community. WSO-UV is a third mission of the SPEKTR (spectrum) series of the Russian Federal Space Program together with Spektr-R (on orbit since 2011) and Spektr-RG (with Russian ART-XC and e-Rosita payloads, launch date is 2019). Its launch date is 2025. The WSO-UV project is led by the Institute of Astronomy of the Russian Academy of Sciences. The main instrument is a high-resolution spectrograph. It is supplemented by a low-resolution spectrograph. The imaging cameras are designed by INASAN (Russia) and the Universidad Complutense de Madrid (Spain). The key scientific drivers of the WSO-UV project are described in (Boyarchuk et al. (2016)). Here we present the science case of the FCU and describe our approach to the ground support of the mission.

2. FCU instrument science case

WSO-UV will work as a space targeted observatory with a Core Program, an Open Program for scientific projects from the world-wide community and na-

tional (Funding Bodies) programs for the project partners. Hereby we briefly summarize the main scientific issues of the FCU. They are (but not limited to): planetary nebulae studies; supernovae studies; variable sources study at a short timescale (order of 40 ms); exoplanetary atmospheres; protostellar jets; comets in UV; the galactic globular clusters; asteroseismology (Sachkov et al. (2004)).

3. FCU preliminary layout

The FCU includes two channels (Sachkov et al. (2014)):

A Far Ultraviolet (FUV) channel with an MCP detector for observations in 115 - 176 nm spectral range. A Near Ultraviolet (NUV) channel with a CCD detector for observations in 174 - 310 nm spectral range.

Main characteristics of the FUV channel are:

- Solar blind detector.
- Diffraction-limited imaging in FUV.
- High sensitivity in photon-counting mode.
- High time resolution.

Main characteristics of the NUV channel are:

- Wide field of view.
- High dynamic range.
- High angular resolution.
- Low resolution field spectroscopy.
- Possibility for extended spectral range: 115–1000 nm.

4. Call for the core program application and ground support for WSO-UV

Because of the fact that preparatory observations are required for several proposals, The WSO–UV Science Team decided to make a first Core Program Call for applications in 2018, several years before the launch date. The PI of such application should have a permanent position in astronomy/astrophysics in Russia or in Spain, countries that fund the WSO–UV project. The members of the team that make an application may include participants from any country. The detailed information on the Call can be found on the web site of the Joint Centre of Ultraviolet Astronomy: http://jcuva.space.

For the successful operation of the WSO–UV space mission we are preparing ground based telescopes with spectroscopic instrumentation. The 2–m telescope

of Terscol observatory will play a significant role as well as 1–m telescopes of Simeiz branch of INASAN (Gorynya et al. (1996)) and SAO RAS. For radial velocity measurements the spectrograph polarimeter will be prepared (Panchuk et al. (2018)).

5. Conclusions

The WSO–UV project is an efficient multipurpose orbital observatory for high and low resolution spectroscopy, high sensitivity imaging and slitless spectroscopy in the ultraviolet. The imaging instrument FCU onboard WSO–UV will be the first UV camera to be flown to a geosynchronous orbit. The WUVS spectrographs will deliver spectroscopic performance on a range of astronomical sources, combining high sensitivity, low background and high resolution at FUV and NUV wavelengths.

References

Boyarchuk, A. A., Shustov, B. M., Savanov, I. S., et al., Scientific problems addressed by the Spektr-UV space project (world space Observatory Ultraviolet). 2016, *Astronomy Reports*, **60**, 1, DOI: 10.1134/S1063772916010017

Gorynya, N. A., Samus', N. N., Rastorguev, A. S., & Sachkov, M. E., A catalog of Cepheid radial velocities measured in 1992-1995 with a correlation spectrometer. 1996, *Astronomy Letters*, **22**, 175

Panchuk, V., Sachkov, M., & Klochkova, V., Spectral and polarimetric facilities for ground support of the WSO-UV Space mission. 2018, in Society of Photo-Optical Instrumentation Engineers (SPIE) Conference Series, Vol. **10702**, *Society of Photo-Optical Instrumentation Engineers (SPIE) Conference Series*, 107022R

Sachkov, M., Ryabchikova, T., Kochukhov, O., et al., Pulsational velocity fields in the atmospheres of two roAp stars HR 1217 and γ Equ. 2004, in Astronomical Society of the Pacific Conference Series, Vol. **310**, *IAU Colloq. 193: Variable Stars in the Local Group*, ed. D. W. Kurtz & K. R. Pollard, 208

Sachkov, M., Shustov, B., & Gómez de Castro, A. I., Instrumentation of the WSO-UV project. 2014, in Proc. SPIE, Vol. **9144**, *Space Telescopes and Instrumentation 2014: Ultraviolet to Gamma Ray*, 914402

Shustov, B., Gómez de Castro, A. I., Sachkov, M., et al., The World Space Observatory Ultraviolet (WSO-UV), as a bridge to future UV astronomy. 2018, *Astrophys. Space Sci.*, **363**, 62, DOI: 10.1007/s10509-018-3280-7

Contrib. Astron. Obs. Skalnaté Pleso **49**, 148 – 150, (2019)

Current status of the Milanković telescope

P. Kostić, O. Vince, S. Samurović and A. Vudragović

Astronomical Observatory Belgrade, Volgina 7, 11060 Belgrade, Serbia

Received: October 28, 2018; Accepted: January 24, 2019

Abstract. The Milanković telescope is a 1.4 m telescope installed at the Astronomical station Vidojevica on a mountain in south Serbia. The telescope was procured through the FP7 REGPOT BELISSIMA project with the support of the Serbian Ministry of Education, Science and Technological Development which started in 2010 and was finished in 2016 by setting up the telescope in the temporary pavilion. With an ultimate goal to make the telescope robotic, we have built a new pavilion and provided several modern instruments. Here, we present our 1.4 m telescope, its past/present status.

Key words: Milanković telescope

1. Introduction

The Milanković telescope is now in its third year of operation at the Astronomical station Vidojevica. During September of last year it was moved from temporary to the new pavilion, under the newly finished dome. In the following days and nights the telescope was collimated and we made the rough pointing model for slewing. Right now (the end of September 2018) the dome is in process of automation after which the telescope pointing model will be made so it could be ready for further normal usage. We present our new pavilion and dome along with some pictures of transferring works.

2. New pavilion and dome

The construction of the new pavilion, which is being carried by a Serbian company, is practically finished. It has three levels: the ground level where the control room is placed, plus two floors. The first floor is an empty room which functions mainly as a thermal isolation between the control room and the second floor, where the telescope is mounted. The new dome was manufactured and mounted by the Italian Gambato company in June 2018. It is a reasonably light construction of 7 meters in diameter, so it can make the full circle for around a minute, which is comparable with the rotation speed of the telescope itself. It has the heating mechanism against the frost in the door and in the azimuth circle. In the next period we intend to make the telescope fully remotely controlled, but the ultimate aim for the future is a fully robotic telescope.

Figure 1. Left: Raising the telescope to the door of the new dome. The tube with the secondary mirror was detached and moved separately. Right: The telescope seen from the new dome.

3. Telescope and instruments

The Milanković telescope is a 1.4 m Nasmyth-Cassegrain reflector with four ports of which two are equipped with de-rotators. The focal length is 11.2 m, except for the one with the de-rotator which is equipped with the field corrector that makes the focal length shorter, 10.5 m, and provides about a half degree field of view without significant optical aberrations. Vince et al. (2018) gave a more detailed review of the telescope and its parts. The telescope, produced by the Austrian ASA Astrosysteme GmbH, was procured through the FP7 REGPOT BELISSIMA project with the support of the Serbian Ministry of Education, Science and Technological Development. The project started in 2010 and was finished in 2016 by setting up the telescope in the temporary pavilion. In June 2018 the primary and secondary mirror were sent by the ASA company to the Carl Zeiss Jena factory for re-aluminization and it came back to the new pavilion with new coating. The instruments for use with Milanković remained the same ones as listed in Samurović et al. (2018) and Vince et al. (2018):

– an ANDOR iKonL CCD camera: 2048×2048 pixels, the pixel size is 13.5×13.5 μm, the field of view at the telescope $9' \times 9'$;

– an Apogee U42 CCD camera: 2048×2048 pixels, the pixel size is 13.5×13.5 μm, the field of view at the telescope $9' \times 9'$;

– an ANDOR iXon3 Ultra 897 CCD camera: 512×512 pixels, the size of the pixel 16×16 μm;

– a Spectrograph SpectraPro 2750 by the Princeton Instruments. Type: Cherny-Turner with 3 gratings 300, 600, 1200 lines mm^{-1}, with resolutions 44, 22, 10 Å mm^{-1} and spectral ranges 1120, 560, 250 Å. The resolving power is $R = 9300$, 5400 and 3200 for slits of 5 μm, 10 μm and 200 μm, respectively.

Acknowledgements. This work was supported by the Ministry of Education, Science and Technological Development of the Republic of Serbia through project no. 176021, Visible and Invisible Matter in Nearby Galaxies: Theory and Observations. We thank the Ministry of Education, Science and Technological Development of the Republic of Serbia for the continued support related to the construction works at the Vidojevica Astronomical Station. We acknowledge the financial support by the European Commission through project BELISSIMA (BELgrade Initiative for Space Science, Instrumentation and Modelling in Astrophysics, call FP7-REGPOT-2010-5, contract No. 256772).

References

Samurović, S., Djurašević, G., Cvetković, Z., Pavlović, R., & Vince, O., Telescope "Milanković": mounting, present and future work. 2018, *Publ. Astron. Obs. Belgrade*, **98**, 333

Vince, O., Samurović, S., Pavlović, R., Cvetković, Z., & Djurašević, G., The first year of the "Milanković" telescope. 2018, *Publ. Astron. Obs. Belgrade*, **98**, 233

Contrib. Astron. Obs. Skalnaté Pleso **49**, 151 – 153, (2019)

CoLiTecVS – a new tool for an automated reduction of photometric observations

Š. Parimucha[1], V.E. Savanevych[2], O.B. Briukhovetskyi[2], S.V. Khlamov[3], A.V. Pohorelov[4], V.P. Vlasenko[2], P.A. Dubovský[5] and I. Kudzej[5]

[1] *Institute of Physics, Faculty of Science, UPJŠ Košice, Slovakia*

[2] *Western Radio Technical Surveillance Center, National Space Agency of Ukraine, Mukachevo, Ukraine*

[3] *Uzhhorod National University, Laboratory of space research, Uzhhorod, Ukraine*

[4] *Kharkiv National University of Radioelectronics, Kharkiv, Ukraine*

[5] *Vihorlat Observatory, Mierová 4, 06601 Humenné, Slovakia*

Received: November 28, 2018; Accepted: January 23, 2019

Abstract. The capabilities of telescopes allow us to make the plotting of light curves a routine task. This one shifts the main attention of an astronomer from the plotting to research. To achieve this goal, we developed a new tool for automated reduction of photometric observations, which includes the computational method for the brightness assessment of the investigated and comparison stars; brightness equalization of astronomical images using an inverse median filter; light curve plotting and its processing using different tools.

Key words: stars: variables – Techniques: photometric, image processing

1. Introduction

CoLiTec application was originally developed for automated detection of objects with nonzero apparent motion (Savanevych et al., 2015). Recently, we have started the major update with the goal to use it in the variable stars research as the tool for automated reduction of CCD images. The new version is called CoLiTecVS[1]. It allows the astronomer to create the light curve of an investigated variable star without manual-data handling between processing steps.

2. CoLiTecVS workflow for the automatic data reduction

CoLiTecVS has the following work-flow: forming the series of frames with the investigated variable star; brightness equalization of frames using master-frames and an inverse median filter; preliminary segmentation of objects on images; estimation of objects brightness and equatorial coordinates; frames identification;

[1] http://www.neoastrosoft.com/colitecvs_en/

automatic selection of the reference stars in the frame; brightness assessment of the investigated star using the developed computational method; preparing the task-file with selected comparison stars; processing of the photometric observations; light curve creation of the investigated variable star. Created light curves can be viewed and analyzed using the specific modules of the CoLiTecVS - PlotViewer or the Virtual Observatory (ViViO).

3. LookSky – the auxiliary tool

To create the task file corresponding to the investigated target on the given telescope the user has to use the additional software called LookSky. Its capabilities are as follows:

- Viewing opened series of frames.
- Selecting investigated target and comparison stars.
- Preparing a task-file for plotting the light curve. It will be used in the future in every reduction of the given target.

The process can be greatly automated using the AAVSO[2] chart for the given target. In one click the software finds the corresponding AAVSO chart, selects the comparison stars in the field of view and take the coordinates and brightness values from the photometry table.

4. Testing on real images

We have performed several tests to ensure the reliability of produced data. We have analyzed archival images taken at the Astronomical Observatory on Kolonica Saddle with several instruments. First, we investigated the possible influence of non-linearity of median filtering on the photometry results. We didn't find measurable influence. Contrary to the background brightness equalization,the inverse median filter usually provides better results than the classical flat-field calibration. Detailed analysis of the inverse median filtering can be found in Dubovský et al. (2017).

The photometry of constant stars obtained by CoLiTecVS was compared with values obtained by the conventional reduction process, i. e. calibration and photometry were performed with C-Munipack[3] software and subsequently the ensemble photometry using MCV software (Kim et al., 2004). We have performed many comparisons with different instruments in different star fields. More than 100 time series were reduced. The typical result is shown in Table 1. The meaning of the methods is as follows: C-Munipack_diff means single differential photometry with C-Munipack software, one comparison star; C-Munipack

[2]http://www.aavso.org

[3]http://c-munipack.sourceforge.net/

Table 1. The mean values and standard deviations of the selected stars measurements in the field of view of cataclysimic variable MASTER OT J174305.70+231107.8

Method	Mean value	Standard deviation
C-Munipack_diff	1.3935	0.0118
C-Munipack + MCV	1.3935	0.0067
CoLiTecVS	1.3939	0.0078
CoLiTecVS + MCV	1.3941	0.0070

+ MCV means ensemble photometry, instrumental magnitudes provided by C-Munipack reduced by MCV software; CoLiTecVS means ensemble photometry, fully automated output of CoLiTecVS; CoLiTecVS + MCV means ensemble photometry, instrumental magnitudes provided by CoLiTecVS reduced by MCV software.

The disadvantage of a single comparison star (C-Munipack_diff method) is clearly visible. The scatter is caused by the parabolic trend connected with extinction. The rest of the light curves are practically equal. So the CoLiTecVS can replace the conventional reduction process with the same precision and accuracy. If the user doesn't trust the automatic process completely, one has still got the option to take instrumental output of CoLiTecVS and play with MCV.

5. Conclusion

A new tool for automated reduction of photometric observations was developed. It includes the computational method for the brightness assessment of the investigated star, comparisons stars and light curve creation. The proposed method of the inverse median filter application can be used for calibration of astronomical images without negative influence on the results of the photometry. Nowadays CoLiTecVS is regularly used for data reduction at the Astronomical Observatory on Kolonica Saddle.

Acknowledgements. This work was supported by the Slovak Research and Development Agency under the contract No. APVV-15-0458.

References

Dubovský, P. A., Briukhovetskyi, O. B., Khlamov, S. V., et al., 2017, *Open European Journal on Variable Stars*, **180**

Kim, Y., Andronov, I. L., & Jeon, Y.-B., 2004, *Journal of Astronomy and Space Sciences*, **21**, 191

Savanevych, V. E., Briukhovetskyi, O. B., Sokovikova, N. S., et al., 2015, *Mon. Not. R. Astron. Soc.*, **451**, 3287

Contrib. Astron. Obs. Skalnaté Pleso **49**, 154 – 158, (2019)

Slovak-Bavarian collaboration on the development of telescope instrumentation

T. Döhring[1], T. Pribulla[2], R. Komžík[2], M. Mann[1], P. Sivanič[2] and M. Stollenwerk[1]

[1] *Aschaffenburg University of Applied Sciences, Würzburger Strasse 45, 63743 Aschaffenburg, Germany (E-mail: thorsten.doehring@h-ab.de)*

[2] *Astronomical Institute of the Slovak Academy of Sciences 059 60 Tatranská Lomnica, The Slovak Republic*

Received: October 24, 2018; Accepted: March 5, 2019

Abstract. Within the project SLOBATCO (Slovak-Bavarian Telescope Collaboration) the Astronomical Institute of the Slovak Academy of Sciences and Aschaffenburg University of Applied Sciences collaborate in the development and commissioning of scientific instrumentation for the new ϕ1.3 m astronomical telescope at the Skalnaté Pleso observatory. The joint project is funded by the Bavarian Academic Center for Central, Eastern and Southeastern Europe (BAYHOST). Planned technical work packages are targeting the filter wheel software for the VIS camera, additional IR filters, and an upgrade of the mirror coating facility by additional sputtering equipment.

Key words: telescope – instrumentation – filter – camera – coating

1. Introduction

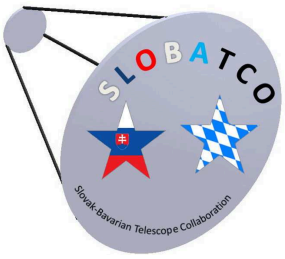

Figure 1. Logo of the SLOBATCO project.

The aim of the project SLOBATCO (Slovak-Bavarian Telescope Collaboration) is the effective combination of experience, expertise, and instrumentation of the Astronomical Institute of the Slovak Academy of Sciences (AI SAS) and

Aschaffenburg University of Applied Sciences for the development and commissioning of a new astronomical telescope and the corresponding scientific instrumentation. The bilateral project is funded by the Bavarian Academic Center for Central, Eastern and Southeastern Europe (BAYHOST). The logo of the SLOBATCO project is depicted in Fig. 1.

Thanks to a grant from the European Regional Development Fund (ITMS No. 26220120029) the Skalnaté Pleso observatory in Slovakia got a new 1.3 m telescope, shown in Fig. 2. The Stellar department of the AI SAS is currently installing this alt-azimuth Nasmyth-Cassegrain telescope (first light was in 2014) at its mountain observatory at Skalnaté Pleso (altitude 1783 m). The new telescope can be operated in a fully remote-controlled mode requiring minimum man-power. Corresponding advanced focal instruments for the new telescope are being developed as well. However, having only a small amount of dedicated staff at the observatory, the instrument development and improvement is a slow process. Therefore the Slovak team is very interested to get support from international partners.

Figure 2. The new 1.3 m telescope at the Skalnaté Pleso Observatory.

Aschaffenburg University of Applied Sciences is a dynamic and growing University of Applied Sciences in Germany; known for its innovative and interdisciplinary approach to education and its close links with the business world. Bachelor´s and Master´s degree programs are offered that have a strong practical focus within the fields of business, law, and engineering. Astronomy is the passion of the participating professors from the faculty of engineering sciences of Aschaffenburg University. Thus, direct access to a quite large professional astronomical telescope by using their technical know-how in an interesting field of research, is particularly motivating for them. So both partners decided to collaborate, proposed the bilateral project SLOBATCO, and finally got the requested funding from BAYHOST.

2. Timeline and research stays within the project

The granted project funding is dedicated to cover only travel expenses. Therefore the project timeline is mainly deflecting the planned visits. The milestones are set related to the two project meetings, one at the AI SAS, held at mid of September 2018 and one project meeting at Aschaffenburg University, held at the end of October 2018. The two bi-directional research stays within the project are illustrated in Fig. 3. A third milestone was the delivery of the final project report, to be submitted by the end of November 2018. Consequently, the project duration is scheduled from September 2018 till November 2018.

Figure 3. Research stays within the SLOBATCO project.

The two project meetings at the Skalnaté Pleso observatory and in Aschaffenburg were foreseen to form up a joint project team and to identify the technical work packages, which can be started within this project and executed within the intended future long-term cooperation. The partners will develop and exchange ideas on further project steps that will be the basis for additional joint funding proposals.

3. Potential technical work packages

Due to the limited financial resources and the limited duration of the project (September to November, 2018) the aim of the project was planning and setting up a specification of the intended future technical work. Up to now, two potential technical work packages have been already identified, covering the development needs for the telescope operation and also the technical expertise of the involved scientists (Döhring et al., 2006); (Pribulla et al., 2015).

3.1. Work package WP1

The large frame CCD camera, shown in Fig. 4, will benefit from the development of dedicated control software which will operate the external shutter and, in parallel, the filter wheel. Up to now, only one fixed filter (J passband) is available for the IR camera, but more specific filters are needed for the intended astronomical observations.

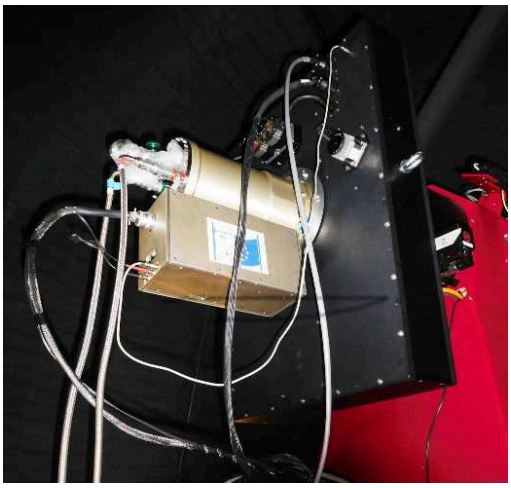

Figure 4. The VIS camera (on the left) with the corresponding filter wheel (black box).

3.2. Work package WP2

It is considered to improve the existing coating facility (see Fig. 5) by installing sputtering technology, especially needed for silver coatings of the primary mirror. Here the expertise of the scientists from Aschaffenburg University will be beneficial. They are operating similar equipment in their laboratory and could produce test coatings (Döhring et al., 2017).

4. Summary and outlook

Already in previous projects, Aschaffenburg University was successfully cooperating with Czech partners from the Czech Technical University in Prague (Hudec & Döhring, 2017). Cross-border networking of scientists and students within Europe will not only give progress to science, but there are also positive political implications with an impact on a prosperous economic development in both countries. Aschaffenburg University has the goal of internationalization as already written in its program. The SLOBATCO project is an excellent

Figure 5. The mirror coating facility at the Skalnaté Pleso observatory.

starting point for the intended long-term cooperation between the Astronomical Institute of the Slovak Academy of Sciences and Aschaffenburg University of Applied Sciences; those partners will also develop innovative ideas for future joint projects.

Acknowledgements. The SLOBATCO project is funded by the Bavarian Academic Center for Central, Eastern and Southeastern Europe (BAYHOST) via grant MB-2018-2/11. This German funding agency BAYHOST supports Bavarian universities and universities of applied sciences through its specific competencies; by supporting their collaboration with academic organizations in our partner countries and by establishing new partnerships.

References

Döhring, T., Loosen, K.-D., & Hartmann, P., The technical challenge of large ELT filters. 2006, in Proc. SPIE, Vol. **6273**, *Society of Photo-Optical Instrumentation Engineers (SPIE) Conference Series*, 62730U

Döhring, T., Probst, A.-C., Emmerich, F., et al., Development of iridium coated x-ray mirrors for astronomical applications. 2017, in Society of Photo-Optical Instrumentation Engineers (SPIE) Conference Series, Vol. **10399**, *Society of Photo-Optical Instrumentation Engineers (SPIE) Conference Series*, 103991C

Hudec, R. & Döhring, T., JEUMICO: Czech-Bavarian astronomical X-ray optics project. 2017, *Contributions of the Astronomical Observatory Skalnate Pleso*, **47**, 170

Pribulla, T., Garai, Z., Hambálek, L., et al., Affordable échelle spectroscopy with a 60 cm telescope. 2015, *Astronomische Nachrichten*, **336**, 682, DOI: 10.1002/asna.201512202

Contrib. Astron. Obs. Skalnaté Pleso **49**, 159 – 170, (2019)

Optical photometry and spectroscopy of V612 Sct: slow classical nova with rebrightenings

D. Chochol[1], S. Shugarov[1,2], Ľ. Hambálek[1], J. Guarro[3] and V. Krushevska[4]

[1] *Astronomical Institute of the Slovak Academy of Sciences 059 60 Tatranská Lomnica, The Slovak Republic, (E-mail: chochol@ta3.sk)*

[2] *Sternberg State Astronomical Institute, Universitetskij Prosp. 13, Moscow 119992, Russia*

[3] *Balmes 2, 08784 Piera, Barcelona, Spain*

[4] *Main Astronomical Observatory of National Academy of Sciences of Ukraine, 27 Akademika Zabolotnoho St. 03680 Kyiv, Ukraine*

Received: October 31, 2018; Accepted: February 1, 2019

Abstract. We present the results of multicolour $UBVR_CI_C$ CCD photometry and optical echelle spectroscopy of the slow classical nova V612 Sct, discovered during its outburst on 2017 June 19.41 UT. The nova reached its brightness maximum $V_{max} = 8.42$ mag and $B_{max} = 9.53$ mag on 2017 July 29.99 UT. The light curve allows to classify it as a slow nova of the J-class with multiple peaks on the decline. We used the V and B light curves to find the rates of decline $t_{3,V} = 105$ d and $t_{3,B} = 224$ d. We estimated by applying MMRD relations the absolute magnitudes of the nova at maximum $MV_{max} = -6.67$ and $MB_{max} = -6.44$. The latter value yields a mass of 0.65 $M_\odot$ for the white dwarf component. We estimated the colour excess $E(B-V) = 0.755$ and found the distance 3.5 kpc to the nova. The study of radial velocities of Hα and Hβ P Cyg absorptions revealed two distinct components of the expanding envelope accelerated by a variable wind with the terminal velocity up to 1900 km s^{-1}. The P Cyg absorptions were most enhanced during rebrightenings.

Key words: novae – photometry – spectroscopy

1. Introduction

Classical novae are cataclysmic variables with 6 to 19 mag brightness increase caused by a thermonuclear event on the surface of the white dwarf. They are semi-detached binaries with orbital periods less than 2 days, in which a matter from a cool component is transferred to a white dwarf. During the optically thick phase of the classical nova outburst the white dwarf photosphere expands to supergiant dimensions and engulfs the binary. Due to a strong wind from a hot source a large part of the envelope is ejected and the photospheric radius shrinks.

Classical novae are usually classified from their photometric appearance as fast or slow according to a time interval in which nova fades by 2 or 3 magnitudes

(t_2, t_3) from its maximum brightness. The fast super-Eddington novae ($t_2 < 13$, $t_3 < 30$ days) have smooth light curves (LCs) with well defined maxima. The slow Eddington novae ($t_2 > 13$, $t_3 > 30$ days) have structured LCs and many of them have standstills at the maximum and dust formation at later stages (Downes & Duerbeck 2000). According to the properties of the LCs during nova declines, Strope *et al.* (2010) proposed seven types of LCs: S (smooth), P (plateau), D (dust dip), C (cusp), O (oscillations), F (flat topped), and J (jitter).

The spectra of classical novae display at maximum light either He/N or Fe II emission lines as the most prominent non-Balmer lines. Fe II spectra are formed in a large circumbinary envelope of gas, whose origin is the secondary star, while He/N spectra are formed in white dwarf ejecta. In hybrid objects both classes of spectra appear sequentially due to changing parameters in the two emitting regions (Williams, 2012).

2. Discovery and ATels spectroscopy

The classical nova V612 Sct (Nova Scuti 2017) = ASASSN-17hx was discovered by Stanek *et al.* (2017a,2017b) with the All Sky Automated Survey for SuperNovae on 2017 June 19.41 UT at mag 14.7 at the coordinates α_{2000} = $18^h31^m45.918^s$, δ_{2000} = -14°18'55.57". According to Kurtenkov *et al.* (2017) the progenitor is the Gaia Source ID 4104113350446549888, located 0.59 arcsec from the position with $G = 19.102$ mag. According to Saito *et al.* (2017), VVVX Ks-band observations taken during July and August 2016 show the presence of a faint source 0.84 arcsec from the reported target position with the Ks = 16.71±0.11 mag and coincide within 0.65 arcsec with the position of the Gaia source.

The first spectra of the nova, taken on June 24, 2017 by Kurtenkov *et al.* (2017) with the 2m RCC telescope at Rozhen Observatory (resolution R ∼ 500) exhibited Hα, Hβ, He I, He II, NII and NIII emission lines. This indicates that the nova is of He/N type, according to the classification of Williams (1992). RVs of absorptions in He I P Cyg profiles give the expansion velocity of 990 km s^{-1}. The medium-resolution (R ∼ 5400) spectra, taken on June 26.1, 29.02 by Williams & Darnley (2017) with the 2-m Liverpool telescope show Balmer and He I P Cyg profiles. The FWHM of Hα emission was 800 km s^{-1}. RVs of Hβ P Cyg profile absorptions were -860 and -520 km s^{-1}. The Mg II and Si II emissions were also present. The ARAS low resolution (R ∼ 580 - 2650) spectroscopy during June 29.8 - July 4.8 shows that He I emissions weakening is accompanied by Fe II emissions appearance. The RVs of P Cyg absorptions extended to –800 km s^{-1} (Berardi *et al.* 2017). High and low resolution spectroscopy at the brightness pre-maximum on July 10, 2018 with 1.82-m and 1.22-m telescopes in Asiago and a 1.5-m telescope at TUBITAK National Observatory shows prominent emissions of Balmer and Paschen series, FeII lines,

SiII, OI and CaII lines, so it is a textbook example of the Fe II nova (Munari *et al.* 2017a). The RVs of P-Cyg absorptions of Fe II multiplet 42 are -451, -359, and -285 km s^{-1}. Interstellar reddening $E(B-V) = 0.68$ was derived from EW of the diffuse interstellar band at 6614 Å. The spectra taken on July 26.61 and 27.58 (a few days before the brightness maximum) by the 2.3-m Vainu Bappu telescope, Kavalur, India show that the P Cyg absorptions developed in Balmer and Fe II lines while the emission component strenghtened (Pavana *et al.* 2017). According to Munari *et al.* (2017b), the peak brightness was reached on July 30.1 UT at $B = 9.65$, $V = 8.44$. The spectra on Aug 12.8 were dominated by Fe II and He I emissions. A sharp absorption at velocity 250 km s^{-1} was presented in the profile of Balmer lines, superimposed on the emission component that extent at its base from about -1000 to +1000 km s^{-1}. The interstellar absorption lines of NaI D1,D2 doublet were splitted into at least 5 distinct components. The total equivalent width indicates a reddening $E(B-V) = 0.62$ following the calibration by Munari & Zwitter (1997). Kuin *et al.* (2017) started the spectroscopic observations of the nova with Swift's UVOT 30-cm telescope on June 30. They derived $E(B-V) = 0.8\pm0.1$ from a significant 2175 Å dip caused by an interstellar extinction. They found the line width FWZI 4600 km s^{-1} from NIII] 1750 Å and Mg II 2800 Å emissions with FWZI 4600 km s^{-1}. In August 9, a large Fe II curtain was present in 1800 - 3800 Å part of the spectrum. The echelle spectrum taken during rebrightening of the nova on September 11, 2017 with the Varese 0.61-m telescope show Balmer and Fe II emission lines with multi-component P Cyg absorptions (Munari *et al.* 2017c). The RVs of Hα P Cyg absorptions were -500, -875, and -1130 km s^{-1} and FWHM of Hα emission 770 km s^{-1}. The ARAS spectra from June, 29 till September, 9 with resolution from 580 to 14000, depending on the spectrograph (Alpy 600, LISA, LHIRES, eShel) covering 3800-7200 Å and S/N 50–100 showed that all lines varied in strength and profile in correlation with the LCs changes (Guarro *et al.* 2017).

3. Observations, data reduction and times of brightness maxima

Our $UBVR_CI_C$ CCD photometric observations of the nova were obtained with the 18-cm Maksutov telescope and the 60-cm telescope located in the pavilions G1 and G2 of the AISAS observatory at Stará Lesná as well as the 50-cm telescope at the Southern Station of the Sternberg State Astronomical Institute of the Moscow University. The data were processed by a standard way using the nearby comparison star TYC 5703 – 0153 – 1. We found its magnitudes: $U = 11.87$, $B = 11.76$, $V = 11.14$, $R_C = 10.80$, $I_C = 10.40$ adopting the sequence of 8 stars around the symbiotic star RS Oph, published by Henden & Munari (2006). All our observations were reduced to the standard Johnson-Cousins system. Our photometric data were completed by the AAVSO International Database photometry and data from other available sources. Our individual V and B observa-

tions of the nova, the data published by Munari *et al.* (2017a,b,c), Kurtenkov *et al.* (2017) and available data of P. Jordanov (http://antares48.byethost7.com/) and N. Ikonnikova (https://istina.msu.ru/conferences/presentations/90612008/) together with the AAVSO V, B and TG, TB CCD data are presented in Fig. 1. Our data show that the nova reached maximum on 2017 July 29.9886 UT (JD 2457964.4886) at $V_{max} = 8.42$ and $B_{max} = 9.53$ mag. After the main maximum I four rebrightenings of the nova, designated by Roman number II-V were detected in 2017. Their dates and JDs were as follows: (II) September 13, 2017, JD2458010.409; (III) October 6, 2017, JD2458033.271; (IV) October 24, 2017, JD2458051.194; (V) November 17, 2017, JD2458075.239. Further rebrightenings of the nova were detected in 2018 after the 3-months gap in observations caused by the position of the nova on the sky in the vicinity of the Sun. Nightly means of our $UBVR_CI_C$ and AAVSO observations taken during the year 2017 are shown in Fig. 2.

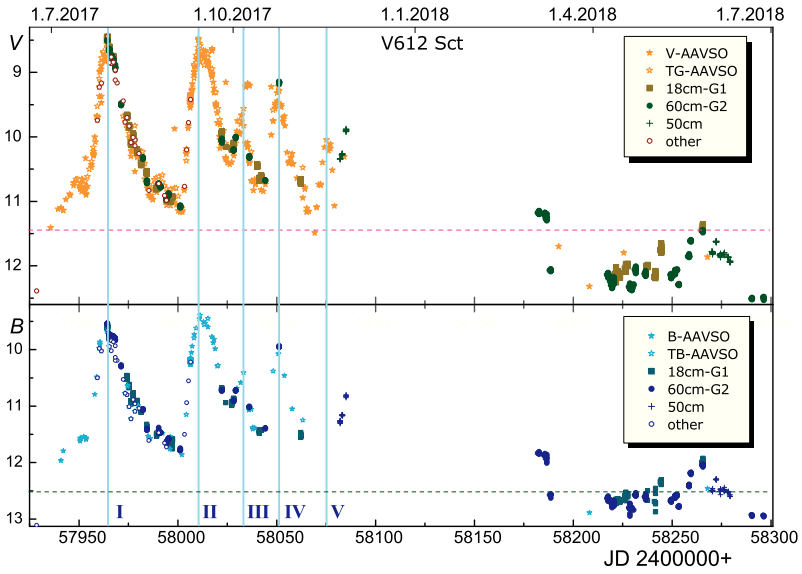

Figure 1. V and B LCs of the nova. The brightness corresponding to t_3 time is indicated by dashed lines. The vertical lines designate brightness maxima I - V.

Our optical echelle spectra in 2017 were obtained with the 60-cm telescope in G1 pavilion of the AISAS observatory at Stará Lesná (17 spectra with the resolution $R \sim 12\,000$) and the 1.3-m telescope of the AISAS observatory at Skalnaté

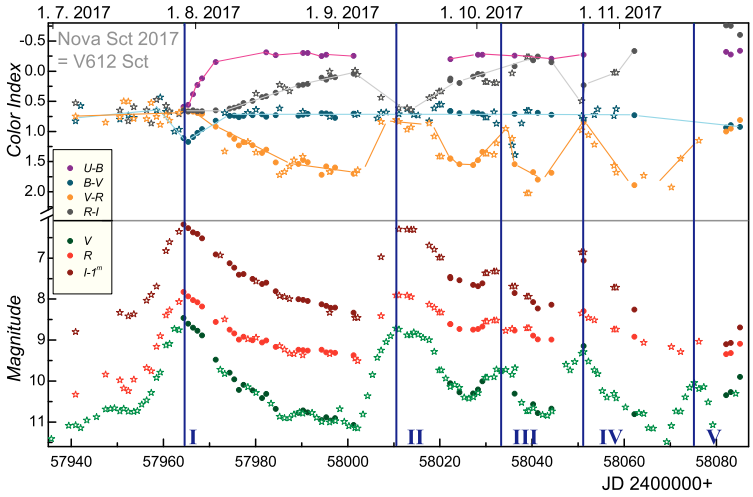

Figure 2. The $UBVR_CI_C$ photometry of the nova in 2017. The nightly means of our and AAVSO data are displayed by circles and asterisks, respectively. The vertical lines designate brightness maxima I - V.

Pleso (1 spectrum with the resolution $R \sim 24\,000$). Our data were completed by the Astronomical Ring for Access to Spectroscopy (ARAS) data, available at http://www.astrosurf.com/aras/Aras_DataBase/Novae/2017_NovaSct2017.htm. In the present paper, we have used 140 ARAS spectra with $R \sim 5\,000$ - 13 000, including 71 spectra taken by the co-author (JG).

4. Basic parameters of the nova and classification

The basic parameters of the nova V612 Sct were determined using the LCs presented in Fig. 1. Due to the large V and B LCs variations after maximum I, that exceeded 2 mag, the rate of decline found from t_2 time is ambiguous. Therefore, we used t_3 time to find the rates of decline $t_{3,V} = 105$ days and $t_{3,B} = 224$ days from V and B LCs, respectively.

We estimated the absolute magnitude of the nova at maximum MV_{max}, MB_{max} using the MMRD (Magnitude at Maximum – Rate of Decline) relations:

1) MV_{max} - t_3 relations of Schmidt (1975)

$$MV_{max} = -11.75 + 2.5 \log t_3, \tag{1}$$

2) MV_{max} - t_3 relations of de Vaucouleurs (1978)

$$MV_{max} = -11.3 + 2.4 \log t_3, \tag{2}$$

3) MV_{max} - t_3 relations of Downes & Duerbeck (2000)

$$MV_{max} = (-11.99 \pm 0.56) + (2.54 \pm 0.35) \log t_3, \tag{3}$$

4) MB_{max} - t_3 relations of Pfau (1976)

$$MB_{max} = -10.67 + 1.80 \log t_3. \tag{4}$$

We have calculated the following values of MV_{max} using these relations: MV^1_{max} = –6.70, MV^2_{max} = –6.45, MV^3_{max} = –6.86 with the unweighted mean: MV_{max} = -6.67 ±0.09. The relation (4) provides MB^4_{max} = –6.44. Van den Bergh & Younger (1987) found that the mean intrinsic value of the $B - V$ colour index for novae at maximum is

$$MB_{max} - MV_{max} = 0.23 \pm 0.06, \tag{5}$$

which leads to the exactly same value of MB_{max} as from the MMRD relation (4). Therefore, MB_{max} = -6.44 ±0.15.

Using this value and the formula given by Livio (1992)

$$MB_{max} = -8.3 - 10.0 \log(M_{wd}/M_{\odot}), \tag{6}$$

we can estimate the mass of the white dwarf component in V612 Sct as M_{wd} = 0.65±0.02 $M_{\odot}$.

The interstellar extinction can be found:

1) from the comparison of the observed colour index at maximum $(B-V)_{max}$ = 1.11, affected by extinction, with the intrinsic colour index $(B-V)^{in}_{max}$ = 0.23. We thus find the colour excess $E(B-V) = 0.88$;

2) from the relation of van den Bergh & Younger (1987), who found that novae two magnitudes below maximum have an unreddened colour index of

$$B - V = -0.02 \pm 0.04; \tag{7}$$

The observed colour of V612 Sct two magnitudes below maximum is $B - V$ = 0.68, which thus yields $E(B-V) = 0.70 \pm 0.04$.

3) from the 2175 Å dip caused by an interstellar extinction in UV Swift spectra (Kuin *et al.* 2017) $E(B-V) = 0.8 \pm 0.1$,

4) from the equivalent width of the diffuse interstellar band at 6614 Å (Munari *et al.* 2017a) $E(B-V) = 0.68$,

5) from the interstellar NaI D1,D2 doublet (Munari *et al.* 2017b) $E(B-V)$ = 0.62,

6) from the comparison of the true position (affected by interstellar reddening) of the nova Sct 2017 in the $(U-B, B-V)$ diagram with its expected

position in the classical novae sequence introduced by Hachisu & Kato (2014) $E(B-V) = 0.85$

The mean value of the reddening is $E(B-V) = 0.755 \pm 0.039$. Corresponding absorption in V is $A_V = 2.34 \pm 0.12$. The distance modulus of the nova is $V_{max} - MV_{max} = 15.08 \pm 0.08$, which yields a corresponding distance to the nova of 3.5 ± 0.3 kpc.

Using the classification scheme of nova LCs (Downes & Duerbeck 2000) and Strope *et al.* (2010), the nova V612 Sct can be classified as a slow nova of J-class with multiple peaks on the decline, similar to V723 Cas, HR Del, V4745 Sgr or V5558 Sgr. The presence of Fe II emission lines (Munari *et al.* 2017b) around the maximum light allows to classify V612 Sct as the Fe II nova (Williams, 2012).

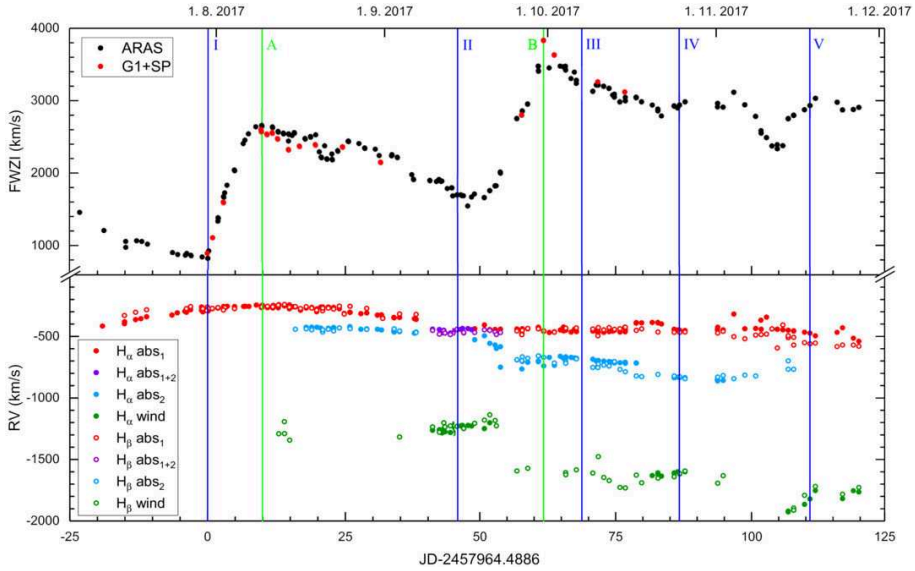

Figure 3. The FWZI of the Hα main emission peak (top). The RVs of the Hα and Hβ P Cyg absorptions (bottom). They arise in expanding inner and outer envelopes marked by the red and blue symbols, respectively. The terminal velocity of the wind is designated by green symbols. The violet symbols denoted the absorptions around maximum II without assigning them to the inner or outer envelope.

5. Hα and Hβ spectroscopy

For fitting of spectral lines and continuum we used the code `fityk` (Wojdyr, 2010). It is a general purpose peak fitting software with graphical interface. It offers many non-linear functions, subtraction of continuum, and can fit an

arbitrary number of peaks simultaneously by the Levenberg-Marquardt least square method. We selected the region of spectrum around the Hα line and fitted continuum by the second-order polynomial. We added a few Gaussian peaks based on the shape of the line, emission and absorption features. The main emission peak was selected to cover the shape of the wings and the intensity at the central wavelength λ_C. We have calculated 3σ distance from λ_C and computed corresponding radial velocity to λ_C-3σ while using the laboratory wavelength for Hα. Then we measured FWZI of the main emission component and expressed it in a velocity scale.

Comparison of the brightness maxima I–V of the nova and FWZI of the Hα emission is demonstrated in Fig. 3 (top). In brightness maximum I, the FWZI of Hα emission lines reached minimum 800 km s^{-1}. The local maximum of FWZI 2600 km s^{-1} (designated as A) was reached 10 days after the maximum I on August 8, 2017 (JD2457974.441). Then the FWZI started to decline and reached the minimal values around the rebrightening maximum II. The maximum of FWZI 3830 km s^{-1} (designated as B) was reached 16 days after the rebrightening II on September 29, 2017 (JD2458026.238). The Hα and Hβ P Cyg absorptions are a useful tool to study the variable outflow from the nova. The RVs of absorptions are presented in Fig. 3 (bottom). We can easily distinguish 2 distinct components of the expanding envelope and variable thick wind with the terminal velocity up to 1900 km s^{-1}.

We have selected spectra taken by our co-author (JG) for the investigation of the evolution of Hα and Hβ profiles. This subset provided good resolution (R = 9000) spectra with large coverage (4050–7500 Å). Also the number of spectra and their temporal cadence (with mean 4 days) was ideal for tracking changes in the line profiles. The evolution of the Hα and Hβ profiles in a normalized intensity scale are displayed in Fig. 4. The evolution of selected Hα profiles around the brightness maximum I and rebrightenings II and III are shown in Fig. 5.

6. Discussion

Appearance of the strong P Cyg absorptions in Balmer lines during the brightness maximum and rebrightenings maxima of the nova V612 Sct can be explained by re-expansion of its photosphere as suggested by Tanaka *et al.* (2011) for V5558 Sgr and similar novae. Csák *et al.* (2005) proposed for the nova V4745 Sgr that the repetitive instabilities of the hydrogen shell burning on the surface of the white dwarf cause a majority of spectral lines to switch back to strong P-Cyg profiles during mini-outbursts similar to their profiles from the main outburst. Episodic fuel burning during rebrightenings was discussed by Pejcha (2009).

The expanding shell of the nova V612 Sct consists of two major components: an inner slow main high-mass envelope in the form of an equatorial ring and an

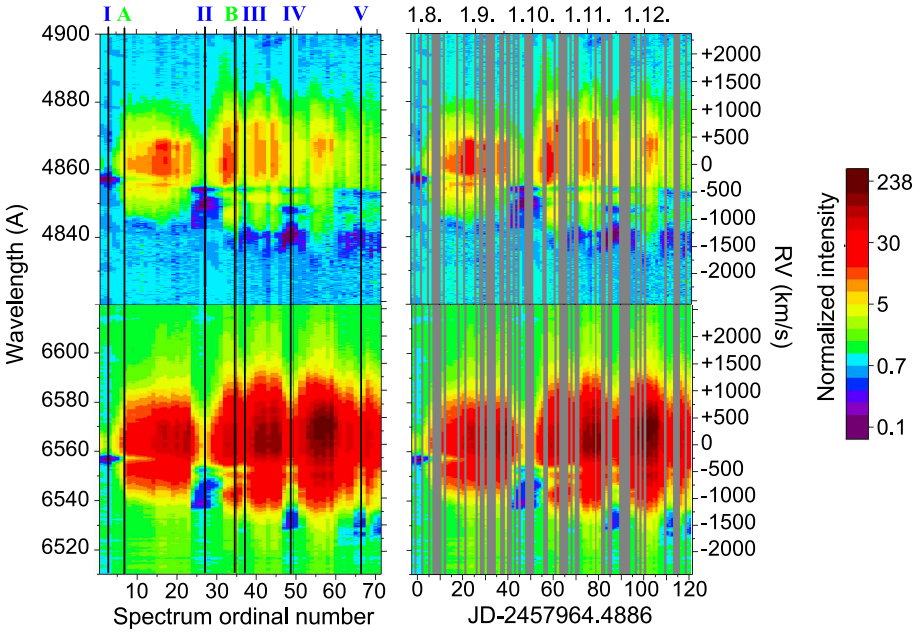

Figure 4. The evolution of the Hα and Hβ profiles in a normalized intensity scale. The profiles on the right side are expressed in a time scale, the missing dates of observations are marked by neutral wedges. The profiles on the left side are expressed in ordinal numbers of the spectra. The brightness maxima I–V and FWZI maxima A, B are marked.

outer fast tenuous low-mass envelope shaped and accelerated by spherical and polar winds. Chochol *et al.* (1997) proposed a similar structure of the expanding shell for the nova V1974 Cyg. Unfortunately, the interpretation of absorptions before the maximum II is not unique. The long-term behaviour of absorptions (red symbols before the maximum II and blue symbols after the maximum II in Fig. 3) could indicate a long-term change of an inclination of the polar outflow, suggesting the precession of the accretion disk with the period of about 170 days. The exact kinematical model of the expanding shell requires the high-resolution spectroscopy in a nebular stage of the nova and direct radio and optical images of the expanding shell.

Kato & Hachisu (2011) proposed two types of nova evolution that can occur in low-mass white dwarfs of $\sim$ 0.5 - 0.7 $M_{\odot}$. The flat peak around maximum, lasting about 9 years, in the symbiotic nova PU Vul suggests evolution with no indication of strong winds. The multipeak, lasting a few hundred days, for slow novae V723 Cas, V5558 Sgr, and HR Del suggest the presence of a transition from static evolution with no optically thick wind to usual evolution with the

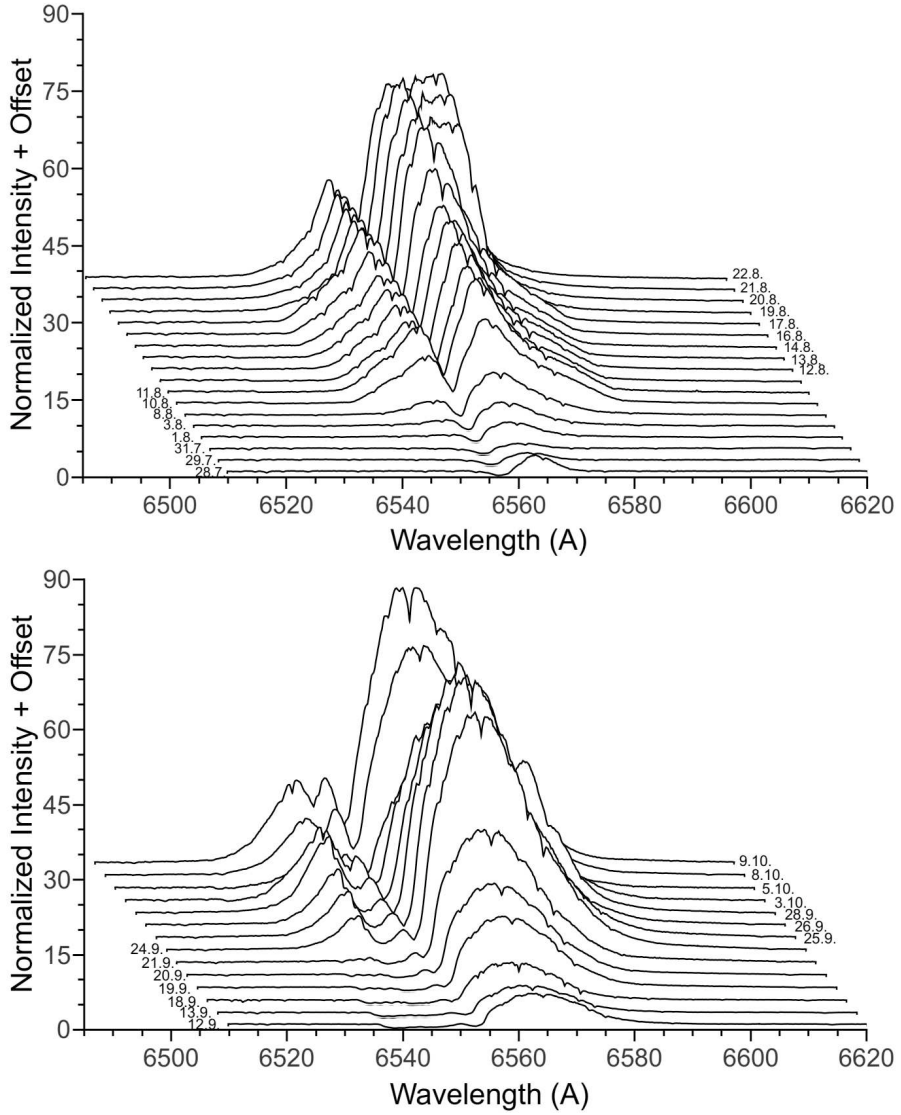

Figure 5. The evolution of selected Hα profiles around the brightness maximum I (top) and rebrightenings II and III (bottom). Individual spectra are shifted in wavelength and normalized intensity for better visibility.

optically thick winds. The presence of a companion deep inside the envelope triggers this transition, accompanied by oscillatory behaviour caused by a relaxation process. The LCs can be fitted by the model of a 0.6 $M_\odot$ WD with solar composition envelope. Our findings of the existence of thick winds in nova V612 Sct and its WD mass of 0.65 $M_\odot$ suggest that it belongs to the same group of slow novae.

Acknowledgements. We acknowledge with thanks the variable star observations from the AAVSO International Database contributed by observers worldwide and used in this research. We would like to thank all observes for spectra available in the ARAS database. This work was supported by the Slovak Research and Development Agency under the contract No. APVV-15-0458, and the VEGA grant 2/0031/18.

References

Berardi, P., Woody, S., Sollecchia, U.: 2017, *ATel*, 10558

Chochol, D., Grygar, J., Pribulla, T. et al.: 1997, *Astron. Astrophys.* **318**, 908

Csák, B., Kiss, L.L., Retter, A. et al.: 2005, *Astron. Astrophys.* **429**, 599

de Vaucouleurs, G.: 1978, *Astrophys. J.* **223**, 351

Downes, R.A. & Duerbeck, H.W.: 2000, *Astron. J.* **120**, 2007

Guarro, J., Berardi, P., Solecchia, U., Lester, T. et al.: 2017, *ATel*, 10737

Hachisu, I. & Kato, M.: 2014, *Astrophys. J.* **785**, 97

Henden, A. & Munari, U.: 2006, *Astron. Astrophys.* **458**, 339

Kato, M. & Hachisu, I.: 2011, *Astrophys. J.* **743**, 157

Kuin, N.P.M., Page, K.L., Williams, S.C., Darnley, M.J. et al.: 2017, *ATel*, 10636

Kurtenkov, A., Tomov, T., Pessev, P.: 2017, *ATel*, 10527

Livio, M.: 1992, *Astrophys. J.* **393**, 516

Munari, U., Hambsch, F.-J., Frigo, A., Castellani, F. et al.: 2017a, *ATel*, 10572

Munari, U., Traven, G., Hambsch, F.-J., Castellani, F. et al.: 2017b, *ATel*, 10641

Munari, U., Ochner, P., Hambsch, F.-J., Frigo, A. et al.: 2017c, *ATel*, 10736

Munari, U. & Zwitter, T.: 1997, *Astron. Astrophys.* **318**, 269

Pavana, M., Anupama, G.C., Selvakumar, G., Kiran, B.S.: 2017, *ATel*, 10613

Pejcha, O.: 2009, *Astrophys. J., Lett.* **701**, 119

Pfau, W.: 1976, *Astron. Astrophys.* **50**, 113

Schmidt, T.: 1957, *Z. Astrophys.* **41**, 182

Saito, R.K., Hempel, M., Minniti, D.: 2017, *ATel*, 10552

Stanek, K.Z., ASAS-SN Team: 2017b, *ATel*, 10524

Stanek, K.Z., Kochanek, C.,S., Chomiuk, L., Strader, J. et al.: 2017a, *ATel*, 10523

Strope, R.J., Schaefer, B.E., Henden, A.A.: 2010, *Astron. J.* **140**, 34

Tanaka, J., Nogami, D., Fujii, M., Ayani, K. et al.: 2011, *Publ. Astron. Soc. Jap.* **63**, 911

van den Bergh, S. & Younger, P.F.: 1987, *Astron. Astrophys.* **70**, 125

Williams, R.E.: 1992, *Astron. J.* **104**, 725

Williams, R.: 2012, *Astron. J.* **144**, 98

Williams, S.C. & Darnley, M.J.: 2017, *ATel*, 10542

Wojdyr, M.: 2010, *J. of Applied Crystallography* **43**, 1126

Contrib. Astron. Obs. Skalnaté Pleso **49**, 171 – 182, (2019)

Selected new results on pulsating variable stars

L. Szabados

Konkoly Observatory, Research Centre for Astronomy and Earth Sciences of the HAS, MTA CSFK Lendület Near-Field Cosmology Research Group, H-1121 Budapest, Konkoly Thege Miklós út 15-17, Hungary

Received: November 9, 2018; Accepted: February 18, 2019

Abstract. Recent progress in the studies of pulsating variable stars is summarized from an observational point of view. A number of unexpected phenomena have been revealed in the case of pulsators in the classical instability strip. These discoveries – lacking theoretical explanation yet – make pulsating stars more valuable objects for astrophysics than before. The emphasis is laid on Cepheids of all kind and RR Lyrae type variables, as well as binarity among pulsating variable stars.

Key words: pulsating variables – radial pulsation – nonradial pulsation – binarity

1. Introduction

This paper is intended to be an update and continuation of the review published in the proceedings of the previous conference held in Tatranská Lomnica on similar topic five years ago (Szabados, 2014). The reader will find repetitions only in unavoidable cases.

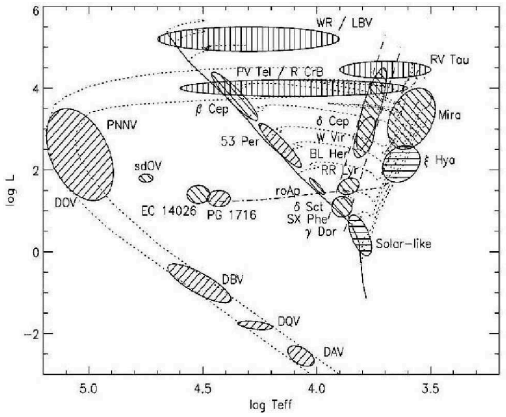

Figure 1. The H-R diagram showing the location of various types of pulsating variables (Jeffery, 2008). Some more types are listed in Table 1.

Table 1. Classification of pulsating variable stars.

Type	Design.	Spectrum	Period	Amplitude in V band (m)	Remark*
Cepheids	DCEP	F-G Iab-II	1-135 d	0.03-2	
	DCEPS	F5-F8 Iab-II	<7 d	<0.5	1OT
	CEP(B)	F5-F6 Iab-II	2-7 d	0.1-1	beat Cepheids
BL Boo	ACEP	A-F	0.4-2 d	0.4-1.0	anomalous Cepheids
W Vir	CWA	FIb	>8 d	0.3-1.2	
BL Her	CWB	FII	<8 d	<1.2	
RV Tau	RV, RVA	F-G	30-150 d	up to 3	
	RVB	F-G	30-150 d	up to 3	var. mean brightness
RR Lyr	RRAB	A-F giant	0.3-1.2 d	0.4-2	
	RRC	A-F giant	0.2-0.5 d	<0.8	1OT
	RR(B)	A-F giant	0.2-1.0 d	0.4-2	double-mode puls.
δ Sct	DSCT	A0-F5 III-V	0.01-0.2 d	0.003-0.9	R+NR
SX Phe	SXPHE	A2-F5 subdw.	0.04-0.08 d	<0.7	Pop. II
γ Dor	GDOR	A7-F7 IV-V	0.3-3 d	<0.1	NR, low degree g-mode
roAp	ROAP	B8-F0 Vp	5-20 min	0.01	NR p-modes
λ Boo	LBOO	A-F	<0.1 d	<0.05	Pop. I, metal-poor
Maia		A			to be confirmed
V361 Hya	RPHS, EC14026	sdB	80-600 s	0.02-0.05	NR, p-mode
V1093 Her	PG1716, Betsy	sdB	45-180 min	<0.02	g-mode
DW Lyn		subdwarf		<0.05	V1093 Her + V361 Hya
GW Vir	DOV, PG1159	HeII, CIV	300-5000 s	<0.2	NR g-modes
ZZ Cet	DAV	DAV	30-1500 s	0.001-0.2	NR g-modes
DQV	DQV	white dwarf	7-18 min	<0.05	hot carbon atmosphere
V777 Her	DBV	He lines	100-1000 s	<0.2	NR g-modes
Solar-like oscill.		F5-K1 III-V	<hours	<0.05	many modes
Mira	M	M, C, S IIIe	80-1000 d	2.5-11	small bolometric ampl.
Small ampl. red var.	SARV	K-M IIIe	10-2000 d	<1.0	
Semi-regular	SR	late type I-III	20-2300 d	0.04-2	
	SRA	M, C, S III	35-1200 d	<2.5	R overtone
	SRB	M, C, S III	20-2300 d	<2	weak periodicity
	SRC	M, C, S I-II	30-2000 d	1	
	SRD	F-K I-III	30-1100 d	0.1-4	
	SRS	late type	5-30 d	0.1-0.6	high-overtone puls.
Long-period irregular	L	late type			slow
	LB	K-M, C, S III			
	LC	K-M I-III			
Protoplan. nebulae	PPN	F-G I	35-200 d		SG, IR excess

* R = radial; NR = non-radial; 1OT = first overtone; SG = supergiant. Spectrum is given for maximum brightness for large amplitude variables.

Table 1. Classification of pulsating variable stars (continued).

Type	Design.	Spectrum	Period	Amplitude in V band (m)	Remark*
53 Per		O9-B5	1-3 d		NR
β Cep	BCEP	O8-B6 I-V	0.1-0.6	0.01-0.3	R + NR
	BCEPS	B2-B3 IV-V	0.02-0.04	0.015-0.025	R + NR
SPB	SPB	B2-B9 V	0.4-5 d	<0.5	high radial order, low degree g-modes
Be	BE, LERI	Be	0.3-3 d		NR (or rotational?)
LBV	LBV	hot SG	30-50 d		NR?
α Cyg	ACYG	Bep-Aep Ia	1-50 d	∼0.1	NR, multiperiodic
BX Cir		B	0.1 d	∼0.1	H-deficient
PV Tel	PVTELI	B-A Ip	5-30 d	∼0.1	He SG, R strange mode
	PVTELII	O-B I	0.5-5 d		H-def. SG, NR g-mode
	PVTELIII	F-G I	20-100 d		H-def. SG, R?
Fast Rotating Puls. B Stars	FaRPB	B	<55 d	0.001-0.004	fast rotators
Blue Large Ampl. Puls.	BLAP	O-B	20-40 min	0.2-0.4	
Binary Evolution Pulsators	BEP				RR Lyr 'impostors'
Heartbeat Variables					binary stars on eccentric orbit

Oscillations are ubiquitous in stars. Hot and cool stars, luminous and low luminosity stars can also pulsate, as is seen in the Hertzsprung-Russell (H-R) diagram showing the location of different types of pulsating variable stars (Fig. 1). Even our Sun is a pulsating variable star in which millions of non-radial oscillation modes have been excited.

Table 1 is an up-to-date overview of different types of pulsating variables whose oscillations are excited by various mechanisms. In the last years, four new types of pulsating variables – listed in the end of Table 1 – were discovered:
- fast rotating pulsating variables,
- blue large amplitude pulsators,
- binary evolution pulsators,
- heartbeat variables.

The first representatives of fast rotating pulsating stars were discovered by Degroote et al. (2009) and Mowlavi et al. (2013). Stars belonging to this new variability type also obey a period-luminosity (P-L) relationship, but its cause differs from that of the P-L relationship for classical pulsating variables (Mowlavi et al., 2016).

Blue large amplitude pulsators vary with a short period, like δ Scuti stars, but with a larger amplitude and their effective temperature is about 30 000 K (Pietrukowicz et al., 2017). Their luminosity corresponds to stars fainter than

those of main sequence stars of similar temperature. Such objects can be formed after merging of two low mass stars.

Binary evolution pulsators resemble RR Lyrae type variables phenomenologically (this is why their nickname is RR Lyrae impostors), but their mass is lower (about half) than that of the RR Lyraes on the horizontal branch of the H-R diagram. Such stars can occur in the instability strip of classical pulsators as a result of mass transfer in a binary system (Pietrzyński et al., 2012). Binary evolution pulsators can mimic Cepheid type behaviour, too. Based on a population synthesis calculation, Karczmarek et al. (2017) concluded that about 0.8% of seemingly RR Lyrae type variables are, in fact, binary evolution pulsators, while the contamination of Cepheids by such impostors is higher, about 5%.

The heartbeat variables are composed of two stars on an eccentric orbit and tidal interaction excites a low amplitude pulsation in at least one of their components. The first such binary star was found in the Kepler field (Welsh et al., 2011), and soon after this discovery, a number of such systems have been identified (Thompson et al., 2012).

Pulsating variable stars are important objects for astrophysics, cosmology, and studies of galactic structure, as well. From the point of view of astrophysics, stellar oscillations provide us with information on internal structure of the stars and their evolutionary phase. The cosmological use of pulsating variable stars is based on the fact that several types of luminous pulsators obey a specific P-L relationship which is indispensable in extragalactic distance determination. The galactic structure can be traced by studying spatial distribution of various types of pulsating stars of different ages/populations within a galactic system.

Importance of pulsating stars is supported by the frequency of occurrence of such variables, as well. About 40% of the designated variable stars in the General Catalogue of Variable Stars (GCVS, Samus et al., 2017) are pulsating variables. Because of the strict criteria, GCVS designation has been assigned to only less than 60 000 variable stars, meanwhile the number of known variables is over half a million. The Variable Star Index (VSX) maintained at the AAVSO website contains 543 564 stars in October 2018, while data on 550737 variable stars have been published in the Gaia Data Release 2 in April 2018, including more than 100 000 RR Lyrae type variables and 10 000 Cepheids (Gaia Collaboration, Brown et al., 2018). Keeping in mind the fact that about 10% of the targets of the Hipparcos astrometric satellite were found to be variable in brightness, the expected number of variable stars exceeds a hundred million among the more than one billion targets of the ESA's Gaia project. Naturally, the number of pulsating stars is also extremely large among the Gaia sample of stars brighter than $20\overset{\mathrm{m}}{.}7$ magnitude.

When observing pulsating stars, temporal coverage (duration of the time series) is a critical aspect for studying multiperiodicity, changes in frequency content, modal amplitudes, etc. Therefore, time consuming photometry of pulsating variables is a realm of small telescopes. If the astroclimate of the observing

site does not allow high-precision photometry, observations of variable stars with a large photometric amplitude are recommended.

A tutorial on the basic notions related to stellar pulsation is available in the pdf version of the author's presentation delivered during the conference (Szabados, 2018).

2. Importance of binarity among pulsating variables

It is a remarkable fact that binarity is important in at least three of the four recently defined types of pulsators mentioned above. In addition, pulsating stars in eclipsing binary systems are invaluable sources of information because such pairs of stars offer a unique possibility for an accurate determination of the mass, radius and luminosity of the components and test predictions of the pulsation theory (see e.g. Pilecki, 2018). Moreover, bright companions can falsify the calibration of the P-L relationship without correcting for their additional light. Therefore an important task is to reveal binary systems among pulsating stars used for standard candles.

A useful hint for binarity is the appearance of the light travel time effect in the $O-C$ diagram due to the orbital motion in a binary system. However, seemingly periodic variations in the pulsation period are insufficient for declaring that the given pulsator is a member in a binary system if the light-time effect solution results in unrealistic stellar parameters, or orbital elements as testified by the case of the RR Lyrae variable Z CVn (Skarka et al., 2018).

A close companion can even trigger stellar oscillations in the other star of the binary system. This happens in the case of heartbeat variables. Another kind of externally triggered pulsation was observed in the symbiotic nova RR Tel preceding its eruption in 1948 (Robinson, 1975).

Now it is clear that long-period variations in the mean brightness of RV Tauri stars (RVB subtype) are also caused by the binarity of these pulsators (Kiss & Bódi, 2017, and references therein).

3. Rapid evolutionary episodes in pulsating variables

In this section, recently observed interesting examples of rapid evolutionary episodes are mentioned continuing the list published in Szabados (2014).

The Type II Cepheid, V725 Sgr, experienced a sudden transition to a red semi-regular variable: its pulsation period increased from about 10 days to 90 days within a century (Percy et al., 2006).

The OGLE photometric survey is a treasure-house for finding peculiar behaviour among various pulsators. For example, Soszyński et al. (2014) revealed three RR Lyrae type variables which experienced mode switching from a double-mode pulsation to a simple fundamental mode oscillation, or vice versa. Their sample consisted of about 38 000 RR Lyrae stars in the Galactic Bulge, so such

rapid transitions are not extremely rare. Similarly, the OGLE project resulted in the discovery of a Cepheid variable, OGLE-SMC-CEP-3043, that stopped its pulsations within 15 years of observation (Soszyński et al., 2015b).

Delta Scuti stars perform both radial and non-radial pulsations and many modes can be excited simultaneously. It is noteworthy that temporal variations occur in both the observed frequencies and the modal amplitudes on a time scale of months to years. A thoroughly studied example is the case of AI CVn (Breger et al., 2017; Breger & Lenz, 2018).

4. New results on classical Cepheids

Cepheids have been considered as extremely stable pulsators for long. Studies based on very accurate photometric data collected by space telescopes, however, revealed that this paradigm has to be revised. Cycle-to-cycle changes occur in the pulsation period and light curve shape of V1154 Cygni (Derekas et al., 2012). In spite of this slight period flickering, the average pulsation period has remained stable on the time scale of decades. From the analysis of Kepler data covering four years Derekas et al. (2017) pointed out that the light curve of V1154 Cyg is modulated. This effect resembles the Blazhko effect commonly appearing among RR Lyrae stars. In the case of V1154 Cyg, the cycle length of the modulation is about 159 days.

The Blazhko effect was revealed in other classical Cepheids, too. Berdnikov et al. (2017) found a strong Blazhko modulation in the light curve of ASAS 160125-51503 with a cycle length of 1242 days. The pulsation of the best known Blazhko Cepheid, V473 Lyrae (Molnár et al., 2013) is subjected to period doubling, as revealed from uninterrupted photometry obtained with the MOST space telescope (Molnár et al., 2017). Such period doubling was recently observed in Blazhko RR Lyrae stars, too.

A part of fundamental-mode Cepheids in both Magellanic Clouds have periodically modulated light curve (Smolec, 2017). Though the amplitude of the modulation is tiny, the phenomenon is intriguing.

In addition to the slightly unstable light curve, the radial velocity phase curve of classical Cepheids is also non-repetitive because variations in the atmospheric velocity gradient result in radial velocity changes (Anderson, 2016).

Most of Cepheids are single-mode pulsators, but a simultaneously excited double-mode oscillation also exists among this type of variable stars and even Cepheids pulsating simultaneously in three radial modes have been identified (Moskalik, 2013). A long-term modulation of the light curve has been observed among the double-mode Cepheids of the Magellanic Clouds (Moskalik & Kołaczkowski, 2009). A characteristic feature of this modulation is that the amplitudes of modes involved vary in an anticorrelated manner.

The period ratio of the firts overtone and the fundamental mode pulsation is sensitive to the atmospheric iron abundance of double-mode Cepheids (Sziládi

et al., 2007). Recently, Sziládi et al. (2018) published formulae allowing calculation of iron abundance of double-mode Cepheids from the Fourier decomposition of the light curve.

The OGLE data show that additional periodic variability exists among first overtone Cepheids in the Magellanic Clouds with a photometric amplitude of 2-5 millimagnitude. The period is in the range of 0.60-0.65 of the value of the main pulsation period (Smolec & Śniegowska, 2016). In the Petersen diagram, three well separated sequences are outlined corresponding to stars that pulsate with this additional periodicity (see left panel of Fig. 2). From the period ratio, the slightly excited oscillation cannot be any radial mode. Pulsation with a similar period ratio has been observed in first overtone RR Lyrae variables. According to Dziembowski's (2016) theoretical calculations, the three new sequences in the Petersen diagram correspond to stars pulsating in non-radial modes of angular degrees 7, 8, and 9.

Anomalous Cepheids are probably old coalesced binaries crossing the instability strip (Soszyński et al., 2015a). Thus they are examples for binary evolution pulsators. Because anomalous Cepheids have separate P-L relationships, their individual representatives can be readily identified in the Magellanic Clouds based on the apparent mean brightness, unlike their Galactic counterparts.

5. New results on Type II Cepheids

Type II Cepheids are low-mass, usually metal-poor pulsators oscillating in the radial fundamental mode. Their pulsation is less stable compared with the oscillation of classical Cepheids. Noticeable light-curve changes occur from one cycle to the other, and the pulsation period can vary rapidly. In addition to these long known interesting facts, other peculiarities have been revealed quite recently (Smolec et al. 2018). The following dynamical phenomena have been identified in Type II Cepheids of the OGLE collections:
- double-mode pulsation in the short period (BL Her) subgroup;
- period doubling behaviour in the BL Her type variables;
- quasi-periodic light-curve modulation in all three (BL Her, W Vir, and RV Tau) subgroups of Type II Cepheids.
- Moreover, period doubling was revealed in Galactic W Vir stars (Plachy, 2018).

DF Cyg turned out to be the first RVb type variable star showing low-dimensional chaos in its pulsation (Plachy et al., 2018). This is only the third known case of chaotically pulsating RV Tauri stars, the other two variables belong to the RVa subgroup.

6. New results on RR Lyrae type variables

In addition to their periodic pulsation, the old RR Lyr type variables situated on the horizontal branch of the H-R diagram also show various other effects worthy

of studying in detail. At the turn of the millennium, RR Lyrae variables were thought to be monoperiodic radial pulsators part of which shows a modulated light curve. Now we know that RR Lyrae stars are multiperiodic with radial and nonradial modes excited. The long known, though still mysterious, phenomenon is the Blazhko effect, a slow, cyclic (not periodic) modulation of the light curve amplitude and phase appearing simultaneously is present in about 50% of these variable stars. It is typical that more than one modulation cycle is present in a given star. A gallery of the Blazhko modulation is published by Benkő et al. (2014). It is promising that new models involving interactions between radial and nonradial modes of oscillation, as well as coupling between the fundamental mode, first overtone and a high-order (9th) radial mode can lead us to the correct explanation of the Blazhko effect (Buchler & Kolláth, 2011). Several months ago Zoltán Kolláth succeeded in calculating a model light curve resembling Blazhko modulated brightness variations.

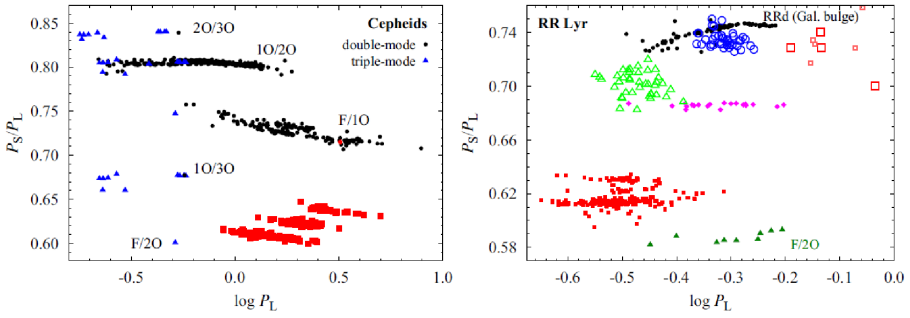

Figure 2. The Petersen diagram for Cepheids (left) and RR Lyrae stars (right) (Smolec et al., 2017).

Double-mode pulsation and nonradial modes are also present in some RR Lyr type variables (Moskalik, 2013). Among the double-mode RR Lyrae variables in the Magellanic Clouds, Soszyński et al. (2016) identified anomalous RRd pulsators, which are characterised by unusual period ratios and modal amplitudes.

Based on Kepler and CoRoT data, new dynamical phenomena have been discovered: period doubling and extra modes in all RR Lyraes pulsating in the first radial overtone, in all double-mode RR Lyraes and all Blazhko modulated fundamental pulsators (Netzel et al., 2015). These additional modes are non-stationary and their frequency ratios are concentrated in narrow intervals (see Fig. 2., right panel). The existence of extra nonradial modes is similar to the phenomenon discussed in Section 4.

Another important aspect of the current RR Lyrae research is the quest for finding binaries among these old pulsators. There is only one undoubted case: TU UMa (Liška et al., 2016), unlike Cepheids in our Galaxy where the occur-

rence of binaries exceeds 60%. The list of suspected binaries among RR Lyrae stars can be found in the online data base maintained by Liška & Skarka.

7. Telescopes, targets, tasks

Observation of pulsating variable stars needs patience and a huge amount of time. Therefore small (up to 1.5 m diameter) telescopes are used for carrying out photometric observations of such variables. Databases of various photometric sky surveys also offer an opportunity to study individual pulsating variable stars or a group of them.

Table 2. Space telescopes used for, or dedicated to photometry.

Mission (duration)	Aperture (cm)	Band (nm)	Remarks
IUE (1978-1996)	45	wide	Fine Error Sensor, no calibration
			0.03; var.; var.; targets for UV spectra
Hipparcos (1989-1993)	29	400-800 (Hp)	Tycho B_T: 350-500 nm; V_T: 460-600 nm
			0.02; 30-380; 3 years; 118 000 (Tycho: 2.5×10^6)
HST (1990-)	240	460-700	Fine Guidance Sensor
			0.001; var.; var.; millions
WIRE (1999-2011)	5.2	$V + R_J$	star tracker
			0.005; $> 10^3$; 21 d; 200 bright stars
INTEGRAL (2002-)	5	Johnson V	Optical Monitoring Camera
			0.04; var.; var.; $> 10^3$
Coriolis (2003-2011)	1.3	wide	on board SMEI satellite
			0.02; $> 10^3$; years; all naked-eye stars
MOST (2003-2014)	15	380-800	limited field (CVZ)
			0.0001; $> 10^3$; up to 60 d; 5000 bright stars
CoRoT (2006-2012)	27	350-1000	very limited field
			0.0001; $> 10^5$; 0.5 year; 120 000
Kepler (2009-2013)	95	400-900	very limited field
			0.00003; $> 10^5$; 4 years; 150 000
BRITE (2013/2014-)	3	550-700	5 satellites: 3 in blue, 2 in red band
		or 390-460	0.001; $> 10^3$; 30-180 d; ∼1000 bright stars
Gaia (2013-)	68	330-1050 (G)	G_{BP}: 330-680 nm; G_{RP}: 640-1050 nm
			0.001-0.020; ∼70; >5 years; 1.6 billion
K2 (2014-2018)	95	400-900	small fields along the Ecliptic
			0.0005; 10^5 ; 80 d; 350 000
TESS (2018-)	4×10.5	600-1000	large field of view
			0.0005; $> 10^4$; 27 d; 200 000
CHEOPS (2019-)	30	400-1100	to be launched
			0.00002; n.a.; n.a.; bright exoplanet host stars

In addition to ground-based equipments, space telescopes dedicated to, or used for, stellar photometry (see Table 2) also produce a large amount of time series photometric data. The typical accuracy (in magnitudes), typical number

of observations per target, length of the data series, and the approximate number of the observed stars are also listed in the second line of the remarks column of Table 2, for each space project. The advantage of space photometric data is twofold: their accuracy is much better than that of ground-based photometry and the time series is uninterrupted, or there are only short gaps. This latter feature is important for identifying the oscillation frequencies present in the observed star.

In view of the tremendous number of recently discovered new variable stars and the ongoing survey of the ESA's astrometric space probe, Gaia, the chance of revealing new variables during our own observations is extremely low. Observers with small telescopes cannot compete with the discovery efficiency of the LSST, either (LSST Science Collab., 2012). However, projects aimed at studying carefully selected individual pulsating variables can be very productive. A not exhaustive list of the features to be investigated from the observational data is as follows:
- the value of the pulsation period can be updated using the $O - C$ method, if prior photometric data are available;
- from detailed photometric study of individual variables one can point out additional periodicities, perform a mode identification, discover slightly excited non-radial (or radial) modes;
- pulsating variables in binary systems can be especially useful targets because of chance of revealing interactions of binarity and pulsation phenomena;
- for Cepheids and RR Lyrae stars, the atmospheric metallicity can be determined from the shape of the light curve via Fourier decomposition (Klagyivik et al., 2013).

If photometric data are insufficient for a reliable analysis, an in-depth spectroscopic study with a larger telescope can be instrumental. In such cases a cooperation between several telescopes/observatories is beneficial.

Many other interesting facts on pulsating variable stars are discussed in detail in the recent handbooks written by Aerts et al. (2010), Balona (2010), Catelan & Smith (2015), and Percy (2007), as well as in the conference proceedings edited by Suárez et al. (2013).

Acknowledgements. The organizers of the conference are thanked for dedicating an invited review to the topic of pulsating variables. This work has been supported by the Lendület Program of the Hungarian Academy of Sciences, project No. LP2018-7/2018 and the Hungarian NKFIH projects K-115 709 and K-129 249.

References

Aerts, C., Christensen-Dalsgaard, J., & Kurtz, D. W.: 2010, *Asteroseismology*, Springer, Dordrecht, Heidelberg, London, New York

Anderson, R. I.: 2016, *Mon. Not. R. Astron. Soc.* **463**, 1707

Balona, L. A.: 2010, *Challenges in Stellar Pulsation*, Bentham Science, Sharjah

Benkő, J. M., Plachy, E., Szabó, R., et al.: 2014, *Astrophys. J., Suppl.* **213**, 31

Benkő, J. M., Kolenberg, K., Szabó, R., et al.: 2010, *Mon. Not. R. Astron. Soc.* **409**, 1585

Berdnikov, L., Kniazev, A. Y., Kravtsov, V. V., & Dambis, A. K.: 2017, *Astrophys. Space Sci.* **362**, 105

Breger, M., Lenz, P.: 2018, *Journal of Astronomical Data* **24**, 1

Breger, M., Montgomery, M. H., Lenz., P., Pamyatnykh, A. A.: 2017, *Astron. Astrophys.* **599**, A116

Buchler, J. R., Kolláth, Z.: 2011, *Astrophys. J.* **731**, 24

Catelan, M., Smith, H. A.: 2015, *Pulsating Stars*, Wiley-VCH, Weinheim

Degroote, P., Aerts, C., Ollivier, M., et al.: 2009, *Astron. Astrophys.* **506**, 471

Derekas, A., Szabó, Gy. M., Berdnikov, L. N., et al.: 2017, *Mon. Not. R. Astron. Soc.* **425**, 1312

Derekas, A., Plachy, E., Molnár, L., et al.: 2012, *Mon. Not. R. Astron. Soc.* **464**, 1553

Dziembowski, W. A.: 2016, *Comm. Konkoly. Obs.* **105**, 23

Gaia Collaboration, Brown, A. G. A. et al.: 2018, *Astron. Astrophys.* **616**, A1

Jeffery, C. S.: 2008, *Comm. Asteroseism.* **157**, 240

Karczmarek, P., Wiktorowicz, G., Iłkiewicz, K., et al.: 2017, *Mon. Not. R. Astron. Soc.* **466**, 2842

Kiss, L. L., Bódi, A.: 2017, *Astron. Astrophys.* **608**, A99

Klagyivik, P., Szabados, L., Szing, A., Leccia, S., & Mowlavi, N.: 2013, *Mon. Not. R. Astron. Soc.* **434**, 2418

Liakos, A.: 2018, *Astron. Astrophys.* **616**, A130

Liška, J., Skarka, M., Mikulášek, Z., et al.: 2016, *Astron. Astrophys.* **589**, A94

URL: LSST Science Collab., 2012:, `http://www.lsst.org/scientists/scibook`

Molnár, L., Szabados, L., Dukes, R. J., Győrffy, Á., & Szabó, R.: 2013, *Astron. Nachr.* **334**, 980

Molnár, L., Derekas, A., Szabó, R., et al.: 2017, *Mon. Not. R. Astron. Soc.* **466**, 4009

Moskalik, P., Kołaczkowski, Z.: 2009, *Mon. Not. R. Astron. Soc.* **394**, 1649

Moskalik, P.: 2013, in *Stellar Pulsations. Impact of New Instrumentation and New Insights*, ed.: Suárez, J. C., Garrido, R., Balona, L. A., & Christensen-Dalsgaard, J., Springer, Heidelberg, New York, Dordrecht, London, 103

Mowlavi, N., Barblan, F., Saesen, S., & Eyer, L.: 2013, *Astron. Astrophys.* **554**, A108

Mowlavi, N., Saesen, S., Semaan, T. et al.: 2016, *Astron. Astrophys.* **595**, L1

Netzel, H., Smolec, R., Moskalik, P.: 2015, *Mon. Not. R. Astron. Soc.* **453**, 2022

Percy, J. R.: 2007, *Understanding Variable Stars*, Cambridge Univ. Press, Cambridge

Percy, J. R., Molak, A., Lund, H., et al.: 2006, *Publ. Astron. Soc. Pac.* **118**, 805

Pietrukowicz, P., Dziembowski, W. A., Latour, M., et al.: 2017, *Nature Astronomy* **1**, 166

Pietrzyński, G., Thompson, I. B., Gieren, W., et al.: 2012, *Nature* **484**, 75

URL: Pilecki, B., 2018, `https://www.pta.edu.pl/pliki/proc/vol6/v6p237.pdf`

Plachy, E., Bódi, A., Kolláth, Z.: 2018, *Mon. Not. R. Astron. Soc.* **481**, 2986

URL: Plachy, E., 2018, `https://www.pta.edu.pl/pliki/proc/vol6/v6p310.pdf`

Robinson, E. L.: 1975, *Astron. J.* **80**, 515

Samus', N. N, Kazarovets, E. V., Durlevich, O. V., Kireeva, N. N, Pastukhova, O. N.: 2017, *ARep* **61**, 80

Skarka, M., Liška, J., Dřevený, R., et al.: 2018, *Mon. Not. R. Astron. Soc.* **474**, 824

Smolec, R.: 2017, *Mon. Not. R. Astron. Soc.* **468**, 4299

Smolec, R. & Śniegowska, M.: 2016, *Mon. Not. R. Astron. Soc.* **458**, 3561

Smolec, R., Dziembowski, W., Moskalik, P., et al.: 2017, *EPJ Web of Conf.* **152**, 06003

Smolec, R., Moskalik, P., Plachy, E., et al.: 2018, *Mon. Not. R. Astron. Soc.* **481**, 3724

Soszyński, I., Smolec, R., Dziembowski, W. A., et al.: 2016, *Mon. Not. R. Astron. Soc.* **463**, 1332

Soszyński, I., Udalski, A., Szymański, M. K., et al.: 2014, *Acta Astron.* **64**, 177

Soszyński, I., Udalski, A., Szymański, M. K., et al.: 2015a, *Acta Astron.* **65**, 233

Soszyński, I., Udalski, A., Szymański, M. K., et al.: 2015b, *Acta Astron.* **65**, 329

Suárez, J. C., Garrido, R., Balona, L. A., & Christensen-Dalsgaard, J. (eds.): 2013, *Stellar Pulsations. Impact of New Instrumentation and New Insights*, Springer, Heidelberg, New York, Dordrecht, London

Szabados, L.: 2014, *Contrib. Astron. Obs. Skalnaté Pleso* **43**, 338

URL: PDF version of Szabados (2018) talk delivered at the conference 'Observing techniques, instrumentation and science for metre-class telescopes II', `https://www.astro.sk/conferences/75AI2018/talks/B04.pdf`

Szabó, R., Benkő, J. M., Paparó, M., et al.: 2014, *Astron. Astrophys.* **570**, A100

Szabó, R., Kolláth, Z., Molnár, L., et al.: 2010, *Mon. Not. R. Astron. Soc.* **409**, 1244

Sziládi, K., Vinkó, J., Poretti, E., et al.: 2007, *Astron. Astrophys.* **473**, 579

Sziládi, K., Vinkó, J., & Szabados, L.: 2018, *Acta Astron.* **68**, 111

Thompson, S. E., Everett, M., Mullally, F., et al.: 2012, *Astrophys. J.* **753**, 86

Welsh, W. F., Orosz, J. A., Aerts, C., et al.: 2011, *Astrophys. J., Suppl. Ser.* **197**, 4

URL: RR Lyrae stars in binary systems, maintained by J. Liška & M. Skarka, `http://rrlyrbincan.physics.muni.cz/`

URL: The AAVSO International Variable Star Index, `http://www.aavso.org/vsx/`

Contrib. Astron. Obs. Skalnaté Pleso **49**, 183 – 188, (2019)

Optical observations of bright supernovae

D.Yu. Tsvetkov[1], **N.N. Pavlyuk**[1], **S.Yu. Shugarov**[1,2] **and I.M. Volkov**[1,3]

[1] *Sternberg Astronomical Institute, M.V. Lomonosov Moscow State University, Universitetskii pr. 13, 119234 Moscow, Russia*

[2] *Astronomical Institute of the Slovak Academy of Sciences 059 60 Tatranská Lomnica, The Slovak Republic*

[3] *Institute of Astronomy of the Russian Academy of Sciences, 48 Pyatnitskaya street, 119017 Moscow, Russia*

Received: November 1, 2018; Accepted: March 20, 2019

Abstract. The program of CCD photometric monitoring of bright supernovae (SNe) has been carried out at 0.4 – 1.0 meter telescopes of the Sternberg Astronomical Institute, Crimean Astrophysical Observatory and Stará Lesná Observatory since 1998. We have observed more than 300 SNe of different types. We present the light curves of SN Ia 2014J, type II SNe 2009af, 2009ay, 2010jl, 2017eaw, type Ibn SN 2015U, and SLSN-I 2017egm. We discuss the physical parameters of the explosions and latest developments of the SN classification.

Key words: supernovae – photometry

1. Introduction

Supernova (SN) outbursts represent the final, explosive stage in the evolution of certain classes of stars. SNe occur in several spectroscopically distinct varieties. Type I SNe are defined by the absence of hydrogen in their optical spectra, while SNe II exhibit strong lines of hydrogen.

Type II SNe is the most common class of exploding stars. They are thought to arise from the death of massive stars with the mass $M > 8M_{\odot}$, when the nuclear burning does not provide sufficient thermal pressure to balance the gravity of the star. Type I SNe are subdivided into types Ia, Ib, Ic on the basis of the intensity of lines in the near-maximum spectra.

SNe of the type II, Ib and Ic are the result of core-collapse of massive stars (CCSN), while SNe Ia are the thermonuclear explosion of a CO white dwarf, which loses stability by accreting matter from the companion (thermonuclear SN).

Recently, new classes were added to this classification scheme. Extremely luminous SNe with maximum luminosity exceeding the absolute magnitude $M_V \sim -21$ mag were discovered. They are dubbed "Superluminous SNe" (SLSN) and divided into classes SLSN-I (without hydrogen) and SLSN-II (with hydrogen).

2. Observations

Light curves and spectra are the basic observational characteristics of SNe.

Obtaining a good-quality light curve requires continuous monitoring of an object for a period from some months to a few years, while the brightness decreases by 5-10 magnitudes. This is an appropriate task for small telescopes with CCD photometers.

We have carried out the program of systematic CCD photometric observations of SNe since 1998. The description of the program and some results were presented by Tsvetkov et al. (2014). Here we present the data for some interesting objects among those studied in the course of this program during the last 5 years. Their light curves are shown in Fig. 1.

3. Results

3.1. SN 2014J

The photometric and spectroscopic observations of this SN were reported by Tsvetkov et al. (2018a). This is a "normal" SN Ia, whose photometric and spectral evolution are typical for this class of SNe. The interstellar extinction in the parent galaxy is very high, with $E(B-V)_{host} = 1.22$, and we found a low value of a ratio between total and selective extinction $R_V = 1.36$. Continous monitoring did not reveal evidence for microvariability with an amplitude and characteristic time as reported by Bonanos & Boumis (2016).

3.2. SNe 2009af and 2009ay

We carried out $BVRI$ photometry for these type II SNe. The results were presented by Tsvetkov (2014). Both objects are characterized by a fast linear brightness decline at early stages of their evolution and a relatively high maximum luminosity. SN 2009af is distinguished by the low brightness drop during the first 200 days after maximum.

3.3. SN 2010jl

Photometric observations of SN IIn 2010jl were reported by Tsvetkov et al. (2016). The data from Fransson et al. (2014) were also plotted in Fig. 1. SN 2010jl was found to be extremely luminous even among type IIn SNe, with $M_{V(max)} \sim -20$ mag. The optical light curves showed slow decline during the first $\sim$ 175 days. After this epoch the light curves flattened, but at phase $\sim$ 300 days they started to decline considerably. We present evidence that SN 2005kd (Tsvetkov, 2008) is the most similar object to SN 2010jl considering the evolution of luminosity.

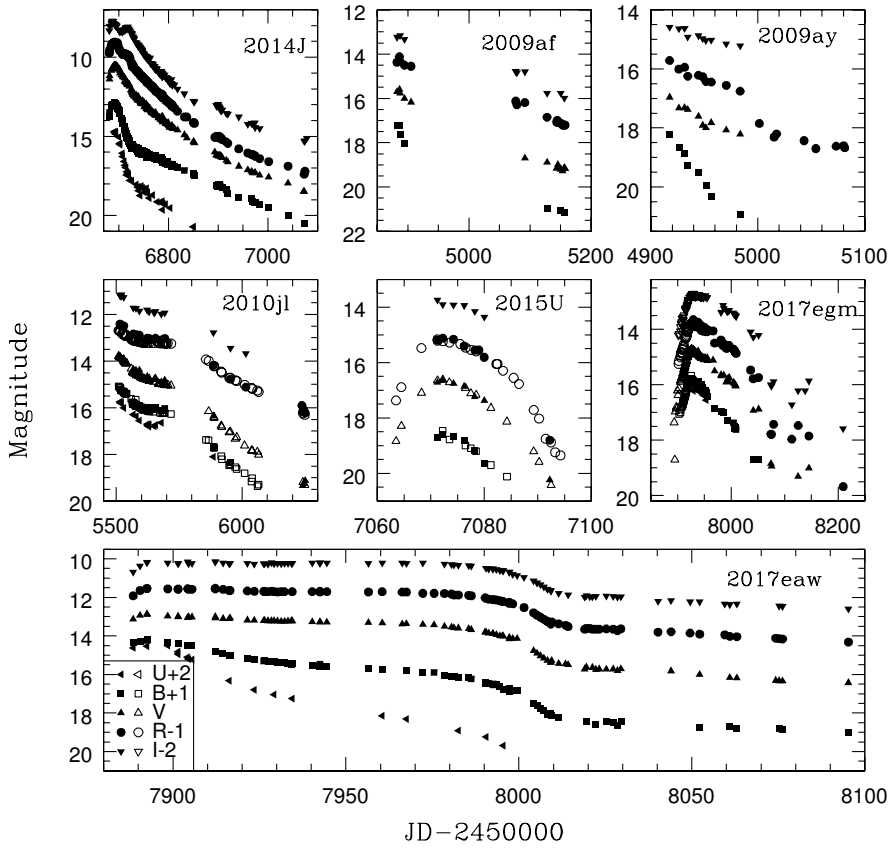

Figure 1. The light curves of selected SNe. The data in different bands are shifted for clear presentation. The shifts are indicated in the bottom plot. Filled symbols show our observations, while open symbols represent data from the literature.

3.4. SN 2015U

The results of photometric monitoring of SN 2015U were presented by Tsvetkov et al. (2015). Observations by Pastorello et al. (2015) were also plotted in Fig. 1. We conclude that SN 2015U exhibits a very high rate of brightness decline, fading by 2.6 mag in the V-band during the first 15 days after maximum. This SN belongs to a rare class of extremely fast declining SNe and is similar to SNe 2002bj (Poznanski et al., 2010), 2005ek (Drout et al., 2013) and 2010X (Kasliwal et al., 2010) regarding the shape of the light curves. The estimate of the peak luminosity for a heavily reddened SN depends strongly on the presently

unknown value of R_V. If we assume $R_V = 3.1$, then SN 2015U reached a peak magnitude of $M_R = -20.15$ mag and was definitely much brighter than all other SNe with similar photometric evolution. If $R_V = 1.5$, then the maximum luminosity of SN 2015U $M_R = -18.8$ mag, which still belongs to the brightest objects among SNe of similar classes.

3.5. SN 2017eaw

We presented *UBVRI* photometry of the supernova 2017eaw in NGC 6946, covering ∼200 days after its maximum (Tsvetkov et al., 2018b). The light curves are typical for type II-P SNe, with a plateau lasting about 100 days. Our first observations were made before the maximum light. We determined the time of maximum to be JD2457892.5. The magnitudes at maximum are $U = 12.5, B = 13.22, V = 12.87, R = 12.54, I = 12.18$. The fast decline after the plateau stage started at about JD2457980, and the final linear tail started at JD245810, with $B = 17.3, V = 15.5, R = 14.5, I = 13.8$ mag. The rates of decline on the tail in the B, V, R, I bands are 0.0054, 0.0106, 0.0092, 0.0090 mag day^{-1}, respectively. Assuming the distance of 6.0 Mpc for NGC 6946 (Efremov et al., 2011) and reddening $E(B-V) = 0.30$ mag, we derive absolute magnitudes of SN 2017eaw at maximum light: $M_U = -17.9, M_B = -16.9, M_V = -17.0, M_R = -17.1, M_I = -17.2$ mag.

The light curve shape with a luminous plateau shows that SN 2017eaw is a normal type II-P SN and its presupernova star was a red supergiant (RSG). SNe II-P show a large variety in their light-curve shapes. The main features of the light curves are determined by the initial radius R, total mass of presupernova M, mass of ^{56}Ni and the energy of explosion E (Kasen & Woosley, 2009). We computed the large grid of models in the parameter space ($R, M,^{56}$Ni, E) to evaluate the best fit model.

For the model calculation, we used the multi-group radiation-hydrodynamics numerical code STELLA (Blinnikov et al., 2006). The preliminary results show that the light curves of SN 2017eaw are best represented by the model with parameters $R = 600R_\odot$, $M = 23M_\odot$, $M_{\rm Ni} = 0.05M_\odot$, $E = 2 \times 10^{51}$ erg.

3.6. SN 2017egm

SN 2017egm was one of the nearest among superluminous SNe of type I. It exploded in a massive, metal-rich spiral galaxy NGC 3191, while most of SLSNe-I discovered earlier were from dwarf, star-forming metal-poor galaxies. We monitored this SN in *UBVRI* bands for more than 200 days after maximum. In Fig. 1 wee plotted also the data from Bose et al. (2018). SN 2017egm reached the peak luminosity of $M_V = -21$ mag. The light curves exhibit linear rise and decline near maximum, while other SLSNe-I show a curvature in their light curves near peaks. On the larger scale, the photometric evolution of SN 2017egm may be considered to be typical for this class of objects.

4. Conclusions

The program of photometric monitoring of SNe with small telescopes proved to be effective. During the last five years we carried out observations of SNe of different types and found some peculiar objects, revealing possibilities for a modification of the existing classification scheme. Comparison of the observed light curves with theoretical models allows to estimate physical parameters of the explosions.

Acknowledgements. The work of D.Tsvetkov was partly supported by the Russian Science Foundation Grant No. 16-12-10519. The work of S.Shugarov was partly supported by Grants VEGA 2/0008/17 and APVV-15-0458. The work of I.Volkov was supported by the scholarship of the Slovak Academic Information Agency (SAIA), by the Russian Science Foundation Grant No.14-12-00146 and Russian Foundation for Basic Research Grant No.18-502-12025.

References

Blinnikov, S. I., Röpke, F. K., Sorokina, E. I., et al., Theoretical light curves for deflagration models of type Ia supernova. 2006, *Astron. Astrophys.*, **453**, 229, DOI: 10.1051/0004-6361:20054594

Bonanos, A. Z. & Boumis, P., Evidence for rapid variability in the optical light curve of the Type Ia SN 2014J. 2016, *Astron. Astrophys.*, **585**, A19, DOI: 10.1051/0004-6361/201425412

Bose, S., Dong, S., Pastorello, A., et al., Gaia17biu/SN 2017egm in NGC 3191: The Closest Hydrogen-poor Superluminous Supernova to Date Is in a Normal, Massive, Metal-rich Spiral Galaxy. 2018, *Astrophys. J.*, **853**, 57, DOI: 10.3847/1538-4357/aaa298

Drout, M. R., Soderberg, A. M., Mazzali, P. A., et al., The Fast and Furious Decay of the Peculiar Type Ic Supernova 2005ek. 2013, *Astrophys. J.*, **774**, 58, DOI: 10.1088/0004-637X/774/1/58

Efremov, Y. N., Afanasiev, V. L., & Egorov, O. V., Ionized gas characteristics in the cavities of the gas and dust disc of the spiral galaxy NGC 6946. 2011, *Astrophysical Bulletin*, **66**, 304, DOI: 10.1134/S1990341311030035

Fransson, C., Ergon, M., Challis, P. J., et al., High-density Circumstellar Interaction in the Luminous Type IIn SN 2010jl: The First 1100 Days. 2014, *Astrophys. J.*, **797**, 118, DOI: 10.1088/0004-637X/797/2/118

Kasen, D. & Woosley, S. E., Type II Supernovae: Model Light Curves and Standard Candle Relationships. 2009, *Astrophys. J.*, **703**, 2205, DOI: 10.1088/0004-637X/703/2/2205

Kasliwal, M. M., Kulkarni, S. R., Gal-Yam, A., et al., Rapidly Decaying Supernova 2010X: A Candidate ".Ia" Explosion. 2010, *Astrophys. J., Lett.*, **723**, L98, DOI: 10.1088/2041-8205/723/1/L98

Pastorello, A., Tartaglia, L., Elias-Rosa, N., et al., Massive stars exploding in a He-rich circumstellar medium - VIII. PSN J07285387+3349106, a highly reddened supernova Ibn. 2015, *Mon. Not. R. Astron. Soc.*, **454**, 4293, DOI: 10.1093/mnras/stv2256

Poznanski, D., Chornock, R., Nugent, P. E., et al., An Unusually Fast-Evolving Supernova. 2010, *Science*, **327**, 58, DOI: 10.1126/science.1181709

Tsvetkov, D. Y., SN 2005kd: Another Very Luminous, Slowly Declining Type IIn Supernova. 2008, *Peremennye Zvezdy*, **28**

Tsvetkov, D. Y., Photometric Observations of Type II Supernovae 2009af and 2009ay. 2014, *Peremennye Zvezdy*, **34**

Tsvetkov, D. Y., Metlov, V. G., Volkov, I. M., et al., Photometric and spectroscopic observations of Supernova 2014J in M82. 2018a, *Contributions of the Astronomical Observatory Skalnate Pleso*, **48**, 511

Tsvetkov, D. Y., Pavlyuk, N. N., Volkov, I. M., & Shugarov, S. Y., Photometric monitoring of bright supernovae. 2014, *Contributions of the Astronomical Observatory Skalnate Pleso*, **43**, 351

Tsvetkov, D. Y., Shugarov, S. Y., & Volkov, I. M., The light curves of type IIn supernova 2010jl. 2016, *Contributions of the Astronomical Observatory Skalnate Pleso*, **46**, 87

Tsvetkov, D. Y., Shugarov, S. Y., Volkov, I. M., et al., Light Curves of the Type II-P Supernova SN 2017eaw: The First 200 Days. 2018b, *Astronomy Letters*, **44**, 315, DOI: 10.1134/S1063773718050043

Tsvetkov, D. Y., Volkov, I. M., & Pavlyuk, N. N., PSN J07285387+3349106 in NGC 2388: an extremely rapidly declining luminous supernova. 2015, *Information Bulletin on Variable Stars*, **6140**

Contrib. Astron. Obs. Skalnaté Pleso **49**, 189 – 196, (2019)

Studying symbiotic stars and classical nova outbursts with small telescopes

A. Skopal

Astronomical Institute of the Slovak Academy of Sciences
059 60 Tatranská Lomnica, The Slovak Republic, (E-mail: skopal@ta3.sk)

Received: November 2, 2018; Accepted: March 5, 2019

Abstract. Symbiotic stars are the widest interacting binaries, whose orbital periods are of the order of years, or even more, while cataclysmic variables are interacting binaries with periods of a few hours. Both systems comprise a white dwarf as the accretor, and undergo unpredictable outbursts. Using the multi-colour photometry and optical spectroscopy obtained with small telescopes, I present examples of the white dwarf outburst in a cataclysmic variable, the classical nova V339 Del, and that in the symbiotic star AG Peg. In this way I highlight importance of observations of bright outbursts using small telescopes.
Key words: stars: binaries: symbiotic – novae, cataclysmic variables – individual: V339 Del, AG Peg

1. Introduction

Symbiotic stars (SSs) and cataclysmic variables (CVs) are interacting binary systems, in which the accretor is a white dwarf (WD). In the former the donor is a red giant, while in the latter an evolved main sequence star. Orbital periods are extremely different, being typically of the order of years for SSs, but only of a few hours for CVs. The red giant in SSs underfills its Roche lobe with a factor of ~ 0.5 (e.g. Mürset & Schmid, 1999), whereas the evolved dwarf donor in CVs fills its Roche lobe. As a result, the WD in SSs accretes from the wind of the giant, while in CVs the accretion runs via the Roche-lobe overflow. A review of CVs can be found in the monograph of Warner (1995) and that on SSs in Kenyon (1986).

A common feature of these types of interacting binaries are their unpredictable outbursts observed on a very different and variable time-scale. The so-called classical nova (CN) outbursts of CVs are characterized by a large brightness amplitude of ∼7–15 mag, whereas the so-called Z And-type outbursts of SSs are as low as $\sim 1-3$ mag in the optical. CN outbursts are caused by the explosive thermonuclear fusion of hydrogen to helium on the WD surface, when the pressure at the base of the accreted matter exerts the critical value (e.g. Bode & Evans, 2008, for a review). In most cases the CN events result from accretion onto the WD at rates of $\sim 10^{-11} - 10^{-8}\, M_\odot\, \mathrm{yr}^{-1}$, which gives the recurrence time of their explosions usually much longer than the human life (Yaron et al., 2005). The energy output from the accreting WD in SSs can be

generated by two different mechanisms. The observed hot component luminosity of $\sim 10^0 - 10^2\,L_\odot$ can be powered solely by the accretion process onto a WD (e.g. EG And, 4 Dra, SU Lyn, see Skopal, 2005a; Mukai et al., 2016), while in other cases, luminosities of a few times $10^3\,L_\odot$ (e.g. Muerset et al., 1991; Skopal, 2005b) are believed to be caused by stable hydrogen nuclear burning on the WD surface (e.g. Paczynski & Rudak, 1980). The latter requires accretion onto a low mass WD at $\sim 10^{-8} - 10^{-7}\,M_\odot\,\mathrm{yr}^{-1}$ (e.g. Shen & Bildsten, 2007).

The nature of outbursts of accreting WDs in SSs is not yet unambiguously established. The low luminosity *accretion powered* WDs could increase their energy output due to transient accretion phenomena connected with a disk instability, as in dwarf novae. Here an example can be a ∼1 mag brightening of Z And in 1997 (see Sokoloski et al., 2006) and/or the erratic activity of the symbiotic star CH Cyg (e.g. Mikolajewska et al., 1988). For the luminous *nuclearly powered* WDs in SSs, the event of outburst can result from an increase in the accretion rate above the level sustaining the stable burning, which leads to blowing optically thick wind from the WD (Hachisu et al., 1996) and the luminosity can increase to the Eddington limit. The wind converts a fraction of the hot WD's radiation to the optical in the form of nebular emission, which causes a brightening in the light curve we indicate as the outburst. In this way, Skopal et al. (2017) explained the recent 2015 outburst of AG Peg.

In this contribution I present examples of the accreting WD outburst in a CV, the classical nova V339 Del (Nova Del 2013), and that in the symbiotic binary AG Peg. This work is based on the optical multicolour photometry and spectroscopy obtained solely with small telescopes collected mostly by amateur astronomers. In this way I demonstrate how such the observations carried out with a high cadence can contribute to worthy science.

2. Observations

2.1. Classical nova V339 Del

Classical nova V339 Del (Nova Delphini 2013) was discovered by Koichi Itagaki on 2013 August 14.584 UT at a visual magnitude of ∼6.8 (Nakano et al., 2013). On Aug. 16.45 UT, after ∼1.85 days of its discovery, the nova peaked at $V \sim 4.43$ (Munari et al., 2013), and became to be an attractive target also for amateur astronomers that resulted in obtaining high-cadence photometric and spectroscopic observations in the optical. Figure 1 shows the AAVSO International Database[1] photometric observations in the B and I_C passbands. Optical spectroscopy for the purpose of this contribution was taken from the *Astronomical Ring for Access to Spectroscopy (ARAS)* database.[2] Here, the spectrum obtained by J. Guarro at the Santa Maria de Montmagastrell Observatory on

[1] https://www.aavso.org/data-download

[2] http://www.astrosurf.com/aras/Aras_DataBase/Novae/Nova-Del-2013.htm

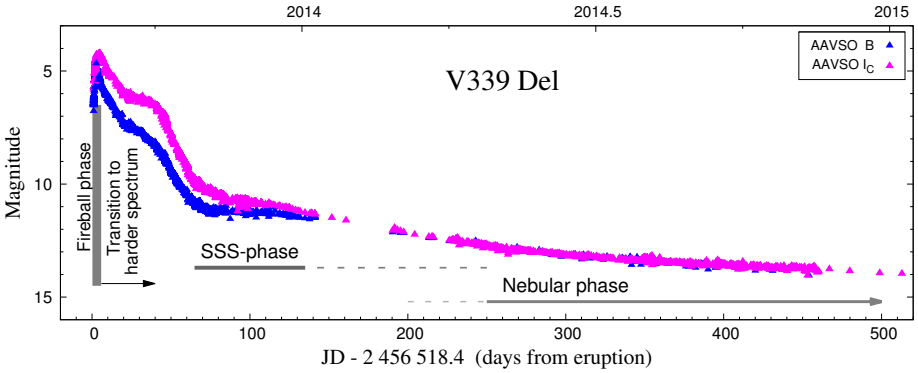

Figure 1. The B and I_C light curves of the nova V339 Del from its explosion (day 0) to day 520 of its life as collected in the AAVSO International Database. Basic phases of the nova evolution are designated by thick gray lines.

August 15.99, 2013, and that secured by M. Fujii at the Fujii Kurosaki Observatory with a 0.4 m telescope on September 13, 2013, were used. The spectra were described in detail by Skopal et al. (2014).

2.2. Symbiotic star AG Peg

AG Peg is a symbiotic binary comprising an M3 III giant (Mürset & Schmid, 1999) and a WD on an 818-d orbit (e.g. Fekel et al., 2000). It erupted around 1850, and rose in brightness from $\sim$ 9 to $\sim$ 6 mag around 1885 (Lundmark, 1921). Afterwards, AG Peg followed a gradual decline to around 2000. Such the evolution represents the slowest nova outburst ever recorded (Kenyon et al., 1993). From around 1997 to June 2015, AG Peg kept its brightness at a constant level, showing just pronounced wave-like orbitally-related variations (see Fig. 2). During June 2015, AG Peg experienced a new outburst (Waagen, 2015). The new outburst was monitored both photometrically and spectroscopically with a high cadence and also in the X-ray domain by the *Swift* satellite. It was found that the 2015 outburst was of the Z And-type (Ramsay et al., 2016; Tomov et al., 2016), during which the enhanced wind from the burning WD converted a fraction of its radiation to the nebular emission causing the observed 2 mag brightening in the light curve (Skopal et al., 2017).

Optical spectroscopy presented in this contribution was performed by K. Graham at his private station using a 0.25 m telescope on October 27, 2013, by U. Sollecchia at the private station in L′Aquila with a 0.20 m telescope on June 26, 2015 and by D. Boyd at the West Challow Observatory using a 0.28 m telescope. Spectra are available at the ARAS database and were described by Skopal et al. (2017).

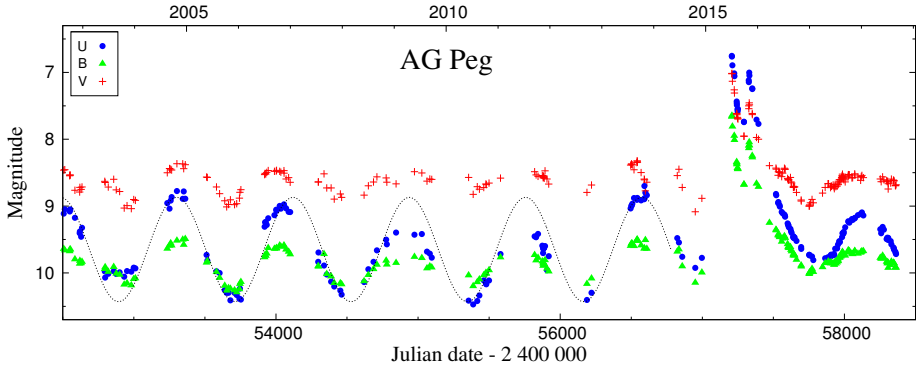

Figure 2. UBV light curves of AG Peg from 2003 to the present. During the quiescent phase the wave-like variation along the orbit is observed (the sine wave with the period of 818 days). Between June 2015 and June 2016, AG Peg showed a new outburst of the Z And-type. Data are from Skopal et al. (2012) and Sekeráš et al. (2019).

3. Analysis and results

During the nuclearly powered outbursts of WDs in CVs and/or SSs, the ejected material reprocesses the inner radiation, originally produced by the nuclear fusion on the WD surface. Because the geometrical and optical properties of the ejecta vary with time, the observed spectrum will be a function of the outburst stage. Generally, at the Earth we can observe the radiation from the WD photosphere, $\theta^2_{\rm WD}\pi B_\lambda(T_{\rm BB})$, whose fraction can be converted to the nebular continuum, $k_{\rm N}\times\varepsilon_\lambda(T_{\rm e})$. In the case of a symbiotic star, an additional component is emitted by the cool giant, which is compared with an appropriate synthetic spectrum, $\mathcal{F}_\lambda(T_{\rm eff})$. As a result, the observed continuum can be expressed as

$$F(\lambda)=\theta^2_{\rm WD}\pi B_\lambda(T_{\rm BB})+k_{\rm N}\times\varepsilon_\lambda(T_{\rm e})+\mathcal{F}_\lambda(T_{\rm eff}), \qquad (1)$$

where $\theta_{\rm WD}=R_{\rm WD}/d$ is the angular radius of the WD photosphere for the distance d. Fitting parameters are $\theta_{\rm WD}$, the blackbody temperature of the hot WD photosphere, $T_{\rm BB}$, the observed emission measure, $k_{\rm N}$, the electron temperature of the nebula, $T_{\rm e}$, and the effective temperature of the cool giant, $T_{\rm eff}$. The volume emission coefficient, $\varepsilon_\lambda(T_{\rm e})$, includes f–f and f–b transitions in the hydrogen plasma. A detailed description of modelling the composite spectrum (1) is given by Skopal (2005b).

3.1. Models SED of V339 Del

During the early stage of the nova evolution, called the 'fireball stage', the expanding shell redistributes the major part of the inner energetic photons into

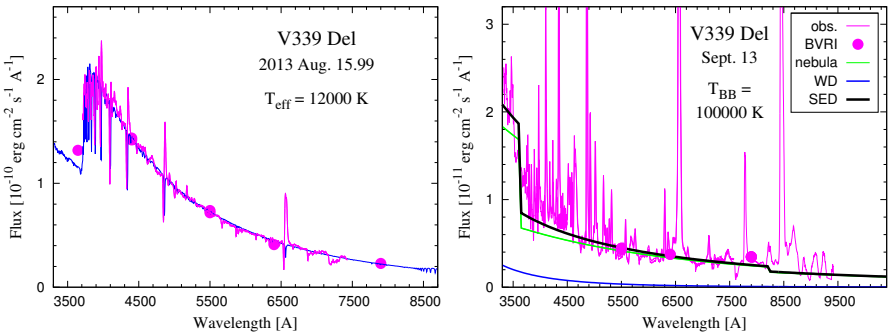

Figure 3. Observed (in magenta: spectrum and photometric flux-points) and models SED of V339 Del during the fireball stage (left) and the transition to harder spectrum (right). Observations were dereddened with $E_{\mathrm{B-V}} = 0.18$ mag (see Skopal et al., 2014).

the optical. The observed spectrum resembles that produced by a star of spectral type A to F. Accordingly, the spectrum of the nova can be compared with an atmospheric model, i.e., the first term in Eq. (1) is replaced by $\theta^2_{\mathrm{WD}}\,\mathcal{F}_\lambda(T_{\mathrm{eff}})$ and the nebular contribution can be neglected. The left panel of Fig. 3 shows the observed spectrum from the optical maximum compared with the atmospheric model calculated for the effective temperature of the WD photosphere of 12 000 K. Corresponding scaling, $\theta_{\mathrm{WD}} \sim 8.3 \times 10^{-10}$, gives the luminosity of $\sim 2.0 \times 10^{39} (d/4.5\,\mathrm{kpc})^2\,\mathrm{erg\,s^{-1}}$.

During the transition to harder spectrum, the ejecta dilutes on the line of sight, the WD photosphere becomes hotter, shifts its maximum to shorter wavelengths and ionizes the outer material giving rise to the nebular emission. Therefore, to model the observed continuum we use the first two terms on the right-hand side of Eq. (1). The right panel of Fig. 3 shows an example of the optical spectrum and its model SED. The nebular continuum radiates at $T_{\mathrm{e}} \sim 40\,000$ K and strongly dominates the optical with a large emission measure of $\sim 3.0 \times 10^{62} (d/4.5\,\mathrm{kpc})^2\,\mathrm{cm^{-3}}$. However, a small contribution of the hot WD photosphere in the optical does not allow to determine its T_{BB}.

3.2. Models SED of AG Peg

In the optical, the contribution from the hot WD in AG Peg (i.e., the first term on the right-hand side of Eq. (1)) is negligible with respect to those from the nebula and the cool giant. Therefore, the method is able to disentangle only these dominant contributions, i.e., to determine variables k_{N}, T_{e} and the giant's spectral type. Fig. 4 shows examples of the optical spectrum from the quiescent phase and that from the very beginning of the 2015 outburst with their models SED. The nebular continuum dominated the optical immediately at the start of the outburst. A factor of ∼12 increase of the emission measure, from ∼0.75

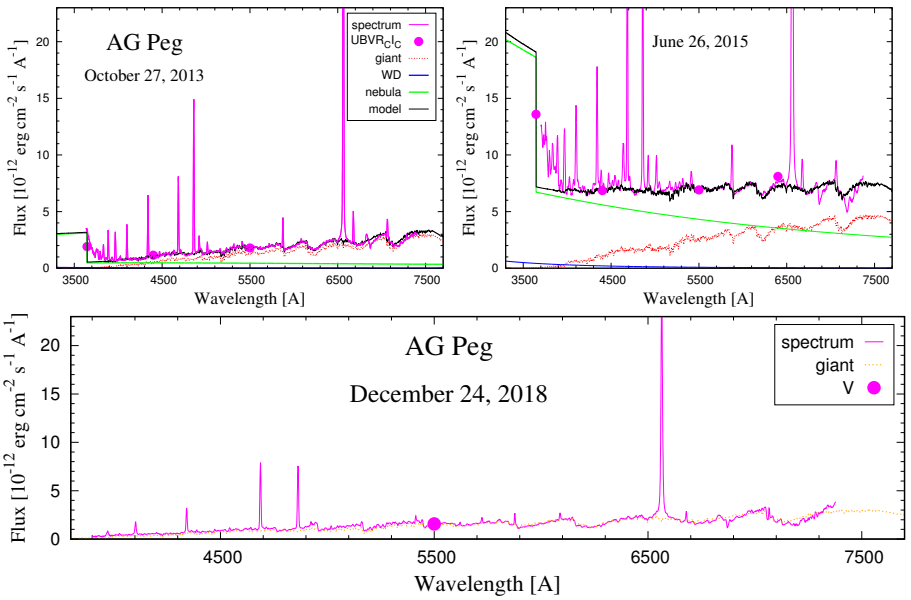

Figure 4. Examples of the AG Peg spectra (magenta) and their models SED (black) from the quiescence (left), the 2015 outburst (right) and 2018 quiescence (bottom). Observations were dereddened with $E_{\mathrm{B-V}} = 0.1$ mag (see Skopal et al., 2017).

to $\sim 9 \times 10^{60}\,(d/0.8\,\mathrm{kpc})^2\,\mathrm{cm}^{-3}$ at these dates corresponds to the observed brightening by ∼2.7 mag (see Skopal et al., 2017, in detail).

4. Conclusion

In this contribution, using examples of the classical nova V339 Del (Nova Delphini 2013) and the symbiotic binary AG Peg, it was shown that bright explosions of accreting WDs in SSs and CVs represent very suitable targets for the science with small telescopes. The following points are relevant.

– An unpredictable sudden change in the brightness of these types of objects is exclusively discovered by photometric monitoring. A discovery of outbursts provides an alert for observation with other facilities (Sect. 2.2).

– Multicolour photometric measurements, when corrected for emission lines, define the continuum flux-points, which allow us to calibrate the spectra that are usually obtained in arbitrary units (Skopal, 2007, Figs. 3 and 4 here).

– High cadence of both photometric and spectroscopic observations as provided by AAVSO and ARAS databases allows a detailed mapping of usually fast events of outbursts (e.g., Fig. 9 of Skopal et al., 2017).

– Disentangling the composite spectra into its individual components of radiation allow us to determine the corresponding physical parameters (Sect. 3).

– Observations with small optical telescopes are useful to complement measurements in other wavelengths.

Accordingly, it is possible to conclude that photometric and spectroscopic observations of bright transients with small telescopes can contribute to worthy science.

Acknowledgements. This research was supported by a grant of the Slovak Academy of Sciences, VEGA No. 2/0008/17, and the Slovak Research and Development Agency under the contract No. APVV-15-0458.

References

Bode, M. F. & Evans, A. 2008, *Classical Novae* (Cambridge: Cambridge University Press)

Fekel, F. C., Joyce, R. R., Hinkle, K. H., & Skrutskie, M. F., Infrared Spectroscopy of Symbiotic Stars. I. Orbits for Well-Known S-Type Systems. 2000, *Astron. J.*, **119**, 1375, DOI: 10.1086/301260

Hachisu, I., Kato, M., & Nomoto, K., A New Model for Progenitor Systems of Type IA Supernovae. 1996, *Astrophys. J., Lett.*, **470**, L97, DOI: 10.1086/310303

Kenyon, S. J. 1986, *The symbiotic stars* (Cambridge: Cambridge University Press)

Kenyon, S. J., Mikolajewska, J., Mikolajewski, M., Polidan, R. S., & Slovak, M. H., Evolution of the symbiotic binary system AG Pegasi - The slowest classical nova eruption ever recorded. 1993, *Astron. J.*, **106**, 1573, DOI: 10.1086/116749

Lundmark, K., Ein neuer Veränderlicher vom P Cygni-Typus. 1921, *Astronomische Nachrichten*, **213**, 93, DOI: 10.1002/asna.19212130604

Mikolajewska, J., Selvelli, P. L., & Hack, M., IUE low resolution observations of the symbiotic star CH Cygni in 1979-1986. 1988, *Astron. Astrophys.*, **198**, 150

Muerset, U., Nussbaumer, H., Schmid, H. M., & Vogel, M., Temperature and luminosity of hot components in symbiotic stars. 1991, *Astron. Astrophys.*, **248**, 458

Mukai, K., Luna, G. J. M., Cusumano, G., et al., SU Lyncis, a hard X-ray bright M giant: clues point to a large hidden population of symbiotic stars. 2016, *Mon. Not. R. Astron. Soc.*, **461**, L1, DOI: 10.1093/mnrasl/slw087

Munari, U., Valisa, P., Milani, A., & Cetrulo, G., Spectroscopy of the very fast Nova Del 2013, already declining past maximum brightness. 2013, *The Astronomer's Telegram*, **5297**

Mürset, U. & Schmid, H. M., Spectral classification of the cool giants in symbiotic systems. 1999, *Astron. Astrophys., Suppl.*, **137**, 473, DOI: 10.1051/aas:1999105

Nakano, S., Itagaki, K., Denisenko, D., et al., Nova Delphini 2013 = Pnv J20233073+2046041. 2013, *Central Bureau Electronic Telegrams*, **3628**

Paczynski, B. & Rudak, B., Symbiotic stars - Evolutionary considerations. 1980, *Astron. Astrophys.*, **82**, 349

Ramsay, G., Sokoloski, J. L., Luna, G. J. M., & Nuñez, N. E., Swift observations of the 2015 outburst of AG Peg - from slow nova to classical symbiotic outburst. 2016, *Mon. Not. R. Astron. Soc.*, **461**, 3599, DOI: 10.1093/mnras/stw1546

Sekeráš, M., Skopal, A., Shugarov, S., et al., Photometry of Symbiotic Stars - XIV. 2019, *Contributions of the Astronomical Observatory Skalnaté Pleso*, **49**, 19

Shen, K. J. & Bildsten, L., Thermally Stable Nuclear Burning on Accreting White Dwarfs. 2007, *Astrophys. J.*, **660**, 1444, DOI: 10.1086/513457

Skopal, A., Accretion-powered symbiotic binaries: EG And and CQ Dra. 2005a, in Astronomical Society of the Pacific Conference Series, Vol. **330**, *The Astrophysics of Cataclysmic Variables and Related Objects*, ed. J.-M. Hameury & J.-P. Lasota, 463

Skopal, A., Disentangling the composite continuum of symbiotic binaries. I. S-type systems. 2005b, *Astron. Astrophys.*, **440**, 995, DOI: 10.1051/0004-6361:20034262

Skopal, A., On the effect of emission lines on UBVR photometry. 2007, *New Astron.*, **12**, 597, DOI: 10.1016/j.newast.2007.04.003

Skopal, A., Drechsel, H., Tarasova, T., et al., Early evolution of the extraordinary Nova Delphini 2013 (V339 Del). 2014, *Astron. Astrophys.*, **569**, A112, DOI: 10.1051/0004-6361/201424284

Skopal, A., Shugarov, S., Vaňko, M., et al., Recent photometry of symbiotic stars. 2012, *Astronomische Nachrichten*, **333**, 242, DOI: 10.1002/asna.201111655

Skopal, A., Shugarov, S. Y., Sekeráš, M., et al., New outburst of the symbiotic nova AG Pegasi after 165 yr. 2017, *Astron. Astrophys.*, **604**, A48, DOI: 10.1051/0004-6361/201629593

Sokoloski, J. L., Kenyon, S. J., Espey, B. R., et al., A "Combination Nova" Outburst in Z Andromedae: Nuclear Shell Burning Triggered by a Disk Instability. 2006, *Astrophys. J.*, **636**, 1002, DOI: 10.1086/498206

Tomov, T. V., Stoyanov, K. A., & Zamanov, R. K., AG Pegasi - now a classical symbiotic star in outburst? 2016, *Mon. Not. R. Astron. Soc.*, **462**, 4435, DOI: 10.1093/mnras/stw2012

Waagen, E. O., Very rare outburst of the symbiotic variable AG Peg. 2015, *AAVSO Alert Notice*, **521**

Warner, B. 1995, *Cataclysmic Variable Stars.* (Cambridge: Cambridge University Press)

Yaron, O., Prialnik, D., Shara, M. M., & Kovetz, A., An Extended Grid of Nova Models. II. The Parameter Space of Nova Outbursts. 2005, *Astrophys. J.*, **623**, 398, DOI: 10.1086/428435

Contrib. Astron. Obs. Skalnaté Pleso **49**, 197 – 203, (2019)

The current active stage of the symbiotic system AG Draconis

R. Gális[1], J. Merc[1,2] and L. Leedjärv[3]

[1] *Institute of Physics, Faculty of Science, P. J. Šafárik University, Park Angelinum 9, 040 01 Košice, Slovak Republic*

[2] *Astronomical Institute, Faculty of Mathematics and Physics, Charles University, V Holešovičkách 2, 180 00 Prague, Czech Republic*

[3] *Tartu Observatory, Faculty of Science and Technology, University of Tartu, Observatooriumi 1, Tõravere, 61602 Tartumaa, Estonia*

Received: November 15, 2018; Accepted: February 12, 2019

Abstract. AG Dra is a strongly interacting binary system which manifests characteristic symbiotic activity of alternating quiescent and active stages. The latter ones consist of the series of individual outbursts repeating at about one-year interval. The current activity of AG Dra was initiated by a minor outburst in May 2015. The new stage of activity of this symbiotic system was confirmed by the following three outbursts in April 2016, May 2017 and in April 2018. The photometric and spectroscopic observations suggest that all these outbursts are of the *hot* type. Such behaviour is considered to be unusual in almost 130-year observation history of this object, because the major outbursts at the beginning of active stages are typically *cool*. In the present work, the current activity of the symbiotic binary AG Dra is described in detail.

Key words: symbiotic stars – outbursts – photometry – spectroscopy

1. Introduction

AG Dra is one of the best studied symbiotic systems. Its cool component is a metal-poor cool giant of spectral type K3 and higher luminosity than that of standard class III (Smith et al., 1996). The hot component of AG Dra is considered to be a white dwarf sustaining a high temperature of $(1\text{-}1.5) \times 10^5$ K and luminosity of $(1 - 5) \times 10^3\,L_\odot$ due to the stable hydrogen burning of the accreted matter on its surface (Mikolajewska et al., 1995; Sion et al., 2012). The giant under-fills its Roche lobe and the WD accretes from the stellar wind of the cool giant. A fraction of the giant's wind is ionised by the WD, which gives rise to the symbiotic nebula (Seaquist et al., 1984).

The period analysis of long-term photometric and spectroscopic observations confirmed the presence of two periods in AG Dra (Hric et al., 2014). The longer one (≈ 550 d) is related to the orbital motion and the shorter one (≈ 355 d) could be due to pulsation of the cool component of this symbiotic system.

AG Dra regularly undergoes quiescent and active stages which consist of several outbursts repeating with about 360 d interval. UV and X-ray observations

showed that there are two types of outbursts: *cool* and *hot* ones (González-Riestra et al., 1999). In the previous work, we demonstrated that the outbursts of AG Dra can also be clearly distinguished according to the behaviour of the prominent emission lines in optical spectra (Leedjärv et al., 2016).

2. Observational data

In this study, we analysed the photometric and spectroscopic observations that cover the ongoing active stage of AG Dra. New photometric measurements were obtained during 261, 155 and 560 nights from Karpov (2017), Vrašťák (2018) and the *AAVSO International Database* (Kafka, 2018), respectively.

Spectroscopic observations of AG Dra were acquired by *ARAS Group*[1] observers mostly in the framework of two observing campaigns which we initiated and coordinated in 2017 and 2018. Although the spectra were obtained with small telescopes (25 - 35 cm, $R \approx 1800$ - 11 000), they provided us valuable information about the recent activity of AG Dra. In total, we used 274 spectra covering the time interval from JD 2 456 765 (April 17, 2014) to JD 2 458 353 (August 23, 2018). Moreover, we analysed new intermediate-dispersion spectra obtained at the Tartu Observatory in Estonia (4 spectra, a 1.5-m telescope, $R \approx 6000$ and 7000) and at the Observatory of the Astronomical Institute of ASCR in Ondřejov (16 spectra, a 2.0-m telescope, $R \approx 13\,000$).

Our analysis was focused on the prominent emission lines in the wavelength regions under study: the hydrogen Balmer lines Hα (λ 6563) and Hβ (λ 4861), the neutral helium He I (λ 6678) line, the ionised helium He II (λ 4686) line, and the Raman-scattered O VI line at λ 6825.

3. Recent outburst activity of AG Dra

After seven years of quiescence following the 2006-08 major outbursts, the symbiotic system AG Dra started to become brighter again toward what appeared to be a new minor outburst during May 2015 (Fig. 1). The outburst activity of AG Dra was definitely confirmed by the following three outbursts in April 2016, May 2017 and in April 2018 (Gális et al., 2018).

3.1. Photometric behaviour

The first, less prominent outburst (G0) was observed in May 2015. The maximum brightness was achieved around JD 2 457 166 (10.7 and 9.6 mag in the B and V filters, respectively). It turned out that it was a minor outburst of AG Dra, a precursor of its activity as it was observed in some of the previous active stages.

[1] http://www.astrosurf.com/aras/Aras_DataBase/Symbiotics.htm

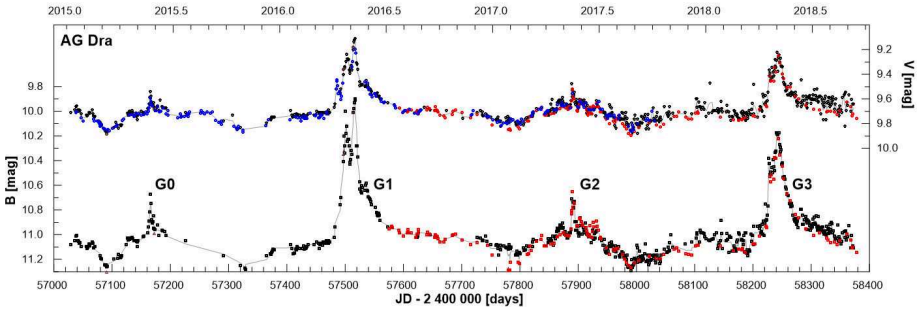

Figure 1. The light curves of the symbiotic system AG Dra during the recent active stage (2015-18) constructed on the basis of the B and V band observations. The photometric measurements depicted by blue, red and black colour were obtained from Karpov (2017), Vrašťák (2018) and *AAVSO* (Kafka, 2018), respectively.

During the second, more prominent outburst (G1), the brightness around JD 2 457 517 (May 8, 2016) reached the maximum of 9.9 and 9.1 mag in the B and V filters, respectively. As in the case of previous outburst (G0), its amplitude ranks this brightening to the minor outbursts of AG Dra.

Such photometric behaviour of the active stage is very unusual. More often, the pre-outbursts of AG Dra are followed by major outbursts, during which the brightness can reach around 8.8 and 8.4 mag in the B and V filters, respectively. A major outburst was not observed only during the activity stage in 1963-66, which was the shortest one in the almost 130-year photometric history of this strongly interacting symbiotic system (Hric et al., 2014).

In May 2017, the third brightening (G2) during the recent activity of AG Dra was detected. It was a very sharp and short-lasting outburst of the *hot* type. Maximal brightness was reached at JD 2 457 890 (10.7 and 9.5 mag in the B and V filters, respectively), similarly to the case of G0.

According to our statistical analysis of photometric observations, we found that time intervals between outbursts of AG Dra vary from 300 to 400 d (without an apparent long-term trend), with a median of $\approx$ 360 d. Therefore we expected the next outburst in the interval from April 21, 2018 (JD 2 458 230) to May 31, 2018 (JD 2 458 270).

Actually, AG Dra manifested the fourth outburst of the ongoing activity stage on May 4, 2018, i.e. 353 days after previous one. The maximum was reached at JD 2 458 243 with brightness of 10.2 and 9.5 mag in the B and V filters, respectively. At the end of July 2018, the brightness of AG Dra almost returned to values typical for quiescence (11.4, 11.1 and 9.8 mag in U, B and V filter, respectively), so the fourth outburst has finished (Merc et al., 2018).

The photometric behaviour suggests that all four recent outbursts of AG Dra

belong to the minor, *hot* type. Such classification is also supported by the EW increase of the studied emission lines detected during all these events.

3.2. Spectroscopic behaviour

We analysed variability of selected emission lines in the optical spectrum of AG Dra during almost 14 years (1997-2011) using own intermediate-dispersion spectroscopic observations (Leedjärv et al., 2016). One of the most interesting features of this variability is the significant increase of the EWs of all the five emission lines considered, but in particular that of Hα and Raman-scattered O VI (λ 6825), during some minor outbursts of this symbiotic system.

On the other hand, the major, *cool* outbursts of AG Dra (e.g. in July 2006) are not specifically distinct in the EWs of hydrogen and helium lines, but the weakening of the Raman-scattered O VI (λ 6825) line is very well seen. A simple interpretation of this behaviour could be that during the *cool* outburst, the temperature of the hot component of the symbiotic system decreased considerably, so that the high excitation original O VI (λ 1032) line faded considerably and its Raman-scattered O VI (λ 6825) counterpart almost disappeared, however leaving the lower excitation emission lines of hydrogen and helium mainly unaffected.

Direct comparison of the spectra of AG Dra obtained during the quiescence stage Q6 (JD 2 456 906) and the recent active stage G (JD 2 457 176) reveals significant increase of the EWs of all studied emission lines during the pre-outburst G0 (Fig. 2). Such spectroscopic behaviour is typical for the *hot* outbursts of this symbiotic system. Moreover, the absorption component observed in the profiles of the emission lines He I (λ 6678), Hα and Hβ completely disappeared during this outburst, which again justifies its *hot* character.

The EWs of emission lines Hα, Hβ, He I (λ 6678) and He II (λ 4686) manifest an even more prominent increase during the minor outburst G1. Such behaviour would suggest that this brightening belongs also to the *hot* outbursts of AG Dra. On the other hand, the EWs of the Raman-scattered O VI (λ 6825) line dropped to deep minimum during this outburst, which was observed only during the major, *cool* outbursts. In this way, the outburst G1 manifested the spectroscopic behaviour of both *hot* and *cool* outbursts of AG Dra (Merc et al., 2017). The open question remains whether it is a new type of outburst or some kind of transition between (or combination of) the *hot* and *cool* outbursts?

Although the third outburst G2 during the recent active stage of AG Dra was similar to the pre-outburst G0 in its brightness, we detected the same prominent increase of all the emission line EWs as in the case of brightening G1. The only exception was the Hα line: its EWs were comparable to ones during the G0 pre-outburst. Other interesting feature of this outburst was a weakening of hydrogen emission lines just before the G2 outburst. Overall, spectroscopic behaviour ranks this brightening to the *hot* outburst of AG Dra.

The last outburst of AG Dra detected in April 2018 was also of the *hot* type. The maxima of the EWs were either comparable to the values reached during

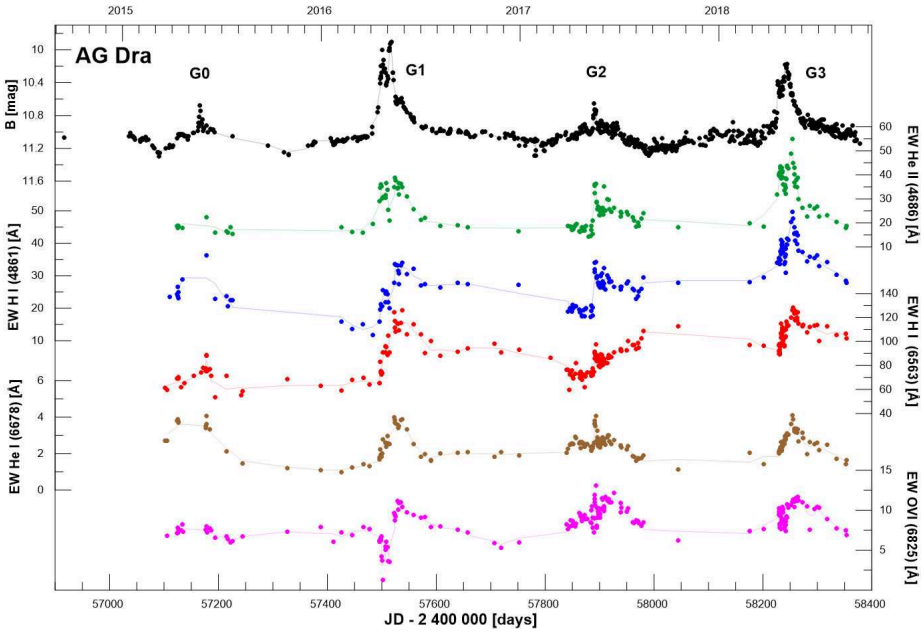

Figure 2. The light curves of AG Dra during the recent active stage in the B band together with the EWs of the studied emission lines. The spectroscopic measurements were obtained from *ARAS* database.

previous outbursts (in the case of Hα, He I (λ 6678) and Raman-scattered O VI (λ 6825) lines) or demonstrated the highest values detected during the ongoing active stage (Hβ and He II (λ 4686) lines).

4. Conclusions

To sum it up, photometric as well as spectroscopic behaviour suggest that the last four outbursts of AG Dra belong to the minor, *hot* type. Such classification is also supported by the results of our analysis of the hot component's temperature during the ongoing active stage of this symbiotic system (more details are given in Merc et al., 2019). On the other hand, some specific effects observed during the outburst G1 (e.g. the almost disappearance of the Raman-scattered O VI lines) are more typical for the *cool* outbursts, despite the fact that the WD's temperature reached the historical maximum during this event.

The future evolution of AG Dra is an open question. Can we expect (finally) a major, *cool* or (again) minor, *hot* outburst? Another possibility is that the symbiotic system will return to quiescence as we already detected such behaviour during the weak activity stage 1963-66. On the basis of our statistical analysis of

photometric observations, we are able to predict the time of the next outburst of AG Dra in the interval from JD 2 458 581 (April 7, 2019) to JD 2 458 625 (May 21, 2019).

In any case, AG Dra clearly demonstrates the importance of a pro/am co-operation in long-term monitoring of symbiotic stars in order to disentangle the nature and mechanisms of their active stages and outbursts.

Acknowledgements. This work was supported by the Slovak Research and Development Agency grant No. APVV-15-0458 and by the Estonian Ministry of Education and Research institutional research funding IUT 40-1. We are grateful to all ARAS members that contributed their spectra to this paper. We acknowledge with thanks the variable star observations from the AAVSO International Database contributed by observers worldwide and used in this research.

References

Gális, R., Merc, J., Vrašťák, M., et al., The fourth outburst during the present active stage of symbiotic binary AG Dra. 2018, *The Astronomer's Telegram*, **11559**, 1

González-Riestra, R., Viotti, R., Iijima, T., & Greiner, J., IUE observations of the high-velocity symbiotic star AG Draconis. III. A compendium of 17 years of UV monitoring, and comparison with optical and X-ray observations. 1999, *Astron. Astrophys.*, **347**, 478

Hric, L., Gális, R., Leedjärv, L., Burmeister, M., & Kundra, E., Outburst activity of the symbiotic system AG Dra. 2014, *Mon. Not. R. Astron. Soc.*, **443**, 1103, DOI: 10.1093/mnras/stu1162

Kafka, S. 2018, Observations from the AAVSO International Database, https://www.aavso.org

Karpov, S. 2017, private communication

Leedjärv, L., Gális, R., Hric, L., Merc, J., & Burmeister, M., Spectroscopic view on the outburst activity of the symbiotic binary AG Draconis. 2016, *Mon. Not. R. Astron. Soc.*, **456**, 2558, DOI: 10.1093/mnras/stv2807

Merc, J., Gális, R., & Leedjärv, L., Recent outburst activity of the super-soft X-ray binary AG Draconis. 2017, *Contributions of the Astronomical Observatory Skalnaté Pleso*, **47**, 192

Merc, J., Gális, R., & Teyssier, F., Study of long-term spectroscopic variability of symbiotic stars based on observations of the ARAS Group, *Contributions of the Astronomical Observatory Skalnaté Pleso*. 2019, *Contributions of the Astronomical Observatory Skalnaté Pleso*, **49**, 228

Merc, J., Gális, R., Vrašťák, M., & Leedjärv, L., The Fourth Outburst during the Ongoing Active Stage of AG Draconis has Finished. 2018, *Research Notes of the American Astronomical Society*, **2**, 142, DOI: 10.3847/2515-5172/aad807

Mikolajewska, J., Kenyon, S. J., Mikolajewski, M., Garcia, M. R., & Polidan, R. S., Evolution of the Symbiotic Binary System AG Draconis. 1995, *Astron. J.*, **109**, 1289, DOI: 10.1086/117361

Seaquist, E. R., Taylor, A. R., & Button, S., A Radio Survey of Symbiotic Stars. 1984, *Astrophys. J.*, **284**, 202, DOI: 10.1086/162399

Sion, E. M., Moreno, J., Godon, P., Sabra, B., & Mikolajewska, J., On the Nature of the Hot Component in the Symbiotic, Supersoft X-Ray Binary AG Draconis. 2012, *Astron. J.*, **144**, 171, DOI: 10.1088/0004-6256/144/6/171

Smith, V. V., Cunha, K., Jorissen, A., & Boffin, H. M. J., Abundances in the symbiotic star AG Draconis: the barium-symbiotic connection. 1996, *Astron. Astrophys.*, **315**, 179

Vrašťák, M. 2018, private communication

Contrib. Astron. Obs. Skalnaté Pleso **49**, 204 – 216, (2019)

ASASSN-18fk: A new WZ Sge-type dwarf nova with multiple rebrightenings and a new candidate for a superhumping intermediate polar

E. Pavlenko[1], K. Niijima[2], P. Mason[3,4], N. Wells[3,4], A. Sosnovskij[1], K. Antonyuk[1], A. Simon[5], N. Pit[1], C. Littlefield[6], H. Itoh[7], S. Kiyota[8], T. Tordai[9], P. Dubovsky[10], T. Vanmunster[11], G. Stone[12], T. Kato[2], A. Sergeev[13,14], V. Godunova[13], E. Lyumanov[1], O. Antonyuk[1], A. Baklanov[1], Ju. Babina[1], K. Isogai[2], Ya. Romanyuk[15], V. Troianskyi[16,17] and V. Kashuba[17]

[1] *Crimean astrophysical observatory of RAS, Republic of Crimea, (E-mail: eppavlenko@gmail.com)*

[2] *Department of Astronomy, Kyoto University, Kyoto 606-8502, Japan*

[3] *New Mexico State University, MSC 3DA, Las Cruces, NM, 88003, USA*

[4] *Picture Rocks Observatory, 1025 S. Solano, Suite D, Las Cruces, NM, 88001, USA*

[5] *Astronomy and Space Physics Department, Taras Shevchenko National University of Kyiv, Volodymyrska str. 60, Kyiv, 01601, Ukraine*

[6] *Department of Physics, University of Notre Dame, 225 Nieuwland Science Hall, Notre Dame, Indiana 46556, USA*

[7] *Variable Star Observers League in Japan (VSOLJ), 1001-105 Nishiterakata, Hachioji, Tokyo 192- 0153, Japan*

[8] *VSOLJ, 7-1 Kitahatsutomi, Kamagaya, Chiba 273-0126, Japan*

[9] *Polaris Observatory, Hungarian Astronomical Association, Laborc utca 2/c, 1037 Budapest, Hungary*

[10] *Vihorlat Observatory, Mierova 4, 06601 Humenne, Slovakia*

[11] *Center for Backyard Astrophysics Belgium, Walhostraat 1A, B-3401 Landen, Belgium*

[12] *American Association of Variable Star Observers, 49 Bay State Rd., Cambridge, MA 02138, USA*

[13] *ICAMER Observatory of NASU, 27 Acad. Zabolotnogo str., Kyiv, 03143, Ukraine*

[14] *Terskol Branch of the Institute of Astronomy, Russian Academy of Science, Terskol, Kabardino-Balkarian Republic, 361605, Russian Federation*

[15] *Main Astronomical Observatory of the National Academy of Sciences of Ukraine, 27 Acad. Zabolotnoho str., Kyiv, 03143, Ukraine*

[16] *Institute Astronomical Observatory, Faculty of Physics, Adam Mickiewicz University in Poznan, ul. Sloneczna 36, PL60-286 Poznan, Poland*

[17] *Astronomical Observatory of Odessa I.I. Mechnikov National University, 1v Marazlievska str., Odesa, 65014, Ukraine*

Received: November 20, 2018; Accepted: February 1, 2019

Abstract. We present the result of a multi-longitude campaign on the photometric study of the dwarf nova ASASSN-18fk during its superoutburst in 2018. It was observed with 18 telescopes at 15 sites during $\sim$ 70 nights within a three-month interval. Observations covered the main outburst, six rebrightenings and 50-d decline to a near-quiescent state. We identify ASASSN-18fk as WZ Sge-type dwarf nova with multiple rebrightenings and show the evolution of the 0.06-d superhump period over all stages of the superoutburst. A strong 22-min brightness modulation that superimposed on superhumps is found during rebrightenings and decline. Some evidence of this modulation in a form of a sideband signal is detected during the very onset of the outburst. We interpret the 22-min modulation as a spin period of the white dwarf and suggest that ASASSN-18fk is a good candidate for a superhumping intermediate polar.

Key words: accretion, accretion disks – cataclysmic variables – stars: dwarf novae – stars: individual: ASASSN-18fk

1. Introduction

Cataclysmic variables (CVs) are close binary systems which consist of an old (K-L) spectral type dwarf and a white dwarf (WD). The orbital periods of most of CVs are distributed between ∼6 hours and ∼76-min period minimum (Hellier, 2001), (Knigge, 2006). There is the 2.15 -3.18 hr "period gap" with a deficiency of CVs within it.

The primary component, that is the WD, is accreting matter from the secondary old-type component, which filled its Roche Lobe and looses material via the inner Lagrangian point see e.g. (Warner, 1995) for CVs in general. Depending on the primary's magnetic field, accretion could occur through an accretion disk (non- magnetic CVs) or accretion stream is channelled onto magnetic poles (magnetic CVs or polars with magnetic field $B = 10^7 - 10^8$ G). Non-magnetic CVs (dwarf novae) display outbursts. SU UMa-type dwarf novae, which occupy a region of orbital periods 76 min – ∼3 hr, possess the two types of outbursts – the normal ones and superoutbursts that are a result of the combination of thermal and tidal instabilities (Osaki, 1989); (Osaki, 1996). Typically, several normal outbursts that are shorter and slightly fainter than superoutbursts occur between two consequtive superoutbursts. The interval between superoutbursts varies between tens of days (SU UMa stars) and years – decades (WZ Sge type stars). More on the WZ Sge-type stars, see (Kato, 2015) for the review of these stars.

During superoutbursts, there are brightness variations (superhumps) with a period of several percent longer than the orbital one. Kato et al. (2009) in-

troduced three stages in the superhump evolution: stage A of the growing superhumps whose period is constant and slightly longer than the period at the next stage B; stage B with a systematically varying period and stage C with a shorter and almost constant period. One of the defining characteristics of WZ Sge-type dwarf novae are "early superhumps", the double-wave modulations during the early stage of the outburst with a period equal to the orbital one (Kato, 2002). Some WZ Sge-type stars may show so-called "late superhumps" – coherent modulation during the slowly fading stage (Kato et al., 2008).

The spin and orbital periods of the WD in magnetic CVs are synchronized (with an exception of four well-established, slightly asynchronous polars (Pavlenko et al., 2018). In the intermediate polars (IPs) the magnetic field of the white dwarf is $B = 10^6 - 10^7$ G and accretion occurs from an accretion ring onto the magnetic poles of the highly asynchronous white dwarf. Among 1166 CVs known up to 2012 (Ritter & Kolb, 2003)], there are 38 of the confirmed IPs with some uncertainty of WZ Sge, see http://asd.gsfc.nasa.gov/Koji.Mukai/-iphome/iphome.htm; Woudt et al. (2012). The orbital periods of the known IPs are distributed between 81 and 1000 min, where the most of them have the orbital period above the period gap. Only eight IPs are placed below the period gap, which include six outbursting members (Woudt et al., 2012). The only outbursting IPs with superhumps are V455 And, CC Scl and possibly WZ Sge.

ASASSN-18fk was discovered on March 17 by the ASASSN-team as a bright star of $12^m.14$. It matched the blue $g = 19^m.6$ SDSS source (VSNET-alert 21987) and according to the CRTS data showed no past outbursts. C. Littlefield reported on the 0.0570(3) d modulation (VSNET-alert 21992) that was preliminary identified as double-wave early superhumps of a likely new WZ Sge-type dwarf nova, ASASSN-18fk. Here, we report results of the multisite campaign of the ASASSN-18fk investigation during the superoutburst and its decline up to the near-quiescent state.

2. Observations

The CCD-photometry of ASASSN-18fk was done in 2018 with 18 telescopes located at 15 observatories during 70 nights (see Table 1). All observations were obtained in unfiltered light. CCD frames were dark subtracted and flat-fielded in the usual manner. Depending on a size of the telescope, time exposure, weather conditions and brightness of the object, the accuracy of a single observation varied between $0^m.005$ and $0^m.007$. All the data were measured relative to the comparison star 148 ($\alpha_{2000} = 12^h08^m53.45^s$, $\delta_{2000} = 19°16'05.6"$) in the AAVSO designation, $V = 14^m.813$, $B - V = 0^m.792$ from the sequence X23128MX (AAVSO) and expressed in the Heliocentric Julian Day (HJD). During the time of our observations, the brightness of ASASSN-18fk decreased from $13^m.3$ to $19^m.5$.

Table 1.: Journal of observations.

HJD 2458000+ (start - end)	Observatory/telescope	CCD	N
195.587 - 195.821	LCO/0.80m	SBIG STL-1001E	1543
199.409 - 199.599	DPV/1m	MII G2-1600	244
199.566 - 199.799	LCO/0.80m	SBIG STL-1001E	1078
200.287 - 200.440	DPV/1m	MII G2-1600	196
200.303 - 200.408	Trt/0.25m	ALCCD 5.2 (QHY6)	263
200.570 - 200.682	LCO/0.80m	SBIG STL-1001E	520
201.423 - 201.627	DPV/1m	MII G2-1600	263
201.501 - 201.572	Trt/0.25m	ALCCD 5.2 (QHY6)	135
202.048 - 202.322	Ioh/0.25m	SBIG ST-9XE	440
202.077 - 202.211	Kis/0.25m	APOGEE F47	263
202.293 - 202.408	Trt/0.25m	ALCCD 5.2 (QHY6)	544
202.388 - 202.511	Van/0.40m	SBIG ST-10XME	89
202.401 - 202.610	DPV/1m	MII G2-1600	254
202.935 - 202.999	Kis/0.25m	APOGEE F47	117
203.000 - 203.209	Kis/0.25m	APOGEE F47	480
203.003 - 203.290	Ioh/0.25m	SBIG ST-9XE	455
203.227 - 203.534	CrAO/0.38m	APOGEE E47	436
203.976 - 203.999	Ioh/0.25m	SBIG ST-9XE	39
204.000 - 204.030	Ioh/0.25m	SBIG ST-9XE	49
204.037 - 204.240	Kis/0.25m	APOGEE E47	468
204.937 - 204.999	Ioh/0.25m	SBIG ST-9XE	80
205.000 - 205.031	Ioh/0.25m	SBIG ST-9XE	51
206.024 - 206.233	Kis/0.25m	APOGEE E47	484
212.227 - 212.453	CrAO/0.38m	APOGEE E47	160
213.224 - 213.547	CrAO/0.38m	APOGEE E47	216
215.311 - 215.584	CrAO/0.38m	APOGEE E47	193
216.238 - 216.503	CrAO/0.38m	APOGEE E47	188
217.284 - 217.445	CrAO/0.38m	APOGEE E47	114
219.229 - 219.338	CrAO/2.6m	APOGEE E47	733
220.247 - 220.379	CrAO/2.6m	APOGEE E47	724
221.288 - 221.425	CrAO/1.25m	ProLine PL23042	847
222.279 - 222.377	CrAO/1.25m	ProLine PL23042	250
223.263 - 223.390	CrAO/1.25m	ProLine PL23042	86
224.270 - 224.387	CrAO/1.25m	ProLine PL23042	293
226.297 - 226.446	CrAO/1.25m	ProLine PL23042	71
228.303 - 228.310	CrAO/1.25m	ProLine PL23042	19
229.262 - 229.380	CrAO/1.25m	ProLine PL23042	272
230.264 - 230.392	CrAO/1.25m	ProLine PL23042	89
230.395 - 230.539	Terskol/0.6m	SBIG STL-1001	296
231.249 - 231.478	Terskol/0.6m	SBIG STL-1001	195
231.257 - 231.390	CrAO/1.25m	ProLine PL23042	179
232.362 - 232.484	CrAO/1.25m	ProLine PL23042	165
233.296 - 233.420	Terskol/0.6m	SBIG STL-1001	269
233.309 - 233.461	CrAO/1.25m	ProLine PL23042	72
234.290 - 234.373	CrAO/1.25m	ProLine PL23042	35
235.363 - 235.465	CrAO/1.25m	ProLine PL23042	138
236.356 - 236.378	CrAO/1.25m	ProLine PL23042	31
237.338 - 237.353	CrAO/1.25m	ProLine PL23042	41
238.288 - 238.308	CrAO/1.25m	ProLine PL23042	45
239.270 - 239.397	CrAO/1.25m	ProLine PL23042	90
239.291 - 239.401	Lisnyky/0.35m	SBIG ST-8XMEI	88
240.338 - 240.340	Lisnyky/0.7m	ProLine PL4710	6

Table 1.: Journal of observations (continued).

HJD 2458000+ (start - end)	Observatory/telescope	CCD	N
240.346 - 240.352	Terskol/0.6m	SBIG STL-1001	222
241.311 - 241.314	Lisnyky/0.7m	ProLine PL4710	5
242.282 - 242.412	CrAO/0.38m	APOGEE E47	63
242.324 - 242.382	Lisnyky/0.7m	ProLine PL4710	166
243.290 - 243.428	CrAO/0.38m	APOGEE E47	66
243.307 - 243.311	Lisnyky/0.7m	ProLine PL4710	5
244.414 - 244.506	Mayaky/0.8m	MicroLine 9000	104
245.251 - 245.525	CrAO/0.38m	APOGEE E47	127
249.315 - 249.507	Lisnyky/0.35m	SBIG ST-8XMEI	179
251.285 - 251.343	CrAO/1.25m	ProLine PL23042	24
252.289 - 252.359	CrAO/1.25m	ProLine PL23042	34
253.413 - 253.487	Mayaky/0.8m	MicroLine 9000	72
254.295 - 254.400	CrAO/1.25m	ProLine PL23042	49
259.331 - 259.380	CrAO/1.25m	ProLine PL23042	24
260.278 - 260.452	CrAO/2.6m	APOGEE E47	259
261.278 - 261.310	CrAO/2.6m	APOGEE E47	43
278.288 - 278.377	CrAO/2.6m	APOGEE E47	121
279.282 - 279.359	CrAO/2.6m	APOGEE E47	107
287.641 - 287.731	McDonald/2.1m	ProEM	1560

Description of columns:

HJD 2458000+ (start-end): beginning and end of an observational run.

Observatory/telescope: LCO - C.Littlefield, DPV - P.Dubovsky, Trt - T.Tordai, Ioh - H.Itoh, Kis - S.Kiyota, Van - T.Vanmunster; CrAO - Crimean Astrophys. Obs., Lisnyky - Lisnyky Obs., Terskol - Terskol Obs., Mayaky - Mayaki Obs., McDonald - Picture Rocks Obs.

CCD: CCD camera type. N: number of observations.

3. Superoutburst and superhumps

The overall light curve of ASASSN-18fk during the superoutburst is presented in Fig. 1. It includes the main outburst, six rebrightenings and the ∼50-d decline to the near-quiescent state. Taking into account the ASASSN data, one could conclude that the superoutburst amplitude was about 7^m and the main outburst lasted for $\sim$ 15 d. The amplitude of rebrightenings was $\sim 3^m$. It seems that $\sim$ 100 d after the start of the outburst, ASASSN-18fk reached its quiescence, or at least appeared close to it.

In the course of the main outburst, rebrightenings and superoutburst decline, the superhumps have been observed. The early superhumps, having a two-humped profile, were detected only for JD 2458195 with a period of 0.057-0.060 d. A further gap in the observations did not allow us to estimate the duration of this stage. Using both the periodogram analysis (Pelt, 1992) and O-C method for the superhump maxima, we identified a stage of growing superhumps A, with a period of 0.06075(2) d and a stage of fully developed superhumps B, with a near-constant mean period of 0.05940(1) d. The stage A lasted for at least about 20 cycles, while stage B – about 60 cycles (see Fig. 2).

The lack of data at the stage of early superhumps did not ensure sufficient accuracy in estimating the period that could be considered as the orbital one, and, hence, in

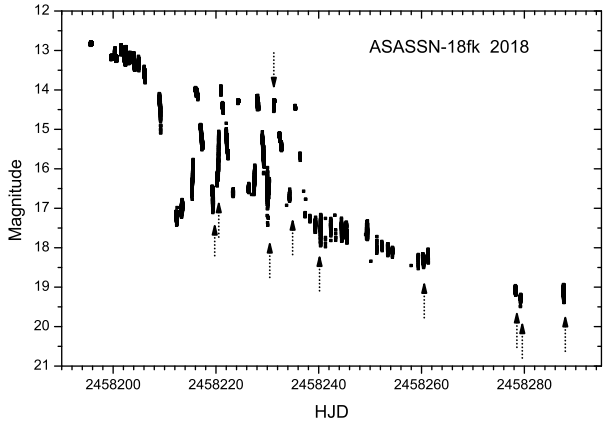

Figure 1. The overall light curve. The dates when the 0.015-d period was detected are shown by arrows.

defining the binary mass ratio, using the method proposed by Kato & Osaki (2013). During the stages of rebrightenings and superoutburst decline, the period of superhumps was 0.059586(7) d and 0.059521(4) d, respectively, that is 0.3% - 0.2% larger than the period during stage B. We suggest that this period probably could be a period of late superhumps similar to what was observed in three WZ Sge-like stars GW Lib, V455 And and WZ Sge (Kato et al., 2008). No orbital periodicity was detected after the main outburst termination.

Taking into account the outburst features described, ASASSN-18fk could be defined as a WZ Sge-type dwarf nova with multiple rebrightenings – type B outburst according to the classification given by Kato (2015).

4. Short-periodic variations

We found that additionally to the 0.06-d superhumps the nights of the best quality displayed a short-term 22-min brightness variability at different stages of the superoutburst – during rebrightenings and superoutburst decline. This modulation was not seen during the main outburst.

We considered a short-term periodicity for these stages separately. We constructed the periodograms for these selected data using the ISDA package (Pelt, 1992) after removing a superhump wave and a trend corresponding to the superoutburst profile. The original light curves for these nights and periodograms for the detrended data are shown in Fig. 3, and in Fig. 4, for the outburst decline stage. All the periodograms contain the strongest peak around 0.015 d (22 min) with an ecxeption of the first night where the 0.015-d period has the second rating. Contrary to the 0.015-d period that was detected at the rebrightening stage, these data contain a signal at the first harmonic of the 0.015-d period which became stronger as ASASSN-18fk approached the quiescence.

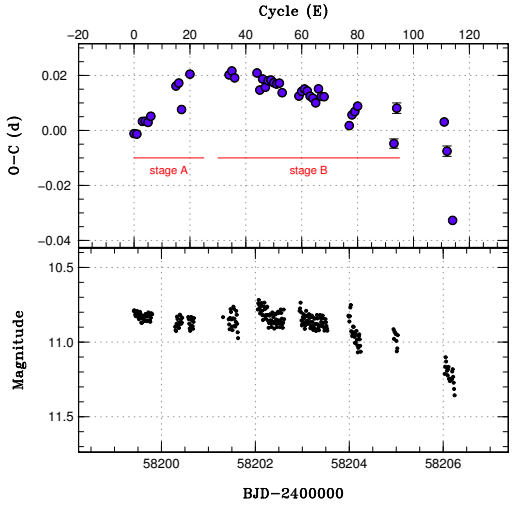

Figure 2. Evolution of superhumps. Upper panel: O-C for the superhump maxima. Stages A and B are marked. Lower panel: a part of the main outburst.

We assume that these short-periodic variations may be related to the spin period of the WD. Therefore, ASASSN-18fk could be classified as an intermediate polar (IP). Another evidence in favor of the IP is a modulation around $\sim 50 d^{-1}$ (for JD=2458195 and JD=2458199) and at $\sim 84 d^{-1}$ (for JD=2458219 and JD=2458260) that coincides with beat frequencies $\omega - \Omega$ and $\omega + \Omega$ between 0.06-d and 0.015-d periods (see Fig.5, Fig.3 and Fig.4), where ω and Ω are spin and orbital frequencies, respectively. The possibility of existence of the spin-orbital sidebands of $\omega \pm \Omega$ for IPs was predicted earlier by Warner (1986) and Wynn & King (1992). Note that although a precise orbital frequency is unknown, we could roughly admit it to be close to the 0.06-d superhump period.

5. The place of ASASSN-18fk among outbursting IPs

Due to our preliminary classification, several questions arise concerning the period coherence, its profile, change of amplitude in the range from rebrightenings to the late decline and place in a space of orbital – spin periods among outbursting IPs.

5.1. Is the 0.015-d periodicity coherent throughout the main outburst, rebrightenings and outburst decline?

Fig. 6 shows the examples of the phase light curves folded on the 0.015-d period for the data between rebrightenings, at the top of the rebrightening and close to the quiescent state.

It is seen that the 0.015-d modulation was highly coherent during the outburst decline, but it was not coherent during the stage of rebrightenings. The magnetosphere

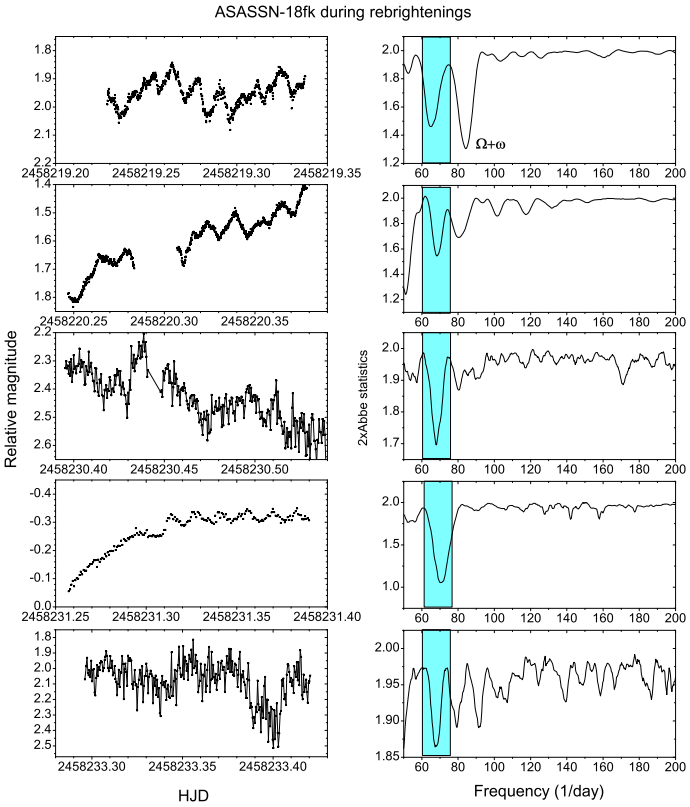

Figure 3. Left: examples of original nightly light curves for the rebrightening stage displaying the 0.015-d period. Right: corresponding periodograms. The region around the 0.015-d period is marked by the blue strip.

radius of the white dwarf varied on a scale of days during rebrightenings and, as a whole, it was smaller than during the late stage of the outburst decline, when the magnetospere was rather "quiet". Obviously, it will produce both different accretion geometry and visibility of accretion regions between these two stages. It is known that another IP, DO Dra, displayed an unstable profile of the spin period and a significant shift of the peak at the spin frequency in periodograms for some nights (Szkody et al., 2002); (Andronov et al., 2008).

5.2. Is a difference between spin profiles at high and low brightness stages common for the IPs?

As shown in Section 4, ASASSN-18fk displayed a one-humped spin profile during rebrightenings and a two-humped one during the outburst decline. Most of the known outbursting IPs exhibit the same behavior. One explanation of this phenomenon was

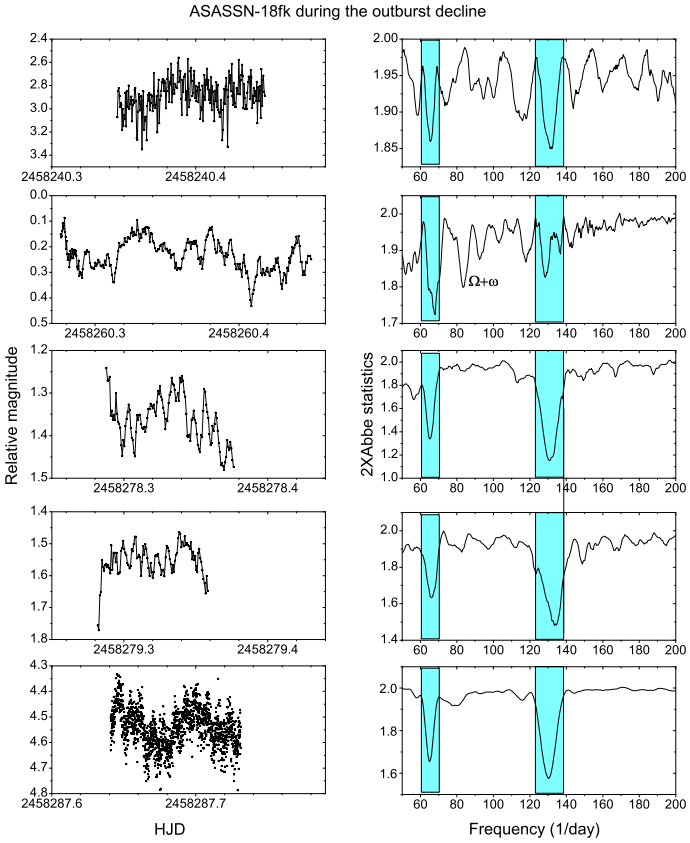

Figure 4. Left: examples of original nightly light curves for the superoutburst decline stage displaying the 0.015-d period. Right: corresponding periodograms.The regions around the 0.015-d period and its first harmonic are marked by the blue strip.

given for XY Ari by Hellier et al. (1997): humps on the spin light curve are associated with two accretion regions on a white dwarf. In quiescence, the magnetosphere radius is rather large and two zones are visible. In outburst, the magnetosphere is reduced by a higher accretion rate and the accretion disk obscures one of the poles. However, as noted by Hellier (2001), "Currently, we do not have enough observational clues to determine why some systems show double-peaked pulses while others are single peaked".

5.3. What is an amplitude of the spin pulse at different stages of the superoutburst?

The mean amplitude of the 0.015-d period was about $0^m.04$ at the stage of rebrightenings and $0^m.09$ during the gradual decline stage. Converting magnitudes into rel-

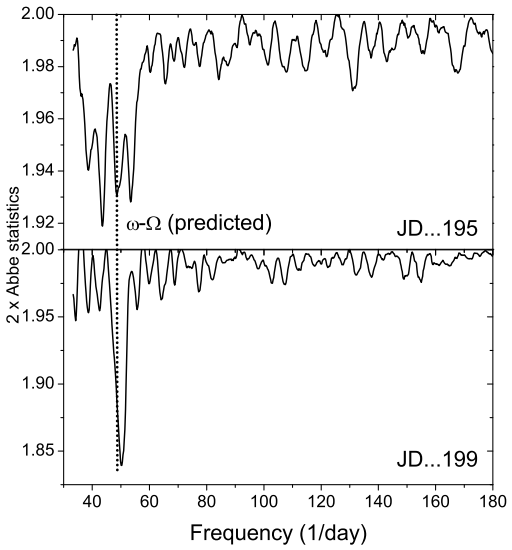

Figure 5. Periodograms for the data during two nights of observations: JD 2458195 (above) and JD 2458199 (below). The dotted line indicates a position of the side-band $\omega - \Omega$ frequency. The last three numbers of JD are given for the date of observations.

ative intensities, we found a dependence of the amplitude of the mean spin pulse of ASASSN-18fk on the mean brightness (see Fig. 7). At the top of the rebrightening, the spin amplitude was three times larger than those between rebrightenings and ∼50 times larger than those at the end of the outburst decline. The tendency of a growing amplitude with brightness is not common for all outbursting IPs. Thus, there is no significant difference in the spin amplitudes for outbursts and quiescence for DO Dra, but there is a similar dependence for XY Ari (Hellier et al., 1997).

5.4. What is a position of ASASSN-18fk in the P_{orb} - P_{spin} diagram?

We used the available data (Woudt et al., 2012) and our estimate for ASASSN-18fk to plot a dependence of the spin period on the orbital one for all IPs below the period gap. Taking into account that the expected orbital period for ASASSN-18fk is slightly lower than the superhump period, we could use the mean superhump period value as an estimate of the orbital one. In this case the spin period is ∼3.8 times smaller than the orbital one, that is close to the values of the known IPs below the period gap (Woudt et al., 2012). The position of ASASSn-18fk among these IPs is shown in Fig. 8. While IPs above the period gap are on or below the line of $P_{spin} = 0.1P_{orb}$ (Hellier, 2001), IPs with the shortest orbital period (excepting EX Hya) are concentrated within a strip on either side of this line. ASASSN-18fk is situated well within this strip.

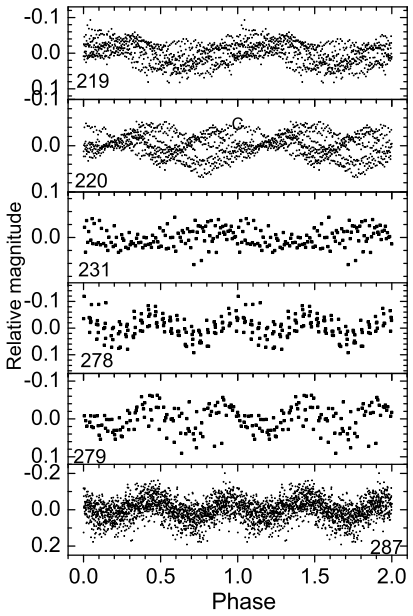

Figure 6. The detrended data folded on the 0.0153492-d period with zero-epoch HJD=2458219.22859. The last three numbers of JD are given for the date of observations. The light curves from the top to bottom correspond to the observations between the first and second rebrightening (JD ...219), during the rise to the second rebrightening (JD ...220), during the top of the fifth rebrightening (JD ...231) and during the superoutburst decline (JD ...278, ...279 and ...287).

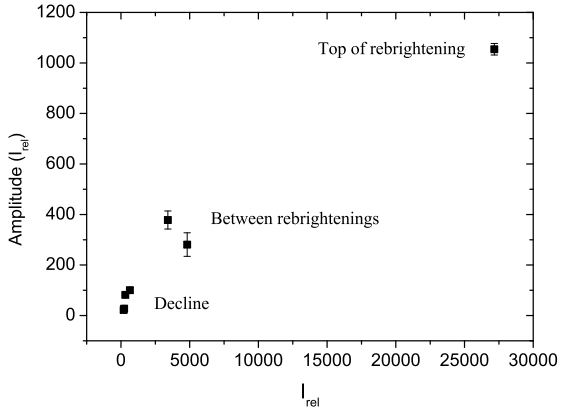

Figure 7. Dependence of the amplitude of the 0.015-d modulation expressed in the relative intensity (I_{rel}) on the mean relative intensity from the decline to the top of rebrightening ($I_{rel} = 10^{10} \times 10^{-0.4m}$).

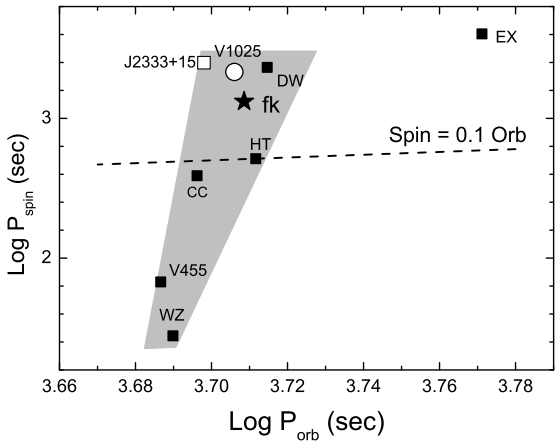

Figure 8. Dependence between spin and orbital periods for the IPs below the period gap. Abbreviations mean: EX = EX Hya; J2333+15 = SDSS J2333+15; V1025 = V1025 Cen; DW = DW Cnc; HT = HT Cam, V455 = V455 And; CC = CC Scl; fk = ASASSN-18fk. SDSS J2333+15 with no information on possible outburst and V1025 Cen are marked by the open square and circle, respectively. The rest are outbursting IPs. ASASSN-18fk is marked by a star symbol. The dashed line corresponds to the $P_{spin} = 0.1P_{orb}$ relation. Gray area indicates location of IPs below the period gap (with an exception of EX Hya).

6. Conclusion

Our main findings for ASASSN-18fk are as follows:

1) ASASSN-18fk is a WZ Sge-type dwarf nova with six rebrightenings and a superhump period of 0.06-d; 2)the one-humped 22-min signal was detected during the rebrightening stage and the two-humped one – during the outburst decline, which is assumed to be the spin period of the white dwarf; 3) spin-orbital sideband periods during the main outburst.

Thus ASASSN-18fk is a first IP among the rare subclass of the superhumping IPs for which evidence of the spin period (the direct spin signal or the spin-orbital sideband signal) was tracked through the main outburst, rebrightenings and near-quiescent state.

References

Andronov, I. L., Chinarova, L. L., Han, W., Kim, Y., & Yoon, J. N., Multiple timescales in cataclysmic binaries. The low-field magnetic dwarf nova DO Draconis. 2008, *Astron. Astrophys.*, **486**, 855, DOI: 10.1051/0004-6361:20079056

Hellier, C. 2001, *Cataclysmic Variable Stars*

Hellier, C., Mukai, K., & Beardmore, A. P., An outburst of the magnetic cataclysmic variable XY ARIETIS observed with RXTE. 1997, *Mon. Not. R. Astron. Soc.*, **292**, 397, DOI: 10.1093/mnras/292.2.397

Kato, T., On the Origin of Early Superhumps in WZ Sge-Type Stars. 2002, *Publications of the Astronomical Society of Japan*, **54**, L11, DOI: 10.1093/pasj/54.2.L11

Kato, T., WZ Sge-type dwarf novae. 2015, *Publications of the Astronomical Society of Japan*, **67**, 108, DOI: 10.1093/pasj/psv077

Kato, T., Imada, A., Uemura, M., et al., Survey of Period Variations of Superhumps in SU UMa-Type Dwarf Novae. 2009, *Publications of the Astronomical Society of Japan*, **61**, S395, DOI: 10.1093/pasj/61.sp2.S395

Kato, T., Maehara, H., & Monard, B., Late Superhumps in WZ Sge-Type Dwarf Novae. 2008, *Publications of the Astronomical Society of Japan*, **60**, L23, DOI: 10.1093/pasj/60.4.L23

Kato, T. & Osaki, Y., New Method of Estimating Binary's Mass Ratios by Using Superhumps. 2013, *Publications of the Astronomical Society of Japan*, **65**, 115, DOI: 10.1093/pasj/65.6.115

Knigge, C., The donor stars of cataclysmic variables. 2006, *Mon. Not. R. Astron. Soc.*, **373**, 484, DOI: 10.1111/j.1365-2966.2006.11096.x

Osaki, Y., A model for the superoutburst phenomenon of SU Ursae MAjoris stars. 1989, *Publications of the Astronomical Society of Japan*, **41**, 1005

Osaki, Y., Dwarf-Nova Outbursts. 1996, *Publications of the Astronomical Society of the Pacific*, **108**, 39, DOI: 10.1086/133689

Pavlenko, E. P., Mason, P. A., Sosnovskij, A. A., et al., Asynchronous polar V1500 Cyg: orbital, spin, and beat periods. 2018, *Mon. Not. R. Astron. Soc.*, **479**, 341, DOI: 10.1093/mnras/sty1494

Pelt, J. 1992, *Irregularly Spaced Data Analysis User Manual*

Ritter, H. & Kolb, U., Catalogue of cataclysmic binaries, low-mass X-ray binaries and related objects (Seventh edition). 2003, *Astron. Astrophys.*, **404**, 301, DOI: 10.1051/0004-6361:20030330

Szkody, P., Nishikida, K., Erb, D., et al., X-Ray/Optical Studies of Two Outbursts of the Intermediate Polar YY (DO) Draconis. 2002, *Astron. J.*, **123**, 413, DOI: 10.1086/324733

Warner, B., Multiple optical orbital sidebands in intermediate polars. 1986, *Mon. Not. R. Astron. Soc.*, **219**, 347, DOI: 10.1093/mnras/219.2.347

Warner, B., Cataclysmic variable stars. 1995, *Cambridge Astrophysics Series*, **28**

Woudt, P. A., Warner, B., Gulbis, A., et al., CC Sculptoris: a superhumping intermediate polar. 2012, *Mon. Not. R. Astron. Soc.*, **427**, 1004, DOI: 10.1111/j.1365-2966.2012.22010.x

Wynn, G. A. & King, A. R., Theoretical X-ray power spectra of intermediate polars. 1992, *Mon. Not. R. Astron. Soc.*, **255**, 83, DOI: 10.1093/mnras/255.1.83

Contrib. Astron. Obs. Skalnaté Pleso **49**, 217 – 227, (2019)

Eruptive stars monitoring and the ARAS database

F. Teyssier

Observatoire Rouen Sud, France
(E-mail: francoismathieu.teyssier@gmail.com)

Received: October 31, 2018; Accepted: December 19, 2018

Abstract. Spectroscopic monitoring of eruptive stars (e.g. symbiotic binaries, classical novae) by amateurs around the world, in both the northern and southern hemispheres, is a fundamental activity of the ARAS (Astronomical Ring for Amateur Spectroscopy) initiative. The group of volunteers demonstrates what can be accomplished with a network of independent, very small telescopes (from 20 to 60 cm), furnished with spectrographs of different resolution, from ∼500 to ∼15000, and covering the range from 3600 to nearly 8000 Å. Acquisition, reduction and analysis of the spectra will be described. The observing program concentrates on bright symbiotic stars (57, to date) and novae (35, to date). The main features of the ARAS activity are rapid response to alerts, long term monitoring and high cadence. A part of the program involves collaborations based on requests from professional teams (e.g. CH Cyg, AG Dra, R Aqr, SU Lyn, V339 Del) for long term monitoring or specific events. Some examples of the evolution of basic observational parameters during outbursts and/or as a function of orbital phase (e.g. radial velocities, equivalent widths or line profiles) are presented. The spectra are gathered in the open access Eruptive Stars Database that has been used for several publications by professional teams.

Key words: novae – symbiotic stars – spectroscopic database

1. Introduction

Eruptive stars spectroscopic monitoring is a part of ARAS (Astronomical Ring for Access to Spectroscopy), an initiative dedicated to promote Amateur spectroscopy, originally intended for Be stars: BESS data base (Neiner et al., 2011).

The program was initiated in 2009 and developed from the 2013 Pisa meeting (multi-wavelength observation of bright novae on the initiative of Steve Shore, Università di Pisa): the aim of the project was the monitoring in all wavelengths of the next bright nova. Nova Del 2013 exploded a few weeks later (August, 14th), was bright (V magnitude at maximum = 4.3) and well placed in the evening sky. Since then, the monitoring of symbiotic stars, novae, dwarf novae and related objects has been coordinated. The program includes: 1. Long term monitoring of more than 50 bright symbiotic stars (orbital variations, outbursts and high states), monitoring of novae outbursts (35 to date), spectroscopic identification of new stars. 2. Collaboration with professional teams either by the

use of the database (e.g. AG Peg outburst, T CrB active state, EG And) or on specific requests (e.g. CH Cyg, BF Cyg, AG Dra, R Aqr, SU Lyn, V694 Mon).

2. Setups and data reduction

The telescopes are mostly reflectors of various types, often Schmidt-Cassegrain, but also Newtonian, Dall-Kirkham, Cassegrain etc. The diameters range usually from 20 to 40 cm, exceptionally to 50 or 60 cm. Various spectroscopes are used. Most of them are produced by the Shelyak Company. Alpy600 is a low resolution slit spectroscope with a resolution of 600 which covers 3800-7500 Å range, particularly appropriate to fainter objects. LISA is a low resolution spectroscope (R = 1000) used by many regular observers. Lhires III has been designed in the context of the Be stars program. It is a slit spectroscope which comes with various gratings (150 to 2400 l/mm) and produces spectra with resolutions ranging from 700 to 15000. eShel is a fibre Echelle spectroscope working in the range 4000 - 7500 Å at a resolution of 11000. Other commercial spectroscopes are used (e.g. DADOS, equipped with two gratings 200 and 900 l/mm, LX-200, similar design to the Lhires III). Last, but not least a few observers have produced their own spectroscopes (slit or Echelle) with excellent results, e.g. Tim Lester (CA) and Joan Guarro (SP).

2.1. Acquisition and reduction

The very small diameter of the telescopes requires excellent tuning of all the equipment, notably focusing and autoguiding, to obtain valuable results with high enough SNR. The spectra, dark subtracted and flat divided, are reduced in most cases by the ISIS software, written by C. Buil [1]. The atmospheric and instrumental response is computed from a reference early A-type star. Figure 1 shows two spectra of AG Peg independently acquired/processed by J. Montier (FR) and J.P. Masviel (FR) using Alpy600 on 2015-09-07.071 and 09.065 UT. This is our target level. However, the atmospheric response remains a difficult issue. Each observing campaign is a school for new observers and the occasion for experienced observers to improve their technique through discussions on our forums (see e.g. ARAS Forum [2]).

2.2. How faint?

Most of the targets from the symbiotic stars program range from mag. V = 7 to 12 and are monitored at resolutions from 600 to 15000 with sufficient exposure time to obtain a SNR of about 100 in the red part of the spectrum. The exposure time can reach 3 hours for that purpose. Due to the spectral energy distribution

[1] http://www.astrosurf.com/buil/isis-software.html
[2] http://spectro-aras.com/forum/index.php

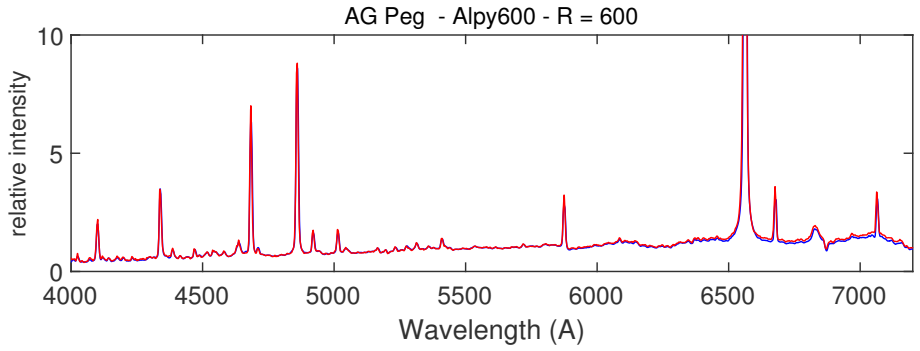

Figure 1. AG Peg - Comparison of two low resolution spectra

of most of the targets, the SNR is 10 - 20 in the blue part of the spectrum. Using a LISA or Alpy600 spectroscopes, spectra of targets with V = 14 can be obtained with a reasonable exposure duration.

3. Symbiotic star monitoring

Symbiotic stars are wide interacting binary systems comprising a cool giant as the donor star and a hot compact star, mostly a white dwarf (WD), accreting from the giant's wind. Their orbital periods run from hundreds of days (S-type systems containing a normal giant) to a few times 10 - 100 years (D-type systems containing a Mira variable). The accreting WD represents a strong source of extreme ultraviolet radiation ($T_h > 10^5$ K, $L_h \approx 10^1$ to 10^4 $L_\odot$) in the binary that ionises a fraction of the wind from the giant giving rise to nebular emission (Skopal et al., 2017). Symbiotic stars are considered as laboratories for many astrophysical phenomena such as winds from red giants, accretion and eruptive processes on compact objects, disks, jets, etc. A number of questions remain unsolved. Already Merrill (1958) suggested that *"persistent observations, both spectroscopic and photometric, for 5 or 10 years of the brightest symbiotics would surely help us to understand their mysterious behaviour and might develop ideas of considerable general interest"*.

In the following section, we present selected results obtained from our spectra.

3.1. Low resolution monitoring of the classical symbiotic star AX Per

AXPer is an eclipsing symbiotic binary comprising a M4.5 III giant and a luminous WD on a 680-d orbit (Fekel et al., 2000b).

David Boyd (UK) has monitored this system since 2014 with a LISA (R = 1000) simultaneously with photometry in the V band, which allows flux cali-

bration of the spectra in, e.g. erg cm^{-2} s^{-1} Å^{-1}. For example, the integrated absolute flux of the forbidden line [Fe VII] λ 6087Å is shown in Fig. 2. The flux variation is strongly different from one cycle to another, but seems to be orbitally related. The maxima are located rather around the inferior conjunction of the giant according to the ephemeris of Fekel et al. (2000a). The monitoring is ongoing, together with higher resolution spectra.

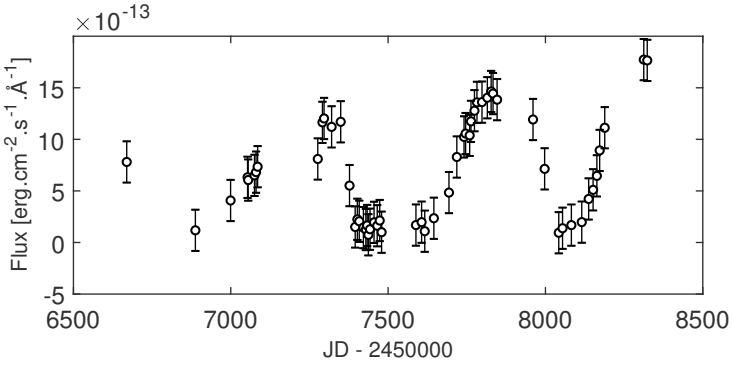

Figure 2. AX Per - [Fe VII] λ6087 Å flux

3.2. Orbital monitoring of CI Cygni

CI Cygni is a prototypical symbiotic star. It hosts a red M5.5III giant and a luminous hot component on a 853-d orbit whose nature remains controversial (e.g. Siviero et al., 2009).

36 Echelle spectra were obtained by F. Teyssier (FR), J. Guarro (SP) and T. Lester (CA) at R = 9000 to 13000 during the orbital cycle 8 according to the ephemeris of Fekel et al. (2000b). The system is in a quiescent state since its last active period 2008-2012 (e.g. Siviero et al., 2009; Teyssier, 2011). Radial velocities of the red giant have been determined by cross-correlation with the M6 III red giant 13 Lyr (using ISIS) within a range of free emission lines (6375-6545 Å). The radial velocity curve (red squares) is shown Fig. 3. The error of each individual measurement is estimated to 2 km s^{-1}. The second curve (blue circles) represents the radial velocity (RV) of the centre of the He II λ 4686 Å emission line. It is located at the anti-phase to the RVs of the giant, and thus can reflect the orbital motion of the hot component.

The orbital elements for the red giant have been computed using Spectroscopic Binary Solver, SBS hereafter (Johnson, 2004). The results shown in Table 1 are in good agreement with published values (Kenyon et al., 1991; Fekel et al., 2000b). The solution computed by SBS proposes an eccentricity of 0.126, at the

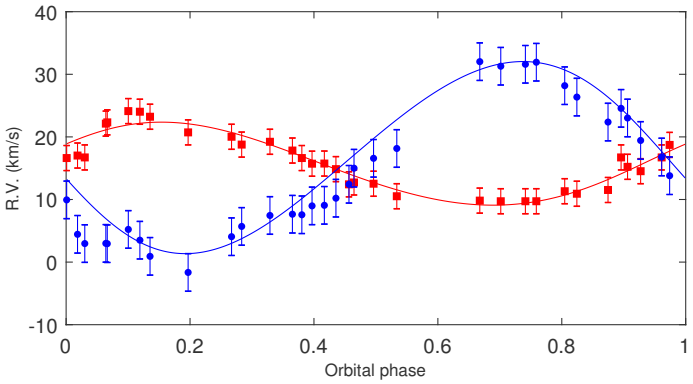

Figure 3. CI Cyg - Radial velocities of the red giant (red squares) and the center of the He II λ4686 Å emission line (blue dots). The orbital phase was calculated according to our solution.

limit of confidence. Similar eccentricities found in the two cited studies and our data reinforced the solution with an eccentric orbit.

Table 1. CI Cygni Orbital elements.

		Kenyon et al. 1991	Fekel et al. 2000b	ARAS this paper
P	(days)	855.25	853.8± 2.9	853.8 [1]
T	(HJD)		2450426.4 ± 59.6	2456512.9 ± 56.8
γ	(km/s)	18.5 ± 0.4	14.96 ± 0.23	15.34 ± 0.24
K1	(km/s)	7.0 ± 0.5	6.70 ± 0.23	6.63 ± 0.37
K2	(km/s)			15.3 ± 0.5
e		0.0	0.109 ± 0.048	0.126 ± 0.05

[1] adopted from Fekel et al., 2000b

As an example, the variation of the Hβ profile at the beginning of the orbital cycle, from phase 0.0 to 0.15 is shown Fig. 4. The classical central absorption seen in many Balmer lines of symbiotic stars is quickly filled in by an emission component. The high cadence coverage through the orbital cycle allows us to detect unexpected events and their precise dating will help to constrain a model.

3.3. CH Cyg

Although as a class, the symbiotic stars are enigmatic, CH Cyg is a particularly intriguing star. It was adopted as a standard star of the spectral class M6 III in the Morgan-Keenan classification until 1963 when a strong blue continuum and

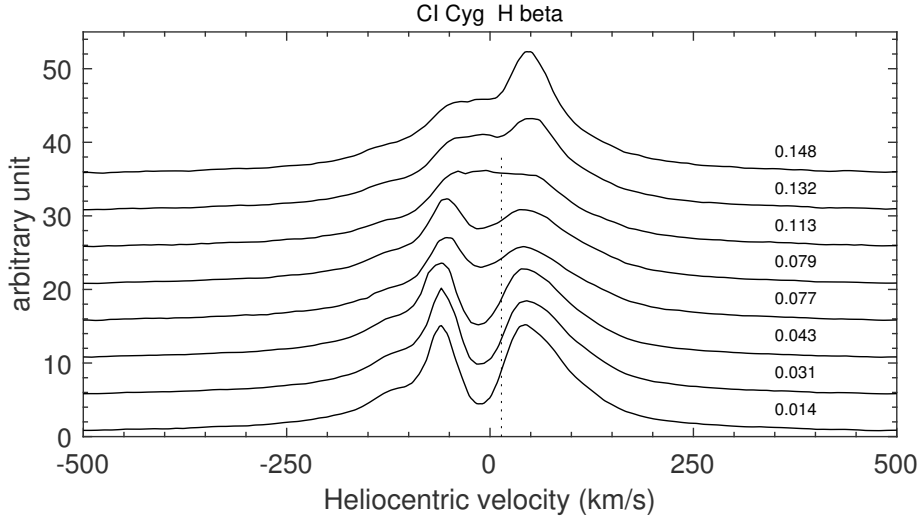

Figure 4. CI Cyg - Hβ profile from phase 0.01 to 0.14 during JD 2457268 to JD 2457383.

HI emission lines appeared in the star spectrum, thus revealing its symbiotic nature. The low luminosity of the hot component is attributed to accretion through a disk, with evidence for strong jets (velocity up to 3000 km s^{-1}). 700 spectra are gathered in the ARAS database, with daily coverage during certain periods. Depending of its activity CH Cyg shows very complex variations. One of them is photometric and spectroscopic flickering on a time scale of minutes. This is illustrated in Fig. 5 with a 2.6 hour time series acquired by P. Somogyi (HU) with a 25 cm telescope equipped with a Lhires III 2400 l/mm (R = 15000). Each spectrum has a duration of 300 sec. and a SNR $\sim$ 30. The left view shows 31 spectra of the Hα line and strong variation of the blue part of the line. The right view represents a statistical study of the variation: the red line is the mean spectrum; the blue line is the variance, multiplied by a factor of 10 and shifted (+1) for clarity. The blue dashed line is the variance of the continuum (3 sigma), computed on 50 points. The flickering is established at a significant level of confidence in the range -20 to -150 km s^{-1}. The radial velocity of the system (-60 km s^{-1}) has been subtracted.

3.4. Publications and collaborations

The database has been used for several publications. The outburst of the symbiotic nova AG Peg in 2015 was studied by Skopal et al. (2017) and Ramsay et al. (2016). The study of the recurrent symbiotic nova T CrB in high state by Iłkiewicz et al. (2016) is widely based on ARAS spectra. On the request of

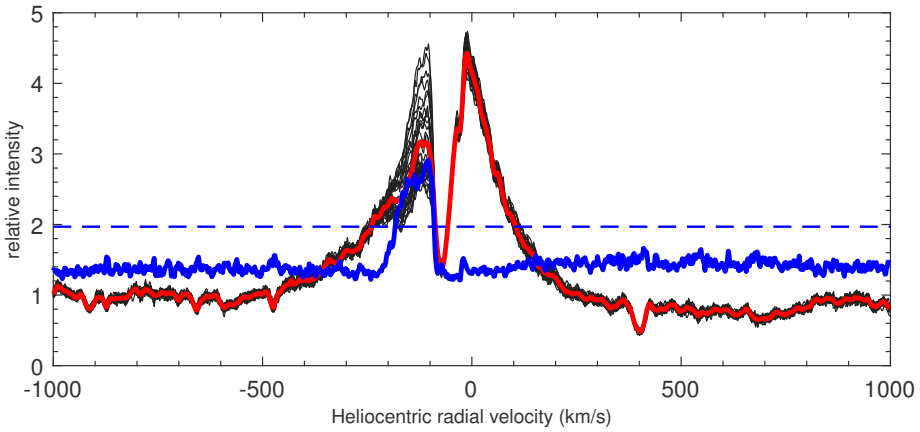

Figure 5. CH Cyg - Hα line rapid variability (see Sect. 3.3).

J. Merc and R. Gális, the activity of the yellow symbiotic AG Dra has been monitored since 2016 with a higher cadence during outburst activity (e.g. Merc et al., 2017; Gális et al., 2018; Merc et al., 2018). The ARAS group also provided spectra of R Aqr in support of HST observations by M. Karovska in 2017. The most recent campaign at the request of A. Lucy and J. Sokoloski sets out to detect new symbiotics among a selected list of faint red giant stars. The interest in monitoring symbiotic stars by the ARAS group was highlighted by A. Skopal during this conference: *Studying symbiotic stars and classical nova outbursts with small telescopes* (this proceedings).

4. Novae observations

Classical novae are thermonuclear explosions that take place in the envelopes of accreting white dwarfs in binary systems. The material piles up under degenerate conditions, driving a thermonuclear runaway (e.g. Casanova et al., 2016).

To date, 35 events have been observed by the ARAS group, with a total number of more than 2000 spectra. In the next sections, we present selected results of three peculiar events.

4.1. Nova Del 2013

The classical Nova Del 2013 (V339 Del) outburst on 2013 August 14th and peaked at mag V = 4.4 on August 16.47 (e.g. Chochol et al., 2014). It has been intensively monitored by the group at resolutions from 600 to 15000. More than 1200 spectra obtained by observers worldwide are stored in the database; for one day, August 15th, 52 spectra were acquired. See e.g. Shore et al. (2013) in-

cluding 41 ARAS observers as co-authors. The spectra have been used in several publications (e.g. Shore et al., 2016; Skopal et al., 2014). Especially, among the various studies of this event, the first resolved images of the expanding fireball have been obtained by the CHARA Array (Schaefer et al., 2014). Six spectra obtained by Olivier Garde have been used to calibrate the observations. Usefulness of our spectra was demonstrated by Schaefer et al. (2014): *"From an analysis of spectra downloaded from the archive of the Astronomical Ring for Access to Spectroscopy, we estimated the outflow speed near the continuum-forming layer to be* $V_{\rm ejection} = 613 \pm 79\, km\, s^{-1}$ ".

4.2. The oscillations of Nova Sct 2017 near maximum

Nova Sct 2017 belongs to the small class of novae showing strong oscillations near maximum instead of the classical, more or less, smooth decrease of luminosity during the first decline. The nova has been monitored at high cadence during all the rebrightenings and fadings. See the contribution of D. Chochol in this proceedings (*Optical photometry and spectroscopy of V612 Sct: slow classical nova with rebrightenings*).

4.3. The narrow lines of Nova Per 2018 = V392 Per

Nova Per 2018 is an extraordinary nova event in an already known dwarf nova V392 Per. Moreover, the evolution of emission lines (Balmer, He I) showed the rare development of narrow lines superposed on a broad component with terminal velocity of $\sim \pm 4000\,\mathrm{km\,s^{-1}}$ or even more. Despite the difficult position in the evening sky of the target, the team obtained 61 spectra of the nova at resolution from 600 to 15000.

5. Identification of "New Stars"

The responsibility and worldwide location of the group allow to obtain identification and confirmation spectra for a number of objects following alerts, with results published in Astronomer's Telegram, CBET, or on the Transient Objects Confirmation Page. As a recent example, Paolo Berardi (IT) obtained the first spectrum of the transient TCP J19544251+1722281 detected by Robert Fidrich (HAA/VSS) on 2018-08-8.938. The spectrum acquired with a Lhires III mounted on a 23 cm telescope is typical of a symbiotic star in outburst (Belczyński et al., 2000), with high ionization lines (e.g. He II) on the red continuum of a red giant. The identification is reported by Munari et al. (2018).

6. Aras Database for Eruptive Stars "asdb"

Spectra are gathered in the ARAS Eruptive stars database [3] and are publicly available. The spectra follow the BESS format specifications, i.e., they must be simple fits spectra with a header including at least a few mandatory keywords (Neiner et al., 2011). For each target, the web page shows the observations with the main information (date, time, observer, observatory, spectral range, duration). The name of each spectrum is built in the form: asdb_x_aaaammdd_hhh.fit', with asdb as reference for the base, x = name of the target, aaaa = year, mm = month, dd = day, hhh = time expressed in fraction of a day. Observer is expressed as a letter code, observatory as a 3 letter code followed by the country in 2 letters. There is a first level validation check prior to adding spectra to this table: identification, wavelength calibration, atmospheric response. Users should verify the quality of the spectra (possibly with the observer concerned). Use of these data in research publications is encouraged subject to the following conditions: *ARAS DataBase Eruptive Stars should be acknowledged and a link to the address of the database should be provided. * Observers contribution should be acknowledged * Observers contributing a significant amount of data or whose data are pivotal to the findings of the paper should be included as co-authors. If you use any ARAS Eruptive stars data in your research, please mention this publication in the references of your article. Any questions about the data may be directed to the author. zip files can be provided.

An Information letter [4] is published every 3 months with the main results and basic analysis. Professional teams using ARAS spectra are kindly asked for contributions to the letter as an educational involvement as most of the observers would like to understand the physics behind their observations.

Acknowledgements. The author warmly thanks Steve Shore for his continuous support, stimulation and his regular notes in the Information Letter, Augustin Skopal for his steady contribution, support and the invitation to this conference. David Boyd is thanked for correction of the English syntax of the text. All ARAS observers who contribute to this program are warmly commended for their tireless efforts.

References

Belczyński, K., Mikołajewska, J., Munari, U., Ivison, R. J., & Friedjung, M., A catalogue of symbiotic stars. 2000, *Astronomy and Astrophysics Supplement Series*, **146**, 407, DOI: 10.1051/aas:2000280

Casanova, J., José, J., García-Berro, E., & Shore, S. N., Three-dimensional simulations of turbulent convective mixing in ONe and CO classical nova explosions. 2016, *Astron. Astrophys.*, **595**, A28, DOI: 10.1051/0004-6361/201628707

[3] $http://www.astrosurf.com/aras/Aras\_DataBase/DataBase\_EruptiveStars.htm$

[4] $http://www.astrosurf.com/aras/novae/InformationLetter/InformationLetter.html$

Chochol, D., Shugarov, S., Pribulla, T., & Volkov, I., Photometry and spectroscopy of the classical nova V339 Del (Nova Del 2013) in the first month after outburst. 2014, *Contributions of the Astronomical Observatory Skalnate Pleso*, **43**, 330

Fekel, F. C., Hinkle, K. H., Joyce, R. R., & Skrutskie, M. F., Infrared Spectroscopy of Symbiotic Stars. II. Orbits for Five S-Type Systems with Two-Year Periods. 2000a, *Astron. J.*, **120**, 3255, DOI: 10.1086/316872

Fekel, F. C., Joyce, R. R., Hinkle, K. H., & Skrutskie, M. F., Infrared Spectroscopy of Symbiotic Stars. I. Orbits for Well-Known S-Type Systems. 2000b, *Astron. J.*, **119**, 1375, DOI: 10.1086/301260

Gális, R., Merc, J., Vrastak, M., et al., The fourth outburst during the present active stage of symbiotic binary AG Dra. 2018, *The Astronomer's Telegram*, **11559**, 1

Iłkiewicz, K., Mikołajewska, J., Stoyanov, K., Manousakis, A., & Miszalski, B., Active phases and flickering of a symbiotic recurrent nova T CrB. 2016, *Mon. Not. R. Astron. Soc.*, **462**, 2695, DOI: 10.1093/mnras/stw1837

Johnson, D. O., Spectroscopic Binary Solver. 2004, *Journal of Astronomical Data*, **10**, 3

Kenyon, S. J., Oliversen, N. A., Mikolajewska, J., et al., On the Nature of the Symbiotic Binary CI Cygni. 1991, *Astron. J.*, **101**, 637, DOI: 10.1086/115712

Merc, J., Gális, R., & Leedjärv, L., Recent outburst activity of the super-soft X-ray binary AG Draconis. 2017, *Contributions of the Astronomical Observatory Skalnate Pleso*, **47**, 192

Merc, J., Gális, R., & Leedjärv, L., Recent outburst activity of the symbiotic binary AG Draconis. 2018, *ArXiv e-prints*, arXiv:1806.05935

Merrill, P. W., 51. Symbiosis in Astronomy: Introductory Report. 1958, in Liege International Astrophysical Colloquia, Vol. **8**, *Liege International Astrophysical Colloquia*, 436–448

Munari, U., Dallaporta, S., Valisa, P., et al., HBHa 1704-05: a bright and newly discovered symbiotic star, currently undergoing an "hot-type" outburst. 2018, *The Astronomer's Telegram*, **11937**, 1

Neiner, C., de Batz, B., Cochard, F., et al., The Be Star Spectra (BeSS) Database. 2011, *Astron. J.*, **142**, 149, DOI: 10.1088/0004-6256/142/5/149

Ramsay, G., Sokoloski, J. L., Luna, G. J. M., & Nuñez, N. E., Swift observations of the 2015 outburst of AG Peg - from slow nova to classical symbiotic outburst. 2016, *Mon. Not. R. Astron. Soc.*, **461**, 3599, DOI: 10.1093/mnras/stw1546

Schaefer, G. H., Brummelaar, T. T., Gies, D. R., et al., The expanding fireball of Nova Delphini 2013. 2014, *Nature*, **515**, 234, DOI: 10.1038/nature13834

Shore, S. N., Cechura, J., Korcakova, D., et al., Continuing spectroscopic observations (3600-8800A) of V339 Del = Nova Del 2013 in the early nebular stage with the Nordic Optical Telescope, Ondrejov Observatory and the ARAS group. 2013, *The Astronomer's Telegram*, **5546**, 1

Shore, S. N., Mason, E., Schwarz, G. J., et al., The panchromatic spectroscopic evolution of the classical CO nova V339 Delphini (Nova Del 2013) until X-ray turnoff. 2016, *Astron. Astrophys.*, **590**, A123, DOI: 10.1051/0004-6361/201527856

Siviero, A., Munari, U., Dallaporta, S., et al., The ongoing 2008-09 outburst of CI Cyg. 2009, *Mon. Not. R. Astron. Soc.*, **399**, 2139, DOI: 10.1111/j.1365-2966.2009.15414.x

Skopal, A., Drechsel, H., Tarasova, T., et al., Early evolution of the extraordinary Nova Delphini 2013 (V339 Del). 2014, *Astron. Astrophys.*, **569**, A112, DOI: 10.1051/0004-6361/201424284

Skopal, A., Shugarov, S. Y., Sekeráš, M., et al., New outburst of the symbiotic nova AG Pegasi after 165 yr. 2017, *Astron. Astrophys.*, **604**, A48, DOI: 10.1051/0004-6361/201629593

Teyssier, F., CI Cygni 2010 Outburst and Eclipse: An Amateur Spectroscopic Survey - First Results From Low Resolution Spectra. 2011, *Journal of the American Association of Variable Star Observers (JAAVSO)*, **39**, 41

Contrib. Astron. Obs. Skalnaté Pleso **49**, 228 – 235, (2019)

Study of long-term spectroscopic variability of symbiotic stars based on observations of the ARAS Group

J. Merc[1,2], R. Gális[1] and F. Teyssier[3]

[1] *Institute of Physics, Faculty of Science, P. J. Šafárik University, Park Angelinum 9, 040 01 Košice, Slovak Republic*

[2] *Astronomical Institute, Faculty of Mathematics and Physics, Charles University, V Holešovičkách 2, 180 00 Prague, Czech Republic*

[3] *Astronomical Ring for Amateur Spectroscopy Group*

Received: November 15, 2018; Accepted: February 14, 2019

Abstract. The importance of small-telescope observations is demonstrated by investigation of long-term outburst activity of the symbiotic systems AG Dra, Z And and AG Peg based on spectroscopic measurements obtained by amateur astronomers organized in the Astronomical Ring for Amateur Spectroscopy. Preliminary results of our ongoing spectroscopic campaign focused on AG Dra are presented. The temperature of the white dwarf is studied based on behaviour of the prominent emission lines, which are well detectable even in low-resolution spectra. The activity of AG Dra is compared to that of two other symbiotic systems - Z And and AG Peg, which have shown outbursts recently. Z And is a prototype of classical symbiotic stars which manifested the outburst at the turn of the years 2017 and 2018. AG Peg is the slowest symbiotic nova with the Z And-type outburst in 2015, 165 years after its nova-like flare-up.
Key words: symbiotic stars – outbursts – spectroscopy

1. Introduction

Symbiotic stars are strongly interacting systems, in which physical mechanisms related to the mass transfer and accretion cause observable activity by manifesting increases of brightness (about 2 – 5 mag) and significant changes in their spectra. These binaries consist of a cool giant of spectral type K - M and a hot compact star, mostly a white dwarf. The mass transfer most likely takes place via the stellar wind of the cool giant, which is also the source of the dense circumbinary envelope of these systems.

Symbiotic systems are wide binaries with orbital periods of hundreds to thousands of days and their stages of activity may last from a few days to decades. Therefore, the long-term photometric as well as spectroscopic observations of these interacting systems are needed to study the physical mechanism responsible for their observed activity. Both amateur and professional astronomers utilizing small telescopes play an important role in such monitoring.

2. Selected symbiotic systems

AG Draconis is one of the best studied symbiotic systems. The cool component is a red giant of early spectral type (K0 - K4), with low metallicity and higher luminosity than that of standard class III (Smith et al., 1996). The hot component is considered to be a white dwarf sustaining a high luminosity and temperature (Mikołajewska et al., 1995). The orbital period of this binary is 551 days (Hric et al., 2014). The system undergoes characteristic symbiotic activity with alternating quiescent and active stages. The latter ones consist of several outbursts repeating at about one-year interval.

Z Andromedae is a prototype of the classical symbiotic systems, which consists of a late-type M4.5 III giant (Mürset & Schmid, 1999) accompanied by a white dwarf. The orbital period of the binary system is 758 days (Mikołajewska & Kenyon, 1996). During more than hundred years of monitoring, the system showed several active stages with changes of brightness ranging from a few tenths of magnitude to about three magnitudes (e.g. Skopal et al., 2000). The system has been in the active stage since 2000.

AG Pegasi is the slowest symbiotic nova, which showed a Z And-type outburst 165 years after its nova-like flare-up (Skopal et al., 2017). The symbiotic system consists of a M3 III giant (Schulte-Ladbeck, 1988) and a white dwarf. The orbital period was determined to be 816.5 days (Fernie, 1985). The brightness of the system began to be recorded before 1820 (although with very low cadence). Its nova-like outburst began in 1850 and maximum brightness was reached around 1885 (Boyarchuk, 1967).

3. Observational data

Astronomical Ring for Amateur Spectroscopy (ARAS) is an initiative dedicated to promotion of amateur astronomical spectroscopy and pro/am collaborations. Observations of the group[1] focus on novae (34, to date) and symbiotic binaries (54, to date). Moreover, Be stars, cataclysmic variables, supernovae and other objects are observed. The network consists of observers equipped with small telescopes (20 to 60 cm) with spectrographs of different resolution (500 to 15000), covering the range from 3500 to nearly 8000 Å. The advantages of the ARAS Group are rapid response to alerts, long-term monitoring and high cadence of observations.

In this work, we used medium resolution spectra of the selected symbiotic stars obtained by 22 individual ARAS observers. These observations were used to study the activity and overall behavior of AG Dra during the ongoing active stage (274 spectra obtained by 17 observers) and to compare the recent evolution of prominent emission lines in its spectra to that of Z And (61 spectra, 6 observers) and AG Peg (111 spectra, 15 observers).

[1] http://www.astrosurf.com/aras/Aras_DataBase/DataBase.htm

4. Analysis and results

All three studied symbiotic binaries manifested Z And-type outbursts recently. In this section, the spectroscopic behaviour of AG Dra, Z And and AG Peg during their last active stages is discussed and compared to their previous activity. Moreover, the temperature of white dwarfs in the symbiotic system is derived based on characteristics of the prominent emission lines in their spectra.

4.1. Recent outburst activity of AG Dra, Z And and AG Peg

AG Dra entered the new active stage in 2015 and since then four outbursts have been observed (upper panel of Fig. 1). After the last outburst, the brightness of AG Dra returned to values typical for its quiescent stage at the end of July 2018 (Merc et al., 2018b).

Leedjärv et al. (2016) showed that it is possible to distinguish between the *cool* and *hot* outbursts of AG Dra (see González-Riestra et al., 1999) according to the behaviour of the prominent emission lines in its optical spectra. The outbursts at the beginning of active stages of AG Dra are usually major, *cool* ones. During the *hot* outbursts, the brightness is more or less linearly correlated with equivalent widths (EWs) and other spectral characteristics of the emission lines. With respect to this behaviour, the activity of AG Dra during the ongoing active stage is very unusual. The increase of the EWs of prominent emission lines observed during all four outbursts suggests their *hot-type* character.

Z And has been active since 2000 and its recent outburst was detected at the turn of the years 2017 and 2018 (middle panel of Fig. 1). The EWs of studied emission lines in spectra of Z And showed significant decline during the recent outburst and their values are anti-correlated with its brightness changes. In the case of AG Dra, such behaviour is typical for the *cool* outbursts. The Raman-scattered O VI and [Fe VII] lines completely disappeared during this outburst. The latter reappeared at the time when O VI lines remained undetectable.

Similar behaviour of emission lines in the spectra of Z And was observed in 2006, when the star underwent the major outburst accompanied by the ejection of bipolar jets (Skopal & Pribulla, 2006). During that outburst, the He II line also practically disappeared. Despite the similarity of the outbursts in 2006 and 2018, no sign of the jet components around the Hα and Hβ lines was observed in the spectra of Z And during the recent one.

AG Peg manifested the outburst in 2015 with very slow decline in brightness lasting for more than a year (bottom panel of Fig. 1). Similar double-peaked structure as in the light curve was also observed in the spectral behaviour of this object. During the outburst, the EWs of studied emission lines increased significantly compared to their quiescence values although the observed increase of EWs was not so steep as for the brightness. The Raman-scattered O VI lines disappeared from the spectra during both outburst maxima.

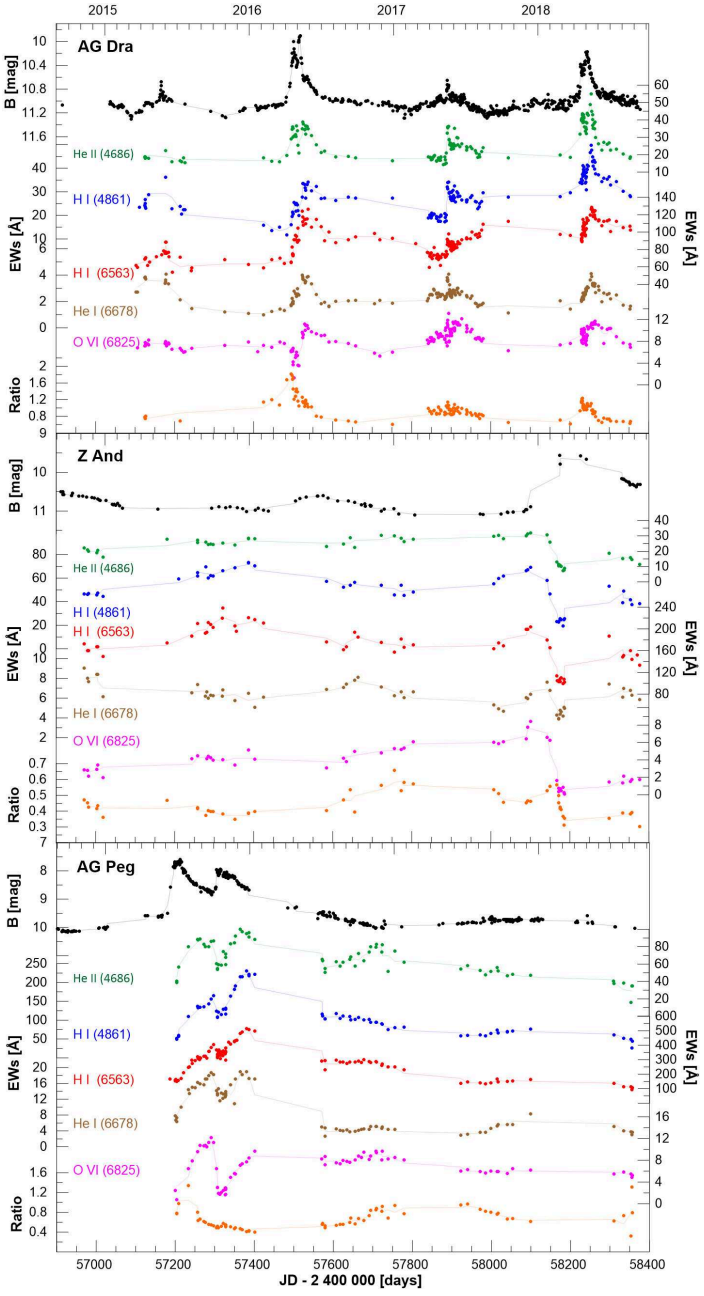

Figure 1. The light curves of studied symbiotic stars in the B filter plotted together with EWs for selected emission lines and the He II/Hβ ratio.

4.2. Temperature evolution of the white dwarfs

The fluxes of He I 4471 Å, He II 4686 Å and Hβ emission lines can be used to derive the temperature of the hot component in symbiotic systems (Iijima, 1981).

Sokoloski et al. (2006) neglected the flux of the He I 4471 Å line in the case of Z And, because $F_{4471} \leq 0.1 F_{H\beta}$. The same relation is valid for AG Dra (Leedjärv et al., 2016; Merc et al., 2018a) and AG Peg (this work). Making this assumption allows us to use the ratio of EWs instead of the fluxes:

$$T_{\rm hot}\,(\text{in}\,10^4\,\text{K}) \approx 14.16\sqrt{\frac{\text{EW}_{4686}}{\text{EW}_{\text{H}\beta}}} + 5.13. \qquad (1)$$

In general, this approximation increases the estimate of the hot component's temperature. Moreover, there are also other phenomena (e.g. the presence of additional ionization mechanisms; the phase dependence of the EWs of low excitation lines on the orbital motion; presence of the absorption component in Hβ line profile) which have to be taken into account in studying the temperature changes of white dwarfs using the He II/Hβ ratio (Merc et al., 2018a).

Counting all these effects, the main findings can be summarized as follows: a) All four recent outburst of AG Dra were of the *hot* type. Moreover, during the outburst in 2016, the historical maximum of the white dwarf's temperature was detected. b) During and after the last outburst of Z And, a decrease in the temperature was observed. c) The outburst of AG Peg in 2015 was accompanied by an increase of the hot component's temperature as in the case of AG Dra.

4.3. The Raman-scattered O VI lines

The Raman-scattered O VI lines are broad emission lines at 6825 and 7082 Å which are a product of Raman-scattering of the photons of the O VI resonance lines at 1032 and 1038 Å off the atoms of neutral hydrogen (Schmid, 1989). They occur almost exclusively in the spectra of symbiotic variable stars.

The Raman-scattered O VI 6825 Å line almost disappeared during the *cool* outburst of AG Dra in 2006, confirming a drop in the hot component's temperature (Leedjärv et al., 2016). The outburst of this symbiotic system in May 2016 manifested the same vanishing of this line although it was not of the *cool* type (Merc et al., 2017). Similar vanishing was observed during the recent outbursts of Z And and AG Peg (the curves of the Raman-scattered O VI EWs are depicted in Fig. 1 by purple color).

In the case of Z And, the minima of the Raman-scattered O VI EWs can be explained by a cooling of the hot component. On the other hand, observations of AG Dra and AG Peg during studied outbursts showed that temperatures of their white dwarfs were high enough to produce original O VI lines. Their values reject the usual interpretation for disappearance of the Raman-scattered O VI lines due to the cooling of the ionizing source. During the outburst of AG Dra

in May 2016, the temperature reached the historical maximum. In the case of AG Peg, the minimum of the Raman-scattered O VI EWs was also observed when the temperature of the hot component was very high. Skopal et al. (2017) suggested that the transient weakening of the Raman-scattered O VI lines during the outburst of AG Peg in 2015 is a result of an increase of mass-loss rate from the hot component which makes the O VI zone optically thick. Probably, a similar effect played a role in the case of AG Dra.

5. Conclusions

The medium-resolution spectra of AG Dra, Z And and AG Peg were used to study the variability and behaviour of the prominent emission lines formed in the circumbinary envelope of these symbiotic systems. In addition, changes in profiles of the spectral lines were studied. The high cadence of the obtained spectra allowed us to study the evolution of the white dwarf's temperature during the outbursts of these systems. Moreover, we have used the same mid-res spectra of AG Dra for radial velocity measurements, which will be presented in our forthcoming paper. Low-resolution spectra play an important role not only in monitoring, but can be used also for spectral energy distribution modelling.

Our results showed the importance of long-term monitoring of symbiotic stars as well as how the pro/am collaborations is essential for investigation of these strongly interacting binaries. The ARAS Group is a perfect example that such collaborations can be very successful and can bring significant results.

Acknowledgements. This work was supported by the Slovak Research and Development Agency grant No. APVV-15-0458. We are grateful to all ARAS members that contributed their observations to this paper, particularly we acknowledge and thank P. Berardi, E. Bertrand, F. Boubault, D. Boyd, Ch. Buil, F. Campos, V. Desnoux, J. Foster, O. Garde, K. Graham, J.G. Flo, S. Charbonnel, T. Lemoult, T. Lester, D. Li, J. Montier, U. Sollecchia, P. Somogyi, O. Thizy, M. Verlinden and A. Wilson. We acknowledge with thanks the variable star observations from the AAVSO International Database contributed by observers worldwide and used in this research. Last but not least, JM would like to thank the conference organizers for the support of his stay at the conference.

References

Boyarchuk, A. A., The Nature of AG Pegasi. 1967, *Soviet Astronomy*, **11**, 8

Fernie, J. D., The Period of AG Pegasi: Having Another Go. 1985, *Publications of the Astronomical Society of the Pacific*, **97**, 653, DOI: 10.1086/131581

González-Riestra, R., Viotti, R., Iijima, T., & Greiner, J., IUE observations of the high-velocity symbiotic star AG Draconis III. . 1999, *Astron. Astrophys.*, **347**, 478

Hric, L., Gális, R., Leedjärv, L., Burmeister, M., & Kundra, E., Outburst activity of the symbiotic system AG Dra. 2014, *Mon. Not. R. Astron. Soc.*, **443**, 1103, DOI: 10.1093/mnras/stu1162

Iijima, T., Temperature determination of exciting stars in highly excited planetary nebulae and symbiotic stars. 1981, in *Photometric and Spectroscopic Binary Systems*, 517

Leedjärv, L., Gális, R., Hric, L., Merc, J., & Burmeister, M., Spectroscopic view on the outburst activity of the symbiotic binary AG Draconis. 2016, *Mon. Not. R. Astron. Soc.*, **456**, 2558, DOI: 10.1093/mnras/stv2807

Merc, J., Gális, R., & Leedjärv, L., Recent outburst activity of the super-soft X-ray binary AG Draconis. 2017, *Contributions of the Astronomical Observatory Skalnate Pleso*, **47**, 192

Merc, J., Gális, R., & Leedjärv, L., Recent outburst activity of the symbiotic binary AG Draconis. 2018a, in *The Golden Age of Cataclysmic Variables and Related Objects IV*, 60

Merc, J., Gális, R., Vrašťák, M., & Leedjärv, L., The Fourth Outburst during the Ongoing Active Stage of AG Draconis has Finished. 2018b, *Research Notes of the American Astronomical Society*, **2**, 142, DOI: 10.3847/2515-5172/aad807

Mikołajewska, J. & Kenyon, S. J., The Inscrutable Hot Component in the Symbiotic Binary Z Andromedae. 1996, *Astron. J.*, **112**, 1659, DOI: 10.1086/118131

Mikołajewska, J., Kenyon, S. J., Mikołajewski, M., Garcia, M. R., & Polidan, R. S., Evolution of the Symbiotic Binary System AG Draconis. 1995, *Astron. J.*, **109**, 1289, DOI: 10.1086/117361

Mürset, U. & Schmid, H. M., Spectral classification of the cool giants in symbiotic systems. 1999, *Astronomy and Astrophysics Supplement Series*, **137**, 473, DOI: 10.1051/aas:1999105

Schmid, H. M., Identification of the emission bands at lambda lambda 6830, 7088. 1989, *Astron. Astrophys.*, **211**, L31

Schulte-Ladbeck, R. E., Near-infrared spectral classification of symbiotic stars. 1988, *Astron. Astrophys.*, **189**, 97

Skopal, A., Chochol, D., Pribulla, T., & Vanko, M., UBV Photometry of the Symbiotic Star Z And During its 2000 Outburst. 2000, *Information Bulletin on Variable Stars*, **5005**, 1

Skopal, A. & Pribulla, T., The first detection of the bipolar jets from the symbiotic prototype Z And. 2006, *The Astronomer's Telegram*, **882**, 1

Skopal, A., Shugarov, S. Y., Sekeráš, M., et al., New outburst of the symbiotic nova AG Pegasi after 165 yr. 2017, *Astron. Astrophys.*, **604**, A48, DOI: 10.1051/0004-6361/201629593

Smith, V. V., Cunha, K., Jorissen, A., & Boffin, H. M. J., Abundances in the symbiotic star AG Draconis: the barium-symbiotic connection. 1996, *Astron. Astrophys.*, **315**, 179

Sokoloski, J. L., Kenyon, S. J., Espey, B. R., et al., A "Combination Nova" Outburst in Z Andromedae: Nuclear Shell Burning Triggered by a Disk Instability. 2006, *Astrophys. J.*, **636**, 1002, DOI: 10.1086/498206

Contrib. Astron. Obs. Skalnaté Pleso **49**, 236 – 240, (2019)

Digging out twin-binary star systems from the ASAS catalogue and determining their physical parameters

V. Bakış[1], O. Sarı[1], G. Yücel[1], E. Sonbaş[2] and H. Bakış[1]

[1] *Department of Space Sciences and Technologies, Akdeniz University, Dumlupınar Boulevard 07058 Antalya, Turkey, (E-mail: volkanbakis@akdeniz.edu.tr)*

[2] *Department of Physics, University of Adıyaman, 02040, Adıyaman, Turkey*

Received: November 6, 2018; Accepted: February 25, 2019

Abstract. We have studied the ASAS catalogue in search of detached binary systems with identical components. The selected systems were photometrically and spectroscopically observed for spectral type determination. The light curves available in the ASAS database were analyzed and the light curve parameters once combined with the spectroscopic information yielded the spectral types of the binary stars in our twin candidate list. The spectral type distribution of twin binaries has shown a clear peak at the F-spectral type. Moreover, it is noteworthy that the number of twins with the A-spectral type is comparable to those with the G-spectral type, which is in contrast to previous studies.

Key words: eclipsing binaries: twin binaries, techniques: photometry, techniques: spectroscopy

1. Introduction

Studies on the mass distributions of binary stars (e.g. Lucy, 2006; Simon & Obbie, 2009) show that the ratio of twins with a mass ratio of q (M_2 / M_1) = 0.98-1.00 is around 3 percent and that the F, G and K spectral species are dominant. Simon & Obbie (2009) has 1 O, 1 B, 3 A, 16 F, 11 G and 3 K-type stars in the example list. This statistics led Simon and Obbie (2009) to make a suggestion that small-mass twins are in binary star populations where the accreation process in the star formation is slower. In addition, the presence of twins with the early-spectral type suggests that binary stars with components with masses larger than 1.6 solar masses may have the same formation mechanism as binary stars with smaller mass stars (Zinnecker & Yorke, 2007), but different mechanisms may also be important (Simon & Obbie, 2009). For this reason, it is obvious that the determination of the spectral type distribution among the twin stars will generally contribute to the understanding of star formation, and, in particular, to the understanding of twin binary stars.

Simon & Obbie (2009)'s statistical work has benefited from the SB9 (Pourbaix et al., 2004) catalog, which is the spectral catalog of binary stars and con-

stantly updated on the internet. Therefore, a systematic search of twin binaries by means of photometric and spectroscopic observing techniques is a necessity to do a more reliable statistics on their parameters.

2. Determination of twins

2.1. The database

The observational database to be investigated for twin binary stars must be free of selection effects such as limitation of a particular spectral type stars or orbital period etc. The ASAS catalogue (Pojmanski, 1997) is very suitable for our purpose since it consists of all sky photometric observations of targets down to 14th magnitude and no orbital period or spectral type limitation exist in the catalogue.

2.2. Binary selection

We needed detached binary stars so that they did not make any mass transfer between the components and the components still have the same mass at their birth. Such binary systems have components that have similar temperature and radii, therefore, the primary and secondary minima in the light curves must be identical. Thus, the ASAS catalogue are searched for such light curves for a preliminary selection.

The observability was also considered during the preliminary selection. The systems to be analyzed must also be observable in Turkey. Thus, we have limited our all sky to a declination of > -32 deg. Assumign the twins are evenly distributed in the sky, the selection of the sky region does not make a selection effect. The declination and right ascension distribution of the selected twin candidates are shown in Fig.1.

2.3. Light curve analysis

The light curves of the selected systems are analyzed with the Wilson-Devinney method (Wilson & Devinney, 2003). The number of analyzed systems is 240. The analysis yielded the the ratio of temperature and radii of the components. The systems with the ratio of temperature and radii in between 0.95-1.00 are selected for observation for a more reliable spectral type determination. Among the analyzed twin candidates, 71 systems are found to be twins. A sample light curve model fitted to a twin candidate is shown in Fig.2.

2.4. Observations of candidate twins

Observations of the selected twin binary candidates are done in two observing sites, TUBITAK National Observatory (TUG) in Antalya and Adıyaman University Observatory in Adıyaman. In TUG, three telescopes are used, a 1.5-m

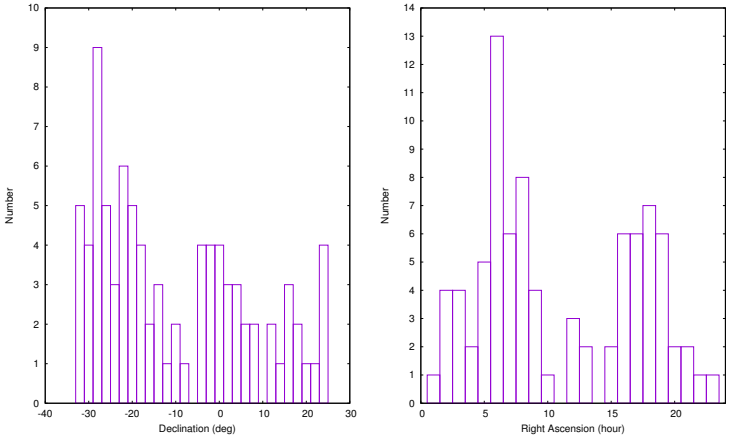

Figure 1. Sky distribution of the targets observed in this study. The left panel is for declination and the right panel is for right ascension. In the panels, the binning of the data was chosen to be 2 deg for declination (*left*) and 1 hr for right ascension (*right*).

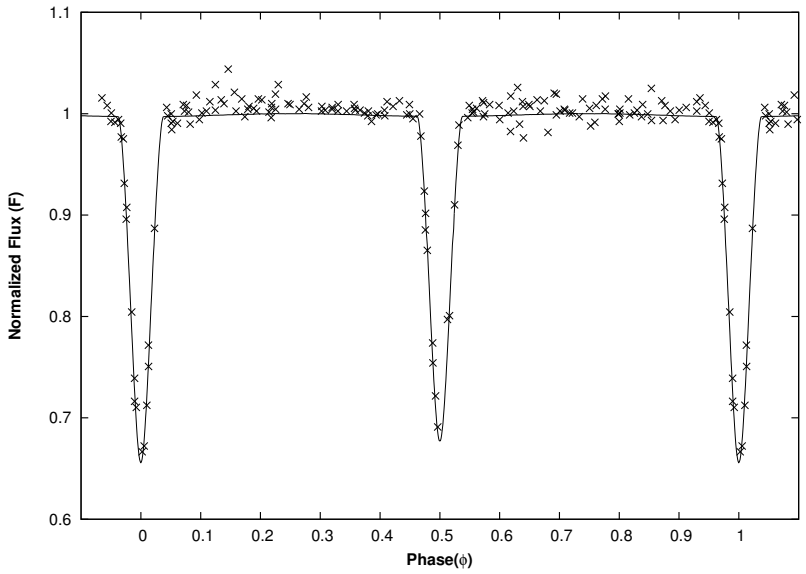

Figure 2. A sample of light curve model of a twin candidate from the ASAS catalogue.

RTT150 telescope and a 0.6-m UBT60 telescope for medium resolution spectroscopy, and a 1-m (T100) telescope for multi-band imaging. In Adıyaman, the 0.6-m telescope is used for only multi-band imaging. A sample spectrum of a 8.46 mag ASAS star is shown in Fig.3.

In photometric observations, $UBVRI$ Johnson filters were used with both telescopes and the telescope standart coefficients are calculated precisely for a reliable absolute photometry. Once the colors (U–B, B–V, V-R and V-I) are obtained, stars without spectroscopic observations are plotted in the color-color diagrams and spectral types together with interstellar extinction were estimated by moving the stars in the opposite direction of interstellar extinction. The interstellar extinction was used to obtain reddening-free colors, which are used to estimate temperatures of the twins.

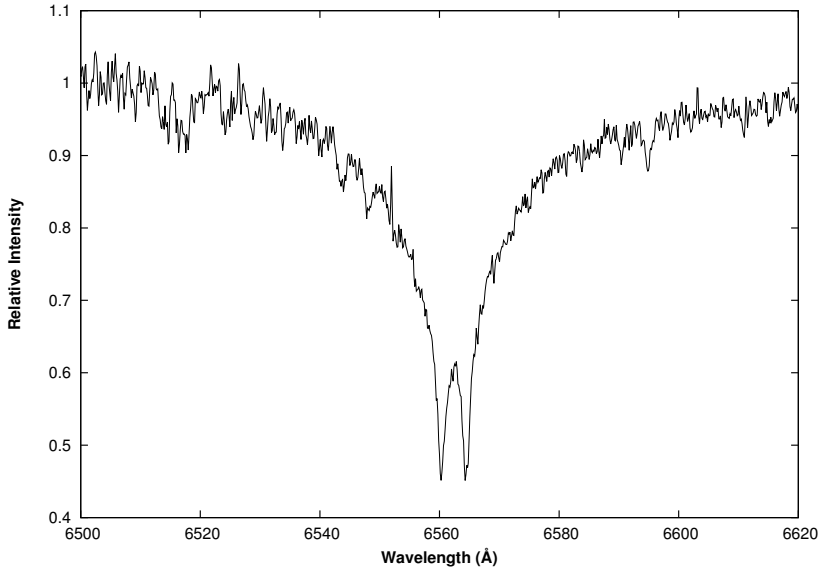

Figure 3. A sample spectrum around the H_α region of an 8.46 mag twin candidate from the ASAS catalogue.

3. Preliminary results

In this project, a total of 71 twin canditates from the ASAS catalogue are determined and observed. Their spectral types are determined either by photometric or spectroscopic data. If a spectral data exists for a system, the spectral type is determined directly from the spectral data otherwise from the colors obtained

by absolute photometry. The spectral type distribution of the twins is shown in Fig. 4. In Fig. 4, a peak at the F-spectral type is clear, which is in agreement with the recent study by Simon & Obbie (2009). However, it is new that the number of twins with the A-spectral type is more than those with the G-spectral type.

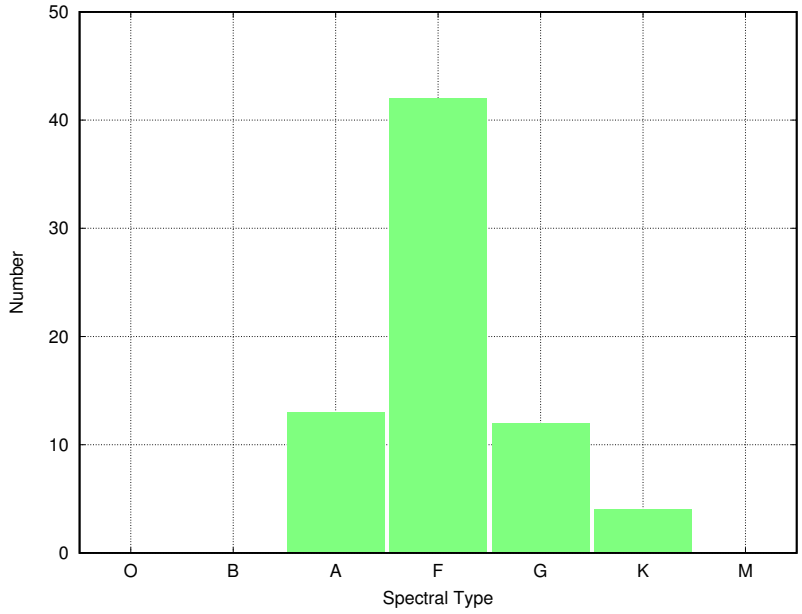

Figure 4. Spectral type distribution of twin binaries in the ASAS catalogue.

Acknowledgements This study is fully supported by the TÜBITAK project under the code 115F029.

References

Lucy, L.B.: 2006, *Astron. Astrophys.* **457**, 629-635

Pourbaix, et al.: 2004, *Astron. Astrophys.* **424**, 727-732

Pojmanski, G.: 1997, *Acta Astron.* **47**, 467-481

Simon, M., Obbie, R.C.: 2009, *Astron. J.* **137**, 3442-3448

Van Hamme, W., Wilson, R.E.: 2007, *Astrophys. J.* **661**, 1129-1151

Wilson, R.E., Devinney, E.J.: 1971, *Astrophys. J.* **166**, 605

Zinnecker, H., Yorke, H.W.: 2007, *Ann. Rev. Astron. Astrophys.* **45**, 481-563

Contrib. Astron. Obs. Skalnaté Pleso **49**, 241 – 245, (2019)

Double eclipsing binaries

P. Zasche

Astronomical Institute, Charles University, Faculty of Mathematics and Physics, CZ-180 00, Praha 8, V Holešovičkách 2, Czech Republic , (E-mail: zasche@sirrah.troja.mff.cuni.cz)

Received: October 10, 2018; Accepted: January 22, 2019

Abstract. Double eclipsing binaries are still quite neglected type of objects. Despite the increasing number of candidates, a thorough study of these interesting systems is still missing. We started our campaign on these stars and even after one season several very interesting results appeared. At first, it seems that almost all of the candidate double eclipsing systems really constitute the rare quadruple stellar systems. Moreover, the final proof of quadruple nature can be done only on the photometric data (studying the period variations of both pairs). As a by-product also a mass estimation can be done using only the photometry, which is quite beneficial and unusual fact in stellar astrophysics. The lack of such systems on the northern hemisphere is also being discussed and a call for a systematic search is presented.

Key words: stars: binaries: eclipsing – stars: fundamental parameters

1. Introduction

Eclipsing binaries still represent the objects of crucial importance for our knowledge about the Universe, about the stellar structure and evolution, and others. Thanks to them we are able to calibrate our evolutionary models, we can derive the interior structure of the stars, derive their radii or study the stellar populations in and outside of our Galaxy (see e.g. Southworth 2012).

During the last decade there have also been discovered a special group of eclipsing binaries called double eclipsing binaries (or sometimes also doubly eclipsing binaries). These systems show two different sets of eclipses with different periods and durations of eclipses. Hence, we can speculate about their connection and consider them as gravitationally bound systems. The other possibility is that these are two independent eclipsing binaries at different distances projected into the same direction by a pure chance. In the dense fields also this possibility cannot easily be ruled out.

However, to prove their bound orbit is, in general, not easy. One way is to measure their radial velocities, and to detect the mutual movement around the common barycenter. For any such detection one needs high-quality spectra to successfully disentangle all the four components and consecutively to detect the mutual movement also the long-time baseline of observations. According to different studies (e.g. Duquennoy & Mayor 1991, or Raghavan et al. 2010),

the outer periods of the third components in multiple-star systems are typically of the order of several years, decades, or centuries. Therefore, any such spectroscopic detection of the quadruple nature is very time consuming. Worth of mention is also the fact that many such systems are relatively faint, hence good spectroscopic observations are still quite tricky.

Another possible method proving that the two binaries are really bound to each other would be to detect there some dynamical perturbation of the two pairs. The easiest for photometric detection is maybe the detection of the changing orientation of the orbital plane of such systems, hence the changing eclipse depth of the binary (or both binaries). Such phenomena were discovered for several dozens of stars nowadays, see e.g. Juryšek et al. (2018), but as far as we know only for one double eclipsing system yet (Hong et al., 2018). The problem is that for detecting such perturbation the movement of the orbital precession should be rather fast (which is typically not the case), which means that the third body should have quite a short orbital period. The shorter the outer period, the more pronounced and faster the nodal precession (Borkovits et al., 2015).

2. Method

However, we introduced a different method. Our method seems to be much more effective and less demanding for high-quality data. We need no spectroscopy, and the use of photometry of large surveys (measuring, for example, the object only once per night) is sufficient. We used a classical and well-known method of period analysis of the eclipses (ETV method) using the hypothesis of a so-called light-time effect to the orbits of both pairs. When we incorporate both binaries into one joint analysis, we can get a complete set of orbital parameters of their mutual orbit. In fact the same method was first used for a well known (and first discovered) system V994 Her, see Zasche & Uhlař (2016).

As a source of photometric data we used mainly the OGLE catalogue (Udalski et al. 2008, and Udalski 2003), accompanied with our own measurements when available. The list of candidate double eclipsing systems was scanned and each system was considered to be potentially interesting. However, only those with adequately detached components having enough data points for subsequent analysis were included into our sample to be analysed.

The main result of our analysis is the first evidence that many of these double eclipsing binary candidates really orbit each other thanks to their ETV analysis. Two most promising examples of our analysis are plotted in Figure 1.

The light curves of both eclipsing binaries were analysed using the program PHOEBE (Prša & Zwitter, 2005). Thanks to this modelling of the light curves, we were able to derive the individual inclination angles of the inner pairs, relative radii of the components, their luminosity ratios, etc. Moreover, using these light

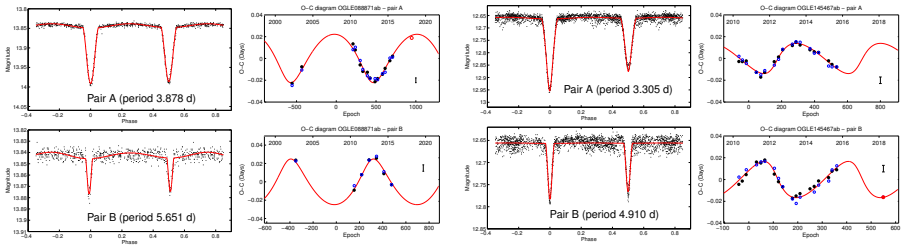

Figure 1. A sample of two systems found in the OGLE database with proved quadruple nature. Their light curves (left) as well as the ETV curves (right) are plotted.

curve templates also the times of the eclipses were derived using a method introduced earlier (Zasche et al., 2014).

From our analysis of ETV there resulted that the selected systems (see Figure 1) really comprise two eclipsing binaries which orbit around each other. Their mutual movement was detected via the ETV signals of both pairs. Hence, using this analysis also the mass ratios of both pairs can easily be computed from the amplitudes of the ETV variations of both pairs (because of knowing the inclination angles for eclipsing binaries $i \approx 90^\circ \Rightarrow \sin i \approx 1 \Rightarrow M_A/M_B = A_B/A_A$). The mass ratio of both binaries is a crucial parameter for any further analysis. However, for a final derivation of the mutual inclination of the orbits one needs precise masses of both pairs, which can only be derived from spectroscopy. And the mutual orientation of the orbits plays a crucial role when discussing about the origin of the system as well as its future dynamical evolution.

Several systems showing their mutual motion have quite good coverage of their ETV diagrams, and can be definitely classified as quadruples. In total, we have detected 10 new proved quadruples. This is for the first time any such large portion of new quadruples using this new technique was detected. As one can see in Figure 1, the two different eclipses are rather deep and therefore the analysis was rather straightforward concerning the ETV analysis. What is still quite problematic was the analysis of their luminosity ratios (i.e. the third light values of both pairs). For other systems, with much worse data coverage or shallower minima, this task is still very questionable and the results inconvincing.

Nowadays we have several dozens of candidates for double eclipsing stars (88 in total), but which were not proved to orbit each other. Can we say something more general about these systems? What can be stated even with the present result is a fact, that certainly almost all of the double eclipsing systems constitute real bound quadruples. Why can we be so sure? We detected in our sample an occurrence rate of more than 40% of quadruples. However, our method is essentially sensitive only to those systems with the outer orbital period of several years. Below one year the result would be inconclusive due to poor data sampling of the ETV curves. And on the other hand, the orbital periods longer

than 10 – 15 years would be also problematic due to the limited time span of our data. However, as it was published earlier (e.g. Duquennoy & Mayor 1991, or Raghavan et al. 2010), the typical periods of the distant components are an order of magnitude longer. Hence our method is quite insensitive to that detection and we only revealed a "tip of an iceberg". Moreover, also the mass ratio, as well as the orientation of the mutual orbit towards the observer, play a role. All of these limitation should be taken into account when trying to estimate the incompleteness fraction. Hence, we believe that practically all double eclipsing systems are parts of the quadruples.

One important aspect of the topic was not discussed. Due to the large photometric surveys OGLE we nowadays know a huge majority of such double eclipsing systems only on the southern sky. As one can see from Figure 2, most of the systems have low declinations and can only be observed from the southern observatories. We really demand more similar systems on the northern sky for prospective photometric observations using the world-wide net of variable star observers (having their instruments mostly on the northern hemisphere). Potentially, surveys like ASAS-SN (Shappee et al. 2014 and Kochanek et al. 2017) can serve as an ideal starting point for finding new candidates also on the northern sky.

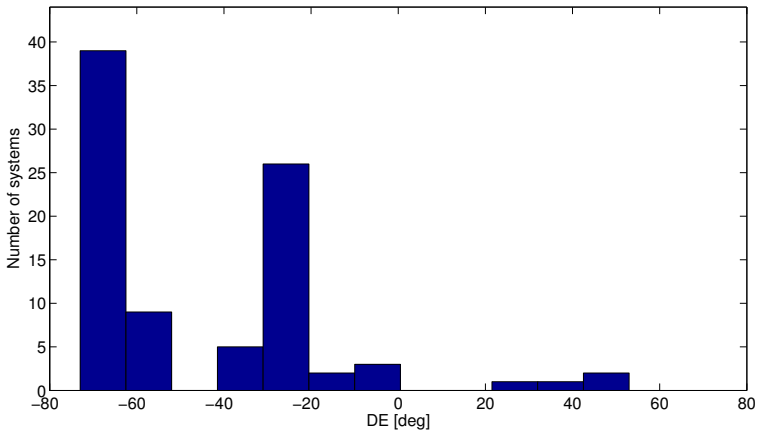

Figure 2. The histogram of declinations for the known candidate double eclipsing systems. The double-peaked shape is caused by the systems located in the Magellanic Clouds and the Galactic bulge from the OGLE survey.

Acknowledgements. The research was supported by the grant MSMT INGO II LG15010. We also thank the OGLE team for making all of the observations easily

public available. We are also grateful to the ESO team at the La Silla Observatory for their help in maintaining and operating the Danish telescope. This research has made use of the SIMBAD and VIZIER databases, operated at CDS, Strasbourg, France and of NASA Astrophysics Data System Bibliographic Services.

References

Borkovits, T., Rappaport, S., Hajdu, T., & Sztakovics, J., Eclipse timing variation analyses of eccentric binaries with close tertiaries in the Kepler field. 2015, *Mon. Not. R. Astron. Soc.*, **448**, 946, DOI: 10.1093/mnras/stv015

Duquennoy, A. & Mayor, M., Multiplicity among solar-type stars in the solar neighbourhood. II - Distribution of the orbital elements in an unbiased sample. 1991, *Astron. Astrophys.*, **248**, 485

Hong, K., Koo, J.-R., Lee, J. W., et al., KMTNet Time-series Photometry of the Doubly Eclipsing Binary Stars Located in the Large Magellanic Cloud. 2018, *Publ. Astron. Soc. Pac.*, **130**, 054204, DOI: 10.1088/1538-3873/aab428

Juryšek, J., Zasche, P., Wolf, M., et al., New inclination changing eclipsing binaries in the Magellanic Clouds. 2018, *Astron. Astrophys.*, **609**, A46, DOI: 10.1051/0004-6361/201730655

Kochanek, C. S., Shappee, B. J., Stanek, K. Z., et al., The All-Sky Automated Survey for Supernovae (ASAS-SN) Light Curve Server v1.0. 2017, *Publ. Astron. Soc. Pac.*, **129**, 104502, DOI: 10.1088/1538-3873/aa80d9

Prša, A. & Zwitter, T., A Computational Guide to Physics of Eclipsing Binaries. I. Demonstrations and Perspectives. 2005, *Astrophys. J.*, **628**, 426, DOI: 10.1086/430591

Raghavan, D., McAlister, H. A., Henry, T. J., et al., A Survey of Stellar Families: Multiplicity of Solar-type Stars. 2010, *Astrophys. J., Suppl.*, **190**, 1, DOI: 10.1088/0067-0049/190/1/1

Shappee, B. J., Prieto, J. L., Grupe, D., et al., The Man behind the Curtain: X-Rays Drive the UV through NIR Variability in the 2013 Active Galactic Nucleus Outburst in NGC 2617. 2014, *Astrophys. J.*, **788**, 48, DOI: 10.1088/0004-637X/788/1/48

Southworth, J., Eclipsing Binary Stars: the Royal Road to Stellar Astrophysics. 2012, in *Orbital Couples: Pas de Deux in the Solar System and the Milky Way*, ed. F. Arenou & D. Hestroffer, 51–58

Udalski, A., The Optical Gravitational Lensing Experiment. Real Time Data Analysis Systems in the OGLE-III Survey. 2003, *AcA*, **53**, 291

Udalski, A., Szymanski, M. K., Soszynski, I., & Poleski, R., The Optical Gravitational Lensing Experiment. Final Reductions of the OGLE-III Data. 2008, *AcA*, **58**, 69

Zasche, P. & Uhlař, R., Updated study of the quintuple system V994 Herculis. 2016, *Astron. Astrophys.*, **588**, A121, DOI: 10.1051/0004-6361/201628153

Zasche, P., Wolf, M., Vraštil, J., et al., Apsidal motion and a light curve solution for eighteen SMC eccentric eclipsing binaries. 2014, *Astron. Astrophys.*, **572**, A71, DOI: 10.1051/0004-6361/201424273

Contrib. Astron. Obs. Skalnaté Pleso **49**, 246 – 251, (2019)

KOREL disentangling of the LMC eclipsing Algol OGLE-LMC-DPV-065

M. Cabezas[1], P. Hadrava[1], R. E. Mennickent[2] and T. Rivinius[3]

[1] *Astronomical Institute of the Czech Academy of Sciences Boční II 1401, 141 31 Praha 4, Czech Republic*

[2] *Departamento de Astronomía, Universidad de Concepción Casilla 160-C, Concepción, Chile*

[3] *ESO - European Organisation for Astronomical Research in the Southern Hemisphere, Casilla 19001, Santiago 19, Chile*

Received: November 1, 2018; Accepted: March 8, 2019

Abstract. We present disentangled orbital parameters and component spectra of the double-periodic eclipsing Algol OGLE-LMC-DPV-065. Direct spectroscopic evidence on a disk-like envelope around the primary star and circumstellar matter in the system is given.

Key words: spectroscopic – binary stars – disentangling – eclipsing binary

1. Introduction

A group of hot Algols shows a long photometric cycle with average about 33 times its orbital period. This group is called Double Periodic Variables (DPVs, Mennickent et al., 2003, 2016, 2017, Poleski et al. 2010). DPVs are semidetached binaries typically consisting of an A/F/G giant star filling its Roche lobe and transferring mass onto a B-type primary surrounded by a circumprimary disk.

The OGLE-LMC-DPV-065 (R.A.$_{2000}$ = 05:20:04.07, Dec.$_{2000}$ = -69:36:39.1; OGLE05200407-6936391) is one of the brightest DPVs in LMC (V =14.74, $B-V=-0.07$), with an orbital period of $P_o = 10^d.031645 \pm 0.000033$ (Poleski et al., 2010). This is an interesting target because the system is eclipsing and shows a change in the long period: from 340 to 210 days in 15 years. In this work we present its orbital solution and the separated spectra obtained using the method of disentangling of spectra.

2. Observations

Our spectroscopic data consist of 27 exposures obtained in overall time of 25 hours of observations in the service mode with the ESO Ultraviolet and Visual Echelle Spectrograph UVES (Dekker et al., 2000) at the Kueyen telescope in the Paranal Observatory. This is a cross-dispersed echelle spectrograph in which the light beam is split into two main spectral regions; the Blue region, covering 3760-4985 Å, and the Red region, covering 5700-7520 Å. This instrument provides an

accurate calibration of the wavelength scale close to 50 m/s and a resolving power of 50 000 and 55 000, respectively, for each region.

In this work we use seven spectral regions containing metallic lines which are not blended and are much narrower than other lines such as those of H and He. To diminish the numerical errors of disentangling we have used an oversampling (compared to the spectrograph resolution and pixel-size of the original detector) of each spectral region in 4096 bins and an average resolution of RV/bin=0.7256 $\mathrm{km\,s^{-1}}$. The details about preparation of the data and operation of the `KOREL` code can be found at the User's guide (Hadrava, 2004b).

3. Results

3.1. Solution of orbital parameters

In order to obtain the radial velocities and orbital parameters we used the `KOREL` code which directly yields also the separated spectra of the components of a multiple stellar system under study. Four solutions of orbital parameters are presented in Table 1. The period was fixed in all of them to $P_o = 10.0316267$ days found from a combination of various photometric data sets. The periastron epoch τ^* given in Table 1 is HJD–2453300.

Table 1. Summary of our different solutions.

Parameter	I	II	III	IV
τ^*	92.31±0.02	92.305±0.004	94.79±0.33	92.35±0.14
K_1 [$\mathrm{km\,s^{-1}}$]	42.60±0.97	42.44±0.33	42.45±0.32	42.92±0.38
K_2 [$\mathrm{km\,s^{-1}}$]	210.5±6.4	214.1±1.8	213.5±1.7	209.1±1.8
q	0.203±0.008	0.198±0.002	0.199±0.002	0.205±0.002
ω [deg]	90	90	178.7±11.6	90
e	0	0	0.021±0.006	0

The first three solutions are based on the same above-described seven spectral regions. Solution I corresponds to the average of the seven `KOREL`-solutions calculated for each spectral region independently. The errors of the parameters are the standard deviations. Solution II is the best fit obtained using the `KOREL` for the multiregion data, that is with all the seven spectral regions as input fitted simultaneously. In this procedure we do not get directly errors of the parameters, but we can find their Bayesian estimate (cf. Hadrava, 2016) using the outputs of `KOREL` which map the χ^2 in two-dimensional cross-sections of the parameter space for each pair of parameters. The above mentioned oversampling of the input data must be taken into account to find the proper number of statistically independent pixels of noise. The errors of the parameters and their correlation coefficients (e.g. $c_{K_1,q} = 0.972$ for the Solution II) can then be calculated from

the moments of the Bayesian probability distribution. Another possibility to estimate the errors of disentangled parameters is to compare them with a solution of radial-velocity curves obtained, e.g., using `FOTEL` (cf. Hadrava, 2004a) from the radial velocities calculated by `KOREL`. It should be, however, noted that the usually given error-bars of published values of parameters yield anyway only very limited information about their uncertainties. For instance, the (Bayesian-probability) weighted mean values (e.g. $\bar{K}_1 = 42.38$ km s^{-1} in the $\{K_1, q\}$-plane of Solution II) generally differ from the values at the deepest minima of χ^2 which may be influenced by an interference of the noise and there may exist several comparable solutions. The inspection of the probability distribution thus yields more reliable information. In both solutions I and II we considered a circular orbit, i.e. we fixed $e = 0$ and $\omega = 90°$.

Table 2. Systemic velocities measured from individual lines.

Spectral line Å	γ_{pri} km s^{-1}	Spectral line Å	γ_{pri} km s^{-1}	Spectral line Å	γ_{sec} km s^{-1}
He I 4143.76	279.22	Si II 4621.42	271.29	Si II 4128.05	281.14
N II 4227.74	276.36	O II 4638.85	276.56	Si II 4130.89	278.43
N II 4236.91	277.24	O II 4641.81	276.86	Fe II 4233.17	280.48
N II 4241.78	272.03	O II 4649.14	276.16	Cr II 4242.36	275.77
O II 4414.88	275.35	O II 4699.21	270.56	Sc II 4246.82	275.29
O II 4416.97	274.26	O II 4705.36	276.68	Ti II 4443.79	277.68
He I 4437.55	276.15	He I 4713.14	278.23	Ti II 4533.96	281.19
N II 4447.04	273.91			Ti II 4549.62	284.99
Si III 4567.84	276.48			Cr II 4558.65	277.75
Si III 4574.76	274.98			Ti II 4563.76	281.19
O II 4590.97	274.64			Ti II 4571.97	282.47
O II 4596.17	273.44			Fe II 4629.34	278.68
N II 4607.15	272.24			Fe II 4731.45	280.79

The Solution III is similar to the Solutions II, but it takes into account a possible eccentricity of the orbit (i.e. $e \neq 0$). The best fit to the multiregion data given in the Solution III indicates a slight asymmetry of the radial-velocity curve corresponding to the eccentricity 0.021. The Bayesian probability distribution in the plane of e and the correlated τ and ω is, however, very irregular and the mean value of the eccentricity $\bar{e} = 0.017$. The periastron longitude is close to 180°, so that the eccentricity should be also seen in photometry. However, our `FOTEL`-solution of the OGLE-photometry (Poleski et al., 2010) limits the eccentricity to 0.0007 ± 0.01. In view of the long-term variability of the system, which indicates the presence of some circumstellar matter, the asymmetry may be due to some other reasons and the marginal evidence for the eccentricity in the currently available data cannot be accepted as real.

In addition to the seven spectral regions containing the narrow 'metal' lines suitable for determination of the orbital parameters we also disentangled the Hα region. The corresponding results are given as the Solution IV. The Hα line is

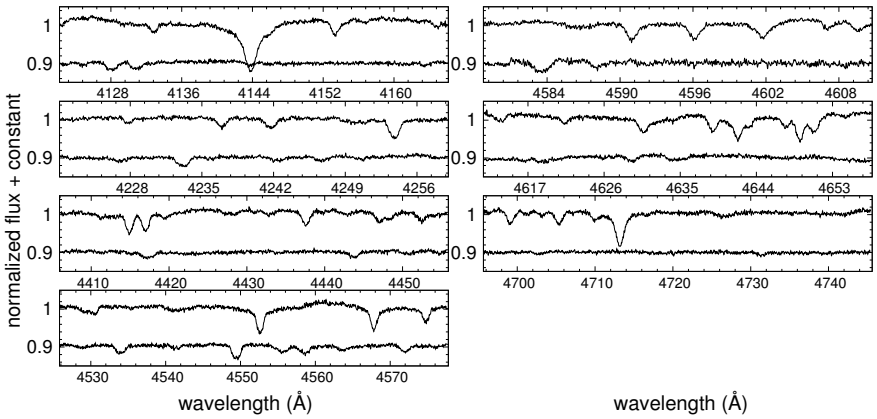

Figure 1. The component spectra in our seven selected regions disentangled using KOREL. For each panel the upper spectrum corresponds to the primary component and the lower spectrum to the secondary component. The wavelength scale is shifted for the mean γ-velocity to correspond to the laboratory wavelengths of the lines.

highly influenced by the circumstellar matter, which may distort the line profiles (as it will be discussed in Section 3.3). In the following we shall thus adopt the Solution II as the most reliable information on the orbital parameters.

The procedure of disentangling does not need any identification of spectral lines and in fact it uses the disentangled mean component spectra as a template to find the changes of radial velocities in the individual exposures. To find the systemic velocity, i.e. the radial velocity of the center of mass of the binary system, we thus adopted an average of radial velocities calculated by Gaussian adjustments for different spectral lines in each disentangled component spectrum shown in Table 2. We arrived at mean values $\gamma_{pri} = 275.1 \pm 2.3$ km s^{-1} for the primary and $\gamma_{sec} = 279.6 \pm 2.8$ km s^{-1} for the secondary component.

3.2. Disentangled spectra

Figure 1 shows the seven selected regions. As we can see, the first component, which is hotter, has strong lines of He I, N II, O II, and Si II. In turn, the colder component has metallic weak lines of Fe II, Si II, Cr II, and Ti II. The separation of these spectra is crucial for our future study in which we plan to determine the spectral type of each component and its physical parameters.

3.3. H$_\alpha$ region

To study the circumstellar matter in the system we also disentangled the region of H$_\alpha$ line. This region is highly contamined by the telluric water-vapour lines, so

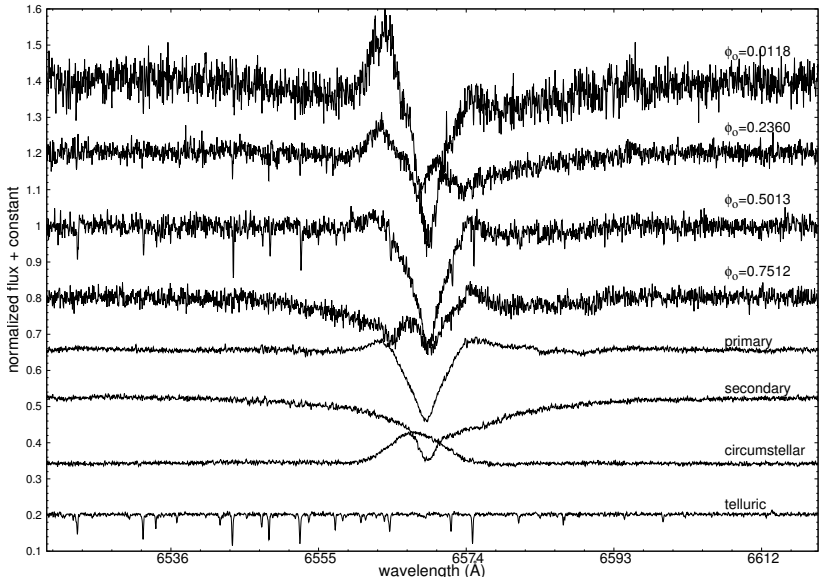

Figure 2. Spectra of DPV 065 in the Hα region. From the top: observed spectra at four different phases, separated spectra of the primary and secondary component, emission of the circumsetallar matter and the telluric lines.

it is advantageous to add into the disentangling also a component moving with the annual motion of the Earth. If we disentangled the region with the three components for the two stars and the tellurics, we arrived at orbital parameters within errors equal to the Solution II; the shape of the disentangled spectra was qualitatively similar to the corresponding component spectra shown in Figure 2. The primary component has a double-peak emission in wings which suggests a disk-shaped envelope. While in the previous solutions of the narrow-line regions the line strengths of the primary component were diminished and those of the secondary enhanced in the exposure taken close to the primary minimum, in the Hα region the emission is enhanced in this phase (in particular in the blue wing – see the top spectrum in Figure 2). Generally, the fit of Hα profile was not much precise and residuals in all phases contained humps revealing inhomogeneities in the circumstellar matter. To improve the fit we included into the disentangling a third component corrotating with the binary with an unknown phase-shift and radial-velocity amplitude. Such an approximation has proved to be useful, e.g., in the case of Cyg X-1 (cf. Figure 7.4 in Hadrava, 2016, and the references therein). This Solution IV (given in Table 1 and displayed in Figure 2) has bit less pronounced emission wings of the primary and instead of it there is a circumstellar emission blob mowing with an amplitude of radial velocity equal to (125.2±0.4) km s^{-1} and ('periastron') longitude 136.8° ± 0.5°. The fit of the

input spectra is much better, despite it is not yet so precise as in the 'metallic' lines.

4. Conclusion

Our KOREL disentangling of spectra of DPV-065 improved the orbital parameters and provided the first spectroscopic evidence of the presence of an accretion disk around the primary star and the circumstellar matter in this system. This interesting system will require a further observational as well as theoretical investigation. In particular, we plan to compare the disentangled spectra with synthetic models.

Acknowledgements. This work has been supported by project GACR 14-37086G. M.C. acknowledges support by the Astronomical Institute of the Czech Academy of Sciences. R.E.M. gratefully acknowledges support by VRID-Enlace 218.016.004-1.0 and the Chilean Centro de Excelencia en Astrofísica y Tecnologías Afines (CATA) BASAL grant AFB-170002.

References

Dekker, H., D'Odorico, S., Kaufer, A., Delabre, B., & Kotzlowski, H., Design, construction, and performance of UVES, the echelle spectrograph for the UT2 Kueyen Telescope at the ESO Paranal Observatory. 2000, in Proc. SPIE, Vol. **4008**, *Optical and IR Telescope Instrumentation and Detectors*, ed. M. Iye & A. F. Moorwood, 534–545

Hadrava, P., FOTEL 4 - User's guide. 2004a, *Publications of the Astronomical Institute of the Czechoslovak Academy of Sciences*, **92**, 1

Hadrava, P., KOREL - User's guide. 2004b, *Publications of the Astronomical Institute of the Czechoslovak Academy of Sciences*, **92**, 15

Hadrava, P., Disentangling of Stellar Spectra. 2016, in Astrophysics and Space Science Library, Vol. **439**, *Astronomy at High Angular Resolution*, ed. H. M. J. Boffin, G. Hussain, J.-P. Berger, & L. Schmidtobreick, 113

Mennickent, R. E., Long Photometric Cycles in Hot Algols. 2017, *Serbian Astronomical Journal*, **194**, 1, DOI: 10.2298/SAJ1794001M

Mennickent, R. E., Otero, S., & Kołaczkowski, Z., Interacting binaries W Serpentids and double periodic variables. 2016, *MNRAS*, **455**, 1728, DOI: 10.1093/mnras/stv2433

Mennickent, R. E., Pietrzyński, G., Diaz, M., & Gieren, W., Double-periodic blue variables in the Magellanic Clouds. 2003, *Astron. Astrophys.*, **399**, L47, DOI: 10.1051/0004-6361:20030106

Poleski, R., Soszyński, I., Udalski, A., et al., The Optical Gravitational Lensing Experiment. The OGLE-III Catalog of Variable Stars. X. Enigmatic Class of Double Periodic Variables in the Large Magellanic Cloud. 2010, *AcA*, **60**, 179

Contrib. Astron. Obs. Skalnaté Pleso **49**, 252 – 257, (2019)

Tracking massive pairs

M. Ratajczak[1,2], A. Pigulski[1] and K. Pavlovski[3]

[1] *Astronomical Institute, University of Wrocław, ul. Kopernika 11, 51-622 Wrocław, Poland*

[2] *Warsaw University Observatory, Aleje Ujazdowskie 4, 00-478 Warszawa, Poland*

[3] *Department of Physics, Faculty of Science, University of Zagreb, Bijenicka cesta 32, 10000 Zagreb, Croatia*

Received: October 18, 2018; Accepted: January 22, 2019

Abstract. The analysis of eclipsing binaries with massive components enables to test stellar evolution models and track selected aspects of the structure of early-type stars. Stellar pairs with B-type components may serve to find tighter constraints on the mechanisms of convective core overshooting or masses of β Cephei-type stars. We present the results of an analysis of several eclipsing binaries – N Sco, LS CMa, and δ Vel – observed by BRITE-Constellation satellites and followed by a wide range of ground-based telescopes.

Key words: binaries: spectroscopic – binaries: eclipsing – stars: oscillations

1. Introduction

Stellar astrophysics is based on the precise determination of fundamental stellar parameters, like masses, radii, and effective temperatures. Detached eclipsing binaries (DEBs) of SB2-type enable determination of these parameters with the required precision of 3% (Torres et al., 2010), and thus allow us to test the predictions of stellar evolution models.

2. Finding constrains on convective core overshooting

Inspection of the catalogue of the detached eclipsing binaries (Southworth, 2015, DEBCat) indicates the lack of massive stars with precise masses and radii. There is only a dozen of systems with well-characterised B-type components. Considering that our knowledge of the evolution of early-type stars on the main sequence (MS) is incomplete, there is a need to find and study binary systems with massive components.

Even if modern evolutionary codes are very advanced, there are still some uncertainties that affect the modelling of stellar structure and evolution. One of the major issues under debate in models of high-mass stars is the convective boundary mixing, called overshooting. It affects the size of convective stellar cores, the size of MS stellar radii, and the MS lifetime. The greater the effect

of convective core overshooting is assumed in the models, the wider the MS, and so the more the TAMS is shifted towards higher luminosity (see Ratajczak et al., 2017, Fig. 1). Finding observational constrains on the convective core overshooting parameters may be possible by tracking DEBs with B-type stars located close to TAMS. By determining the masses and radii of massive components of these systems and comparing them with the models, we aim at limiting the parameters of convective core overshooting.

The analysed sample consists of bright DEBs with B-type components mostly observed by BRITE (Weiss et al., 2014; Pablo et al., 2016), for which spectroscopy was carried out using a wide range of spectrographs. The outcome of the survey resulted in a dozen of systems, many of which turned out to be less evolved than expected, residing closer to ZAMS than thought. A few promising systems are still under analysis. We have also performed analysis of fainter targets not observed by BRITE, namely HD 161160, HD 153387, HD 93004, HD 82422, HD 326440, HD 145614, and V743 Cep.

3. Selected BRITE targets – N Sco and LS CMa

One of the peculiar objects from the BRITE sample is N Sco (HD 148703, $V = 4.23$ mag), which was not classified as an eclipsing binary to date, just considered as a variable star.

BRITE photometry revealed eclipses in the data, which were confirmed by the Solar Mass Ejection Imager (Jackson et al., 2004, SMEI) data taken between 2003 and 2011. The orbital period of N Sco is $P \sim 223.88$ d. and the system is highly eccentric with $e = 0.93$. Spectroscopic data were obtained using the following spectrographs: BACHES (Kozłowski et al., 2014), PUCHEROS (Vanzi et al., 2012), FIDEOS (Vanzi et al., 2018), and HRS/SALT (Bramall et al., 2010). High-resolution HRS spectra were used to detect the spectral lines of the secondary component at the highest radial velocity (RV) separation. The preliminary analysis of the system was presented by Ratajczak & Pigulski (2018).

N Sco turned out to be the most eccentric eclipsing binary with massive components. Its high eccentricity is a puzzle possibly giving a new perspective on the formation and evolution of such systems.

Another intriguing system from BRITE is LS CMa (HD 52670, $V = 5.63$ mag), which was already classified as an eclipsing binary, but with an unknown orbital period. The object was observed by the BRITE-Toronto satellite and the data enabled to determine the orbital period of $P \sim 70.048$ d. We have also detected an additional periodic signal with frequency $f = 0.624$ c/d, confirmed by the SMEI observations. The BRITE light curve of LS CMa is presented in Fig. 1.

Ground-based spectroscopic observations of the target resulted in 44 spectra in total (using CHIRON, PUCHEROS, BACHES, and FIDEOS spectrographs) taken in order to determine the RVs of the components and their masses.

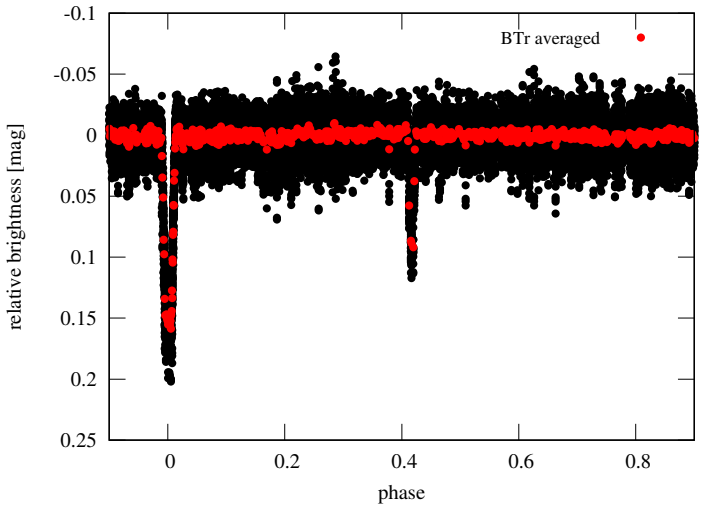

Figure 1. The BRITE light curve of LS CMa. Red points indicate averaged data from the BRITE-Toronto satellite.

4. Mass determination of β Cephei-type stars

β Cephei-type stars are important test-beds of massive stars asteroseismology. The mass estimation of a given β Cephei-type star sets constrains on several aspects of stellar structure modelling.

There are a few examples of β Cephei-type stars in eclipsing binary systems of SB1 type (eg. EN Lac, V381 Car, λ Sco, V916 Cen). Since a direct dynamical mass determination of these stars is not possible, it is crucial to detect spectral lines of secondary (fainter) components and thus estimate the masses of both stars – including a β Cephei-type one.

We have investigated the possibility of detection the secondary's spectrum if its contribution to the total flux of the system is about 2% when we consider B- and A-type stars in a system and about 0.1% when the system consists of B- and F-type stars (Ratajczak et al., 2017). All this under assumption that the spectral observations are obtained when the stars are in quadrature phases, because the chance to detect the secondary's lines is the highest at these phases.

Tests on the synthetic spectra yielded that a signal-to-noise ratio (SNR) of 500 is required in the first case (B- and A-type components) and 8 000 in the other (B- and F-type components). Such high SNR can be achieved only by adding many high-SNR spectra. The power of this method is also proven in the spectral disentangling technique described by Kolbas et al. (2015), where the authors show that it is possible to resolve a stellar component that contributes only 1% to the total light of the triple system.

To test their method of spectral disentangling on our data we have studied δ Vel (HD 74956, $V = 1.95$ mag), the brightest known DEB. The system is well described in the literature by eg. Kervella et al. (2009) and was a subject of photometric, spectroscopic, and astrometric studies.

We have analysed the δ Vel photometric data obtained by BRITE (see Fig. 2), as well as by the SMEI satellite. Our analysis confirmed the estimated orbital period of the system ($P = 45.15$ d.) and the lack of detectable additional periodic signal in both components.

The spectra of the system were obtained with the BESO spectrograph on the Bochum 1.5-m Hexapod Telescope at the Cerro Armazones Observatory. The spectra of the individual components were extracted with the method of spectral disentangling using a time series of 65 spectra. Atmospheric parameters of each individual component (disentangled spectra) were derived from an optimal fit using a precalculated grid of synthetic spectra and a genetic optimisation algorithm. The fitting was performed in the 4400 – 4650 Å spectral region, for the fixed surface gravity values and the light ratio estimated by Mérand et al. (2011). The analysis reveals effective temperatures of the components of $T_1 = 10\,250$ K, $T_2 = 9\,450$ K, and a projected rotational velocity of $v \sin i_1 = 130$ km s^{-1}, $v \sin i_2 = 138$ km s^{-1}, for the primary and secondary, respectively. These values are in agreement with the estimations presented by Mérand et al. (2011). The best fits to the spectra are presented in Fig. 3.

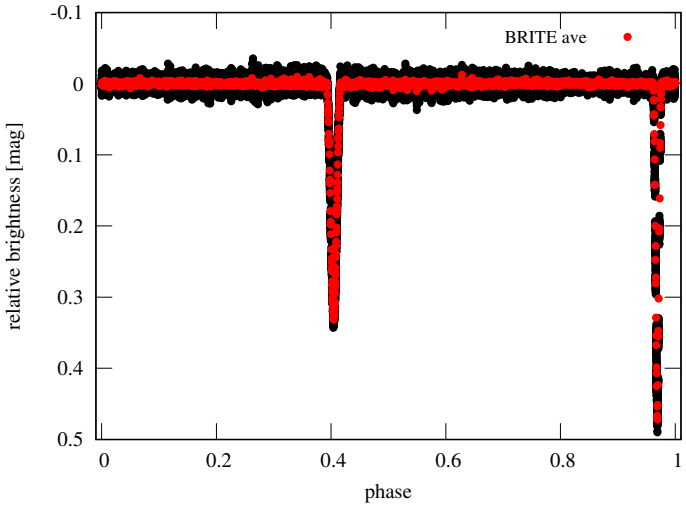

Figure 2. BRITE light curve of δ Vel. Red points indicate averaged data.

We have also studied the following SB1 systems with β Cephei components: EN Lac, V381 Car, and the β Cephei binary pair itself. The analysis of about

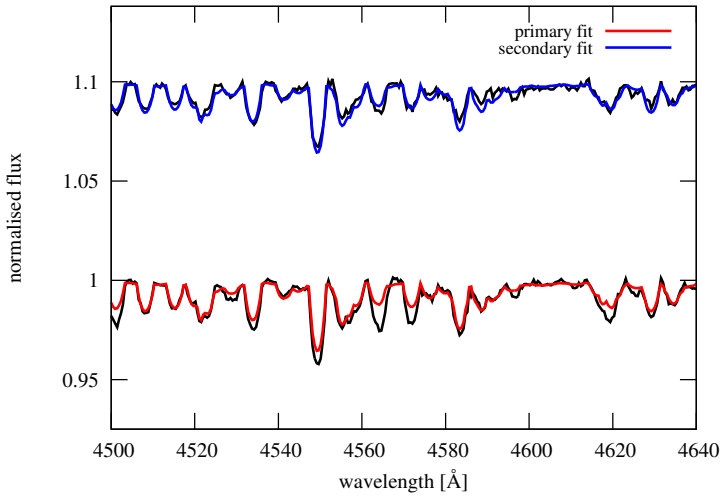

Figure 3. The most optimal fits to disentangled spectra of δ Vel components. The spectra of the secondary are shifted for clarity of the plot.

1 000 spectra of EN Lac was carried out in order to disentangle the system components, but due to pulsations it is a challenging task, so the target needs further investigation. We have also performed the simulations of the β Cephei binary system, which reveals that the secondary component contributes about 2% to the total flux of the system (at $\lambda = 5\,500$ Å). More than a thousand spectra were obtained for the target and the technique of adding spectra in quadrature phases is being implemented. We have also performed spectral disentangling for the V381 Car system, which reveals a weak secondary spectrum. The detailed analysis of that object will be described elsewhere.

Acknowledgements. MR acknowledges support by the National Science Center through the grant 2015/16/S/ST9/00461, AP through the grant 2016/21/B/ST9/01126, KP was supported by the Croatian Science Foundation under the grant 2014-09-8656. The authors thank prof. R. Chini for putting spectra of δ Vel at their disposal. The analysis was based on data collected by the BRITE Constellation satellite mission, designed, built, launched, operated and supported by the Austrian Research Promotion Agency (FFG), the University of Vienna, the Technical University of Graz, the Canadian Space Agency (CSA), the University of Toronto Institute for Aerospace Studies (UTIAS), the Foundation for Polish Science and Technology (FNiTP MNiSW), and the National Science Centre (NCN). This work is supported by the ERC through a Starting Grant. Some of the observations reported here were obtained with the Southern African Large Telescope (SALT).

References

Bramall, D. G., Sharples, R., Tyas, L., et al., The SALT HRS spectrograph: final design, instrument capabilities, and operational modes. 2010, in Proc. SPIE, Vol. **7735**, *Ground-based and Airborne Instrumentation for Astronomy III*, 77354F

Jackson, B. V., Buffington, A., Hick, P. P., Kojima, M., & Tokumaru, M., Comparison of Solar Mass Ejection Imager (SMEI) White Light Observations with IPS Velocity. 2004, *AGU Fall Meeting Abstracts*, SH21A

Kervella, P., Thévenin, F., & Petr-Gotzens, M. G., The nearby eclipsing stellar system δ Velorum . I.... 2009, *Astron. Astrophys.*, **493**, 107

Kolbas, V., Pavlovski, K., Southworth, J., et al., Spectroscopically resolving the Algol triple system. 2015, *Mon. Not. R. Astron. Soc.*, **451**, 4150, DOI: 10.1093/mnras/stv1261

Kozłowski, S. K., Konacki, M., Ratajczak, M., et al., BACHES - a compact échelle spectrograph for radial-velocity surveys with small telescopes. 2014, *Mon. Not. R. Astron. Soc.*, **443**, 158, DOI: 10.1093/mnras/stu1148

Mérand, A., Kervella, P., Pribulla, T., et al., The nearby eclipsing stellar system δ Velorum. III. Self-consistent fundamental parameters and distance. 2011, *Astron. Astrophys.*, **532**, A50, DOI: 10.1051/0004-6361/201116896

Pablo, H., Whittaker, G. N., Popowicz, A., et al., The BRITE Constellation Nanosatellite Mission: Testing, Commissioning, and Operations. 2016, *Publ. Astron. Soc. Pac.*, **128**, 125001, DOI: 10.1088/1538-3873/128/970/125001

Ratajczak, M. & Pigulski, A., Massive Eclipsing Binaries Observed by BRITE. 2018, in *3rd BRITE Science Conference*, ed. G. A. Wade, D. Baade, J. A. Guzik, & R. Smolec, 118–122

Ratajczak, M., Pigulski, A., & Pavlovski, K., B-type stars in eclipsing binaries. 2017, in *Second BRITE-Constellation Science Conference, Proceedings of PAS volume 5*, ed. K. Zwintz & E. Poretti, 128–133

Southworth, J., DEBCat: A Catalog of Detached Eclipsing Binary Stars. 2015, in Astronomical Society of the Pacific Conference Series, Vol. **496**, *Living Together: Planets, Host Stars and Binaries*, ed. S. M. Rucinski, G. Torres, & M. Zejda, 164

Torres, G., Andersen, J., & Giménez, A., Accurate masses and radii of normal stars: modern results and applications. 2010, *Astronomy and Astrophysics Review*, **18**, 67, DOI: 10.1007/s00159-009-0025-1

Vanzi, L., Chacon, J., Helminiak, K. G., et al., PUCHEROS: a cost-effective solution for high-resolution spectroscopy with small telescopes. 2012, *Mon. Not. R. Astron. Soc.*, **424**, 2770

Vanzi, L., Zapata, A., Flores, M., et al., Precision stellar radial velocity measurements with FIDEOS... 2018, *Mon. Not. R. Astron. Soc.*, **477**, 5041

Weiss, W. W., Rucinski, S. M., Moffat, A. F. J., et al., BRITE-Constellation: Nanosatellites for Precision Photometry of Bright Stars. 2014, *Publ. Astron. Soc. Pac.*, **126**, 573

Contrib. Astron. Obs. Skalnaté Pleso **49**, 258 – 263, (2019)

A relation between the brightness maxima separation and mass ratio in contact binaries

B. Debski

Astronomical Observatory of the Jagiellonian University
Orla 171, 30-244 Krakow, Poland (E-mail: bartlomiej.debski@uj.edu.pl)

Received: November 15, 2018; Accepted: February 11, 2019

Abstract. A new effect concerning the light curves of contact binaries is presented. The separation between the brightness maxima tends to be larger than half of the orbital phase, if the primary minimum is defined as during which the more massive star is being eclipsed.
Key words: stars – contact binaries – starspots

1. Introduction

The W UMa-type contact binaries are one of the most most peculiar examples of the interacting binary stars. According to their canonical model (Lucy, 1968), they consist of two (near) main sequence stars, both of which overfill their inner critical Lagrangian surface. It leads to sharing a common convective envelope, as well as to the interchange of both energy and mass (Flannery, 1976). Such configuration should result in an equal surface temperature for a whole binary with a brightness distribution dictated by the gravitational and limb darkenings.

The light curves of contact binaries are known to have minima of similar depths due to eclipses and prominent maxima between them due to the tidal distortion of the components. These light curves are known also for their intrinsic variability, which is commonly explained with the photospheric phenomena (starspots). The occurence of such a starspot introduces many interesting asymmetries to the light curve. One of them is the O'Connell effect, i.e. the difference between the height of the maxima. Other effect is tied to the brightness minima and the evolution of the starspot. As the starspot changes its location, the minima change their depths. It might be even the case that the minimum which once was the deeper one for some time is the shallower one (see Fig. 1, the KIC 9283826 have been phased using elements from the Kepler Eclipsing Binary Catalogue, KEBC, Prša et al., 2011). That in turn opens up a debate on the naming convention of the minima. Namely, which is the 'primary' one?

There are two definitions of the 'primary' minimum. First, purely phenomenological, identify the primary minimum as the deeper one. In the second definition the primary minimum is the one during which the more massive component of a binary is being eclipsed. Here, the more massive component is also called the 'primary component'. In case of contact binaries, the more massive

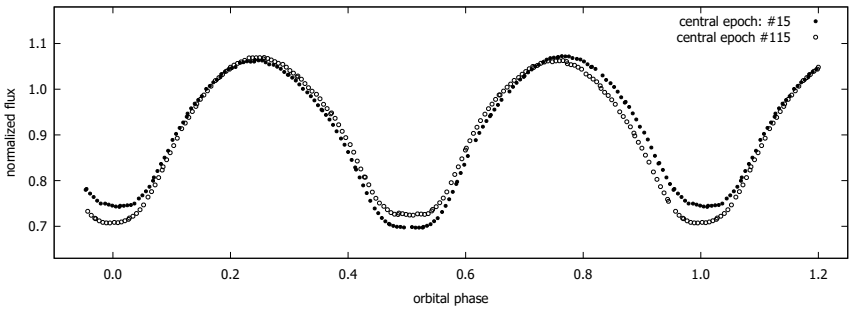

Figure 1. A comparison of the phase curves of KIC 9283826 taken with the Kepler Spacecraft in the Long Cadence mode. The first curve (solid circles) comes from a range of orbital epochs 10-21, while the second curve covers a range of epochs 110-121.

component is also the larger one. Together with the second definition it implies that, with a proper inclination, the total eclipse, which corresponds to the flat-bottom minimum in the light curve, is always during the secondary minimum. In this work the primary star is the more massive one and we employ the second definition of the primary minimum.

During our preliminary studies on Kepler light curves (Debski et al., 2015) we found that the positions of brightness maxima hardly ever lie exactly on the orbital phases $\phi = 0.25$ and $\phi = 0.75$. One could argue that such a feature is also caused by a starspot-related light curve distortion, but the effect exists even in light curves with no noticeable O'Connell effect. Since this new effect was initially found in the high-precision Kepler light curves, the measurement error also cannot be the cause.

We define the separation as $S = \phi_{max_{II}} - \phi_{max_I}$, where ϕ_{max_I} and $\phi_{max_{II}}$ are the positions in phase of the primary and secondary maximum, respectively. While conducting the aforementioned preliminary studies, we found presumptive evidence for a possible connection between the mass ratio and the maxima separation. Namely, the light curves of contact binaries with a mass ratio $q = \frac{M_2}{M_1} < 1$ had the separation between the brightness maxima always larger than half of the orbital phase, $S > 0.5\,\phi$ (here M_1 and M_2 are masses of the primary and secondary components, respectively).

2. Observational data

In this study we used two different observational samples. The first one (a.k.a the *Kepler sample*) consists of 49 objects from the KEBC. All objects in the Kepler sample have light curves resembling contact binaries, almost equal minima depths and a prominent tidal distortion effect. The most important trait

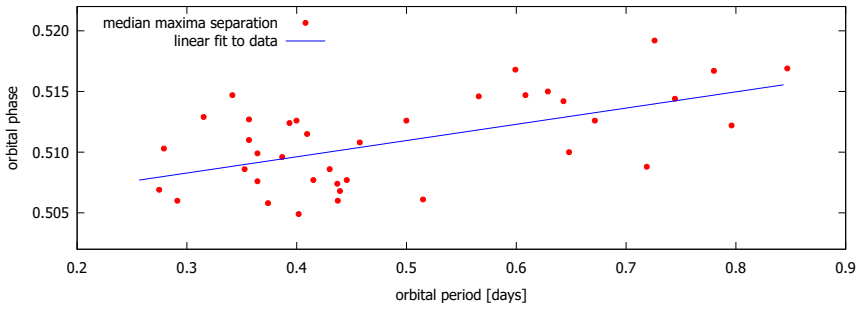

Figure 2. Median Maxima Separation in the Kepler sample as a function of the orbital period. The correlation coefficient is $r = 0.51$, while the slope of the fitted linear function is $b = 0.0134 \pm 0.0040$.

is that all the objects in the Kepler sample have very similar inclinations, close to $i = 90°$. This fact reduces the possible influence of the inclination on the observables. The second sample (hereafter the *Suhora sample*, Kreiner et al., 2003) is build with 42 objects observed in *UBVRI* Bessel filters and all have spectroscopically determined mass ratios (Lu et al., 2001).

2.1. Kepler light curves

Because most of the objects in *KEBC* don't have a measured mass ratio q, we settled on ensuring a proper light curve phasing to satisfy $q = M_2/M_1 < 1$. In order to do so, we focused our attention on light curves with a flat-bottom minimum. As mentioned before, having the secondary eclipse a flat-bottom one, it is to be expected to have a binary with a mass ratio $q < 1$.

The criteria of choosing objects into our sample from the *KEBC* were as follows: 1) the light curve must be flagged as an FB (flat-bottom minimum), 2) the light curve must have the shape typical for a contact binary, i.e. a great ellipsoidal effect present and not obvious beginning and end of the minimum profile, 3) minima must have similar depths, since both components should have similar surface temperatures. The rule of thumb was to throw away light curves with a minima depth difference larger than 0.1 of the normalized flux. We searched the database for objects with the orbital period less than $P = 1\,day$ and the morphology parameter $morph > 0.6$.

We measured the separations of the maxima in every subsequent orbital period for every object, while the measured phase curves were binned dynamically. The size of the bin varied, so that the phase curve would consist of at least 120 datapoints. Since the maxima separations were varying in time, for every object we calculated its Median Maxima Separation (MMS). We found that for

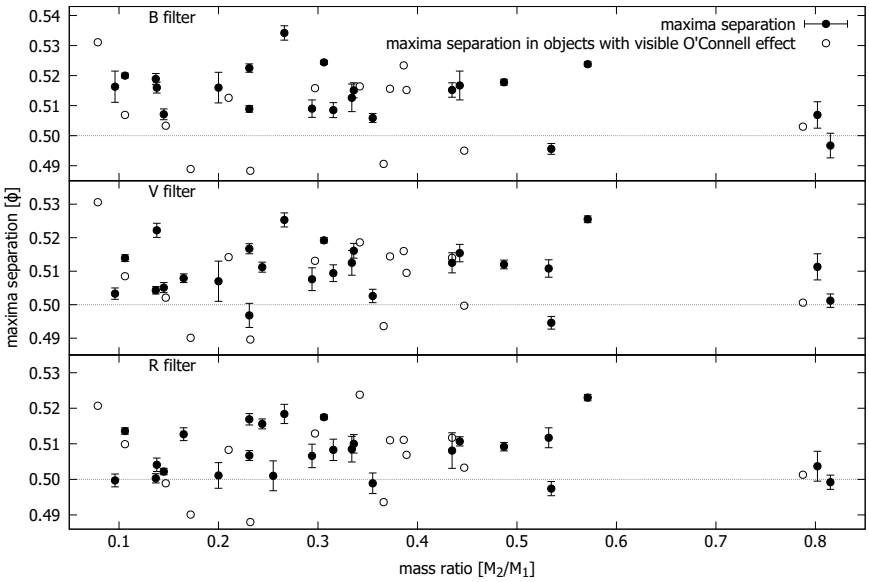

Figure 3. Measured maxima separations in the Suhora sample in the selected filters.

all objects in the sample the MMS was larger than half of the orbital phase, $MMS > 0.5\,\phi$, if their mass ratio was set as $q < 1$ (see Fig. 2).

2.2. Multicolor & spectroscopic observations

Objects in the next sample were all rephased so that their mass ratio would be $q < 1$ and their maxima positions were found by fitting the Gaussian functions to the narrow, selected parts of their phase curves. We measured maxima separations in every filter and found that, in general, the maxima separations were again $S > 0.5\,\phi$. Only the light curves with a noticeable O'Connell effect were not following this rule. We presented the results in selected filters in Fig. 3. There is no visible correlation between the separation of the maxima and the mass ratio, possibly due to the high diversity of the sample in inclination. There is a visible trend in the color: in general, the redder the filter, the smaller the maxima separation.

3. Numerical simulations

We designed a grid of synthetic light curves with the Wilson-Devinney code (Wilson & Devinney, 1971). We found that the main factor shaping the distribution of maxima separations was the limb darkening. The influence of gravitational brightening was smaller, but also non-negligible. Because of that, we

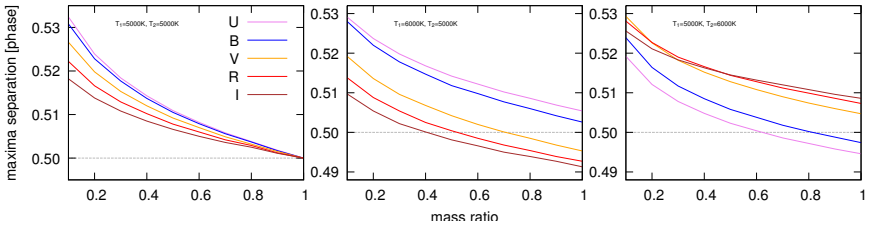

decided to extend the simulations from binaries with a components of equal surface temperatures, to extreme cases of temperature inequality. In the simulations the temperatures are taken with a $1000\,K$ step, but we do not simulate binaries with a temperature difference between the components larger than $1000\,K$. Our grid covers contact binaries with a range of mass ratios ($q \in (0.1, 1)$, step 0.1), fill-out factors ($ff \in (0, 100\%)$, step 10%) and inclinations ($i \in (20°, 90°)$, step $2°$ for $i \geq 70°$ and $10°$ for $i < 70°$). The fill-out factor ff here is defined as follows: $ff = (\Omega_s - \Omega_{L_1})/(\Omega_{L_2} - \Omega_{L_1}) \cdot 100\%$, where Ω_s is the pseudopotential of the binary surface, while Ω_{L_1} and Ω_{L_2} are the pseudopotentials of the equipotential surfaces crossing Lagrangian points L_1 and L_2 respectively. An excerpt from the simulated maxima separations is presented in Fig. 3.

The most interesting insight from the simulations is that the maxima separation for contact binaries with components of equal temperatures indeed are larger than half of the orbital phase, if $q < 1$. The same holds even for highly unequal temperatures of the components, but only in case of $ff = 0\%$. Moreover, the lower the mass ratio, the maxima separation should be larger. Interestingly, the separation of the maxima also grows significantly larger for lower inclinations. When compared in different filters, maxima separation differs, as it should, if it is caused predominantly by the limb darkening.

4. Summary

The main conclusion of this study is that the maxima separation in the light curves of contact binaries hardly ever equal to the half of the orbital phase of the system. If one defines a primary minimum as the one during which the more massive star is being eclipsed, then it is possible to point at it by phasing the light curve so that the maxima separation would be $S > 0.5\,\phi$. The primary minimum will then sit at phase $\phi = 0.0$. According to our simulations, this criterion works for all cases of $T_1 \leq T_2$. In case of $T_1 = T_2 + 1000\,K$, the criterion works always for $ff = 0\%$.

The simulations show that for very low mass ratios maxima separation should grow rather large, up to $S > 0.52\,\phi$ and larger. This is not the case in the Suhora sample. The lack of trend there may lead to at least two scenarios: 1) low-mass contact binaries have some hidden traces of photospheric phenomena, not visible straight in the light curves yet influencing the maxima

separation or 2) models of contact binaries and/or limb darkening coefficients in these are faulty. The second scenario is particularly worrisome, as many studies of contact binaries rely on the accuracy of the Wilson-Devinney code.

Another opportunity rises with the multicolor observations of the maxima separation effect. The simulations showed that the maxima separation is greater in bluer filters in case of components of equal surface temperatures or the primary being the hotter one. The separation S becomes larger for redder filters only if the secondary is hotter than the primary. Interestingly, almost all objects from the Suhora sample (from those which show no O'Connell effect) have *color separation*, that is $S_B - S_R$ (maxima separation in the B filter minus the separation in the R filter) larger than zero, which means that in their case the primary is most likely the hotter one. That holds even if the secondary minimum is the deeper one, which makes *color separation* a promising tool for studying a temperature ratio in the binary.

Acknowledgements. This work has been supported by a Polish National Science Centre Grant 2016/23/N/ST9/01218 and the Polish Ministry of Science and Higher Education grant 7150/E-338/M/2018.

References

Debski, B., Zola, S., & Baran, A., Light Curve Morphology: The Evolution of the O'Connell Effect and the Maxima Separation. 2015, in Astronomical Society of the Pacific Conference Series, Vol. **496**, *Living Together: Planets, Host Stars and Binaries*, ed. S. M. Rucinski, G. Torres, & M. Zejda, 293

Flannery, B. P., A Cyclic Thermal Instability in Contact Binary Stars. 1976, *Astrophys. J.*, **205**, 217, DOI: 10.1086/154266

Kreiner, J. M., Rucinski, S. M., Zola, S., et al., Physical parameters of components in close binary systems. I. 2003, *Astron. Astrophys.*, **412**, 465, DOI: 10.1051/0004-6361:20031456

Lu, W., Rucinski, S. M., & Ogłoza, W., Radial Velocity Studies of Close Binary Stars. IV. 2001, *Astron. J.*, **122**, 402, DOI: 10.1086/321131

Lucy, L. B., The Structure of Contact Binaries. 1968, *Astrophys. J.*, **151**, 1123, DOI: 10.1086/149510

Prša, A., Batalha, N., Slawson, R. W., et al., Kepler Eclipsing Binary Stars. I. Catalog and Principal Characterization of 1879 Eclipsing Binaries in the First Data Release. 2011, *Astron. J.*, **141**, 83, DOI: 10.1088/0004-6256/141/3/83

Wilson, R. E. & Devinney, E. J., Realization of Accurate Close-Binary Light Curves: Application to MR Cygni. 1971, *Astrophys. J.*, **166**, 605, DOI: 10.1086/150986

Contrib. Astron. Obs. Skalnaté Pleso **49**, 264 – 270, (2019)

Using wide hot subdwarf binaries to constrain Roche-lobe overflow models

J. Vos[1], M. Vučković[2], X. Chen[3,4,5], Zh. Han[3,4,5], T. Boudreaux[6], B.N. Barlow[6], R. Østensen[7] and P. Németh[8,9]

[1] *Institut für Physik und Astronomie, Universität Potsdam, Germany, (E-mail: astro@jorisvos.eu)*

[2] *Instituto de Física y Astronomía, Universidad de Valparaiso, Chile*

[3] *Yunnan Observatories, Chinese Academy of Sciences, P. R. China*

[4] *Key Laboratory for the Structure and Evolution of Celestial Objects, P. R. China*

[5] *Center for Astronomical Science, Chinese Academy of Sciences, P. R. China*

[6] *Department of Physics, High Point University, NC, USA*

[7] *Department of Physics, Astronomy, and Materials Science, Missouri State University, MO, USA*

[8] *Astronomical Institute of the Czech Academy of Sciences, Czech Republic*

[9] *Astroserver.org, 8533 Malomsok, Hungary*

Received: November 1, 2018; Accepted: March 27, 2019

Abstract. Hot subdwarf B (sdB) stars are evolved core helium burning stars that have lost most of their hydrogen envelope due to binary interaction on the red giant branch. As sdB stars in wide binary systems can only be created by stable Roche lobe overflow, they are a great test sample to constrain the theoretical models for stable mass loss on the red giant branch. We present here the findings of a long term monitoring program of wide sdB+MS binaries.

We found two main features in the orbital parameters. The majority of the systems have eccentric orbits with systems on longer orbital period having a higher eccentricity. As these systems have undergone mass loss near the tip of the RGB, tidal circularisation theory predicts them to be circularized. Our observations suggest that efficient eccentricity pumping mechanisms are active during the mass loss phase. Secondly we find a strong correlation between the mass ratio and the orbital period. Using binary evolution models, this relation is used to derive both an upper and lower limit on the initial mass ratio at which RLOF will be stable. These limits depend on the core mass of the sdB progenitor.

Key words: stars: subdwarfs – stars: binaries: spectroscopic – stars: fundamental parameters – stars: evolution

1. Introduction

Hot subdwarf B-type (sdB) stars are core He burning stars with a very tiny hydrogen envelope ($M_{\rm H} < 0.02 M_{\odot}$). The current consensus is that they can

only be formed through binary interaction in a binary in which the primary is a red giant near the tip of the red giant branch (RGB). There are three main formation channels for sdB stars. sdBs in short period binaries are formed through a common envelope ejection, while sdBs in wide binaries are formed through stable Roche-lobe overflow (RLOF). Single sdB binaries can be formed by the merger of two white dwarf stars.

The evolution of a typical subdwarf star in the Herzsprung-Russel diagram is shown in the left panel of Fig. 1. The sdB progenitor ascends the red giant branch until it starts the binary interaction phase near the tip of the RGB, and loses its envelope. This model shows an early flasher where He is ignited under degenerate conditions very fast after leaving the RGB. Due to neutrino cooling the He-flashes take place in a shell outside the core and work their way inwards until the star starts central He burning. This is shown in the right panel of Fig. 1. After the core He-burning phase, the subdwarf stars undergoes a phase of stable He-shell burning where it heats up and becomes an sdO star. As the star is too light to burn heavier elements, it then moves on to the white dwarf cooling track.

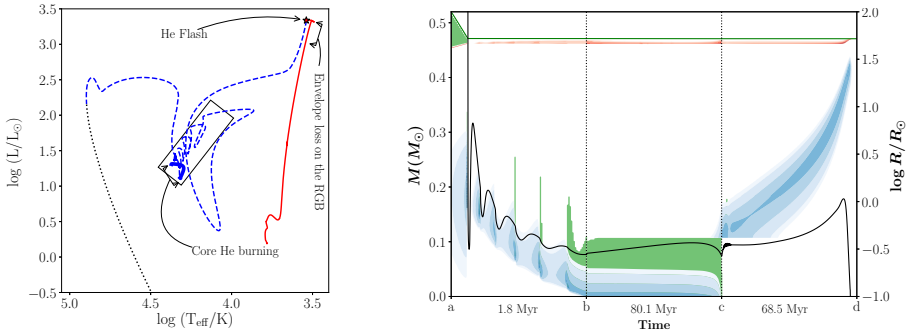

Figure 1. Left: The evolution of a typical hot subdwarf star in the HR diagram. The main sequence and red giant branch are indicated in red full line. The He burning phase is indicated by blue dashed line, of which the core He burning phase is shown in full blue line. The white dwarf cooling track is indicated in black dotted line. Right: The profile from the sdB star during the Helium burning phase. He burning regions are shown in blue color, while H burning regions are shown in red. The convective zones in the star are shown in green. The full black line shows the radius of the sdB star. The figure is split in three stages: He flashes (a-b), stable He core burning (b-c) and stable He shell burning (c-d) with the time the star spends in each of them indicated below the figure. Figures calculated with the MESA stellar/binary evolution code (Vos, 2015)

Because an sdB star can only be formed though binary interaction mechanisms, they are ideal objects to study these mechanisms. When considering low

mass stars($M < 2M_{\odot}$), roughly 15% of the binary stars will interact on the red giant branch (Vos et al., 2017). However, many of the interaction mechanisms are not understood from first principles, e.g. the stability of mass loss, the exact treatment of the CE phase, the mass loss fractions during stable RLOF and many more. With this project we aim to use hot subdwarf stars as a test sample for binary interaction models.

2. The wide sdB+MS sample

A long term project to monitor wide sdB+MS binaries was started in 2009 using the HERMES spectrograph at the 1.2m Mercator telescope in La Palma and in later stages extended to the southern hemisphere using CHIRON at the 1.5m SMARTS and FEROS at the 2.2m MPG telescope. In combination with dedicated programs at the smaller telescopes there is also a long running bad weather program using UVES at the 8.2m VLT telescope.

Currently 19 systems have sufficient phase coverage to solve the orbital parameters (Vos et al., 2012, 2013, 2017, 2019). In combination with two sdB binaries solved by Barlow et al. (2013), one by Deca et al. (2018) and one solved from photometry by Otani et al. (2018) the total sample contains 23 systems of which 21 with a known mass ratio. In the following subsections the more interesting results of this survey are summarized.

2.1. Period and eccentricity distribution

The distribution of the orbital periods of the sdB+MS sample is shown in the left panel of Fig. 2. The orbital periods range from around 450 days up to 1400 days with a peak around 1000 days. Original model predictions for the orbital periods of sdB binaries formed by the stable RLOF channel peaked at 100 days (Han et al., 2002, 2003). Based on these observations, Chen et al. (2013) adapted the original models by including a more realistic treatment of angular momentum and the inclusion of atmospheric RLOF. The improved models match very well with the observed period distribution.

The eccentricity of these systems is unexpected. All of the wide sdB+MS binaries have undergone a mass loss phase in their past, at which point the sdB progenitor filled its Roche lobe. Tidal interaction theory clearly shows that all of these systems should have circularised long before the onset of RLOF. To explain the observed eccentricity, an eccentricity pumping process is necessary that is active during or after the mass loss phase. Vos et al. (2015) tested several such processes and found that a combination of two was able to explain the observed eccentricities: a) phase dependent mass loss where more mass is lost near apastron than near periastron leading to an increase in eccentricity of the orbit, and b) the interaction of a stable circumbinary disk formed during the mass loss phase with the binary which can further increase the eccentricity of the orbit.

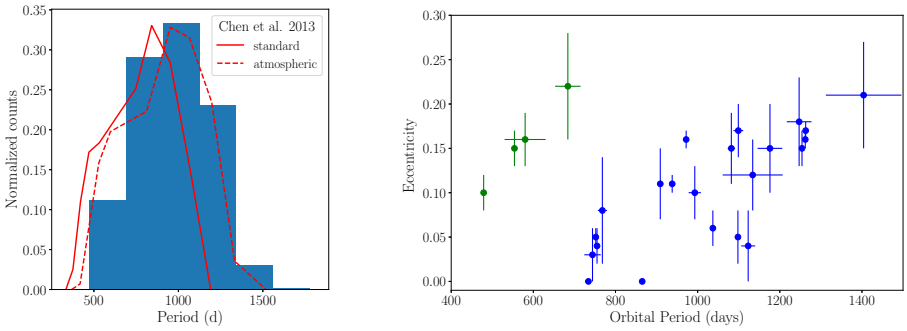

Figure 2. Left: The distribution of orbital periods in blue, and the predicted distribution by Chen et al. (2013) in red line. The dotted red line indicates models which include atmospheric RLOF (Figure taken from Vos et al. (2019)). Right: the eccentricity vs the orbital period for all solved wide sdB+MS binaries. There is an indication for the existence of systems at shorter orbital periods which have higher eccentricity, indicated in green. This second group is selected by eye based on its different location in both the Period - Eccentricity and the Period - Mass ratio distribution (See also Fig. 3).

Orbits with significant non-zero eccentricity are not uncommon in binary systems containing an evolved component. In fact, the majority of the long period post-AGB, S-type and Ba stars in long period binaries have significant eccentric orbits, with eccentricities as high as 0.6 (e.g. Vos et al., 2017; Oomen et al., 2018). The eccentricity pumping mechanisms in Vos et al. (2015) can offer an explanation for these systems as well.

2.2. Mass ratio - period relation

One of the most interesting results from this project up till now is the discovery of a strong correlation between the mass ratio and the orbital period in the wide sdB+MS sample shown in the left panel of Fig 3. Taking into account that the sdB mass is well constrained to $M_{\rm sdB} = 0.47 \pm 0.05 M_{\odot}$, this means that sdB stars with low mass companions have short orbital periods and those with high mass companions have long orbital periods.

This P-q relation can be used to derive a stability criterion for RLOF. Using the current mass of the sdB, which is related to the orbital period (Chen et al., 2013), and the mass ratio, the mass of the companion can be determined. By assuming a likely progenitor mass between 1 and 2 $M_{\odot}$ for the sdB, the initial mass ratio at the start of mass loss can be derived. As the current sdB mass is the same as the core mass of the sdB progenitor (which is a red giant at the start of RLOF), a relation between the initial mass ratio at the start of mass loss and the core mass of the sdB progenitor is found. This clearly shows an

upper limit depending on the core mass, leading to a stability criterion of:

$$q_c = M_{\rm sdB}^{-2} - 0.25 M_{\rm sdB} - 2.55 \quad (1)$$

This stability criterion together with the relation between the initial mass ratio and the core mass at the start of RLOF is shown in the right panel of Fig. 3. The initial mass ratio is shown for sdB progenitors with 2 different initial masses: 1.2 and 1.6 $M_\odot$. The exact initial mass can not be determined from the current evolution models, thus a range between 1 and 2 $M_\odot$ was used in the derivation of the stability criterion.

The 3 systems plotted in green squares in the left plot of Fig. 3 are not included in the derivation of the stability criterion. Due to their separate location in both the period - eccentricity and period - mass ratio distribution it is likely that they are formed by a different channel. The shorter orbital period indicates that they likely descend from higher mass sdB progenitors ($M > 2M_\odot$) that ignited He under non-degenerate conditions. This also explains why there are only few of them found. For an extended discussion see Vos et al. (2019).

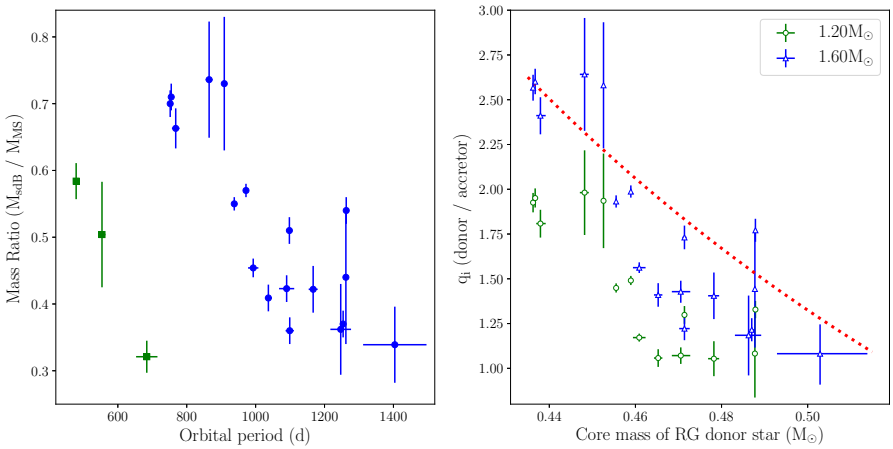

Figure 3. Left: The orbital period vs the mass ratio of all solved wide sdB+MS binaries. There is a strong correlation between the period and mass ratio, and there are again a second group visible (green squares, same systems as in Fig. 2). Right: The initial mass ratio in function of the core mass of the sdB progenitor at the start of the RLOF phase. The initial mass ratio is shown for 2 different sdB progenitor masses: 1.2 and 1.6 $M_\odot$. A clear upper limit is visible determined by the stability of RLOF. The derived stability criterion is shown in red dashed line. Figures adapted from Vos et al. (2019).

3. Conclusions

Hot subdwarf binaries are useful systems to study binary interactions mechanisms. Due to the reasonable brightness and the need for observations spread over a long time, small and medium sized telescopes are ideal for this survey project. Currently two main results from this survey are the discovery that the majority of the systems are eccentric, which indicates that eccentricity pumping mechanisms are at play during or after the mass loss phase. The second result is the discovery of a strong correlation between orbital period and mass ratio, which is linked directly to the stability of RLOF. Based on this correlation the first observational stability criterion for mass loss on the red giant branch was derived.

References

Barlow, B. N., Liss, S. E., Wade, R. A., & Green, E. M., Two New Long-period Hot Subdwarf Binaries with Dwarf Companions. 2013, *Astrophys. J.*, **771**, 23, DOI: 10.1088/0004-637X/771/1/23

Chen, X., Han, Z., Deca, J., & Podsiadlowski, P., The orbital periods of subdwarf B binaries produced by the first stable Roche Lobe overflow channel. 2013, *Mon. Not. R. Astron. Soc.*, **434**, 186, DOI: 10.1093/mnras/stt992

Deca, J., Vos, J., Németh, P., et al., Evolutionary constraints on the long-period subdwarf B binary PG 1018-047. 2018, *Mon. Not. R. Astron. Soc.*, **474**, 433, DOI: 10.1093/mnras/stx2755

Han, Z., Podsiadlowski, P., Maxted, P. F. L., & Marsh, T. R., The origin of subdwarf B stars - II. 2003, *Mon. Not. R. Astron. Soc.*, **341**, 669, DOI: 10.1046/j.1365-8711.2003.06451.x

Han, Z., Podsiadlowski, P., Maxted, P. F. L., Marsh, T. R., & Ivanova, N., The origin of subdwarf B stars - I. The formation channels. 2002, *Mon. Not. R. Astron. Soc.*, **336**, 449, DOI: 10.1046/j.1365-8711.2002.05752.x

Oomen, G.-M., Van Winckel, H., Pols, O., et al., Orbital properties of binary post-AGB stars. 2018, *ArXiv e-prints*

Otani, T., Oswalt, T. D., Lynas-Gray, A. E., et al., Orbital Characteristics of the Subdwarf-B and F V Star Binary EC 20117-4014 (=V4640 Sgr). 2018, *Astrophys. J.*, **859**, 145, DOI: 10.3847/1538-4357/aab9bf

Vos, J. 2015, Exploring the evolution of wide hot-subdwarf binaries, PhD thesis, University of Leuven, Belgium

Vos, J., Østensen, R. H., Degroote, P., et al., The orbits of subdwarf B + main-sequence binaries. I. The sdB+G0 system PG 1104+243. 2012, *Astron. Astrophys.*, **548**, A6, DOI: 10.1051/0004-6361/201219723

Vos, J., Østensen, R. H., Marchant, P., & Van Winckel, H., Testing eccentricity pumping mechanisms to model eccentric long-period sdB binaries with MESA. 2015, *Astron. Astrophys.*, **579**, A49, DOI: 10.1051/0004-6361/201526019

Vos, J., Østensen, R. H., Németh, P., et al., The orbits of subdwarf-B + main-sequence binaries. II. Three eccentric systems; BD +29°3070, BD +34°1543 and Feige 87. 2013, *Astron. Astrophys.*, **559**, A54, DOI: 10.1051/0004-6361/201322200

Vos, J., Østensen, R. H., Vučković, M., & Van Winckel, H., The orbits of subdwarf-B + main-sequence binaries. III. The period-eccentricity distribution. 2017, *Astron. Astrophys.*, **605**, A109, DOI: 10.1051/0004-6361/201730958

Vos, J., Vučković, M., Chen, X., et al., The orbital period-mass ratio relation of wide sdB+MS binaries and its application to the stability of RLOF. 2019, *Mon. Not. R. Astron. Soc.*, **482**, 4592, DOI: 10.1093/mnras/sty3017

Contrib. Astron. Obs. Skalnaté Pleso **49**, 271 – 277, (2019)

Evolution of 2MASS J16211735+4412541 light curve in the quiescent state

S. Zola[1,2], W. Ogloza[2], M. Drozdz[2], P. Szkody[3], B. Debski[1], G. Stachowski[2], A. Kobak[4] and J. Krüger[5]

[1] *Astronomical Observatory, Jagiellonian University, ul. Orla 171, 30-244 Krakow, Poland, (E-mail: szola@oa.uj.edu.pl)*

[2] *Mt. Suhora Observatory, Pedagogical University, ul. Podchorazych 2, 30-084 Krakow, Poland*

[3] *Department of Astronomy, University of Washington, Box 351580, Seattle, WA 98195, USA*

[4] *Centre for Astronom, Faculty of Physics, Astronomy and Informatics, Nicolaus Copernicus University, ul. Grudziadzka 5, 87-100 Torun, Poland*

[5] *Astronomical Observatory Institute, Faculty of Physics, Adam Mickiewicz University, ul. Sloneczna 36, 60-286 Poznan, Poland*

Received: October 30, 2018; Accepted: January 24, 2019

Abstract. We report follow-up multifilter observations of the binary 2MASS J16211735+4412541 taken in BVRI colors in 2017 and 2018. We present the evolution of the shape of the light curve, as well as the preliminary results from modelling the system. Based on these and a spectrum showing double peaked Balmer emission lines, we infer that the system still contains an accretion disk and not a bare white dwarf.

Key words: stars:individual: 2MASS J16211735+4412541 – binaries:eclisping – cataclysmic variables

1. Introduction

2MASS J16211735+4412541 is a short-period eclipsing binary (P=0.21^d) which was classified as a contact system based on its light curve as gathered by large surveys. In June 2016 it unexpectedly brightened by about 2 magnitudes and stayed in this high state for about 2 weeks. The shape of the light curve changed during the outburst, but within a week the system returned to its pre-outburst state. Following the initial alert by Drake et al. (2016), this event drew much attention from observers and resulted in the posting of several pieces of information about its properties in the Astronomer's Telegrams (Maehara (2016); Scaringi et al. (2016); Zejda & Pejcha (2016); Thorstensen (2016)). Less than two weeks later, on June 12, the light curve taken in the R filter displayed the usual, pre-outburst shape, typical of an eclipsing binary system with a close configuration (Zola et al., 2016).

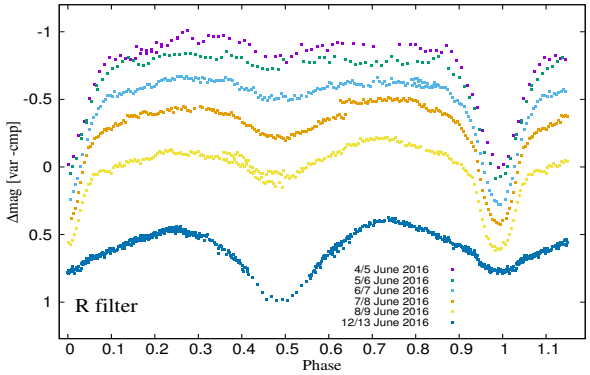

Figure 1. Changes of the light curve shape during the 2016 outburst. Only R filter data are shown here.

We monitored the outburst starting from June 4, first with the 35 cm Maksutov telescope in Krakow, and from June 6 also with the 50 cm telescope at the same site and the 60 cm at the Mt. Suhora observatory. In Fig. 1 we show the light curve of the system taken at outburst (June 4-8, 2016) and that taken on June 12, when the system returned to its low state. During the outburst, the depths of the minima were reversed, with the one which was shallower in the low state becoming the deeper one. The shape of the light curve appeared distorted, and changing rapidly while the system brightness was declining. The depth of the deeper (outburst) minimum was decreasing and once the system returned to the low state it again became the less deep one, as observed in the pre-outburst state. Furthermore, the decline was so fast that it was impossible to match the level of the light curve at the same phase taken at the beginning and the end of a night (see Fig. 1).

The first model of the system was published by Kjurkchieva et al. (2017), who analyzed the system light curve and arrived at the conclusion that due to enhanced mass transfer, a temporary disk was being created around the white dwarf which, after some time, entirely accreted leaving the system consisting of a main sequence star and a bare white dwarf. A diskless model of the binary in quiescence was also proposed by Qian et al. (2017) with brightening being due to mass transfer bursts. The study by Zola et al. (2017) based on photometry, spectroscopy and data taken by SWIFT concluded that this cataclysmic type variable does harbour an accretion disk even more than a year after the outburst. Kimura et al. (2018) arrived at a similar model of a high inclination system with an accretion disk in both high and low states.

2. Spectroscopic Observation

Two spectra were obtained with the Double Imaging Spectrograph on the Apache Point Observatory 3.5m telescope on April 17, 2018, using 10 min exposures for each. The grating settings, calibration and reduction were identical to those in Zola et al. (2017). The red spectra (Fig. 2) show deep doubling of the Balmer lines, clearly indicative of an accretion disk viewed at relatively high inclination.

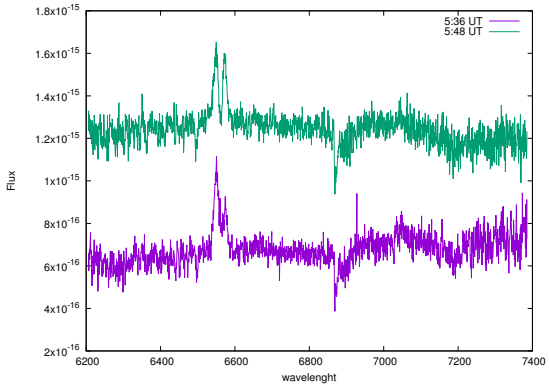

Figure 2. Spectra of 2MASS J16211735+4412541 obtained with the APO 3.5m telescope (red) on April 17, 2018. The shape of the H_α line changed between the two consecutive spectra taken at 5:36 UT (top) and at 5:48 UT (bottom). The top spectrum is offset for clarity.

3. Photometric Observations and Light Curve Modeling

In the beginning and ending of the 2017 and 2018 observing seasons we collected a complete multicolor light curve of J1621 using two telescopes: the 50 cm telescope at the Astronomical Observatory of the Jagiellonian University in Krakow and the 60 cm telescope at the Mt. Suhora Observatory of the Pedagogical University. Both telescopes are equipped with Apogee CCDs and a set of wide-band filters. Light curves in B and V filters were taken at the Mt. Suhora observatory, while those in R and I filters at the Krakow site. A series of calibration images were taken every night. Reduction of observations were performed in a standard way, with calibration images for bias, dark and flatfield (taken on sky) done with the IRAF package, while extraction of magnitudes with the CMunipack package (an interface to the DAOPHOT program) using the aperture method. The resulting light curves (phase versus differential magnitudes) gathered in 2017 and 2018 are shown in Figs. 3 and 4. Note the different depths of the pri-

mary (phase 0) minima between May 2017 and August 2018 (the most recent observations). On all dates, the depth of the primary minimum grows toward shorter wavelengths and in the U filter this minimum becomes deeper (see the left panel of Fig. 4) than the secondary one. The most recent light curves in R and I filters may be taken as typical of a close or contact system.

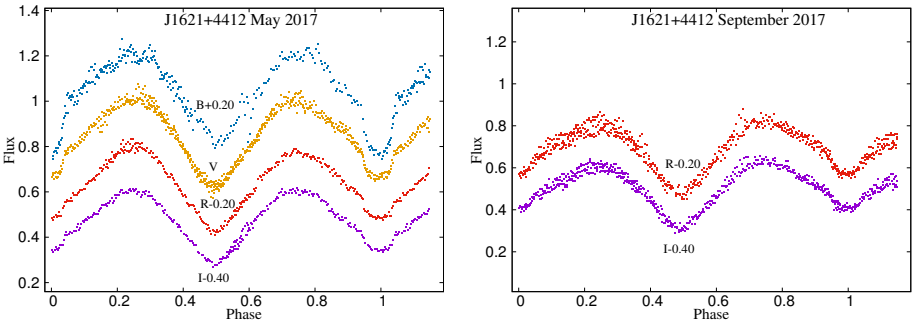

Figure 3. The light curves of 2MASS J16211735+4412541 taken in May (left panel) and September (right panel) 2017.

We phased the newly gathered light curves and recalculated magnitude differences into flux normalizing it to 1 at the first quadrature. We also analyzed the BVR light curves published by Qian et al. (2017). The ephemeris listed in Zola et al. (2017) was used for phasing and the primary minimum corresponds to the minimum which was deeper during the outburst. While doing light curve modelling, we applied the disk model and followed the same procedure as outlined in Zola et al. (2017). The program we used for light curve simulation is a modified Wilson-Devinney code altered by adding a phenomenological disk model that surrounds the star eclipsed at phase 0. The disk is assumed to be optically thick and its vertical thickness grows linearly with radius. The secondary star is assumed to fill in the Roche lobe. This model accounts for effects due to the presence of the disk, e.g. obscuration of primary and secondary stars by the disk, self obscuration of the disc face. The search for the best fit is done by the Monte Carlo search method. Further details were given in Zola (1991) and Zola (1992).

The theoretical model lines and the observed data (gathered in April 2016 and March 2018) are shown in Fig. 5.

We were able to obtain fits of reasonable quality to all quiescent light curves within the disk model. Even the fit derived to the sparse U filter data resembles the observations pretty well. Comparing the current system parameters with those obtained during the outburst, its is obvious that both the accretion disk and the accreting white dwarf are cooling, plausibly as a result of decreasing mass transfer rate. The temperature of the accreting component, the accretion

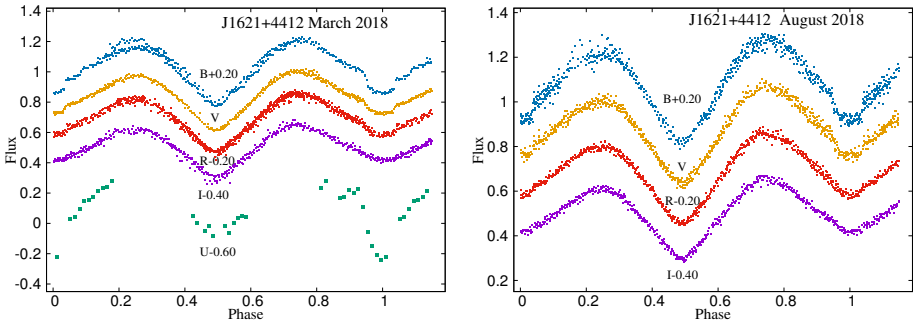

Figure 4. Light curve of 2MASS J16211735+4412541 gathered in March (left panel) and in August 2018 (right panel).

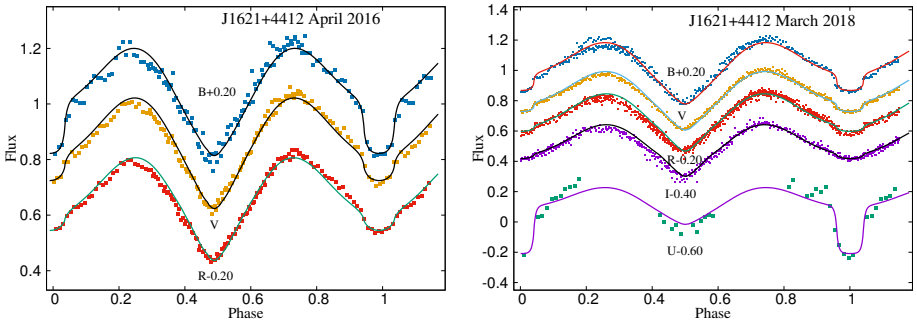

Figure 5. Model light curves (continuous lines) plotted along observed ones (square symbols). The pre-outburst (April 2016) LC is shown in the left panel, while that taken in March 2018 in the right one.

disk size (in units of components separation) and its light contribution to the system total light (at phases of full accretion disk visibility) derived from modelling are presented in Table 1.

4. Conclusions

– We have gathered multicolor light curves of J16211735+4412541 during quiescence twice in the 2017 and 2018 observing seasons. The most recent one was taken in August 2018, more than 2 years after the 2016 outburst. One can notice the decreasing depth of the primary minimum with time, especially well seen in the B filter, indicating cooling of the accreting white dwarf and the surrounding accretion disk.

Table 1. White dwarf temperature, the size of an accretion disk and the disk light contribution in B and R filters.

Date	T_1 [K]	r_d	l_d [B]	l_d [R]	remarks
Apr 2016	11 360	0.32	16%	5%	this work
Jun 6 2016	44 600	0.39	53%	44%	Zola et al. 2017
Aug 2016	14 350	0.45	10%	7%	Zola et al. 2017
Mar 2017	28 180	0.44	5%	10%	this work
May 2017	16 830	0.34	16%	6%	this work
Sep 2017	11 440	0.28	–	4%	this work
Mar 2018	16 850	0.29	4%	1%	this work
Aug 2018	11 430	0.33	9%	2%	this work

– The light curves are asymmetric, exhibiting an O'Connell effect with a lower level of the first quadrature. A cool spot located on the surface of the secondary, mass losing star could be the reason. An additional, smaller in quantity, rise of the flux in the descending part of the primary minimum may be due to a hot spot on the accretion disk.

– The properties of the target light curve and clearly visible double peaked Balmer emission lines lead to the conclusion that there is an accretion disk still present in the system two years after the outburst. A similar shape of the pre-outburst light curve indicates that it was presumably also present in April 2016, about two months before the outburst.

Acknowledgements. This work was partially supported by the NCN grant No. 2016/23/N/ST9/01218. PS acknowledges support from NSF grant AST 1514737.

References

Drake, A. J., Djorgovski, S. G., Mahabal, A. A., et al., CRTS discovery of an outburst from a short period binary system. 2016, *The Astronomer's Telegram*, **9112**

Kimura, M., Kato, T., Maehara, H., et al., On the nature of long-period dwarf novae with rare and low-amplitude outbursts. 2018, *Publ. Astron. Soc. Jap.*, **70**, 78, DOI: 10.1093/pasj/psy073

Kjurkchieva, D. P., Popov, V. A., Vasileva, D. L., & Petrov, N. I., The newly discovered eclipsing cataclysmic star 2MASS J16211735 + 4412541 and its peculiarity. 2017, *New Astronomy*, **52**, 8, DOI: 10.1016/j.newast.2016.10.001

Maehara, H., KWS pre-discovery observations of CSS160603:162117+441254 = 2MASS J16211735+4412541. 2016, *The Astronomer's Telegram*, **9113**

Qian, S.-B., Han, Z.-T., Zhang, B., et al., A New Stellar Outburst Associated with the Magnetic Activities of the K-type Dwarf in a White Dwarf Binary. 2017, *Astrophys. J.*, **848**, 131, DOI: 10.3847/1538-4357/aa8bb8

Scaringi, S., Mason, E., Van Winckel, H., & Escorza, A., Spectroscopic classification of 2MASS_J16211735+4412541. 2016, *The Astronomer's Telegram*, **9122**

Thorstensen, J., Time-resolved spectroscopy of CSS160603:162117+441254. 2016, *The Astronomer's Telegram*, **9141**

Zejda, M. & Pejcha, O., CSS160603:162117+441254 shows deep eclipses during the ongoing outburst. 2016, *The Astronomer's Telegram*, **9132**

Zola, S., RZ Oph - The Algol-type, long-period binary star with a thick accretion disk. 1991, *Acta Astronomica*, 213

Zola, S., KU Cyg - The Algol-type binary with an accretion disk. 1992, *Acta Astronomica*, 213

Zola, S., Ciprini, S., Debski, B., et al., CSS160603:162117+441254: pretending to be a contact system again. 2016, *The Astronomer's Telegram*, **9167**

Zola, S., Szkody, P., Ciprini, S., et al., Observational Study of an Unusual Cataclysmic Binary 2MASS J16211735+4412541. 2017, *Astron. J.*, **154**, 276, DOI: 10.3847/1538-3881/aa9565

Contrib. Astron. Obs. Skalnaté Pleso **49**, 278 – 286, (2019)

Surface inhomogeneities of the eclipsing binary ER Vul

İ. Özavcı, E. Bahar and H.V. Şenavcı

Department of Astronomy and Space Sciences, Faculty of Science, Ankara University, Tandoğan 06100 Ankara, Turkey, (E-mail: iozavci@ankara.edu.tr)

Received: November 2, 2018; Accepted: January 24, 2019

Abstract. We performed Doppler imaging of the eclipsing binary ER Vul using time-series mid-resolution (R $\sim$ 13500) spectra of the system. The spectra were acquired via the echelle spectrograph attached to the 0.4m Kreiken Telescope at the Ankara University Kreiken Observatory. We applied Least-Squares Deconvolution (LSD) technique in order to enhance SNRs of the velocity profiles to better resolve the spot signatures. We determined the mass ratio, q, as 0.949(19) and masses of the primary and secondary components as 1.108 (33) and 1.052 (34), respectively. The reconstructed images of both components show that cool spots are preferably located at high latitudes. We also investigated the chromospheric activity behaviour with the help of the spectral synthesis method. Both photospheric and chromospheric activity variations along with the orbital phase are in accordance with each other.

Key words: stars: activity – binaries: eclipsing – stars: imaging.

1. Introduction

RS CVn-type systems have remarkable significance in better understanding the dynamo mechanism working in close binary stars due to their strong magnetic activity. One of them, ER Vul, is a short-period RS CVn-type eclipsing binary system that has several activity-related studies in the literature after its classification by Hall (1976). The variability in the light curves of the system outside eclipses was attributed to the cool spot activity on both components (Olah et al., 1994; Ekmekçi et al., 2002; Wilson & Raichur, 2011; Pop & Vamoş, 2013). The activity of both components of ER Vul was confirmed by Çakırlı et al. (2003), who also revealed that the secondary star is more active than the primary one using the equivalent width (hereafter EQW) variations of H_α excess emission with the help of the spectral subtraction method. Using the high resolution spectroscopic data obtained from the Canada-France Hawaii Telescope (CFHT), Shkolnik et al. (2005) determined some orbital parameters of the system from radial velocity measurements and investigated the activity behaviour with the help of the Ca II emissions. They mentioned that the emissions are consequences of the activity of both components as well as a broad stream flowing toward the secondary. The Doppler images of the system obtained by Piskunov (1996) and Piskunov et al. (2001) showed large temperature difference as well as

the presence of a hot spot at sub-stellar points on both components. Piskunov (2008) revealed a non-axisymmetric dynamo action by analyzing the Doppler images of ER Vul. The most recent Doppler imaging study of the system was carried out by Xiang et al. (2015) using the code `DoTS`. They mentioned that the active regions were almost found in the hemisphere facing the other component, while they found no remarkable concentration of spots at the sub-stellar points.

In this work, we analyzed the mid resolution time-series spectroscopic data of the short-period RS CVn-type eclipsing binary ER Vul via the Doppler imaging and spectral synthesis methods in order to study the activity behaviour and determine some orbital parameters of the system. In addition to the long-term star-spot activity of ER Vul, we also presented the performance of a small telescope (D=0.4m) equipped with a mid-resolution spectrograph in point of image reconstruction of such active binary systems.

2. Observations and data reduction

The mid-resolution time series spectra of ER Vul were obtained between 1 and 19 July 2018, using the Shelyak *eShel* spectrograph attached to the 0.4m Kreiken Telescope at the Ankara University Kreiken Observatory. We obtained seventeen spectra of the system with an average resolution of R ∼13500 that cover the wavelength range between 4340 Å and 7400 Å. The data was taken using the exposure time of 3600 seconds that gives SNR values between 58 and 99. We also observed three slowly rotating and non-active template stars HD 143761 (G0V), HD 32147 (K3V) and HD 139777 (G1.5V) that are required by Doppler imaging (photospheres of the primary and secondary components and the spot temperature) and spectral synthesis methods (photospheres of the primary and secondary components). The data reduction as well as the wavelength calibration procedures were carried out with the help of the `AudeLA` software (Klotz et al., 2012). The normalization of the spectra was performed using our own code that was developed in `Python`.

We used the signal enhancing Least-Squares Deconvolution (LSD) technique by Donati et al. (1997) to better resolve the spot signatures on both components during Doppler imaging process. The linelist required by the LSD technique was obtained from the Vienna Atomic Line Database (Kupka et al., 1999), considering log g and $T_{\rm eff}$ of ER Vul. We obtained the SNR values of LSD profiles between 1500 and 1900. Considering the resolving power of the spectral data, we set the increment per pixel to 10 km s^{-1} during the calculation of LSD profiles.

3. Analysis

3.1. Orbital solution and Doppler imaging

We determined the RVs of both components of ER Vul by fitting synthetic rotation profiles to the LSD profiles (see Şenavcı et al., 2018, for more details). An example of a fitted LSD profile is given in Fig. 1. The radial velocity analysis of ER Vul was performed using the `rvfit` code developed by Iglesias-Marzoa et al. (2015). The RV data together with the model are also plotted in Fig. 1, while the parameters obtained from the RV analysis are given in Table 1.

We used the Doppler imaging code `DoTS` (Collier Cameron, 1997) to reveal the spot pattern on the surfaces of both components of ER Vul. The code is based on two temperature model to mimic the spotted and unspotted photosphere and uses the Maximum-Entropy Method (MEM) to find the best fitting spot distribution across the stellar surface by means of a spot filling factor. The LSD profiles and best fit models are shown in Fig. 2, while the surface reconstructions of the primary and the secondary components are in Fig. 3.

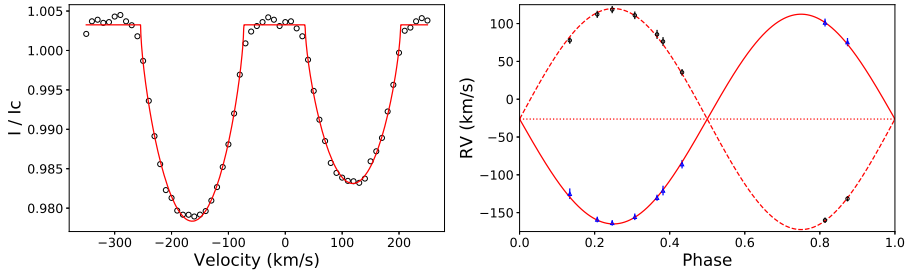

Figure 1. Left panel: An example of LSD profile (open circles) at phase 0.247 and the theoretical fit (red solid line) used in RV determination. Right panel: RV curve of ER Vul. The open blue triangles and open black circles represent the RV data of primary and secondary components of ER Vul, respectively. The solid and dashed red lines belong to the RV fit to the data.

3.2. Spectral subtraction

We also investigated the chromospheric activity behavior of ER Vul with the help of the spectral subtraction technique that was first suggested by Barden (1985). In this context, we determined the EQWs of the H_α excess emission for each spectrum considering the flux contribution from both components depending on the orbital phase and hence the eclipses. The details of the code used concerning the spectral subtraction process can be found in the study by Şenavcı

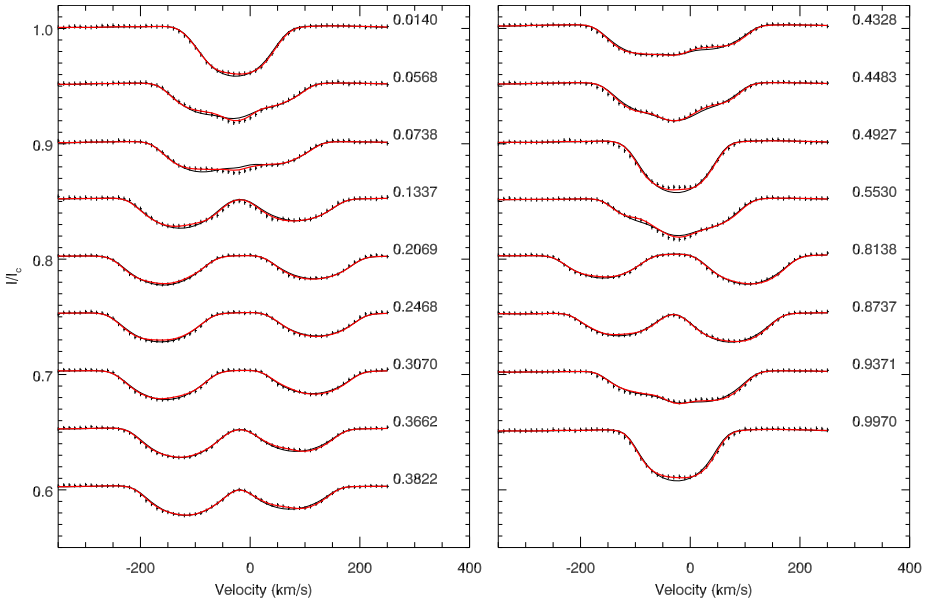

Figure 2. Phase-ordered LSD profiles of ER Vul. Black solid lines represent the synthetic velocity profiles generated using the system parameters, while the red solid lines show the maximum entropy regularized models of ER Vul.

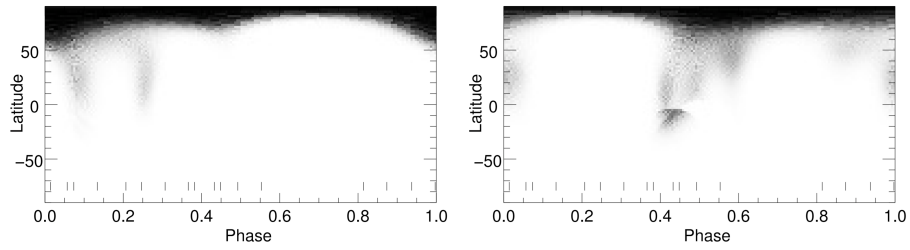

Figure 3. The Mercator projection of reconstructed image for the primary (left panel) and the secondary (right panel) component of the ER Vul system.

et al. (2018). An example of H_α excess emission obtained for two different orbital phases using spectral subtraction is shown in Fig. 4.

4. Discussion and conclusion

We have presented an activity investigation of both components of the RS CVn type eclipsing binary ER Vul, using time-series mid-resolution spectra of the

Table 1. Some physical parameters of ER Vul and comparisons from the literature.

Parameter	Value	Reference
$q = M_2/M_1$	0.949 ±0.019	This Study
	0.960 ±0.050	a
K_1 (km s^{-1})	138.67 ±2.06	This Study
	139.30 ±4.60	a
	135.20 ±0.63	b
K_2 (km s^{-1})	146.13 ±1.90	This Study
	144.30 ±5.20	a
	142.82 ±0.76	b
i [°]	66.63	c
V_γ [km s^{-1}]	-26.26 ±1.24	This Study
	-28.30 ±3.30	a
$T_0(HJD)$	2445220.40964	This Study
$P(d)$	0.698095	This Study
$T_{\rm eff,1}(K)$	6000	c
$T_{\rm eff,2}(K)$	5750	c
$a(R_\odot)$	4.28 ±0.04	This Study
M_1 $(M_\odot)$	1.108 ±0.033	This Study
M_2 $(M_\odot)$	1.052 ±0.034	This Study

Note: Reference: a. Çakırlı et al. (2003), b. Shkolnik et al. (2005), c. Harmanec et al. (2004).

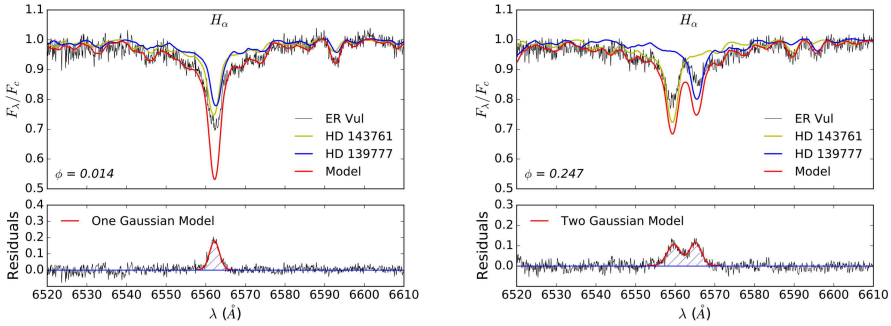

Figure 4. The spectral subtraction of the H$_\alpha$ line obtained at phases 0.014 (left panel) and 0.247 (right panel) of ER Vul. The yellow and blue solid lines show the spectra of the primary and secondary components, respectively, while the red solid line represents the total flux. The bottom panels show the residuals from the fit as well as the area of excess emission.

system with the help of the Doppler imaging and spectral subtraction techniques. The resolution of the spectral data (R $\sim$ 13500) used in this study may not be sufficient for such Doppler imaging purposes. However, both the high $v \sin i$ value of the system (84 km/s and 78 km/s for the primary and secondary, respectively) and the resolving power allow us to resolve star spots larger than 13 degrees, which can be considered as a good resolution for such a telescope and spectrograph system. The exposure time of 3600 seconds used during the observations corresponds to $\sim$ 6% of the orbital period of ER Vul, which causes the phase smearing phenomenon and hence leads to another limitation for the reconstructed surface images. The effects of phase smearing on the surface reconstruction was investigated in detail in the study by Şenavcı et al. (2018) that includes the Doppler imaging of the RS CVn type SV Cam using the code `DoTS`. They found that the long exposure times do not lead to considerable uncertainties for large spots, while the spot features smaller than 12 degrees that correspond to longest exposure times can be artefacts. In our case, the exposure time of 3600 seconds corresponds to 21.5 degrees (0.06 in orbital phase units). Therefore, we may infer that the spot features smaller than 21.5 degrees may not be reliable, while there is no smaller feature present in the reconstructed maps as seen from Fig. 3. It is clear from Fig. 3 that the primary and secondary components show high latitude spots as well as the extensions from lower latitudes. These distributions of spots for both the primary and secondary are consistent with the results that was obtained by Xiang et al. (2015). The spots location on the hemisphere facing to each other are also compatible with their surface maps.

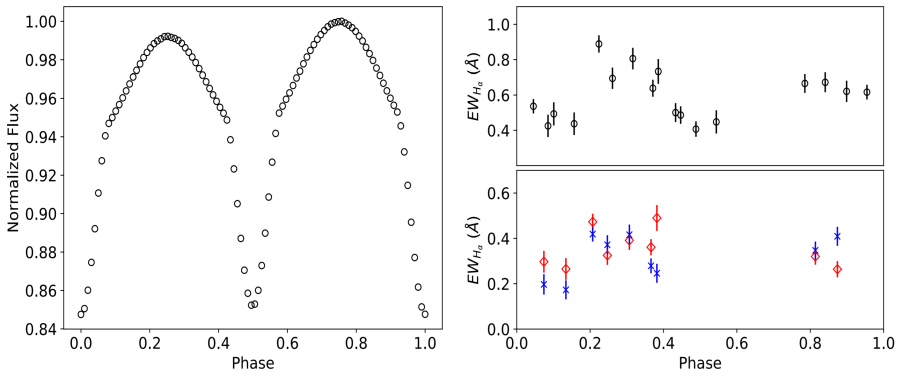

Figure 5. Left panel:The light curve generated by `DoTS` code, using the DI map. Upper right panel: The variation of H_α excess emission coming from both components along with the orbital phase. Lower right panel: The EQW variation of primary (red diamonds) and secondary (blue crosses) component.

As seen from Fig. 5, the EQW variation of the H_α line along with the orbital phase has the highest value at around phase ϕ=0.25, while the minimum excess emission occurs at around phase ϕ=0.50. The lower right panel of Fig. 5 shows the EQW variation of H_α excess emission obtained individually from both components. A similar behaviour can be clearly seen, with a slightly higher emission from the primary. This result is not compatible with the one obtained by Çakırlı et al. (2003), who mentioned that the secondary component is more active. Besides, Gunn & Doyle (1997) also mentioned that the secondary component is more active than the primary, while Newmark (1990) found that the primary is the more active one. Such a behaviour may be a consequence of the interaction between the magnetic fields of both components as suggested by Uchida & Sakurai (1985).

The light curve shown in the left panel of Fig. 5 was generated with the help of the code `DoTS`, using the resultant surface maps of both primary and secondary components obtained from Doppler imaging. The lower light level seen at phase ϕ=0.25 compared to ϕ=0.75 indicates a higher distribution of spots visible at ϕ=0.25. It also confirms the variation of H_α excess emission. This result suggests that both photospheric and chromospheric regions are associated with each other.

Acknowledgements. The authors acknowledge the support by The Scientific and Technological Research Council of Turkey (TÜBİTAK) through the project 1001 - 115F033.

References

Barden, S. C., A study of short-period RS Canum Venaticorum and W Ursae Majoris binary systems - The global nature of H-alpha. 1985, *Astrophys. J.*, **295**, 162, DOI: 10.1086/163361

Çakırlı, Ö., İbanoğlu, C., Frasca, A., & Catalano, S., Hα variations of the RS CVn type binary ER Vulpeculae. 2003, *Astron. Astrophys.*, **400**, 257, DOI: 10.1051/0004-6361:20021885

Şenavcı, H. V., Bahar, E., Montes, D., et al., Star-spot distributions and chromospheric activity on the RS CVn type eclipsing binary SV Cam. 2018, *Mon. Not. R. Astron. Soc.*, **479**, 875, DOI: 10.1093/mnras/sty1469

Collier Cameron, A., Eclipse mapping of late-type close binary stars. 1997, *Mon. Not. R. Astron. Soc.*, **287**, 556, DOI: 10.1093/mnras/287.3.556

Donati, J.-F., Semel, M., Carter, B. D., Rees, D. E., & Collier Cameron, A., Spectropolarimetric observations of active stars. 1997, *Mon. Not. R. Astron. Soc.*, **291**, 658, DOI: 10.1093/mnras/291.4.658

Ekmekçi, F., Özeren, F. F., & Ak, H., Chromospherically active binary systems, RT And and ER Vul: 1995-1998 observations and spot distributions. 2002, *Astronomische Nachrichten*, **323**, 31, DOI: 10.1002/1521-3994(200203)323:1¡31::AID-ASNA31¿3.0.CO;2-2

Gunn, A. G. & Doyle, J. G., Environments of active close binaries. I. ER Vulpeculae. 1997, *Astron. Astrophys.*, **318**, 60

Hall, D. S., The RS CVn Binaries and Binaries with Similar PROPERTIÉS. 1976, in Astrophysics and Space Science Library, Vol. **60**, *IAU Colloq. 29: Multiple Periodic Variable Stars*, ed. W. S. Fitch, 287

Harmanec, P., Božić, H., Thanjavur, K., et al., An improved ephemeris and physical elements of ER Vul. 2004, *Astron. Astrophys.*, **415**, 289, DOI: 10.1051/0004-6361:20034614

Iglesias-Marzoa, R., López-Morales, M., & Jesús Arévalo Morales, M., The rvfit Code: A Detailed Adaptive Simulated Annealing Code for Fitting Binaries and Exoplanets Radial Velocities. 2015, *Publ. Astron. Soc. Pac.*, **127**, 567, DOI: 10.1086/682056

Klotz, A., Delmas, R., Marchais, D., Pujol, M., & Jasinski, C., The AudeLA software. 2012, in Astronomical Society of India Conference Series, Vol. **7**, *Astronomical Society of India Conference Series*, .15

Kupka, F., Piskunov, N., Ryabchikova, T. A., Stempels, H. C., & Weiss, W. W., VALD-2: Progress of the Vienna Atomic Line Data Base. 1999, *Astron. Astrophys., Suppl.*, **138**, 119, DOI: 10.1051/aas:1999267

Newmark, J. S. 1990, Coordinated optical and ultraviolet observations of short period RS CVn and W UMa type stars, PhD thesis, Pennsylvania State University, University Park.

Olah, K., Budding, E., Kim, H.-L., & Etzel, P. B., The active close binary system ER Vulpeculae. 1994, *Astron. Astrophys.*, **291**, 110

Piskunov, N., Doppler imaging of eclipsing binaries. 1996, in IAU Symposium, Vol. **176**, *Stellar Surface Structure*, ed. K. G. Strassmeier & J. L. Linsky, 45

Piskunov, N., Doppler imaging. 2008, *Physica Scripta Volume T*, **133**, 014017, DOI: 10.1088/0031-8949/2008/T133/014017

Piskunov, N., Vincent, A., Duemmler, R., Ilyin, I., & Tuominen, I., Doppler Imaging of Eclipsing Binary Systems ER Vul and TY Pyx (CD-ROM Directory: contribs/piskunov). 2001, in Astronomical Society of the Pacific Conference Series, Vol. **223**, *11th Cambridge Workshop on Cool Stars, Stellar Systems and the Sun*, ed. R. J. Garcia Lopez, R. Rebolo, & M. R. Zapaterio Osorio, 1285

Pop, A. & Vamoş, C., Orbital period modulation of the eclipsing binary system ER Vulpeculae: Real or not? 2013, *New Astronomy*, **23**, 27, DOI: 10.1016/j.newast.2013.02.003

Shkolnik, E., Walker, G. A. H., Rucinski, S. M., Bohlender, D. A., & Davidge, T. J., Investigating Ca II Emission in the RS Canum Venaticorum Binary ER Vulpeculae Using the Broadening Function Formalism. 2005, *Astron. J.*, **130**, 799, DOI: 10.1086/431364

Uchida, Y. & Sakurai, T., Magnetodynamical processes in interacting magnetospheres of RS CVn binaries. 1985, in IAU Symposium, Vol. **107**, *Unstable Current Systems and Plasma Instabilities in Astrophysics*, ed. M. R. Kundu & G. D. Holman, 281–285

Wilson, R. E. & Raichur, H., Distance and temperature from absolute light curves of three eclipsing binaries. 2011, *Mon. Not. R. Astron. Soc.*, **415**, 596, DOI: 10.1111/j.1365-2966.2011.18741.x

Xiang, Y., Gu, S., Cameron, A. C., & Barnes, J. R., Doppler images of the eclipsing binary ER Vulpeculae. 2015, *Mon. Not. R. Astron. Soc.*, **447**, 567, DOI: 10.1093/mnras/stu2458

Contrib. Astron. Obs. Skalnaté Pleso **49**, 287 – 292, (2019)

Deriving photospheric parameters and elemental abundances for a sample of stars showing the FIP effect

B. Seli[1,2], **L. Kriskovics**[1] **and K. Vida**[1]

[1] *Konkoly Observatory, Research Centre for Astronomy and Earth Sciences, Hungarian Academy of Sciences, 1121 Budapest, Konkoly Thege Miklós út 15-17, Hungary*

[2] *Eötvös University, Department of Astronomy, 1518 Budapest, Pf. 32, Hungary*

Received: October 31, 2018; Accepted: January 21, 2019

Abstract. One puzzling question in solar physics is the difference between elemental abundances in the photosphere and the corona. Elements with low first ionization potential (FIP) can be overabundant in the corona compared to the photosphere under certain circumstances. The same phenomenon has been observed on a handful of stars, while a few of them show the inverse effect. But not all the stars in the original sample had precise photospheric abundances derived from optical spectra, so for some the solar values were adopted. In this work we make homogeneous abundance measurements from optical spectroscopy.

We collected spectra of 16 stars showing the FIP effect with the 1-m RCC telescope of Konkoly Observatory, with resolution of $\lambda/\Delta\lambda \sim 21\,000$. We determine the fundamental astrophysical parameters ($T_{\rm eff}$, $\log g$, $[M/H]$, $\xi_{\rm mic}$, $v \sin i$) and individual elemental abundances with the SME spectral synthesis code using MARCS2012 model atmosphere and spectral line parameters from the Vienna Atomic Line Database (VALD).

Key words: Stars: abundances – Stars: atmospheres – Stars: fundamental parameters – Techniques: spectroscopic

1. Introduction

When working on X-ray spectra, solar physicists found a discrepancy between the abundances of several elements compared to the known photospheric values. In the solar corona, elements with low first ionization potential (FIP) are enhanced by approximately a factor of 4 (Laming, 2015, and references therein). This phenomenon – the FIP effect – was later observed on a handful of stars. The magnitude of the effect shows a spectral type dependence, for stars cooler than K5 the inverse FIP effect was observed, where the low FIP elements are depleted in the corona.

However, for some of these stars the photospheric composition is unknown or the available data were collected from several different sources. Substituting

Table 1. The observed sample. Mean S/N was calculated with the DER_SNR algorithm (Stoehr et al., 2008).

star	number of spectra	S/N	star	number of spectra	S/N
EK Dra	17	77	β Com	5	140
EQ Peg A	24	39	ϵ Eri	42	100
EV Lac	23	23	κ Cet	20	113
GJ 338 A	31	69	ξ Boo A	5	124
GJ 338 B	27	66	ξ Boo B	5	58
Sun	3	99	π^1 UMa	6	143
70 Oph A	5	122	π^3 Ori	40	151
70 Oph B	15	80	χ^1 Ori	35	105

the stellar elemental composition with the solar abundance pattern makes it impossible to determine whether the coronal abundances are caused by the FIP effect or if those elements are just over/underabundant in that particular star. In this work we present new fundamental parameters and elemental abundances derived from new homogeneous optical measurements for stars that are known to show the FIP effect.

2. Data

We selected our target stars showing the FIP effect from Table 2 in Laming (2015). We excluded objects that are not visible from Hungary, as well as faint targets (fainter than $V \sim 8^m$) to ensure sufficient S/N. Our final observed sample consists of 16 main-sequence stars with spectral types ranging from F6 to M3. The full list can be seen in Table 1.

Observations were made with the 1-m RCC telescope of Konkoly Observatory, equipped with an echelle spectrograph with $\lambda/\Delta\lambda \sim 21\,000$ mean resolution. The observations were carried out in March, June, August and November 2017. The quality of most spectra is sufficient for spectral synthesis, while for the fainter stars we have to combine spectra collected on the same night to ensure a high enough S/N.

Data reduction was carried out with the standard IRAF tasks. A ThAr spectral lamp was used for wavelength calibration. 28 echelle orders were extracted from each image uniformly, but we restrict our analysis to the 5000–7000 Å wavelength range, because below 5000 Å the S/N gradually decreases while the region after 7000 Å is dominated by telluric absorption lines.

3. Spectral synthesis

We used the Spectroscopy Made Easy (SME) code (Valenti & Piskunov, 1996) with MARCS2012 model atmosphere to calculate the necessary parameters from the continuum normalized spectra. We downloaded spectral line data from the Vienna Atomic Line Database (VALD; Piskunov et al., 1995) using the "extract stellar" option.

Before fitting the individual elemental abundances, the fundamental parameters of the stars are needed. These are effective temperature ($T_{\rm eff}$), surface gravity ($\log g$), metallicity ([M/H]), microturbulence ($\xi_{\rm mic}$) and projected rotational velocity ($v \sin i$). Another necessary parameter is macroturbulent velocity ($\xi_{\rm mac}$), but since it is hard to disentangle the contribution of $\xi_{\rm mac}$ from the other line broadening effects, we chose to apply the following empirical relation from Valenti & Fischer (2005) rather than fitting $\xi_{\rm mac}$:

$$\xi_{\rm mac} = 3.5 + (T_{\rm eff} - 5777)/650 \tag{1}$$

The following initial parameters were used: $\log g = 4.5$ dex (since all stars in the sample are dwarfs), $[M/H] = 0$ dex, $\xi_{\rm mic} = 1\,{\rm km\,s^{-1}}$, $v \sin i = 20\,{\rm km\,s^{-1}}$ and $T_{\rm eff}$ inferred from spectral type. In general, no reasonable fit can be achieved if we iterate all parameters at once, so we fit them in the following order: first $\xi_{\rm mic}$ and $v \sin i$ simultaneously, then $T_{\rm eff}$, then $[M/H]$ and $\xi_{\rm mic}$. After this step we fit $\log g$ with a line list containing only the Na D and Mg b lines, since their strong line wings are more sensitive to gravity. Then we proceed by downloading a new line list from VALD with the parameters derived so far. With this we fit $T_{\rm eff}$ once again, then $[M/H]$. The results can be seen in Table 2, and Figure 1 shows an example of the observed and synthetic spectrum of π^3 Ori.

After these steps we fit the individual elemental abundances (along with $[M/H]$), namely C, Na, Mg, Al, Si, S, Ca, Ti, Mn, Fe, Ni and Ba. Some interesting elements whose coronal abundance can be derived from X-ray spectra have no transitions in the observed wavelength range, so their abundances cannot be determined. The result can be seen in Figure 2 for 8 stars from the sample. While most elements show no deviation from the solar scale, there is a clear Ba enhancement for all these stars. According to D'Orazi et al. (2009) young stars tend to have higher Ba abundance, based on empirical results. All stars appearing in Figure 2 are younger than the Sun with the oldest one being β Com with age of $\sim$2.5 Gyr, which explains the observed overabundance. To check if any of these 8 stars could be Ba dwarfs we fit other s-process elements, although with larger uncertainties. It turns out that the abundances of La and Ce are high, while the Y and Zr content is approximately solar, which disproves the idea. Al abundances also seem to be higher than solar, but since there are only a few and relatively weak Al lines to fit, it is likely not a real physical effect.

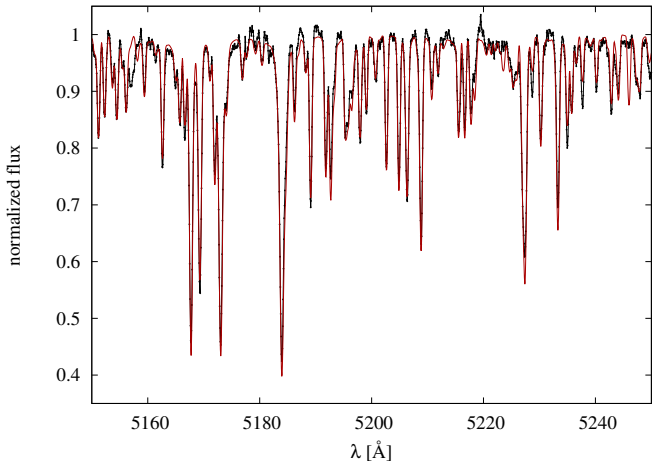

Figure 1. Observed (black) and synthetic (red) spectrum of π^3 Ori near the Mg triplet.

3.1. Error estimation

SME is robust enough to give almost identical results for all spectra collected from the same star on the same night. This means that the standard deviations calculated from multiple observations are small (e.g. 5 K in $T_{\rm eff}$) and can only be used for consistency check. So the uncertainties of the derived parameters have to be obtained by different means, for example by seeing how much each parameter can be altered before it affects the determination of the other parameters during the fit. The expected average uncertainties are 50 K in $T_{\rm eff}$, 0.1 dex in $\log g$, 0.1 dex in $[M/H]$, 0.3 km s^{-1} in $\xi_{\rm mic}$ and 3 km s^{-1} in $v \sin i$.

After comparing our results with available literature data, it seems that our $\log g$ values are usually lower by $\sim$0.1 dex. However that should have little effect on the derived abundances. Running the abundance fitting procedure with 0.2 dex difference in $\log g$ modifies the final abundances by $\sim$0.08 dex. 200 K change in $T_{\rm eff}$ results in $\sim$0.07 dex difference, while 0.6 km s^{-1} change in $\xi_{\rm mic}$ gives $\sim$0.05 dex.

4. Conclusion

It appears that a metre-class telescope equipped with a mid-high resolution spectrograph is enough to determine elemental abundances for bright enough stars with the spectral synthesis method. We have collected spectra of 16 stars that show the FIP effect, and carried out the abundance analysis for 8 of them. The remaining stars are the fainter ones with noisier spectra, so for them the

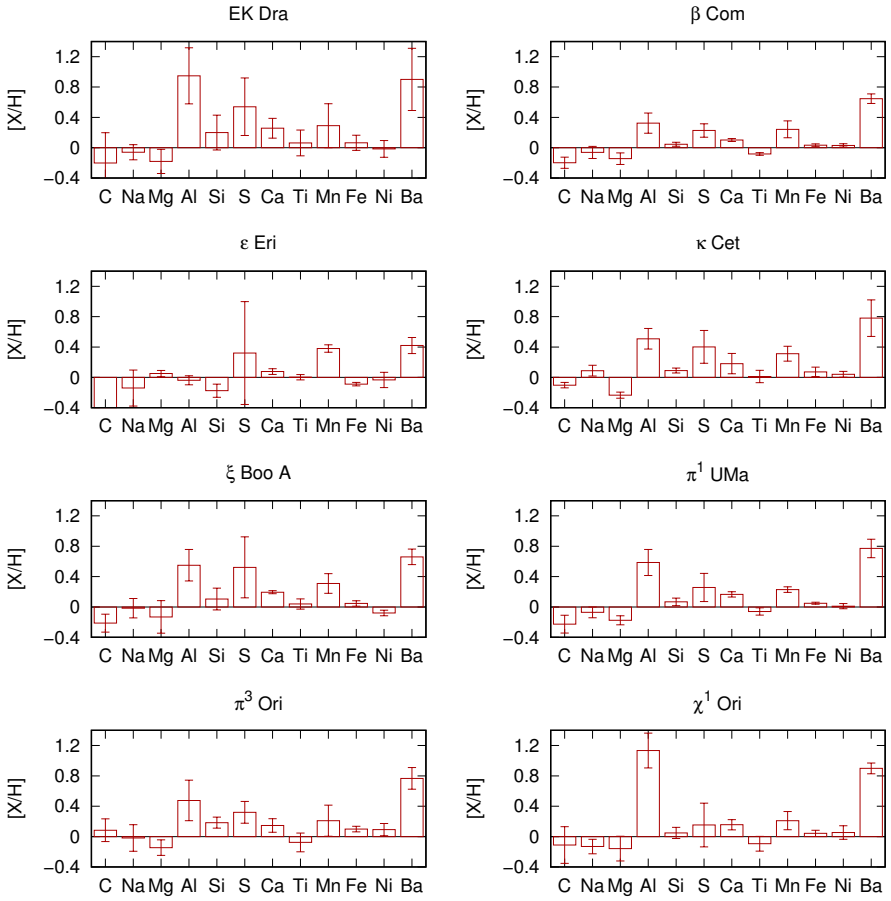

Figure 2. Elemental abundances relative to the solar values (derived in this work). Error bars shown are multiplied by 10 for illustration purposes.

spectral synthesis will be more challenging. In the future we also plan to gather the available X-ray abundances to recalculate the FIP bias for these stars.

Acknowledgements. Authors are grateful to Konkoly Observatory, Hungary, for hosting two workshops on Elemental Composition in Solar and Stellar Atmospheres (IFIPWS-1, 13–15 Feb, 2017 and IFIPWS-2, 27 Feb–1 Mar, 2018) and acknowledge the financial support from the Hungarian Academy of Sciences under grant NKSZ 2018_2. The authors acknowledge the Hungarian National Research, Development and Innovation Office grant OTKA K-113117 and the Lendület grant LP2012-31 of the Hungarian Academy of Sciences. KV is supported by the Bolyai János Research Scholarship of the Hungarian Academy of Sciences. This work has made use of the VALD database,

Table 2. Fundamental parameters derived from the spectra.

star	$T_{\rm eff}$ [K]	$\log g$ [dex]	$[M/H]$ [dex]	$\xi_{\rm mic}$ [km s^{-1}]	$v \sin i$ [km s^{-1}]
EK Dra	5780	4.46	−0.06	1.32	21.2
β Com	5980	4.37	−0.09	0.92	13.3
ϵ Eri	5150	4.32	−0.07	0.91	12.8
κ Cet	5780	4.39	−0.01	0.83	12.5
ξ Boo A	5670	4.56	−0.16	1.32	14.1
π^1 UMa	5880	4.39	−0.18	0.98	16.9
π^3 Ori	6320	4.37	−0.12	1.06	20.0
χ^1 Ori	5940	4.44	−0.10	0.54	17.2

operated at Uppsala University, the Institute of Astronomy RAS in Moscow, and the University of Vienna. Authors are grateful to Borbála Cseh for her helpful suggestions related to Ba stars.

References

D'Orazi, V., Magrini, L., Randich, S., et al., Enhanced Production of Barium in Low-Mass Stars: Evidence from Open Clusters. 2009, *Astrophys. J.*, **693**, L31, DOI: 10.1088/0004-637X/693/1/L31

Laming, J. M., The FIP and Inverse FIP Effects in Solar and Stellar Coronae. 2015, *Living Reviews in Solar Physics*, **12**, 2, DOI: 10.1007/lrsp-2015-2

Piskunov, N. E., Kupka, F., Ryabchikova, T. A., Weiss, W. W., & Jeffery, C. S., VALD: The Vienna Atomic Line Data Base. 1995, *Astron. Astrophys., Suppl.*, **112**, 525

Stoehr, F., White, R., Smith, M., et al., DER_SNR: A Simple & General Spectroscopic Signal-to-Noise Measurement Algorithm. 2008, in Astronomical Society of the Pacific Conference Series, Vol. **394**, *Astronomical Data Analysis Software and Systems XVII*, ed. R. W. Argyle, P. S. Bunclark, & J. R. Lewis, 505

Valenti, J. A. & Fischer, D. A., Spectroscopic Properties of Cool Stars (SPOCS). I. 1040 F, G, and K Dwarfs from Keck, Lick, and AAT Planet Search Programs. 2005, *Astrophys. J., Suppl.*, **159**, 141, DOI: 10.1086/430500

Valenti, J. A. & Piskunov, N., Spectroscopy made easy: A new tool for fitting observations with synthetic spectra. 1996, *Astronomy and Astrophysics Supplement Series*, **118**, 595

Contrib. Astron. Obs. Skalnaté Pleso **49**, 293 – 300, (2019)

INASAN NEO finder (INF) project

A. Shugarov, M. Nalivkin, S. Naroenkov and I. Savanov

Institute of Astronomy of the Russian Academy of Sciences, 48 Pyatnitskaya st. 119017, Moscow, Russia

Received: October 31, 2018; Accepted: March 10, 2019

Abstract. The INF (INASAN Near Earth Objects Finder) project is a dedicated network of robotic telescopes to detect 10 m asteroids coming to the near Earth Space. The main features of the project are a short cadence time (1 h) of all-sky survey, a moderate limiting magnitude (19^m) without filters and a possibility of carrying out the additional scientific program. The INF multiaperture telescope consists of 8 VT-78d telescopes on a fast mount. The VT-78d telescope provides a unique combination of parameters: the aperture (250 mm), the fast focal ratio f/1.58, the field of view (10 deg diameter, 78.5 deg^2) and the D_{80} image quality (5 arcsec). The INF total field of view is 574 deg^2 (298 Mpixels) with a 5.2 $\mathrm{arcsec\,pixel}^{-1}$ scale. According to our estimates the INF will discover about 7330 NEOs of 10 m size in 5 years in the case of everyday operation (8 hour per night).

Key words: Near Earth Objects – Wide field telescopes

1. Introduction

After the Chelyabinsk event it is evident that not only large asteroids but also >10 m size bodies pose a substantial hazard (Shustov et al., 2017; Shugarov et al., 2018). The number of Neart-Earth objects with sizes more than 20-m is estimated at 7.7 million (Emel'yanenko & Naroenkov, 2015).

The current programs of ground-based surveys, such as the Catalina Sky Survey, Pan-STARRS and ZTF, typically focused on 100 m class objects. Up to date it is impossible to make a complete catalogue to predict a collision of decameter size bodies with the Earth in advance. The only way to protect the Earth against such bodies and/or to mitigate is to detect NEOs in the near-Earth Space and to warn about a possible collision.

The Asteroid Terrestrial-Impact Last Alert System (ATLAS) is an example of a successful system designed to detect 30-50 m impactors about one week in advance (Tonry et al., 2018).

INASAN proposes to build a dedicated network of robotic telescopes to detect 10 m class NEOs entering the near-Earth space. Several hours of warning time provided by the INF project is sufficient to decrease risks, the larger warning time implies a dramatically larger cost of the system.

The INF project main features are a short cadence time (1 h) of all-sky survey and a moderate limiting magnitude (19^m) without filters, with the possibility of carrying out the additional scientific program.

The main advantage of INF over other similar projects, such as SuperWASP (Pollacco et al., 2006), ADAM-WFS (Vereš et al., 2014) and GWAC (Claret, 2018), is a better combination of the field of view, sensitivity and the spatial resolution (pixel scale).

Table 1. INF comparison with other similar projects.

Parameter	INF	SuperWASP	ADAM-WFS	GWAC
Telescope aperture, mm	250	200	300	180
Pixel format	6k × 6k	2k × 2k	4k × 4k	4k × 4k
Field of view, deg^2	574	482	100	5000
Field of view of single tube, deg^2	72	60	25	164
Pixel scale, arcsec pixel^{-1}	5.2	13.7	4.36	11.2
All-sky servey	1 h @ 19^m	40 min @ 15^m	2 h @ 17.5^m	2 min @ 16^m

Besides NEOs detection, INF has potential to work on other scientific programs such as gravitational wave events electromagnetic counterparts, variable stars, supernovae, gamma ray bursts and monitoring of space debris.

In this paper we describes the optical parameters of the system and system performance. Data processing software, which is a very important part of such project, is beyond the scope of this article.

2. INF architecture

The INF multiaperture telescope (Fig. 1) consists of eight VT-78d telescopes at one fast-track mount ASA DDM160. INF multiaperture telescope main parameters are presented in Table 1.

Table 2. INF main parameters.

Parameter (8x telescopes)	Value
Telescope aperture	250 mm
Field of view	17.6 × 35.2 574 deg^2
Pixel format	12k × 24k
Number of pixels	298 Mpixel
Pixel scale	5.2 arcsec pixel^{-1}
Readout time	<1 s
All sky @ 10 s exposure	10 min @ 18.3^m
All sky @ 30 s exposure	20 min @ 18.9^m
All sky @ 100 s exposure	1 h @ 19.4^m

Figure 1. INF multiaperture telescope: 8 x VT-78d's on the ASA DDM160 mount.

For fast repointing INF will be installed in a "shell type" dome. To provide 24 h operation and to detect NEOs coming from 2π sr (night sky), several INF multiaperture telescopes are required to be installed in the northern and southern hemispheres at sites with low sky background.

It is possible to put a filter change mechanism with one specific filter for each telescope. All telescopes can be aligned by a special mechanism to look at one field in order to perform multicolor photometry or improve telescope sensitivity (20.4^m for 100 s exposure).

For specific scientific tasks (Beskin et al., 2010) INF can be used for high time resolution photometry with a frame rate up to 44 Hz.

2.1. VT-78D wide field telescope

VT-78d telescope (Table 3) is a new generation (Terebizh, 2016) wide field telescope designed by V. Terebizh (INASAN patent 162010 (RU)). VT-78d optics consists of simple optical elements with all spherical surfaces and simple types of glasses.

The telescope provides a unique combination of aperture (250 mm), field of view (10 deg) and D_{80} image quality (5 arcsec).

The optical quality throughout the field of view allows us to use a 6k × 6k detector with small pixel instead of a 4k × 4k one, which are commonly used for similar projects. The typical FWHM is expected at the level of one pixel over the whole field of view of 10 deg. The other benefit of the 6k × 6k detector is improvement in the pixel background noise, which is the main limitation factor for such a wide field system with a long (up to 100 s) exposure time.

Table 3. VT-78d main optical parameters.

Parameter	Value
Entrance pupil diameter	250 mm
Effective diameter	212 mm
Effective focal length	395 mm
F-ratio	F/1.58
Field of view angular diameter	10 deg
Field of view linear diameter	69.5 mm
Scale	1.915 μm arcsec^{-1}
Spectral range	450-850 nm
D_{80} in integral light, center-edge	8-10 μm, 4-5 arcsec
Maximum distortion at 550 nm	0.45 %

The telescope limiting magnitude vs exposure time for a non-moving object is shown in Fig. 2. Calculation was done using the detector with 90 % quantum efficiency, without filters, seeing of 1.5 arcsec and sky background of 20.5^m arcsec^{-2}. The main limitation factor for a long (up to 100 s) exposure time are the sky background and proper motion of the object. For moderate weather conditions and for a fast moving object the limiting magnitude will be lower.

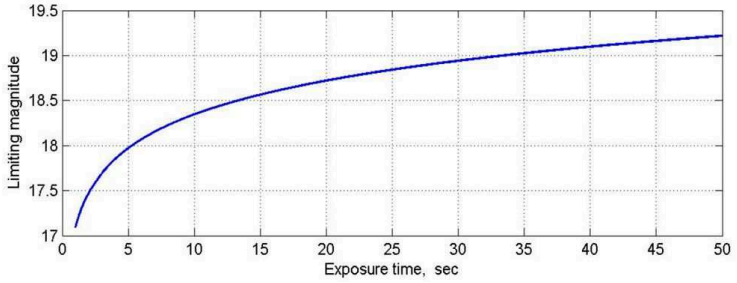

Figure 2. VT-78d limiting magnitude (SNR = 7) vs exposure time.

The telescope was designed to be used with a modern scientific CMOS GSENSE 6060BSI (6k×6k, 61×61 mm) detector. The CMOS has a rolling shutter with global reset architecture, provides up to a 44 Hz frame rate, 4.6 e- rms noise, 14 bit digitization. The back illuminated version has the peak quantum efficiency of 95%.

2.2. INF system performance

The position of INF on a survey merit diagram is shown in Fig. 3. The ideal system capable of detecting 10 m class NEOs should have:

– short cadence time (< 1 h);

– limiting magnitude of 19^m and fainter to detect 10 m NEOs at a reasonable distance;

– reasonable angular resolution of the telescope to prevent contamination.

INF seems to be an efficient instrument to detect 10 m class NEOs. The ATLAS project is optimized for detection of 50 m class NEOs with a cadence time of about 1 day.

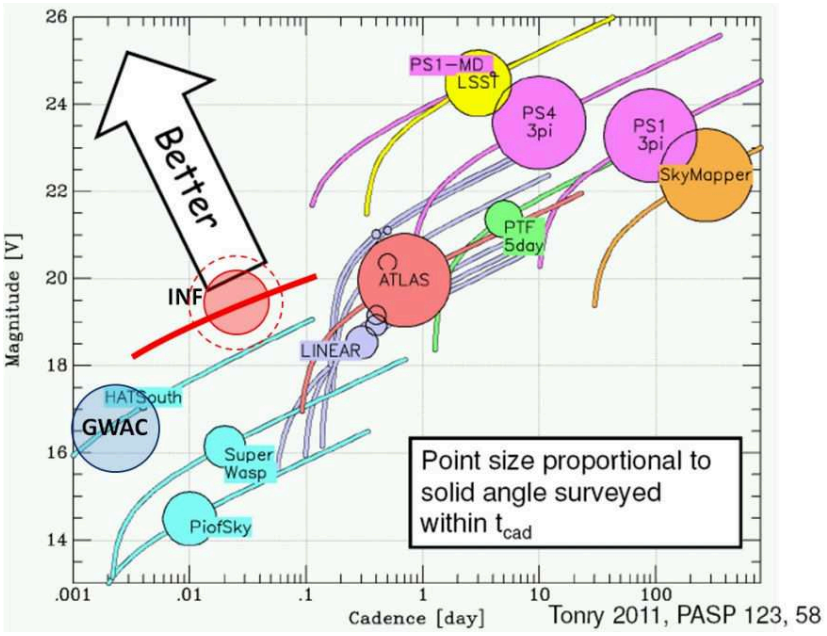

Figure 3. INF on the survey merit diagram (Tonry, 2011).

To calculate visibility zones of a NEO, the following parameters should be taken into account (Shugarov, 2013):

– the size and albedo of the NEO, the phase angle and the distance to the Sun and the observer;

– the main characteristics of a telescope and a detector;

– the background illumination, i.e., zodiacal light and scattered light in the telescope;

– exposure time.

To determine the NEO visibility zone, the criterion of a significant signal to noise ratio (SNR) was used. The significance is determined by a specific task. To perform a reliable detection and to take into account the INF's moderate pixel scale, we suggest to use the criteria SNR > 9.

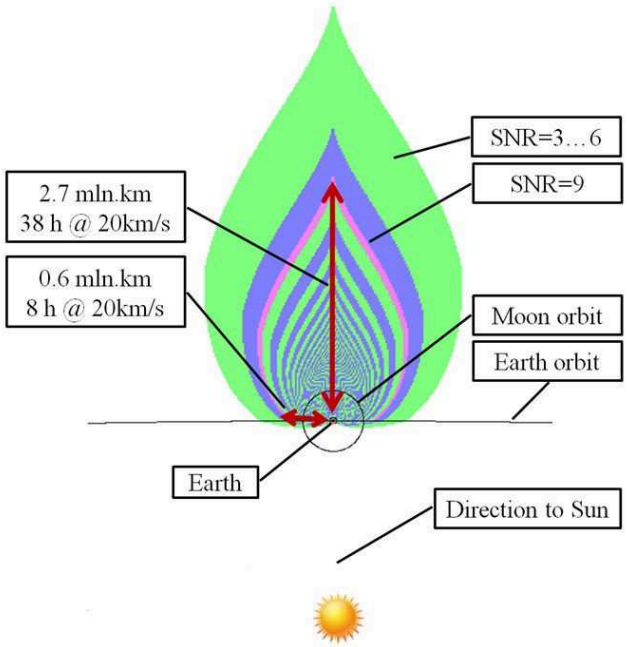

Figure 4. INF visibility zone for 10 m NEOs with 100 s exposure.

In Fig. 4 the visibility zone for a 10 m NEO with 0.15 albedo for 100 s exposure time is shown. Isophote bands of constant SNR are shown with a step of 3 units. A separate pink isophote is given for SNR = 9 which corresponds to a reliable detection. The INF is practically unable to operate at the day-time hemisphere because of the phase angle and background light. The sharp peak in the detection distance around the opposite direction to the Sun is due to a micro reflectivity effect that is typical for asteroids.

For 10 m class bodies the INF will provide a visibility zone of 0.6-2.7 million km from the Earth. The world wide network of INF telescopes can provide a warning time of 6-30 h and possibility to detect a good share (∼80%) of 10 m class NEOs coming from the night sky.

The discovery rate for the INF project was estimated using the NEA population model by Granvik, Morbidelli and Bottke. According to our estimates the INF will discover ∼7330 NEOs in 5 years in the case of everyday operation

(8 hour per night) with a limiting magnitude of 19.7^m. A model distribution of discovered NEOs on the sky is shown in Fig. 5.

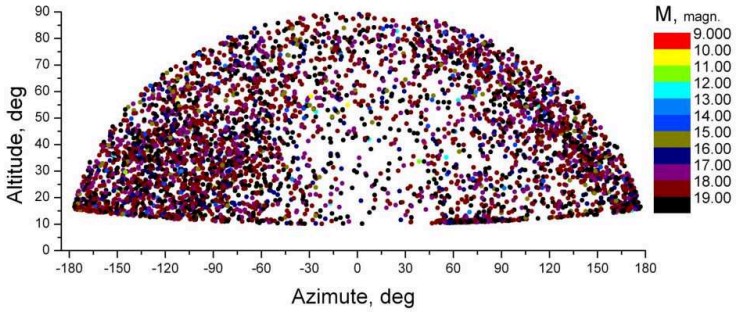

Figure 5. Distribution of possible near Earth asteroids in the (Az-Alt) plane that could be detected by INF.

2.3. INF prototype

INASAN is finishing the construction of a prototype of the INF multiaperture telescope. The prototype consists of 2 identical wide-field telescopes equipped with 4k×4k CCD cameras on the fast-track mount. First light is expected in 2019. The INF prototype consists of:

- 2 VT-78d telescopes, 2 FLI ML16803 CCD cameras;
- 2 FLI Atlas focusers, ASA DDM85PRO mount;
- ScopeDome 3m full robotic dome;
- control computer and equipment;
- observation planning software;
- data processing software.

3. Conclusion

The INF project combines sensitivity and survey efficiency. According to our calculations today it is one of the most efficient projects to detect 10 m class NEOs with a warning time of 6-30 h.

Combination of the survey rate (one sky per hour), limiting magnitude (19^m), possibility of multicolor photometry and fast photometry makes the INF project suitable for many scientific programs. The first light of the INF prototype (2x tubes) is expected in 2019 at the Zvenigorod observatory of INASAN.

References

Beskin, G., Bondar, S., Karpov, S., et al., From TORTORA to MegaTORTORA–Results and Prospects of Search for Fast Optical Transients. 2010, *Advances in Astronomy*, **2010**, 171569, DOI: 10.1155/2010/171569

Claret, A., The Svom mission. 2018, in COSPAR Meeting, Vol. **42**, *42nd COSPAR Scientific Assembly*, E1.15–15–18

Emel'yanenko, V. V. & Naroenkov, S. A., Dynamical features of hazardous near-Earth objects. 2015, *Astrophysical Bulletin*, **70**, 342, DOI: 10.1134/S199034131503013X

Pollacco, D. L., Skillen, I., Collier Cameron, A., et al., The WASP Project and the SuperWASP Cameras. 2006, *Publications of the Astronomical Society of the Pacific*, **118**, 1407, DOI: 10.1086/508556

Shugarov, A., Shustov, B., & Naroenkov, S., System of observation of day-time asteroids (SODA). 2018, *Open Astronomy*, **27**, 132, DOI: 10.1515/astro-2018-0023

Shugarov, A. S., Simulation of the detection zone of dangerous celestial bodies for space-based systems. 2013, *Solar System Research*, **47**, 296, DOI: 10.1134/S0038094613040187

Shustov, B. M., Naroenkov, S. A., & Efremova, E. V., On population of hazardous celestial bodies in the near-Earth space. 2017, *Solar System Research*, **51**, 38, DOI: 10.1134/S0038094617010038

Terebizh, V. Y., On the Capabilities of Survey Telescopes of Moderate Size. 2016, *Astron. J.*, **152**, 121, DOI: 10.3847/0004-6256/152/5/121

Tonry, J. L., An Early Warning System for Asteroid Impact. 2011, *Publ. Astron. Soc. Pac.*, **123**, 58, DOI: 10.1086/657997

Tonry, J. L., Denneau, L., Heinze, A. N., et al., ATLAS: A High-cadence All-sky Survey System. 2018, *Publ. Astron. Soc. Pac.*, **130**, 064505, DOI: 10.1088/1538-3873/aabadf

Vereš, P., Tóth, J., Jedicke, R., et al., Automatic detection of asteroids and meteoroids. A Wide Field Survey. 2014, *Meteoroids 2013*, 307

Contrib. Astron. Obs. Skalnaté Pleso **49**, 301 – 306, (2019)

Spectral observations and photometry of the near-Earth object (25916) 2001 CP44

I.M. Volkov[1,2], S.I. Barabanov[1], I.V. Nikolenko[1], S.V. Kryuchkov[1] and A.V. Sergeev[3]

[1] *Institute of Astronomy of the Russian Academy of Sciences, 48 Pyatnitskaya street, 119017Moscow, Russia, (E-mail: hwp@yandex.ru)*

[2] *Sternberg Astronomical Institute, Lomonosov Moscow State University, Universitetskij Ave. 13, 119992 Moscow, Russia, (E-mail: kravts@yandex.ru)*

[3] *Terskol Filial branch of Institute of Astronomy, Russian Academy of Sciences (TF IA RAS), Terskol peak, Russia*

Received: November 1, 2018; Accepted: February 11, 2019

Abstract. During the demonstrational experiment on quasi-simultaneous observation of asteroid 2001 CP44 with meter-class telescopes the variations of the colour indices of the object with the period P=0^d.19165(9) were discovered. This value is close to the previously defined rotation period of the asteroid. We elaborated methods for the rapid measurement of a large number of physical and mineralogical characteristics.

Key words: Minor planets, asteroids: individual:2001 CP44 – techniques: photometric – techniques: spectroscopic

1. Introduction

We present the spectral and photometrical quasi-simultaneous observations of 2001 CP44 = 25916 NEO asteroid which were conducted with the help of the 2-m Zeiss telescope situated on the peak Terskol (Caucasus, Mt. Elbrus) and the 1-m Zeiss Mt. Koshka (Crimea) Cassegrain. We obtained a new value of the period of the optical variations, colour indices, the taxonomic class and some other characteristics of the object. We present the methods and the results of data processing, the comparison analysis of light curves in different pass-bands. The taxonomic class is obtained from the spectral observations and mean colour indices analysis. Some recommendations on the methods of simultaneous spectral and photometric observations are given. The first demonstrational experiment using several telescopes, the so-called observation network of INASAN, was first conducted by us in Ibragimov et al. (2013).

2. Observations and data reduction

The continuous photometric runs were obtained in June 11-13, 2018 in the $BV(RI)c$ - system with the 1-m reflector and FLI PL0900 CCD at Mt. Koshka

(Crimea). The magnitudes of comparison stars were obtained by special observations of the 1081491 standard star from Landolt (2009) with the Zeiss-600 telescope and the VersArray 512UV CCD at Mt. Koshka on August 23, 2018. The details of our photometric system and instrumentation one can find in Volkov et al. (2011).

Spectroscopic observations were fulfilled on June 12, 13 and 15, 2018 on the peak Terskol with the 2-m reflector and a Multi Mode Cassegrain Spectrometer (MMCS). MMCS was designed for spectroscopic observations of faint objects at the
Cassegrain focus ($f/8$) of the telescope Zeiss-2000. It has a modular design which allows quick transformation from its echelle to prism mode. The collimator is a parabolic mirror with a diameter of 75 mm and a focal length of $f = 600$ mm. The spectrometer has a wide range of resolutions from $R = 100$ to $R = 15000$ and the spectral range 3700 - 8000Å. We used a 45° crown glass prism in combination with a $f = 150$ mm Schmidt-Cassegrain camera, which provided $R = 100$ at the hydrogen line $H\gamma$. The limiting magnitude of our spectroscopy and photometry comes up to 17 mag in V.

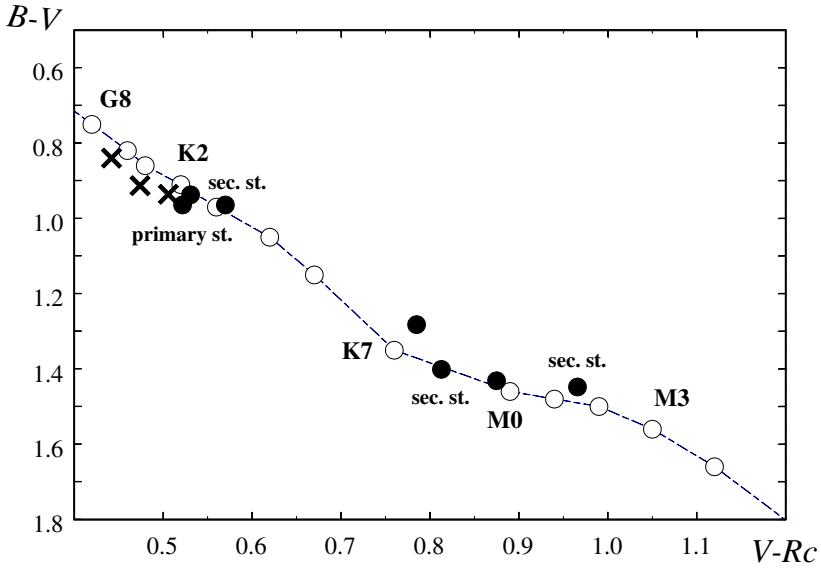

Figure 1. The $B - V, V - Rc$ diagram for the asteroid and the stars in the field. Crosses - mean colour indices of the asteroid for three consecutive nights. Black circles point stars position. Unsigned black circles - the position of check stars. The dashed line connecting empty circles - normal colour indices sequence for fifth-luminosity class stars.

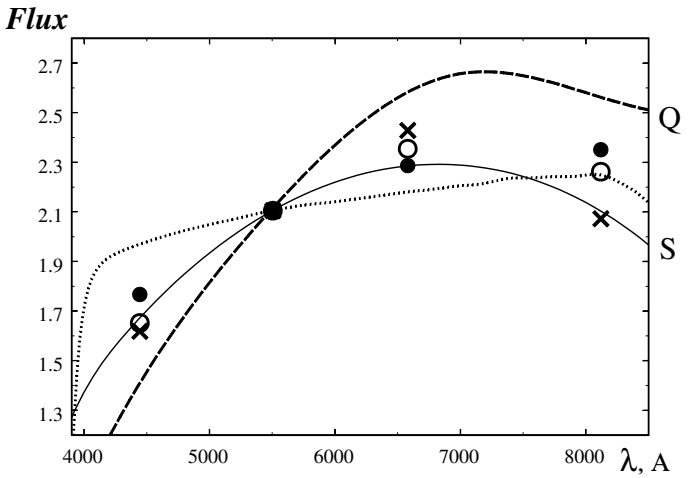

Figure 2. Frequent points - smoothed spectrum of the asteroid in relative units normalized on Sun's spectrum. Empty, full circles and crosses - photometrical measurements in $BVRcIc$ in three consecutive nights. The reasons for the discrepancy between spectroscopy and photometry are not fully understood. The taxonomic S-class presents photometric measurements by the best way.

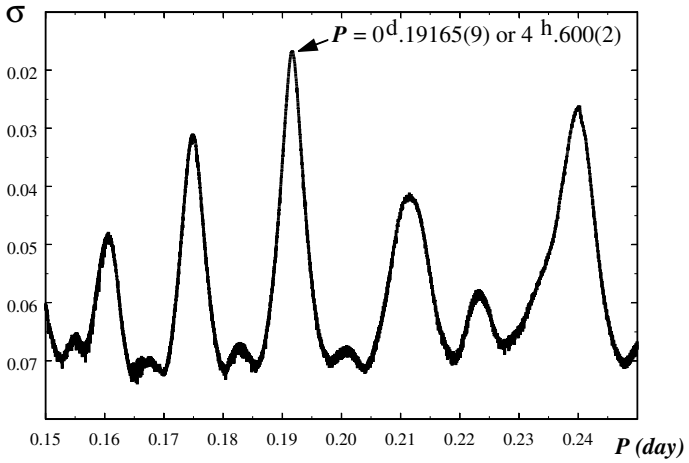

Figure 3. A periodogram for all of asteroid observations constructed by a moving average method. The ordinate σ characterizes the mean deviation of the observation points relative to the center of mass of the phase curve. The curves were constructed for all period values from the interval indicated on the abscissa axis with a step of 0.00001 day. Aliases are smaller in amplitude than the true period. The value of σ in the maximum characterizes the scatter of the mean curve in Fig. 4.

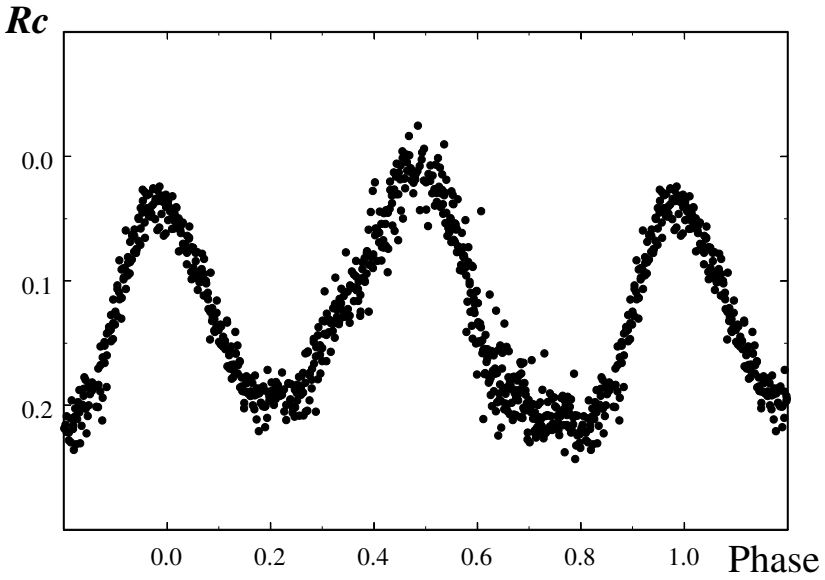

Figure 4. All our *Rc* observations phased with a 4.6 hour period.

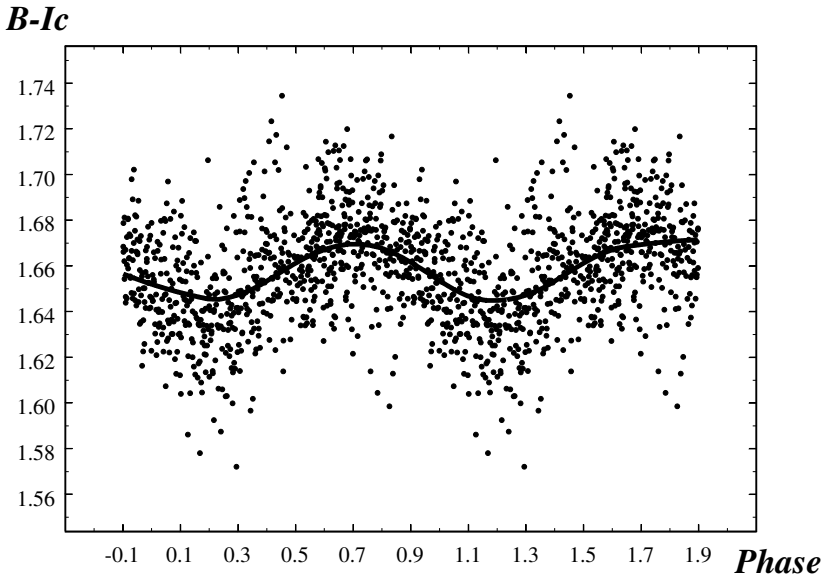

Figure 5. Phased with 4.6 hour period $B - Ic$ observations.

3. Comparison of photometry and spectrometry

We present the results of our multicolour photometry in Fig. 1. It seems that the colour indices change a little from night to night. Fig. 2 demonstrates the comparison of our photometric and spectral observations with each other and with two taxonomic classes - S and Q, Tholen (1989). All data are normalized on the Sun spectrum. The magnitudes in different pass-bands were normalized on Sun's magnitudes and on the V magnitudes of the asteroid. The scatter of measurements at different nights reflects both the errors of the observations of standard stars and the real changes in the colour indices. Our photometry shows that 2001 CP44 belongs to the S taxonomic class. This result coincides well with Ieva et al. (2014).

Measurable changes in the colour indices were revealed, which correlate well with the period of the rotation of the asteroid found in present investigation, P=0^d.19165(9), see Fig. 4 and Fig. 5. Note that the light curve of the asteroid is characterized by two humps in a period and the colour index wave has only one hump in a period. The $B-Ic$ index was chosen for demonstration as it changes much more than other colour indices. A full amplitude of the variations is $0.^m02$. In our opinion, the explanation of this phenomenon lies in the heterogeneity of the substance of the reflectivity of the surface of the asteroid associated with the collision history of this small body. Perhaps there was a collision with another asteroid, part of the substance of which initially formed a cloud of dust and then settled on the surface of the asteroid. So in the place of impact the concentration of the substance of the impactor is maximal and it gradually decreases outwards. However, it is likely that there may be other explanations that will be considered by us in a more detailed study of this unusual phenomenon in the future.

The albedo of 2001 CP44 was determined earlier and has a value of 0.177 (ssd.jpl.nasa.gov). This value corresponds well to the S class derived from our photometry, which means it consists of ordinary chondrites. In the case of an unknown albedo, it can be estimated using, for example, a polarimeter. Now we are preparing one in order to start such observations with the 1-m telescope on Mt. Koshka. It is important to note that iron-nickel asteroids can be used in the future as a source of minerals.

4. Conclusions

In this paper, we proposed a configuration of three one-meter class telescopes to determine all the basic physical and mineralogical features of the asteroids that are brighter than 17 mag. We demonstrate its applicability for the study of asteroid 25916, whose visibility was favorable in June 2018. The variability of colour indices was found. This phenomenon seems to be quite rare and requires a separate study.

Acknowledgements. This study was partly supported by the scholarship of the Slovak Academic Information Agency(IMV), RNF grant 14-12-00146 and RFBR grant 18-502-12025(IMV). This work was partly supported by the Program of Presidium of RAS No.28. We are grateful to our referee M.Husárik for valuable suggestions and remarks leading to significant improvement of our paper.

References

Ibragimov, M., Barabanov, S., Bakanas, E., et al., Project on coordinated observations of Hazardous objects: background, creation and first experience. 2013, *Ecological Bulletin of the BSEC Research Centers, Kuban State University, Krasnodar*, No. **4**, Issue 2, 60

Ieva, S., Dotto, E., Perna, D., et al., Low delta-V near-Earth asteroids: A survey of suitable targets for space missions. 2014, *Astron. Astrophys.*, **569**, A59, DOI: 10.1051/0004-6361/201322283

Landolt, A. U., UBVRI Photometric Standard Stars Around the Celestial Equator: Updates and Additions. 2009, *Astron. J.*, **137**, 4186, DOI: 10.1088/0004-6256/137/5/4186

Tholen, D. J., Asteroid taxonomic classifications. 1989, in *Asteroids II*, ed. R. P. Binzel, T. Gehrels, & M. S. Matthews, 1139–1150

Volkov, I. M., Bakanas, E. S., Nikolenko, I. V., Ivanov, A. L., & Lysenko, V. E., Photometric observations of selected small bodies, made in 2009-2011, using a high-precision BVRI photometer on the Zeiss-1000 telescope on Mt. Koshka. (in Russian). 2011, *Bulletin of Siberian State Aerospace University, Krasnoyarsk*, **6**, 129

Contrib. Astron. Obs. Skalnaté Pleso **49**, 307 – 319, (2019)

Small telescopes and their application in space debris research and space surveillance tracking

J. Šilha

Faculty of Mathematics, Physics and Informatics of Comenius University in Bratislava, Slovakia (E-mail: jiri.silha@fmph.uniba.sk)

Received: November 15, 2018; Accepted: February 4, 2019

Abstract. Space debris is an essential threat to the satellite infrastructure. Possible collisions with even small particles, e.g. 1 cm of size, can cause catastrophic events when the parent body, a spacecraft or an upper stage, breaks up into hundreds of small fragments. The space debris research and space surveillance tracking (SST) helps to discover, monitor and characterize these objects, identify their origins and support their active removal.

There are two major observations strategies recognized for optical observations. The optical surveys aim to discover new objects for cataloguing or for statistical purposes. The follow-up observations are performed for catalogued objects to improve their orbits or to investigate their physical characteristics. A majority of the systems are focused on the high orbital regions when objects' orbits have mean motion less than $\sim$ 10 revolutions per day. For lower altitudes, so-called Low Earth Orbits (LEO), more complex tracking capabilities of the system are needed.

In our work we present applications of small telescopes in space debris area, their usage for surveys, tracking and cataloguing. We discuss the world's largest optical SST networks, individual space debris research telescopes as well as the space debris research program at the domestic 70-cm telescope installed at the Astronomical and Geophysical Observatory in Modra (AGO), Slovakia, which belongs to and is operated by the Faculty of Mathematics, Physics and Informatics of Comenius University in Bratislava, Slovakia. We present products provided by these systems.

Key words: space debris – research – telescopes

1. Introduction

In the last 60 years the human space activities created an expansive population of unused and unwanted objects in the close vicinity of the Earth. This population is known as space debris (alternatively orbital debris) and poses a huge threat to the present and future space missions. Research and regular tracking is important to understand and protect against it. These objects move in various types of geocentric orbits, from low Earth orbits of several hundreds kilometres above the Earth's surface to geosynchronous orbits at the heights of about 35,800 km above the surface.

1.1. Space debris sources

The creation of space debris objects is a direct consequence of human space activities. The largest, and also easiest to monitor, are non-functional payloads and spared rocket bodies (R/Bs). More than 97 % of total mass situated on the Earth orbit is concentrated in this type of debris along with functional spacecrafts (Liou, 2011). The mass of the International Space Station (ISS) is not included. The most abundant portion of objects larger than 10 cm are fragments from payloads and rocket bodies, fragmentation debris. Shapes, sizes and material types of this kind of debris differ from piece to piece. Many additional objects can be discharged during a spacecraft's launch - heat covers, launch adapters and objects lost by astronauts are all part of mission-related debris. All aforementioned objects can reach brightness and sizes detectable by the ground-based optical systems.

A specific type of debris are particles with small additional velocities, released from spacecrafts caused by unknown mechanisms, called anomalous debris. One of the representatives of anomalous debris is multilayer insulation (MLI), a material used as a thermal protection for sensitive systems placed on board of spacecrafts. During a breakup event, or under the influence of space environment (impacts from small particles, extreme ultraviolet radiation), the MLI parts can degrade and be released to the space environment.

1.2. Space debris spatial distribution

Spatial distribution of the debris population is directly associated with orbits used for satellite operations. The Low Earth orbit (LEO) is the most populated. Satellites on LEO have mean altitudes lower than 2,000 km above the surface, which corresponds to orbital periods P below 2.2 hours. According to the website www.space-track.org (hereafter public catalogue) of the United States Strategic Command (USSTRATCOM) (see also section 2.1), almost 80 % of catalogued objects are situated on LEO. Medium Earth orbits (MEO) have P from 2.2 hours to 24 hours and a wide range of eccentricities. Global navigation satellite systems' (GNSS), like European navigation system Galileo, US Global Position System (GPS) and Russian Globalnaya navigatsionnaya sputnikovaya sistema (GLONASS), are part of GNSS operate on MEO orbits. GNSS have circular orbits with $P \sim 12$ hours and orbital inclinations between 60° to 70°. Eccentric MEO orbits, marked as a geosynchronous transfer orbit (GTO) and Molniya orbits, are very common too. MEO is mostly populated by rocket bodies, fragmentation debris and mission-related debris. A unique type of the orbit is the geosynchronous Earth orbit (GEO). GEO has $P \sim 24$ hours, low inclinations (i from 0° to 15°) and low eccentricities. According to the public catalogue (see section 2.1) about 7 % of the catalogued objects are placed on GEO, mostly payloads and rocket bodies. For better visualization of the spatial distribution see Fig.1.

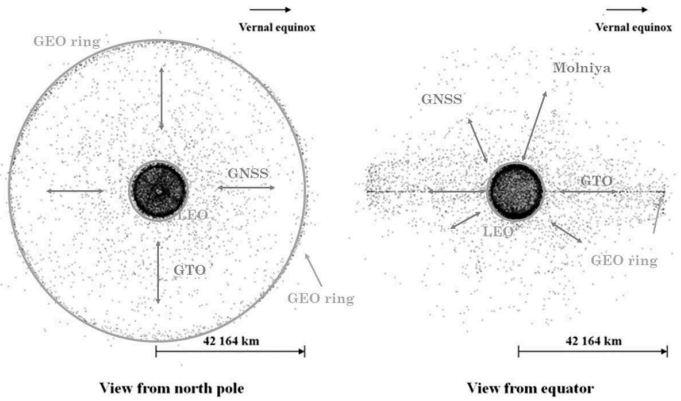

Figure 1. Space debris spatial distribution. Data generated by the using public catalogue www.space-track.org (Šilha , 2012).

1.3. Optical observations

Two major observation strategies are recognized for space debris optical observations. Optical surveys aim to discover new objects for cataloguing or for statistical data collection. Tracking (follow-ups, FUPs) of and observations on catalogued objects are performed to improve their orbits or investigate their physical characteristics. A majority of optical systems are focused on high orbital regions where objects' orbits have mean motion less than ~ 10 revolutions per day. Moreover, more complex system capabilities are needed for LEO tracking.

Space debris research helps to improve the understanding of creation mechanisms of space debris. The research characterizes the debris dynamical (e.g. orbital elements) and physical properties (e.g. surface material); it analyses the attitude information (e.g. through light curves) for supporting the debris mitigation efforts, deals with the models of the spatial distribution for small populations (from μm to cm), etc. In general, space debris research is performed by using optical, radar and in-situ techniques.

So-called space surveillance and tracking (SST) is responsible for regular tracking by using optical (passive and active) and radar systems. This service requires orbit determination and maintenance of a catalogue. When compared to the research function, SST is a service which requires a network of sensors coupled with the real-time data acquisition and processing (Šilha et al., 2017a).

2. Surveillance networks

To cover a large part of a specific orbital region one needs to use the network of dedicated sensors. For the SST application, there are several networks which

provide constant monitoring of debris.

2.1. USSTRATCOM network

The primary network and the source of orbital elements providing the most extensive data set is operated by the United States Strategic Command (USSTRATCOM). It consists of several ground-based radar and optical sensors and one space-based telescope. The USSTRATCOM network covers all orbital regions, from LEO up to GEO. The network has been operational since 1957 and it focuses on tracking objects larger than 10 cm in diameter by using radar and optical means. The USSTRATCOM's catalogue contains the mean osculating elements in a form of TLE (Two-Line Elements) and it is publicly available at www.space-track.org. In June 2018 the public catalogue contained orbital data for almost 17,000 objects from which almost 80% were situated on LEO. Fig. 1 was generated by using the public catalogue data.

2.2. The International scientific optical network

The largest civilian network performing the SST function is the International scientific optical network (ISON) operated by the Keldych Institute of Applied Mathematics, Russian Academy of Sciences, Russia. There are more than three dozen of observation facilities worldwide contributing to the ISON network. ISON is continuously increasing its coverage and currently contains 90 telescopes with apertures in range from 0.125 m to 2.6 m (Mokhnatkin et al., 2017). A majority of the telescopes' operators are from academic institutions. ISON focuses on the cataloguing and research of objects on higher orbits and Near Earth Asteroids (NEA). Three ISON telescopes, a 64-cm AT-64 (a), a 2.6-m ZTSh in Nauchniy-1 (b) and a new 50-cm VT-40/500 in Ussuriysk (c) are shown in Fig. 2. The 2.6-m ZTSh telescope, situated in Nauchny, is the telescope with the largest aperture from all sensors contributing to ISON.

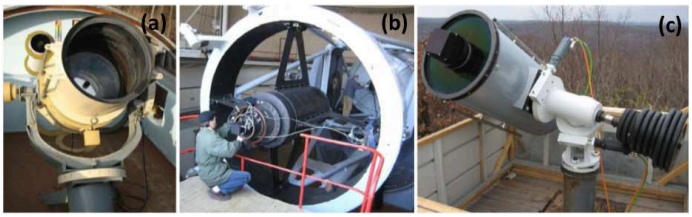

Figure 2. Examples of ISON telescopes for the faint fragment observations: a 64-cm AT-64 (a) and a 2.6-m ZTSh in Nauchniy (b) and a new 50-cm VT-40/500 in Ussuriysk (c) (Molotov et al., 2014).

The geographic distribution of the ISON telescopes and its cooperating telescopes as to 2017 are plotted in Fig. 3. Most of the ISON telescopes are situated in the Russian Federation but are continuously deployed to other locations such as South and North America, Australia and Africa.

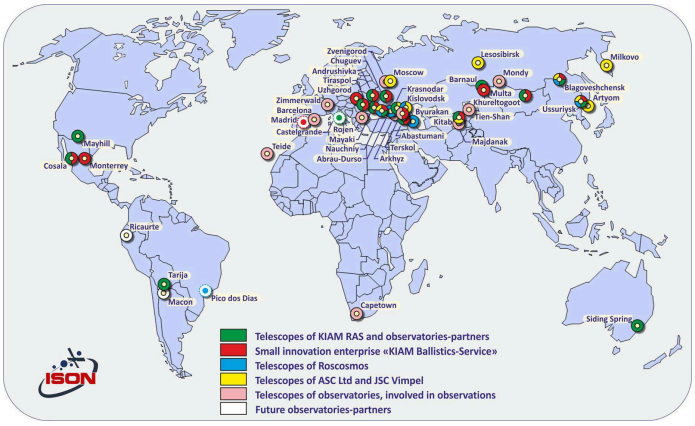

Figure 3. Geographical distribution of sensors participating to the ISON (Mokhnatkin et al., 2017).

3. Research telescopes

A single sensor is not able to cover any mentioned population completely and is usually used to acquire statistical information about a specific orbital region by using sky surveys, or to acquire scientific data for a specific object. This data can be further used for the improvement of the space debris model such as ESA MASTER (Flegel et al., 2011) and NASA ORDEM (Krisko et al., 2015), or to study physical characteristics of selected objects. There are dozens of telescopes dedicated to the research of space debris. This section discusses only a representative fraction of it. Some of these presented systems can also perform the SST functions.

Basic characteristics of presented systems are listed in Table 1. The 1-m ESA Space Debris Telescope (ESASDT) is situated at the Optical Ground Station (OGS), Canary Islands, Tenerife (Spain) and is operated by the European Space Agency (ESA). The MODEST telescope (Michigan Orbital DEbris Survey Telescope) is situated at Cerro Tololo Inter-American Observatory (CTIO) in Chile and is operated by the University of Michigan in cooperation with the National Aeronautics and Space Administration (NASA). ZIMLAT (Zimmerwald Laser and Astrometry Telescope) is situated at the the Swiss Optical Ground Station

Table 1. Configurations of selected optical telescopes used for the space debris research.

Operator	*ESA*	*NASA*	*AIUB*	*FMPI*
Telescope	*ESASDT*	*MODEST*	*ZIMLAT*	*AGO70*
Telescope design	Ritchey-Chretien	Curtis Schmidt	Ritchey-Chretien	Newton
Mount	Equatorial (English/Yoke)	Equatorial (Cross-axis)	Alt-azimuth	Equatorial (Open fork)
Camera	CCD	CCD	CCD/sCMOS*	CCD
Dimension	4096 x 4096	2048 x 2048	2048 x 2064	1024 x 1024
Primary mirror [m]	1.00	0.61	1.00	0.70
Focal length [mm]	4500.0	2135.0	4000.0	2962.0
Focal ratio	f/4.5	f/3.5	f/4.0	f/4.2
FOV [arc-min]	42.0 x 42.0	78.0 x 78.0	25.0 x 25.0	28.5 x 28.5
iFOV [arc-sec/pix]	0.62	2.30	0.70	1.67

*configuration with sCMOS not listed

and Geodynamics Observatory Zimmerwald (Switzerland) and is operated by the Astronomical Institute of the University of Bern (AIUB). The last listed telescope is a 70-cm Newton telescope (hereafter AGO70) of the Faculty of Mathematics, Physics and Informatics, Comenius University (FMPI) situated at the Astronomical and Geophysical Observatory in Modra, Slovakia (AGO).

Fig. 4 depicts all four telescopes, namely ESA OGS (a), NASA MODEST (b), AIUB's ZIMLAT (c) and FMPI's AGO70 (d).

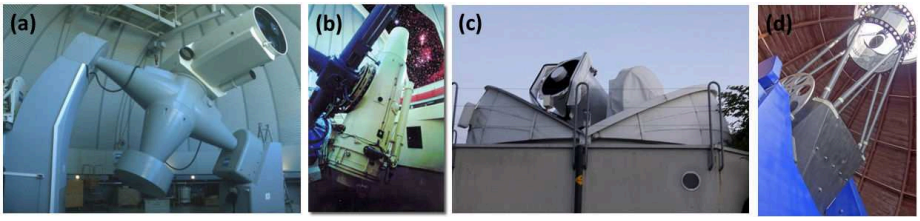

Figure 4. Selected optical telescopes used for the space debris research. Plotted is ESA OGS (a), NASA MODEST (b), AIUB's ZIMLAT (c) and FMPI's AGO70 (d). Photo credit: www.esa.int (a) and orbitaldebris.jsc.nasa.gov (b).

3.1. ESA ESASDT

For almost two decades the ESA OGS has dedicated its observation program to the continuous surveys of the GEO ring (Schildknecht et al., 2004). Additionally,

surveys of GTO and Molniya orbits (Šilha et al., 2017b) are also performed. In 2004, Schildknecht et al. (2004) presented a discovery of a new population of objects: High Area-to-Mass Ration (HAMR) objects. As the name suggests, these objects have very high area-to-mass ratio (AMR), specifically above 1 m^2/kg. This population also showed a rapid change in orbital elements over time, mostly in eccentricity and inclination. This dramatic orbital change could be explained trough the AMR parameter and the solar radiation pressure as showed in Schildknecht et al. (2008). However, the origin and material type of HAMR objects remains unknown.

In 2017, Vananti et al. (2017) published the work where authors presented photometric and spectroscopic data of HAMR objects acquired by ESA OGS. They defined three categories of populations according to the colour indices B-V and R-I as plotted in Fig.5a. The authors confronted the defined categories with the reflectance spectra obtained for given objects and they classified the categories even further. High values of the R-I index are typical for category I, values for B-V index are between 0.8-1.3 and this category has monotonic increase in reflectance spectra with a concave-up shape. Category II has very high values for both the B-V index and R-I index - between 0.4-0.8 with monotonic increasing in reflectance spectra with concave-down shape. Category III has the low values for B-V and R-I indices and spectra relatively flat with possible negative shape in the blue range. Examples of reflectance spectra for categories II and III obtained for real objects E08152A and S95300, as well for representative materials gold and silver coating foil obtained in laboratory, are plotted in Fig.5b and Fig.5c, respectively.

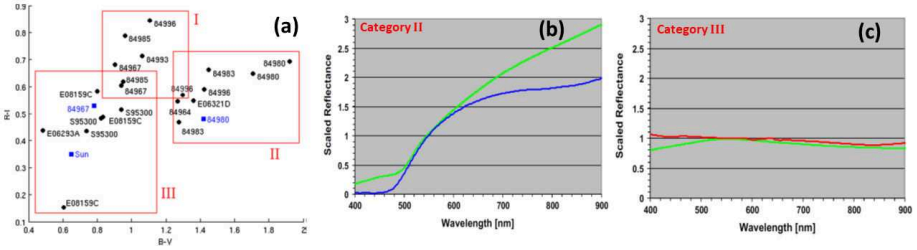

Figure 5. A diagram B-V vs. R-I of the observed HAMR space debris objects (a), reflectance spectra of the object 84980 (green) and gold MLI (blue) (b), and reflectance spectra of object S95300 (green) and silver MLI measured in laboratory (red) (Vananti et al., 2017).

3.2. NASA MODEST

The NASA MODEST system primary focuses on regular GEO surveys to monitor the population status over time. Each observed object is analyzed and classified as a correlated (CT) or un-correlated target (UCT) - whether the object is or is not in the public catalogue. Additionally, the preliminary orbital elements, assuming a circular orbit, such as inclination, right ascension of ascending node and mean motion are obtained. Once the FUP is performed, all six orbital elements are determined. Each object has extracted brightness in the R-filter. Consequently, also the size distribution of the observed population by assuming the Bond albedo of 0.175 is estimated. Fig. 6 plots the absolute magnitude distribution of GEO objects as observed by the MODEST telescope in years 2007-2010 (Seitzer et al., 2011). The absolute magnitude is calculated by correcting the measured magnitude to the zero-phase angle. Fig. 6 also indicates the size of an object by assuming the Lambertian sphere. For transformation from the absolute magnitude to the physical size, see e.g. Šilha (2012).

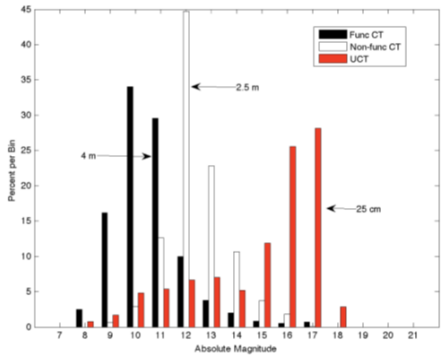

Figure 6. A histogram of R-magnitudes of GEO objects detected during 2007-2010 with the 0.6-m MODEST (Seitzer et al., 2011).

3.3. AIUB ZIMLAT

ZIMLAT is a hybrid system which is used either for SLR to cooperative targets, targets equipped with SLR retroreflectors (RR/RRA), or for optical observations (astrometric positions and magnitudes) of debris and Near Earth Asteroids (NEA). During daytime the system operates in an SLR mode only. During the night time the available observation time is shared between SLR and CCD/sCMOS (Šilha et al., 2016).

ZIMLAT focuses on the SST, as well as on the space debris research. It acquires astrometric data daily to support AIUB's cataloguing and photometric light curve catalogue used to monitor the rotation properties of space debris.

In Šilha et al. (2018) the authors presented the ZIMLAT space debris light curve database, which contained almost 2000 light curves for 400 individual objects situated on orbits from LEO to GEO. Once the light curve was pre-processed, three apparent attitude motion types for an object according to its light curve shape were distinguished. In case the light curve contains no pattern that would relate to the object's own rotation the object was classified as *stable* object. There were cases when a dominant pattern was present in the light curve, but no repetition was visible. Such objects were referred to as *slow rotators*. Finally, once the light curves contained a periodic pattern and the apparent period could be extracted, the object was marked as a *rotator*. The results obtained by ZIMLAT for the LEO population are plotted in Fig. 7. Almost 97 % of observed LEO objects showed stable or slow rotating behaviour and only 3 % of all observed LEO objects could be marked as rotators.

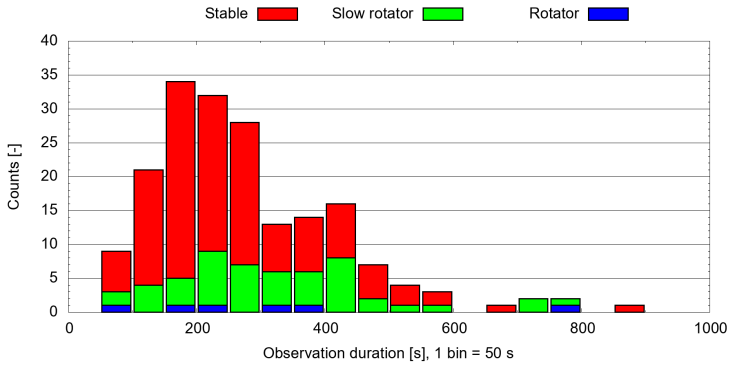

Figure 7. Distribution of acquired light curves durations for LEO objects. The width of one bin is 50 s (Šilha et al., 2018).

3.4. FMPI AGO70

FMPI's AGO70 is a relatively young system, installed at AGO in September 2016. Its observation program is dedicated to the space debris research, as well as to SST. There can be distinguished three major observation programs at AGO70 - the astrometry to support SST, instrumental photometry to characterize the debris attitude states, and absolute photometry to characterize the debris surface properties.

The system has been primarily developed thanks to the European Space Agency's (ESA) Plan for European Cooperating States (PECS) program, namely

trough the contract no. 4000117170/16/NL/NDe, which supported the development of the system's software, hardware and observation programs (Šilha et al., 2018).

To evaluate the AGO70's performance for the SST application, Šilha et al. (2018) acquired 20 nights of observations of GNSS (Global Navigation Satellite System) satellites with the goal to identify and remove epoch bias (a constant epoch registration time shift in the measurements) from the astrometric measurements and to quantify the astrometric accuracy of the AGO70s data. This analysis has been performed by AIUB and it shows that for the last two months of observations in May and June 2018, the system behaved consistently, providing measurements with astrometric accuracies of 0.8-0.9 arc-sec. A systematic epoch bias, which reached consistent value of around 67.7 ms, has been identified. Results of the analysis for the specific night can be seen in Fig.8, where the system's astrometric accuracy (Fig.8a) and epoch bias (Fig.8b), as determined by AIUB, are plotted.

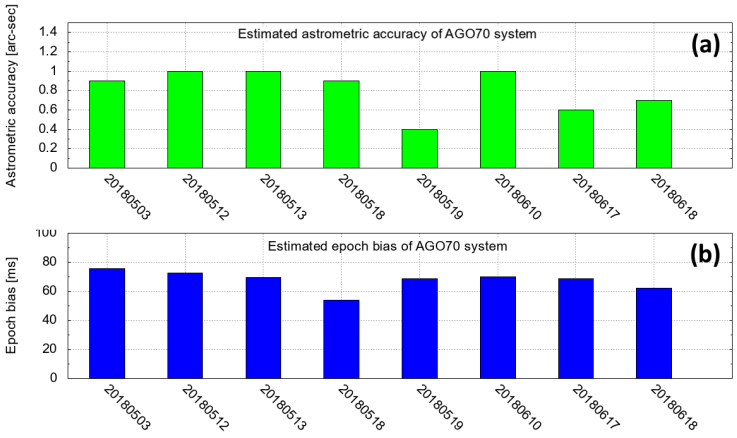

Figure 8. Estimated astrometric accuracy (a) and epoch bias (b) of AGO70 system. Data obtained from AGO70s GNSS measurements processed by AIUB (Šilha et al., 2018).

During the total duration of the observation campaign, which took place between May 2017 and June 2018, Šilha et al. (2018) acquired 339 light curves for 148 individual space debris objects. The example of a light curve for a non-operational satellite Gorizont 7 and its reconstructed phase diagram are plotted in Fig. 9. The satellite was observed in August 2017. To obtain the phase diagram and the apparent rotation period of 76.28s±0.005s the authors used a phase dispersion minimization method (Stellingwerf, 1978). From all observed

objects, for more than 55% the apparent rotation periods could be extracted. For more details refer to Šilha et al. (2018).

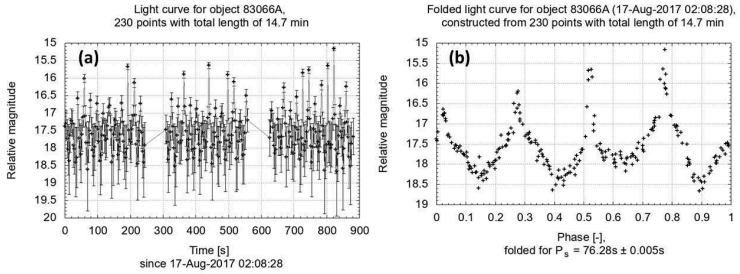

Figure 9. A light curve (left) and a folded light curve (right) acquired by the AGO 70cm telescope for the non-operational satellite Gorizont 7 (1983-066A).

4. Summary

Space surveillance of space debris is essential for space operations safety and long-term sustainability. Surveillance networks such as USSTRATCOM and the Russian ISON are widely using optical sensors/telescopes, which discover new objects and maintain their own catalogues. Both systems' data is publicly available and largely used by different subjects, from governmental entities and space agencies to academic researchers.

Individual research telescopes such as ESA OGS or FMPI's AGO70 can support surveillance functions, but they primarily focus on observations to acquire the physical characteristics of unknown debris objects. They can provide information about the surface material by using multi-band colour photometry and spectroscopy. Brightness variation, captured on photometric series (light curves) provide the information about the rotational properties, which is essential for the future active debris removal missions. A long-term monitoring of a specific orbital region through the optical surveys supports space debris models.

Small optical telescopes play a crucial role in space debris research and space surveillance tracking. Their role in space safety will increase in the next few years due to the large privatization of the space industry, which will bring new challenges like the mega-constellation projects. Therefore, it is important to constantly perform development of the dedicated telescopes, like AGO70.

References

Flegel, S. K., and 6 colleagues, Multi-layer insulation model for MASTER-2009, 2011, Acta Astronautica 69, 911, DOI: 10.1016/j.actaastro.2011.06.015.

Krisko, P. H., Flegel, S., Matney,M.J., Jarkey, D. R., Braun, V., ORDEM 3.0 and MASTER-2009 modeled debris population comparison, Acta Astronautica, Volume 113, 2015, Pages 204-211, DOI: 10.1016/j.actaastro.2015.03.024.

Liou, J.-C., An active debris removal parametric study for LEO environment remediation, 2011, Advances in Space Research 47, 1865, DOI: 10.1016/j.asr.2011.02.003.

Mokhnatkin, A., and 6 colleagues, Performance analysis of the large space debris tracking telescope in the north Caucas after the second first light, 2017, Proceedings of 7th European Conference on Space Debris, Darmstadt, Germany, 17 April 2017 - 21 April 2017.

Molotov, I., and 7 colleagues, Current status of the ISON optical network, 2014, 40th COSPAR Scientific Assembly, held 2-10 August 2014, in Moscow, Russia, Abstract id. PEDAS.1-3-14.

Schildknecht, T., and 7 colleagues, Optical observations of space debris in GEO and in highly-eccentric orbits, 2004, Advances in Space Research 34, 901, DOI: 10.1016/j.asr.2003.01.009.

Schildknecht, T., Musci, R., Flohrer, T., Properties of the high area-to-mass ratio space debris population at high altitudes, 2008, Advances in Space Research 41, 1039, DOI: 10.1016/j.asr.2007.01.045.

Seitzer, P., and 6 colleagues, A Search For Optically Faint GEO Debris, 2011, Advanced Maui Optical and Space Surveillance Technologies Conference E22.

Šilha, J., and 6 colleagues, Comparison of ENVISAT's Attitude Simulation and Real Optical and SLR Observations in order to Refine the Satellite Attitude Model, 2016, Advanced Maui Optical and Space Surveillance Technologies Conference 54.

Šilha, J., and 9 colleagues, Conceptual Design for Expert Coordination Centres Supporting Optical and SLR Observations in a SST System, 2017, Proceedings of 7th European Conference on Space Debris, Darmstadt, Germany, 17 April 2017 - 21 April 2017.

Šilha, J., Schildknecht, T., Hinze, A., Flohrer, T., Vananti, A., An optical survey for space debris on highly eccentric and inclined MEO orbits, 2017 Advances in Space Research 59, 181, DOI: 10.1016/j.asr.2016.08.027.

Šilha, J., and 22 colleagues, Slovakian Optical Sensor for HAMR Objects Cataloguing and Research, 2018, International Astronautical Congress 2018, Bremen, Germany.

Šilha, J., Identification of the Artificial Objects in Close Vicinity of the Earth, 2012, PhD thesis, Faculty of Mathematics, Physics and Informatics, Comenius university in Bratislava, Slovakia.

Šilha, J., Pittet, J.-N., Hamara, M., Schildknecht, T., Apparent rotation properties of space debris extracted from photometric measurements, 2018, Advances in Space Research 61, 844, DOI: 10.1016/j.asr.2017.10.048.

Stellingwerf, R. F., Period determination using phase dispersion minimization, 1978, The Astrophysical Journal 224, 953, DOI: 10.1086/156444.

Vananti, A., Schildknecht, T., Krag, H., Reflectance spectroscopy characterization of space debris, 2017, Advances in Space Research 59, 2488, DOI: 10.1016/j.asr.2017.02.033.

Contrib. Astron. Obs. Skalnaté Pleso **49**, 320 – 329, (2019)

Galactic astronomy and small telescopes

T. Zwitter

University of Ljubljana, Faculty of Mathematics and Physics, Jadranska 19, 1000 Ljubljana, Slovenia (E-mail: tomaz.zwitter@fmf.uni-lj.si)

Received: December 16, 2018; Accepted: January 24, 2019

Abstract. The second data release of ESA's Gaia satellite (Gaia DR2) revolutionised astronomy by providing accurate distances, proper motions, apparent magnitudes, and in many cases temperatures and radial velocities for an unprecedented number of stars. These new results, which are freely available, need to be considered in virtually any stellar research project, as they provide crucial information on luminosity, position, motion, orbit, and colours of observed targets. Ground-based spectroscopic surveys, like RAVE, Gaia-ESO, Apogee, LAMOST, and GALAH, are adding more measurements of radial velocities and, most importantly, chemistry of stellar atmospheres, including abundances of individual elements. We briefly describe the new information trove, together with some warnings against blind-folded use.

Even though it may seem that Gaia is already providing any information that could be collected by small telescopes, the opposite is true. In particular, we discuss a possible reach of a ground-based photometric survey using a custom filter set. We demonstrate that it can provide valuable information on chemistry of observed stars, which is not provided by Gaia or other sky surveys. A survey conducted with a small telescope has the potential to measure both the metallicity and alpha enhancement at a ~ 0.1 dex level for a large fraction of Gaia targets with temperatures between 4500 and 7500 K, a valuable goal for galactic archaeology.

Key words: galactic archaeology – photometric surveys

1. Introduction

Our Galaxy is a typical barred spiral galaxy. So understanding its structure, evolution, and origin is an important endeavour and the goal of galactic archaeology (Freeman & Bland-Hawthorn, 2002). Many questions can be answered only by studying our Galaxy, as even detection of individual stars in nearby galaxies can be a difficult task. On the other hand, we are located inside our Galaxy, so its more than 10^{11} stars are distributed all over the sky and are in many cases obscured by interstellar dust clouds. Knowledge of distances and 3-dimensional motions is crucial to derive luminosities and orbits of observed stars. Orbits are important, as they allow identification of a given star as a member of a particular galactic component, i.e. the thin or thick disks, bulge or halo. Stars on bound orbits in the halo are moving in a low density environment, so they get perturbed only twice per Galactic orbit during their passages through

the Galactic plane. Their kinematic properties, like the total energy, total angular momentum and the size of its z-component maintain a nearly constant value. As a consequence, present orbits of stars in the halo can have their origins traced to individual dwarf galaxies which were cannibalised by our Galaxy some 12 billion years ago (Helmi & de Zeeuw, 2000). Unfortunately, this type of kinematic reasoning does not work in a higher-density environment of a galactic disc. Studies of origin of individual disk stars should therefore rely on measurements of chemistry of their atmospheres, which remains constant throughout their lives (except for material dredge-ups late in their lives). So one could hope to identify stellar siblings with an origin in a common star cluster which has now long-gone. This is the idea behind chemical tagging (De Silva et al., 2007, 2015; Kos et al., 2018).

In this contribution we first briefly review recent space and ground-based stellar sky surveys, which now provide a firm observational basis for galactic archaeology. We urge the users to use the new and freely available datasets in their daily research activities. Finally, we connect these datasets with the reach of surveys using small telescopes, in particular we discuss how stellar chemistry can be studied through a photometric survey which uses a customised filter set.

2. Gaia satellite of ESA

April 25, 2018, is an important date, as from then on astronomers have access to the second data release of the satellite Gaia of the European Space Agency (Gaia DR2, Brown et al., 2018). The release vastly expanded the available number (Table 1) and accuracy (Table 2) of astrometric, but also photometric and radial velocity measurements. Gaia DR2 profoundly changed every area of astronomy: parallaxes, for example, are now available for 1.3 billion stars at a typical accuracy of 0.03 mas at the bright end, which can be compared to already very impressive but much smaller and less accurate parallaxes for 2 million stars at a 0.3 mas level, published in Gaia's first data release (Brown et al., 2016).

New information should benefit virtually any stellar research project. In many cases it provides a good handle on absolute magnitude, colour, spatial position and orbit of the observed object(s), a completely novel situation in astronomy where such information has been largely limited to members of star clusters, or other spatially confined groups where a suitable standard candle could be found. Finally, the field stars are joining the game of disentangling detailed physics and Galactic orbits.

The data trove of Gaia should be, however, used responsibly. First, Gaia is not measuring distances but parallaxes. Relation between the two can be non-trivial, as thoroughly discussed by Bailer-Jones et al. (2018). Some of the reported parallaxes are negative which *is* a correct statistical data treatment. In many cases this puts a firm lower limit on the true distance of the observed

Table 1. The number of stars in the Gaia DR2 with a cited type of information (Brown et al., 2018).

Type of information	Number of stars
Position and brightness on the sky	1,692,919,135
Red colour photometry	1,383,551,713
Blue colour photometry	1,381,964,755
Parallax and proper motion	1,331,909,727
Surface temperature	161,497,595
Reddening along the line of sight	87,733,672
Radius and luminosity	76,956,778
Radial velocity	7,224,631
Variable sources	550,737
Orbits of Solar system objects	14,099

object, which can be a valuable piece of information. Some parallaxes are very large, 59 of them have a value larger than the parallax of Proxima Centauri. Still, this does not mean they are closer, but that the reported value is a result of an automated procedure which can get confused by spurious alignment with sources which are resolved by Gaia only in some observations and not in others. It is important to note that there is no universal recipe to mitigate such cases, but that the users can perform custom tests which will effectively resolve such issues on parallaxes and/or proper motions. A useful example is discussed in figure C4 of Lindegren et al. (2018).

Energy and angular momentum of a stellar Galactic orbit cannot be computed without knowledge of the velocity vector. While proper motion and parallax measurements provide accurate values of velocity components along the sky plane, radial velocity can be measured only by spectroscopy, except for nearby stars where perspective acceleration could be used (Prusti et al., 2016; de Bruijne & Eilers, 2012). Gaia mission measures radial velocities with an onboard spectrograph and Gaia DR2 contains an unprecedented set of radial velocities for 7,2 million objects with a typical error of ~ 1 km s^{-1} (Cropper et al., 2018; Katz et al., 2018; Sartoretti et al., 2018). This error can be compared to the error budget on velocities along the sky plane. Table 3 illustrates the error budget for a Solar type and for a red clump star, both at a distance of 1 kpc, if interstellar extinction can be neglected. The next to last line shows that for stars at rest their velocities along the sky plane are determined to ~ 0.1 km s^{-1}, while the last line demonstrates that for fast moving stars the uncertainties on their distance increase the errors on their velocities along the sky plane to more than 1 km s^{-1}. So at least for slowly moving stars and for the ones in clusters it is desirable that the radial velocity component has an error similar to errors of velocities along the sky plane, i.e. ~ 0.1 km s^{-1}. Note also that any studies of dynamics *inside* star clusters greatly benefit from accurate velocities, as escape

Table 2. Typical uncertainties of Gaia DR2 (Brown et al., 2018). G magnitude is a white light measurement by Gaia, while G_{BP}, G_{RP} and G_{RVS} are integral measurements in its blue, red and Gaia-RVS bands; mas stands for milli-arc-second.

Data product or source type	Typical uncertainty
Five-parameter astrometry (position & parallax)	0.02-0.04 mas at $G < 15$
	0.1 mas at $G = 17$
	0.7 mas at $G = 20$
	2 mas at $G = 21$
Five-parameter astrometry (proper motion)	0.07 mas yr^{-1} at $G < 15$
	0.2 mas yr^{-1} at $G = 17$
	1.2 mas yr^{-1} at $G = 20$
	3 mas yr^{-1} at $G = 21$
Mean G-band photometry	0.3 mmag at $G < 13$
	2 mmag at $G = 17$
	10 mmag at $G = 20$
Mean $G_{\rm BP}$ and $G_{\rm RP}$ band photometry	2 mmag at $G < 13$
	10 mmag at $G = 17$
	200 mmag at $G = 20$
Median radial velocity over 22 months	0.3 km s^{-1} at $G_{\rm RVS} < 8$
	0.6 km s^{-1} at $G_{\rm RVS} = 10$
	1.8 km s^{-1} at $G_{\rm RVS} = 11.75$
Systematic radial velocity errors	< 0.1 km s^{-1} at $G_{\rm RVS} < 9$
	0.5 km s^{-1} at $G_{\rm RVS} < 11.75$

velocity from a cluster seldom supersedes a few km s^{-1}.

3. Ground based spectroscopic surveys

Ground-based spectroscopic surveys designed to complement Gaia include RAVE, Gaia-ESO, Apogee, GALAH, and LAMOST. All but the last one measure radial velocities at a level better than or comparable to Gaia, but for a much smaller number of stars. Internal precision of Apogee is better than 0.1 km s^{-1} (Nidever et al., 2015), and the accuracy is ~ 0.3 km s^{-1} (Anguiano et al., 2018). GALAH survey currently observed more than half-a-million stars with a typical accuracy of their radial velocity of ~ 0.15 km s^{-1} (Zwitter et al., 2018), as it includes also effects of convective blueshift and gravitational redshift of light emerging from a stellar atmosphere. It published also medians of observed spectra that are nearly noiseless, as they are obtained from a large number of observed spectra belonging to the same bin in stellar parameter space with a width of 50 K in temperature, 0.2 dex in gravity, and 0.1 dex in metallicity.

Table 3. Typical errors on distance, proper motion and velocity along the sky plane for a star at a distance of 1 kpc if effects of interstellar reddening can be neglected. Errors on velocity along the sky plane depend on actual velocity of the object: $\sigma(V_\mu)_1$ lists the error if the object is at rest and the error is driven by the proper motion uncertainty; and $\sigma(V_\mu)_2$ is for an object with a velocity of 50 km s^{-1} along the sky plane, where the error is driven by the distance error.

Parameter	Symbol	Solar type star	Red clump star
Absolute V magnitude	M_V	4.83	0.5
$V - I_C$ colour	$V - I_C$	0.70	1.06
Apparent G magnitude	G	14.5	10.1
Parallax error	$\sigma_{\tilde{\omega}}$	30 μas	40 μas
Distance error	$\sigma_{distance}$	3%	4%
Proper motion error	σ_μ	17 μas yr^{-1}	22 μas yr^{-1}
Velocity error along the sky plane	$\sigma(V_\mu)_1$	0.08 km s^{-1}	0.11 km s^{-1}
Velocity error along the sky plane	$\sigma(V_\mu)_2$	1.5 km s^{-1}	2 km s^{-1}

Publicly released 1181 median spectra have a resolving power of 28,000 and trace the F-G-K stars with metallicities between −0.6 and +0.3 dex.

All of the mentioned ground-based spectroscopic surveys determine values of stellar parameters and in many cases also abundances of individual elements. The GALAH survey recently published what is currently the largest set of abundances of up to 23 chemical elements, which now includes 342,682 stars (Buder et al., 2018). This chemical information is crucial in complementing the excellent astrometric and photometric information from Gaia.

4. Proposal for a dedicated photometric survey

Gaia can judge on chemical composition of stars from two sources of information. It can use its radial velocity spectrograph (RVS) which collects several tens of spectra for stars brighter than $V \sim 15$. By adding up all spectra of a given star the combined spectrum yields radial velocity and – for bright-enough sources ($V \lesssim 12.5$) – also metallicity. Experience from the RAVE survey, which observed in the same wavelength range as Gaia RVS, shows that metallicity is driven by strong lines of the Calcium triplet, so that it is very difficult to separate iron abundance ([Fe/H]) from alpha enhancement ([α/Fe]) for relatively faint stars with noisy spectra (Zwitter et al., 2008; Kunder et al., 2017). The second source of chemistry for Gaia is star's spectral energy distribution which is sampled by low dispersion BP and RP spectra. Wavelength span of an effective resolution element (defined as 76% energy extent of the along-scan line spread function) varies from 9.1 nm at 330 nm to 24.5 nm at 640 nm and to 61.5 nm at 1050 nm (Prusti et al., 2016). Assuming the star is observed 100 times during the mission its total exposure time for the BP and RP instruments equals 442 seconds, each.

These low dispersion spectra can be used to determine values of astrophysical parameters for fainter stars than with the RVS instrument. As explained in Bailer-Jones (2011) and Prusti et al. (2016) for FGKM stars at $G = 15$ with less than two magnitudes extinction, effective temperature can be estimated to ~ 150 K, extinction to ~ 0.1 mag, surface gravity to ~ 0.3 dex, and metallicity [Fe/H] to ~ 0.2 dex. Ground-based spectroscopic surveys (RAVE, Apogee, Gaia-ESO, LAMOST, GALAH) have been useful in providing metallicities and in some cases element abundances, but cumulatively they now include less than 5 million stars, a small fraction of 160 million stars brighter than $G = 17$ with effective temperatures published by Gaia DR2. Here we propose a way to extend results on chemistry to fainter stars than doable by Gaia and to obtain iron abundances ([Fe/H]) and alpha-enhancement (α/Fe] separately. This is vital, as iron and alpha element abundances form a basis for stellar population studies (e.g. Krumholz et al., 2018), and present a useful chemical clock (e.g. Freeman & Bland-Hawthorn, 2002).

Star's chemistry can be inferred by measuring its brightness in 3 specific photometric filter bands centred on and off the prominent metallic lines. We use three readily available industrial photometric filters, which have however never been used in astronomy. Band A (394 ± 5 nm) is centred on the Ca II H&K lines, so it is sensitive to abundance of alpha elements ([α/Fe]), band B (430 ± 5 nm) contains many strong Fe I lines, so it is sensitive to metallicity ([Fe/H]), while band C (450 ± 5 nm) lacks any strong metallic lines. Bands have a width of 10 nm, thus moderately sized telescopes can be used. These are hard coated OD 4 10 nm bandpass filters in the Edmund Optics catalogue (items #65-192, #65-198, and #65-201). Their wide availability means that results obtained by different instruments can complement each other.

We build on the fact that luminosity and effective temperature of the source is now known from Gaia, so we can use the colour-colour vs. chemistry relationship holding at this particular position in the luminosity-temperature plane. These relationships can be established by a data driven approach using detailed chemical abundances of benchmark stars measured by ground-based spectroscopic surveys. The GALAH survey (Buder et al., 2018) and other observations by the Hermes spectrograph at the 4-m AAO telescope, which now contain accurate chemical abundances for up to 30 chemical elements and for $\sim 650,000$ stars, can be used, together with the results from RAVE and Gaia-ESO surveys.

Figure 1 illustrates properties of the proposed dataset for main sequence stars (as defined by Pecaut & Mamajek, 2013) using Kurucz models of stellar atmospheres (Munari et al., 2005). AB magnitudes in the three filters are combined into two spectral indices: $A - C$ (top panel) and $B - C$ (bottom panel). For each panel we plot the difference in magnitude if a star with Solar abundances and with a given effective temperature is mistaken for another similar (but not identical) type of object. Solid lines plot the difference if we observe a non-enhanced metal poor star of the same temperature, and dashed lines are for an alpha enhanced metal poor star. Finally, the dotted lines check on the

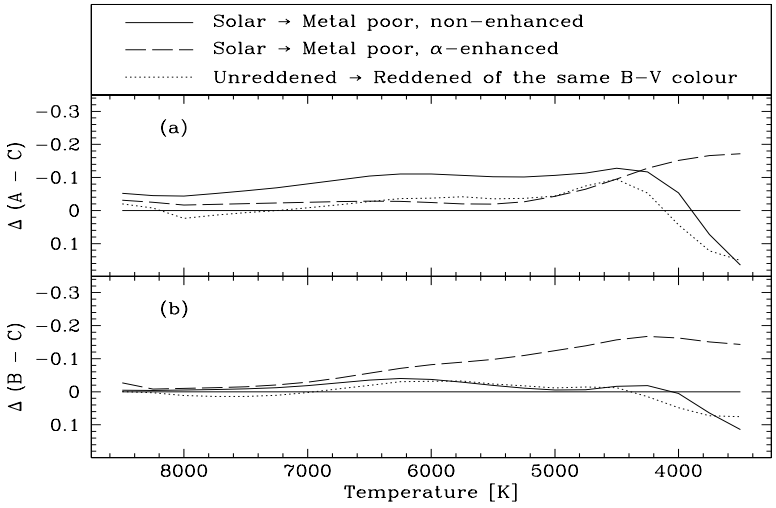

Figure 1. Change in the $A - C$ spectral index (panel a) and $B - C$ spectral index (panel b) as a function of effective temperature for main sequence stars. Three types of changes are plotted: (i) solid lines: observation of a metal poor non-enhanced star ([Fe/H] $= -0.4$, [α/Fe] $= 0.0$) instead of a Solar type one ([Fe/H] $= 0.0$, [α/Fe] $= 0.0$) with the same temperature; (ii) dashed lines: observation of a metal poor α-enhanced star ([Fe/H] $= -0.4$, [α/Fe] $= +0.4$) instead of a Solar type one ([Fe/H] $= 0.0$, [α/Fe] $= 0.0$) with the same temperature; (iii) dotted lines: observation of two Solar type stars which have the same observed $B - V$ colour, but one is reddened ($A_{\rm V} = 0.155$ mag) and the other is not. Horizontal line traces zero values.

influence of interstellar reddening: a star with Solar abundances with a given temperature is replaced with a reddened main sequence star ($A_V = 0.155$ mag) of Solar composition but with an intrinsically higher effective temperature, so that the observed $B - V$ colours of both stars are the same.

Absorption lines in the wavelength range of filter A are mostly lines of calcium, an α element. So the $A - C$ index (Fig. 1a) is sensitive to metal content, in the sense that the flux in filter A increases in the absence of absorption lines. This is true if all elements, including calcium, have a lower abundance (solid line in the top panel). But if calcium abundance is increased to Solar levels in a metal poor α-enhanced star ([Fe/H] $= -0.4$, [α/Fe] $= +0.4$), the $A - C$ index stays virtually the same as for a star with Solar abundances. Behaviour of the $B - C$ index (Fig. 1b) is different. Its values are increased for a metal poor α-enhanced star. So a combination of $A - C$ (Fig. 1a) and $B - C$ (Fig. 1b) indices allows a *separate* judgement of the iron abundance ([Fe/H]) and alpha enhancement ([α/Fe]) values.

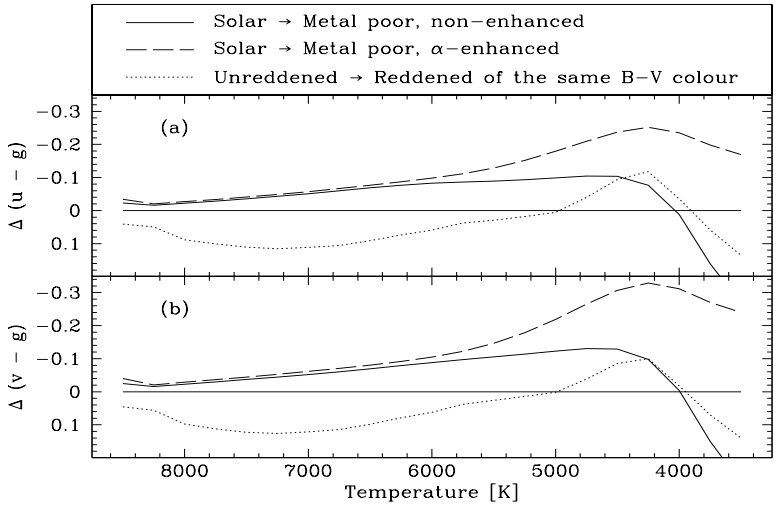

Figure 2. The same as Fig. 1 but for a Sloan $u - g$ index (panel a) and $v - g$ index (panel b). Pairwise behaviour of solid and dashed lines is virtually the same for both panels, so one cannot use the two spectral indices to distinguish changes in metallicity and alpha enhancement. Sloan bands are very blue, so they are sensitive to reddening (dotted lines) which can overshadow changes due to chemistry.

Values of temperature are known from Gaia, but with a typical error of ~ 150 K (Prusti et al., 2016). Derivation of more accurate values is hampered by unknown values of interstellar extinction which is strongly correlated with temperature. As an example, we compare stars with Solar abundances but with two different temperatures: an undereddened star and one which suffers from moderate interstellar reddening ($A_V = 0.155$, $R = 3.1$) and has the same reddened $B - V$ colour as the unreddened star. Typically, this implies that a reddened main sequence star is ~ 160 K hotter than the unreddened one. Results are shown with a dotted line in Fig. 1. Clearly the influence of reddening is moderate, except for stars cooler than 4750 K which have a steeply increasing flux in the range of A and B filters.

Approach outlined here is different from existing photometric surveys (e.g. SkyMapper) which use standard Sloan filters in an attempt to determine both the values of stellar parameters and chemistry, with the result that filters are not optimised for chemical analysis. So these surveys find it difficult to separate abundances of iron and alpha group elements, a vital starting point for any stellar population studies. Note also that the LSST survey uses a similar unoptimised filter set and may be saturated for most stars observed by Gaia.

The situation is illustrated in Figure 2 which is equivalent to Figure 1, ex-

cept that results for the Sloan indices $u - v$ and $g - v$, as implemented by the SkyMapper survey (Bessell et al., 2011), are presented. Both indices have almost identical solid and dashed curve shapes, so one can use them to determine general metallicity, but there is little hope to separate alpha enhancement and iron abundance. This agrees with recent results of Casagrande et al. (2019) who emphasise usefulness of SkyMapper for metallicity, but do not mention alpha enhancement determination. Note also that amplitudes of dotted curves in Fig. 2 are much larger than in Fig. 1, so measurement of metallicity using Sloan u and g filters which are bluer than A and B filters, is quite sensitive to damaging effects of interstellar reddening.

5. Conclusions

Gaia DR2 presents a profound change in the way research in astronomy is being done, so it should be used by virtually any astronomer. Still, it is important this information trove is used responsibly, taking into account all the information which was provided along with the data release. Complementary ground-based spectroscopic surveys are adding valuable information on chemistry of observed targets. The last months are bursting with activity, the Gaia DR2 paper (Brown et al., 2018) is the most cited paper in the field of astronomy and astrophysics published this year. Among the many significant results one could point to a disagreement between the value of the Hubble constant as determined from local Cepheids by Gaia and HST and between the value suggested by Planck observations of the early Universe (Riess et al., 2018), discovery of a perturbation and oscillation of the Galactic disk by a passage of a dwarf galaxy between 300 million and 900 million years ago (Antoja et al., 2018; Bland-Hawthorn et al., 2018), formation of the thick disc (Helmi et al., 2018), rich details of Hertzsprung-Russell diagrams (Babusiaux et al., 2018), and new studies of stellar clusters which are now relieved from uncertainties regarding their membership (e.g. Kos et al. 2018, 2018a).

Despite the tremendous success Gaia cannot do it all. Very accurate values of radial velocities and abundances of individual chemical elements are largely left to be determined by the ongoing spectroscopic ground-based surveys. An additional possibility which is briefly discussed above, is a photometric survey using dedicated filters which should be able to indicate metallicity and alpha enrichment of observed targets. This is achieved through the use of dedicated photometric filters which are narrower than resolution elements of Gaia's BP and RP instruments. Such a survey is within reach of a small telescope, which could therefore make a very significant contribution to Galactic astronomy.

Acknowledgements. The author acknowledges financial support of the Slovenian Research Agency (core funding P1-0188 and research project N1-0040).

References

Anguiano, B., et al. 2018,*Astron. Astrophys.*, **620**, A76

Antoja, T., et al. 2018, *Nature*, **561**, 360

Babusiaux, C., et al. 2018, *Astron. Astrophys.*, **616**, A10

Bailer-Jones, C.A.L. 2011, *Mon. Not. R. Astron. Soc.*, **411**, 435

Bailer-Jones, C.A.L., et al. 2018, *Astron. J.*, **156**, 58

Bessell, M., et al. 2011, *Publ. Astron. Soc. Pac.*, **123**, 789

Bland-Hawthorn, J., et al. 2018, *Mon. Not. R. Astron. Soc.*, in press, arXiv:1809.02658

Brown, A.G.A, et al. 2016, *Astron. Astrophys.*, **595**, A2

Brown, A.G.A, et al. 2018, *Astron. Astrophys.*, **616**, A1

Buder, S., et al. 2018, *Mon. Not. R. Astron. Soc.*, **478**, 4513

Casagrande, L., et al. 2019, *Mon. Not. R. Astron. Soc.*, **482**, 2770

Cropper, M. et al. 2018, *Astron. Astrophys.*, **616**, A5

de Bruijne, J.H.J, Eilers, A.-C. 2012 *Astron. Astrophys.*, **546**, A61

De Silva, G.M., et al. 2007, *Astron. J.*, **133**, 1161

De Silva, G.M., et al. 2015, *Mon. Not. R. Astron. Soc.*, **449**, 2604

Freeman, K., Bland-Hawthorn, J. 2002, *Ann. Rev. Astron. Astrophys.*, **40**, 487

Helmi, A., dr Zeeuw, P.T. 2000, *Mon. Not. R. Astron. Soc.*, **319**, 657

Helmi, A., et al. 2018, *Nature*, **563**, 85

Katz, D. et al. 2018, *Astron. Astrophys.*, in press, arXiv:1804.09372

Kos, J., et al. 2018, *Mon. Not. R. Astron. Soc.*, **473**, 4612

Kos, J., et al. 2018a, *Mon. Not. R. Astron. Soc.*, **480**, 5242

Krumholz, M.R., et al. 2018, *Ann. Rev. Astron. Astrophys.*, in press, arXiv:1812.01615

Kunder, A., et al. 2017, *Astron. J.*, **153**, 75

Lindegren, L., et al. 2018, *Astron. Astrophys.*, **616**, A2

Munari, U., et al. 2005, *Astron. Astrophys.*, **442**, 1127

Nidever, D.L., et al. 2015, *Astron. J.*, **150**, 173

Pecaut, M.J., Mamajek, E.E. 2013, *Astrophys. J., Suppl. Ser.*, **208**, 9

Prusti, T., et al. 2016, *Astron. Astrophys.*, **595**, A1

Riess, A.G., et al. 2018, *Astrophys. J.*, **861**, 126

Sartoretti, P., et al. 2018, *Astron. Astrophys.*, **616**, A6

Zwitter, T., et al. 2008, *Astron. J.*, **136**, 421

Zwitter, T., et al. 2018, *Mon. Not. R. Astron. Soc.*, **481**, 645

Contrib. Astron. Obs. Skalnaté Pleso **49**, 330 – 333, (2019)

YETI - The Young Exoplanet Transit Initiative

M. Mugrauer

Astrophysical Institute and University Observatory Jena, Schillergäßchen 2, 07745 Jena, Germany (E-mail: markus@astro.uni-jena.de)

Received: October 31, 2018; Accepted: January 23, 2019

Abstract. The Young Exoplanet Transit Initiative (YETI, Neuhäuser et al., 2011) is a world-wide collaboration of up to 2 m-class telescopes to continuously monitor the photometry of stars, which are members of young (age $\lesssim 100$ Myr) nearby ($d \lesssim 2$ kpc) open star clusters.

Although the telescopes of the YETI network exhibit only small diameters, a photometric precision on the few milli-mag level is reached, which allows the detection of young transiting exoplanets and the precise measurement of their transit light curves, which is the primary goal of YETI. In addition, as secondary science of this initiative, for all stars, located in the observed fields of view, their photometric variability of any kind is investigated within a range of time between minutes up to years.

So far, several open star clusters could already be monitored in many photometric campaigns, successfully carried out over at least three subsequent years. Each of these YETI campaigns typically lasts for about two weeks, sufficiently long to detected all transit events of young exoplanets, which revolve on close-in orbits around the observed target stars. For detected transiting planet-candidates their radii are derived from the obtained transit light curves and follow-up observations are carried out to rule out false positive scenarios and eventually to determine the masses of these companions. The radius and mass determination of detected young exoplanets allows to probe their internal structure, and eventually will constrain planet formation and evolutionary models and their time-scales.

In a talk, presented at the conference *Observing techniques, instrumentation and science for metre-class telescopes II* on 26 September 2018, I gave an overview of YETI and presented first results obtained during the last years in the course of this initiative. Furthermore, in my talk I reported on upcoming follow-up observations, proposed and scheduled for detected planet-candidates at 10 m class telescopes.

Key words: exoplanets – photometry – transit observations

1. First results of YETI

Although the photometric monitoring of the young open star clusters, conducted in the course of YETI, was just recently finished, and data-reduction and analysis are still ongoing for several clusters, first results of this project were already published during the last years, based on observations carried out at the observatories that cooperate within the YETI network.

So far, a large amount of imaging data could be taken for YETI using this telescope network. For example, at the University Observatory Jena the YETI clusters were observed in hundreds of nights using the instruments (STK, CTK, and RTK, Mugrauer & Berthold, 2010; Mugrauer, 2009, 2016) operated at the observatory, which results in about 1.6 TB of science data that could be recorded for YETI at this observing site since 2009.

In those YETI clusters, which were the first to be investigated and whose data have already been fully analyzed, transiting planet-candidates were reported. Among them, 2 planet-candidates in the young open star cluster Trumpler 37 (Errmann et al., 2013, 2014), one candidate in NGC 7243 (Garai et al., 2016), as well as a young transiting exoplanet-candidate of the weak-lined T Tauri star CVSO 30 in 25 Ori (Raetz et al., 2016). In addition, close to this young star a direct imaging planet-candidate was reported, which was detected with the adaptive optics imager NACO/VLT, and whose spectroscopic properties were determined with the integral field spectrograph SINFONI/VLT (Schmidt et al., 2016). Hence, if confirmed, CVSO 30 could be the first system known with both a close-in transiting exoplanet and a directly imaged planet on a wider orbit. Furthermore, an interesting transit-signal was found in the light curve of a member of IC 348, which is probably a grazing eclipsing binary, composed of a K0 pre-main-sequence star with a low-mass companion with a mass close to the stellar/substellar mass-border (Fritzewski et al., 2016). Further observations are needed to characterize the true nature of the detected transit-signal, and in particular for mass determination.

Meanwhile, also additional planet-candidates could be revealed among members in other YETI clusters but data analysis is still ongoing. In order to rule out false-positive detections for all identified presumable planet host stars, follow-up high contrast adaptive optics imaging observations, multi-band photometric monitoring, low-resolution spectroscopy, and eventually also radial-velocity measurements are carried out, which are currently ongoing.

Beside the detection of young exoplanets, which is the primary science goal of YETI, the photometric variability of the stars, located within the observed field of views, is investigated as secondary science. In the course of YETI so far several rotating and flaring T-Tauri stars could be identified and their photometric variability, as well as the distribution of their rotational periods and flaring rates, were investigated (e.g. GM Cep in Trumpler 37, Chen et al., 2012). Furthermore, many new eclipsing binary stars and pulsating variables were detected, and their orbital and/or physical properties could be determined.

2. Online material

The slides of my talk are available online for download in the pdf-format at:
`https://www.astro.uni-jena.de/Users/markus/26092018/talk.pdf`

A list of all publications, referenced on the slides in my talk, is summarized in the following section.

References

Baraffe, I., Chabrier, G., Allard, F., & Hauschildt, P. H., Evolutionary models for solar metallicity low-mass stars: mass-magnitude relationships and color-magnitude diagrams. 1998, *Astron. Astrophys.*, **337**, 403

Baraffe, I., Chabrier, G., Barman, T. S., Allard, F., & Hauschildt, P. H., Evolutionary models for cool brown dwarfs and extrasolar giant planets. The case of HD 209458. 2003, *Astron. Astrophys.*, **402**, 701, DOI: 10.1051/0004-6361:20030252

Bate, M. R., Bonnell, I. A., & Bromm, V., The formation of a star cluster: predicting the properties of stars and brown dwarfs. 2003, *Mon. Not. R. Astron. Soc.*, **339**, 577, DOI: 10.1046/j.1365-8711.2003.06210.x

Burrows, A., Marley, M., Hubbard, W. B., et al., A Nongray Theory of Extrasolar Giant Planets and Brown Dwarfs. 1997, *Astrophys. J.*, **491**, 856, DOI: 10.1086/305002

Chen, W. P., Hu, S. C.-L., Errmann, R., et al., A Possible Detection of Occultation by a Proto-planetary Clump in GM Cephei. 2012, *Astrophys. J.*, **751**, 118, DOI: 10.1088/0004-637X/751/2/118

de Boer, J., Salter, G., Benisty, M., et al., Multiple rings in the transition disk and companion candidates around RX J1615.3-3255. High contrast imaging with VLT/SPHERE. 2016, *Astron. Astrophys.*, **595**, A114, DOI: 10.1051/0004-6361/201629267

Errmann, R., Neuhäuser, R., Marschall, L., et al., The stellar content of the young open cluster Trumpler 37. 2013, *Astronomische Nachrichten*, **334**, 673, DOI: 10.1002/asna.201311890

Errmann, R., Torres, G., Schmidt, T. O. B., et al., Investigation of a transiting planet candidate in Trumpler 37: An astrophysical false positive eclipsing spectroscopic binary star. 2014, *Astronomische Nachrichten*, **335**, 345, DOI: 10.1002/asna.201412047

French, M., Becker, A., Lorenzen, W., et al., Ab Initio Simulations for Material Properties along the Jupiter Adiabat. 2012, *Astrophys. J., Suppl.*, **202**, 5, DOI: 10.1088/0067-0049/202/1/5

Fritzewski, D. J., Kitze, M., Mugrauer, M., et al., Long-term photometry of IC 348 with the Young Exoplanet Transit Initiative network. 2016, *Mon. Not. R. Astron. Soc.*, **462**, 2396, DOI: 10.1093/mnras/stw1797

Garai, Z., Pribulla, T., Hambálek, Ľ., et al., Search for transiting exoplanets and variable stars in the open cluster NGC 7243. 2016, *Astronomische Nachrichten*, **337**, 261, DOI: 10.1002/asna.201512310

Mayer, L., Quinn, T., Wadsley, J., & Stadel, J., Formation of Giant Planets by Fragmentation of Protoplanetary Disks. 2002, *Science*, **298**, 1756, DOI: 10.1126/science.1077635

Mugrauer, M., CTK: A new CCD Camera at the University Observatory Jena. 2009, *Astronomische Nachrichten*, **330**, 419, DOI: 10.1002/asna.200811186

Mugrauer, M., CTK-II & RTK: The CCD-cameras operated at the auxiliary telescopes of the University Observatory Jena. 2016, *Astronomische Nachrichten*, **337**, 226, DOI: 10.1002/asna.201512302

Mugrauer, M. & Berthold, T., STK: A new CCD camera at the University Observatory Jena. 2010, *Astronomische Nachrichten*, **331**, 449, DOI: 10.1002/asna.201011349

Neuhäuser, R., Errmann, R., Berndt, A., et al., The Young Exoplanet Transit Initiative (YETI). 2011, *Astronomische Nachrichten*, **332**, 547, DOI: 10.1002/asna.201111573

Raetz, S., Schmidt, T. O. B., Czesla, S., et al., YETI observations of the young transiting planet candidate CVSO 30 b. 2016, *Mon. Not. R. Astron. Soc.*, **460**, 2834, DOI: 10.1093/mnras/stw1159

Schmidt, T. O. B., Neuhäuser, R., Briceño, C., et al., Direct Imaging discovery of a second planet candidate around the possibly transiting planet host CVSO 30. 2016, *Astron. Astrophys.*, **593**, A75, DOI: 10.1051/0004-6361/201526326

Spiegel, D. S. & Burrows, A., Spectral and Photometric Diagnostics of Giant Planet Formation Scenarios. 2012, *Astrophys. J.*, **745**, 174, DOI: 10.1088/0004-637X/745/2/174

Contrib. Astron. Obs. Skalnaté Pleso **49**, 334 – 340, (2019)

Planet-star tidal interactions with precise transit timing

G. Maciejewski

Centre for Astronomy, Faculty of Physics, Astronomy and Informatics, Nicolaus Copernicus University, Grudziadzka 5, 87-100 Toruń, Poland, (E-mail: gmac@umk.pl)

Received: November 2, 2018; Accepted: March 7, 2019

Abstract. Theoretical calculation and some indirect observations show that massive exoplanets on the tightest orbits – so-called hot Jupiters – must undergo orbital decay due to tidal dissipation within their host stars. This orbital evolution could be observationally accessible through precise transit timing over the course of decades. Meter-class telescopes are recognised as excellent instruments for such follow-up observations. They usually provide photometric time series of millimagnitude or even sub-millimagnitude precision for stars brighter than ∼12 mag. Such observations allow us to determine individual mid-transit times with errors between 20 and 40 s, and when they are combined together, the averaged timing precision down to or even below 10 s can be achieved over time scales of months. The rate of planetary in-spiralling may not only help us to understand some aspects of evolution of planetary systems, but can also be used as a probe of the stellar internal structure. Since 2017 we have run a regular observing campaign aimed at transit timing for a sample of best candidates for in-falling planets. Among them there is WASP-12 b, transits of which exhibit a pronounced departure from a linear ephemeris. New observations allow us to confirm the rapid decay rate for that planet, and to place constraints on the tidal dissipation efficiency in other systems.

Key words: planet-star interactions – stars: individual: HAT-P-23, WASP-12 – planets and satellites: individual: HAT-P-23 b, WASP-12 b

1. Introduction

The tidal force, which is raised by one body on the other, is proportional to the mass of the body rising the tide, and inversely proportional to the cube of the distance between both bodies. Thus, massive exoplanets on the tightest orbits, with orbital separations as small as several stellar radii, are recognised as great laboratories for studies of star-planet tidal interactions outside the Solar Sytem. Such planets, called hot Jupiters, are expected to be spiralling towards host stars because of the dissipative nature of tides, caused by the friction of the tidally induced fluid flow (Levrard et al., 2009). In such systems, the host star usually rotates slower than the orbital period of the planet. There is a phase lag in the tidal response that results in transferring the orbital angular momentum into the

star – the orbit shrinks and the star spins up. The dissipation of energy, which is stored in the equilibrium tides, is thought to occur in stellar zones where the viscosity is induced by the turbulent convective motions (Zahn, 1966; Goldreich & Nicholson, 1977). The tidal dissipation can be boosted by radiative damping of the dynamical tides that are produced near radiative-convective boundaries (see Goldreich & Nicholson, 1989, for further references).

The efficiency of tidal dissipation in the host star can be characterised with the dimensionless tidal quality parameter $Q'_\star = \frac{3}{2}Q_\star/k_2$ (Goldreich & Soter, 1966), where $Q_\star$ is the inverse of the phase lag between the tidal potential and the tidal bulge (or the ratio of energy stored in tidal distortion to energy dissipated in one tidal cycle), and k_2 is the second order tidal Love number. A smaller value of $Q'_\star$ translates into a stronger or more efficient tidal dissipation and vice versa. Theoretical studies of turbulent damping of equilibrium tides predict $Q'_\star$ of 10^8–10^9 for main-sequence stars (Penev & Sasselov, 2011). The studies of binary stars in stellar clusters show that $Q'_\star$ might be of order 10^6 (e.g. Meibom & Mathieu, 2005). A statistical analysis of the destruction rate of hot Jupiters yields $Q'_\star > 10^7$ (Penev et al., 2012). In other studies, Jackson et al. (2008) and Husnoo et al. (2012) obtained $Q'_\star \sim 10^{6.5}$, while Hansen (2010) found $10^7 < Q'_\star < 10^9$. An investigation of orbital parameters for a sample of hot planets allowed Bonomo et al. (2017) to conclude that Q'_* must exceed 10^6–10^7. Penev et al. (2018) studied hot-Jupiter systems with known stellar rotation periods and found that the tidal quality parameter may also depend on the amplitude and frequency of the tidal excitation, and it must be in the range of 10^5 to 10^7.

Orbital decay can be detected through transit timing over a course of decades. Following the formalism of Goldreich & Soter (1966), the cumulative shift in transit times $T_{\rm shift}$ after time T can be estimated by the formula

$$T_{\rm shift} = -\frac{27}{4}\frac{\pi}{Q'_\star}\frac{1}{P_{\rm orb}}\left(\frac{M_{\rm p}}{M_\star}\right)\left(\frac{a}{R_\star}\right)^{-5} T^2\,, \qquad (1)$$

where $P_{\rm orb}$ is the orbital period, $M_{\rm p}$ is the planet's mass, $M_\star$ and $R_\star$ are the host star's mass and radius, and a is the semi-major axis of the planet's orbit. For some planets, the predicted value of $T_{\rm shift}$ is of order 100 s after ten years if $Q'_\star = 10^6$ is assumed (e.g., Birkby et al., 2014).

So far, the only candidate for a spiralling-in exoplanet is WASP-12 b (Hebb et al., 2009). The planet has a mass of $\sim$1.4 $M_{\rm Jup}$ (Jupiter mass) and a bloated radius of $\sim$1.9 $R_{\rm Jup}$ (Jupiter radius). It orbits its F/G host star with a period of 1.09 d. Maciejewski et al. (2016) employed the method of precise transit timing to detect the apparent shortening of the orbital period. Departure from a linear transit ephemeris by $\sim$5 minutes was observed in the course of 8 years. This finding translates into the rate of orbital period shortening of $\sim 2.6\times10^{-2}$ s yr^{-1}, giving $Q'_\star = 2.5\times10^5$. Although transit times were found to follow the quadratic ephemeris very well, there is still an alternative scenario in which the observed

period shrinkage is *de facto* part of a long-period cycle caused by either a tidally induced apsidal precession of a slightly eccentric orbit (Ragozzine & Wolf, 2009) or dynamical interactions with a planetary companion (Maciejewski, 2018).

Being motivated by the case of the WASP-12 system, we have initiated a systematic transit timing monitoring programme for a sample of hot giant exoplanets for which period shrinkage could be detected in the course of a decade (Maciejewski et al., 2018). In this note, we announce results obtained for the WASP-12 system. We place them in a wider context by comparing them to results obtained for another system of our sample – HAT-P-23, in which there is a 2.1 $M_{\rm Jup}$ planet orbiting an early G dwarf star with a period of 29 hours (Bakos et al., 2011).

2. Results

New mid-transit times were determined from photometric time series acquired between March 2016 and September 2018 with 0.6–2.0 m telescopes located in Spain, Germany, Bulgaria, and Poland (see Maciejewski et al., 2018, for details). The transit timing residuals against the linear ephemerides in the form:

$$T_{\rm mid}(E) = T_0 + P_{\rm orb} \times E\,, \tag{2}$$

where E is a transit number from the reference epoch T_0, are shown for both planets in Fig. 1. The new transit times for HAT-P-23 b reveal no departure from the linear ephemeris. To place a constraint on the rate of the orbital decay for HAT-P-23 b , and hence on $Q'_\star$, a quadratic ephemeris in the form was fitted:

$$T_{\rm mid} = T_0 + P_{\rm orb} \times E + \frac{1}{2}\frac{dP_{\rm orb}}{dE} \times E^2\,, \tag{3}$$

where $\frac{dP_{\rm orb}}{dE}$ is the change in the orbital period between succeeding transits. The best-fit parameters and their uncertainties were derived from the posterior probability distributions of those parameters generated with the Markov Chain Monte Carlo algorithm. We employed 100 chains, each of which was 10^4 steps long after discarding the first 1000 trials. The value of $Q'_\star$ was calculated after rearranging Eq. (1) to the form

$$Q'_\star = -\frac{27}{2}\pi \left(\frac{M_{\rm p}}{M_\star}\right) \left(\frac{a}{R_\star}\right)^{-5} \left(\frac{dP_{\rm orb}}{dE}\right)^{-1} P_{\rm orb}\,. \tag{4}$$

Since the value of $\frac{dP_{\rm orb}}{dE}$ was found to be indistinguishable from 0 within 2σ, we found that $Q'_\star$ of HAT-P-23 must be greater than 5.6×10^5 at the 95% confidence level (Maciejewski et al., 2018).

The new transit times for WASP-12 b were found to follow the quadratic ephemeris very well. The best-fit model has the reduced χ^2 of 0.9 and yields

$$\frac{dP_{\rm orb}}{dE} = (-9.67 \pm 0.73) \times 10^{-10} \quad \text{days per epoch}^2\,. \tag{5}$$

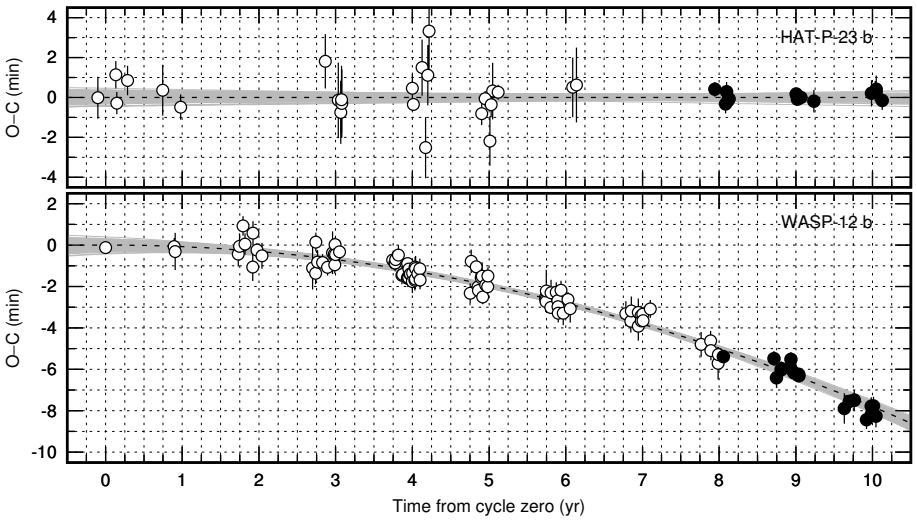

Figure 1. Upper panel: timing residuals against the linear ephemeris for HAT-P-23 b. Values from the new observations, which are taken from Maciejewski et al. (2018), are marked with dots, while the literature values are plotted with open circles. A dashed line marks the zero value. The ephemeris uncertainties are illustrated by grey lines that are drawn for 100 sets of parameters, randomly chosen from the Markov chains. Bottom panel: the same as in the upper panel but for WASP-12 b with the difference that the dashed line in the bottom panel displays the best-fit quadratic trend in transit times, and the grey lines sketch the uncertainties of the quadratic ephemeris.

This value is consistent within error bars with and more precise than values of $(-8.9 \pm 1.4) \times 10^{-10}$ and $(-10.2 \pm 1.1) \times 10^{-10}$ days per epoch^2 reported by Maciejewski et al. (2016) and Patra et al. (2017), respectively. Following eq. (4), we obtained

$$Q'_\star = (1.82 \pm 0.32) \times 10^5 \,. \tag{6}$$

3. Concluding discussion

Chernov et al. (2017) demonstrated that the rate of the orbital shrinkage of WASP-12 b might be consistent with theoretical predictions which assume the host star is a dwarf. In this scenario, the WASP-12 system would be nowadays observed in the final stage of its existence, which appears to be unlikely (Patra et al., 2017). On the other hand, Weinberg et al. (2017) found that the observed rate of orbital decay could only be explained if WASP-12 were a subgiant – a star during the transition phase between the end of the main-sequence stage and the beginning of stable hydrogen burning in a shell on the red-giant branch. This scenario is supported by the stellar properties, which are consistent with

a $\sim$1.2 $M_\odot$ subgiant star. Models of the internal structure of subgiants predict that the efficiency of the tidal dissipation is boosted by several orders of magnitude due to nonlinear wave-breaking of the dynamical tide near the star's centre (Barker & Ogilvie, 2010). If this mechanism operates in WASP-12, the calculations of Barker & Ogilvie (2010) yield $Q'_\star \approx 1.9 \times 10^5$ that is in an excellent agreement with our empirical $Q'_\star \approx 1.8 \times 10^5$. The high value of $Q'_\star \approx 10^8$ would have prevented the planet from spiralling inward over the course of $\sim$4 Gyr of WASP-12's evolution on the main sequence. The evolutionary changes in the star's interior structure would then trigger a rapid orbital decay that is observed nowadays (Barker & Ogilvie, 2010; Weinberg et al., 2017).

For the HAT-P-23 system, the model of Essick & Weinberg (2016) predicts $Q'_\star \approx 6.7 \times 10^5$, which is not rejected by our empirical constraint of $Q'_\star > 5.6 \times 10^5$. On the other hand, Penev et al. (2018) obtained $Q'_\star \approx 3 \times 10^6$ assuming that HAT-P-23, with its rotational speed observed nowadays, has been spun up by tides being raised by its hot giant planet. Further precise transit timing data are expected to empirically verify the proposed models.

A mechanism that drives the rapid orbital decay of WASP-12 b still remains a puzzle. New transit times follow the quadratic ephemeris very well, making the alternative scenarios, such as the apsidal precession or dynamical perturbations from a planetary companion, less likely.

Acknowledgements. The author acknowledges the financial support from the National Science Centre, Poland, through grant no. 2016/23/B/ST9/00579.

References

Bakos, G. Á., Hartman, J., Torres, G., et al., HAT-P-20b-HAT-P-23b: Four Massive Transiting Extrasolar Planets. 2011, *Astrophys. J.*, **742**, 116, DOI: 10.1088/0004-637X/742/2/116

Barker, A. J. & Ogilvie, G. I., On internal wave breaking and tidal dissipation near the centre of a solar-type star. 2010, *Mon. Not. R. Astron. Soc.*, **404**, 1849, DOI: 10.1111/j.1365-2966.2010.16400.x

Birkby, J. L., Cappetta, M., Cruz, P., et al., WTS-2 b: a hot Jupiter orbiting near its tidal destruction radius around a K dwarf. 2014, *Mon. Not. R. Astron. Soc.*, **440**, 1470, DOI: 10.1093/mnras/stu343

Bonomo, A. S., Desidera, S., Benatti, S., et al., The GAPS Programme with HARPS-N at TNG . XIV. Investigating giant planet migration history via improved eccentricity and mass determination for 231 transiting planets. 2017, *Astron. Astrophys.*, **602**, A107, DOI: 10.1051/0004-6361/201629882

Chernov, S. V., Ivanov, P. B., & Papaloizou, J. C. B., Dynamical tides in exoplanetary systems containing hot Jupiters: confronting theory and observations. 2017, *Mon. Not. R. Astron. Soc.*, **470**, 2054, DOI: 10.1093/mnras/stx1234

Essick, R. & Weinberg, N. N., Orbital Decay of Hot Jupiters Due to Nonlinear Tidal Dissipation within Solar-type Hosts. 2016, *Astrophys. J.*, **816**, 18, DOI: 10.3847/0004-637X/816/1/18

Goldreich, P. & Nicholson, P. D., Turbulent viscosity and Jupiter's tidal Q. 1977, *Icarus*, **30**, 301, DOI: 10.1016/0019-1035(77)90163-4

Goldreich, P. & Nicholson, P. D., Tidal friction in early-type stars. 1989, *Astrophys. J.*, **342**, 1079, DOI: 10.1086/167665

Goldreich, P. & Soter, S., Q in the Solar System. 1966, *Icarus*, **5**, 375, DOI: 10.1016/0019-1035(66)90051-0

Hansen, B. M. S., Calibration of Equilibrium Tide Theory for Extrasolar Planet Systems. 2010, *Astrophys. J.*, **723**, 285, DOI: 10.1088/0004-637X/723/1/285

Hebb, L., Collier-Cameron, A., Loeillet, B., et al., WASP-12b: The Hottest Transiting Extrasolar Planet Yet Discovered. 2009, *Astrophys. J.*, **693**, 1920, DOI: 10.1088/0004-637X/693/2/1920

Husnoo, N., Pont, F., Mazeh, T., et al., Observational constraints on tidal effects using orbital eccentricities. 2012, *Mon. Not. R. Astron. Soc.*, **422**, 3151, DOI: 10.1111/j.1365-2966.2012.20839.x

Jackson, B., Greenberg, R., & Barnes, R., Tidal Evolution of Close-in Extrasolar Planets. 2008, *Astrophys. J.*, **678**, 1396, DOI: 10.1086/529187

Levrard, B., Winisdoerffer, C., & Chabrier, G., Falling Transiting Extrasolar Giant Planets. 2009, *Astrophys. J., Lett.*, **692**, L9, DOI: 10.1088/0004-637X/692/1/L9

Maciejewski, G., WASP-12 b - an exoplanet falling onto its host star? 2018, in XXXVIII Polish Astronomical Society Meeting, Vol. **7**, *XXXVIII Polish Astronomical Society Meeting*, ed. A. Różańska, 113–117

Maciejewski, G., Dimitrov, D., Fernández, M., et al., Departure from the constant-period ephemeris for the transiting exoplanet WASP-12. 2016, *Astron. Astrophys.*, **588**, L6, DOI: 10.1051/0004-6361/201628312

Maciejewski, G., Fernández, M., Aceituno, F., et al., Planet-Star Interactions with Precise Transit Timing. I. The Refined Orbital Decay Rate for WASP-12 b and Initial Constraints for HAT-P-23 b, KELT-1 b, KELT-16 b, WASP-33 b and WASP-103 b. 2018, *Acta Astron.*, **68**, 371, DOI: 10.32023/0001-5237/68.4.4

Meibom, S. & Mathieu, R. D., A Robust Measure of Tidal Circularization in Coeval Binary Populations: The Solar-Type Spectroscopic Binary Population in the Open Cluster M35. 2005, *Astrophys. J.*, **620**, 970, DOI: 10.1086/427082

Patra, K. C., Winn, J. N., Holman, M. J., et al., The Apparently Decaying Orbit of WASP-12b. 2017, *Astron. J.*, **154**, 4, DOI: 10.3847/1538-3881/aa6d75

Penev, K., Bouma, L. G., Winn, J. N., & Hartman, J. D., Empirical Tidal Dissipation in Exoplanet Hosts From Tidal Spin-up. 2018, *Astron. J.*, **155**, 165, DOI: 10.3847/1538-3881/aaaf71

Penev, K., Jackson, B., Spada, F., & Thom, N., Constraining Tidal Dissipation in Stars from the Destruction Rates of Exoplanets. 2012, *Astrophys. J.*, **751**, 96, DOI: 10.1088/0004-637X/751/2/96

Penev, K. & Sasselov, D., Tidal Evolution of Close-in Extrasolar Planets: High Stellar Q from New Theoretical Models. 2011, *Astrophys. J.*, **731**, 67, DOI: 10.1088/0004-637X/731/1/67

Ragozzine, D. & Wolf, A. S., Probing the Interiors of very Hot Jupiters Using Transit Light Curves. 2009, *Astrophys. J.*, **698**, 1778, DOI: 10.1088/0004-637X/698/2/1778

Weinberg, N. N., Sun, M., Arras, P., & Essick, R., Tidal Dissipation in WASP-12. 2017, *Astrophys. J., Lett.*, **849**, L11, DOI: 10.3847/2041-8213/aa9113

Zahn, J. P., Les marées dans une étoile double serrée (suite). 1966, *Annales d'Astrophysique*, **29**, 489

Contrib. Astron. Obs. Skalnaté Pleso **49**, 341 – 345, (2019)

Photometric study of the asynchronous polar V1432 Aql in 2017-2018 at the Crimean Astrophysical Observatory

A. Baklanov and D. Baklanova

Crimean Astrophysical Observatory of RAS
298409 Nauchny, Crimea, Russia, (E-mail: baklanov@craocrimea.ru)

Received: October 31, 2018; Accepted: January 30, 2019

Abstract. We present the results of our research of the eclipsing asynchronous polar V1432 Aql. Photometric observations were obtained during 21 nights in 2017-2018 using the 38-cm telescope of the Crimean Astrophysical Observatory. We obtained 22 moments of dips associated with the orbital variability of the binary system and 40 minima associated with self-eclipses of accretion columns in the binary system. We found out that accretion in the system occurs at least on three accreting areas. According to our observations, the spin period of the white dwarf is 0.1405429(102) days in 2017 and 0.1404547(29) days in 2018. The improved orbital period is 0.140234676(15) days.

Key words: cataclysmic variables – accretion – stars: individual: V1432 Aql

1. Introduction

V1432 Aquilae (RX J1940.1-1025) belongs to a unique subclass of variable stars – asynchronous polars. To date, only four objects of this type are known (Ritter & Kolb, 2015).

This star is unique in this subtype. First, the V1432 Aql is the only one of these objects for which, thanks to a successful orientation of the system's orbit, eclipses and self-eclipses of accretion columns can be observed. And secondly, this is the only asynchronous system, in which the rotation period of the white dwarf exceeds the orbital period. The presence of eclipses allows us to determine the value of the orbital period with a high accuracy photometrically, P_{orb} = 3.365 hours. In addition to the usual eclipses of V1432 Aql, which were usually called "dips" (deep narrow "dips" on the light curve), the star has self-eclipses of the accretion column with a smaller depth and wider width. Andronov & Baklanov (2007) found that the accretion in the system occurs simultaneously into two poles. Rana et al. (2005) found three maxima in the X-ray during the spin period.

2. Observations

Observations were carried out at the Crimean Astrophysical Observatory with the 38-cm telescope using an Apogee Alta E47 CCD camera. To increase the accuracy of determining extremes, we obtained our observations in unfiltered light. Totally, our observations covered 6 nights (1281 points) in 2017 and 13 nights (3452 points) in 2018. Fig. 1 shows individual light curves of V1432 Aql in 2017 – 2018.

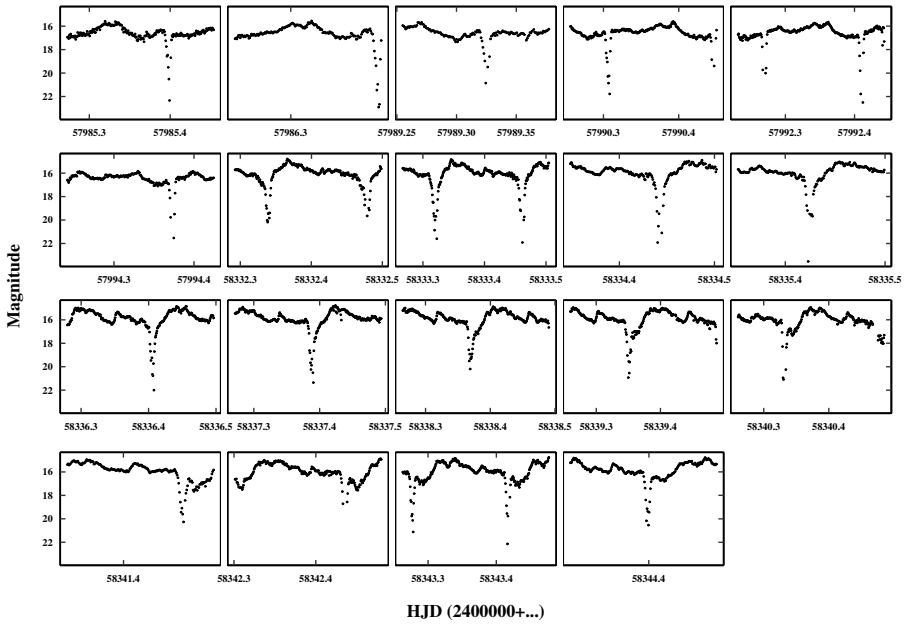

Figure 1. Individual light curves of V1432 Aql in 2017 – 2018.

3. Four types of minima

On the light curve, we can see the minima related to both the eclipse in the system and the self-eclipses of the accretion columns. Using the program MAVKA-OM (Andrych et al., 2017) (the method of asymptotic parabolas (Andronov, 1994)), 62 minimum moments with their errors were determined. All the moments of the minima were plotted on the diagram $(O-C)$ in Fig. 2 using the ephemeris obtained by Littlefield et al. (2015):

$$2454289.51352(4) + 0.1402347644(18) \times E.$$

All minima can be divided into four types.

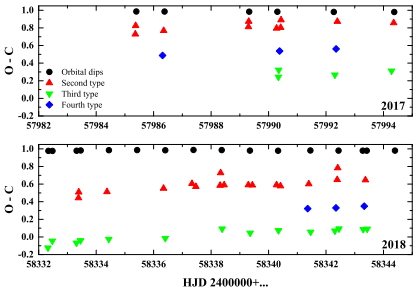

Figure 2. $(O-C)$ diagrams for four types of minima.

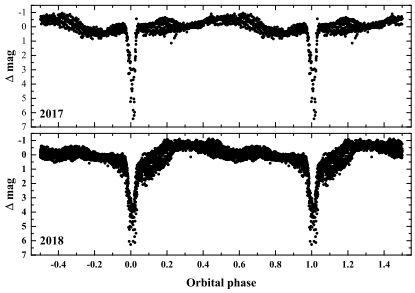

Figure 3. Orbital phase curves of V1432 Aql in 2017 and 2018

The first group of minima is parallel to the abscissa axis and corresponds to the orbital variability and is associated with eclipses of the white dwarf in the system. $(O-C)$ values of this type of minima systematically differ from 0. The $(O-C)$ average value is 0.9836 and 0.9817 in 2017 and 2018, respectively, which indicates that the orbital ephemeris of Littlefield et al. (2015) requires improvements.

The second group of minima, the most numerous, is located at an angle to the first group, which indicates that their period is rather larger than the orbital period. We associate this group of minima with the self-eclipses of the first accretion column (see Fig. 3).

The third group of minima is also located at an angle to the first group and shifted relative to the second group by 0.5 of the orbital period. We associate this group of minima with the self-eclipse of the second accretion column.

The fourth group of minima is inclined to the first group and is shifted relative to the second group by 0.7. This group can be associated with the self-eclipse of the third accretion column, or another bright accretion structure. This is the rarest type of minima, and contains only 6 points. We were able to identify these eclipses reliably only in a few consecutive nights, perhaps because the phenomenon causing this minimum is temporary and depends on the spin-orbit beat phase.

4. Orbital variability

Since the first type of minima on the $(O-C)$ diagram systematically differs from 0, we specified the value of the orbital period using the initial epoch of the minima by Littlefield et al. (2015). The adjusted period was 0.140234676(15) days. Phase curves with the improved orbital period are shown in Fig. 3.

5. Improvement of the spin period

To improve the spin period of the white dwarf in the system, we performed a periodogram analysis of the non-eclipse part using a 5-th order trigonometric polynomial fit realized in the program MCV (Andronov & Baklanov, 2004). The periodograms are shown in Fig. 4. The maxima of the periodogram correspond to 0.1405429 and 0.1404547 days in 2017 and 2018, respectively. The values of the periods were improved by the method of differential corrections (Andronov, 1994) and amounted to 0.1405429(102) and 0.1404547(29) days in 2017 and 2018, respectively. Mean phase curves using these periods are shown in Fig. 5. Between August 2017 and August 2018, the spin period decreased by 0.0000882(106) days (7.6 seconds = 8.3σ) or 0.063% of the orbital period.

As we see, mean spin phase curves in 2017 and 2018 are different. First of all, this difference is caused mostly by observations at different phases of the spin-orbital beat period. We can't exclude other causes, but these need additional study.

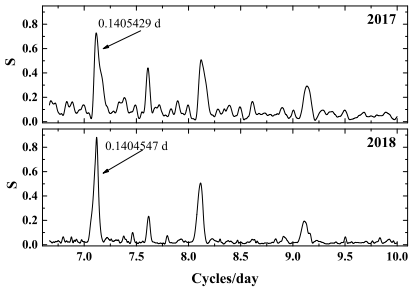

Figure 4. Periodograms for non-eclipsed parts of light curves in 2017 and 2018.

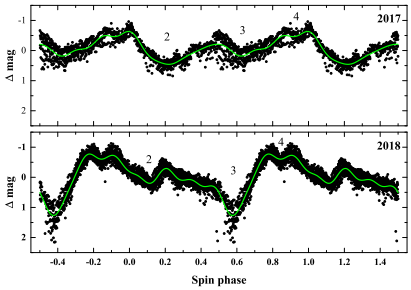

Figure 5. Spin phase curves of V1432 Aql in 2017 and 2018, excluding eclipses. Numbers corresponds to the group of minima and are described in section 3.

6. Conclusion

Our study confirms the complex structure of the accretion stream in V1432 Aql. We demonstrated that in the system there could be self-eclipses of at least three accretion columns. The improved orbital period is 0.140234676(15) days. We also obtained the rotation period of the synchronizing white dwarf in the system in August 2017 and August 2018 – 0.1405429(102) and 0.1404547(29), respectively. During the year, the period of the white dwarf slightly decreased by more than 7.5 ± 1 seconds.

References

Andronov, I. L., (Multi-) Frequency Variations of Stars. Some Methods and Results. 1994, *Odessa Astronomical Publications*, **7**, 49

Andronov, I. L. & Baklanov, A. V., Algorithm of the artificial comparison star for the CCD photometry. 2004, *Astronomical School's Report*, **5**

Andronov, I. L. & Baklanov, A. V., Capture radius and synchronization of the white dwarf in the unique magnetic cataclysmic system V1432 Aql. 2007, *Astrophysics*, **50**, 105, DOI: 10.1007/s10511-007-0012-z

Andrych, K. D., Andronov, I. L., & Chinarova, L. L., Statistically Optimal Modeling of Flat Eclipses and Exoplanet Transitions. The Wall-Supported Polynomial" (WSP) Algoritms. 2017, *Odessa Astronomical Publications*, **30**, 57, DOI: 10.18524/1810-4215.2017.30.118521

Littlefield, C., Mukai, K., Mumme, R., et al., Periodic eclipse variations in asynchronous polar V1432 Aql: evidence of a shifting threading region. 2015, *Mon. Not. R. Astron. Soc.*, **449**, 3107, DOI: 10.1093/mnras/stv462

Rana, V. R., Singh, K. P., Barrett, P. E., & Buckley, D. A. H., X-Ray Emission and Optical Polarization of V1432 Aquilae: An Asynchronous Polar. 2005, *Astrophys. J.*, **625**, 351, DOI: 10.1086/429283

Ritter, H. & Kolb, U., The Ritter-Kolb Catalogue and its Impact on Research into CVs, LMXBs and related Objects. 2015, *Acta Polytechnica CTU Proceedings*, **2**, 21

Contrib. Astron. Obs. Skalnaté Pleso **49**, 346 – 348, (2019)

Modelling of stellar surfaces in single and binary star systems

M. Fedurco, M. Čokina and Š. Parimucha

Institute of Physics, Faculty of Natural Sciences, P. J. Šafárik University, Jesenná 5, 040 01, Košice, Slovakia

Received: November 19, 2018; Accepted: March 15, 2019

Abstract. A precise and time effective method for generating stellar surfaces is a crucial step in creating the light curves of single and binary star systems. In the case of rotationally deformed components of single star systems and tidally deformed components of close binaries, spherical symmetry is no longer usable for generating stellar surfaces, which increases complexity of the task. However, exploitation of axial and planar symmetries of such stellar components proved to be a powerful tool in reducing overall computational time necessary to generate a stellar surface. We present one of the possible approaches to this issue that includes usage of symmetry vectors that enabled us to effectively perform the surface discretization and calculation of surface parameters such as the local effective temperature or gravity acceleration.

Key words: binary stars – single stars – computational astrophysics

1. Introduction

Stellar surface in hydrostatic equilibrium can be described as the equipotential surface defined by the appropriate potential function. Hovewer, especially in the case of components of binary systems, the solution of such potential function for the equipotential surface has to be found implicitly. Such approach is computationally demanding and thus the number of surface points evaluated should be minimized.

2. Construction of the stellar surfaces

Axial and planar symmetries of single and binary stellar surfaces enabled us to greatly reduce the surface area of the star that needs to be evaluated. It is especially important in the case of components of binary systems where surface points have to be solved implicitly. Moreover, triangulation of such reduced surface becomes much more efficient since the computational time of the Delaunay triangulation (Barber et al., 1996) scales with the square of the number of triangulated points.

Symmetries of stellar surfaces can be also utilized to avoid calculation of quantities characterizing stellar surface on the whole surface. Such quantities as

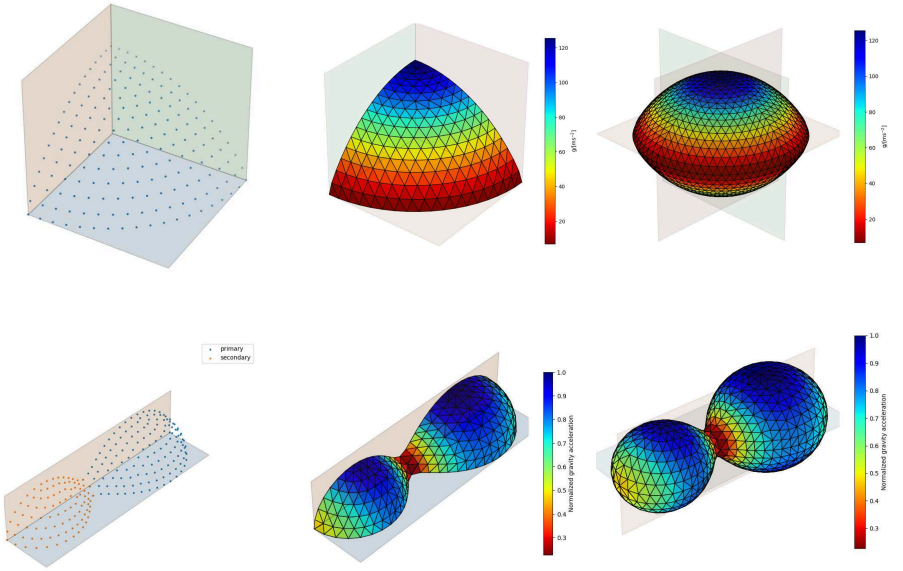

Figure 1. This set of figures illustrates construction of the stellar surface for a rotationally deformed single star (top row) and an over-contact binary system (bottom row) utilizing displayed planar symmetries. The left column shows the equipotential surface points that were subsequently triangulated (middle column) using the Delaunay triangulation. The rest of the surface is completed using before mentioned planar symmetries (right column).

gravity acceleration, gradient of surface potential, local effective temperature, etc. need to be evaluated only on the one eighth resp. one quarter of the surface and then mirrored to the rest of the surface faces using the "symmetry vector" which maps evaluated surface faces to all its symmetrical counterparts on the rest of the surface.

3. Triangulation of over-contact binary surfaces

One of the limitations of the Delaunay triangulation is the ability to triangulate only convex surfaces. However, the neck of the over-contact system is not a convex surface. We solved this problem by equalizing the radial component of the surface points which effectivelly transformed the surface point mesh into a convex spherical surface (Fig. 2b,c) which was triangulated and resulting faces were then remapped into the original concave point mesh (Fig. 2d).The main

advantage of this transformation is that it maintains relative positions of surface points which is crucial during the triangulation process.

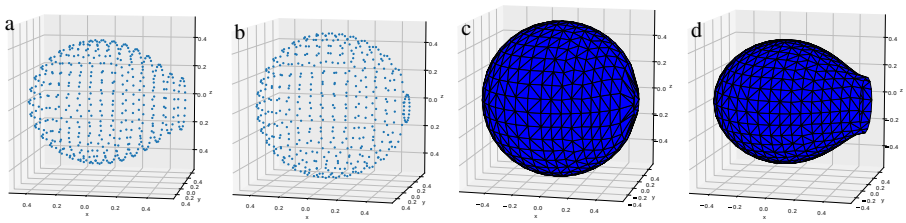

Figure 2. This series of figures illustrates an approach to triangulation of over-contact binary systems. Figures a) and b) show surface points of the component before and after the transformation which enabled us to use the Delaunay triangulation method (figure c)). The resulting surface of the over-contact component is on display in figure d).

4. Conclusions

This approach utilizes a novel approach to the problem of generation of the single and binary stellar surfaces. Compared to the other algorithms utilized in software packages such as PHOEBE (Horvat et al., 2018) and ROCHE (Pribulla, 2012), this approach requires far less evaluations of surface points and faces in order to produce the stellar surface with the same resolution. This algorithm will be implemented in the upcoming software package dedicated to a modelling of eclipsing binaries with pulsating components.

Acknowledgement

This contribution has been supported by the Slovak Research and Development Agency under the contract No. APVV-15-0458. The research of M.F. was supported by the internal grant No. VVGS-PF-2018-758 of the Faculty of Science, P. J. Šafárik University in Košice.

References

Barber, C.B., Dobkin, D.P., Huhdanpaa, H.T., 1996, ACM Trans. on Mathematical Software, 22(4):469-483

Horvat, M., Conroy, K. E., Pablo, H., et al., 2018, The Astrophysical Journal Supplement Series, 237, 26

Pribulla, T., 2012, From Interacting Binaries to Exoplanets: Essential Modeling Tools, 282, 279-282

Contrib. Astron. Obs. Skalnaté Pleso **49**, 349 – 351, (2019)

Analysis of exoplanetary system WASP-118

P. Gajdoš[1], M. Vaňko[2], Š. Parimucha[1] and M. Fedurco[1]

[1] *Institute of Physics, Faculty of Science, Pavol Jozef Šafárik University, Košice, Slovakia*

[2] *Astronomical Institute of the Slovak Academy of Sciences 059 60 Tatranská Lomnica, The Slovak Republic*

Received: October 17, 2018; Accepted: January 28, 2019

Abstract. We present a new study of a recently discovered exoplanetary system WASP-118. The system consists of an F-type star and a close-in giant planet (an inflated hot Jupiter). Using Kepler-K2 observations, we redetermined the orbital and physical parameters of the system. Our results are in good agreement with the values published in the literature. The precise times of all transits were determined, however, no significant transit timing variations were detected. Our analysis of an upper mass limit allows us to include additional Earth-mass planet(s) near to mean-motion resonance(s).

Key words: planetary systems - eclipses - methods: numerical - planets and satellites: individual: WASP-118 b

1. Introduction

The parent star of hot Jupiter WASP-118 b, discovered in 2016 and confirmed by Hay et al. (2016), is a 2.38 Gyr-old F6-type star with a radius of 1.696 $R_\odot$ and a mass of 1.320 $M_\odot$. The 2^{nd} Gaia Data Release gives a distance of 380.5 pc (Gaia Collaboration et al., 2018). Močnik et al. (2017) found γ Dor pulsations in the light curve (LC) of WASP-118 with a period of 1.9 day and a semi-amplitude of $\sim$ 200 ppm.

WASP-118 was observed during Campaign 8 of the Kepler K2 mission (from 3 Jan to 23 Mar 2016). We used de-trended short-cadence data (PDCSAP_FLUX), sampled every 58.8 seconds. During the observation period 19 transits were observed.

2. Light curve and TTV analysis

For our light curve (LC) analysis, we used the same approach as in our paper Gajdoš et al. (2017):

1. We extracted parts of the LC around detected transits.
2. We aligned and stacked all 19 LCs together to obtained the template of transit.

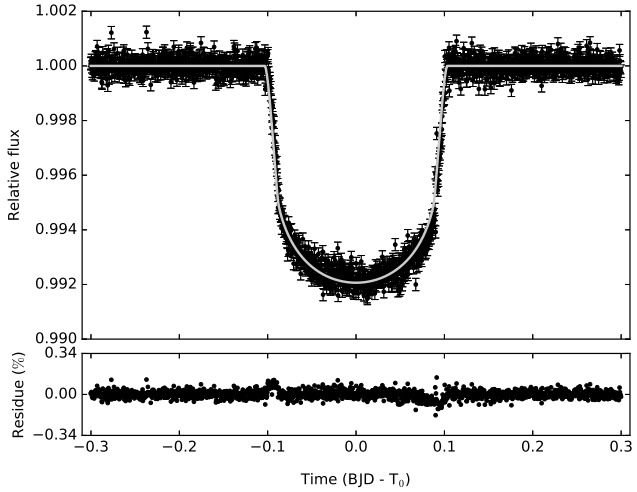

Figure 1. Template of transit WASP-118 b.

3. We used our software implementation of the Mandel & Agol (2002) model and MCMC simulation for the determination of transit parameters and to obtain template of transit.

4. For each of 19 individual transits, the time of the transit was determined using template from step 3. We constructed an O-C diagram.

Table 1. Parameters of exoplanet WASP-118 b.

Parameter	Hay et al. (2016)	Močnik et al. (2017)	This paper
T_0 [HJD]*	6787.81423(62)	6787.81256(2) **	6787.81249(68)
P [d]	4.0460435(44)	4.0460407(26)	4.0460654(43)
a [au]	0.05453(48)	0.05450(49)	0.05356(99)
$r_{\rm P}$ [$R_\oplus$]	16.141(404)	15.630(150)	14.940(268)
i [°]	88.70(90)	88.24(14)	89.86(18)
χ^2	116249.01	19040.62	17746.10

* in HJD - 2450000; ** original value 7423.04483 shifted to the same epoch

We did not observe any significant periodic variations on the O-C diagram. The periodic TTV signal with an amplitude greater than 100 s over the observing period seems to be unlikely.

We put upper constraint on the mass of a potential perturbing planet in the system with refined assumptions: maximal variance in the O-C diagram (100 s) as the amplitude of possible TTV and the orbits of both planets are circular and coplanar.

We used MERCURY6 code (Chambers, 1999) to produce 20000 synthetic O-C diagrams for different configurations of the mass and orbital period of a hypothetical planet.

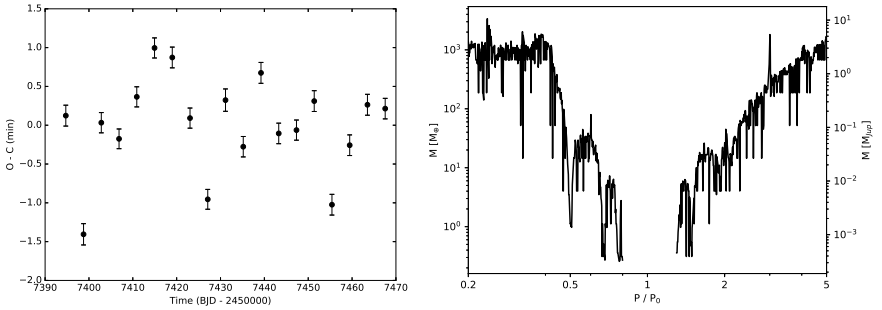

Figure 2. The O-C diagram for transit timing of WASP-118 b, plotted according to the new linear ephemeris (*left*). The upper-mass limit of a hypothetical additional planet in the WASP-118 system (*right*).

3. Discussion and conclusion

We redetermined the basic parameters of exoplanet WASP-118 b. We also determined the accurate times of all transits of this planet to analyse possible TTVs. We concluded that our values of the planetary parameter are, in general, consistent with previously published papers.

The obtained O-C diagram showed no significant periodic variation. We put upper limit of the mass of a potential planet in the system which could generate the TTV signal. We observed that in this system there could exist also the earth-mass planet near to the mean-motion resonance. To better specify the mass limit of a potential perturbing planet, the high-quality photometric observations of transits during a long observing period are needed. Radial velocity measurements would also be helpful.

Acknowledgements. This paper was supported by the grant of the Slovak Research and Development Agency with number APVV-15-0458. M.V. would like to thank the project VEGA 2/0031/18. The research of P.G. was supported by the VVGS-PF-2017-724 internal grant of the Faculty of Science, P. J. Šafárik University in Košice.

References

Chambers, J. E. 1999, MNRAS, 304, 793

Gaia Collaboration, Brown, A. G. A., Vallenari, A., et al. 2018, A&A, 616, A1

Gajdoš, P., Parimucha, Š., Hambálek, Ľ., & Vaňko, M. 2017, MNRAS, 469, 2907

Hay, K. L., Collier-Cameron, A., Doyle, A. P., et al. 2016, MNRAS, 463, 3276

Mandel, K., & Agol, E. 2002, ApJL, 580, L171

Močnik, T., Hellier, C., Anderson, D. R., Clark, B. J. M., & Southworth, J. 2017, MNRAS, 469, 1622

Contrib. Astron. Obs. Skalnaté Pleso **49**, 352 – 354, (2019)

Analysis of KOI 2700b: the second exoplanet with a comet-like dusty tail

An improved tail model

Z. Garai

Astronomical Institute of the Slovak Academy of Sciences
059 60 Tatranská Lomnica, The Slovak Republic, (E-mail: zgarai@ta3.sk)

Received: October 26, 2018; Accepted: January 29, 2019

Abstract. The *Kepler* object KOI 2700b was discovered recently as the second exoplanet with a comet-like dusty tail. Previously, we aimed at verifying the disintegrating-planet scenario of KOI 2700b by modeling its light curve and to put constraints on various tail and planet properties, as was done in the case of KIC 12557548b. Here, we describe an improved tail model with five free parameters and its application in the case of γ-alumina 1 micron grains.
Key words: planets and satellites: general – planet-star interactions – scattering

1. Introduction

The *Kepler* object KOI 2700b (KIC 8639908b) was discovered by Rappaport et al. (2014) as the second exoplanet with a comet-like dusty tail. It exhibits a distinctly asymmetric transit profile, likely indicative of the emission of dusty effluents and reminiscent of KIC 12557548b (Kepler 1520b), the first exoplanet with a comet-like dusty tail (Rappaport et al., 2012). Garai (2018) aimed at verifying the disintegrating-planet scenario of KOI 2700b by modeling its light curve and to put constraints on various tail and planet properties, as was done in the case of KIC 12557548b (Budaj, 2013). Here, we describe an improved tail model and its application.

2. Data analysis

We used the phase-folded and binned transit light curve of KOI 2700b, presented by Garai (2018), and we also adopted the analysis procedure from this work, but with an improvement. Four free parameters were originally adjusted simultaneously during the fitting procedure – the orbital inclination angle i [deg], the dust density at the beginning of the ring $\rho(0)$ [g.cm^{-3}], the planet to star radius ratio $R_{\rm p}/R_{\rm s}$, and the density exponent $A2$. One more free parameter – the transit midpoint phase shift of the synthetic light curve with respect to the observed light curve ($\Delta\varphi_0$) – was adjusted only before the modeling process

and then was kept fixed to its best value. This parameter reflects the unknown mid-transit time of the planet. Garai (2018) describes that every synthetic light curve was shifted in phase by $\Delta\varphi_0 = -0.235$. The advantage of this treatment is that it saves computing time; on the other hand, one cannot exclude the possibility that uncertainties on the resulting parameters are underestimated.

In our analysis procedure we used the transit midpoint phase shift of the synthetic light curve with respect to the observed light curve as a next free parameter. We prepared a parameter range and stepping for $\Delta\varphi_0$ similarly, as it was described in the case of other free parameters by Garai (2018). During the first iteration we used the range of $[-0.215, -0.255]$ and the stepping of 0.005. During the next iteration we reduced the range of the parameter $\Delta\varphi_0$ and at the same time we used finer stepping in the parameter range. We selected the best value of the parameter $\Delta\varphi_0$, found in the previous iteration, as a midpoint $(\tilde{x})$ of the new parameter range. As the second iteration we used the parameter range of $\tilde{x}_{\Delta}\varphi_0 \pm 0.008$ and stepping of 0.002. During the last (third) iteration we similarly applied the parameter range and stepping of $\tilde{x}_{\Delta}\varphi_0 \pm 0.004$ and 0.001, respectively. Other parameters were applied during this analysis procedure as it was described by Garai (2018). A formal, quantitative goodness-of-fit was measured via determination of reduced χ^2 ($\chi^2_{\rm red}$). The best fit corresponds to the minimum value of $\chi^2_{\rm red}$. To derive uncertainties on the resulting parameters we applied Monte Carlo simulations as it was described by Garai (2018).

To save the computing time, we applied our improved tail model in the case of γ-alumina 1 micron grains only. In this case, we can compare only the results for γ-alumina 1 micron grains, i.e. results, obtained via the original four-free-parameter model with our results, obtained via the five-free-parameter model.

3. Results and Conclusions

Applying γ-alumina 1 micron grains, Garai (2018) obtained the following fitted parameters. The orbital inclination angle $i = 87 \pm 0.6$ [deg], the dust density at the beginning of the ring $\rho(0) = 0.2190 \pm 0.0005$ ($\times 10^{-15}$) [g.cm^{-3}], the planet to star radius ratio $R_{\rm p}/R_{\rm s} = 0.007 \pm 0.006$, and the density exponent $A2 = -8.0 \pm 0.2$. In this case the reduced χ^2 was $\chi^2_{\rm red} = 1.093$.

Applying our five-free-parameter model, we obtained the following fitted parameters. The orbital inclination angle $i = 87 \pm 0.7$ [deg], the dust density at the beginning of the ring $\rho(0) = 0.2185 \pm 0.0008$ ($\times 10^{-15}$) [g.cm^{-3}], the planet to star radius ratio $R_{\rm p}/R_{\rm s} = 0.007 \pm 0.005$, the density exponent $A2 = -8.0 \pm 0.2$ and the transit midpoint phase shift of the synthetic light curve with respect to the observed light curve $\Delta\varphi_0 = -0.237 \pm 0.003$. In this case the reduced χ^2 was $\chi^2_{\rm red} = 1.109$.

The fitted parameters and their uncertainties are comparatively summarised in Tab. 1. We can see that the fitted parameters and their uncertainties are very similar in both cases. The reduced χ^2 values are also comparable. This means

Table 1. Comparison of the fitted parameters and their uncertainties. *This parameter was fixed to its best value.

Parameter	Garai (2018)	This work
i [deg]	87 ± 0.6	87 ± 0.7
$\rho(0)$ ($\times 10^{-15}$) [g.cm^{-3}]	0.2190 ± 0.0005	0.2185 ± 0.0008
$R_\mathrm{p}/R_\mathrm{s}$	0.007 ± 0.006	0.007 ± 0.005
$A2$	-8.0 ± 0.2	-8.0 ± 0.2
$\Delta\varphi_0$	-0.235^*	-0.237 ± 0.003

that to include the parameter $\Delta\varphi_0$ into the model as a next free parameter is not necessary. On the other hand, we have to note that we applied the improved tail model only in one case from 15 (Garai, 2018). The full comparison can change this conclusion, but this needs a lot of computing time.

Acknowledgements. This work was supported by the VEGA grant of the Slovak Academy of Sciences No. 2/0031/18.

References

Budaj, J., Light-curve analysis of KIC 12557548b: an extrasolar planet with a comet-like tail. 2013, *Astron. Astrophys.*, **557**, A72, DOI: 10.1051/0004-6361/201220260

Garai, Z., Light-curve analysis of KOI 2700b: the second extrasolar planet with a comet-like tail. 2018, *Astron. Astrophys.*, **611**, A63, DOI: 10.1051/0004-6361/201629676

Rappaport, S., Barclay, T., DeVore, J., et al., KOI-2700b – A Planet Candidate with Dusty Effluents on a 22 hr Orbit. 2014, *Astrophys. J.*, **784**, 40, DOI: 10.1088/0004-637X/784/1/40

Rappaport, S., Levine, A., Chiang, E., et al., Possible Disintegrating Short-period Super-Mercury Orbiting KIC 12557548. 2012, *Astrophys. J.*, **752**, 1, DOI: 10.1088/0004-637X/752/1/1

Contrib. Astron. Obs. Skalnaté Pleso **49**, 355 – 357, (2019)

Structural changes in DPVs related to the long cycle

J. Garcés[1], R.E. Mennickent[1], G. Djurašević[2,3] and R. Poleski[4,5]

[1] *Universidad de Concepción, Departamento de Astronomía, Casilla 160-C, Concepción, Chile*

[2] *Astronomical Observatory, Volgina 7, Belgrade, 11060, Serbia*

[3] *Isaac Newton Institute of Chile, Yugoslavia Branch, 11060, Belgrade, Serbia*

[4] *Warsaw University Observatory, Al. Ujazdowskie 4, PL-00-478 Warszawa, Poland*

[5] *Department of Astronomy, Ohio State University, 140 W. 18th Ave., Columbus, OH 43210, USA*

Received: October 31, 2018; Accepted: March 18, 2019

Abstract. Recent studies indicate changes in the morphology of the light curve of OGLE-LMC-DPV-097 directly related to the long cycle. These are explained by changes in the structure of the accretion disk and temperatures of the bright and hot spot. In this report we present a preliminary study of a new galactic DPV, OGLE-BLG-ECL-157529, that has similar behavior.

Key words: binaries: eclipsing - stars: close - binaries.

1. Introduction

Double periodic variables (DPVs) are a sub-class of Algol binary systems. They exhibit two photometric cycles: an orbital period, typical of eclipsing binaries, and a long cycle of unknown origin. The latter lasts in average about 33 times the orbital period (Mennickent et al., 2003). Studies indicate that a B-type star (gainer) surrounded by an accretion disk with a late-type giant star (donor) filling its Roche lobe are the components in DPVs systems (Mennickent et al., 2016). Previous research shows that the donor is a potentially magnetic active star, as is the case of the DPV V393 Sco (Mennickent et al., 2012; Mennickent, Schleicher & San Martin-Perez 2018). Possibly the accretion flow is modulated as a result of a magnetic dynamo cycle, where the radius of the donor changes, as shown in Applegate models (Schleicher & Mennickent, 2017).

Recently we reported a change in the light curve morphology of DPV-097 (see Garcés et al., 2018). Now we present a new DPV in the bulge of the Milky Way with similar behavior. OGLE-BLG-ECL-157529 (I = 13.035, α=17:53:08, δ=-32:46:27), has an orbital period of 24.7991558 ± 0.000202 [d] and a variable long period that descends from 867 to 742 [d] in the photometric time series (15 years) taken from the OGLE-II/III/IV project data bases (provided by the OGLE team) and described by Soszyński et al., 2016. We disentangled the light

curve into an orbital and long-cycle using the Fourier decomposition algorithm described by Mennickent et al., 2012.

Table 1. Results of the analysis of ECL-157529 considering the OGLE II light curves. * Results from Garcés et al., 2018 for DPV-097. A comparison of both objects can be visualized.

	OGLE-LMC-DPV-097*				OGLE-BLG-ECL-157529			
Quanty	**Asc***	**Max***	**Des***	**Min***	**Asc**	**Max**	**Des**	**Min**
$\Sigma(O-C)^2$	0.0481	0.0464	0.1662	0.1692	0.1662	0.0481	0.1692	0.0464
i [°]	74.3	75.1	74.4	74.4	85.20	85.44	85.13	85.40
T_d [K]	4030	5580	5210	6870	3460	4550	3675	3670
T_h [K]	14000	14000	14000	14000	18630	18750	18760	18740
T_c [K]	4930	4980	4910	4950	6650	6650	6650	6650
$A_{hs} = T_{hs}/T_d$	1.63	1.70	1.14	1.71	1.78	1.67	1.20	1.81
$A_{bs} = T_{bs}/T_d$	1.78	1.17	1.16	1.76	1.51	1.52	1.81	1.58
$M_{\rm h}[M_\odot]$	5.51	5.51	5.51	5.51	7.26	7.26	7.26	7.26
$M_{\rm c}[M_\odot]$	1.10	1.10	1.10	1.10	1.45	1.45	1.45	1.45
$R_{\rm h}[R_\odot]$	3.65	3.64	3.65	3.65	4.95	4.95	4.92	4.91
$R_{\rm c}[R_\odot]$	7.75	7.75	7.75	7.75	18.44	18.44	18.44	18.44
$R_{\rm d}[R_\odot]$	15.28	15.40	11.20	7.49	34.34	34.14	35.94	32.69
$\rm d_e[R_\odot]$	1.36	1.06	2.53	0.95	6.65	2.95	2.65	6.99
$\rm d_c[R_\odot]$	3.09	3.41	3.16	2.60	3.38	2.22	5.15	10.40

Fixed Parameters: $q = M_{\rm c}/M_{\rm h} = 0.20$ mass ratio, temperature of one component. **Quantities:** $\Sigma(\rm O-C)^2$ sum of squares of residuals between observed and synthetic light curves, i orbit inclination. $\rm T_d$, $\rm T_c$, $\rm T_h$ temperature of the disk-edge, donnor (Cooler) and gainer (Hotter) respectively. $\rm A_{hs}$, $\rm A_{bs}$ hot and bright spots temperature coefficients. $M_{\rm h}$, $M_{\rm c}$, $R_{\rm d}$, $R_{\rm h}$, $R_{\rm c}$ stellar masses and mean radii of disk and stars in solar units. $\rm d_e$, $\rm d_c$, disk thicknesses (at the edge and at the center).

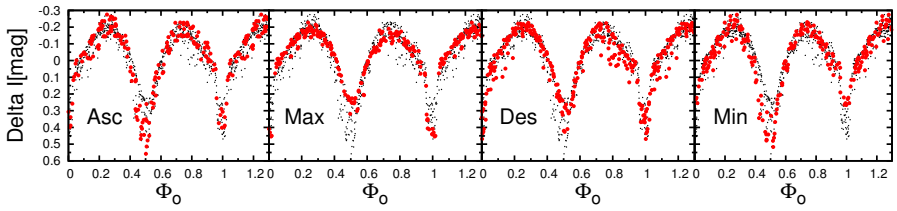

Figure 1. Black dots represent the disentangled orbital light curve of OGLE-157529. Red dots represent the same but at different branches of the long cycle (See Sec. 2).

2. Model

For OGLE-157529, the long cycle phases (ϕ_l) are defined using a constant long period of 867 [d] and considering only OGLE II I-band data (See Fig. 1), where the ascendent (Asc) branch corresponds to $0.6 < \phi_l \leq 0.9$, maximum (Max) to $0.9 < \phi_l \leq 1.1$, descendent (Des) to $0.11 < \phi_l \leq 0.35$ and Minimum (Min) to $0.35 < \phi_l \leq 0.60$.

We applied theoretical models to the light curve on the different branches of the long cycle using a program developed by Djurašević (1992a, 1992b). Our models assume an optically and geometrically thick disk with a radial temperature profile that follows the distribution proposed by Zola (1991), synchronous rotation for both stellar components and q = 0.2 based on complete studies performed on differents DPVs (Mennickent, Otero & Kołaczkowski, 2016).

3. Conclusion

We found changes in the light curve of OGLE-157529 related to the different stages of the long cycle. As for our previous study in DPV-097, this could be explained mainly by structural changes of the accretion disk and the temperatures of the hot and bright spot. The most significant change for OGLE-157529 is the disk thickness, while for DPV-097 is the disk radius (See Table 1).

The OGLE database allows us to investigate for the first time this type of phenomena on DPVs and a complete study of this interesting object is in preparation.

Acknowledgements. JG and REM acknowledge support by VRID-Enlace 216.016.002-1.0 and the BASAL (CATA) PFB06/2007. G.D. acknowledges the financial support of the Ministry of Education and Science of the Republic of Serbia through the project 176004 "Stellar Physics". The OGLE project has received funding from the Polish National Science Centre grant MAESTRO no. 2014/14/A/ST9/00121. REM acknowledges grant FONDECYT 1190621.

References

Djurašević, G.,: 1992a, *Astrophys. Space Sci.* **196**, 267

Djurašević, G.,: 1992b, *Astrophys. Space Sci.* **197**, 17

Garcés L., J., Mennickent, R., Djurašević, G., et al.,: 2018, *Mon. Not. R. Astron. Soc.* **477**, L11

Mennickent, R.E., Pietrzyński, G., Diaz, M., et al.,: 2003, *Astron. Astrophys.* **399**, L47

Mennickent, R.E., Djurašević, G., Kołaczkowski, Z., et al.,: 2012, *Mon. Not. R. Astron. Soc.* **421**, 862

Mennickent, R. E., Otero, S. and Kołaczkowski, Z.: 2016, *Mon. Not. R. Astron. Soc.* **455**, 1728

Mennickent, R.E., Schleicher, D.R.G., San Martin-Perez, R.,: 2018, *Publ. Astron. Soc. Pac.* **130**, 094203

Schleicher, D. R. G. and Mennickent, R. E.: 2017, *Astron. Astrophys.* **602**, A109

Soszyński, I., Pawlak, M., Pietrukowicz, P., et al.,: 2016, *Acta Astron.* **66**, 131

Zola, S.: 1991, *Acta Astron.* **41**, 213

Contrib. Astron. Obs. Skalnaté Pleso **49**, 358 – 362, (2019)

Follow-up observations of variable stars at the Terskol Observatory within the Gaia project

V. Godunova[1], A. Simon[2], V. Reshetnyk[2], I. Izviekova[1,2], I. Sokolov[3], Yu. Bufan[1,4], V. Kozlov[1], O. Sergeev[1,3] and V. Taradii[1]

[1] *ICAMER Observatory of NASU, 27 Acad. Zabolotnogo str., Kyiv, 03143, Ukraine (E-mail: godunova@mao.kiev.ua)*

[2] *Astronomy and Space Physics Department, Taras Shevchenko National University of Kyiv, 60 Volodymyrska str., Kyiv, 01601, Ukraine*

[3] *Terskol Branch of the Institure of Astronomy of RAS, Terskol Settl., 361605, Kabardino-Balkarien Republik, Russian Federation*

[4] *Astronomical Observatory of the Ivan Franko National University of Lviv, 8 Kyryla i Methodia str., Lviv, 79005, Ukraine*

Received: November 7, 2018; Accepted: February 6, 2019

Abstract. We report on optical observations of stellar objects (SNe, CVs, YSOs, etc.), which were detected within the framework of the Gaia mission. The telescopes Zeiss-2000 and Zeiss-600 at the Terskol Observatory provide good enough opportunities especially for follow-up studies of these objects. Photometric observations have been used to perform a quick analysis of the imaging data in order to reveal short- or long-term variability in the brightness of Gaia transients. Appropriate software developed has been applied for processing and analysis of datasets gathered in 2016-2018 for more than 40 objects; a lot of them have been continuously observed over the years. In this paper, we present some results obtained for transients Gaia17dce, Gaia18aen, and Gaia18cct.

Key words: variable stars – photometry – light curves – transients – Gaia

1. Introduction

Nowadays, analysis of observational datasets gathered by the Gaia satellite is worldwide well advanced. Research groups in many countries work together to achieve the best possible results by investigating a wide variety of transient events and stellar activity, which have been detected by the space telescope. However, interpretations and theoretical models which are based on space data require verification and additional observations to be performed using ground-based instruments.

During the last three years, the facilities of the Terskol Observatory in the Northern Caucasus (43° 16′ 29″ N, 42° 30′ 03″ E, 3143 *m* asl) have been heavily used for follow-up photometry of Gaia transients. The available optical telescopes with diameters up to 2 m open up good opportunities for long-term

monitoring of asteroids and stellar objects (Tarady et al., 2010). By providing observations of newly detected transients (SNe, CVs, YSOs, etc.), the Terskol Observatory contributes significantly to their classification and a better understanding of star formation and evolution.

2. Observations and results

Research activities at the Terskol Observatory (IAU code B18) are now highly focused on BVRI photometry (including long-term monitoring) of transients detected by ESA Gaia, DPAC and the Photometric Science Alerts Team *(gsaweb.ast.cam.ac.uk/alerts)*. As for the objects to be of the most importance, the following selection criteria are applied:

- (very) recently detected transients (G mag down to 18.8);
- a high emphasis on unclassified objects;
- objects that show unusual (intriguing) light curves.

Since 2016, a lot of Gaia transients have been observed at the Terskol Observatory: Gaia16asm, Gaia16bkf, Gaia16bkn, Gaia16blg, Gaia16bnz, Gaia16bvs, Gaia16bvt, Gaia17akp, Gaia17agr, Gaia17agj, Gaia17aqm, Gaia17asz, Gaia17bqo, Gaia17ctl, Gaia17cty, Gaia17cuh, Gaia17cvx, Gaia17cxa, Gaia17dev, Gaia17dcx, Gaia17ddg, Gaia17dce, Gaia17ddi, Gaia17ddp, Gaia18aak, Gaia18aen, Gaia18aes, Gaia18afb, Gaia18akt, Gaia18aip, Gaia18ajz, Gaia18arm, Gaia18arn, Gaia18axl, Gaia18azl, Gaia18avw, Gaia18cct, Gaia18cfs, Gaia18chm, etc.

More than 8000 photometric measurements of these objects were recorded; images were taken mainly with the Zeiss-600 telescope. For sources of magnitude G∼16, a photometric accuracy of better than 0.05 mag was achieved for V, R, I passbands, while the errors in B values are somewhat larger. The follow-up data points obtained have been uploaded to the Cambridge Photometric Calibration Server *(http://gsaweb.ast.cam.ac.uk/followup)*. The co-processing of photometric data from many observing sites results in a detailed light curve coverage that allows one to investigate the object′s distinctive features (Wyrzykowski et al., 2018).

Here we provide some findings for the three unclassified transients.

Gaia17dce

This bright blue hostless transient was discovered by Gaia on 2017-11-27 at magnitude G = 16.67. There was no progenitor object on archival images. We detected Gaia17dce on the images taken on 2017-12-01 with the 2-m telescope. Using the AAVSO catalogue for photometric calibration we obtained the following magnitudes of the source (not corrected for the Galactic foreground extinction): B = 17.41 ± 0.07, V = 17.12 ± 0.08, R = 17.13 ± 0.05 (MJD 58088.71).

Additional observations of this unclassified object, which were performed at Terskol from 2017-12-13 to 2017-12-17, showed that its R-band brightness has

fallen down by more than 4 mags within the four days; the light curve depicted small variations within 0.2 mag on a time scale of hours (Fig. 1). Taking into account a sudden increase in brightness by at least 5 mags and a rapid decay 20 days later, we suggest that Gaia 17dce is a cataclysmic variable star. It is significant to note that we did not detect Gaia17dce in CCD images taken on 2017-12-17 (limiting R mag > 22.0), on 2018-04-25 (limiting R mag > 21.0), and on 2018-07-17 (limiting R mag ~ 21.0).

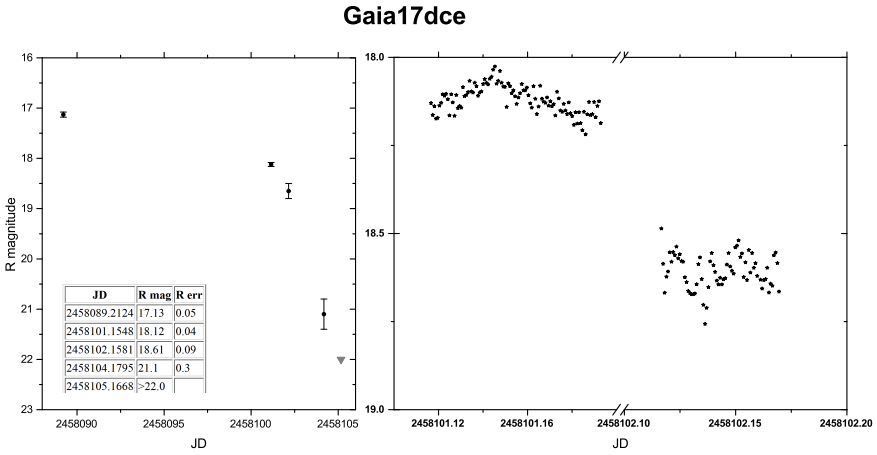

Figure 1. *Left*: R-band photometry for Gaia17dce performed in December 2017 with the 2-m telescope at the Terskol Observatory. *Right*: R-band observations of Gaia17dce on December 13 and 14, 2017. Notes: 1) due to the instrumental errors, measurements of December 14 were smoothed using the boxcar averaging (of three points); 2) the grey triangle indicates the limiting R magnitude of about 22.0; 3) the NOMAD catalog was used for photometric calibration.

Gaia18aen

A $\sim$ 1 mag increase in brightness of this object was detected by Gaia on 2018-01-17, when its G magnitude reached 11.33. This bright emission line star in the Galactic plane apparently did not show any significant variability until December 2017. Moreover, it was noticed by Wray (1966) and indicated as WRAY15-136.

BVRI photometry of Gaia18aen was performed at Terskol with the 0.6-m telescope in February-March 2018. All the follow-up data points were uploaded to the Cambridge Photometric Calibration Server. Fig. 2 shows multi-band observations of Gaia18aen, which were acquired in 2018 by Gaia and by the three ground-based observers. The light curve demonstrates the decaying oscillations on a time scale of months, with the general decline of the object's brightness to the baseline. So far, the revealed variability does not allow the unambiguous classification of Gaia18aen; it is assumed to be an YSO or a nova.

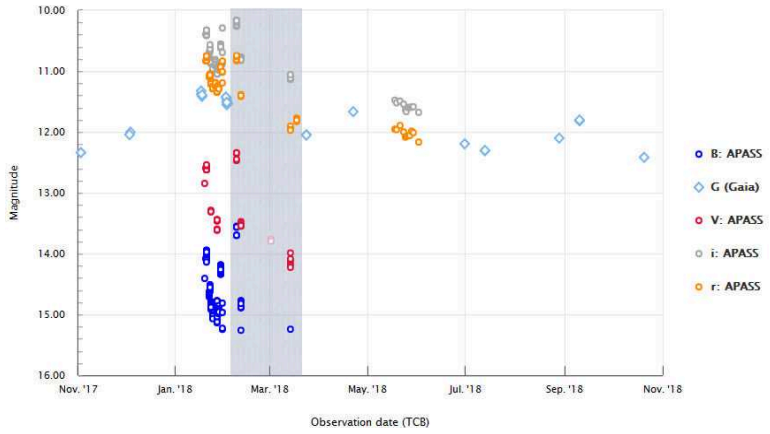

Figure 2. Multi-band follow-up observations of Gaia18aen in 2018. The shaded area depicts the time span containing observations from Terskol. *(Image from http://gsaweb.ast.cam.ac.uk/alerts).*

Gaia18cct

A long-term rise of 0.4 mag in brightness of this Gaia source was announced on 2018-08-10. Based on the Gaia′s photometry (Fig. 3, the inset), which showed a slow falling (over more than one year) and than a slow rising (over the period of about one year) of the brightness of the object, Gaia18cct was primarily assumed to be a microlensing event or a Mira. In this case, however, one should take into account that Gaia18cct appears near the direction of the Galactic anticenter and is apparently located at the outer edge of the Milky Way.

Since 2018-08-14, Gaia18cct has been continuously observed at Terskol; data processing has been made using the Cambridge Photometric Calibration Server. Fig. 3 demonstrates that the source brightness remained approximately constant over the observed four-month period, with insignificant changing colors. Thus, the results obtained show clearly that further observations of Gaia18cct are needed in order to classify its variability.

3. Conclusions

Three-year observations of Gaia transients at the Terskol Observatory have yielded new data and findings. Photometric observations acquired with the aid of the 0.6-m and 2-m telescopes have been continuously uploaded on the Cambridge Photometric Calibration Server. Being collected along with datasets gathered worldwide, they can be used by the astronomical community for a further analysis. This is an outstanding example how a more systematic, integrated use of small and medium-aperture telescopes leads to better information about transient events in the Universe.

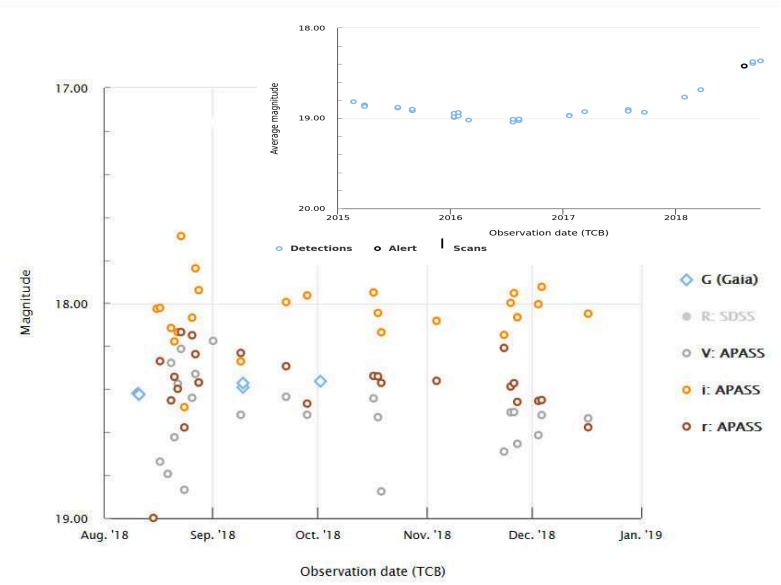

Figure 3. Multi-band follow-observations of Gaia18cct in August-December 2018 at Terskol with the 0.6-m telescope. *The inset*: Lightcurve of Gaia18cct from Gaia's observations. *(Images from http://gsaweb.ast.cam.ac.uk/alerts).*

Acknowledgements. We acknowledge the use of the Cambridge Photometric Calibration Server *(http://gsaweb.ast.cam.ac.uk/followup)* developed and maintained by Lukasz Wyrzykowski, Sergey Koposov, Arancha Delgado, and Pawel Zielinski, funded by the European Union's Horizon 2020 research and innovation programme under grant agreement No 730890 (OPTICON).

References

Tarady, V., Sergeev, O., Karpov, M., Zhilyaev, B., & Godunova, V., Observations with small and medium-sized telescopes at the Terskol Observatory. 2010, *ArXiv e-prints*, arXiv:1003.4875

Wray, J. D. 1966, A Study of Hα-emission Objects in the Southern Milky Way, PhD thesis, Northwestern University.

Wyrzykowski, Ł., Rybicki, K., Kruszyńska, K., et al., Gaia mission and its transients. 2018, in *XXXVIII Polish Astronomical Society Meeting*, 364–367

Contrib. Astron. Obs. Skalnaté Pleso **49**, 363 – 366, (2019)

Long-term spectroscopic survey of T Tauri stars in the Taurus-Auriga star-forming region

T. Pribulla[1], M. Vaňko[1], J. Budaj[1], Z. Garai[1], E. Guenther[2], Ľ. Hambálek[1], R. Komžík[1] and E. Kundra[1]

[1] *Astronomical Institute of the Slovak Academy of Sciences*
059 60 Tatranská Lomnica, The Slovak Republic, (E-mail: lhambalek@ta3.sk)
[2] *Thüringer Landessternwarte*
Sternwarte 5, D-07778 Tautenburg, Germany

Received: November 2, 2018; Accepted: March 17, 2019

Abstract. Long-term spectroscopic monitoring of 22 T Tauri stars located in the Taurus-Auriga star-forming region (SFR) is presented. The medium and high-dispersion spectra were obtained at the Stará Lesná (SLO), Skalnaté Pleso (SPO) and Tautenburg observatory (TLS) during 2015–2018. The broadening function technique was used to determine the radial and projected rotational velocities of the stars and to study multiplicity of objects. The analysis was also focused on the determination of atmospheric parameters such as $\log g$, $T_{\rm eff}$ and [Fe/H]. The nature of the objects was assessed by measuring the equivalent with of the H_α and Li I 6708 lines. Their membership was checked using the *Gaia* DR2 parallaxes and estimated model distances.

Key words: Stars: Variables – Stars: T Tauri – Stars: Pre-main sequence

1. Observation and data reduction

We have found many bona fide T Tauri stars (originally designated as members of the nearest known SFR Taurus-Auriga) in the literature without much information and/or contradicting physical parameters. We have focused only on objects classified as weak-line T Tauri stars. We have hand-picked stars with $V < 11$ mag because of our observation limit. Altogether 168 spectra have been obtained with medium and high-dispersion spectrographs:

(i) At SLO with a 60 cm, $f/12.5$ Zeiss Cassegrain telescope equipped with a fiber-fed échelle spectrograph eShel (see Pribulla et al., 2015) with 4150–7600 Å spectral range, and $R = 11\,000$. ThAr calibration unit provides about $100\,\mathrm{m\,s^{-1}}$ accuracy in radial-velocity.

(ii) At SPO with a 1.3 m, $f/8.36$ Nasmyth-Cassegrain telescope equipped with a fiber-fed échelle spectrograph similar to the MUSICOS design (see Baudrand & Bohm, 1992). The spectral range of the instrument is 4250–7375 Å, and $R = 38\,000$.

(iii) At TLS with the 2 m Alfred Jensch telescope and a $f/46$ Coudé échelle spectrograph. These spectra cover 4510–7610 Å with $R = 31\,500$.

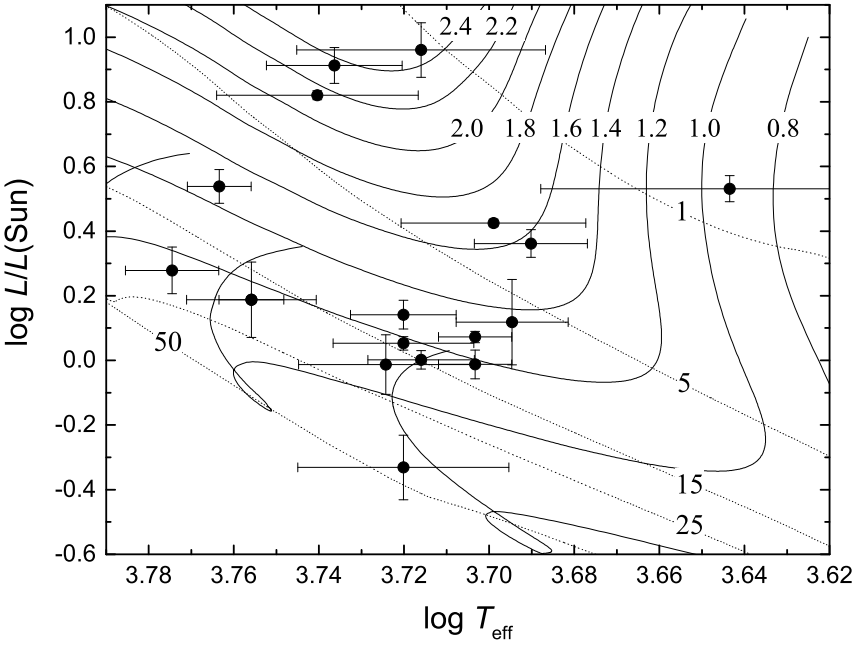

Figure 1. Positions of our targets in the HR diagram with evolutionary tracks from 2.4 to 0.8 $M_\odot$ (solid curves) and isochrones from 1 to 50 Myr (dotted curves). The evolutionary tracks/isochrones for the solar metallicity from the Pisa Stellar Models by Tognelli et al. (2011) are shown.

The raw data from SLO and SPO were reduced using `IRAF` package tasks, Linux shell scripts and `FORTRAN` programs as described in Pribulla et al. (2015). Data were reduced with standard dark and flat-field frames. Bad pixels were cleaned using a bad pixel mask, cosmic hits were removed using the program of Pych (2004). Order positions were defined by fitting Chebyshev polynomials to the tungsten-lamp and blue LED spectrum. In the following step, scattered light was modelled and subtracted. Aperture spectra were then extracted for both the object and the ThAr lamp and then the resulting spectra were wavelength calibrated. Spectra obtained at TLS were also reduced under the `IRAF` environment (e.g. Guenther et al., 2009).

2. Evolution stage

The *ubvyβ* photometry data taken from Paunzen (2015) were used as input for the `TempLogG TNG` software (Kaiser, 2006) with different calibrations to derive

the temperature $T_{\rm eff}$, [Fe/H] and $\log g$. We have calculated luminosity from the *Gaia* DR2 parallax (Lindegren et al., 2018) and the reddening from Meištas & Straižys (1981); Chavarría-K et al. (2000); Grankin (2013); Herczeg & Hillenbrand (2014). The de-reddening method was based on the Strömgren-Crawford $ubvy\beta$ photometric system (Crawford, 1975; Schuster & Nissen, 1989). To deduce the age of stars, we used the evolutionary tracks (Figure 1) for solar metallicity from the Pisa Stellar Models (PSM) by Tognelli et al. (2011). We have found that all stars in our sample are younger than 70 Myr. This is close or inclusive to the 10–100 Myr interval for the post T Tauri stars defined by Jensen (2001). The errors, mainly due to the effective temperature, translated into the uncertainty in the mass are of about $\pm 0.2\,{\rm M}_{\odot}$. We have measured the equivalent widths (EW) of H_{α} and Li I 6708 lines using the `IRAF` package. Radial velocities $v \sin i$ were extracted using the broadening function technique (see Rucinski, 1992). We list the results in Table 1. The spectral type of targets was adopted from the available literature.

Table 1. Results of modelling for different targets. Negative values of EW denote emission. Formal errors are given only if several sources/determinations were available. Further details are given in the text.

Star	Age [Myr]	[Fe/H] [dex]	$T_{\rm eff}$ [K]	$\log g$ (cgs)	Sp. type	EW H_{α} [mÅ]	EW Li [mÅ]	$v \sin i$ [km s^{-1}]
HD 285281	1-8	−0.111	4800(600)	4.4(5)	K1		423	80
V1298 Tau	7-12	+0.010	5170(150)	4.57(28)	K1	254	376	31
HD 284135		−0.555	5700(230)	4.1(4)	G3	824	193	74
HD 284149	15-25	−0.650	6070(170)	4.16(21)	G1	720	169	30
HD 281691	8-18	+0.191	5160(210)	4.61(26)	G8	145	342	25
HD 284266	15-30	−0.134	5850(230)	4.4(4)	K0	408	239	34
HD 284503	10-20	−0.232	5430(260)	4.2(4)	G8	125	274	44
HD 284496	12-20	−0.230	5430(100)	4.2(7)	K0	297	288	28
HD 285840	20-70		5640(40)	4.45	K1		214	25
HD 285957	3-13	+0.059	4940(260)	4.79(25)	K1	155	411	28
HD 283798	17-21	+0.595	5760(130)	4.7(4)	G7	380	243	29
HD 283782	<3	+0.082	4900(700)	4.72(29)	K1	−3937	237	77
HD 30171	2-4	−0.353	5390(260)	4.0(5)	G5	706	273	112
HD 31281	8-12	−0.558	5500(400)	4.0(5)	G1	970	167	83
HD 286179	10-35	−0.153	5800(300)	4.6(4)	G3	1316		22
HD 286178			4490(90)	4.6	K1	211	166	46
HD 283447	2-4		4050(50)	4.7	K3	−1397	500	47
HD 283572	2-5		5340(60)	4.5	G5	899	274	82
HD 285778	8-15	−0.352	5300(250)	4.0(5)	K1	510	269	21
HD 283518	<2		3770	4.8	K3		517	74

Acknowledgements. This work was supported by VEGA grant no. 2/0031/18.

References

Baudrand, J. & Bohm, T., MUSICOS - A fiber-fed spectrograph for multi-site observations. 1992, *Astron. Astrophys.*, **259**, 711

Chavarría-K, C., Terranegra, L., Moreno-Corral, M. A., & de Lara, E., Photometric observations of weak-line T Tauri stars . II. WTTS in Taurus-Auriga, Orion and Scorpius OB2-2. 2000, *Astron. Astrophys., Suppl.*, **145**, 187

Crawford, D. L., Empirical calibration of the ubvy,beta systems. I. The F-type stars. 1975, *Astron. J.*, **80**, 955

Grankin, K. N., Magnetically active stars in Taurus-Auriga: Photometric variability and basic physical parameters. 2013, *Astronomy Letters*, **39**, 251

Guenther, E. W., Hartmann, M., Esposito, M., et al., A substellar component orbiting the F-star 30 Arietis B. 2009, *Astron. Astrophys.*, **507**, 1659

Herczeg, G. J. & Hillenbrand, L. A., An Optical Spectroscopic Study of T Tauri Stars. I. Photospheric Properties. 2014, *Astrophys. J.*, **786**, 97

Jensen, E. L. N., Can Post T Tauri Stars Be Found? Yes! 2001, in Astronomical Society of the Pacific Conference Series, Vol. **244**, *Young Stars Near Earth: Progress and Prospects*, ed. R. Jayawardhana & T. Greene, 3

Kaiser, A., Determination of Fundamental Parameters with Stroemgren Photometry. 2006, in Astronomical Society of the Pacific Conference Series, Vol. **349**, *Astrophysics of Variable Stars*, ed. C. Aerts & C. Sterken, 257

Lindegren, L., Hernández, J., Bombrun, A., et al., Gaia Data Release 2. The astrometric solution. 2018, *Astron. Astrophys.*, **616**, A2

Meištas, E. & Straižys, V., Interstellar extinction in the Taurus dark clouds. II. 1981, *Acta Astronomica*, **31**, 85

Paunzen, E., A new catalogue of Strömgren-Crawford uvbyβ photometry. 2015, *Astron. Astrophys.*, **580**, A23

Pribulla, T., Garai, Z., Hambálek, L., et al., Affordable échelle spectroscopy with a 60 cm telescope. 2015, *Astronomische Nachrichten*, **336**, 682

Pych, W., A Fast Algorithm for Cosmic-Ray Removal from Single Images. 2004, *Publ. Astron. Soc. Pac.*, **116**, 148

Rucinski, S. M., Spectral-line broadening functions of WUMa-type binaries. I - AW UMa. 1992, *Astron. J.*, **104**, 1968

Schuster, W. J. & Nissen, P. E., Uvby-beta photometry of high-velocity and metal-poor stars. II - Intrinsic color and metallicity calibrations. 1989, *Astron. Astrophys.*, **221**, 65

Tognelli, E., Prada Moroni, P. G., & Degl'Innocenti, S., The Pisa pre-main sequence tracks and isochrones. A database covering a wide range of Z, Y, mass, and age values. 2011, *Astron. Astrophys.*, **533**, A109

Contrib. Astron. Obs. Skalnaté Pleso **49**, 367 – 372, (2019)

Photometric observations of the asteroid 3200 Phaethon using small and middle telescopes

A. Kartashova[1], M. Husárik[2], O. Ivanova[2,3,4], G. Kokhirova[5], E. Bakanas[1], I. Sokolov[6], U.Kh. Khamroev[5] and A.A. Ibragimov[5]

[1] *Institute of Astronomy, Russian Academy of Sciences, Pyatnitskaya str. 48, 119017 Moscow, Russian Federation (E-mail: akartashova@inasan.ru)*

[2] *Astronomical Institute of the Slovak Academy of Sciences, 059 60 Tatranská Lomnica, Slovakia*

[3] *Main Astronomical Observatory of the NAS of Ukraine, 27 Akademika Zabolotnoho str., 03143 Kyiv, Ukraine*

[4] *Astronomical Observatory, Taras Shevchenko National University of Kyiv, Ukraine*

[5] *Institute of Astrophysics of the Academy of Sciences of the Republic of Tajikistan, St. Bukhoro 22, 734042, Dushanbe, Tajikistan*

[6] *Terskol Branch of Institute of Astronomy, Russian Academy of Sciences, Terskol, Elbrus ave., 81-33, Tyrnyauz, Kabardino-Balkaria Republic, 361623 Russian Federation*

Received: November 2, 2018; Accepted: March 28, 2019

Abstract. The main aim of photometrical observations of the asteroid 3200 Phaethon was searching for its low-level cometary activity (possible coma and/or dust tail) in the pre-perihelion passage. We performed observational runs with telescopes ranging from 0.61-m to 2-m and BVR color imaging. Three longer photometric series were used for modeling of the 3D shape of Phaethon. The color indices and size of the asteroid were estimated.
Key words: asteroids – 3200 Phaethon – photometry

1. Introduction

Near-Earth asteroid 3200 Phaethon is an outstanding small body in the Solar System. Its perihelion distance is 0.14 au, quite close to the Sun, and leads to a systematic strong heating of the surface. Phaethon reveals cometary activity (Jewitt, 2012), and is considered as a parent body of the Geminid meteor shower (Williams & Wu, 1993; Ryabova et al., 2019). These three features make Phaethon a legitimate target for space-probe exploration (Arai, 2018).

2. Results from photometry

Observations of the asteroid 3200 Phaethon were obtained from October to December 2017 with the 2-m telescope at the Terskol Observatory (Caucasus,

Russia), the 1-m telescope at the Sanglokh Observatory (Tajikistan), and the 0.61-m telescope at the Skalnaté Pleso Observatory (Slovakia). The photometric data were obtained through the B, V, and R broadband filters. The reduction of the raw data using bias subtraction, dark and flat field correction was applied in a standard way. The color indices, absolute magnitude, and effective diameter of the asteroid with uncertainties one can see in Tab. 1. For calculation of the effective diameter we applied the formula

$$\log p_V = 6.259 - 2\log D - 0.4H, \tag{1}$$

where D is the diameter of the asteroid in kilometers, p_V the geometric albedo, and H the absolute V-band magnitude (Bowell et al., 1989).

Table 1. Photometric results of 3200 Phaethon from October to December 2017. Table contains heliocentric and geocentric distances and the solar phase angle, respectively. Then color indices, the absolute magnitude, and the effective diameter of the asteroid with uncertainties. For all diameter estimates we used the value of albedo of 0.1066 (Tedesco et al., 2004). In the last column there are listed the acronyms for Sanglokh, Skalnaté Pleso, and Terskol, respectively.

Date	r	Δ	α	$B-V$	$V-R$	H	D	Obs.
	au	au	deg	mag	mag	mag	km	
Oct 28	1.640	0.977	34.0	0.69	0.35	14.37	5.52	San
				±0.07	±0.04	±0.03	±0.08	
Oct 29	1.630	0.957	34.0	0.66	0.36	14.35	5.57	San
				±0.13	±0.06	±0.09	±0.22	
Nov 15	1.444	0.603	32.4	–	0.43	14.42	5.38	SPO
				–	±0.02	±0.03	±0.08	
Nov 17	1.422	0.566	31.9	0.59	0.43	14.40	5.43	San
				±0.11	±0.07	±0.06	±0.15	
Nov 22	1.357	0.461	30.4	0.62	0.35	14.36	5.54	SPO
				±0.02	±0.02	±0.02	±0.05	
Nov 23	1.346	0.443	30.1	0.64	0.36	14.37	5.50	SPO
				±0.04	±0.03	±0.04	±0.09	
Nov 27	1.294	0.367	28.3	0.65	0.33	14.35	5.58	SPO
				±0.02	±0.02	±0.02	±0.05	
Dec 02	1.226	0.273	25.0	0.65	0.35	14.33	5.62	Ter
				±0.01	±0.01	±0.01	±0.02	
Dec 13	1.061	0.089	29.6	0.63	0.35	14.22	5.92	Ter
				±0.01	±0.02	±0.02	±0.06	

For comparison our results with other authors we can use the ALCDEF database[1]. Color indices we can compare with values from papers of Pan et al. (2012), Jewitt (2013), and Ansdell et al. (2014). Our determined colors are in

[1]http://alcdef.org/

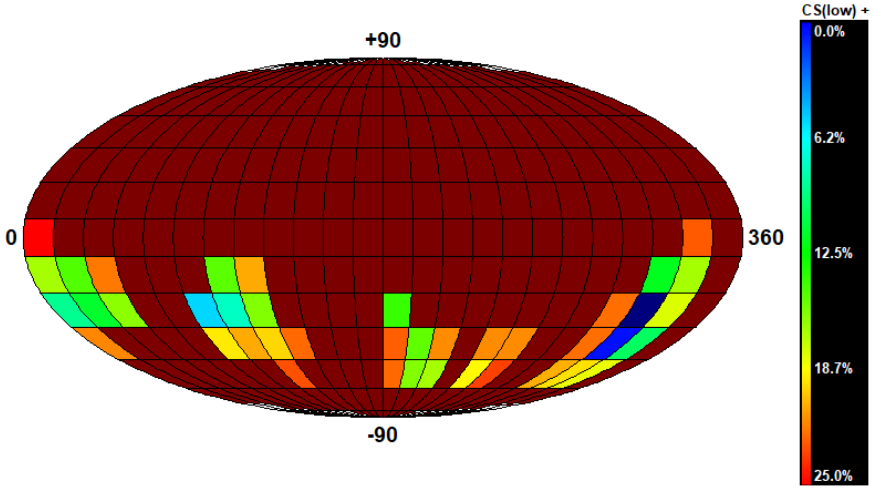

Figure 1. χ^2 residuals between the synthetic and observed lightcurves of the asteroid for spin-vector coordinates covering the entire celestial sphere. The dark blue region represents the pole location with the lowest χ^2, which increases as the color goes from green to yellow and, finally, to red.

good agreement with published values. Absolute magnitudes H have been published by many authors. The values are in the interval from 13.96 to 14.60 mag, but only one is reviewed with three decimal places. It is value 14.345 mag (Pravec et al., 2012). Our H values determined in all nights are very similar to that value.

Also we derived a convex 3D shape model of Phaethon based on 51 previously published in the DAMIT database (Hanuš et al., 2016) and our 3 lightcurves

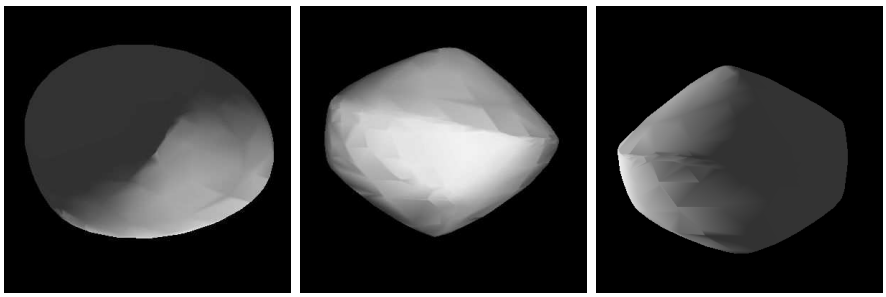

Figure 2. The 3D shape model of Phaethon. On the left there is shown a north pole view, in the middle and right the equatorial viewing and illumination geometry with rotational phases 90° apart.

(November 22 and 27, and December 02, 2017). We have used the robust method, the so-called lightcurve inversion described by Kaasalainen & Torppa (2001) and Kaasalainen et al. (2001). It allows us to determine the sidereal period and pole solutions and recover a detailed convex 3D shape model. The sidereal rotational period was estimated at the value of $3.603\,96 \pm 0.000\,01$ hr. This value is almost the same as computed by Hanuš et al. (2016) and reviewed in the ALCDEF database.

Next, the north pole coordinates were computed. In Fig. 1 there is shown the possible location of the north pole at the ecliptic longitude $\lambda_{\rm p} = 315^\circ \pm 10^\circ$ and latitude $\beta_{\rm p} = -31^\circ \pm 10^\circ$. From that it follows that the sense of rotation of Phaethon is retrograde. The first estimates of the spin axis orientation were published by Krugly et al. (2002) and Ansdell et al. (2014), but the currently accepted, most probable value is that of Hanuš et al. (2016). Our estimate is very similar. The latest published position of the north pole of Phaethon at $(318^\circ \pm 5^\circ, -47^\circ \pm 5^\circ)$ is from the article by Hanuš et al. (2018). Our determined 3D shape model has the ratios at $a/b = 1.11$ and $b/c = 1.04$ (Fig. 2), but that we cannot compare with data from the ALCDEF database.

3. Conclusion

Despite many attempts to obtain signs of Phaethon's cometary activity, no trace of it has been detected. But our photometry in all observed nights showed that Phaethon should be actually larger than 5.1 km as it was previously published. The analysis from the Arecibo radar confirmed that Phaethon is really larger and has the diameter of approx. 6 km (Taylor et al., 2018) and an almost spherical 3D shape[2]. Results of multi-color photometry show a bluish surface for Phaethon. It is in contrast with typical cometary nuclei that are slightly reddish in general (Tedesco & Desert, 2002). Zheltobryukhov et al. (2018) estimated the geometric albedo of Phaethon to be 0.075 ± 0.007 in the R filter, which appears to be consistent with dark F-type asteroids. Also our data confirmed the taxonomy F-type of Phaethon. Note that Phaethon was classified as Tholen F-type by Tholen (1984).

Acknowledgements. AK thanks for the support, in part, from the RFBR grant No. 16-02-00805-a. OI is supported, in part, by the project the SASPRO Program, REA grant agreement No. 609427, and the Slovak Academy of Sciences (Grant Vega No. 2/0023/18). MH thanks Grant VEGA No. 2/0023/18. Observations at the Skalnaté Pleso Observatory were acquired under the realisation of the project ITMS No. 26220120029, based on the supporting operational Research and development program financed from the European Regional Development Fund.

[2]https://www.jpl.nasa.gov/news/news.php?feature=7030

References

Ansdell, M., Meech, K. J., Hainaut, O., et al., Refined Rotational Period, Pole Solution, and Shape Model for (3200) Phaethon. 2014, *Astrophys. J.*, **793**, 50, DOI: 10.1088/0004-637X/793/1/50

Arai, T., An Overview of the DESTINY+ mission: Flyby of Geminids parent (3200) Phaethon and in-situ dust analyses. 2018, in COSPAR Meeting, Vol. **42**, *42nd COSPAR Scientific Assembly*, B1.1–43–18

Bowell, E., Hapke, B., Domingue, D., et al., Application of photometric models to asteroids. 1989, in *Asteroids II*, ed. R. P. Binzel, T. Gehrels, & M. S. Matthews, 524–556

Hanuš, J., Vokrouhlický, D., Delbo', M., et al., (3200) Phaethon: Bulk density from Yarkovsky drift detection. 2018, *Astron. Astrophys.*, **620**, L8, DOI: 10.1051/0004-6361/201834228

Hanuš, J., Delbo', M., Vokrouhlický, D., et al., Near-Earth asteroid (3200) Phaethon: Characterization of its orbit, spin state, and thermophysical parameters. 2016, *Astron. Astrophys.*, **592**, A34, DOI: 10.1051/0004-6361/201628666

Jewitt, D., The Active Asteroids. 2012, *Astron. J.*, **143**, 66, DOI: 10.1088/0004-6256/143/3/66

Jewitt, D., Properties of Near-Sun Asteroids. 2013, *Astron. J.*, **145**, 133, DOI: 10.1088/0004-6256/145/5/133

Kaasalainen, M. & Torppa, J., Optimization Methods for Asteroid Lightcurve Inversion. I. Shape Determination. 2001, *Icarus*, **153**, 24, DOI: 10.1006/icar.2001.6673

Kaasalainen, M., Torppa, J., & Muinonen, K., Optimization Methods for Asteroid Lightcurve Inversion. II. The Complete Inverse Problem. 2001, *Icarus*, **153**, 37, DOI: 10.1006/icar.2001.6674

Krugly, Y. N., Belskaya, I. N., Shevchenko, V. G., et al., The Near-Earth Objects Follow-up Program. IV. CCD Photometry in 1996-1999. 2002, *Icarus*, **158**, 294, DOI: 10.1006/icar.2002.6884

Pan, S., Abe, S., & Kinoshita, D., Rotation Period and Lightcurve Analysis of Asteroid (3200) Phaethon. 2012, in LPI Contributions, Vol. **1667**, *Asteroids, Comets, Meteors 2012*, 6294

Pravec, P., Harris, A. W., Kušnirák, P., Galád, A., & Hornoch, K., Absolute magnitudes of asteroids and a revision of asteroid albedo estimates from WISE thermal observations. 2012, *Icarus*, **221**, 365, DOI: 10.1016/j.icarus.2012.07.026

Ryabova, G. O., Avdyushev, V. A., & Williams, I. P., Asteroid (3200) Phaethon and the Geminid meteoroid stream complex. 2019, *Mon. Not. R. Astron. Soc.*, DOI: 10.1093/mnras/stz658

Taylor, P. A., Marshall, S. E., Venditti, F., et al., Radar and Infrared Observations of Near-Earth Asteroid 3200 Phaethon. 2018, in Lunar and Planetary Science Conference, Vol. **49**, *Lunar and Planetary Science Conference*, 2509

Tedesco, E. F. & Desert, F.-X., The Infrared Space Observatory Deep Asteroid Search. 2002, *Astron. J.*, **123**, 2070, DOI: 10.1086/339482

Tedesco, E. F., Noah, P. V., Noah, M., & Price, S. D., IRAS Minor Planet Survey V6.0. 2004, *NASA Planetary Data System*, **12**, IRAS

Tholen, D. J. 1984, Asteroid taxonomy from cluster analysis of photometry, PhD thesis, University of Arizona, Tucson

Williams, I. P. & Wu, Z., The Geminid meteor stream and asteroid 3200 Phaethon. 1993, *Mon. Not. R. Astron. Soc.*, **262**, 231, DOI: 10.1093/mnras/262.1.231

Zheltobryukhov, M., Chornaya, E., Kochergin, A., et al., Umov effect in asteroid (3200) Phaethon. 2018, *Astron. Astrophys.*, **620**, A179, DOI: 10.1051/0004-6361/201833408

Contrib. Astron. Obs. Skalnaté Pleso **49**, 373 – 376, (2019)

Elemental abundance analysis of single and binary late-B stars using sub-meter class telescopes: HR 342, HR 769, HR 1284, and HR 8705

T. Kılıçoğlu[1] and R. Monier[2]

[1] *Ankara University, Faculty of Science, Department of Astronomy and Space Sciences, 06100, Ankara, Turkey, (E-mail: tkilicoglu@ankara.edu.tr)*

[2] *LESIA, UMR 8109, Observatoire de Paris et Université Pierre et Marie Curie Sorbonne Universités, place J. Janssen, Meudon, Paris, France*

Received: October 19, 2018; Accepted: February 22, 2019

Abstract. We test the capabilities of 0.4 m telescopes equipped with an échelle spectrograph to derive fundamental parameters and elemental abundances of four late-B type stars: HR 342, HR 769, HR 1284, and HR 8705. The medium resolution ($R \sim 14\,000$) spectra covering the wavelength range of 4380-7350 Å of the four stars have been obtained using the 40-cm-telescope in Ankara University Kreiken Observatory (AUKR). Using spectrum synthesis, we were able to derive the abundances of eleven chemical elements. We find that these stars do not show remarkable departures from the solar abundances, except for HR 8705 and the primary component of HR 1284, which exhibit slight underabundances of a few elements, i.e., O, Mg, Al, Si, and Fe. We also find that HR 1284 is probably a newly recognized spectroscopic binary star. In order to model the spectrum of this object, one of us (TK) has developed a new graphic interface which allows us to synthesize the composite spectrum of binary stars.

Key words: chemical abundance analysis – chemically peculiar stars – early type stars – stars: individual: HR 342, HR 769, HR 1284, HR 8705

1. Introduction

The atmospheres of chemically peculiar (CP) late-B stars are useful laboratories to test the theory of atomic diffusion. We have recently started a project aiming at observing and analysing high resolution spectra of about 100 slowly rotating late-B stars in order to find new CP stars. In order to decide which objects should be monitored at a higher resolution with larger telescopes, we are currently observing these objects using a 40-cm telescope equiped with a medium resolution échelle spectrograph. We present here the abundance analysis of HR 342, HR 769, HR 1284, and HR 8705 and the detection of a new binary object (HR 1284). We also present a new interface which allows us to synthesize the spectrum of detached SB2 binaries.

2. Observations and analysis

The targets have been observed using the Shelyak eShel spectrograph mounted on the 40-cm telescope in Ankara University Kreiken Observatory (AUKR) in 2017. The spectra span the spectral range 4380-7350 Å with a medium resolution, i.e., $R \sim 14000$. The atmospheric parameters were initially estimated from Johnson (BV) magnitudes with the calibrations of Flower (1996) and then refined by modelling H_β lines. The fundamental parameters of the stars were also estimated from a $\log g$–$T_{\rm eff}$ diagram (Fig. 1) and are collected in Table 1.

The model atmospheres were calculated using ATLAS12 (Kurucz, 2005) and the synthetic spectra were computed using SYNSPEC49/SYNPLOT (Hubeny & Lanz, 1995). The linelist was first constructed from R. Kurucz's gfall.dat and then updated by using VALD, NIST, and recent publications. We iteratively adjusted the synthetic spectra to the observed spectra until the best fit was achieved in order to derive the elemental abundances.

During the analysis, we have found that HR 1284 (HD 26171) is most likely a newly recognized SB2 star, where the lines of the secondary component are barely visible. One of us (TK) modified SYNPLOT into a new interface (called SYNPLOTBIN) to model the composite spectrum of this binary star. The observed spectrum is compared to the composite synthetic spectrum together with the synthetic spectra of each component in Fig. 2. In the lower panel of Fig. 2, Mg I triplet around 5175 Å, Fe I line at 5328.038 Å, and Na I doublet around 5890 Å belonging to the secondary component are distinguishable in the observed composite spectra of the system.

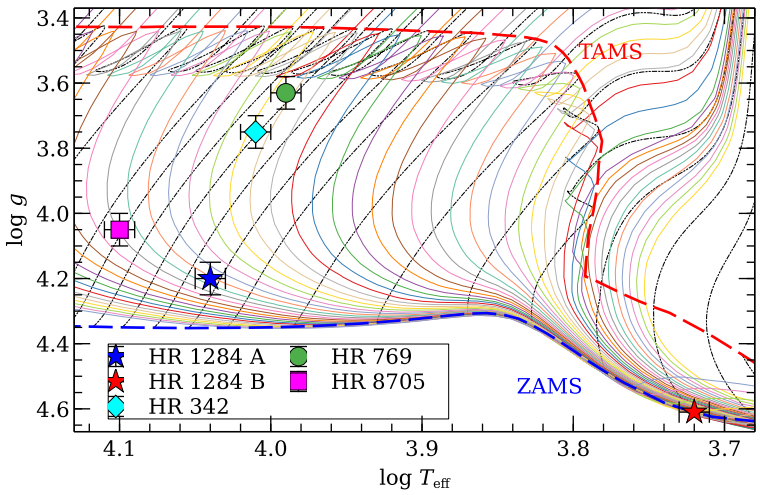

Figure 1. Stars on the theoretical $\log g$–$\log T_{\rm eff}$ diagram (tracks taken from Bressan et al. 2012).

Table 1. Fundamental parameters of the targets

Star	Sp.T.	$T_{\rm eff}$ (K)	$\log g$ (cgs.)	M ($M_\odot$)	Age (Myr)
HR 342	B9.5V	10250 ± 250	3.75 ± 0.05	3.00 ± 0.10	325 ± 20
HR 769	B9.5V	9800 ± 200	3.63 ± 0.05	3.05 ± 0.10	340 ± 20
HR 1284 A	B9.5V	11000 ± 300	4.20 ± 0.05	2.67 ± 0.10	200 ± 20
HR 1284 B	K1V	5200 ± 300	4.61	0.90 ± 0.02	200 ± 20
HR 8705	B8V	12500 ± 500	4.05 ± 0.05	3.40 ± 0.10	158 ± 20

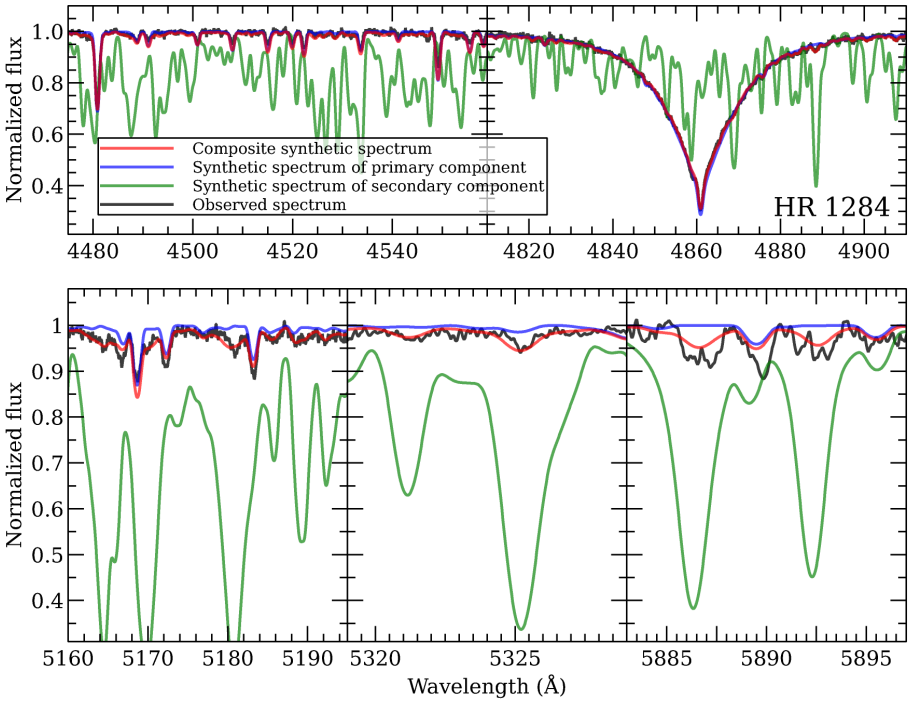

Figure 2. Observed spectra of HR 1284 and synthesized spectra for its components.

3. Results and conclusion

We have derived the abundances of 11 elements for four bright stars with uncertainties ranging from ±0.10 and ±0.25 dex (Fig 3, right). The chemical patterns of the stars do not depart significantly from the solar composition except for HR 8705 and the primary component of HR 1284, which exhibit slight under-

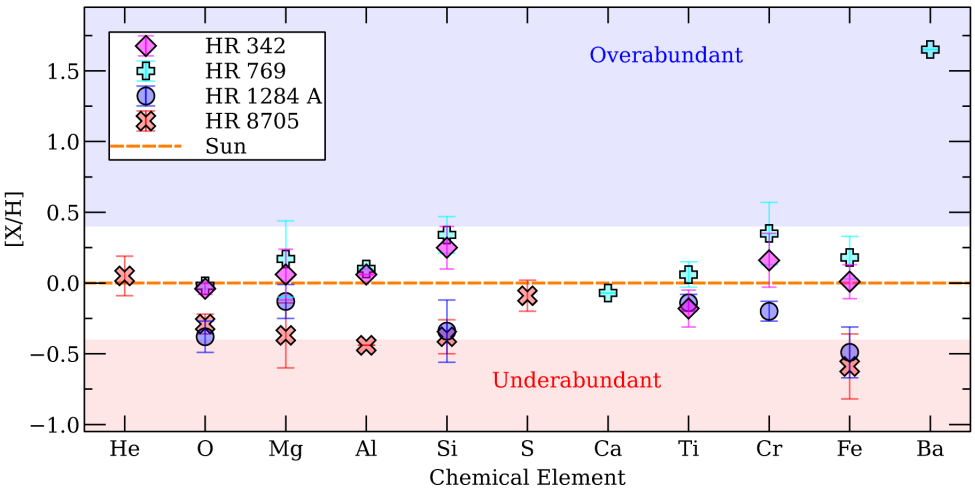

Figure 3. Abundance pattern of the target stars.

abundances of a few elements, such as O, Mg, Al, Si, and Fe. We could detect a very shallow Ne I 6402 Å line only in the spectra of HR 8705, indicating a slight enhancement of Neon. Higher resolution spectra of these two stars, obtained using larger telescopes, will help clarify their natures.

This demonstrates the usefulness of small telescopes equipped with medium resolution spectrographs to derive abundances for certain chemical elements and sort out putative candidates for CP stars to be observed afterwards at higher resolution with meter class telescopes.

References

Bressan, A., Marigo, P., Girardi, L., et al., PARSEC: stellar tracks and isochrones with the PAdova and TRieste Stellar Evolution Code. 2012, *Mon. Not. R. Astron. Soc.*, **427**, 127, DOI: 10.1111/j.1365-2966.2012.21948.x

Flower, P. J., Transformations from Theoretical Hertzsprung-Russell Diagrams to Color-Magnitude Diagrams: Effective Temperatures, B-V Colors, and Bolometric Corrections. 1996, *Astrophys. J.*, **469**, 355, DOI: 10.1086/177785

Hubeny, I. & Lanz, T., Non-LTE line-blanketed model atmospheres of hot stars. 1: Hybrid complete linearization/accelerated lambda iteration method. 1995, *Astrophys. J.*, **439**, 875, DOI: 10.1086/175226

Kurucz, R. L., ATLAS12, SYNTHE, ATLAS9, WIDTH9, et cetera. 2005, *Memorie della Societa Astronomica Italiana Supplementi*, **8**, 14

Contrib. Astron. Obs. Skalnaté Pleso **49**, 377 – 379, (2019)

Hydrodynamics of supernova remnants: interaction with interstellar medium

P. Kostić, S. Knežević and B. Vukotić

Astronomical Observatory, Volgina 7, P.O.Box 74 11060 Belgrade, Serbia

Received: October 27, 2018; Accepted: January 29, 2019

Abstract. We study the large scale interaction of the supernova remnants with clouds of interstellar gas. Optical proper motion measurements and Hα emission in supernova remnants are discussed, especially for the 1.4 m telescope "Milanković" and astroclimate conditions at the Astronomical station Vidojevica near Prokuplje, Serbia. We present our hydrodynamical simulation that is used to estimate the observables. The simulation implements a fractal density structure of interstellar clouds. We analyse how such clouds influence the expansion of the remnants and shock properties in order to estimate the distance to the remnants. From distributions of density and temperature behind the shock we calculate the resulting Hα emission and discuss how such emission can be used to probe the interstellar medium properties.

Key words: supernova remnants – numerical simulation

1. Introduction

Supernova remnants (SNRs) are a critical connection between stellar objects and interstellar medium (ISM). They disperse products of stellar evolution over a significant spatial scales while shaping the ISM and interacting with giant molecular clouds. The studies of such objects are crucial for understanding the evolution of galaxies.

A supernova remnant forms as a collisionless shock wave when supernova ejecta sweep the surrounding ISM. These magneto-hydrodynamic shocks accelerate charged particles to high speeds, which produces a very energetic radiation. Shock waves as well as SNR interiors are vastly observed from radio to X-ray parts of the electromagnetic spectrum. In addition, SNRs and their shocks are successfully modeled with hydrodynamical simulations.

A numerous empirical and theoretical studies of SNRs have indicated that ISM properties are of great significance for SNR evolution (e.g., see Pavlović et al., 2018). Dense ISM parts, such as molecular clouds, slow down the shock-wave changing the emission features and shape of the remnant. A lifetime of a typical SNR is of the order 10^4 years. The observed features of such long-lived objects can only be put into the right evolutionary context using the data from numerical models. Contemporary SNR simulations model the ISM either as homogeneous medium or as assembly of the homogeneous clumps. However,

ISM has a much more complex structure and ISM density distribution can be described as a fractal, turbulence driven medium.

This work discusses the possibility for observing the interactions between SNRs and clumpy ISM with small, meter-class telescopes, especially with the 1.4 m telescope "Milanković", recently commissioned at the Astronomical station Vidojevica, near the town of Prokuplje in southern Serbia. To comprehend the connection between the ISM structure and observables we present a numerical model of SNRs interaction with a fractal-structured medium.

2. Astronomical station Vidojevica

The largest instrument at the Astronomical station Vidojevica is a 1.4 m reflector "Milanković". Typical astro-climate conditions on the site give clear sky seeing median of 1.15 arcsec (Jovanovic et al., 2012). On a displayed figure of a numerical simulation of SNR evolution in a fractal ISM the SNR-cloud interaction features emerge on scales of up to 20 pc. With the telescope "Milanković" such features, in Hα, could be observed up to a 70 kpc distance if bright enough. If we consider that older remnants (older than $\sim 10^4$ years) are less bright than younger ones, the small telescopes can be used to observe remnants in the Milky Way. Apart from that, the long term projects of proper motion observations might be more feasible on smaller telescopes. Observed proper motions in combination with predicted shock speeds from simulations might give distance estimates to SNRs.

Our grid-based 2D hydrodynamical numerical simulation is based on the MUSCL-Hancock finite volume scheme with the HLLC Riemann solver (Toro, 2009). The ISM is modeled as a fractal cloud, ie. a cloud with fractal density distribution (Elmegreen, 1997).

3. Summary

- Fractal distribution of ISM density can influence the properties of SNRs.
- Such properties have a potential to be observed even with small, meter-class telescopes in the Milky Way.
- Numerical hydrodynamical simulations can link the SNR observables to ISM properties.

Acknowledgements. The authors acknowledge the financial support by the Ministry of Education, Science and Technological Development of the Republic of Serbia through the project #176021 "Visible and invisible matter in nearby galaxies: theory and observations".

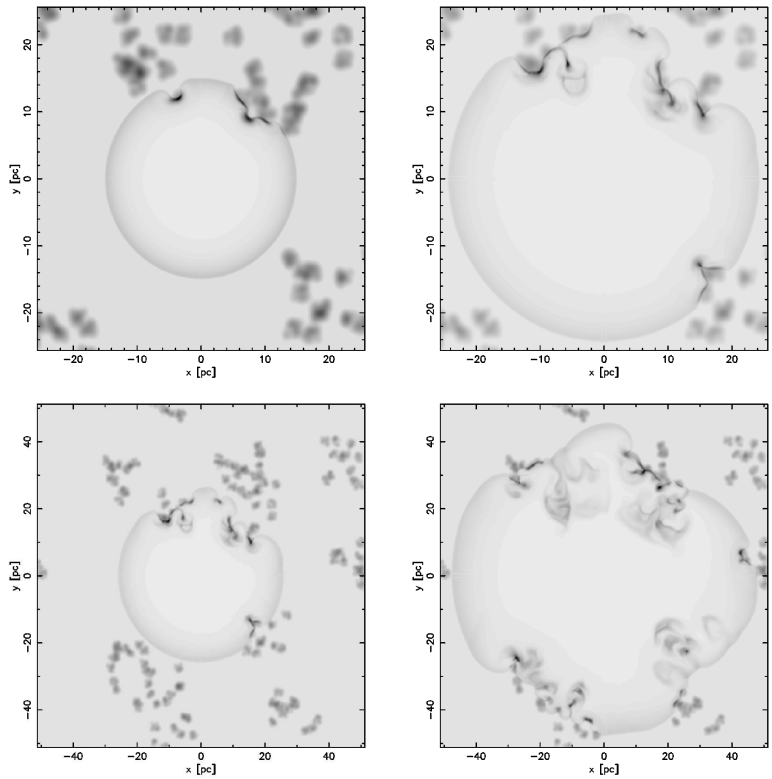

Figure 1. A simulation frame of density distribution for SNR expanding into the fractal ISM. A test simulation on a 400×400 grid, time instances after the supernova explosion are: 3000 yr (upper left), 8000 yr (upper right), 9000 yr (lower left) and 30000 yr (lower right).

References

Elmegreen, B. G., Intercloud Structure in a Turbulent Fractal Interstellar Medium. 1997, *Astrophys. J.*, **477**, 196, DOI: 10.1086/303705

Jovanovic, M., Stojanovic, M., Martinovic, N., et al., Astronomical Station Vidojevica: Astro-Climate. 2012, *Publications de l'Observatoire Astronomique de Beograd*, **91**, 83

Pavlović, M. Z., Urošević, D., Arbutina, B., et al., Radio Evolution of Supernova Remnants Including Nonlinear Particle Acceleration: Insights from Hydrodynamic Simulations. 2018, *Astrophys. J.*, **852**, 84, DOI: 10.3847/1538-4357/aaa1e6

Toro, E. F. 2009, *Riemann Solvers and Numerical Methods for Fluid Dynamics: A Practical Introduction, 3rd edn.* (Berlin, Heidelberg: Springer-Verlag)

Contrib. Astron. Obs. Skalnaté Pleso **49**, 380 – 383, (2019)

Search for extrasolar planets around white dwarfs

V.N. Krushevska[1], Y.G. Kuznyetsova[1], O.A. Veles[1], M.V. Andreev[1,2], Y.O. Romanyuk[1], Z. Garai[3], T. Pribulla[3], J. Budaj[3], S. Shugarov[3,4], E. Kundra[3], Ľ. Hambálek[3] and P. Dolinský[5]

[1] *Main astronomical observatory, NASU, 27, Akademika Zabolotnoho street, Kyiv, 03680, Ukraine*

[2] *ICAMER, NASU, 27, Akademika Zabolotnoho Street, Kyiv, 03680, Ukraine*

[3] *Astronomical Institute of the Slovak Academy of Sciences 059 60 Tatranská Lomnica, The Slovak Republic*

[4] *Sternberg Astronomical Institute,, University avenue 13, Moscow, 119992, Russia*

[5] *Slovak Central Observatory, Hurbanovo, Slovakia*

Received: November 28, 2018; Accepted: February 18, 2019

Abstract. We present a project aimed at detection of exoplanets orbiting around white dwarfs (WDs) using the method of transits. For our research we have selected some objects based on an indication of the presence of extrasolar giant planets around them. We have already started the long-term photometric observations using available telescopes in the northern hemisphere.

Key words: white dwarfs, extrasolar planets

1. Introduction

Presently, the search for extrasolar planets around other stars is at the top of astrophysical investigations. One of the most productive methods of search is the transit method that is based on photometric observations. The main requirement for a transit observation - the planet orbit plane is oriented nearly along the line of sight. Probability of such planet orbit orientation is proportional to the ratio of the planet radius to the star radius.

The simplest variant is to search for Jupiter-like planets on short period orbits. At the moment, the largest number of exoplanets was discovered around F-G stars with masses close to the solar mass. Majority of planets have their orbital periods from 1 to 100 days.

We present a project to search for planets near white dwarfs. This is very important because by the statistical presence or absence of planets in WDs, one can judge about the fate or evolution of planetary systems around near-solar-mass stars after the red giant stage. Besides, the small size of WDs and the very large width of the lines in the spectrum of WDs (a relatively flat spectrum

without sharp lines) will provide an opportunity to identify the thin absorption lines of the atmospheres of the planets during eclipses.

2. The main idea of project

The main aim of the project is detection of exoplanets orbiting around WDs using the transit method. Nowadays there are about 20 thousand known WDs brighter than 19^m (Kleinman, S.J. et al., 2013). In the case if a WD has a transiting exoplanet we will definitely register significant brightness decrease of the central star. We can do it even if the eclipse is not total, since the sizes of a giant planet and a WD are comparable. Characteristic sizes of WD diameters have values close to the Earth diameter.
We consider the following arguments for the possible presence of planets in systems of WDs:
1. One of the first exoplanets was discovered in the system PSR B1620-26 "pulsar+WD"(Thorsett, S.E. et al., 1993).
2. Presence of planet remnants in systems of WDs (Farihi, J. et al., 2017).
3. Discovery of planets in two systems of subdwarfs V391 Pegasi and Kepler-70 (KOI-55) that experienced a stage of red giants (Silvotti, R. et al., 2007), (Charpinet, S. et al., 2011).
4. Discovery of disintegrating minor planets orbiting the WD1145+017 (Vanderburg, A. et al., 2015).

Advantages of extrasolar planet search around WD:
1. Prevalence of WDs (3%-10% from the number of all stars).
2. Easy to detect (a full or partial eclipse), which significantly reduces the requirements for the photometric precision.

Factors that complicate the extrasolar planet searching around WD:
1. Very low luminosity of WDs (absolute values are in the range 10^m - 15^m).
2. Quite small durations of eclipses (minutes).

Most of extrasolar planets have masses similar or greater than the Jovian mass and are at distances less than 0.5 AU from host stars. This fact increases the probability of finding extrasolar planets around WDs. According to our estimates, possible transit phenomena for close star-planet systems with WDs range from minutes to dozen of minutes.

3. Objects

For our research we used the data from the Sloan Digital Sky Survey DR7 White Dwarf Catalog, containing 20 thousand WDs. We collected information on magnitudes of the WDs obtained in the filters *u*, *g*, *r*, *i*, *z*, and calculated *u*-*g*,

g-r, *g-i*, and *g-z* values. Fig. 1 shows that some WDs are far from the main group of objects. In our opinion such excess value may be due to the fact that during the object observation with one of the filters the WD was eclipsed, possibly, by an exoplanet.

From noted WDs we have selected several objects that are visible in the northern latitudes: SDSS J070546.78+393453.4, SDSS J220823.66-011534.0, SDSS J131156.70+544455.8, SDSS J085612.42+143756.9.

We have already started the long-term photometric observations using the telescopes of MAO NAS of Ukraine, the Terskol observatory of Northern Caucasus, the telescopes of the AI SAS and Slovak Central Observatory. However, it is necessary to carry out many new observations and analyze the periodograms obtained from light curves to receive reliable results.

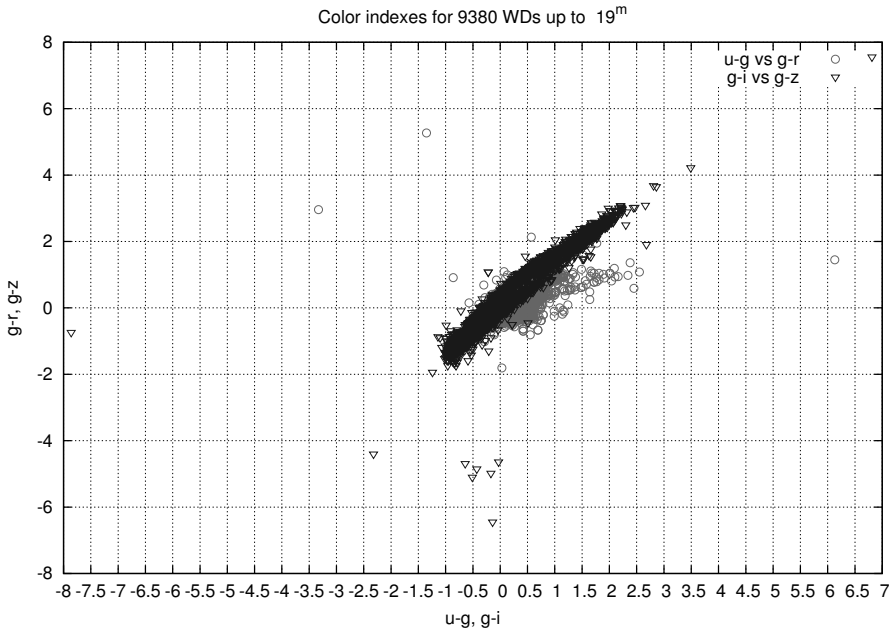

Figure 1. Distribution of white dwarfs by the color index.

4. Conclusions

The development of this method and its testing will allow us to discover new exoplanets, or estimate the limits of distribution probability of giant planets in systems of WDs. Observational data obtained using meter-class telescopes fully

satisfy the requirements of the task. In the near future we also plan to use the data from astronomical catalogues.

We welcome everyone who is interested in this problem and wants to join our team for work on this project.

References

Charpinet, S. et al.: 2011, *Nature* **480**, 496

Farihi, J. et al.: 2017, *Nature Astronomy* **1**, 1

Kleinman, S.J. et al.: 2013, *Astrophys. J., Suppl. Ser.* **204**, 1

Silvotti, R. et al.: 2007, *Nature* **449**, 189

Thorsett, S.E. et al.: 1993, *Astrophys. J., Lett.* **412**, L33

Vanderburg, A. et al.: 2015, *Nature* **526**, 546

Contrib. Astron. Obs. Skalnaté Pleso **49**, 384 – 389, (2019)

A search for additional bodies in short period eclipsing binary stars

A.I. Bogomazov[1], M.A. Ibrahimov[2], V.S. Kozyreva[1], B.L. Satovskii[3], V.N. Krushevska[4], Y.G. Kuznyetsova[4], S.A. Ehgamberdiev[5], B.M. Hafizov[5], R.G. Karimov[5], E.R. Gaynullina[5], A.V. Khalikova[5], O.U. Parmonov[5], T.R. Irsmambetova[1] and A.V. Tutukov[2]

[1] *M. V. Lomonosov Moscow State University, P. K. Sternberg Astronomical Institute, 13, Universitetskij prospect, Moscow, 119991, Russia*

[2] *Institute of astronomy, Russian Academy of Sciences, 48, Pyatnitskaya ulitsa, Moscow, 119017, Russia*

[3] *AstroTel Ltd., 1A, Nizhegorodskaya ulitsa, Moscow, 109147, Russia*

[4] *Main Astronomical Observatory, National Academy of Sciences of Ukraine, 27, Akademika Zabolotnoho street, Kyiv, 03143, Ukraine*

[5] *Ulugh Beg Astronomical Institute, Uzbek Academy of Sciences, 33, Astronomicheskaya ulitsa, Tashkent, 100052, Uzbekistan*

Received: November 1, 2018; Accepted: February 25, 2019

Abstract. We describe here the formulation of our search for additional bodies in fifteen short period eclipsing binary stars and some results obtained by now. We intended to use two methods: transits across the surface of one or both stars (in order to detect planets) in the binary and a timing of eclipses of central binary stars (that can indicate the presence of a stellar mass body in the system). Observations were carried out using ground based photometry with 50-60 cm telescopes in 2013-2017. Until now no transits had been detected in our data. But at the same time we found several candidates for additional bodies in four systems. Further data processing will be performed.

Key words: eclipsing binary stars

1. Introduction

We present a list of eclipsing binary stars that are used to search for potentially existing planetary systems, or additional stellar components. The presence of eclipses increases the probability that the observer is in the orbital plane of the system, since it is natural to expect that protoplanetary disks and planets are located in, or close to this plane (Tutukov & Bogomazov, 2012). Our target binaries can be found in Table 1. Planets in them could be detected with the transit method using 1-meter class telescopes. Also there is a possibility to search for additional bodies using the light time effect, its precision for ground based telescopes allows us to find brown dwarfs or new stars in binary systems.

Table 1. A list of systems to explore. Data from the General Catalogue of Variable Stars (Samus' et al., 2017). "System" is the name of a target binary, "RA" is its right ascension, "Dec" is its declination, P_{orb} is the orbital period, m_{max} is the stellar magnitude at the maximum, m_{min} is the stellar magnitude at the primary minimum, "Type" is the light curve type.

System	RA	Dec	P_{orb}	m_{max}	m_{min}	Type
AC Boo	14 56 28.34	+46 21 44.1	0.3524485	10.14	10.67	EW
CV Boo	15 26 19.58	+36 58 53.6	0.8469938	10.65	11.48	EA
AR CrB	15 59 18.58	+27 52 15.1	0.397352	10.84	11.45	EW
GU Her	16 32 05.52	+30 23 09.7	4.342921	11.5	12.3	EA/DM
V1097 Her	17 33 27.97	+26 55 47.9	0.360847	10.76	11.30	EW
TZ Lyr	18 15 49.67	+41 06 37.9	0.5288269	10.87	11.85	EB/D
V0563 Lyr	18 45 06.63	+40 11 11.5	0.577639[a]	10.96	11.47	EW
V2364 Cyg	19 22 11.75	+49 28 34.4	0.5921376	11.20	11.84	EW
CG Cyg	20 58 13.45	+35 10 29.6	0.63114100	9.73	10.86	EA/SD/RS
SW Lac	22 53 41.66	+37 56 18.6	0.3207209	8.51	9.39	EW/KW
AB And	23 11 32.09	+36 53 35.1	0.3318912	9.49	10.46	EW
AP And	23 49 30.70	+45 47 21.3	1.5872910	11.3	11.9	EA
CO And	01 11 24.84	+46 57 49.4	1.8276678	11.1	12.1	EA
V0873 Per	02 47 08.21	+41 22 31.9	0.2949039	10.8	11.5	EW
HS Aur	06 51 18.47	+47 40 24.2	9.815377	10.16	10.90	EA

[a] By Beltraminelli et al. (1999).

For our photometric observations we used two 60-cm Zeiss-600 telescopes and one 50-cm AMT-1 telescope (the R filter was used everywhere): at the South Station of M. V. Lomonosov Moscow State University in Nauchnii, Crimea (Zeiss-600), and at the Maidanak observatory of the Ulugh Beg Astronomical Institute of Uzbek Academy of Sciences (AMT-1 and Zeiss-600). These sites have excellent (Maidanak) and good (Crimea) astronomical climate, so we were provided with very high quality observations, typical errors were about a few thousandths of stellar magnitude. Usual time of unbroken monitoring was 5-7 hours per night, that allowed us to find a lot of times of minima for our target objects.

2. First results

For V0873 Per, CV Boo, AR CrB, and AB And we obtained evidence in favour of the existence of additional bodies in them using the light time effect, see Table 2 for the summary of our results.

V0873 Per. The system was observed in September-November 2013 and in August-September 2014 at both observatories (Bogomazov et al., 2016a). We obtained 28 times of minima (more than 50% of times of minima existed for V0873 Per in January 2016 at the time of publication). Combining our times of minima with times of minima from the literature we found that the system

contains a new body candidate with the lower limit of mass $m_3 \sin i_3 \approx 0.2 M_\odot$ (its orbital period is about 300 days), in addition to the body candidate with the lower mass limit $m_4 \sin i_4 \approx 0.06 M_\odot$ (its orbital period is about 4 years) found by Kriwattanawong & Poojon (2015).

According to Table 6 by Holman & Wiegert (1999), circumbinary bodies should have stable orbits on long timescales if their semi-major axes are $\gtrsim$ 4 separations of the central binary (i.e., the orbital period of the additional companion is $\gtrsim 8$ orbital periods of the central binary) in all models considered by them. This criterion was met for all third and fourth bodies suggested by us in this manuscript, except the candidate for the third body in CV Boo.

CV Boo. We obtained 14 times of minima during May-July 2014 with practically highest possible precision. The data showed a variation of times of minima on a timescale of about 70 days. We combined our times of minima with the data from the literature and found that the system possesses a secular variation of the orbital period (Figure 2 and Equation 2 by Bogomazov et al., 2016b). The $(O-C)_2$ values were calculated as the difference between observed (our+literature) times of minima and the theoretical curve for the secular variation, $(O-C)_2$ could be statistically satisfactory explained by the influence of a third star with a mass of $m_3 \sin i_3 \approx 0.4 M_\odot$ in an eccentric orbit ($e \approx 0.9$) with the orbital period of ≈ 75 days (Figures 3 and 4 by Bogomazov et al., 2016b).

This candidate can be in a chaotic zone, or near it (if the orbit is wider than its projection), see Figure 1 by Shevchenko (2015), the suggested third body's projection of the orbit has the following parameters for this Figure: $\mu = M_2/(M_1 + M_2) \approx 0.5$, $r_p = 2a_b$, where $M_{1,2}$ are masses of the primary and secondary stars correspondingly, r_p is the periastron distance of the third body, a_b is the semi-major axis of the central binary's orbit. At the same time it is far from the unlimited chaotic diffusion, see Figure 4 by Shevchenko (2015), the ratio of orbital periods of the candidate body and the central binary is about 80, whereas the body is expected to be possibly ejected from the system if it is $\lesssim 5$. So, CV Boo is an interesting example to test its dynamical evolution.

In a previous investigation Torres et al. (2008) claimed no orbital period variations in CV Boo, because they analysed a lot of times of minima with low precision (photo plates and visual observations), but later more CCD observation were made. Their radial velocity studies could miss this companion because of the following reasons. The orbital velocity of the binary's center of masses around the triple's center of masses is $\approx 170 - 190$ km s^{-1} in the periastron, its radial projection is $\approx 130 - 140$ km s^{-1}. In the apastron it is $\approx 8 - 10$ km s^{-1}, its radial projection is $\approx 6 - 8$ km s^{-1}. These quantities are valid for parameters obtained using both our times of minima and times of minima from the literature. Velocities of the binary's components are close to 300 km s^{-1} and their radial projections can be much higher than the radial velocities caused by the influence of the third body. In addition, almost all radial velocity points were obtained in different orbital phases of the central binary. Since the candidate's orbit is highly elliptical, most of the time the orbital velocity of the binary should be much less

than during the periastron passage. The radial projection of the orbital velocity can be only less than the orbital velocity and in some positions within the orbit it can be almost zero. Only a few radial velocity measurements were made near the periastron passage of the suggested body, may be there are no such points, because the epoch of the passage was found with an uncertainty. If one takes into account parameters of the third body only from our observations, radial velocities are less than values above, therefore the third's companion influence could be missed even easier. It is essential to note that residuals of the radial velocity by Torres et al. (2008) in comparison to the model could be up to 16 km s^{-1}, see Table 3; potentially they could be attributed to the suggested influence of the tertiary companion, or to errors that exceed that influence. A new careful radial velocity investigation with a special attention to the periastron passages of the suggested candidate is very important to confirm/reject the existence of the body.

AB And. In October 2013 and August 2014 we observed 45 times of minima of AB And (Kozyreva et al., 2018b). Combining them with data from the literature we found and corrected errors in the treatment of old times of AB And minima made by Li et al. (2014). The correction helped us to arrange models concerning time variations of minima. We studied the secular evolution of the central binary's orbital period and also we found that the system possibly possesses two additional low mass stellar companions.

AR CrB. We collected times of minima from our observations of the system in 2013, 2014, 2016, 2017 (Kozyreva et al., 2018a). Combining them with times of minima from the literature we found that the orbital period of AR CrB could possess periodical variations that can be explained by the gravitational influence of a third companion in a highly eccentric orbit ($e \approx 0.7$) around the central binary. The period of mentioned variation is about 5000 days, it is comparable to the duration of all observations of AR CrB, so potentially there can not be a periodic variation, but a secular change of the orbital period. If our data are not included into consideration the orbital period can be accepted to be stable (Alton & Nelson, 2018) due to the lack of information about the system. Using their radial velocity estimates of the masses of the central binary components, the lower limit of the mass of the suggested third body can be estimated as $m_3 \sin i_3 = 0.07 M_\odot$. Future observations are required to clarify the character of the suggested variation of the orbital period of AR CrB.

3. Alternative explanations of variations of orbital periods in studied binaries

Photometric observations practically are able to find almost only candidates to additional bodies that should be confirmed or rejected using other methods, e.g. radial velocity studies. The O'Connell (1951) effect (whose nature has not been adequately studied yet) can complicate the precise determination of times

Table 2. Obtained results. "System" is the name of a target binary, "$m_{3,4} \cdot \sin i_{3,4}$" is the lower limit of a new companion's mass, "P" is the orbital period of a new companion, e is the eccentricity of its orbit.

System	$m_{3,4} \cdot \sin i_{3,4}$	P, days	e
V0873 Per (3rd)[a]	$0.2M_\odot$	297 ± 15	0-0.05
V0873 Per (4th)[b]	$0.06M_\odot$	1475 ± 113	0.19 ± 0.09
CV Boo[c]	0.4-0.5$M_\odot$	76.2 ± 1.5	0.90 ± 0.04
AB And (3rd)[d]	$0.1M_\odot$	21650 ± 100	0.87
AB And (4th)[e]	0.4-05$M_\odot$	38700 ± 1990	0.41
AR CrB[f]	$0.07M_\odot$	5360 ± 50	0.7

[a] Bogomazov et al. (2016a).
[b] Kriwattanawong & Poojon (2015).
[c] Bogomazov et al. (2016b).
[d] Kozyreva et al. (2018a).
[e] Kozyreva et al. (2018a).
[f] Kozyreva et al. (2018b).

of minima. Transits of planets, or partial eclipses by stars, can potentially be confused with each other and with star spots, binaries that possess one (or both) companions with high magnetic fields potentially can change their quadrupole gravitational momentum with time and, therefore, they are able to show quasi-periodic time variations (Applegate, 1992) that can look similar to the light time effect, and even a mass transfer between components can show quasi-periodical variations of the orbital period of the binary (Liu et al., 2018).

Remaining work over data obtained in our observations is under way, we are going to study the possible presence of additional bodies in all binaries from our target list. Our results can be used for subsequent observations using other methods, because in our photometric study we can find only candidates for such bodies, because mentioned processes can be confused with the gravitational influence of additional bodies.

References

Alton, K. B. & Nelson, R. H., CCD photometry, Roche modelling and period analysis of the W UMa eclipsing binary star system AR CrB. 2018, *Mon. Not. R. Astron. Soc.*, **479**, 3197, DOI: 10.1093/mnras/sty1693

Applegate, J. H., A mechanism for orbital period modulation in close binaries. 1992, *Astrophys. J.*, **385**, 621, DOI: 10.1086/170967

Beltraminelli, N., Dalmazio, D., Remis, J., & Manna, A., B and V Photoelectric Light Curves and First Ephemeris of NSV 11321, a New W UMa System. 1999, *Information Bulletin on Variable Stars*, **4696**

Bogomazov, A., Ibrahimov, M., Satovskii, B., et al., Timing of eclipsing binary V0873 Per: a third body candidate. 2016a, *Astrophys. Space Sci.*, **361**, 4, DOI: 10.1007/s10509-015-2591-1

Bogomazov, A., Kozyreva, V., Satovskii, B., et al., Light equation in eclipsing binary CV Boo: third body candidate in elliptical orbit. 2016b, *Astrophys. Space Sci.*, **361**, 390, DOI: 10.1007/s10509-016-2976-9

Holman, M. J. & Wiegert, P. A., Long-Term Stability of Planets in Binary Systems. 1999, *Astron. J.*, **117**, 621, DOI: 10.1086/300695

Kozyreva, V., Ibrahimov, M., Gaynullina, E., et al., Timing of AB And eclipses. 2018a, *New Astronomy*, **58**, 29, DOI: 10.1016/j.newast.2017.07.005

Kozyreva, V., Irsmambetova, T., Ibrahimov, M., et al., Timing of AR CrB eclipses. 2018b, *Information Bulletin on Variable Stars*, **6235**, DOI: 10.22444/IBVS.6235

Kriwattanawong, W. & Poojon, P., A photometric study of a weak-contact binary: V873 Per. 2015, *New Astronomy*, **36**, 50, DOI: 10.1016/j.newast.2014.10.004

Li, K., Hu, S.-M., Jiang, Y.-G., Chen, X., & Ren, D.-Y., Period variation and four color light curves investigation of AB And. 2014, *New Astronomy*, **30**, 64, DOI: 10.1016/j.newast.2014.01.004

Liu, L., Qian, S.-B., & Xiong, X., A new mechanism of long-term period variations for W UMa-type contact binaries. 2018, *Mon. Not. R. Astron. Soc.*, **474**, 5199, DOI: 10.1093/mnras/stx3138

O'Connell, D. J. K., The so-called periastron effect in close eclipsing binaries ; New variable stars (fifth list). 1951, *Publications of the Riverview College Observatory*, **2**, 85

Samus', N., Kazarovets, E., Durlevich, O., Kireeva, N., & Pastukhova, E., General catalogue of variable stars: Version GCVS 5.1. 2017, *Astronomy Reports*, **61**, 80, DOI: 10.1134/S1063772917010085

Shevchenko, I. I., Chaotic Zones around Gravitating Binaries. 2015, *Astrophys. J.*, **799**, 8, DOI: 10.1088/0004-637X/799/1/8

Torres, G., Vaz, L. P. R., & Sandberg Lacy, C. H., Absolute Properties of the Spotted Eclipsing Binary Star CV Boötis. 2008, *Astron. J.*, **136**, 2158, DOI: 10.1088/0004-6256/136/5/2158

Tutukov, A. & Bogomazov, A., The search for planets around eclipsing binary stars. 2012, *Astronomy Reports*, **56**, 775, DOI: 10.1134/S1063772912100071

Contrib. Astron. Obs. Skalnaté Pleso **49**, 390 – 392, (2019)

Eclipse timing variation of candidate long-period triple systems

A. Kurtenkov[1] **and V.A. Popov**[2,3]

[1] *Institute of Astronomy and NAO, Bulgarian Academy of Sciences, 72 Tsarigradsko Shose Blvd., 1784 Sofia, Bulgaria*
(E-mail: al.kurtenkov@gmail.com)

[2] *Department of Physics, Shumen University, 115 Universitetska Str., 9712 Shumen, Bulgaria*

[3] *IRIDA Observatory, Rozhen NAO, Bulgaria*

Received: November 1, 2018; Accepted: February 11, 2019

Abstract. The continuous photometric monitoring within the original Kepler mission allowed for the identification of a number of eclipsing binaries that display considerable eclipse timing variations (ETV). In their work on candidate triple systems in the Kepler field Conroy et al. (2014) drew a selection of 31 systems with ETV curves, whose shapes within the 1400-day monitoring period are seemingly parabolic. There are several possible explanations, including mass transfer, the Applegate effect, and a third component with a period considerably longer than 1400 days. We tried to determine the cause of the parabolic ETV curves by timing minima of 8 systems from this selection in 2017 and 2018, thus checking whether the ETV curves preserve their parabolic shapes or show signs of periodicity a further 1500 days after the original Kepler data. Results from the 30 cm IRIDA-South and the 50/70 cm Schmidt telescopes at the Rozhen observatory (Bulgaria) are presented.

Key words: eclipsing binaries – celestial mechanics

1. Introduction

Eclipse timing variation (ETV) of eclipsing binaries can be caused by a number of factors. Some of these physically change the orbital period of the binary (e.g. mass transfer or the Applegate effect), while others only shift the minima times by influencing the geometry of the system (e.g. a light travel time effect caused by a tertiary component or apsidal motion).

With its high photometric precision and a long time base, the Kepler mission (Borucki et al., 2010) gives an unprecedented opportunity to study ETV of eclipsing binaries. Conroy et al. (2014) investigated ETVs of over 1000 binaries while searching for third-body signals. Within this work they also selected 31 systems with seemingly parabolic ETV curves. The authors suggest mass transfer as a probable factor for these systems, because a constant change of the period over time would result in a parabolic ETV curve. However, long-period

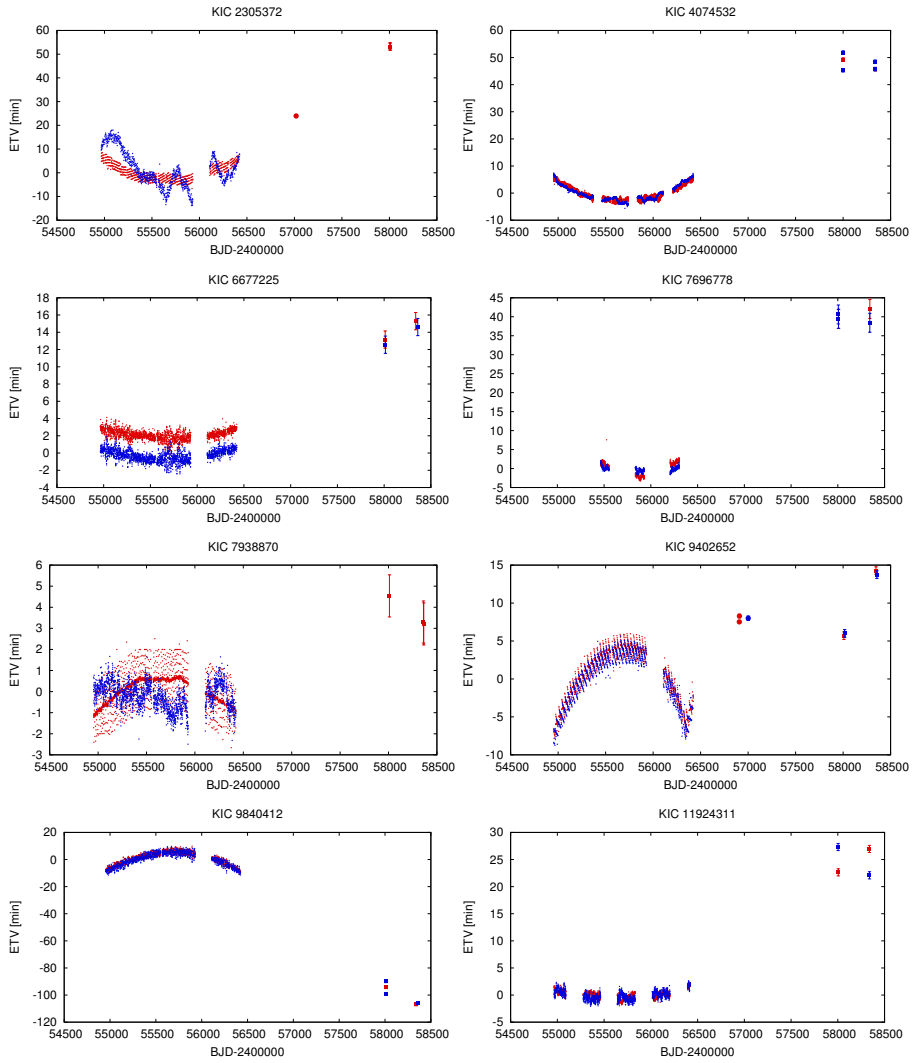

Figure 1. The obtained ETV values *(large squares)* plotted alongside the Kepler ETV data *(small circles)*. ETV values calculated from minima times obtained by Zasche et al. (2015) are included for KIC 2305372 and KIC 9402652 *(large circles)*. Primary and secondary minima are indicated in red and blue, respectively.

tertiary components would cause periodic ETV curves, parts of which may appear to have a parabolic shape. These tertiary components would have to orbit the binaries at periods much larger than the 1400-day base of the original Kepler mission. We selected 8 of these 31 systems and timed their minima in 2017 and 2018 in order to determine the actual reason for the ETV.

2. Observations and results

Time series observations of the selected eclipsing binaries were obtained in the Johnson V-band, covering a phase interval of ∼0.1 near each minimum. We used the 30 cm IRIDA-South telescope at Rozhen NAO in Bulgaria (f/5 with a focal reducer), equipped with an ATIK 4000M CCD camera (2048×2048 pixels, yielding a $35.5' \times 35.5'$ FOV) and the 50/70 cm Schmidt telescope at Rozhen NAO, equipped with a FLI PL 16803 CCD camera (4096×4096 px, yielding a $74' \times 74'$ FOV). Time resolution was a priority, therefore lower exposure times were preferable. The lightcurves around the minima were then fitted with 2^{nd} and 4^{th} degree polynomials to obtain the minima times. The calculated ETV values were plotted on the ETV curves (Fig.1) after applying the barycentric JD correction. The obtained minima times are to be presented in a separate paper.

In at least 6 of the 8 systems the ETV values 6 years after the Kepler mission do not lie on the extrapolated parabola. Instead, the sign of the second derivative of the ETV curve changes over the whole baseline, which indicates periodicity in the ETV signal. The test shows that in most cases the apparently parabolic ETV curve actually is a fragment of a periodic curve, probably due to the light-travel-time effect, caused by a long-period third component. Systems KIC 2305372 and KIC 9402652 were previously investigated by Zasche et al. (2015) and our results are in accordance with theirs.

Acknowledgements. This work was supported by grant DFNP-17-13 of the Young Scientists Support Program of the Bulgarian Academy of Sciences. Partial support under Bulgarian NSF contract DN 18/13 is acknowledged. Based on data obtained at the IRIDA Observatory, Bulgaria.

References

Borucki, W. J., Koch, D., Basri, G., et al., Kepler Planet-Detection Mission: Introduction and First Results. 2010, *Science*, **327**, 977, DOI: 10.1126/science.1185402

Conroy, K. E., Prša, A., Stassun, K. G., et al., Kepler Eclipsing Binary Stars. IV. Precise Eclipse Times for Close Binaries and Identification of Candidate Three-body Systems. 2014, *Astron. J.*, **147**, 45, DOI: 10.1088/0004-6256/147/2/45

Zasche, P., Wolf, M., Kučáková, H., et al., Ten Kepler Eclipsing Binaries Containing the Third Components. 2015, *Astron. J.*, **149**, 197, DOI: 10.1088/0004-6256/149/6/197

Contrib. Astron. Obs. Skalnaté Pleso **49**, 393 – 396, (2019)

Spectropolarimetry of the solar spicules using the 53-cm coronagraph of the Abastumani Astrophysical Observatory

T. Kvernadze[1], G. Kurkhuli[1], G. Kakauridze[2], B. Kilosanidze[2], V. Kulijanishvili[1] and E. Khutsishvili[1]

[1] *Abastumani Astrophysical Observatory, Ilia State University, Georgia*
[2] *Institute of Cybernetics, Georgian Technical University, Georgia*

Received: November 5, 2018; Accepted: March 7, 2019

Abstract. In this paper we present the test spectropolarimetric observations of the spicules in the Hα and He I D3 multiplet for different high chromospheric altitudes from 5000 km to 7000 km using the innovative Polarization-Holographic Imaging Stokes Polarimeter (PHISP) mounted on the 53-cm coronagraph of the Abastumani Astrophysical Observatory (Georgia). The laboratory tests and first spectropolarimetric observations show that the resulting uncertainties are estimated to be of the order of 10^{-3}.

Key words: Solar chromosphere – solar spicules – spectropolarimetry – polarization holography

1. Introduction

The solar spicules are thin and very dynamic needle-shaped plasma jet structures, best seen at the solar limb, whose magnetic properties are not well constrained to date. The magnetic field in spicules has been determined using direct analyses of spectral lines in polarized light, mostly using the He I spectral multiplets (Lopez Ariste and Casini, 2005; Trujillo Bueno et al., 2005; Centeno et al., 2010; Orozco Suarez et al., 2015; Ramelli et al., 2011). The polarization signals in these multiplets are generated by the joint action of the transversal Zeeman effect and scattering polarization modified by the Hanle effect.

Here we present the test spectropolarimetric observations of the spicules in the Hα and He I D3 multiplet for different chromospheric altitudes using the innovative Polarization-Holographic Imaging Stokes Polarimeter (PHISP) mounted on the 53-cm coronagraph of the Abastumani Astrophysical Observatory (Georgia), depicted in Figure 1.

Polarization-holography was first proposed by Kakichashvili (1972, 1974). This method was used to develop a unique polarization optical element providing instant and full analysis of the polarization state of an incoming light in the visual and near infrared spectral ranges (Kilosanidze & Kakauridze, 2007; Kilosanidze & Kakauridze, 2009; Kakauridze & Kilosanidze, 2011). The PHISP

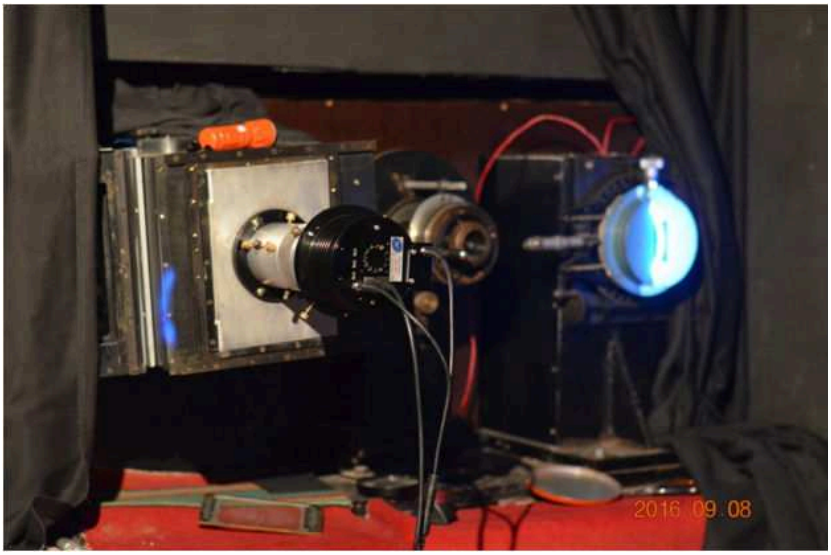

Figure 1. The PHISP mounted at the spectrograph of the 53-cm coronagraph of the Abastumani Astrophysical Observatory (Georgia).

is designed on the basis of such element being the only polarization optical part of the instrument (Kvernadze et al., 2016).

2. Method, design, calibration and test observations

The polarization-holographic element decomposes incident light into circular and linear diffraction orders. As a result we get two orthogonal circularly polarized beams with intensities I_{+c} and I_{-c}, two linearly polarized beams with intensities $I_{+1,45}$ and $I_{-1,45}$ and position angle $+45°$, two linearly polarized beams with intensities $I_{+1,90}$ and $I_{-1,90}$ and position angle $+90°$ and also none diffracted beam with a state of polarization identical to incoming beam and with intensity I_0.

The measurements of intensities of diffracted orders allow us to determine all four Stokes parameters through the following relations:

$$\begin{aligned} I_\lambda &= k_{+c,\lambda} I_{+c} + k_{-c,\lambda} I_{-c}, \\ Q_\lambda &= (k_{+c,\lambda} I_{+c} + k_{-c,\lambda} I_{-c}) - 2k_{90,\lambda} I_{90}, \\ U_\lambda &= 2k_{45,\lambda} I_{45} - (k_{+c,\lambda} I_{+c} + k_{-c,\lambda} I_{-c}), \\ V_\lambda &= k_{+c,\lambda} I_{+c} - k_{-c,\lambda} I_{-c}, \end{aligned} \tag{1}$$

where k terms are coefficients connected with absorption of light in an element, diffraction efficiency of an element and the optoelectronic transformations by

the photo-detectors. The values of these coefficients are determined experimentally during calibration. The principal scheme of PHISP and configuration of diffraction orders is shown in Figure 2 (Kvernadze et al., 2016).

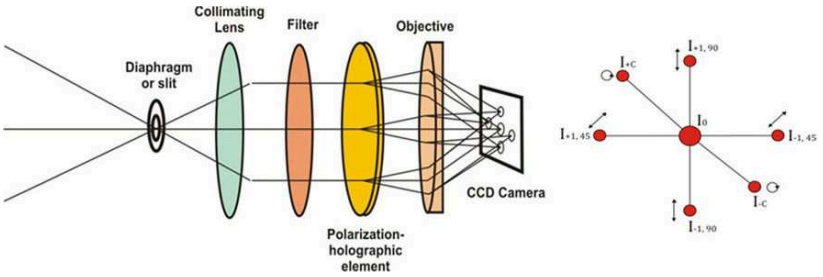

Figure 2. Principal scheme of PHISP and configuration of diffraction orders.

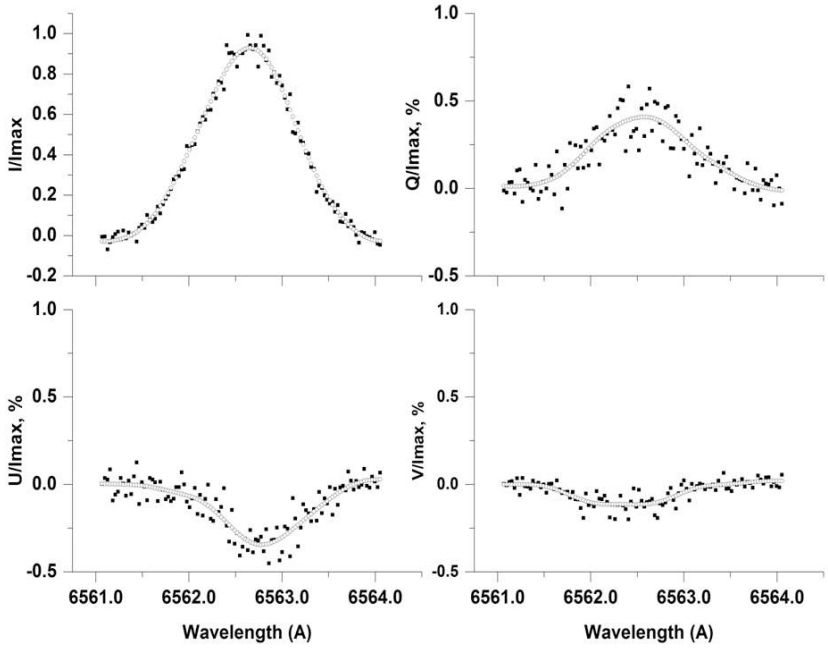

Figure 3. Observed Hα Stokes profiles normalized to Imax value.

For calibration purposes the special spectropolarimetric observations of the photosphere near the solar center were carried out in the Hα and D3 absorbtion lines immediately after the observations of the spicules with identical setup of the telescope and the polarimeter. The polarizer were placed in front of the spectrograph slit and rotated by 15° in the range of 0°-360° to obtain linear

polarization light beam with different phase angles. The spectral line minima were used to calculate the calibration parameters. The measured intensities and known values of the Stokes parameters of every position of the polarizer were used in the formulas above to calculate the calibration coefficients (Kilosanidze et al., 2015).

The intensity profiles of the spicules were transformed to the Stokes profiles using the calibration coefficients. The resulting normalized Stokes profiles are depicted below (Fig. 3). Also fitted curves are shown which are calculated using a spline smoothing algorithm. The residuals between measurements and fitted curves show that the uncertainties are of the order of 10^{-3}.

Acknowledgements. This work was supported by the grant # AR/209/6-120/14 of the Georgian National Science Foundation.

References

Centeno, R., Trujillo Bueno, J., and Asensio Ramos, A. 2010, ApJ, 708, 1579.

Kakichashvili, Sh. 1972, J. Opt. Spectrosc., 33, 324.

Kakichashvili, Sh. 1974, Sv. J. Q. El., 4, 795-798.

Kilosanidze, B. and Kakauridze, G. 2007, Appl. Opt. 46(7), 1040-1049.

Kilosanidze, B. and Kakauridze, G. 2009. Proc. SPIE, 7358.

Kakauridze, G. and Kilosanidze, B. 2011. Proc. SPIE, 7957, 7957-28.

Kilosanidze, B., Kakauridze, G., Kvernadze, T. & Kurkhuli, G. 2015, SPIE 9652.

Kvernadze, T., Kurkhuli, G., Kilosanidze, B., Kakauridze, G. et al. 2016, Solar Polarization Workshop 8, Firenze, Italy.

Lopez Ariste, A. and Casini, R. 2005, A and A, 436, 325.

Orozco Suarez, D., Asensio Ramos, A., Trujillo Bueno, J. 2015, The Astrophysical Journal Letters, Volume 803, Issue 2, L18, 5.

Ramelli, R., Trujillo Bueno, J., Bianda, M., Asensio Ramos, A. 2011, Solar Polarization Workshop 6, ASP Conference Series, Vol. 437, 109.

Trujillo Bueno, J., Merenda, L., Centeno, R., Collados, M. and Landi Degl Innocenti, E. 2005, ApJL, 619, L191.

Contrib. Astron. Obs. Skalnaté Pleso **49**, 397 – 399, (2019)

Variability analysis of δ Scuti candidate stars

E. Pakštienė[1], R. Janulis[1], A. Drazdauskas[1], L. Klebonas[1,2], Š. Mikolaitis[1], G. Tautvaišienė[1], R. Minkevičiūtė[1] and V. Bagdonas[1]

[1] *Astronomical Observatory, Institute of Theoretical Physics and Astronomy, Vilnius University, Saulėtekio av. 3, 10257 Vilnius, Lithuania (E-mail: erika.pakstiene@tfai.vu.lt)*

[2] *Mathematisch-Naturwissenschaftliche Fakultät, Universität Bonn, Wegelerstraße 10, 53115 Bonn, Germany*

Received: October 31, 2018; Accepted: February 15, 2019

Abstract. The Hipparcos catalogue contains stars suspected to be δ Scuti variables for which extensive groundbased observations and characterisation of variability are **desired**. We obtained 24 215 CCD images with the 35/51 cm Maksutov-type robotic telescope at the Molėtai Astronomical Observatory (MAO, Lithuania) of thirteen δ Scuti candidates selected from the Hipparcos catalogue in order to characterize their variability. We confirm that twelve of them are variables and pulsate with frequencies typical for δ Scuti-type stars. Five of them may be hybrid δ Scuti-γ Doradus pulsators. One more candidate is a variable star with longer periods of pulsations which are intrinsic to γ Doradus-type pulsators.

Key words: oscillations (including pulsations) – stars: variables: delta Scuti

1. Introduction

Though δ Scuti type stars belong to one of most numerous group of pulsators, much more observational information about this type of stars is necessary in order to improve their models and uncover details about processes happening beneath their surfaces. Therefore we selected 13 δ Scuti candidates from the Handler (2002) study suitable for observations with telescopes of the Molėtai Astronomical Observatory (MAO) in Lithuania.

2. Observations

Observations were performed with the 35/51 cm Maksutov-type MAO telescope and the Apogee Alta U47 CCD camera. We used the Y filter of the medium-band Vilnius photometric system. Its effective wavelength is at 466 nm and the width is 26 nm. The observations were carried out in a semi-robotic mode, i.e. the telescope was changing the pointing and took exposures of different fields of the sky according to the beforehand prepared script. This mode allowed us to observe light variations of stars in 5–7 different fields of the sky during the same night with a cadence of 15–30 minutes. We obtained 24 215 CCD images.

3. Data reduction and analysis

The observed images were first processed with the Muniwin program (Hroch 2014), which is built on the basis of a software package DAOPHOT for doing stellar photometry in crowded stellar fields (Stetson 1987). The LCs were analysed using a process of their Fourier decomposition into sinusoidal components (Fourier 1822). We used a software Period04 (Lenz & Breger 2005) for decomposition of LCs, obtaining amplitude spectra and for prewhitening procedures in order to find all frequencies, amplitudes and phases of pulsations in light curves, spectral windows (SW) and a noise level. As single-site observations were used for analysis, SWs have high side-lobes of 1 c/d aliases. The length of the LCs also differs, thus the FWHM of the central peak in SWs vary between 0.0374 c/d (HIP 106223) and 0.1558 c/d (HIP 11090). The worst SW was obtained for HIP 74155, since it had the smallest set of data points and big (2–5 days) gaps between runs.

First of all we calculated an amplitude spectrum with Period04 and identified the highest amplitude peak at frequencies higher than 2 c/d assuming that the low frequencies may be caused by instrumental or weather instabilities. After that we calculated a sinusoid with the identified frequency and used a least square fitting method improving the amplitude and phase, simultaneously. Then we checked a significance of the extracted frequency by comparing an amplitude of the signal with the mean amplitude of residual in a box ± 10 c/d around the extracted frequency, i.e., we calculated a signal-to-noise ratio (S/N) at the extracted frequency. The signal was assumed as significant if its S/N$\geq$4, according to Breger et al. (1993).

4. Results

In Table 1 we listed the extracted frequencies according to their extraction succession. Considering the amplitude spectra of pulsations we confirm that twelve of investigated stars are variables and pulsate with frequencies typical for δ Scuti type stars. Moreover, five of them (HIP 2923, HIP 5526, HIP 11090, HIP 115856, and HIP 106219) may be hybrid δ Scuti-γ Doradus pulsators, as they simultaneously show high-frequency pulsations typical for the δ Scuti stars and significant low-frequency oscillations (between 0.5422 c/d and 1.3778 c/d) characteristic for the γ Doradus stars. Yet, the firm detection of low frequencies needs more observational data. One more star, HIP 106223, pulsates just with low frequencies typical for variables of γ Doradus type stars. Positions of these stars in the $\log L/L_{\odot}$ versus $\log T_{\rm eff}$ diagram (the values were taken from the *Gaia* DR2) confirm our conclusions. A more detailed description of the analysis was published in Pakštienė et al. (2018).

Table 1. Observed signals in amplitude spectra.

Freq. c/d	Ampl. mmag	Phase	Noise mmag	S/N	Freq. c/d	Ampl. mmag	Phase	Noise mmag	S/N
		HIP 2923					HIP 74155		
15.0271	8.41	0.764	1.45	5.81	11.7619	14.15	0.847	2.99	4.73
16.0973	7.28	0.277	1.25	5.84			HIP 101473		
11.7260	6.24	0.987	1.26	4.94	6.0374	7.24	0.997	1.79	4.04
6.7078	6.02	0.845	1.40	4.30	4.3081	5.64	0.038	1.34	4.20
11.4043	4.71	0.262	1.09	4.32			HIP 106219		
		HIP 5526			11.3007	6.66	0.113	0.74	8.95
9.3431	24.19	0.806	4.77	5.07	10.8018	2.91	0.042	0.69	4.19
5.1385	20.46	0.557	4.23	4.84	14.2773	2.45	0.210	0.52	4.74
8.5147	17.92	0.788	3.26	5.50			HIP 106223		
9.7283	13.21	0.291	2.70	4.89	1.1429	31.09	0.194	2.84	10.95
5.5947	12.46	0.849	2.58	4.82			HIP 107786		
12.5515	8.22	0.255	1.86	4.41	15.4817	9.87	0.932	2.08	4.75
		HIP 5659					HIP 113487		
9.4932	16.45	0.049	2.90	5.67	21.9102	23.01	0.327	3.73	6.16
10.2439	11.49	0.629	2.45	4.69	17.2064	11.40	0.012	2.82	4.04
9.8508	12.46	0.674	1.98	6.30			HIP 115093		
7.0028	8.95	0.814	1.82	4.92	11.4318	10.61	0.784	2.18	4.87
		HIP 11090					HIP 115856		
15.8617	11.30	0.387	1.63	6.94	9.1109	14.08	0.917	1.75	8.06
28.7418	5.34	0.453	1.19	4.47	16.9660	7.48	0.068	1.28	5.86
		HIP 17585			18.6810	5.81	0.676	1.11	5.24
13.1631	13.99	0.887	3.33	4.20					

Acknowledgements. This research has made use of the SIMBAD database and NASA's Astrophysics Data System (operated at CDS, Strasbourg, France), and was funded by the grant from the Research Council of Lithuania (LAT-08/2016).

References

Breger, M., Stich, J., Garrido, R., et al., Nonradial Pulsation of the Delta-Scuti Star Bu-Cancri in the Praesepe Cluster. 1993, *Astron. Astrophys.*, **271**, 482

Fourier, J. J. 1822, Théorie analytique de la chaleur (in French), Paris: Firmin Didot, Pére et fils, OCLC 2688081

Hroch, F. 2014, Munipack: General astronomical image processing software, Astrophysics Source Code Library

Lenz, P. & Breger, M., Period04 User Guide. 2005, *Communications in Asteroseismology*, **146**, 53, DOI: 10.1553/cia146s53

Pakštienė, E., Janulis, R., Tautvaišienė, G., et al., Variability Analysis of δ Scuti Candidate Stars. 2018, *Publ. Astron. Soc. Pac.*, **130**, 084201, DOI: 10.1088/1538-3873/aac5cf

Stetson, P. B., DAOPHOT - A computer program for crowded-field stellar photometry. 1987, *Publ. Astron. Soc. Pac.*, **99**, 191, DOI: 10.1086/131977

Contrib. Astron. Obs. Skalnaté Pleso **49**, 400 – 405, (2019)

Search for new variable stars in the northern sky

E. Pakštienė[1], R. Janulis[1], A. Drazdauskas[1], L. Klebonas[1,2], Š. Mikolaitis[1], G. Tautvaišienė[1], R. Minkevičiūtė[1] and V. Bagdonas[1]

[1] *Astronomical Observatory, Institute of Theoretical Physics and Astronomy, Vilnius University, Saulėtekio av. 3, 10257 Vilnius, Lithuania (E-mail: erika.pakstiene@tfai.vu.lt)*

[2] *Mathematisch-Naturwissenschaftliche Fakultät, Universität Bonn, Wegelerstraße 10, 53115 Bonn, Germany*

Received: October 31, 2018; Accepted: February 15, 2018

Abstract. With the aim to find and characterize new variable stars, we obtained 24 470 CCD images in 13 fields of 0.4 square degrees with a 35/51 cm Maksutov-type semi-robotic telescope at the Molėtai Astronomical Observatory of Vilnius University. From photometric time series of 3604 stars analysed, we found 11 periodic variable stars and 70 slowly varying stars with so far undefined periodicity.

Key words: Methods: data analysis – Catalogs – stars: oscillations

1. Introduction

In order to prepare optimal input catalogues for space missions, extensive ground-based observations and characterisation of possible target objects are necessary. With the aim to search for new variable stars in selected fields of the northern sky which will be observed by the NASA TESS and ESA PLATO space missions, in 2016 we started a spectroscopic and photometric survey (SPFOT, Mikolaitis et al. 2018) and present here some of our results.

2. Observations and method of analysis

Observations were performed at the Molėtai Astronomical Observatory (MAO, Lithuania) with a 35/51 cm Maksutov-type telescope and the Apogee Alta U47 CCD camera. A field of view of this instrument is 0.39 deg^2. We observed 13 fields with several different exposure times (short exposures for the variability analysis of brighter stars and the longer ones in order to analyse fainter objects). The observational data were collected in a period between JD 2457597.4 and JD 2457649.4. The shortest and longest light curves were 18 and 52 days, respectively. A majority of the light curves had about 30 days. The observations and methodology of data reduction are described in more details by Pakštienė et al. (2018), Pakštienė et al. (2019).

The observed images were processed and light curves of 3598 stars till about *Gaia G* 15 mag were derived with a *Muniwin* program (also known as *C* –

Munipack project), which originated from the *Munipack* package (Hroch 2014). More information about the software may be found on its website (*http://c-munipack.sourceforge.net/*). The most common value of the mean error ($\mathrm{ERR_{mean}}$) of every observed point and the most common value of the standard deviation ($\mathrm{STD_{LC}}$) of the observed light curves were obtained in a range of 0.05–0.1 mag and 0.075–0.125 mag, respectively. Both $\mathrm{ERR_{mean}}$ and STD served as indicators of observation quality for non-variable stars, but a large STD also indicated a possible stellar variability. At the same time all LCs were inspected for variability visually to reveal stars with large amplitudes of variability. For searching of smaller amplitude periodic variations we applied the mathematical tools such as the Fourier transform (FT) (Fourier 1822) and the Lomb-Scargle (LS) periodogram (Lomb 1976; Scargle 1982). We assumed that a star may be variable when a power of signal in the Lomb-Scargle periodogram exceeds a calculated detection limit for a case when false alarm probability (FAP) is 1/100. Then we applied Fourier decomposition method using the Period04 program (Lenz & Breger 2005) for a more detailed analysis of possible periodic variables.

A method of trending parameter (TR) was used for searching of long periodic variable star candidates or irregular variables. Such stars show slow changes of magnitude or their LCs have a one way trend. In the case of such variable stars we derived different magnitudes at different times. Since quality of the data was different for individual stars we reduced the reliability of magnitude differences by errors of observations, i.e. by $\mathrm{STD_{LC}}$ and $\mathrm{ERR_{mean}}$. Therefore, we calculated an observed trending parameter ($\mathrm{TR_O}$) using the following equation:

$$\mathrm{TR_O} = \frac{\mathrm{mag_{max}} - \mathrm{mag_{min}}}{\mathrm{STD_{LC}} \cdot \mathrm{ERR_{mean}}},$$

where $\mathrm{mag_{max}}$ and $\mathrm{mag_{min}}$ are differential magnitudes determined at phases when a star was faintest and brightest, respectively.

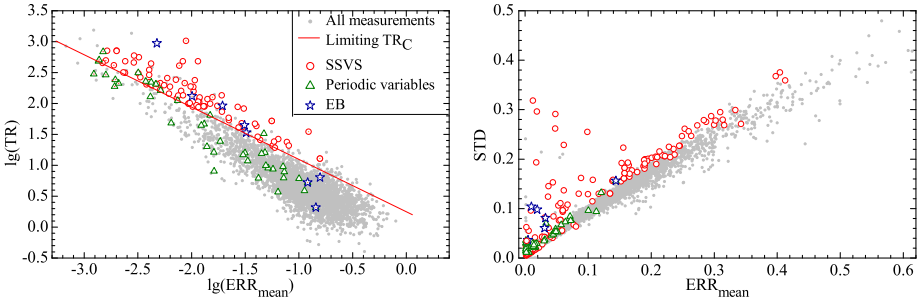

Figure 1. Dependencies of TR and STD parameters on the $\mathrm{ERR_{mean}}$. See the text for more explanations.

The left panel of Fig. 1 shows a dependence of the TR_O parameter on the ERR_{mean} for our observed data set in a logarithmic scale. The red line corresponds to the calculated limit of trending parameter (TR_C) for possibly slowly varying stars, which should appear above that line. A majority of the points in Fig. 1 lay below the limiting TR_C parameter, however some stars have $TR_O > TR_C$ parameters than others with the same ERR_{mean}. Those lifted stars may have trending or slowly varying LCs. In order to recognize potential variable stars we computed a difference between observed $\log(TR_O)$ and calculated $\log(TR_C)$ at a certain ERR_{mean}: $\log(TR_{O/C}) = \log(TR_O) - \log(TR_C)$.

A larger value of $\log(TR_{O/C})$ gives a higher probability that a star is variable. The right panel of Fig. 1 shows a dependence of STD_{LC} on ERR_{mean} (STD(ERR)). Every star which appears above the densest part of STD(ERR) or STD(MAG) dependencies may be variable.

From the right panel of Fig. 1 we can see that such diagrams are sensitive to high amplitude variations (e.g. typical to eclipsing binary stars or δ Cep type stars). We also find there other stars with larger STD than normal, but they do not show any long or short periodic variability. Often those stars have a close neighbour on the sky.

3. New variable stars

Using the described methods we found 81 new candidates of variable stars. 11 of them were found using more than one method. They were analysed in more detail and the results are going to be published in a forthcoming paper (Pakštienė et al. 2019) which is in preparation. The remaining 70 stars were identified as possible variable stars with slow changes in brightness or with irregular variability which cannot be analysed using their amplitude spectra yet. They were selected using the method of trending parameters. The stars with the positive values of $\log(TR_{O/C})$ were attributed to a group of suspected slowly variable stars (SSVS). These stars are shown in Fig. 1 as the red circles lying above the calculated theoretical limit of the trending parameter (the red line in Fig. 1). A list of SSVS with their *Gaia G* magnitudes and *Gaia* coordinates taken from *Gaia* DR2 (Gaia Collaboration et al. 2016, Andrae et al. 2018, Gaia Collaboration et al. 2018) is presented in Table 1. We also picked up luminosities and effective temperatures from the Gaia DR2 catalogue where they were determined from parallaxes and three broad-band photometric measurements (Gaia Collaboration et al. 2016, Andrae et al. 2018, Gaia Collaboration et al. 2018), and compared these values with the Padova stellar evolutionary tracks with different masses (*http://pleiadi.pd.astro.it/*). This way we estimated approximate types of the stars and present them in the last column of Table 1. Some stars were unclassified since their luminosities were not present in the Gaia DR2 catalogue. A majority of the stars have masses smaller than 2.5 $M_\odot$, except for two red giant branch stars (524845214033292800 and 525091745154747904), which

Table 1. A list of suspected slowly variable stars.

Gaia ID	*Gaia G*, [mag]	RAJ2000	DEJ2000	Type[1]
525000859345992960	11.1388	18.0104986371	64.9650940284	MS
524998561542119296	11.1148	18.2651249861	64.9818074356	–
525107310116118528	10.2701	18.3510046419	65.3658881455	RG
525134866626773120	9.2636	18.4228266234	65.6166143921	SG
525091745154747904	11.2388	18.5474162089	64.9931044943	RG
524809995303314176	10.7714	18.5798221174	64.9279842501	MS/SG
525141772934253440	8.227	18.6043442775	65.7375027813	RG
525101434600987136	9.231	18.6061094894	65.2666027345	RG
525104389538474624	9.9243	18.6398231349	65.3681037685	RG
524904347144651392	10.8524	18.6742139351	65.0115400097	MS
524903071529044480	12.111	18.7722224484	64.9207124999	SG/RG
524938466365442688	8.8105	19.0149649408	65.3089116997	RG
524950664072456192	9.6144	19.0787520855	65.6565664824	RG
524888507305367552	10.6168	19.1267052896	64.8583234924	MS
524910699393690112	10.4527	19.1668881276	65.1461946054	MS/SG
524791303605806208	12.5398	19.2301447391	64.6828686697	SG
524933793441182080	11.764	19.3408466046	65.1944293021	MS
524894176662153216	9.8406	19.3586934038	64.9326999485	MS/SG
524935683226651520	11.056	19.3726466587	65.2851335846	–
524887613952295424	11.5937	19.3911079915	64.8214608609	SG/RG
524897127297039104	11.8808	19.3972701036	65.0403010267	MS
524923451159818240	9.5236	19.5136935576	65.2096488369	–
524893558187004032	11.4837	19.6315309338	65.0217548205	–
524929906487427712	10.3878	19.6892888954	65.362794943	MS/SG
524929051797262208	12.3722	19.7226064568	65.2726434851	MS
524925886398044288	12.374	19.7653883266	65.2333253279	SG/RG
524916093872620160	12.2165	19.8082810858	65.01069596	MS
524841262663818112	9.2175	19.8592736896	64.7205464169	MS/SG
524845214033292800	11.5191	19.8686201483	64.9262839528	RG
524924546368250624	11.7148	19.973093738	65.17397557	SG
524843324247702528	13.8064	20.0108416357	64.8297480449	–
524840128792064128	9.9412	20.0737982867	64.7619369824	MS/SG
524838548238275840	10.9242	20.0867153652	64.7241493734	SG
524879745571182848	12.8106	20.1083943669	65.2381994037	SG
524864283689156864	11.6354	20.1717913294	64.8518494965	SG
524869502067395584	12.1572	20.1933373926	64.9716598875	RG
524863974451536256	9.2463	20.2396816824	64.8181902335	RG
524880054808824064	11.1258	20.253494167	65.2663650418	RG
524866620151264256	11.6951	20.2614831216	64.9732018464	SG
524866620151263616	14.195	20.2700508062	64.9739792466	SG
524876859353184896	11.5323	20.2917155956	65.1443171012	MS
339010221170297472	14.0669	35.3336181038	41.2208428331	MS
338956074518570368	9.0222	35.3557119786	41.0924924935	MS
338965557806325632	9.3653	35.4621374032	41.327516872	MS
338963668020721536	9.6547	35.4624127663	41.2628849615	RG
1694320377289305600	12.3535	226.978800471	69.9148327953	SG
1694356871626759680	10.5961	227.930460635	69.6908196763	MS/SG
1694369756528664192	10.2955	228.029397185	69.9367877523	MS
1694358658333159296	12.9441	228.110310003	69.7548509882	MS
1752703796186541696	13.4423	308.416400591	9.7394910823	MS
1752936445975336704	8.4602	308.509720864	10.2531709392	RG
1752933765915721600	7.4819	308.583145863	10.2681214277	RG
1798520785015411840	9.9592	322.35426006	25.0236963089	RG
1798520892390900096	11.2096	322.368208015	25.047902805	MS
1784031180267825024	12.0245	322.444538562	16.2766138823	SG/RG
1798286829556897664	10.6325	322.447691171	24.6026164616	MS/SG
1798286902572778880	10.4316	322.485531726	24.6057297405	RG
1798287521048300672	10.4966	322.514082756	24.6546389142	RG
1772025406644569600	8.7811	322.759697159	16.3007606979	RG
1798232781688454272	13.3126	322.791905621	24.4678215496	SG/RG
1915157669982159744	12.8614	344.508903545	34.3592328576	SG
1914407837411240832	10.8739	344.694745194	34.3730383476	MS
1913321760441573248	9.5265	349.365342282	36.1495604234	MS/SG
1913310937123996928	8.7682	349.389579137	36.0055655426	RG
1913296437314414208	9.8338	349.405599182	35.9047151378	RG
1913291901828961024	11.6621	349.478195832	35.7936387363	MS
1913301415179710336	10.0586	349.629225625	35.9813449457	MS
1913404086374653184	9.1121	349.848263381	36.3364204108	RG
1913347319790018816	9.2237	350.002915174	36.0433222975	MS
2824707704618848896	12.0161	352.321691849	19.5538765948	SG

[1] MS - main sequance stars; SG - subgiant branch stars; RG - red giant branch stars.

may be more massive. Periodicity of these stars is undefined yet and they require further long term photometric and spectrometric observations in order to analyse their variability.

4. Conclusions

We used several methods for searching of variable stars, i.e. we used the Fourier transform spectra, Lomb-Scargle periodograms, dependencies of trending parameters and standard deviations of LCs on measurement errors. Using the described methods we analysed light curves of 3598 stars and found 81 new variable stars, 70 of them were found using a method of trending parameters and attributed to suspected slowly varying stars. We have shown that the method of trending parameters may be productive in searching of stellar variability in relatively short light curves, when amplitude spectra, such as Fourier Transform spectra or Lomb-Scargle periodograms, are not effective. We recommend to observe the newly discovered slowly varying stars presented in this contribution and also to check effectiveness of the proposed method of trending parameters.

Acknowledgements. This research has made use of the SIMBAD database and NASA's Astrophysics Data System (operated at CDS, Strasbourg, France), and was funded by a grant from the Research Council of Lithuania (LAT-08/2016).

References

Andrae, R., Fouesneau, M., Creevey, O., et al., Gaia Data Release 2. First stellar parameters from Apsis. 2018, *Astron. Astrophys.*, **616**, A8, DOI: 10.1051/0004-6361/201732516

Fourier, J. J. 1822, Théorie analytique de la chaleur (in French), Paris: Firmin Didot, Pére et fils, OCLC 2688081

Gaia Collaboration, Brown, A. G. A., Vallenari, A., et al., Gaia Data Release 2. Summary of the contents and survey properties. 2018, *Astron. Astrophys.*, **616**, A1, DOI: 10.1051/0004-6361/201833051

Gaia Collaboration, Prusti, T., de Bruijne, J. H. J., et al., The Gaia mission. 2016, *Astron. Astrophys.*, **595**, A1, DOI: 10.1051/0004-6361/201629272

Hroch, F. 2014, Munipack: General astronomical image processing software, Astrophysics Source Code Library

Lenz, P. & Breger, M., Period04 User Guide. 2005, *Communications in Asteroseismology*, **146**, 53, DOI: 10.1553/cia146s53

Lomb, N. R., Least-squares frequency analysis of unequally spaced data. 1976, *Astrophys. Space Sci.*, **39**, 447, DOI: 10.1007/BF00648343

Mikolaitis, Š., Tautvaišienė, G., Drazdauskas, A., et al., Spectroscopy of Dwarf Stars Around the North Celestial Pole. 2018, *Publ. Astron. Soc. Pac.*, **130**, 074202, DOI: 10.1088/1538-3873/aabfb6

Pakštienė, E., Janulis, R., Drazdauskas, A., et al., Search for variable stars in the northern sky:Analysis of photometric time series for 3598 stars. 2019, *arXiv e-prints* [[arXiv]1902.06357]

Pakštienė, E., Janulis, R., Tautvaišienė, G., et al., Variability Analysis of δ Scuti Candidate Stars. 2018, *Publ. Astron. Soc. Pac.*, **130**, 084201, DOI: 10.1088/1538-3873/aac5cf

Scargle, J. D., Studies in astronomical time series analysis. II - Statistical aspects of spectral analysis of unevenly spaced data. 1982, *Astrophys. J.*, **263**, 835, DOI: 10.1086/160554

Contrib. Astron. Obs. Skalnaté Pleso **49**, 406 – 410, (2019)

H_α orbital variations of the symbiotic star EG And from optical spectroscopy

N. Shagatova[1], A. Skopal[1], M. Sekeráš[1], F. Teyssier[2], S.Yu. Shugarov[1,3], R. Komžík[1], Z. Garai[1], E. Kundra[1] and M. Vaňko[1]

[1] *Astronomical Institute of the Slovak Academy of Sciences 059 60 Tatranská Lomnica, The Slovak Republic, (E-mail: nshagatova@ta3.sk)*

[2] *67 rue Jacques Daviel, 76100 Rouen, France*

[3] *P.K. Sternberg Astronomical Institute, M.V. Lomonosov Moscow State University, Russia*

Received: October 31, 2018; Accepted: March 18, 2019

Abstract. In this contribution, we explore the orbital variability of the Hα-line emission and absorption components of the symbiotic system EG And.

We have found that the equivalent width of the core emission is the largest at the orbital phase $\varphi \approx 0.4$ and the smallest at $\varphi \approx 0.2$. This probably reflects an asymmetric distribution of the cool giant wind at the orbital-plane area. Furthermore, the core emission equivalent width has a secondary maximum at $\varphi \approx 0.1$. The strongest absorption in the profile is measured around the inferior conjunction of the white dwarf, $\varphi \approx 0.4$. This suggests that the ionized region is partially optically thick in the Hα line.

Key words: symbiotic binary stars – stellar spectral lines – stellar mass loss

1. Introduction

EG And is an eclipsing symbiotic star with no recorded outbursts (Stencel, 1984; Crowley et al., 2008). The binary system consists of a white dwarf accretor that ionizes a fraction of the neutral wind from a red giant donor. The presence of the ionized and neutral region in the binary star and its high orbital inclination of $\approx 80^\circ$ (Vogel et al., 1992) causes the observed orbitally-related variations in the Hα line profile (e.g. Smith, 1980). To identify the physical properties of the ionized region, we used the advantage of the long-term monitoring of this source with the orbital period of 483 days (Kenyon & Garcia, 2016) by small optical telescopes.

2. H_α orbital variability

We use 90 optical spectra obtained during years 2015 - 2018 by 60 cm and 1.3 m telescopes at the Stará Lesná (G1 in the figures) and Skalnaté Pleso (SP) observatories, complemented with those available at the Astronomical Ring for Access

to Spectroscopy Data Base (*www.astrosurf.com/aras/Aras_DataBase/Symbiotics.htm*) to fit the Hα line profile by three Gaussian functions corresponding to the core emission, broad wings emission and the central absorption. The resulting fits do not perfectly match the observed Hα line profile (Fig. 1). The most important source of errors of equivalent widths are the errors of the heights of the Gaussian components that are typically higher than 10%. This is caused mainly by the fact that we did not allow the height of the core emission component to vary freely, otherwise the fitting procedure would converge to unrealistically high values. Therefore, our equivalent widths' values can be considered as lower estimates.

The resulting equivalent widths of the core emission and absorption are plotted in Fig. 2. Both quantities are strongest at $\varphi \approx 0.4$ and weakest at $\varphi \approx 0.2$, reflecting the asymmetry of the circumstellar matter density distribution with respect to the binary star axis. Another interesting feature is the secondary maximum of the core emission equivalent width at $\varphi \approx 0.1$. Its existence probably reflect a complex wind flow, as suggested by hydrodynamical simulations of symbiotic stars (e.g. Walder & Folini, 2000). Moreover, solely the fact that we see an emission in the Hα line at orbital phases near the eclipse of the white dwarf by the red giant means that the size of the ionized region exceeds the size of the giant star, as was also found in the study of Kondratyeva et al. (2018).

The maximum of both emission and absorption component at $\varphi \approx 0.4$ reflects a higher density region on the line of sight. This causes a higher emissivity and also absorbing ability, because of shortening the recombination time in the ionized medium. In other words, the fraction of the H^0 atoms in the H^+ zone increases, which makes this part of the nebula partially optically thick in the Hα transition. A similar interpretation was given by Blanco & Mammano (1995) to explain the HeI 587.6 nm orbital variability of EG And. From the presence of the emission component during the inferior conjuction of the giant, they infer that the nebula has to be larger than the obscuring region. At the same time, the absorption component becomes invisible, indicating that the densest part of the nebula, where the absorption occurs, is occulted by the red giant.

Our dataset covers almost two orbital cycles of the system. However, measured equivalent widths from the two different orbital cycles overlap only between the orbital phase 0.6 and 0.8. Outside this range, the data from different cycles are rather complementary. The agreement between the comparable parts of the dataset supports the orbitally-related properties of the Hα line profile.

3. Conclusion

By quantifying the orbital variability of the emission and absorption components of the Hα line separately, we identified several properties of the nebula in EG And. The changes of the absorption component revealed that the ionized

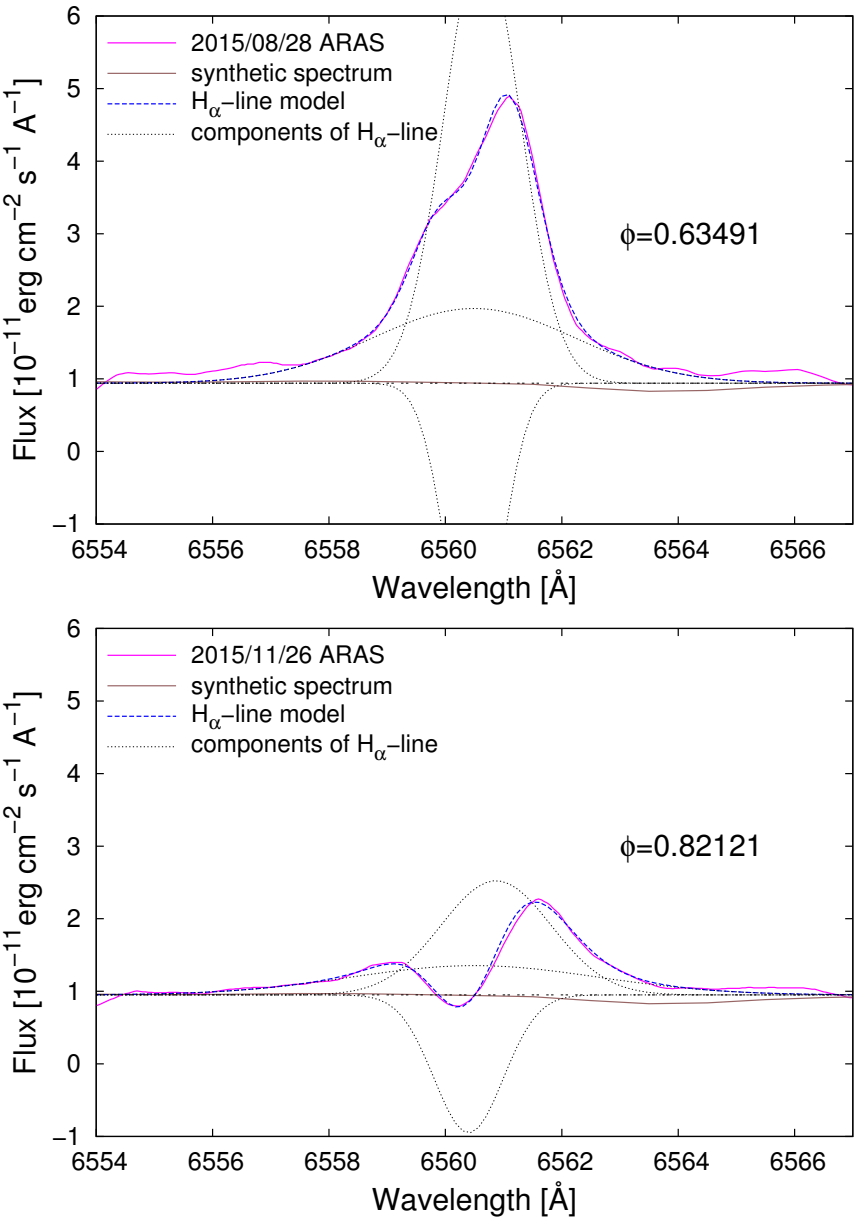

Figure 1. An example of the fit of the Hα line profile by three Gaussian components relatively far from the eclipse (top) and near the eclipse (bottom) of the white dwarf.

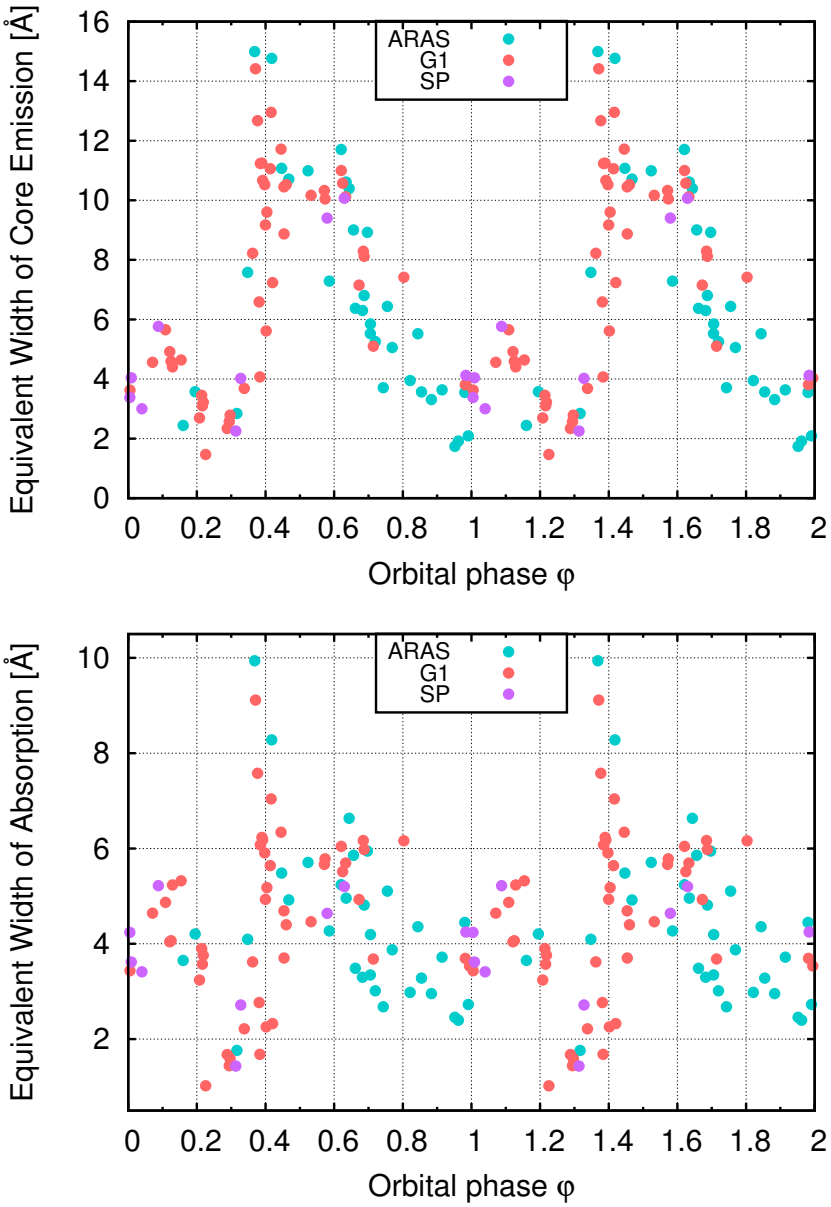

Figure 2. The orbital variabity of equivalent widths of the core emission (top) and absorption (bottom) components of the Hα line profile. We used the time of inferior conjunction of the red giant $MJD = 50683.2$ ($\varphi = 0$) according to Fekel et al. (2000).

region is partially optically thick in the Hα line, while the emission component presence during eclipse shows that the nebula is larger in size than the red giant.

Acknowledgements. This research was supported by a grant of the Slovak Academy of Sciences, VEGA No. 2/0008/17, and the Slovak Research and Development Agency under the contract No. APVV-15-0458.

References

Blanco, C. & Mammano, A., A giant's envelope in the eclipsing symbiotic EG Andromedae. 1995, *Astron. Astrophys.*, **295**, 161

Crowley, C., Espey, B. R., & McCandliss, S. R., EG And: Far Ultraviolet Spectroscopic Explorer and Hubble Space Telescope STIS Monitoring of an Eclipsing Symbiotic Binary. 2008, *Astrophys. J.*, **675**, 711, DOI: 10.1086/524127

Fekel, F. C., Joyce, R. R., Hinkle, K. H., & Skrutskie, M. F., Infrared Spectroscopy of Symbiotic Stars. I. Orbits for Well-Known S-Type Systems. 2000, *Astron. J.*, **119**, 1375, DOI: 10.1086/301260

Kenyon, S. J. & Garcia, M. R., EG Andromedae: A New Orbit and Additional Evidence for a Photoionized Wind. 2016, *Astron. J.*, **152**, 1, DOI: 10.3847/0004-6256/152/1/1

Kondratyeva, I. N., Rspaev, F. K., Reva, I. V., & Krugov, M. A., Photometric and Spectral Studies of the Object EG And. 2018, *Astrophysics*, **61**, 310, DOI: 10.1007/s10511-018-9538-5

Smith, S. E., The symbiotic star HD 4174. 1980, *Astrophys. J.*, **237**, 831, DOI: 10.1086/157930

Stencel, R. E., Changes in the ultraviolet spectrum of EG Andromedae. 1984, *Astrophys. J., Lett.*, **281**, L75, DOI: 10.1086/184289

Vogel, M., Nussbaumer, H., & Monier, R., Absolute radius of an M giant. 1992, *Astron. Astrophys.*, **260**, 156

Walder, R. & Folini, D., Complex Wind Dynamics and Ionization Structure in Symbiotic Binaries. 2000, in Astronomical Society of the Pacific Conference Series, Vol. **204**, *Thermal and Ionization Aspects of Flows from Hot Stars*, ed. H. Lamers & A. Sapar, 331

Contrib. Astron. Obs. Skalnaté Pleso **49**, 411 – 414, (2019)

Mass-outflow from the active symbiotic binary BF Cyg during its 2015 and 2017 bursts

A. Shchurova[1], A. Skopal[1], S.Yu. Shugarov[1,2], M. Sekeráš[1], R. Komžík[1], E. Kundra[1] and N. Shagatova[1]

[1] *Astronomical Institute of the Slovak Academy of Sciences 059 60 Tatranská Lomnica, The Slovak Republic, (E-mail: ashchurova@ta3.sk)*

[2] *P.K. Sternberg Astronomical Institute, M.V. Lomonosov Moscow State University, Russia*

Received: November 13, 2018; Accepted: March 29, 2019

Abstract. In this contribution we present observations of the symbiotic star BF Cygni during its current active phase. Our photometric monitoring indicated 1-mag bursts during 2015 and 2017 on the time-scale of weeks with gradual fading to the pre-outburst level for more than 1 year. During these events, our spectra show signatures of a variable mass-outflow and formation of a highly-collimated bipolar mass ejection.

Key words: stars: binaries: symbiotic – individual: BF Cygni

1. Introduction

Symbiotic stars are the widest interacting binaries with orbital periods of, typically, a few years. They consist of a red giant and a white dwarf (WD) accreting from the giant's wind. According to behaviour of their long-term optical light curves we distinguish between the so-called quiescent and active phases. The latter are characterized by a few magnitudes brightening with signatures of a mass-outflow on the time-scale from months to years (Kenyon, 1986).

BF Cygni is an eclipsing symbiotic binary with the orbital period of ∼757 days, consisting of a hot WD accreting from the wind of an M5III giant companion. A historical light curve shows three types of eruptions: a slow symbiotic nova outburst (in 1895), Z And-type outbursts (in 1920, 1989) and short-term orbitally-dependent flares (e.g. Skopal et al., 1997, and references therein).

2. Observations

Our observations were carried out at the Stará Lesná observatory of the Astronomical Institute of the Slovak Academy of Sciences. Multicolour photometry was carried out with the photoelectric photometer (till January 2016) and CCD detectors at the foci of 0.6 and 0.18 m telescopes. The Echelle medium-resolution spectroscopy ($R \approx 11000$) was obtained with another 0.6 m telescope. The spectra were dereddened with $E_{\mathrm{B-V}} = 0.35$ mag. Basic treatment was done using

the *IRAF*-package software. The spectra were converted to fluxes with the aid of the (near-)simultaneous $(U)BVR_{\rm C}I_{\rm C}$ photometry corrected for emission lines.

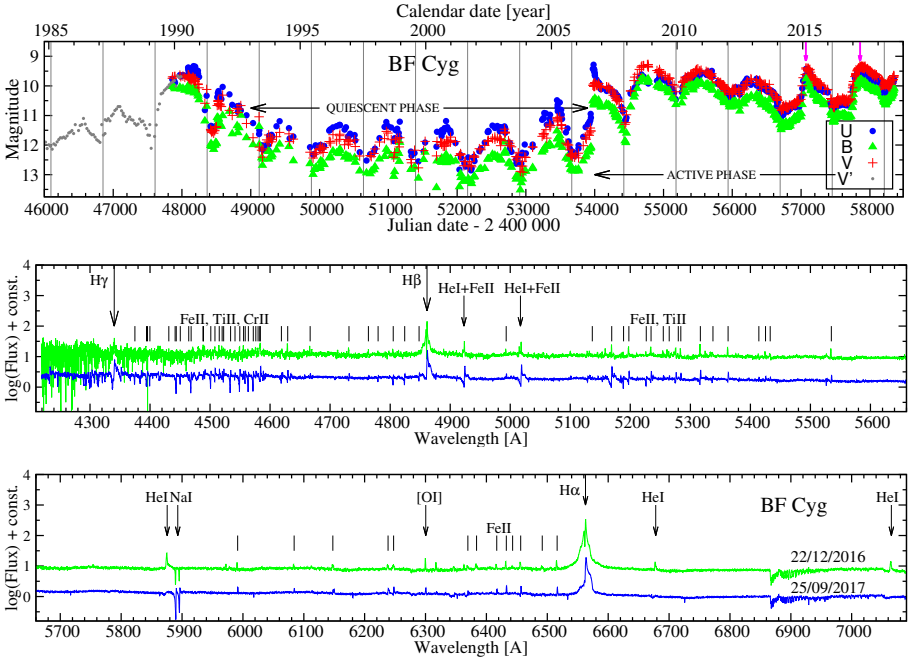

Figure 1. Top: UBV light curves of BF Cyg from its 1989 outburst. Vertical lines represent times of the spectroscopic conjunctions with the giant in front according to the ephemeris $JD_{\rm sp.conj.} = 2\,451\,395.2 + 757.2 \times E$ (Fekel et al., 2001). The 2015 and 2017 flare-like bursts are marked by vertical arrows. Part of the visual light curve V' prior to the 1989 outburst was taken from Leibowitz & Formiggini (2006). Bottom: Comparison of the spectrum from the beginning of the 2017 burst (green line) and that after its maximum (blue line). The most pronounced lines are marked by arrows.

3. Results

Figure 1 shows the UBV light curves of BF Cyg from its 1989 outburst, throughout the following quiescence until the last 2006 outburst, after which the star persists in an active phase to date (2018.8). The quiescent light curve is characterized by the wave-like orbitally-related variations, the nature of which was originally ascribed to the reflection effect (e.g. Kenyon, 1986), but later suggested to be caused by apparent variation of the emission measure of a partially optically thick symbiotic nebula due to the orbital motion (Skopal, 2001). Dur-

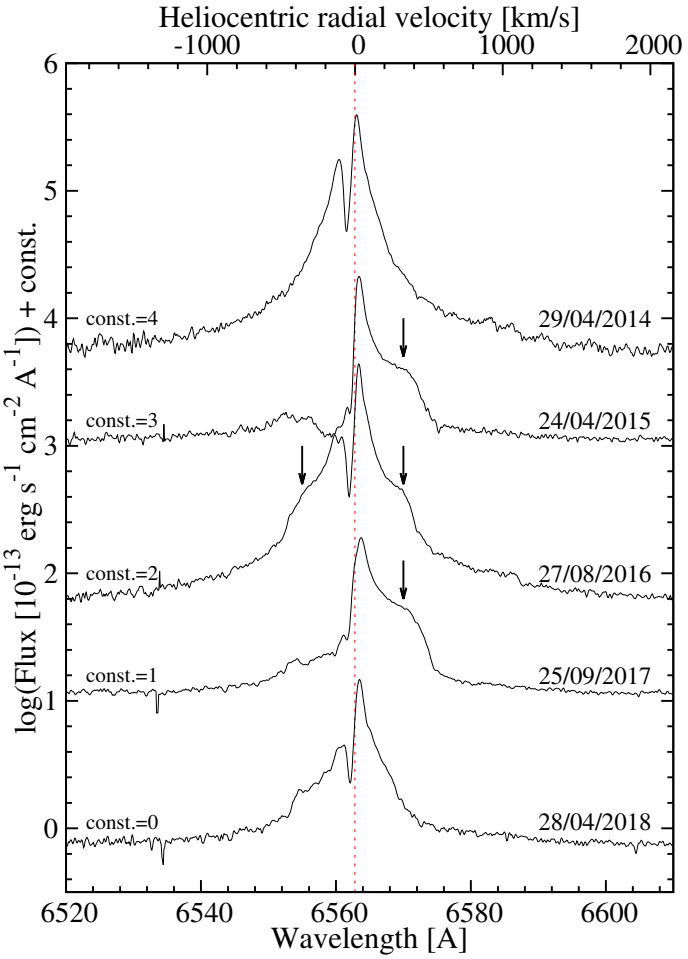

Figure 2. Variation in the Hα profile before and during the 2015 and 2017 bursts. Satellite emission components are marked by arrows.

ing active phases, a cool disk-like pseudophotosphere expanding from the central star creates around the WD (Skopal, 2005). As a result, profiles of minima (eclipses) reflect the geometry of the hot component pseudophotosphere, which can be different at different levels of the activity. For example, during the 1989 outburst of BF Cyg, we observed a rather narrow and deep minimum (eclipse), while during the current activity the minima are much more complex in the profile (see Fig. 1).

At the beginning of 2015 and 2017, BF Cyg showed small 1-mag bursts that peaked at $V \sim 9.3$ with following gradual decline to the pre-outburst brightness

lasting for ∼1 year. Our spectroscopic observations indicate an increase of the mass-outflow during both the 2015 and 2017 bursts. Around the light maximum, blue-shifted absorption component developed in the profiles of most of spectral lines. They indicate a mass-outflow at a few times $100\,\mathrm{km\,s^{-1}}$. Because the orbital inclination of BF Cyg is high, this can be ascribed to the expansion of the cool pseudophotosphere concentrated at/around the equatorial plane. In addition, a strong satellite emission component developed at the red side of hydrogen lines, while during the decline, satellite components developed on both sides of the line (Fig. 2). Such the evolution suggests formation of a highly-collimated bipolar mass ejection from BF Cyg as during the 2009-2012 period (see Skopal et al., 2013).

4. Conclusion

During the 2015 and 2017 bursts, the enhanced mass-outflow was indicated by development of P Cyg profiles and satellite emission components in hydrogen lines. These observational events could be caused by expansion of the equatorially concentrated ejection and the bipolarly-collimated outflow – jets.

Acknowledgements. This research was supported by a grant of the Slovak Academy of Sciences, VEGA No. 2/0008/17, and the Slovak Research and Development Agency under the contract No. APVV-15-0458.

References

Fekel, F. C., Hinkle, K. H., Joyce, R. R., & Skrutskie, M. F., Infrared Spectroscopy of Symbiotic Stars. III. First Orbits for Three S-Type Systems. 2001, *Astron. J.*, **121**, 2219, DOI: 10.1086/319966

Kenyon, S. J. 1986, *The symbiotic stars* (Cambridge: Cambridge University Press)

Leibowitz, E. M. & Formiggini, L., Multiperiodic variations in the last 104-yr light curve of the symbiotic star BF Cyg. 2006, *Mon. Not. R. Astron. Soc.*, **366**, 675, DOI: 10.1111/j.1365-2966.2005.09895.x

Skopal, A., What mimics the reflection effect in symbiotic binaries? 2001, *Astron. Astrophys.*, **366**, 157, DOI: 10.1051/0004-6361:20000217

Skopal, A., Disentangling the composite continuum of symbiotic binaries. I. S-type systems. 2005, *Astron. Astrophys.*, **440**, 995, DOI: 10.1051/0004-6361:20034262

Skopal, A., Tomov, N. A., & Tomova, M. T., Discovery of collimated ejection from the symbiotic binary BF Cygni. 2013, *Astron. Astrophys.*, **551**, L10, DOI: 10.1051/0004-6361/201321030

Skopal, A., Vittone, A., Errico, L., et al., A photometric and spectroscopic study of the symbiotic binary BF CYG. 1997, *Mon. Not. R. Astron. Soc.*, **292**, 703, DOI: 10.1093/mnras/292.3.703

Contrib. Astron. Obs. Skalnaté Pleso **49**, 415 – 419, (2019)

Activity of rapidly rotating dwarf LO Peg an giant FK Com

I. Savanov, S. Naroenkov, M. Nalivkin and A. Shugarov

Institute of Astronomy of the Russian Academy of Sciences 48 Pyatnitskaya st. 119017, Moscow, Russia

Received: October 31, 2018; Accepted: March 6, 2019

Abstract. In 2017-2018, using a robotic wide-field telescope at the Zvenigorod Observatory of INASAN, we carried out new observations of several active late type stars including a rapidly rotating dwarf LO Peg and a rapidly rotating giant – king of spin FK Com. New observations of stars carried out in the V filter allowed to obtain new data for the long-term variability cycles of these objects. Significant changes in the shape of the power spectrum were noted after taking into account our new observations. From the light curves we made restoration of the temperature inhomogeneities on stellar surfaces and determined positions of the active longitudes. The obtained measurements indicate the ongoing evolution of moving active regions and the switching phenomenon(flip-flop) of the positions of active longitudes for FK Com.
Key words: stars – activity – spots – cycles

1. Introduction

The robotic wide-angle monitoring system of the near-earth space of the Zvenigorod observatory of INASAN allows us to carry out photometric observations of cosmic objects according to the plan.

The system is equipped with the Davis Vantage pro2 meteorological observing station, the AAG CloudWatcher cloud cover detector and the Starlight Xpress all-sky camera. This configuration of the equipment, when used in conjunction with specially developed software, made it possible to create a robotic wide-angle optical system operating automatically. To control and obtain information from weather sensors, the software module Control program of weather conditions was designed.

The Veloce RH–200 telescope equipped with a set of Johnson UBVRI photometric filters was used. Observations were performed with the FliProline 16803 CCD with the camera chip size of 4096 x 4096 pixels, the pixel size was 9 x 9 μm. The exposure time (from 20 to 60 s) was chosen for each filter and night individually. The observed data was primarily processed that means subtracting the averaged bias frame, subtracting the dark current frame, and dividing the image frames into the flat field frames. The photometry of stars was conducted with the differential method. Frame reduction was conducted in the MaxImDL program package. The accuracy of a single measurement was about $0.^m009$.

During mentioned below photometric runs in 2017-2018 no flares on FK Com and LO Peg were recorded.

1.1. LO Peg

LO Peg is a K3 young star and belongs to the most studied fast-rotating stars of late spectral types (Karmakar et al., 2016). Its estimated age is 10 – 300 Myr. The star is a member of the AB Dor star group possessing a general spatial motion and for which there is an independent estimation of age, 30 – 150 Myr. The equatorial rotation speed of this star is 65 km s^{-1}, which suggests that it can be referred to ultrafast rotators of late spectral types. In recent years, numerous papers have been published on photometric and polarimetric studies of this star.

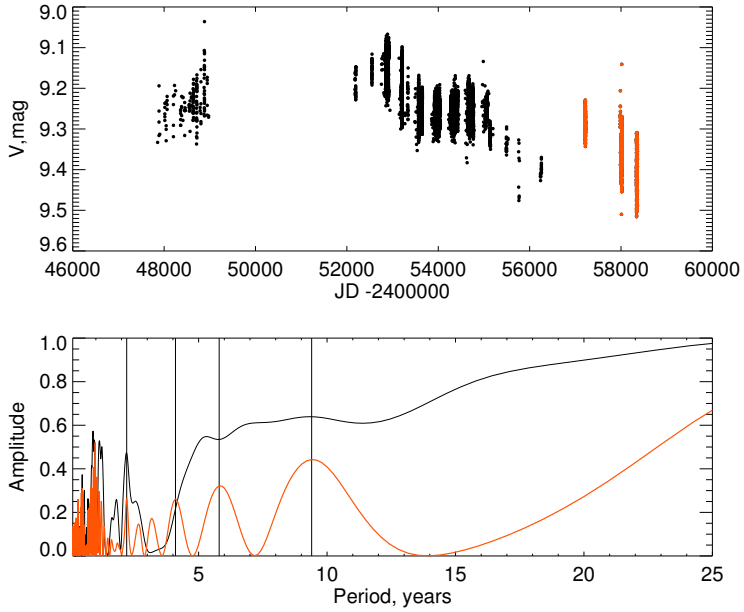

Figure 1. Top: observations of the star in the V filter (red dots are observations with a 20 cm telescope), the middle panel: amplitude power spectrum, the thick line – from the whole data set, the thin line –except for the observations of 2017. The cycles of a long–term variability of 2.2, 4.1, 5.8, and 9.4 yrs are shown with vertical lines.

New observations of LO Peg carried out in the V filter allowed the long – term variability cycles to be determined more precisely. Currently, the data set under consideration includes 15,251 single measurements. The amplitude power spectrum built from them is shown in the lower diagram (red line). We

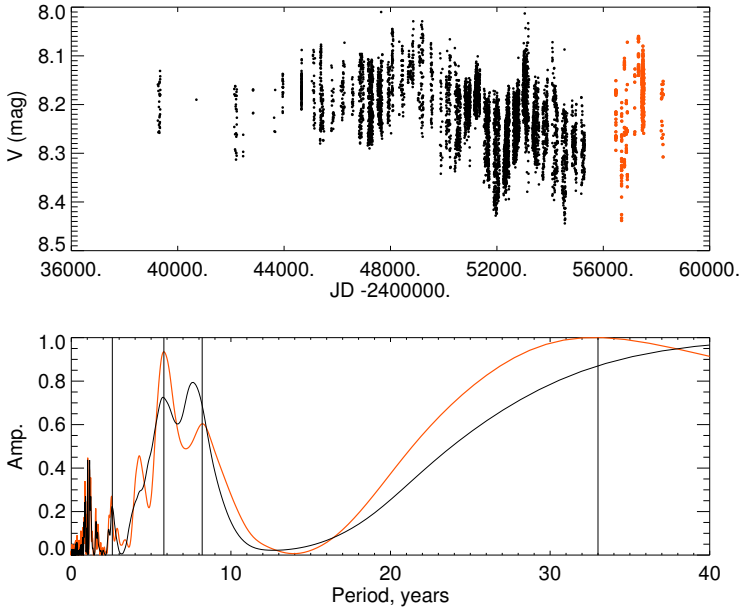

Figure 2. Top: observations of FK Com in the V filter (red dots are observations with a 20 cm telescope), the bottom panel: amplitude power spectrum, the thick red line – from the whole data set, the black thin line –except for the observations of 2017. The cycles of a long–term variability of 2.2, 5.5, 9.2 and 33 yrs are shown with vertical lines.

can notice significant changes in the power spectrum shape after taking into account the new observations of 2017-2018. In the region of the long – term variability cycles greater than 5 yrs, only two cycles appeared at 5.8 and 9.4 years (the power spectrum constructed from the data before our observations is represented in this figure by the black line). Our recent observations indicate that the brightness of the star has stopped to increase without reaching a level of stable brightness, and began to decrease again.

1.2. FK Com

FK Comae Berenices (FK Com, HD117555) is an ultra – fast spinning, heavily spotted, yellow giant. This single star is thought to be a recent binary merger, and is exceptionally active by measure of its intense ultraviolet (UV) and X-ray emissions, and proclivity to a flare (Puzin et al., 2016).

The spectral type of FK Com is estimated as G4III, the projection of the stars rotation velocity on the line of sight is 159 km/s. We present an analysis of new photometric observations of FK Com. Based on our new observational

data and the data from the literature sources we performed an analysis of a complete set of the available photometric data.

From the calculated amplitude power spectrum we can notice significant changes in the power spectrum peaks in the region 6 – 8 years (the peak corresponding to the period of about 6 years became dominant) and in the region of the long – term variability peak of 33 years became visible.

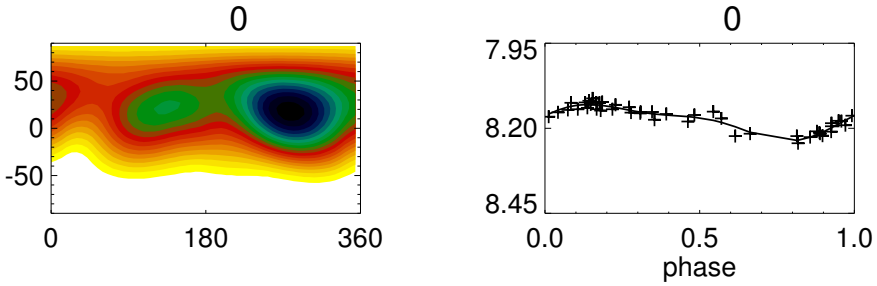

Figure 3. A spot filling factor distribution on FK Com in 2016 (left) and corresponding light curves (right). In the images the darker area implies a higher spot filling factor. Observed light curves are shown as crosses, and the fit as the solid line.

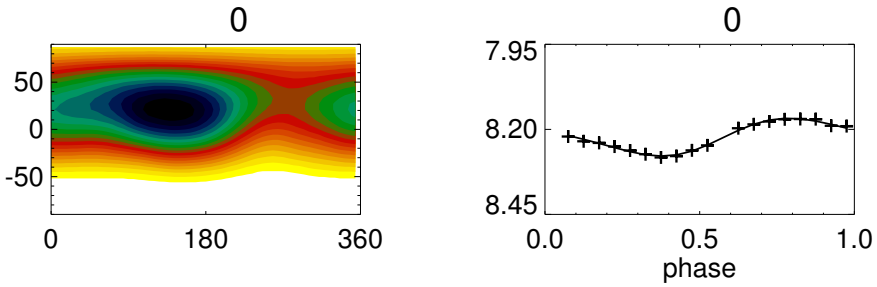

Figure 4. A spot filling factor distribution on FK Com in 2018 (left) and corresponding light curves (right).

From our observations obtained in 2016 and 2018 we made an analysis of surface temperature inhomogeneities of FK Com. To determine the large-scale spot distribution on this star, we apply an inversion technique to the light curves using a two-temperature approximation (Savanov & Strassmeier, 2008). In contrast to direct modelling of light curves, the inversions do not involve any assumptions about spot shapes, numbers, or latitudes. The inversion of the light curve results in the distribution of the spot filling factor over the stellar surface,

i.e., a stellar image (Fig. 3 for 2016 and Fig. 4 for 2018). We adopted values of 5000 K and 4000 K for the photosphere and spot temperatures, respectively, like in our previous investigations (Puzin et al., 2016). We assumed that the star is spotless at V = 8.04 mag. The inclination of the rotational axis to the line of sight is chosen to be 50 degrees. From the stellar images, we recover spot longitudes with the maximum spot filling factor (see details in Puzin et al. (2016)). The accuracy of the spot longitudes depends on the broadness of the light-curve minimum and is on average 0.05 in phase. When two minima are seen in the light curves, two spot concentrations are recovered in the images (in our case one of them is strongly pronounced, the position of the second one is determined less accurately). Our map for observations in 2016 is constructed on the basis of 44 original measurements in filter V, while for the 2018 season 18 averaged values from 377 original measurements were used.

Data in Fig. 3 and Fig. 4 allow us to make a conclusion about the the transition of the star to a new stage of activity in the considered time interval. The shape of the light curve changed, and the dominating activity switched to the opposite longitude. Thus, there is a change in FK Com in positions of the active longitude equal to about 0.5 in phase units, occurred in interval between 2016 and 2018, but it still belongs to system A (a 9.5 year long cycle – Puzin et al. (2016)).

Acknowledgements. This work has been supported by a RFBR Grant 17-52-45048 Flares from F to M - type stars.

References

Karmakar, S., Pandey, J. C., Savanov, I. S., et al., LO Peg: surface differential rotation, flares, and spot-topographic evolution. 2016, *Mon. Not. R. Astron. Soc.*, **459**, 3112, DOI: 10.1093/mnras/stw855

Puzin, V. B., Savanov, I. S., Dmitrienko, E. S., et al., Spots and activity cycles of the star FKCom–2013-2015 data analysis. 2016, *Astrophysical Bulletin*, **71**, 189, DOI: 10.1134/S1990341316020061

Savanov, I. S. & Strassmeier, K. G., Light-curve inversions with truncated least-squares principal components: Tests and application to HD 291095 = V1355 Orionis. 2008, *Astronomische Nachrichten*, **329**, 364, DOI: 10.1002/asna.200710963

Contrib. Astron. Obs. Skalnaté Pleso **49**, 420 – 423, (2019)

Gaia18aak is a new SU UMa-type dwarf nova

A. Simon[1], E. Pavlenko[2], S. Shugarov[3,4], V. Vasylenko[1], I. Izviekova[1], V. Reshetnyk[1], V. Godunova[5], Yu. Bufan[5,6], A. Baransky[7], O. Antonyuk[2], V. Baklanov[2], V. Troianskyi[8,9], S. Udovichenko[9] and L. Keir[9]

[1] *Astronomy and Space Physics Department, Taras Shevchenko National University of Kyiv, 60 Volodymyrska str., Kyiv, 01601, Ukraine (E-mail: andrew_simon@univ.kiev.ua)*

[2] *Crimean Astrophysical Observatory of RAS, Republic of Crimea*

[3] *Astronomical Institute of the Slovak Academy of Sciences 059 60 Tatranská Lomnica, The Slovak Republic*

[4] *Sternberg Astronomical Institute, Moscow State University, Universitetskij pr., 13, Moscow, 119991, Russia,*

[5] *ICAMER Observatory of NASU, 27 Acad. Zabolotnogo str., Kyiv, 03143, Ukraine*

[6] *Astronomical Observatory of the Ivan Franko National University of Lviv, 8 Kyryla i Methodia str., Lviv, 79005, Ukraine*

[7] *Astronomical Observatory, Taras Shevshenko National University of Kyiv, Volodymyrska str. 60, Kyiv, 01601, Ukraine*

[8] *Institute Astronomical Observatory, Faculty of Physics, Adam Mickiewicz University in Poznan, ul. Sloneczna 36, PL60-286 Poznan, Poland*

[9] *Astronomical Observatory of Odessa I.I. Mechnikov National University, 1v Marazlievska str., Odessa, 65014, Ukraine*

Received: November 1, 2018; Accepted: February 5, 2019

Abstract. We report the discovery of a new SU UMa-type dwarf nova, Gaia18aak/ AT2018C, based on its optical observations, which were performed at five observatories (Lisnyky/Kyiv, Terskol, CrAO, Mayaki/Odessa and Stará Lesná, Slovakia) with six small telescopes. The observational campaign started just after the alert was published by ESA Gaia, DPAC and the Photometric Science Alerts Team (http://gsaweb.ast.cam.ac.uk/alerts); the object was very intensely observed during the first month. After this there was organized a four-month monitoring in order to test outburst activity of the object.

We detected the 0.0647-d (or 0.0692-d) superhump period during five nights of the superoutburst. Furthermore, we found the only possible outburst during the subsequent 100 nights.

Key words: variable stars – CV's – GAIA

1. Introduction

Dwarf novae (DN) are a subclass of cataclysmic variables (CV), which are close binary systems and consist of a white dwarf (WD) and an old (K-L) spectral type dwarf. The old-type component fills its Roche lobe and its matter accretes onto the WD through the inner Lagrangian point, creating an accretion disk around the primary component (Warner, 1995). There are two special subclasses among DN: SU UMa-type and WZ Sge-type dwarf novae.

SU UMa-type dwarf novae produce two types of outbursts - normal outbursts with typical duration of 2-5 days and an amplitude of 2-3 mag and superoutbursts that have longer duration and a higher amplitude. The main difference of superotbursts from normal outbursts is the presence of light variability with periods that only by some percent differ from the orbital period - superhumps. Usually several normal outbursts occurred between two neighbor superoutbursts. The time between two superoutbursts is called a supercycle. A WZ Sge-type DN differs from an SU UMa-type DN by a longer supercycle that can last from several years to decades (Kato, 2015).

Gaia18aak (AT2018C) was discovered as a blue hostless transient on 2018-01-01 and reported on 2018-01-03 by Delgado et al. (2018) on behalf of the Gaia Alerts team. The alerting magnitude of the object was G = 16.48 with coordinates (ep=J2000) α = 04 12 01.22, δ = +76:00:57.31. On the images from 2017-12-20 the object was fainter than the limiting magnitude G = 21.5. We started to observe Gaia18aak from 2018-01-09 and detected variations with a period of about 0.068^d and an amplitude of 0.15^m (Simon et al., 2018). Later, on 2018-01-13 the Asiago Transient Classification Program (Tomasella et al., 2014) reported the spectroscopic classification of AT2018C (= Gaia18aak) (Tomasella et al., 2018) that gave them an opportunity to classify Gaia18aak as a cataclysmic variable.

We present the result of our monitoring of Gaia18aak in order to specify its classification.

2. Observations and data reduction

UBVRcIc photometry of Gaia18aak was carried out at six small telescopes at five observational sites (Lisnyky (Kyiv), Terskol, CrAO, Mayaki (Odessa) and Stará Lesná, Slovakia). We provided observations in *UBVRcIc*-bands for color estimation and in the integral light (marked as "Clear") for period estimation. Images obtained in unfiltered light are close to images obtained in the *Rc*-band. All frames were bias and dark subtracted and flat-fielded in the standard manner using MaxIm DL and V. Goranskij (http://www.vgoranskij.net/software/) WinFit packages. These packages were also used to measure the brightness of variable, comparison and check stars. As the reference star we used a star from APASS DR9 catalogue (Henden et al., 2016) with equatorial coordinates

(ep=J2000) α = 04 12 53.78544, δ = +75 59 39.0336 and magnitudes $B = 15^m.541$, $V = 14^m.860$, $r' = 14^m.671$, $i' = 14^m.500$. In this work we present nightly and longterm variability in the *R*-band and no color analysis will be done. In case of absence of data in the *R*-band for several nights, data in integral light or in the *I*-band were taken.

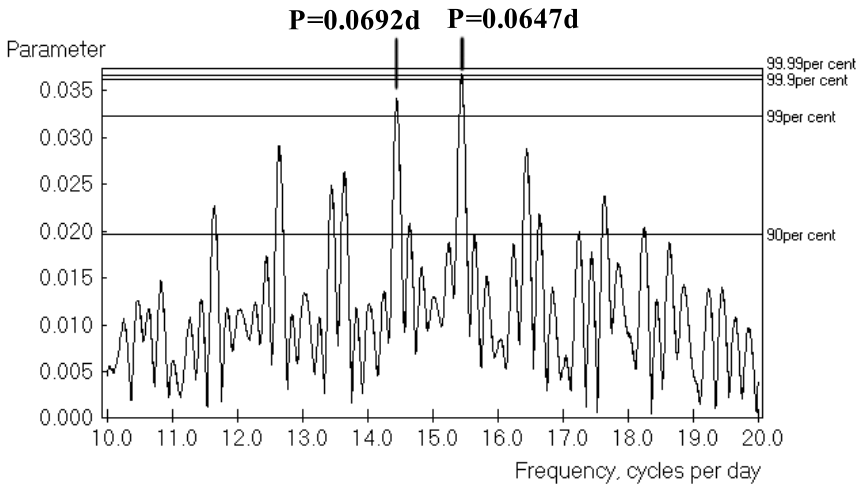

Figure 1. A five-night periodogram.

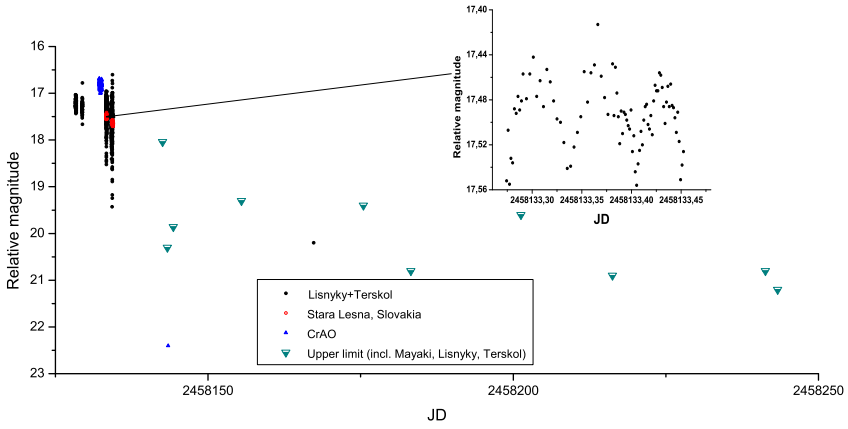

Figure 2. The light curve of Gaia18aak for the whole period of observations. *The inset*: Variability of Gaia18aak on January 14, 2018 (JD=2458133).

3. Results

All our data can be divided into two groups: during the superoutburst and after it. During the superoutburst we obtained data from five nights: 2018-01-09, 10, 13, 14 and 15. For all of these data we provided a periodogram analysis and obtained a period of 0.0647 days (or the aliased one 0.0692 d)(see Fig. 1). We should notice that this period is typical for SU UMa stars (Kato et al., 2009). The next data from 2018-01-24 showed that the object already was $m = 22^m.4$ in an unfiltered image. Also we should note that the latest observations from 2018-10-16 and 17 showed no sign of the object and the limiting magnitude on the images was $m = 22^m.3$. Given this fact, we can estimate the duration of the superoutburst to be less than 23 days with the amplitude higher than 6^m.

After the superoutburst on all images there were no Gaia18aak detected except one night on 2018-02-17 when the object reached $m = 20^m.2$. We suppose that on this date we detected an ordinary outburst. All the photometric data are presented in Fig. 2.

4. Conclusions

The periodogram analysis for the combined five nights yields the best period of 0.0647 d (or the aliased one 0.0692 d). The multi-site campaign confirmed our preliminary suggestion that GAIA 18aak is a new SU UMa-type dwarf nova.

Acknowledgements. We acknowledge ESA Gaia, DPAC and the Photometric Science Alerts Team (http://gsaweb.ast.cam.ac.uk/alerts). S. Shugarov thanks the grants VEGA 2/0008/17 and APVV 15-0458.

References

Delgado, A., Harrison, D., Hodgkin, S., et al. 2018, *Transient Name Server Discovery Report*, **2018-5**, 1

Henden, A. A., Templeton, M., Terrell, D., et al., VizieR Online Data Catalog: AAVSO Photometric All Sky Survey (APASS) DR9 (Henden+, 2016). 2016, *VizieR Online Data Catalog*, II/336

Kato, T. 2015, *PASJ.*, **67**, 10842, DOI: 10.1093/pasj/psv077

Kato, T., Imada, A., Uemura, M., et al. 2009, *Publications of the Astronomical Society of Japan*, **61**, S395, DOI: 10.1093/pasj/61.sp2.S395

Simon, A., Pavlenko, E., & Vasylenko, V. 2018, *The Astronomer's Telegram*, **11155**

Tomasella, L., Benetti, S., Cappellaro, E., et al. 2014, *Astronomische Nachrichten*, **335**, 841, DOI: 10.1002/asna.201412068

Tomasella, L., Benetti, S., Cappellaro, E., & Turatto, M. 2018, *The Astronomer's Telegram*, **11168**

Warner, B. 1995, *Cambridge Astrophysics Series*, **28**

Contrib. Astron. Obs. Skalnaté Pleso **49**, 424 – 426, (2019)

First glance at the recently discovered symbiotic star HBHA 1704-05 during its current outburst

A. Skopal[1], M. Sekeráš[1], E. Kundra[1], R. Komžík[1], S.Yu. Shugarov[1,5], C. Buil[2], P. Berardi[3] and A. Zubareva[4,5]

[1] *Astronomical Institute of the Slovak Academy of Sciences 059 60 Tatranská Lomnica, The Slovak Republic, (E-mail: skopal@ta3.sk)*

[2] *Castanet Tolosan Observatory, 6 place Clemence Isaure, 31320 Castanet Tolosan, France*

[3] *Bellavista Observatory, Via Carlo De Paulis 15, 67100 L'Aquila, Italy*

[4] *Institute of Astronomy, Russian Academy of Sciences, Russia*

[5] *P.K. Sternberg Astronomical Institute, M.V. Lomonosov Moscow State University, Russia*

Received: November 1, 2018; Accepted: January 24, 2019

Abstract. In this contribution we introduce our photometric and spectroscopic observations of the newly (August 9, 2018) discovered outburst of the emission-line star, HBHA 1704-05, whose photometric variability and the spectrum during the outburst are both characteristic for a symbiotic star.

Key words: stars: binaries: symbiotic – individual: HBHA 1704-05

1. Introduction

Symbiotic stars are the widest interacting binaries consisting of a cool giant and a white dwarf (WD) accreting from the giant's wind. Their orbital periods can range from about one year to a few hundred years. During the so-called quiescent phase, the symbiotic system does not change its brightness significantly, except for a wave-like $\sim 0-1$ mag variation in their light curves along the orbit. Their spectrum can be similar to that of a normal red giant with superposed emission lines and a faint blue continuum in the optical. Therefore, their nature as a symbiotic star can be easily overlooked (see Sokoloski et al., 2017). Sometimes they experience unpredictable outbursts characterized by $\sim 1-3$ mag brightening in the optical with signatures of a mass-outflow that reveals their real nature.

According to "Transient Object Followup Reports" of CBAT[1] the star TCP J19544251+1722281 brightened from $V = 12.0$ on July 31.945, 2018 to $V = 10.7$ on August 8.938, 2018. The brightening was confirmed by the on-line ASASSN database for the SR variable ASASSN-V J195442.95+172212.6 as a possible symbiotic star in the outburst. On August 11, 2018, Munari et al. (2018) reported that this object coincides with an emission line star HBHA 1704-05 in

[1] http://www.cbat.eps.harvard.edu/unconf/followups/J19544251+1722281.html

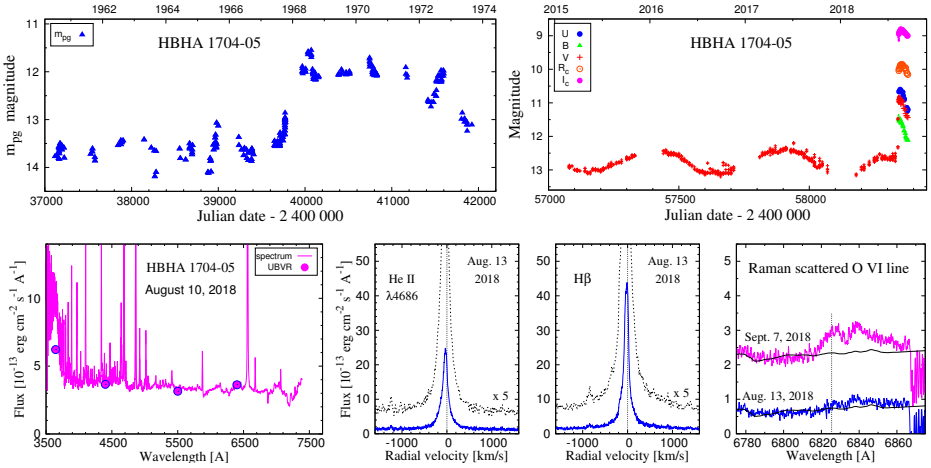

Figure 1. Top left: The historical light curve of HBHA 1704-05 obtained from photographic plates of the Moscow's archive. Top right: The V light curve measured within the ASASSN program indicating a new outburst from August 9, 2018. Bottom: The energy distribution between 350 and 740 nm and line profiles of He II 4686 Å, Hβ and Raman scattered O VI 6825 Å. The spectra were dereddened with $E_{B-V} = 0.22$ mag.

the catalog of Kohoutek & Wehmeyer (1999) and is currently undergoing a "hot-type" outburst.[2] In the spectrum, they found features of an M-type giant, a strong nebular continuum with superposed emission lines of highly ionized elements (e.g., He II 4686 Å and [Ne V] 3426 Å). In this contribution we present examples of our photometric and spectroscopic monitoring of HBHA 1704-05 during the first month of its outburst.

2. Observations

We started to monitor HBHA 1704-05 from August 12, 2018. Our multicolour $UBVR_CI_C$ CCD photometry was carried out by the 0.6 m telescope at the Stará Lesná observatory (pavilion G2), while the optical spectra were obtained by the 0.6 m and 1.3 m telescopes at the Stará Lesná (pavilion G1) and Skalnaté Pleso observatories, respectively. Our spectroscopic observations were complemented with those available at the *Astronomical Ring for Access to Spectroscopy (ARAS)* database.[3] Here, the spectra obtained by P. Berardi at the Bellavista Observatory on August 9.856, 2018 (436–740 nm) and that made by Ch. Buil at the Castanet Tolosan observatory on August 10.932 (350–507 nm) were used.

[2]Originally classified as the 2nd-type of outbursts of symbiotic binaries (see Skopal, 2005)
[3]http://www.astrosurf.com/aras/Aras_DataBase/Symbiotics/TCPJ19544251+1722281.htm

3. Results

Figure 1 shows main photometric and spectroscopic characteristics of the newly discovered symbiotic star HBHA 1704-05. The ASASSN V light curve shows a wave-like variation – a typical feature of the light variability of symbiotic stars during quiescent phases, which is connected with the orbital motion. This suggests the orbital period of ≈500 days. The new outburst of HBHA 1704-05 was indicated by a rapid ∼1.5 mag increase in V at the beginning of August 2018 (Munari et al., 2018), which we confirmed by our $UBVR_{\rm C}I_{\rm C}$ photometry. Inspection of the Moscow's archive of photographic plates revealed another 2-mag-outburst in 1968.

Our low-resolution spectra (350 – 740 nm) indicate the presence of a strong nebular continuum with a prominent Balmer jump in emission, although features of a late type giant can be recognized in the long-wavelength part of the spectrum. The presence of strong He II 4686 Å and gradual emergence of the Raman scattered O VI 6825 Å lines on our medium-resolution spectra suggest a high temperature of the central ionizing source. The flux ratio $F_{4686}/F_{\beta} \sim 0.5$ on August 13, 2018, corresponds to ∼170 000 K.

4. Conclusion

Our preliminary analysis showed that the current outburst of HBHA 1704-05 is of a Z And-type and is very similar to that recently (2015) observed for AG Peg (see Skopal et al., 2017).

Acknowledgements. This research was supported by a grant of the Slovak Academy of Sciences, VEGA No. 2/0008/17, and the Slovak Research and Development Agency under the contract No. APVV-15-0458.

References

Kohoutek, L. & Wehmeyer, R., Catalogue of H-alpha emission stars in the Northern Milky Way. 1999, *Astron. Astrophys., Suppl.*, **134**, 255, DOI: 10.1051/aas:1999101

Munari, U., Dallaporta, S., Valisa, P., et al., HBHa 1704-05: a bright and newly discovered symbiotic star, currently undergoing an "hot-type" outburst. 2018, *The Astronomer's Telegram*, **11937**

Skopal, A., Disentangling the composite continuum of symbiotic binaries. I. S-type systems. 2005, *Astron. Astrophys.*, **440**, 995, DOI: 10.1051/0004-6361:20034262

Skopal, A., Shugarov, S. Y., Sekeráš, M., et al., New outburst of the symbiotic nova AG Pegasi after 165 yr. 2017, *Astron. Astrophys.*, **604**, A48, DOI: 10.1051/0004-6361/201629593

Sokoloski, J. L., Lawrence, S., Crotts, A. P. S., & Mukai, K., Flows and Shocks: Some Recent Developments in Symbiotic Star and Nova Research. 2017, *ArXiv e-prints* [arXiv1702.05898]

Contrib. Astron. Obs. Skalnaté Pleso **49**, 427 – 429, (2019)

Modeling of accretion disk-originated features in the high resolution spectra of U Sge

Ö. Taşpınar, H. Bakış and V. Bakış

Department of Space Sciences and Technologies, Akdeniz University, 07058 Antalya, Turkey, (E-mail: ozlemtaspinar@akdeniz.edu.tr)

Received: October 31, 2018; Accepted: March 18, 2019

Abstract. U Sge (HD 181182) belongs to the group of short period Algol-type binaries with a period of 3.38 days. One hundred and eleven high-resolution spectra of U Sge, which are known to exhibit H_α emission, were obtained at (TÜBİTAK) National Observatory in Turkey. The emission and absorption structures of the system have been analysed. The astrophysical parameters of the system have been obtained by means of analysing the spectral and photometric data. Accordingly, the primary component is a B7-8 spectral type main-sequence star, while the secondary component is a G2 spectral type giant. The cool secondary component has filled its Roche lobe and is transferring material through the L_1 point onto the hot primary component. The effects of both components and the transferring material were detected in the H_α lines. In order to determine these effects, the SHELLSPEC code, which uses an LTE approximation, has been used. The circumstellar structure around U Sge is due to a very low density disk, transferring material, a hot spot where the transferring material from the secondary impacts onto the primary and the magnetic activity from secondary itself. Moreover, all of these effects on the system are highly variable in just a few orbital cycles.

Key words: binary stars – mass transfer – accretion disk

1. Introduction

U Sagittae is the brightest eclipsing binary of the Algol-type with a total primary eclipse. It has been actively studied by photometry as well as by spectroscopy. Observations of U Sge have revealed the presence of variable circumstellar gas in the system. In this study, we determined the physical parameters of the system and the components. We then investigated the variability on H_α spectra and physical properties of the accretion regions in the U Sge using the SHELLSPEC code (Budaj and Richards, 2004).

2. Observations and Analysis of Data

The spectroscopic observations of U Sge were carried out with the Coudè-Èchelle Spectrograph ($R \sim 40000$) at the RTT150 telescope of (TÜBİTAK) National Ob-

servatory. The spectra were reduced by using the IRAF software. The Strömgren b-band ($\lambda_{max} = 4670$ Å) photometry was taken by McNamara and Feltz (1976).

The SHELLSPEC code requires the synthetic spectrum of the components in order to model the circumstellar material. We computed the model atmospheres for the spectrum of the secondary component, where the primary component is totally eclipsed, using the ATLAS9 code written by Kurucz (1993). Synthetic spectra of the secondary component were produced for 17 different èchelle orders at this phase using the SYNTHE code. In this way, model atmosphere parameters of the secondary component were determined.

The spectra of U Sge were analysed with the Fourier spectra disentangling code KOREL (Hadrava, 1995). The light contributions of the components used in the disentangling procedure were taken from the light curve solution which was performed by using the WD code (Wilson and Devinney, 1971). The atmospheric model parameters of the primary component were obtained by fitting synthetic spectrum on He I and Mg II lines of the primary component.

3. Modeling of the Circumstellar Matter

The free parameters for modeling of accretion disk are thickness, inner and outer radius, temperature and density. The models were generated by altering these parameters. The results of the H_α modeling are shown in Fig. 1. It is seen that the distribution of circumstellar matter is highly variable in different epochs at the same phase (see the top panel of Fig. 1).

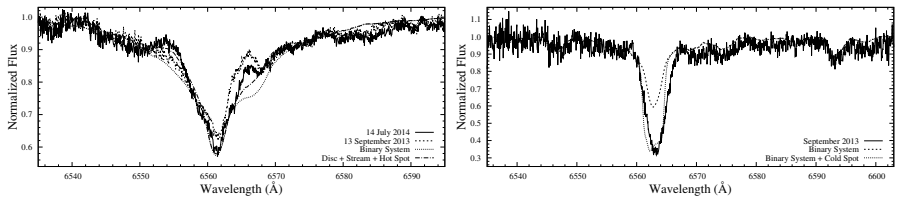

Figure 1. Variability of the circumstellar matter in different epochs at the same phase (ϕ= 0.25) (*top*) and two different models for ϕ= 0.003 (*bottom*).

At the orbital phase ϕ=0.003, the synthetic H_α spectral line calculated for the secondary component is shallower than the observed H_α line implying an excess absorption (see bottom panel of Fig. 1).

This extra absorption may indicate a presence of additional matter in front of the star along our line of sight or chromospheric activity of the secondary star. A model of a cold low density absorbing gas, which is shown as a cold spot in Fig. 1 (bottom panel), around the secondary component as a consequence of the chromospheric activity fits the observed spectrum.

Table 1. Physical parameters of the component stars and the disk.

Parameter (unit)	Value
Stellar parameters	
$T_{eff1,2}$ (effective temperature, K)	12250 ± 50, 5500 ± 50
$\log g_{1,2}$ (surface gravity, cgs)	4.00 ± 0.06, 3.25 ± 0.09
$v \sin i_{1,2}$ (rotation velocity, km/s)	70 ± 5, 80 ± 5
Disk parameters	
a (thickness, $R_\odot$)	0.82 ± 0.02
R_{in} (inner radius, $R_\odot$)	6.20 ± 0.20
R_{out} (outer radius, $R_\odot$)	9.50 ± 0.40
ρ (density, cgs)	$10^{-14} \leqq \rho \leqq 10^{-12}$
$T_{\rm disk}$ (disk temperature, K)	8000 ± 500

4. Conclusions

By modeling the circumstellar matter, we obtained physical parameters of the accretion disk which are given in Table 1. In this study a total of 111 spectra of U Sge were obtained in 14 observing nights between September 2013 and August 2014. The features of the H_α spectra were found to be highly variable in the course of the observing period. As Albright and Richards (1995) suggessted, we also confirmed that circumstellar features in H_α spectra are stable over timescales of days, but vary significantly over timescales of weeks. Investigation of the U Sge system in this study may be important with regards to understanding the mass transfer process in active Algol-type binary systems.

Acknowledgements. This work is fully supported by the Scientific and Technological Research Council of Turkey (TÜBİTAK) under project code 112T928.

References

Albright, G.E., Richards, M.T.: 1995, *Astrophys. J.* **441**, 806

Budaj, J., Richards, M.T.: 2004, *Contrib. Astron. Obs. Skalnaté Pleso* **34**, 167

Kurucz, R.L.: 1993, *CD-ROM No.18* **102**, 1539

McNamara, D.H., Feltz, K.A.: 1976, *Publ. Astron. Soc. Pac.* **88**, 688

Hadrava, P.: 1995, *Astron. Astrophys., Suppl. Ser.* **114**, 393

Wilson, R.E., Devinney, E.J.: 1971, *Astrophys. J.* **166**, 605

Contrib. Astron. Obs. Skalnaté Pleso **49**, 430 – 433, (2019)

Investigating the OB associations in CMa using eclipsing binary systems: Preliminary results on LV CMa

E. Tunç and V. Bakış

Department of Space Sciences and Technologies, Akdeniz University, Dumlupınar Boulevard 07058 Antalya, Turkey
(E-mail: volkanbakis@akdeniz.edu.tr)

Received: October 31, 2018; Accepted: March 15, 2019

Abstract. In this study, an eclipsing binary of a short orbital period ($P = 1^{\rm d}.1834857$) LV CMa ($V = 8^{\rm m}.7$) is selected as a candidate member of an association in the direction of CMa OB1/R1 region. Light curves in $UBVR_cI_c$ photometric bands were obtained and low-resolution ($R \sim 5500$) spectra were collected. Preliminary results show that the system is a detached binary containing at least one B spectral type star. It seems that LV CMa has no connection with the nearby OB associations or stellar clusters.

Key words: eclipsing binaries – associations

1. Introduction

There have been some opposing views about determining the physical boundaries, ages and distances of young stellar groups in the CMa constellation (for details, see Gregorio-Hetem, 2008). In a brief summary, it would be appropriate to mention that CMa consists of three stellar associations (SAs): two of them are located at the same position with a distance of 1.15 kpc from the Sun, hence named together as CMa OB1/R1. Another one, known as CMa OB2 (Kopylov, 1958), is centered at 740 pc away from the Sun. The predicted ages are 3 Myr and 100 Myr for CMa OB1/R1 and OB2, respectively (Clariá, 1974 a; Clariá, 1974 b; Eggen, 1981). A couple of studies on early-type eclipsing binaries (EBs) in CMa revealed the existence of differences between the ages of members and nearby SAs.

For example, in the case of FM CMa, a well-known member of OB1/R1, the photometric distance and age of the system is found to be 980 ±130 pc and 30 ±10 Myr (Zejda *et al.*, 2018), which is in agreement with the values of CMa OB1/R1. Also, another early-type binary LT CMa was investigated by Bakış *et al.* (2010) and they found that the distance to LT CMa is 535 ±45 pc and its age is 35 ±5 Myr, meaning that it is closer than FM CMa, but has a similar age. We see a picture that early-type stars with the similar age are located around the CMa OB1/R1 association. So, our main motivation in this research is to investigate how star forming regions evolve with respect to the distance

through the SAs in the vicinity of CMa by examining early-type EBs, which are likely to be members.

Despite the fact that determining precise boundaries of SAs and, consequently, their radii is a difficult task, discoveries of new members located in the outer frontiers of SAs may lead us to review our knowledge about star forming scenarios. In this aim, we have selected LV CMa (HD 53931), which is a relatively bright ($V = 8\overset{\mathrm{m}}{.}7$), early-type (B9.5V) EB with a short orbital period ($P = 1\overset{\mathrm{d}}{.}1834857$). According to the GAIA parallax (Gaia Collaboration *et al.*, 2016) of LV CMa, it is located at a distance of 510 ±18 pc from the Sun, revealing that it has a similar distance as LT CMa and also their lines of sight in the sky are close to each other. This encouraged us to question the possibility of a dynamical relationship of LV CMa with other early-type stars around.

2. Observations

Photometric observations were carried out between 2016 and 2017 in a total of six nights. The data were collected with AUT25, a 25 cm Ritchey-Chrétien type of telescope which is equipped with a back-illuminated CCD camera and $UBVR_cI_c$ photometric filters. Bias, dark subtraction and flat field correction were applied to the raw data. Subsequently, aperture photometry was performed with the aperture chosen to be three times the *FWHM* of the stellar profile. The orbital period was calculated with the up-to-date ephemerides provided by Kreiner (2004) to form light curves (LCs). Also, a new time of the secondary minimum was extracted from our observations. An example LC can be found in Fig. 1.

Spectroscopic observations were carried out in 2016 with the low-resolution ($R \sim 5500$) Faint Object Spectrograph and Camera (TFOSC) installed at the Cassegrain focus of the 1.5 m RTT150 telescope of TUBITAK National Observatory of Turkey. TFOSC covers a wavelength range between 3300 Å and 12000 Å in 11 spectral orders. An example spectral region of LV CMa, which was observed at orbital phase near the primary minimum, is shown in Fig. 1.

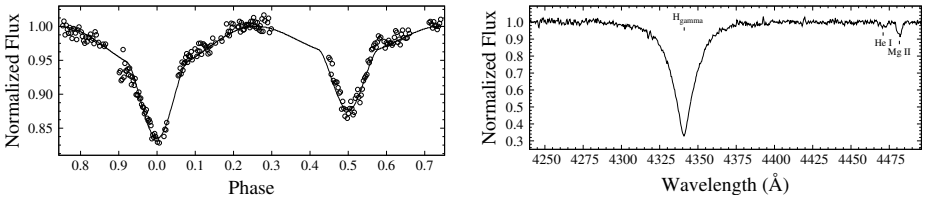

Figure 1. The best fitting model for a V-band light curve (left) and the observed spectrum of LV CMa around H_γ, He I and Mg II lines (right).

Table 1. Light curve solutions for LV CMa.

Parameter	Primary	Secondary
i (°)	68.1 ± 0.4	
e	0	
ω (°)	0	
q	0.80 ± 0.05	
$T_{\rm eff}$ (K)	9300	8200 ± 95
Ω	3.97 ± 0.04	4.30 ± 0.08
$L/L_{\rm total}$	0.64 ± 0.02	0.36 ± 0.02
$r_{\rm mean}$	0.322 ± 0.004	0.253 ± 0.007
$d_{\rm parallax}$ (pc)	510 ± 18	

3. Analysis

To begin with, we analyzed the LC of LV CMa using the Wilson-Devinney (WD) code (version 2015) with Mod 2, which was provided for detached binaries. The V-band LC was used to check if reliable convergence of free parameters can be reached using different input parameters. Unfortunately we weren't able to determine the mass ratio (q) of the system from radial velocity curves due to unevenly distributed data over the orbital revolution, so we used a q-search method. For each q value assigned as a fixed-parameter, a convergent solution was obtained and sum of squared deviations (χ^2) from the model was calculated. The value with minimum χ^2 is adopted as the mass ratio of LV CMa. By setting q, $T_{\rm eff,1}$ (adopted from GAIA DR2), P, $T_{\rm o}$, $A_{1,2}$, $g_{1,2}$, and $F_{1,2}$ (under a radiative atmospheres assumption) as fixed parameters (linear limb darkening coefficients are adopted from van Hamme, 1993) we modeled the LC (see Fig. 1). Our best fitting model parameters are given in Tab. 1. The uncertainities given in the table are calculated by the WD code. The parallax of LV CMa is also adopted from GAIA DR2 (Gaia Collaboration *et al.*, 2018), as we decided it would be convenient to use it instead of the photometric distance which can be vulnerable to effects of interstellar medium.

4. Preliminary Results

By investigating the low-resolution spectrum of LV CMa, we confirm that at least one of the components in the system is a B-spectral type star, as the spectrum at the primary minimum includes He I lines (see Fig. 1). Although the secondary star is in the front as the conjunction occurs, this weak He I line seen in the spectrum could be from the primary star's spectrum since the inclination of the orbit is as low as 68 degrees, where $\sim$60 per cent of light of the primary is still visible by the observer. A collection of the spectra covering the whole orbital cycle would help us to characterize the components in the system. For

now, we keep the temperature of the primary components as given in the GAIA catalogue.

The spectrum at the primary minimum also tells us about the approximate center of mass velocity of the system, which is $\sim -21\,\mathrm{km/s}$. This velocity, when combined with the proper motion and distance of the system, would give us information about the space velocity components of LV CMa as $U = 20\,\mathrm{km/s}$, $V = 3\,\mathrm{km/s}$ and $W = -11\,\mathrm{km/s}$. These velocity components correspond to neither space velocity components of CMa OB1 ($U = -40.3\,\mathrm{km/s}$, $V = -4.6\,\mathrm{km/s}$ and $W = -21.3\,\mathrm{km/s}$) nor those of LT CMa ($U = -25.2\,\mathrm{km/s}$, $V = -7.3\,\mathrm{km/s}$ and $W = -12.5\,\mathrm{km/s}$).

Acknowledgements. Spectroscopic observations with TFOSC were granted by the TUBITAK National Observatory with the project code 12ARTT150-255.

References

Bakış, V., Bulut, İ., Bilir, S., Bakış, H., Demircan, O., Hensberge, H.: 2010, *Publ. Astron. Soc. Jpn.* **62**, 1291

Clariá, J.J.: 1974 a, *Astron. J.* **79**, 1022

Clariá, J.J.: 1974 b, *Astron. Astrophys.* **37**, 229

Eggen, O.J.: 1981, *Astrophys. J.* **247**, 507

Gaia Collaboration *et al.*: 2016, *Astron. Astrophys.* **595**, 1

Gaia Collaboration *et al.*: 2018, *Astron. Astrophys.* **616**, 1

Gregorio-Hetem, J.: 2008, *Handbook of Star Forming Regions, Vol. II*, ASP Monograph Publications, San Francisco

Kopylov, I.M.: 1958, *Sov. Astron.* **2**, 359

Kreiner, J.M.: 2004, *Acta Astron.* **54**, 207

van Hamme, W.: 1993, *Astron. J.* **106**, 2096

Wilson, R.E., Devinney, E.J.: 1971, *Astrophys. J.* **166**, 605

Zejda, M. *et al.*: 2018, **in preparation**, Study of Eclipsing Binary and Multiple Systems in OB Associations. VI. CMa OB1 Member FM Canis Majoris

Contrib. Astron. Obs. Skalnaté Pleso **49**, 434 – 438, (2019)

V839 Cep - a new massive eclipsing variable with apsidal motion in the field of Trumpler 37

I.M. Volkov[1,2], L.A. Bagaev[2], A.S. Kravtsova[2] and D. Chochol[3]

[1] *Institute of Astronomy of the Russian Academy of Sciences, 48 Pyatnitskaya street, 119017 Moscow, Russia, (E-mail: hwp@yandex.ru)*

[2] *Sternberg Astronomical Institute, Lomonosov Moscow State University, Universitetskij Ave. 13, 119992 Moscow, Russia, (E-mail: kravts@yandex.ru)*

[3] *Astronomical Institute of the Slovak Academy of Sciences 059 60 Tatranská Lomnica, The Slovak Republic, (E-mail: chochol@ta3.sk)*

Received: October 31, 2018; Accepted: January 30, 2019

Abstract. Our precise UBV photometric light curves of a poorly studied Algol-type eclipsing binary V839 Cep were used to derive relative and absolute parameters of the system. The masses of the components 3.3 ± 0.2 $M_\odot$, 4.4 ± 0.3 $M_\odot$, radii 1.9 ± 0.1 $R_\odot$, 2.9 ± 0.1 $R_\odot$, effective temperatures $14150 \pm (300)$ K, $15700 \pm (300)$ K and inclination of the orbit 88.15 ± 0.02 deg were determined. The Eclipse Time Variation (ETV) diagram revealed the apsidal motion in the system with $\dot{\omega}_{obs} = 0.027(9) \mathrm{deg\,yr}^{-1}$, $U = 13600(4500)$ years.

Key words: stars: binaries: eclipsing – stars: binaries: close – stars: interstellar reddening – stars: fundamental parameters

1. Introduction

The eclipsing binary GSC 3964 0741 = V839 Cep ($P = 9.^{\mathrm{d}}96$, $V = 9.65$ mag, $e = 0.11$) was discovered by Otero et al. (2006). The light curve of the system is characterized by the shift of the secondary minimum relatively to the phase 0.5, indicating the ellipticity of the orbit. No photoelectric Light Curves (LCs) of this eclipsing binary have been published yet. The analysis of the observations is complicated by the fact that the eclipsing binary has a bright visual companion ($\Delta V = 1.1$ mag) separated by $0.2''$. Moreover, the main component of the eclipsing binary could be variable.

2. Observations and data reduction

In 2008-2018 we obtained $UBVRI(RcIc)$ photometry of the object with the 0.6-m telescope equipped with a Hamamatsu R2949S photomultiplier, changed later by a G4-9000 CCD at Stará Lesná Observatory (Slovakia) and 1-m and 0.6-m reflectors of Simeiz observatory in Crimea (equipped with CCD FLI PL09000 and VersArray 512UV). The derived colour indices $U - B, B - V$ indicate a

strong interstellar absorption, $E(B-V) = 0.66(1)$, Av = 2.1. The normal colour indices of the star, $(U-B)_0 = -0.61$ and $(B-V)_0 = -0.18$, correspond to the spectral class B4. Although the star is located on the celestial sphere in 4.5 deg from the centre of Trumpler 37 open cluster, which is rich with variable and multiple stars, we found that the object does not belong to it. According to WEBDA (http://webda.physics.muni.cz) the distance of the cluster is 835 pc, much more than 550 pc found in this work. Two editions of Gaia data releases give 370 pc and 714 pc, significantly different from each other and from our estimate, probably due to the fact that the object is visual double.

3. LC solution and absolute parameters

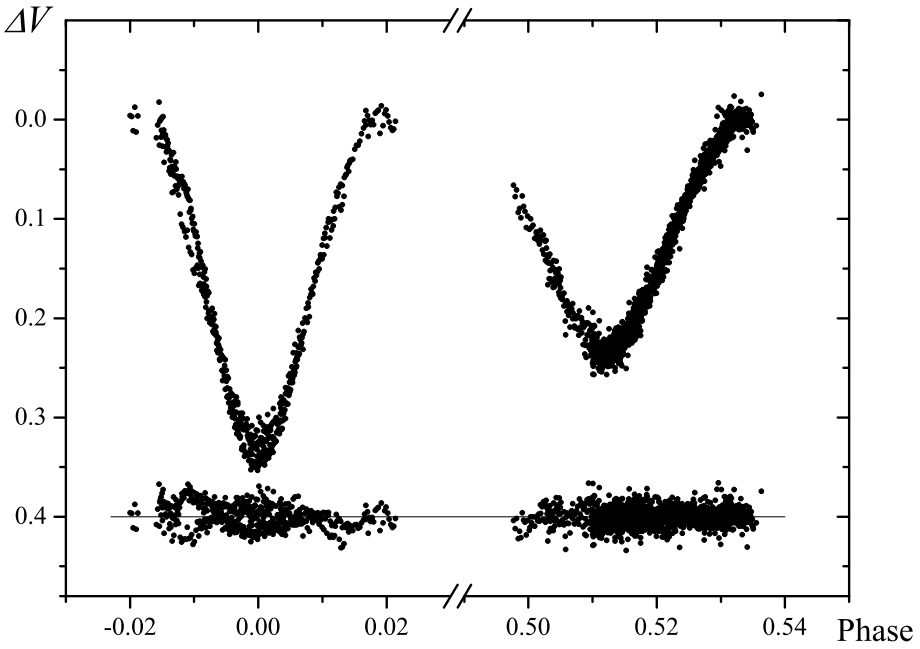

Figure 1. The V observations for V839 Cep. Residuals from the best fit are shown at the bottom of the picture.

The phased LC for the star in the V-band is presented in Fig 1. The observations in $RI(RcIc)$-bands are not completed and will be published in a forthcoming paper. The solution of the LC's were performed by a method described in our previous works on this theme, Volkov & Khaliullin (2002), Volkov & Volkova (2009) is presented in Table 1. We derived the absolute parameters

Table 1. The light curve solution. Parameters of the components: relative radii r_1, r_2, inclination i, eccentricity e, periastron longitude ω, luminosity of main component L_1, third light L_3, limb darkening coefficients u_1, u_2 and error σ.

Parameter	Primary
r_1	0.050 ± 0.001
r_2	0.074 ± 0.001
i (deg)	88.15 ± 0.02
e	0.112 ± 0.003
ω (deg)	80.4 ± 0.8
$L_1 = 1 - L_2 - L_3$	0.267 ± 0.003
L_3	0.269 ± 0.003
$u_1 = u_2$	0.29
σ (mag)	0.0097

of the binary using a non-direct method of Volkov et al. (2017). We derived the temperatures of the components from the $(U - B,\ B - V)$ diagram. We used the Flower (1996) calibration. The results are presented in Table 2.

Table 2. The absolute parameters derived by the non-direct method.

Parameter	Primary	Secondary
M ($M_\odot$)	3.3 ± 0.2	4.4 ± 0.3
R ($R_\odot$)	1.9 ± 0.1	2.9 ± 0.1
$\log g$	4.39 ± 0.04	4.17 ± 0.04
$T(K)$	$14150 \pm (300)$	$15700 \pm (300)$
M_{bol}	-0.47 ± 0.07	-1.77 ± 0.06
d (pc)	550 ± 40	

4. Apsidal motion

We present in Fig. 2 the ETV diagram for the object. We found by a least squares method P1 = $9.^d963364(3)$ and P2 = $9^d.963357(2)$. These values are sufficiently reliable to state that the system demonstrates the apsidal motion: $\dot{\omega}_{obs} = 0.027(9)\,\mathrm{deg\,yr^{-1}}$, $U = 13600(4500)$ years. The theoretical rate of the apsidal motion: $\dot{\omega}_{obs} = 0.021(5)\,\mathrm{deg\,yr^{-1}}$ is close to the obtained value.

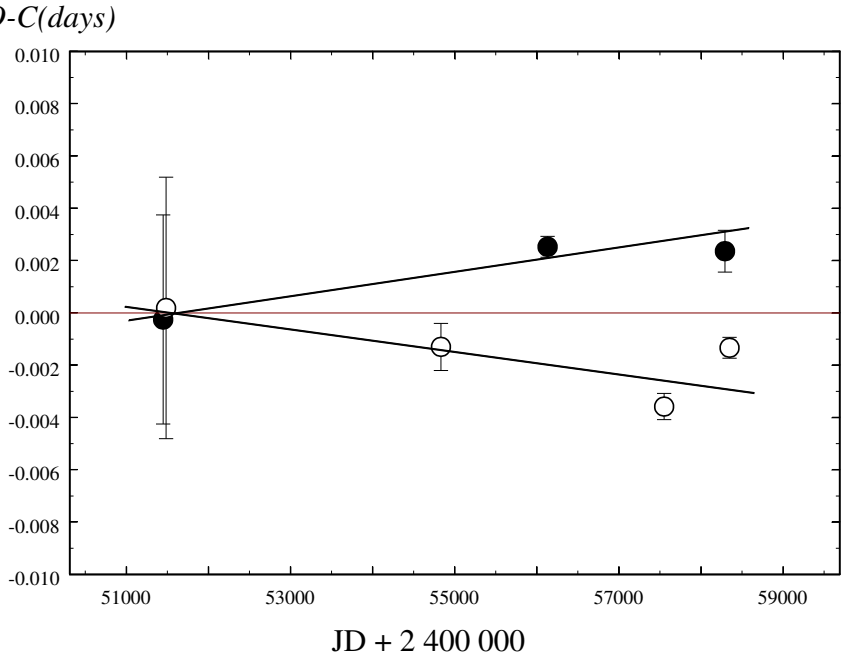

Figure 2. The ETV diagram, constructed with the mean from the P1 and P2 periods for primary (filled circles) and secondary (open circles) minima times. The initial epochs are: Min I=HJD 2451448.6476(21), Min II=HJD 2451483.6403(12).

5. Conclusions

We found the absolute parameters of the components of the eclipsing binary V839 Cep and discovered the apsidal motion in the system. Due to the orientation of the elliptical orbit of the eclipsing star, a more luminous component is eclipsed in the shallow minimum. The analysis was strongly complicated by the physical variability of the dominant (more massive and luminous) component.

Acknowledgements.

This study was partly supported by the scholarship of the Slovak Academic Information Agency (IMV, ASK), RNF grant 14-12-00146, RFBR grant 18-502-12025(IMV) and VEGA grant 2/0031/18 (DC).

References

Flower, P. J., Transformations from Theoretical Hertzsprung-Russell Diagrams

to Color-Magnitude Diagrams: Effective Temperatures, B-V Colors, and Bolometric Corrections. 1996, *Astrophys. J.*, **469**, 355, DOI: 10.1086/177785

Otero, S. A., Wils, P., Hoogeveen, G., & Dubovsky, P. A., 50 New Eccentric Eclipsing Binaries Found in the ASAS, Hipparcos and NSVS Databases. 2006, *Information Bulletin on Variable Stars*, **5681**

Volkov, I. M., Chochol, D., Grygar, J., Mašek, M., & Juryšek, J., Orbital period changes in RW CrA, DX Vel and V0646 Cen. 2017, *Contributions of the Astronomical Observatory Skalnate Pleso*, **47**, 29

Volkov, I. M. & Khaliullin, K. F., Apsidal Motion in the Eclipsing Binary GG Ori. 2002, *Astronomy Reports*, **46**, 747, DOI: 10.1134/1.1508067

Volkov, I. M. & Volkova, N. S., The physical parameters and orbit of the eclipsing binary system GSC 4596 1254 = SAO 3282. 2009, *Astronomy Reports*, **53**, 136, DOI: 10.1134/S106377290902005X

Contrib. Astron. Obs. Skalnaté Pleso **49**, 439 – 443, (2019)

Cool spotted binary system IN Vir (HD116544)

I.M. Volkov[1,2], A.S. Kravtsova[2], T. Pribulla[3], J. Budaj[3], Z. Garai[3], Ľ. Hambálek[3], R. Komžík[3] and E. Kundra[3]

[1] *Institute of Astronomy, Russian Academy of Sciences, Pyatnitskaya Str., 48, 109017 Moscow, Russia, (E-mail: hwp@yandex.ru)*

[2] *Sternberg Astronomical Institute, Lomonosov Moscow State University, Universitetskij Ave. 13, 119992 Moscow, Russia*

[3] *Astronomical Institute of the Slovak Academy of Sciences 059 60 Tatranská Lomnica, The Slovak Republic*

Received: October 31, 2018; Accepted: February 28, 2019

Abstract. High-precision spectral and photometrical observations of the binary IN Vir were carried out during 2015-2018. Basic geometrical and physical parameters were derived. The multicolour photometry made it possible to estimate the orbital inclination of the system, the size and the temperature of the cold spots. Solar like cycles due to chromospheric activity were found. Light Curves (LC)'s form changes with time.

Key words: stars: individual: IN Vir – stars: binaries – methods: observational – techniques: spectroscopy, techniques: photometry

1. Introduction

IN Vir is an X-ray source discovered by EXOSAT (Giommi et al., 1991). The optical variability of the star with the period of 8.15 days was found by Cutispoto et al. (1992). The star was classified as an RS CVn variable with K4 IV + G8 V components. A Doppler-imaging analysis was used to construct a map of spots on the surface of the cooler component (Strassmeier, 1997). The period of the spectral binary from the radial velocity curve was derived as $8^d.22$.

2. Échelle spectroscopy

Medium and high-dispersion spectroscopy of IN Vir was obtained with two spectrographs. At the Stará Lesná observatory observations were performed in the G1 pavilion using a 60 cm, f/12.5 Zeiss Cassegrain telescope equipped with a fiber-fed échelle spectrograph eShel (see Thizy & Cochard, 2011; Pribulla et al., 2015) and having a maximum resolving power of R 11 000. The observations were also performed with a 1.3 m, f/8.36, Nasmyth-Cassegrain telescope, equipped with a fiber-fed échelle spectrograph, at the Skalnaté Pleso observatory.

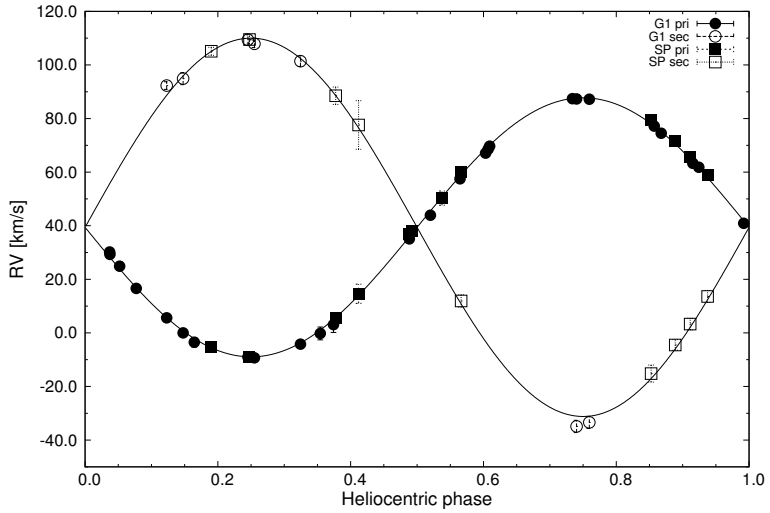

Figure 1. RV measurements of the primary and secondary component of IN Vir

3. CCD photometry

Photometrical observations were made in 100+ nights during 2015-2018 with the Zeiss-600 and Zeiss-1000 telescopes in Simeiz Observatory on Mt. Koshka (Crimea). We used a CCD camera FLI PL09000 with the $BV(RI)c$ filter set mounted at a 1 m reflector and the VersArray512UV camera with $UBVRI(Rc)$ filters at a 60 cm telescope. We've obtained measurements in 100+ nights in four years. We analyzed photometric data using the methods described in our earlier works (see Volkov & Volkova, 2009). All observations were corrected for differential atmospheric extinction.

4. Data Analysis

4.1. Broadening functions and radial velocities

Spectra of IN Vir were analyzed using the broadening-function (hereafter BF), a technique developed by Rucinski (1992). The BFs have been determined in the 4900-5510 Å spectral range (free of hydrogen Balmer lines and telluric lines) for both spectrographs. BFs were extracted using HD185144 (K0V) as the template. The extracted BFs clearly show two components: a fairly-rapidly-rotating primary and a faint slow-rotating secondary. To determine the radial velocities, the BFs were modelled by two limb-darkened rotational profiles (see Pribulla et al., 2015). The orbital period of the eclipsing pair was optimized. A circular orbit was assumed. The resulting best parameters are given in Table 1 and the corresponding fit is plotted in Fig. 1.

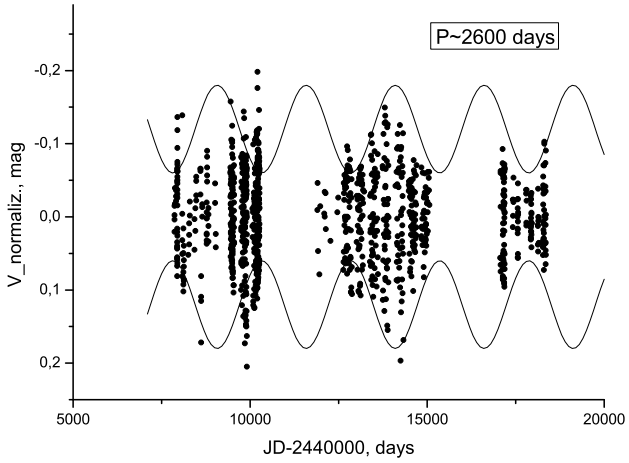

Figure 2. Long-term variability of IN Vir in V. Envelopes show solar-like activity cycles. The mean stellar magnitude is set equal to 0 for each year.

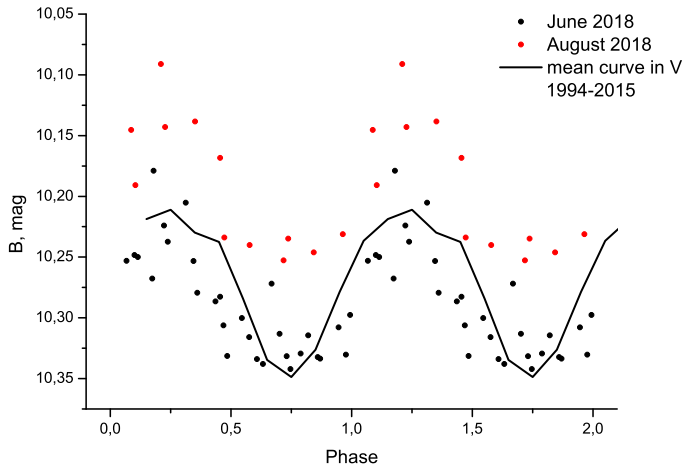

Figure 3. The B - LC during June to August 2018. It demonstrates a nearly flat bottom and narrow peak in maximum. Mean V - LC in 1994-2015 is also presented.

4.2. Photometric variability

We've determined the spectral class of IN Vir as K2 using our $UBVRI$ observations and Popper (1980) calibration. The value of interstellar extinction is nearly zero. We used Hipparcos, ASAS Pojmanski (2002), and Strassmeier (1997) data in combination with our V-observations. A general picture of the variability in V is presented in Fig. 2. The amplitude of the variability changes with time and resembles the chromospheric activity of the Sun. The approximate period of this activity is about 7 years.

Table 1. Spectroscopic elements of the primary and secondary components of IN Vir.

Parameter	Value	σ
P [d]	8.18977	0.00014
T_0 [HJD]	2 457 929.565	0.005
V_0 [km s^{-1}]	+39.38	0.15
K_1 [km s^{-1}]	48.35	0.21
K_2 [km s^{-1}]	70.6	0.6
q	0.685	0.007
$m_1 \sin^3 i$ [M$_\odot$]	0.848	0.016
$m_2 \sin^3 i$ [M$_\odot$]	0.581	0.007
$v_{1rot} \sin i_1$ [km s^{-1}]	24.6	0.5
$v_{2rot} \sin i_1$ [km s^{-1}]	≤ 8	
i [°]	55 - 68	
$r_1 \sin i$ [R$_\odot$]	4.1	0.2
$r_2 \sin i$ [R$_\odot$]	1.6	0.2

From 1994 to 2015, the photometric period, average brightness and the form of LC (not amplitude) remained unchanged. One can suppose a stable configuration of cold spots for 20 years. The photometric period of 8.1321 days during these years did not coincide with the orbital period. This probably indicates that the double system is not fully synchronized. The behavior of variability has changed in the last 2.5 years. At the present time we observe the active period with rapid changes in mean brightness (see Fig. 3).

Comparing the LCs in different bands and taking into account that there are no eclipses in the system, we derived the orbital inclination of the binary to be $55 - 68°$. Further we found that the spectrum of cold spots during the stable configuration corresponds to K5 and the spots occupy 24% of the surface.

5. Conclusions

Using high-precision spectral and photometric observations we have determined the reliable parameters of the binary system IN Vir: masses, velocities, sizes,

temperatures of the components, parameters of the orbit. The period of photometric variability is non-equal to the orbital one. The solar-like chromospheric activity of the K2 IV component is found. The star demonstrates long, till 20 years, intervals of a relatively stable configuration of the spots, and active periods with rapid changes on its surface.

Acknowledgements. The authors thank V. Kollár for his technical assistance. This work has been supported by the VEGA grant of the Slovak Academy of Sciences No. 2/01038/18, by the Slovak Research and Development Agency under the contract No. APVV-015-458 and by the realization of the Project ITMS No. 26220120009, based on the Supporting Operational Research and Development Program financed from the European Regional Development Fund (Pribulla); RFBR 11-02-01213a, 18-502-12025 grants, RNF grant 14-12-00146 (I.M.Volkov); scholarship of the Slovak Academic Information Agency SAIA (Volkov, Kravtsova).

References

Cutispoto, G., Pallavicini, R., Pasquini, L., Rodono, M., & Tagliaferri, G., Photometry of Serendipitous X-ray Sources Detected by EXOSAT. 1992, in Astronomical Society of the Pacific Conference Series, Vol. **26**, *Cool Stars, Stellar Systems, and the Sun*, ed. M. S. Giampapa & J. A. Bookbinder, 119

Giommi, P., Tagliaferri, G., Beuermann, K., et al., The EXOSAT high Galactic latitude survey. 1991, *Astrophys. J.*, **378**, 77, DOI: 10.1086/170408

Pojmanski, G., The All Sky Automated Survey. Catalog of Variable Stars. I. 0h-6h Quarter of the Southern Hemisphere. 2002, *Acta Astronomica*, **52**, 397

Popper, D. M., Stellar masses. 1980, *Ann. Rev. Astron. Astrophys.*, **18**, 115, DOI: 10.1146/annurev.aa.18.090180.000555

Pribulla, T., Garai, Z., Hambálek, L., et al., Affordable échelle spectroscopy with a 60 cm telescope. 2015, *Astronomische Nachrichten*, **336**, 682, DOI: 10.1002/asna.201512202

Rucinski, S. M., Spectral-line broadening functions of WUMa-type binaries. I - AW UMa. 1992, *Astron. J.*, **104**, 1968, DOI: 10.1086/116372

Strassmeier, K. G., Doppler imaging of stellar surface structure. III. The X-ray source HD 116544 = IN Virginis. 1997, *Astron. Astrophys.*, **319**, 535

Thizy, O. & Cochard, F., Spectrographs for small telescopes. 2011, in IAU Symposium, Vol. **272**, *Active OB Stars: Structure, Evolution, Mass Loss, and Critical Limits*, ed. C. Neiner, G. Wade, G. Meynet, & G. Peters, 282–283

Volkov, I. M. & Volkova, N. S., The physical parameters and orbit of the eclipsing binary system GSC 4596 1254 = SAO 3282. 2009, *Astronomy Reports*, **53**, 136, DOI: 10.1134/S106377290902005X

Contrib. Astron. Obs. Skalnaté Pleso **49**, 444 – 446, (2019)

Deep optical photometry of two nearby elliptical galaxies: NGC 4473 and NGC 4697

A. Vudragović and S. Samurović

Astronomical Observatory Belgrade, Serbia (E-mail: ana@aob.rs)

Received: October 17, 2018; Accepted: January 23, 2019

Abstract. We present deep optical photometry of two nearby elliptical galaxies, NGC 4473 and NGC 4697, obtained with a new 1.4m Milanković telescope, mounted at the Astronomical Station Vidojevica (Serbia). For both galaxies we derive surface brightness profiles up to 7 and 3 effective radii, respectively (limited solely by our field of view) to obtain deep color (B-V) gradients. Also, we perform 2D decomposition of galaxy images into Sersic components.
Key words: galaxies – photometry

1. Introduction

The problem of dark matter (DM) emerged from studies of galaxies and in the past decades a lot of effort has been put into constraining the amount of this invisible matter. In our paper (Samurović, S. and Vudragović, A. 2018, MNRAS, in press), we test Newtonian and MOND methodologies on two nearby early-type galaxies (ETGs, hereafter): NGC 4473 and NGC 4697. The motivation for obtaining deep photometry came from the fact that galaxy color can be used to compare the mass-to-light ratio from the stellar population synthesis (SPS) models to the estimated dynamical mass-to-light ratio. To that end, we obtained the images of NGC 4473 and NGC 4697 in the B- and V-band to infer their colors as far from the centre as possible.

2. Observations and data reduction

Observations of two targeted galaxies NGC 4473 and NGC 4697 were carried out in two wavelength bands (B and V) on three consecutive nights (19 - 21 April 2018) using an Apogee U42 CCD camera attached to the 1.4 m Milankovic telescope mounted at the Astronomical Station Vidojevica. We took 24 (22) images and 26 (23) images in B (V) band of NGC 4473 and NGC 4697 galaxy, respectively. Exposure time was 180s in most of the images and occasionally 300s.

Data reduction was done in IRAF, following the standard procedure. Astrometric solution was obtained using the Astrometry software (Lang et al., 2010). The mosaic creation was done with mscred package in IRAF, based on the astrometric solution. A list of stars was generated from mosaics in both B- and

V-band using Sextractor (Bertin & Arnouts, 1996). Aperture photometry was measured in IRAF with the phot task from the apphot package. Matching stars from The Fourth U.S. Naval Observatory CCD Astrograph Catalog (UCAC4: Zacharias et al., 2013) to the stars in our list, we have found 5 and 9 stars in common for NGC 4473 and NGC 4697, respectively and calculated magnitude zero-points.

3. Results

We obtained deep photometry in the B- and V-bands for NGC 4473 and NGC 4697 (Fig 1.). Previous (B-V) colors of these two galaxies were measured up to $\sim 3R_e$ for NGC 4473 (Idiart et al., 2002) and $\sim 1R_e$ for NGC 4697 (Poulain & Nieto, 1994). We have measured color of NGC 4473 and NGC 4697 up to $\sim 7R_e$ ($= 218''$) and $\sim 2.7R_e$ ($= 263''$), respectively.

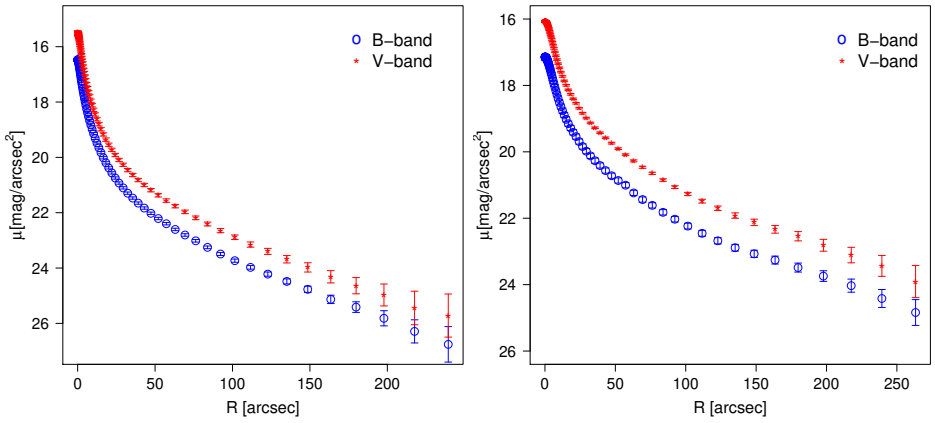

Figure 1. Surface brightness profiles of NGC 4697 and NGC 4473, from left to right. The B-band is marked with blue circles and the V-band with red stars.

Further, we used the Galfit code (Peng et al., 2010) to study the structure of these two galaxies in detail. Both galaxies are fitted with multicomponent Sersic profiles: NGC 4473 was successfully fitted with three Sersic components (two disks and a pseudo-bulge), while for NGC 4697 two Sersic components were sufficient to describe all the structure. Fitted parameters are listed in Table 1.

The interesting case of NGC 4473 requires further investigation: two Sersic components are aligned and this is often the case for fast rotators, but the third component that is orthogonal to these two components came as a surprise. This structure may be the ongoing merger and it would be interesting to analyze its chemical composition with respect to the other two components to see if it is of external origin.

Table 1. Best-fitting parameters in the V-band are given for both galaxies. Columns: (1) multiple Sersic components labeled with 1, 2 and 3 (the third component is presented only for NGC 4473), (2) effective surface brightness, (3) effective radius, (4) Sersic index, (5) minor-to-major axis ratio and (6) position angle of the galaxy measured in the counter-rotating direction from the vertical axis (north is up in the images).

Component	$\mu_{\rm eff}$ [mag/$''^2$]	$R_{\rm eff}$ [$''$]	n	b/a	PA
NGC 4473					$\chi^2 = 199$
Sersic1	19.00	12.8	2.71	0.51	94.51
Sersic2	22.20	67.8	0.99	0.59	92.79
Sersic3	20.18	6.5	1.05	0.87	176.09
NGC 4697					$\chi^2 = 12$
Sersic1	22.32	106.16	0.86	0.51	59.65
Sersic2	19.92	23.72	1.95	0.61	69.72

Acknowledgements. This work was supported by the Ministry of Education, Science and Technological Development of the Republic of Serbia through project no. 176021, "Visible and Invisible Matter in Nearby Galaxies: Theory and Observations". We acknowledge the financial support by the European Commission through project BELISSIMA (BELgrade Initiative for Space Science, Instrumentation and Modelling in Astrophysics, call FP7-REGPOT-2010-5, contract No. 256772). We thank the technical operators at the Astronomical Station Vidojevica (ASV), Miodrag Sekulić and Petar Kostić for their excellent work.

References

Bertin, E. & Arnouts, S., SExtractor: Software for source extraction. 1996, *Astron. Astrophys., Suppl.*, **117**, 393, DOI: 10.1051/aas:1996164

Idiart, T. P., Michard, R., & de Freitas Pacheco, J. A., New UBVRI colour distributions in E-type galaxies . I. The data. 2002, *Astron. Astrophys.*, **383**, 30, DOI: 10.1051/0004-6361:20011699

Lang, D., Hogg, D. W., Mierle, K., Blanton, M., & Roweis, S., Astrometry.net: Blind Astrometric Calibration of Arbitrary Astronomical Images. 2010, *Astron. J.*, **139**, 1782, DOI: 10.1088/0004-6256/139/5/1782

Peng, C. Y., Ho, L. C., Impey, C. D., & Rix, H.-W., Detailed Decomposition of Galaxy Images. II. Beyond Axisymmetric Models. 2010, *Astron. J.*, **139**, 2097, DOI: 10.1088/0004-6256/139/6/2097

Poulain, P. & Nieto, J.-L., UBVRI photoelectric photometry of bright southern early-type galaxies. 1994, *Astron. Astrophys., Suppl.*, **103**, 573

Zacharias, N., Finch, C. T., Girard, T. M., et al., The Fourth US Naval Observatory CCD Astrograph Catalog (UCAC4). 2013, *Astron. J.*, **145**, 44, DOI: 10.1088/0004-6256/145/2/44

Contrib. Astron. Obs. Skalnaté Pleso **49**, 447 – 449, (2019)

Search for dwarf galaxy candidates in M 106

A. Vudragović, S. Samurović and O. Vince

Astronomical Observatory Belgrade, (E-mail: ana@aob.rs)

Received: October 17, 2018; Accepted: February 21, 2019

Abstract. We present preliminary results of a search for dwarf galaxy candidates in the 24′ x 24′ field of view around M 106 galaxy. Total of 107 images were taken in the V-band with the new 1.4 m Milanković telescope (Serbia, near Prokuplje) and 27 images in the L-band. We confirm presence of the satellites from previous studies and find new candidate galaxies.

Key words: galaxies – satellites – photometry

1. Introduction

Nearby galaxies offer unique possibility to study their local environment in unprecedented details. To address the "missing satellites" problem, a systematic study of the low surface brightness objects is needed. Observations carried out using amateur telescopes with hours-long exposures revealed a plethora of dwarf galaxies in the Local Volume (Karachentsev et al., 2015).

We believe that there are numerous low surface brightness galaxies surrounding nearby massive galaxies yet to be discovered using long exposures with modest-sized telescopes. To that end, we have imaged the nearby galaxy M 106, searching for the possible low surface brightness satellite candidates.

2. Observations

We carried out observations in two wavelength bands (V and L) on three nights (11, 20 and 23 April 2018) using the Apogee U42 camera attached to the 1.4 m Milanković telescope mounted at the Astronomical Station Vidojevica. With our small field-of-view (FOV, hereafter) of 8.3′ × 8.3′, we created a mosaic of 3 × 3 images centered on the galaxy, to get 24′ × 24′ area around M 106 galaxy. In each intrinsic FOV we took 10 images dithered slightly (by 0′.3). And on the other nights, 27 images were taken again in V- and L-bands, respectively. Unfortunately, the number of 27 exposures of 180s across such a wide FOV wasn't enough to reduce the noise sufficiently. Finally, we have used 80 images in the V-band only, each of 180s exposure.

Data reduction was done in IRAF, following the standard procedure. Astrometric solution was obtained using Astrometry software (Lang et al., 2010). The mosaic creation was done using mscred package in IRAF, based on the astrometric solution. Objects were found and extracted using Sextractor (Bertin & Arnouts, 1996).

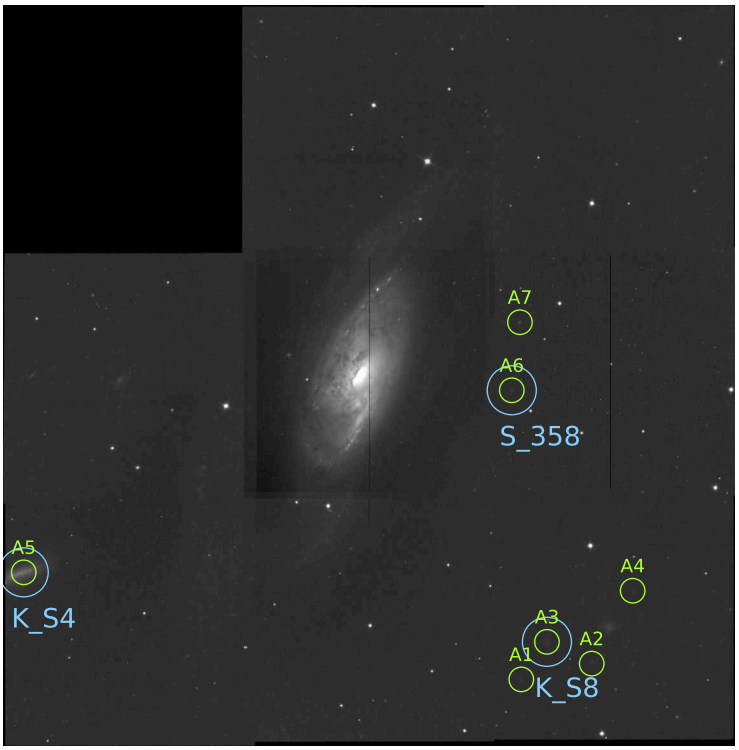

Figure 1. V-band image: Potential satellite galaxies are marked with smaller green circles. Larger blue circles correspond to the previously known satellites (see Table 1).

3. Results

Celestial coordinates of satellite candidates were cross-matched against the SDSS DR14 photometric catalog to get $g - r$ color. We had two requests for candidate galaxies: (1) color $g-r < 0.8$, to exclude possible background galaxies (Fukugita et al., 1995) and (2) a half-light Petrosian radius in the r-band $R_{50}{}^{r} > 3''$, which corresponds to 150 pc. In this way, the potential list of candidates was downsized to 6 objects, yet another candidate galaxy was added with $R_{50}{}^{r} = 2.5''$ (A7 object in Table 1), since it appears as an extended object and with the right color $g - r < 0.8$, it seems to be a plausible candidate. All candidates are marked in Fig 1 with green circles and are listed in Table 1. Large blue circles show objects that were found before: K_S4 and K_S8 are dwarves from Kim et al. (2011) and S_358 is a dwarf galaxy reported by Spencer et al. (2014).

It would be interesting in the future to obtain spectroscopic confirmation of candidate dwarf galaxies and to expand the FOV to at least half of the M 106 virial radius ($\sim 2^o \times 2^o \approx 260\text{kpc} \times 260\text{kpc}$), where most of the satellites should

Table 1. Galaxy candidates data: (1) Object labels same as in Fig 1., (2, 3) Celestial coordinates in the J2000 epoch, (4) objID from the SDSS DR14 photometric catalog, (5) Petrosian radius R_{50} in arcseconds in the r-band and (6) g-r color from the SDSS DR14 photometric catalog.

Name	RA [h:m:s]	DEC [d:m:s]	SDSS-DR14 objID	$R_{50}[''']$	g-r
A1	12:19:28.045	47:28:19.56	1237661434308329731	3.1	0.49
A2	12:19:41.887	47:27:50.55	1237661434308329632	3.0	0.25
A3	12:19:33.184	47:27:05.92	1237661434308329605	8.6	0.52
A4	12:19:50.121	47:25:27.18	1237661434308330070	3.2	0.49
A5	12:17:49.84	47:24:33.13	1237661434308198442	26.9	0.87
A6	12:19:27.353	47:18:43.93	1237661434308329730	3.9	0.4
A7	12:19:29.290	47:16:28.28	1237661357007503592	2.5	0.33

reside (Moore et al., 1999).

Acknowledgements. This work was supported by the Ministry of Education, Science and Technological Development of the Republic of Serbia through project no. 176021, "Visible and Invisible Matter in Nearby Galaxies: Theory and Observations". We acknowledge the financial support by the European Commission through project BELISSIMA (BELgrade Initiative for Space Science, Instrumentation and Modelling in Astrophysics, call FP7-REGPOT-2010-5, contract No. 256772). We thank the technical operators at the Astronomical Station Vidojevica (ASV), Miodrag Sekulić and Petar Kostić, for their excellent work.

References

Bertin, E. & Arnouts, S., SExtractor: Software for source extraction. 1996, *Astron. Astrophys., Suppl.*, **117**, 393, DOI: 10.1051/aas:1996164

Fukugita, M., Shimasaku, K., & Ichikawa, T., Galaxy Colors in Various Photometric Band Systems. 1995, *Publ. Astron. Soc. Pac.*, **107**, 945, DOI: 10.1086/133643

Karachentsev, I. D., Riepe, P., Zilch, T., et al., New low surface brightness dwarf galaxies detected around nearby spirals. 2015, *Astrophysical Bulletin*, **70**, 379, DOI: 10.1134/S199034131504001X

Kim, E., Kim, M., Hwang, N., et al., A wide-field survey of satellite galaxies around the spiral galaxy M106. 2011, *Mon. Not. R. Astron. Soc.*, **412**, 1881, DOI: 10.1111/j.1365-2966.2010.18022.x

Lang, D., Hogg, D. W., Mierle, K., Blanton, M., & Roweis, S., Astrometry.net: Blind Astrometric Calibration of Arbitrary Astronomical Images. 2010, *Astron. J.*, **139**, 1782, DOI: 10.1088/0004-6256/139/5/1782

Moore, B., Ghigna, S., Governato, F., et al., Dark Matter Substructure within Galactic Halos. 1999, *Astrophys. J., Lett.*, **524**, L19, DOI: 10.1086/312287

Spencer, M., Loebman, S., & Yoachim, P., A Survey of Satellite Galaxies around NGC 4258. 2014, *Astrophys. J.*, **788**, 146, DOI: 10.1088/0004-637X/788/2/146

Contrib. Astron. Obs. Skalnaté Pleso **49**, 450 – 452, (2019)

A highly eccentric spectroscopic binary star: HD 5624

M. Yılmaz[1], S.O. Selam[1], H. Izumiura[2], I. Bikmaev[3], B. Sato[4], V. Keskin[5] and E. Kambe[2]

[1] *Ankara University, Dep. of Astronomy and Space Sciences, Ankara, Turkey*

[2] *Okayama Astrophysical Observatory, Honjo, Okayama, Japan*

[3] *Kazan Federal University, Dep. of Astronomy and Satellite Geodesy, Kazan, Russia*

[4] *Tokyo Institute of Technology, Ookayama, Meguro-ku, Tokyo, Japan*

[5] *Ege University, Dep. of Astronomy and Space Sciences, İzmir, Turkey*

Received: October 26, 2018; Accepted: January 16, 2019

Abstract. In this study, we present an orbital solution for precise radial velocity (PRV) measurements of HD 5624. We obtained high resolution spectroscopic data using the Coude Echelle Spectrograph (CES) equipped with an iodine (I_2) absorption cell to the 1.5 m RTT150 telescope at TÜBİTAK National Observatory (TUG) and performed a spectroscopic analysis to obtain orbital parameters. The best fit Keplerian orbit was obtained with an eccentricity of $e = 0.64$, the mass of the companion is less than $0.5 M_{\odot}$ and a period of $P = 2392$ days.

Key words: stars – spectroscopic binary – radial velocity

1. Introduction

Since the first discovery of a planetary companion around a solar-like star in 1995 (Mayor & Queloz, 1995), more than 3700 exoplanets have been discovered (see `http://exoplanet.eu/`) and their number is still increasing every year. However, many exoplanet surveys have been focused on G and K type main sequence stars. However, planetary systems in more massive stars, especially around intermediate-mass stars ($1.3-5 M_{\odot}$), are particularly important for improving the giant planet formation theory and constraints on the time scale. Also, planets around intermediate-mass stars provide a snapshot of the changes in a dynamical configuration of the planetary system during evolution of the host star. Based on this motivation, we started in 2007 a precise Doppler survey at TUG within the framework of an international collaboration between Turkey, Russia, and Japan. For the past ten years, we have been monitoring the RV measurements of 50 G−K type giants and found that a few stars show significant radial velocity variations between 1 and 10 $\mathrm{km\,s^{-1}}$ (Yılmaz et al., 2017).

In this study, we present precise RV measurements and preliminary orbital characteristic of the HD 5624 giant star for the first time.

2. Observations and data reduction

PRV observations of HD 5624 were obtained using the CES equipped with an I_2-cell to the 1.5 m RTT150 telescope at TUG. The CES spectra covered a wavelength region from 3500 Å to 8000 Å, with resolving power $R \sim$55000. We obtained signal-to-noise ratios S/N = 70-120 per pixel, with an exposure time of 1800 seconds for the target.

The extraction of echelle data from raw CCD images was carried out using the IRAF software packages in the standard way. Following the data reduction, precise RV measurements of the target were derived from the observed star $+I_2$ spectrum using a specific IDL code, which is based on the analysis technique described by Butler et al. (1996).

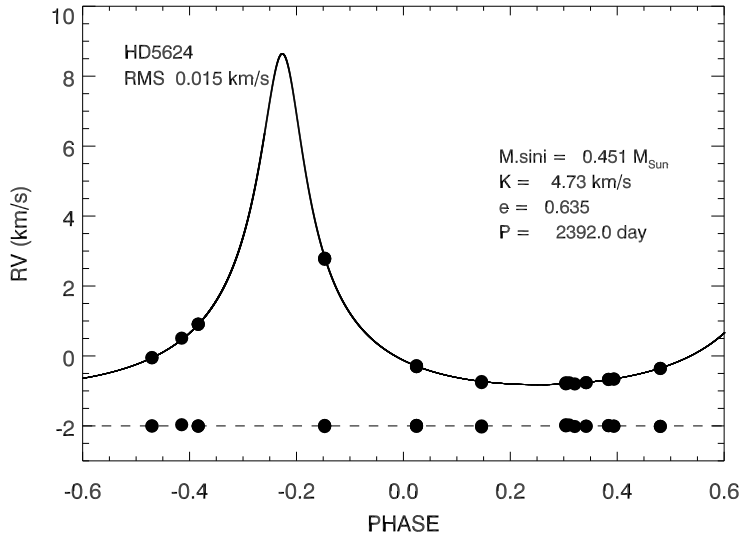

Figure 1. The radial velocities and the best Keplerian orbit (solid line) for HD 5624.

3. Analysis

RV data of HD 5624 show a variability of about 5 km s^{-1}, which indicates that this star is most probably a spectroscopic binary. There are no clear spectroscopic indications for binarity of this star in the literature before. Therefore, we performed the Lomb-Scargle (L-S) periodogram analysis to search for periodicity in the observed RV data first and found a significant periodicity at 2400 days, with a confidence level higher than 99.9% .

In order to obtain orbital parameters of the target, we used the RVLIN code (Wright & Howard, 2009). The best fit Keplerian orbit was obtained with an eccentricity of $e = 0.64$ and a period of 2392 days by estimating the stellar mass

Table 1. Orbital parameters for HD 5624.

Parameter	value	error
P (days)	2392	4.5
K_1 ($\mathrm{km\,s^{-1}}$)	7.73	1.19
e	0.63	0.06
ω (deg)	2.45	0.76
T_p (BJD-2450000)	8383.56	4.31
$m_2 \sin i$ ($M_\odot$)	0.45	0.08
a (AU)	4.62	0.07
RMS ($\mathrm{m\,s^{-1}}$)	15	-

to be 1.85 $M_\odot$. Uncertainties of the orbital parameters were derived using the bootstrapping procedure (see Table 1). The *rms* of the residuals to the best Keplerian fits are about 15 ms^{-1}, which is in the agreement with our radial precision.

4. Conclusion and discussion

It has been understood from the RV measurements of this star that the target shows extremely large RV variation. The analysis of the RV measurements indicates that the most likely origin of the observed periodicity is the Keplerian motion of the companion. This star is most probably a member of a binary star. The mass of the companion is less than $0.5M_\odot$ and has a highly eccentric (e $\sim$0.64) orbit. The derived orbital parameters are listed in Table 1.

Acknowledgements. This work was supported by The Scientific and Technological Research Council of Turkey (TÜBİTAK), the project number 114F099. The authors would like to thank both TÜBİTAK National Observatory (TUG) and KFU for supports in using RTT150.

References

Butler, R. P., Marcy, G. W., Williams, E., et al., Attaining Doppler Precision of 3 M s-1. 1996, *Publ. Astron. Soc. Pac.*, **108**, 500, DOI: 10.1086/133755

Mayor, M. & Queloz, D., A Jupiter-mass companion to a solar-type star. 1995, *Nature*, **378**, 355, DOI: 10.1038/378355a0

Wright, J. T. & Howard, A. W., Efficient Fitting of Multiplanet Keplerian Models to Radial Velocity and Astrometry Data. 2009, *Astrophys. J., Suppl.*, **182**, 205, DOI: 10.1088/0067-0049/182/1/205

Yılmaz, M., Sato, B., Bikmaev, I., et al., A Jupiter-mass planet around the K0 giant HD 208897. 2017, *Astron. Astrophys.*, **608**, A14, DOI: 10.1051/0004-6361/201731184

Contrib. Astron. Obs. Skalnaté Pleso **49**, 453 – 455, (2019)

Photometric investigation of contact binaries near the short period limit – 1SWASPJ161335.80-284722.2.

M. Zejda[1], S.-B. Qian[2,3], L.-Y. Zhu[2,3] and X.-H. Fang[2,3]

[1] *Department of Theoretical Physics and Astrophysics, Masaryk University, Kotlářská 2, CZ 611 37 Brno, Czech Republic*

[2] *Yunnan Observatories, Chinese Academy of Sciences, P.O. Box 110, Kunming, 650216, People's Republic of China*

[3] *Key laboratory of the structure and evolution of celestial objects, Chinese Academy of Sciences, P.O. Box 110, Kunming, 650216, People's Republic of China*

Received: December 17, 2018; Accepted: February 27, 2019

Abstract. A new period distribution of W UMa type (EW) contact binaries indicates that the short-period limit for EWs is around 0.2 days. Close binary stars with orbital periods near to this limit are an important source to understand the formation and evolution of contact binaries. Recently, some close binary stars with orbital periods in the range of 0.2 to 0.23 days were monitored and their light curves were analyzed using the W-D method. We present here one example of such studies – an analysis of 1SWASPJ161335.80-284722.2, its photometric solutions and period changes.

Key words: contact binary – photometry

1. Introduction

W UMa type contact binaries consist of two cool components and they share a common convective envelope. Both components are late evolutive main-sequence stars, spectral types usually F to K. They have nearly the same effective temperature, although their masses are usually quite different. The exhibited light curves are continuous and have a small difference between the eclipse depths of the two minima, and the depths usually change a little with wavelength variation. Binnendijk (1970) described two subtypes of W UMa systems. The two categories evolve in a similar way but under different circumstances. The details of evolution in contact relation between A- and W-type were discussed several times, e.g. Gazeas & Stepien (2008). However, the complex solution is still missing.

Rucinski (1992) found that the period distribution of main sequence contact binaries shows a sharp cut-off at about 0.22 days. During the last two decades several systems with shorter period have been unveiled. A recent study by Qian et al. (2017) indicates that the short-period limit for EWs is around 0.20 days.

We analyse the period distribution in the VSX database (2018) and in several surveys ASAS[1], CRTS[2], KEPLER[3] and OGLE BLG[4]. The result, displayed in Figure 1, is influenced by a different selection effect, however the most numerous surveys show similar results, which confirmed the 0.20 d value.

The study of short-period close binaries ($P \leq 0.22$ d) is still important. It is crucial to understand the evolution of low mass stars and to investigate the cause of the period cut-off.

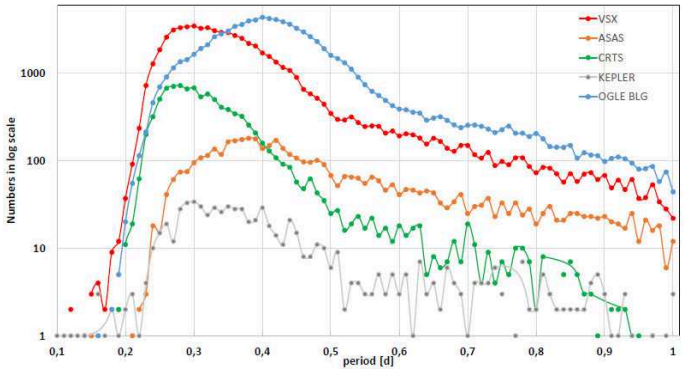

Figure 1. Numbers of EWs contact binaries in the VSX and selected surveys.

2. 1SWASPJ161335.80-284722.2

J161335 is a W-subtype of a late-type W UMa close binary with a very short orbital period. Its variability was reported first by Norton et al. (2011), who presented light curves and periods of 53 candidates for short period eclipsing binaries identified by SuperWASP. Lohr et al. (2012) revised the orbital period as 19852.817 s (= 0.22977796 d) and pointed out that the orbital period is decreasing as $\dot{P}/P$=-3.210^{-6} yr^{-1}.

CCD photometric observations of the system J161335 were obtained in 2015-2016, using the 2.4-m Thai National Telescope and 1-m telescope at the South African Astronomical Observatory. Analysing these data we obtained six sets of photometric parameters using the W-D program. Some deviations between the 2015 and 2016 results may be caused by the uncertain activity of a dark spot. The photometric solutions obtained in 2016 were averaged as the final results. It suggests that J161335 is a W-type contact binary with a fill-out factor nearly = 18.9 %. The less massive component holds an approximately 200 K higher temperature than the more massive one. By considering the spectral type of

[1]http://www.astrouw.edu.pl/asas/
[2]http://nesssi.cacr.caltech.edu/DataRelease/
[3]https://keplerscience.arc.nasa.gov/
[4]http://ogle.astrouw.edu.pl/

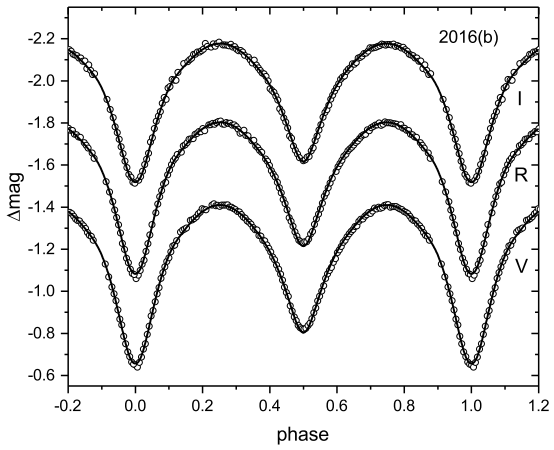

Figure 2. A fit of our observations made in 2016 to the theoretical light curves calculated by using the W-D code. The phases of those observations were calculated with the following linear ephemeris, Min I = HJD 2457117.42272 + 0.229778 × E. (Eq. 1).

the more massive component K7, its mass can be estimated as $M_2 = 0.61 M_\odot$. The derived average mass ratio $q = 1.10$ reveals that the mass of the other component is $M_1 = 0.55 M_\odot$. The detailed parameters will be published soon.

Furthermore, the analysis of an O-C diagram shows not only a decreasing period, but also small amplitude cyclic variations ($P_3 = 4.65$ years) caused very probably by a third, low-mass ($M_3 \sin i = 0.138(7) M_\odot$), very cool stellar companion.

Acknowledgements. This work is partly supported by the Grant Agency of the Czech Republic 16-01116S, the National Natural Science Foundation of China (Nos. 11573063, 11611530685) and the Key Science Foundation of Yunnan Province (No. 2017FA001). The authors would like to thank Dr. M. E. Lohr for kindly providing the timings of eclipses inferred from the SuperWASP data.

References

Binnendijk L.: 1970, *VA* **12**, 217

Gazeas, K., Stepien, K.: 2008, *Mon. Not. R. Astron. Soc.* **390**, 1577

Lohr, M. E., Norton, A. J., Kolb, U. C., et al.: 2012, *Astron. Astrophys.* **542**, A124

Norton, A. J., Payne, S. G., Evans, T., et al.: 2011, *Astron. Astrophys.* **528**, A90

Qian, S. B., Zhang, B., Soonthornthum, B., et al.: 2015, *Astron. J.* **150**, 117

Qian S.-B., He J.-J., Zhang J., et al.: 2017, *RAA* **17**, 087

Rucinski, S.M.: 1992, *Astron. J.* **103**, 960

URL: Variable Star Index, `http://cdsarc.u-strasbg.fr/viz-bin/cat/B/vsx`

Contrib. Astron. Obs. Skalnaté Pleso **49**, 456 – 458, (2019)

Progress in optical monitoring of a sample of FR II-type QSOs

S. Zola[1,2], G. Bhatta[1], A. Kuzmicz[3], M. Jamrozy[1], W. Ogloza[2], M. Drozdz[2], M. Siwak[2], G. Stachowski[2], D.E. Reichart[4] and D.B. Caton[5]

[1] *Astronomical Observatory, Jagiellonian University, ul. Orla 171, 30-244 Krakow, Poland (E-mail: szola@oa.uj.edu.pl)*

[2] *Mt. Suhora Observatory, Pedagogical University, ul. Podchorazych 2, 30-084 Krakow, Poland*

[3] *Center for Theoretical Physics, Polish Academy of Sciences, Al. Lotnikow 32/46, 02-668 Warsaw, Poland*

[4] *University of North Carolina at Chapel Hill, Chapel Hill, North Carolina NC 27599, USA*

[5] *Dark Sky Observatory, Department of Physics and Astronomy, Appalachian State University, Boone, NC 28608, USA*

Received: October 29, 2018; Accepted: February 25, 2019

Abstract. We present results derived from a monitoring program of a sample of FR-II type radio quasars. The variabilities detected in their densely covered light curves, which have being gathered over a period of more than 9 years, are analyzed with statistical methods (LSP and WWZ). We found no statistically significant, strictly coherent periodicities in our data.

Key words: galaxies: photometry – galaxies: nuclei, – quasars:individual: J0713+3656, J0952+2353, J1007+1248, HB1156+631, HB1525+267, J1504+6856, HB1721+343, J2042+7508

1. Introduction

The variability of quasars over the entire electromagnetic spectrum became known soon after their discovery. Radio observations of optically selected samples of quasars showed that 10-40% of objects are powerful radio sources. The orientation of the radio jet axis toward us can have dramatic effects on the observed source structure, apparent jet speed, and other characteristics. At a large inclination angle the observed core-jet emission is largely depressed and generally weaker than the extended steep-spectrum radio lobe emission, and as such a lobe-dominated radio quasar is observed. Several studies suggested that the flux changes may be correlated with the mass of the central supermassive black hole (e.g. Wilhite et al., 2007). Many observational projects were undertaken to study the quasars' variability with two approaches: the analysis of data from large surveys which provide data on numerous objects, or based on specific

samples of a smaller number of targets. In this project we follow the latter approach to investigate a small sample of carefully chosen radio-loud quasars. The selected quasars possess an extended (angular size $\lesssim$ 20") classical FRII (Fanaroff & Riley, 1974) radio morphology, i.e. core and two lobes that are ended with prominent hotspots. Since our sample of targets is seen at intermediate or high angles, the optical observations most likely represent the accretion disk emission (see Bhatta et al., 2018, for a discussion).

2. Optical observations

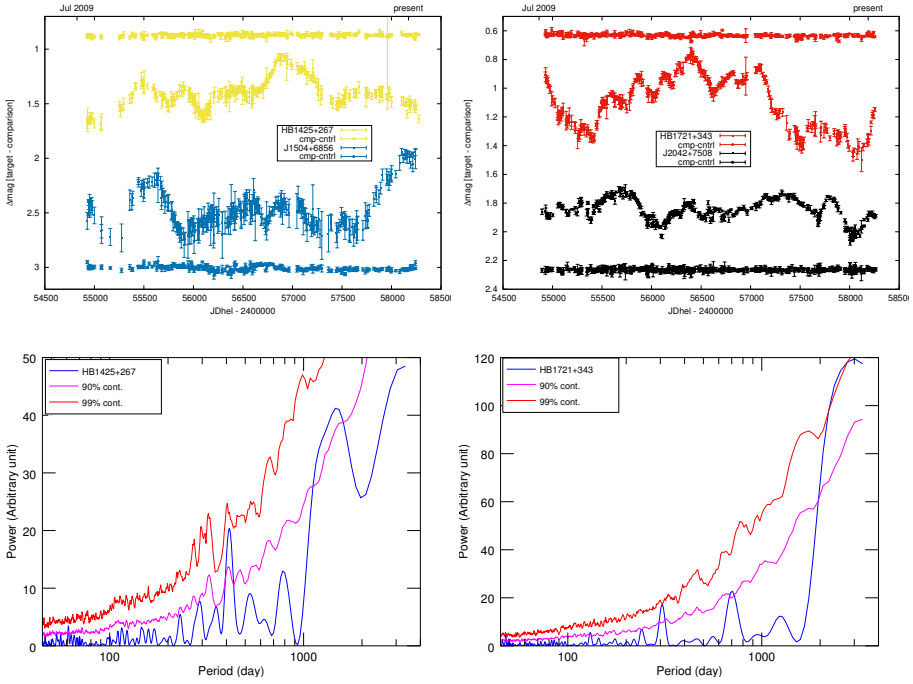

Figure 1. The light curves of four monitored radio-quasars in the R-filter(top panels). Lomb-Scargle periodograms of two sources are shown in the bottom panels.

We started an observing program aimed at long-term monitoring of a sample of 8 radio-quasars in 2009. The motivation for undertaking these observations have been given in detail in Zola et al. (2012). The chosen sample consists of objects located in the northern hemisphere, bright enough to allow photometric measurements with small telescopes with an accuracy better than a few hundredths of a magnitude. Observations in the R-filter are being taken primarily with two telescopes located in Poland: the 60 cm reflector at the Mt. Suhora Observatory of the Pedagogical University and the 50 cm Cassegrain telescope of the Astronomical Observatory of the Jagiellonian University in Krakow. To

avoid large gaps in the case of cloudy weather at the Polish sites, we gather data with two telescopes operated by the SKYNET Robotic Telescope Network: DSO-17 (40 cm) and/or RRRT (60 cm). The light curves of four targets, spanning more than 9 years, are shown in Fig. 1 (top panels).

3. Preliminary results from statistical analysis of light curves

Two standard tools were applied to reveal possible coherent periods in the runs: the Lomb-Scargle periodogram (Lomb, 1976; Scargle, 1982) and Weighted Wavelet Z-transform (WWZ; Foster, 1996) The statistical significance of the spectral features observed in the LSP were estimated using the Monte Carlo simulations method described by Timmer & Koenig (1995). A large number of light curves were simulated using the power spectral slope of 1.4 (see Bhatta et al., 2018) and subsequently sampled similarly to real observations. The 90% and 99% confidence contours for two our targets are shown in the bottom panels of Fig. 1 by the magenta and red lines, respectively. Our preliminary analysis indicates that the lower frequency spectral features primarily show the underlying red noise and none of the peaks exceed the 99% confidence level.

Acknowledgements. This work was partially supported by the NCN grants No: 2017/26/D/ST9/01178 (GB) and 2018/29/B/ST9/01793 (SZ and MJ).

References

Bhatta, G., Stawarz, L., Markowitz, A., et al., Signatures of the Disk–Jet Coupling in the Broad-line Radio Quasar 4C+74.26. 2018, *The Astrophysical Journal*, **866**, 132

Fanaroff, B. L. & Riley, J. M., The morphology of extragalactic radio sources of high and low luminosity. 1974, *Mon. Not. R. Astron. Soc.*, **167**, 31P

Foster, G., Wavelets for period analysis of unevenly sampled time series. 1996, *Astron. J.*, **112**, 1709, DOI: 10.1086/118137

Lomb, N. R., Least-squares frequency analysis of unequally spaced data. 1976, *Astrophys. Space Sci.*, **39**, 447

Scargle, J. D., Studies in astronomical time series analysis. II - Statistical aspects of spectral analysis of unevenly spaced data. 1982, *Astrophys. J.*, **263**, 835

Timmer, J. & Koenig, M., On generating power law noise. 1995, *Astron. Astrophys.*, **300**, 707

Wilhite, B. C., Brunner, R. J., Schneider, D. P., & Vanden Berk, D. E., The Effect of Variability on the Estimation of Quasar Black Hole Masses. 2007, *Astrophys. J.*, **669**, 791

Zola, S., Kuzmicz, A., Jamrozy, M., et al., Optical monitoring of FRII-type radio quasars. 2012, *The Bulletin of the Astronomical Society of India*, 239

Contrib. Astron. Obs. Skalnaté Pleso **49**, 459 – 461, (2019)

Improvement of positional accuracy of Solar system bodies ground-based observations with CCD-imaging of close approaches of them with Gaia stars

D.A. Bikulova

Pulkovo observatory of the Russian Academy of Sciences, Saint-Petersburg, Russia

Received: October 24, 2018; Accepted: February 13, 2019

Abstract. Current release of the Gaia mission provides representation of a new reference frame on an unprecedent level of accuracy. This astrometric catalogue is practically free of systematic errors with respect to astrometric ground-based observations. First applications Gaia DR1 and Gaia DR2 as a reference in an analysis of CCD-observations of asteroids and planetary satellites demonstrated small decrease of formal positional errors. The basic reasons are unaccounted systematic effects of telescope projection and offsets caused by atmospheric dispersion. As a result, positional error of the Solar system bodies' observations performed with the "Saturn" 1-m telescope at Pulkovo Observatory ($F/D = 4$) is in the range of 20 – 80 mas. A frame-to-frame astrometric transformation gives the error level less than 5 – 30 mas. One of possible ways to transfer subpixel accuracy to the final positions of the Solar system bodies are observations of close approaches of satellites or asteroids to the Gaia stars. The main idea is that systematic displacements caused by atmospheric effects and telescope optics that occur in close approaches (< 10 arcsec) are the same for asteroids and the Gaia stars. This makes it possible to significantly improve the quality of ground-based astrometry of the Solar system bodies, taking into account the fairly dense distribution of Gaia stars across the celestial sphere.

Key words: Solar system bodies – close approaches – astrometry

1. Introduction

Tidal evolution of planetary satellites' orbits and motion of asteroids in unstable resonances require the accuracy of astrometry of a 10 mas level. Traditional ground-based observations and processing technique mainly give us 50 - 100 mas. Improvement of the accuracy may be done with observations of the well known sort of events - close approaches of Solar system bodies to Gaia stars (Kopal, 1959). Gaia astrometry has provided us with dense and high precision realization of the reference frame to solve the mentioned task.

2. Observational program and technique of data analysis

Our objects of interest are planetary satellites and selected asteroids.

Planetary satellites:Jupiter: Europe, Ganymede, Callisto, Himalia, Elara, Pasiphae, Carme; Saturn: Mimas, Saturn-Enceladus, Tethys, Dione, Rhea, Titan, Hyperion, Iapetus, Phoebe, Janus, Epimetheus, Helene, Telesto, Calypso, Atlas, Prometheus, Pandora, Pan; Uranus: Ariel, Umbriel, Titania, Oberon; Neptune: Triton, Nereid.

Selected asteroids: Venus: 33342 1998 WT24, 322756 2001 CK32, 417217 2005 YS; Earth: 164207 2004 GU9, 419624 2010 SO16, 459872 2014 EK24, 439898 2000 TG2, 439908 2000 XH47, 449097 2012 UT68; Mars: 5261 Eureka, 121514 1999 UJ7, 311999 2007 NS2, 385250 2001 DH47, 391595 2007 UR2, 16834 1997 WU22, 83982 Crantor, 101429 1998 VF31, 154020 2002 CA10, 261938 2006 OB5, 359170 2009 CN5, 387505 1998 KN3, 439898 2000 TG2, 439908 2000 XH47, 449097 2012 UT68; Neptune: 309239 2007 RW10, 385571 Otrera, 385695 2005 TO74, 310071 2010 KR59, 316179 2010 EN65.

A simulated sum of exposures taken according to a scheme of such appulse observations of a typical asteroid is seen in the left panel of figure 1.

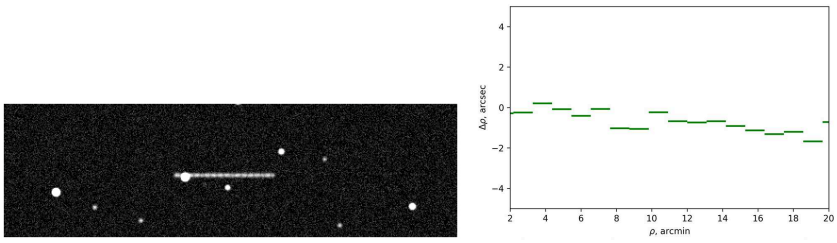

Figure 1. Left panel: Simulation of images taken during a close approach. Right panel: An analysis of several images taken with the Saturn 1-meter telescope (Pulkovo Observatory).

A shapelet decomposition was used for the celestial object image fitting. The efficiency of shapelet decomposition technique is demonstrated in many applications (i.e. Khovrichev et al., 2018).

A standard astrometric reduction of these images with Gaia DR2 as an astrometric calibrator has been done. As a result, residuals for angular distances between stars of each pair in the image were calculated. The right panel of figure 1 shows how the residuals depend on the value of angular distance. As we see, they systematically change with angular distance. This demonstrates advantage of astrometry of close approaches of asteroids to Gaia stars against traditional procedures of determination asteroids coordinates (Morgado et al., 2016).

The procedure of processing of the image taken for the case of close approaches of asteroids to Gaia stars is similar to the method of astrometry of binary stars (Buchheim, 2008).

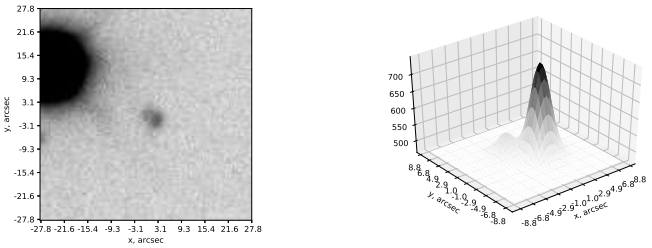

Figure 2. A close approach of U4 Oberon to Gaia2574476038004764800 at 2018-09-23T22:23:32.100 taken with the Saturn1m telescope of Pulkovo Observatory

An part of the CCD-frame taken during the close approach of U4 Oberon to the Gaia star($G = 14.964$) is shown in the left panel of figure 2. The right panel of this figure provides the results of the shapelet decomposition. The ρ value is 3.090 arcsec at the central moment. As a result, the positional accuracy of 10 mas was achieved.

3. Conclusions

The results of simulations and testing observations of appulses performed with the Pulkovo Observatory 'Saturn' 1m telescope demonstrates the high potential of the method considered. Presented technique (observations of appulses and shapelet decompositions) allows us to improve the positional accuracy of ground-based observations of Solar system bodies with small telescopes up to 5-10 mas. Appulse-based orbits of the objects of interest will be calculated as soon as necessary quantity of observations have been performed.

References

Buchheim, R. K., CCD Measurements of Visual Double Stars. 2008, *Society for Astronomical Sciences Annual Symposium*, **27**, 13

Khovrichev, M. Y., Apetyan, A. A., Roshchina, E. A., et al., Searching for Binary Systems Among Nearby Dwarfs Based on Pulkovo Observations and SDSS Data. 2018, *Astronomy Letters*, **44**, 103, DOI: 10.1134/S1063773718010024

Kopal, Z. 1959, *Close binary systems* (Chapman & Hall)

Morgado, B., Assafin, M., Vieira-Martins, R., et al., Astrometry of mutual approximations between natural satellites. Application to the Galilean moons. 2016, *Mon. Not. R. Astron. Soc.*, **460**, 4086, DOI: 10.1093/mnras/stw1244

Contrib. Astron. Obs. Skalnaté Pleso **49**, 462 – 468, (2019)

The role of small telescopes as a ground-based support for exoplanetary space missions

P. Kabáth[1], M. Skarka[1,2], S. Sabotta[3] and E. Guenther[3]

[1] *Astronomical Institute of the Czech Academy of Sciences 251 65 Ondřejov, The Czech Republic, (E-mail: petr.kabath@asu.cas.cz)*

[2] *Department of Theoretical Physics and Astrophysics, Masaryk Univerzity, Kotlářská 2, 61137 Brno, Czech Republic*

[3] *Thüringer Landessternwarte Tautenburg, Sternwarte 5, 07778 Tautenburg, Germany*

Received: November 6, 2018; Accepted: January 29, 2019

Abstract. Small telescopes equiped with modern instrumentation are gaining on importance, especially, in the era of exoplanetary space missions such as TESS, PLATO and ARIEL. A crucial part of every planet hunting mission is now a ground-based follow-up of detectd planetary candidates. Mid-sized telescopes with apertures of 2 to 4-m with an existing instrumentation become more and more valued due to increasing need for observing time.

In this paper, a brief overview on the follow-up process for exoplanetary space missions will be given. Requirements for the ground-based follow-up instrumentation will be discussed. Some of existing 2-m class telescope facilities and their capability and potential for the follow-up process of exoplanetary candidates will be presented. A special focus will be put on existing 2-m class telescopes in central Europe.

Key words: techniques: radial velocities – (stars:) planetary systems – techniques: spectroscopic

1. Introduction

The first exoplanetary space mission CoRoT was launched in 2006 and was dedicated to asteroseismology and exoplanets detection (Auvergne et al., 2009). CoRoT, a 28-cm aperture telescope equipped with 4 CCDs, has detected over 30 exoplanets. All CoRoT planets are fully characterized and their masses and radii are known with high accuracy. Furthermore, several hundreds of CoRoT candidates are still in the follow-up verification process. Among the first reported exoplanets was also at that time the smallest rocky planet CoRoT-7b (Léger et al., 2009). However, CoRoT space mission is also a great example to demonstrate the need for a ground-based follow-up for space missions, and especially, the need for medium-sized telescopes with up-to-date instrumentation. CoRoT instrument was equipped with prisms which were used with manufactured masks for the selected stars to provide colour information for the target stars. The extra information was useful for analyzing of stellar variability, but

the stellar PSF was spread over numerous pixels thus increasing the probability of false positive detections due to blends. Therefore, an extensive follow-up observing was performed with photometric and spectroscopic instruments (Deeg et al., 2009).

Mid-sized telescopes with apertures up to 4-m with Echelle spectrographs or CCD imagers played an important role in the follow-up process like in the case of CoRoT-7 (Pont et al., 2011). In the following section, the false positives rejection process will be described. The third section will present an example of a mid-sized telescope equipped with the Ondřejov Echelle Spectrograph (OES) and the Observatory in Ondřejov and how it can help as a ground-based support for space missions and future plans and outlook will be discussed in the Conclusions section.

2. Source and type of false positives

Once an exoplanetary candidate is reported from the space mission photometric data, where a transit was detected, the planet verification process begins. The initial task is to determine the stellar parameters such as temperature $T_{\rm eff}$ and stellar radius R. For this step, a mid-size telescope with medium resolution spectrographs can be of great help. Furthermore, we can obtain information about the spectral type of the star when the parameters are combined with e.g. Gaia data. This work can be performed with 2-m class telescopes and their instrumentation.

The next step is to determine the size of the planetary candidate from the combination of spectroscopic and photometric data. But still, the planetary candidate can be a false positive. This could be due to a contaminant, which is close to the target star and unresolved. Detailed follow-up with high resolution imaging is required. For such observations, typically larger telescopes with AO instruments are used (Schmitt et al., 2016). In some cases, contaminant stars are detected and the system is marked as a false positive. The transit can also happen on the contaminant system which leads to dillution of the transit depth (Ligi et al., 2018).

Another step is to determine the radial velocities in two opposite phases to analyze the radial velocity amplitude. From the amplitude determination, it can be decided about the nature of the system because typical radial velocity amplitudes of exoplanetary orgin are below km/s with some exceptions, such as WASP-18b (Hellier et al., 2009). If the candidate passes this test, it can be followed-up spectroscopically to determine radial velocities and thus then to obtain a mass limit and orbital parameters (Bouchy et al., 2009; Loeillet et al., 2008; Gandolfi et al., 2010; Léger et al., 2009). For the precise radial velocity measurements a stable instrument on all sizes of telescope apertures can be used. For small planets of Earth-size around solar type stars the required accuracy of radial velocity measurement is in cm/s regime limiting the avail-

able instrumentation (Pepe et al., 2010). However, Jupiter-sized planets can be followed-up by 2-m class telescopes comfortably, as was done also for the first exoplanet orbiting the solar type star 51 Peg (Mayor & Queloz, 1995). Later many planets were confirmed with the help of 2-m class telescopes (Endl et al., 2002; Döllinger et al., 2007).

Only after the last described step, the planet is fully characterized and we know its mass and radius. An interesting illustration why the follow-up process is so needed for space missions are the estimates of false positives provided for CoRoT by Almenara et al. (2009), for Kepler by Santerne et al. (2012); Fressin et al. (2013) and for TESS by Santerne et al. (2013). In addition, the PLATO space mission team estimated how much time is needed for the spectroscopic ground-based follow-up with different aperture sizes. The amount of time estimated for 2-m class telescopes is about 50 nights per year. In reality, perhaps much more time will be needed. Therefore, a 2-m class telescope with a decent spectrograph will be soon very valuable. Especially now, when the TESS space mission team delivered the first list with candidates and the first planet has already been confirmed Gandolfi et al. (2018).

3. Example of 2-m class facility

There are several 2-m class telescopes in Europe. The first exoplanet was detected by a 1.93-m telescope with the ELODIE instrument at the Observatoire de Haute Provence (Mayor & Queloz, 1995; Baranne et al., 1996). Another facility with a 2-m Alfred Jensch telescope at Thüringer Landessternwarte is located in Thuringia in Tautenburg, Germany. Another Zeiss built telescope of 2-m class is located at the Rozhen observatory in Bulgaria.

We present here the Perek 2-m telescope located at Ondřejov Observatory 30 kilometers southeast from Prague, Czech Republic. The Perek telescope was inaugurated as a second Zeiss telescope in 1967 and it is operated by the Czech Academy of Sciences. The location is characterized by typical central European weather and a typical amount of usable telescope time versus observed time is presented in Fig.1. Usually, the observing time when the telescope was open and science data were obtained is about 20-30 % of all nights per year, when the observing night is defined as with the Sun 12° below the horizon. Therefore, the available nights number is between 75-110. The typical seeing value for Ondřjov is between 2 – 3 arcsec. The telescope is equipped with two instruments, first being the single order spectrograph and the newer instrument Ondřejov Echelle Spectrograph (OES) with a slit used mainly for spectroscopic ground-based support of exoplanetary missions, such as K2, TESS and later PLATO and ARIEL. Fig.2 presents a comparison of similar instruments on 2-m class telescopes and their wavelength coverage and resolving power with HARPS/N instruments included for illustration.

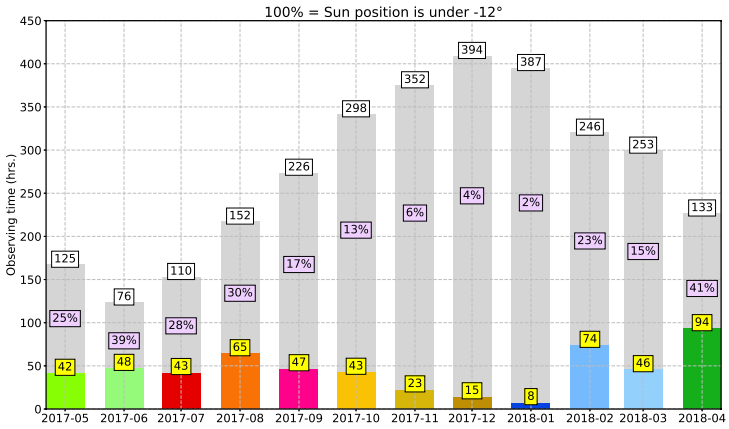

Figure 1. Yearly histogram of available hours of observing for 2017-2018 period (Sun 12° below the horizon) versus observed hours.

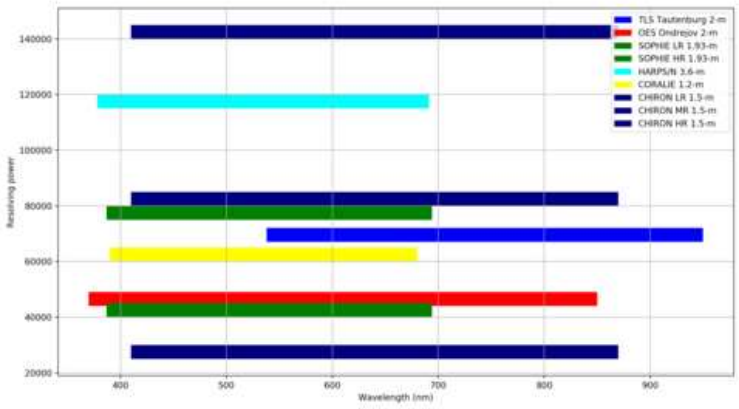

Figure 2. A representative sample of instruments used for exoplanet research on 2-m class telescopes with HARPS/N instruments presented for comparison.

Table 1. Instrumental characteristics of OES

Parameter	value
Slit width	2” on the sky
Spectral range	360–950 nm
Echelle	54.5 g/mm
Blaze angle (θ)	69°
Spectral resolution	50,000 (500 nm)
Limiting magnitude	13 Vmag

Brief characteristics of the OES spectrograph can be found in Tab. 1. OES can monitor a broad range of wavelengths from approximately 360 nm to 950 nm. The accuracy in radial velocities is demonstrated in Fig. 3 where measurement of a G-type radial velocity standard star HD109358 (V mag = 4.25) can be found. Typical accuracy over one night is better than 100 m/s and even a long term stability of radial velocity measurements spanning over one year is about 300 m/s, for more detail see Kabath et al. (2018), where also first scientific results of false positives rejection are presented. Typically, the performance for a star of V mag = $8-9$ of spectral type A is around 1 km/s, but this is of course due to the characteristics of the A stars. The limit of OES in terms of magnitudes is 12.5 mag obtained in 1.5 hrs. exposure with SNR 7.

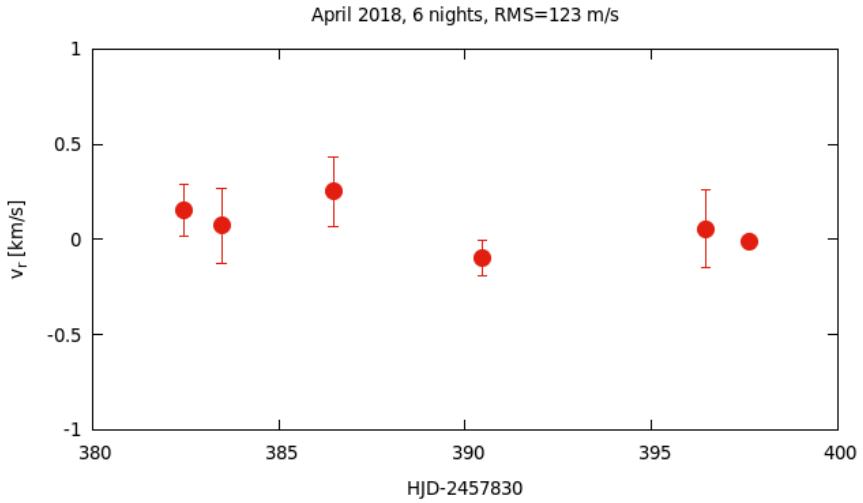

Figure 3. A radial velocity curve for 6 nights of spectroscopic time series for standard HD 109358. Data were taken over a period of 6 nights in April 2018. The RMS corresponds to 123 m/s.

These parameters make the OES spectrograph a valuable instrument for the ground-based support of exoplanetary space missions. The reached sensitivity offers a use of OES especially for a planetary candidate validation process and characterization of a small sample of hot Jupiters orbiting bright stars. Space mission TESS already delivered the first candidate alert list and the median brightness of the stars in the list is about 10.5 mag. In the first place, OES will be able to validate and contribute to characterization of a selected sample from TESS exoplanet candidates, which will be soon observable from the northern latitudes. The first confirmed TESS exoplanet has Vmag = 5.7 (Gandolfi et al., 2018). Therefore, a significant contribution is expected from all 2-m class facilities equipped with spectrographs offering high accuracy in radial velocities.

4. Conclusions

TESS space mission (Ricker et al., 2015) was successfully launched in April 2018 and now the first exoplanet was confirmed Gandolfi et al. (2018); Huang et al. (2018) and many more are coming. In the second half of the next decade, the PLATO space mission should be launched in 2026. The PLATO space mission will be searching for transits of extrasolar planets and it will be monitoring the stellar activity of million bright stars up to magnitude 11. According to the PLATO red book (PLATO red book, 2017) several thousands of candidates and later confirmed planets are to be expected. Not much later after PLATO another exoplanetary space mission ARIEL should be launched in 2028 (Tinetti et al., 2018). The ARIEL space mission should be searching for signatures of exo-atmospheres, however, a ground-based segment will be needed to support ARIELs operations even well before ARIEL's launch. Observational effort to confirm newly detected exoplanets will be thus growing and demand for observing time on 2-m class facilities will be rapidly increasing.

Acknowledgements. PK would like to acknowledge the support from GACR international grant 17-01752J and some travel cost to visit collaborators from ERASMUS+ grant Agreement no. 2017-1-CZ01-KA203-035562. EG and SS acknowledge the DFG grant GU 646/20. MS acknowledges financial support of Postdoc@MUNI project CZ.02.2.69/0.0/0.0/16_027/0008360. We acknowledge the use of IRAF and SIMBAD. We would like to thank the referee for improving the quality of this paper.

References

Almenara, J. M., Deeg, H. J., Aigrain, S., et al. 2009, A&A, 506, 337

Auvergne, M., Bodin, P., Boisnard, L., et al. 2009, A&A, 506, 411

Baranne, A., Queloz, D., Mayor, M., et al. 1996, Astron. Astrophys., Suppl., 119, 373

Bouchy, F., Moutou, C., Queloz, D., & CoRoT Exoplanet Science Team 2009, Transiting Planets, 253, 129

Cabrera, J., Barros, S. C. C., Armstrong, D., et al. 2017, A&A, 606, A75

Deeg, H. J., Gillon, M., Shporer, A., et al. 2009, A&A, 506, 343

Döllinger, M. P., Hatzes, A. P., Pasquini, L., et al. 2007, A&A, 472, 649

Endl, M., Kürster, M., Els, S., et al. 2002, A&A, 392, 671

Fressin, F., Torres, G., Charbonneau, D., et al. 2013, ApJ, 766, 81

Gandolfi, D., Hébrard, G., Alonso, R., et al. 2010, A&A, 524, A55

Gandolfi, D., Barragan, O., Livingston, J., Fridlund, M., Justesen, B., A., et al. 2018, A&A, 619, 10

Hellier, C., Anderson, D. R., Collier Cameron, A., et al. 2009, Nature, 460, 1098

Huang, Ch., Burt, J., Vanderburg A., Günther, N., A., Shporer, A., et al. 2018, arXiv:1809.05967v1 , submitted to AAS Letter

Kabath, P., Skarka, M., Sabotta, S., Guenther, E., Klocova, T., et al. 2018, submitted Astron. J.

Léger, A., Rouan, D., Schneider, J., et al. 2009, A&A, 506, 287

Ligi, R., Demangeon, O., Barros, S., et al. 2018, Astron. J., 156, 182

Loeillet, B., Bouchy, F., Deleuil, M., et al. 2008, A&A, 479, 865

Mayor, M., & Queloz, D. 1995, Nature, 378, 355

Plato definition study report, 2017, ESA-SCI(2017)1

Pepe, F. A., Cristiani, S., Rebolo Lopez, R., et al. 2010, Proc. SPIE, 7735, 77350F

Pont, F., Aigrain, S., & Zucker, S. 2011, Mon. Not. R. Astron. Soc., 411, 1953

Ricker, G. R., Winn, J. N., Vanderspek, R., et al. 2015, Journal of Astronomical Telescopes, Instruments, and Systems, 1, 014003

Schmitt, J. R., Tokovinin, A., Wang, J., et al. 2016, Astron. J., 151, 159

Santerne, A., Díaz, R. F., Moutou, C., et al. 2012, A&A, 545, A76

Santerne, A., Daz, R. F., Almenara, J.-M., et al. 2013, in SF2A-2013: Proceedings of the Annual meeting of the French Society of Astronomy and Astrophysics, ed. L. Cambresy, F. Martins, E. Nuss, & A. Palacios, 555-560

Tinetti, G., Drossart, P., Eccleston, P., et al. 2018, Experimental Astronomy,

Contrib. Astron. Obs. Skalnaté Pleso **49**, 469 – 474, (2019)

Ground-based observations for the BRITE-Constellation Satellites

E. Paunzen[1] **and K. Zwintz**[2]

[1] *Department of Theoretical Physics and Astrophysics, Masaryk University, Kotlářská 2, CZ-611 37 Brno, Czech Republic, (E-mail: epaunzen@physics.muni.cz)*

[2] *Universität Innsbruck, Institut für Astro- und Teilchenphysik, Technikerstrasse 25/8, A-6020 Innsbruck, Austria, (E-mail: Konstanze.Zwintz@uibk.ac.at)*

Received: November 16, 2018; Accepted: January 24, 2019

Abstract. BRITE (BRIght Target Explorer) Constellation is a network of five nano-satellites to investigate stellar structure and evolution of the brightest stars in the sky and their interaction with the local environment. Micropulsation, wind phenomena, and other forms of stellar variability are recorded via high precision photometry in two wavelength regions (red and blue). The success of this mission is also very much depending on supportive ground-based observations, especially spectroscopy. We review the variety of such needed observations together with already published results. Furthermore, we describe the aims and tasks of the BRITE-Constellation Ground-Based Observing Team.

Key words: Space vehicles – Stars: variables: general – Astronomical data bases

1. Introduction

BRITE-Constellation is a group of five nano-satellites, launched in 2013 and 2014, aimed at obtaining continuous time-series high precision photometry in the blue and red wavelength regime for the brightest (typically $V < 6$ mag) stars in the sky (Weiss et al., 2014).

The scientific goals of the mission are mainly related to the investigation of the variability of upper main sequence stars, i.e. hot massive stars. These stars show a variety of variability types which are caused by pulsations, mass loss, rotation, stellar winds, and interactions in binary and multiple systems (Aerts & Sterken, 2006).

However, for a comprehensive study, often, further ground-based observations are needed. The advantage of studying bright stars is, for example, that spectroscopic observations either exist in archives or can be easily obtained even with a small or medium-size telescope.

The BRITE-Constellation Ground-Based Observing Team (GBOT) was founded in 2012 to support collaborations between BRITE-Constellation PIs

Table 1. BRITE-Constellation satellites in orbit.

Country	Satellite Name	ID	Launch	P_{orb} (min)	Filter
AUT	UniBRITE	UBr	2013-02-25	100.37	red
AUT	BRITE-Austria "TUG-SAT-1"	BAb	2013-02-25	100.36	blue
CAN	BRITE-CA1 "Toronto"	BTr	2014-06-19	98.24	red
POL	BRITE-PL2 "Heweliusz"	BHr	2014-08-19	97.10	red
POL	BRITE-PL1 "Lem"	BHr	2013-11-21	99.57	blue

and ground-based observers worldwide. Its mission is to maximize the scientific output of the BRITE-Constellation project.

In this article we will give a few examples of how such additional observations helped to significantly improve the analysis. Furthermore, we will describe the GBOT in more detail.

2. The BRITE-Constellation Satellites

Here, we will give a short overview of the BRITE-Constellation satellites. A much more detailed description can be found in Pablo et al. (2016).

The origin of BRITE-Constellation can be traced directly to two developments: the Canadian micro-satellite project Microvariability and Oscillation of Stars (MOST, Matthews, 2004) and the beginning of the nano-satellite program at the Space Flight Laboratory (SFL) of the University of Toronto in the early 2000s. The MOST mission, proposed in 1997 and launched on 30 June 2003, is still delivering photometric data of the highest quality (Mikulášek et al., 2016). Based on the experience accumulated during this mission, a consortium of researchers from Austria, Canada and Poland was formed. Finally, in the years 2013 and 2014, six satellites were launched from which five are fully functioning. An overview of these satellites are listed in Table 1. In the following, we itemise the basic relevant properties of the mission and its instrument:

- Aperture: 3 cm.
- Size: 20x20x20 cm.
- Bright stars with $V < 4$ mag.
- Two wavelength regions: 400 - 450 nm (blue filter) and 550 - 700 nm (red filter).
- Nearly all-sky coverage.
- One field observed up to half a year.
- Field-of-view has a diameter of about 24° x 24°.

From 2013 to October 2018, 520 stars in 34 campaigns were successfully observed (Pigulski, 2018). The scientific output is manifold (Baade, 2018) and extends from Luminous Blue Variables at the hot and red supergiants at the cool luminous end, both with mostly slow variations, to δ Scuti, γ Doradus, and rapidly oscillating Ap stars at the low-luminosity/rapid-variability end. Furthermore, rotational induced variability and eclipsing binaries have been successfully investigated with BRITE-Constellation data (Paunzen & Rode-Paunzen, 2017; Ratajczak & Pigulski, 2018). The whole project is a major success and it can be hoped that the overlap with targets from the TESS mission (Ricker et al., 2014), will further result in several additional scientific investigations.

3. Some results from ground based support observations

In this section, a short overview of selected results of joint efforts using BRITE-Constellation and additional ground-based data is given. In principle, all types of supportive observations, for example, photometric (Stachowski et al., 2015), polarimetric (Neiner et al., 2017), and spectroscopic (Richardson et al., 2017) data strengthen the individual scientific cases. In the following, we have selected five different star groups showing the success of the GBOT.

β Cephei stars: A simultaneous ground and space-based photometric study of ν Eridani was presented by Handler et al. (2017). In this scientific case, ground-based Strömgren *uvy* photometry allowed a mode identification using the amplitude ratios and phase shifts of the different filters. Although this is also, in principle, possible with the two wavelength regions covered by the BRITE-Constellation data, light curves in additional filters help to put tight constraints on the pulsational models.

Be stars: The variability of this star group caused by mass-loss and circumstellar material can be investigated using BRITE-Constellation and other space-based photometric data (Baade et al., 2018). Additional spectroscopic observations, for example of the Hα profiles, help characterizing the disk around these stars. Especially studying the emission line and radial velocity changes are crucial for modelling the close stellar environment.

γ Doradus stars: Zwintz et al. (2017) presented a detailed analysis of 43 Cygni. High-resolution and high signal-to-noise ratio spectroscopic data obtained at the 1.2 m Mercator telescope with the HERMES spectrograph were used to determine the fundamental atmospheric parameters and chemical composition of this object. With these astrophysical parameters and the 156-days long data set obtained with the BRITE-Toronto satellite, they derived the mode identification, asymptotic period spacing, and near-core rotation rate on the basis of a suite of MESA/GYRE models. Only with the combination of photometry and spectroscopy it was possible to determine the near-core rotation rate and find indications of the presence of a significant chemical gradient in the stellar interior.

O-type supergiants: Stochastically-triggered photospheric light variations were detected in V973 Scorpii (Ramiaramanantsoa et al., 2018) on the basis of BRITE-Constellation observations. The variations on a time scale between 5 and 10 days can be best traced by continuous photometric data over many cycles. To connect this phenomenon to the amount of stellar wind and mass-loss, additional low as well as medium-resolution spectra are needed.

Rapidly oscillating Ap stars: This object class is very demanding in terms of photometric accuracy because the amplitudes of variability hardly reach a few mmags. Weiss et al. (2016) analysed α Circini, one of the prototypes of this variability class. Only with the combined BRITE-Constellation and archival long-term ground-based data, it was possible to study the pulsational and rotational period of this object.

4. The BRITE-Constellation Ground-Based Observing Team

In the following, we give an overview of the main tasks and information which can be found at the website http://www.brite-constellation.at:

- Overview of ground-based observations for completed, ongoing, and future BRITE-Constellation observations.
- Ground-based observing proposals for BRITE-Constellation targets.
- Sub-teams of GBOT and their PIs.
- List of ground-based facilities that already contributed with ground-based observations.
- Information from archives, databases, and the literature.
- Other relevant information (e.g. publications).
- List of GBOT members.

The collaboration with GBOT is open for the whole community. The contact person for any inquiries is Konstanze Zwintz (konstanze.zwintz@uibk.ac.at).

References

Aerts, C. & Sterken, C., eds. 2006, Astronomical Society of the Pacific Conference Series, Vol. **349**, *Astrophysics of Variable Stars*

Baade, D., Bright BRITE Science Results. 2018, in *3rd BRITE Science Conference*, ed. G. A. Wade, D. Baade, J. A. Guzik, & R. Smolec, 15–20

Baade, D., Pigulski, A., Rivinius, T., et al., Short-term variability and mass loss in Be stars. III. BRITE and SMEI satellite photometry of 28 Cygni. 2018, *Astron. Astrophys.*, **610**, A70, DOI: 10.1051/0004-6361/201731187

Handler, G., Rybicka, M., Popowicz, A., et al., Combining BRITE and ground-based photometry for the β Cephei star ν Eridani: impact on photometric pulsation mode identification and detection of several g modes. 2017, *Mon. Not. R. Astron. Soc.*, **464**, 2249, DOI: 10.1093/mnras/stw2518

Matthews, J. M., Probing Rotation in Pulsating Stars from Space (Invited Review). 2004, in IAU Symposium, Vol. **215**, *Stellar Rotation*, ed. A. Maeder & P. Eenens, 189

Mikulášek, Z., Paunzen, E., Zejda, M., et al., Fine detrending of raw Kepler and MOST photometric data of KIC 6950556 and HD 37633. 2016, *Bulgarian Astronomical Journal*, **25**, 19

Neiner, C., Wade, G. A., Marsden, S. C., & Blazère, A., The BRITE spectropolarimetric program. 2017, in *Second BRITE-Constellation Science Conference: Small satellites - big science, Proceedings of the Polish Astronomical Society volume 5, held 22-26 August, 2016 in Innsbruck, Austria. Polish Astronomical Society, Bartycka 18, 00-716 Warsaw, Poland*, ed. K. Zwintz & E. Poretti, 86–93

Pablo, H., Whittaker, G. N., Popowicz, A., et al., The BRITE Constellation Nanosatellite Mission: Testing, Commissioning, and Operations. 2016, *Publ. Astron. Soc. Pac.*, **128**, 125001, DOI: 10.1088/1538-3873/128/970/125001

Paunzen, E. & Rode-Paunzen, M., BRITE photometry of seven B-type stars. 2017, in *Second BRITE-Constellation Science Conference: Small satellites - big science, Proceedings of the Polish Astronomical Society volume 5, held 22-26 August, 2016 in Innsbruck, Austria. Edited by Konnstanze Zwintz and Ennio Poretti. Polish Astronomical Society, Bartycka 18, 00-716 Warsaw, Poland, pp.180-185*, ed. K. Zwintz & E. Poretti, 180–185

Pigulski, A., Statistical Overview of BRITE Targets Observed So Far. 2018, in *3rd BRITE Science Conference*, ed. G. A. Wade, D. Baade, J. A. Guzik, & R. Smolec, 21–30

Ramiaramanantsoa, T., Ratnasingam, R., Shenar, T., et al., A BRITE view on the massive O-type supergiant V973 Scorpii: hints towards internal gravity waves or sub-surface convection zones. 2018, *Mon. Not. R. Astron. Soc.*, **480**, 972, DOI: 10.1093/mnras/sty1897

Ratajczak, M. & Pigulski, A., Massive Eclipsing Binaries Observed by BRITE. 2018, in *3rd BRITE Science Conference*, ed. G. A. Wade, D. Baade, J. A. Guzik, & R. Smolec, 118–122

Richardson, N. D., Russell, C. M. P., St-Jean, L., et al., The variability of the BRITE-est Wolf-Rayet binary, γ^2 Velorum-I. Photometric and spectroscopic

evidence for colliding winds. 2017, *Mon. Not. R. Astron. Soc.*, **471**, 2715, DOI: 10.1093/mnras/stx1731

Ricker, G. R., Winn, J. N., Vanderspek, R., et al., Transiting Exoplanet Survey Satellite (TESS). 2014, in Proc. SPIE, Vol. **9143**, *Space Telescopes and Instrumentation 2014: Optical, Infrared, and Millimeter Wave*, 914320

Stachowski, G., Ogloza, W., Drozdz, M., & Zakrzewski, B., Photometric Observations of Selected BRITE Target Stars at Mt. Suhora Observatory. 2015, in Astronomical Society of the Pacific Conference Series, Vol. **496**, *Living Together: Planets, Host Stars and Binaries*, ed. S. M. Rucinski, G. Torres, & M. Zejda, 316

Weiss, W. W., Fröhlich, H.-E., Pigulski, A., et al., The roAp star α Circinus as seen by BRITE-Constellation. 2016, *Astron. Astrophys.*, **588**, A54, DOI: 10.1051/0004-6361/201526997

Weiss, W. W., Rucinski, S. M., Moffat, A. F. J., et al., BRITE-Constellation: Nanosatellites for Precision Photometry of Bright Stars. 2014, *Publ. Astron. Soc. Pac.*, **126**, 573, DOI: 10.1086/677236

Zwintz, K., Van Reeth, T., Tkachenko, A., et al., Constraining the near-core rotation of the γ Doradus star 43 Cygni using BRITE-Constellation data. 2017, *Astron. Astrophys.*, **608**, A103, DOI: 10.1051/0004-6361/201731784

Contrib. Astron. Obs. Skalnaté Pleso **49**, 475 – 483, (2019)

WET stars and planets: telescope network observations of mCP stars and exoplanets

D.L. Holdsworth[1,2]

[1] *Jeremiah Horrocks Institute, University of Central Lancashire, Preston PR1 2HE, UK (E-mail: dlholdsworth@uclan.ac.uk)*

[2] *Center for Space Research, North-West University, Mafikeng Campus, Private Bag X2046, Mmabatho 2745, South Africa*

Received: December 1, 2018; Accepted: January 14, 2019

Abstract. The Whole Earth Telescope (WET) and similar global telescope networks are discussed. In particular this work focuses on the recent contribution of such networks to the study of magnetic A-type stars with particular attention given to pulsating variable stars. In addition, telescopes that are part of such networks have the ability to provide similar observations for the study of multi-planetary systems.

Key words: asteroseismology – stars: chemically peculiar – planets and satellites: general

1. Introduction

The Whole Earth Telescope (WET) is an international collaboration between 45 observatories which aims to to provide near-continuous photometric observations of variable stars. The broad longitudinal coverage of the network, a shown in Fig. 1, allows a star to be monitored by one site in the east, then picked up by a more westerly observatory as it starts to set at the first location. This system, in principle, allows for uninterrupted observations leading to a 100 % duty cycle which would otherwise be unobtainable from the ground.

The WET was founded in the 1980s with the primary goal of observing pulsating white dwarf stars. Although multi-site campaigns had successfully observed variable stars before the foundation of the WET, the WET is unique as it works as a single instrument. During observations at each site, information is continuously fed-back to headquarters (HQ) at Mt. Cuba Observatory and the University of Delaware (see `http://www.physics.udel.edu/gp/darc/2015new/index.html` for details) so that if an observatory site monitoring the primary star is clouded over, a second over-lapping site can switch from a secondary target to the primary to obtain continuous coverage.

At the end of each night, the data are sent back to HQ for uniform reduction and analysis with the in-house data reduction packages MAESTRO and WQED (with details available on the WET web pages). Standard data reduction steps are applied, as well as correction for primary extinction. The final light curves consist of differential photometry, with time stamps in BJD.

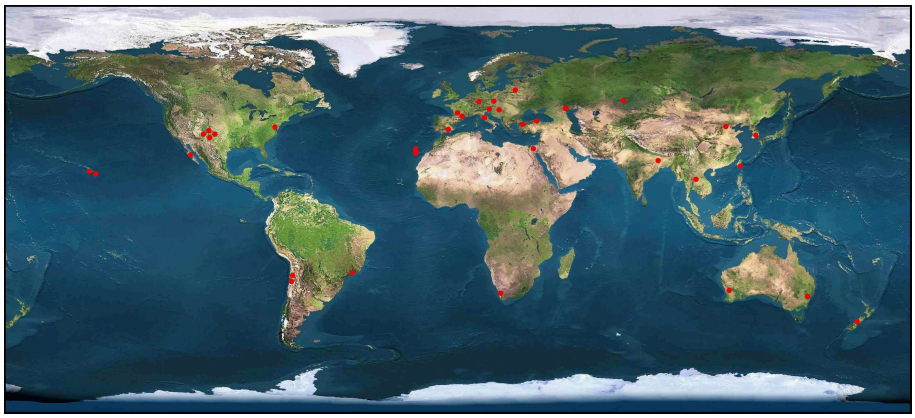

Figure 1. The locations of the observatories, marked by red circles, that have agreed to contribute to Whole Earth Telescope observations.

For a more detailed discussion of the WET, I refer the reader to Sullivan (2001) and Provencal et al. (2014).

2. Observations of magnetic chemically peculiar stars

The magnetic chemically peculiar (mCP) stars span the spectral types of late B to early F. They are characterised by slow rotation, strong global magnetic fields and over-abundances of elements such as Sr, Eu, Cr and rare earth elements whose abundances can be up to one million times that of the Sun (Ryabchikova et al., 2004). The magnetic field in these stars confines the chemical abundances in spots, typically around the magnetic poles, which leads to a light curve modulated with the rotation period of the star. This modulation is evident as the magnetic axis is misaligned with the rotational axis resulting in oblique rotation (Stibbs, 1950).

The rotation periods of the mCP stars have a broad range, from less than a day to, potentially, hundreds of years (Mathys, 2017). The cause for these short rotation periods, when compared to their non-magnetic counterparts, is thought to be magnetic breaking (Abt & Morrell, 1995; Stępień, 2000).

In the late 1970s, Kurtz (1978) observed rapid oscillations in the very peculiar Przybylski's star (HD 101065). With further exploration of other mCP stars, he was able to define the class of rapidly oscilllating Ap (roAp) stars (Kurtz, 1982). The pulsations in these stars are thought to be driven by the κ-mechanism acting in the H I ionisation zone causing the excitation of high-overtone, low degree, pressure (p-) modes (Balmforth et al., 2001; Saio, 2005). However, it is also possible that turbulent pressure in the atmospheres of these stars can also excite pulsations (Cunha et al., 2013), which helps to explain the

observed frequencies which cannot be driven by the κ-mechanism. The pulsation periods of the roAp range from $5 - 24$ min, with peak-to-peak amplitudes up to 34 mmag in B-band observations (Smalley et al., 2015; Joshi et al., 2016; Holdsworth et al., 2018a). It is thought that the magnetic field suppresses low-frequency pulsations in Ap stars (Saio, 2005), although recent K2 observations analysed by Bowman et al. (2018) suggest that this might not be the case.

The pulsation axis in the roAp stars is closely aligned with the magnetic one which leads to a modulation of the pulsation amplitude as the star rotates. This is evident in Fig. 2. This modulation in the amplitude causes a frequency multiplet in the amplitude spectrum of the light curve, and holds information on the geometry of the mode. For a non-distorted mode, a modulated dipole pulsation (i.e. $\ell = 1$) results in a frequency triplet, and a quadrupole ($\ell = 2$) mode shows a quintuplet in the amplitude spectrum.

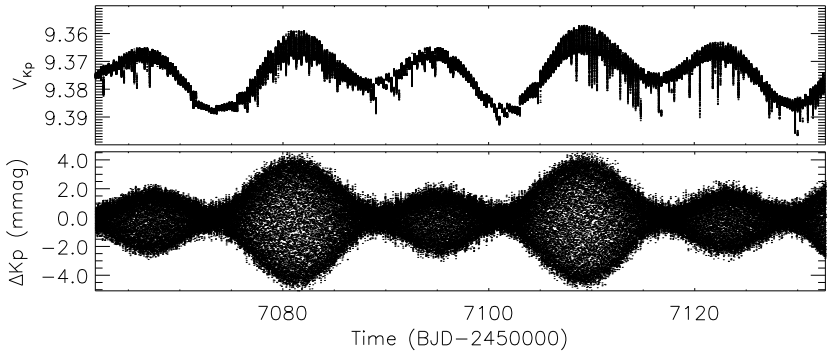

Figure 2. K2 observations of the roAp star HD 24355. The top panel shows the light curve. Evident is the rotational modulation due to surface spots (with a period of about 28 d) and also the $\sim$ 6 h drift in the spacecraft pointing. The lower panel shows the light curve with the low-frequency signals removed. The modulation seen is that of the pulsation envelope which coincides with the spot modulation. Figure from Holdsworth et al. (2016).

If the amplitude of the pulsation goes to zero over the rotation cycle, the line of sight to the star coincides with a pulsation node. When this occurs, we expect a phase change of the pulsation by π-rad as we are now observing the opposite pulsation pole. This is, again, the expected case for a non-distorted mode. Fig. 3 shows examples of the non-distorted case (lower three panels) along side that of a distorted quadrupole pulsation (top panel; HD 24355).

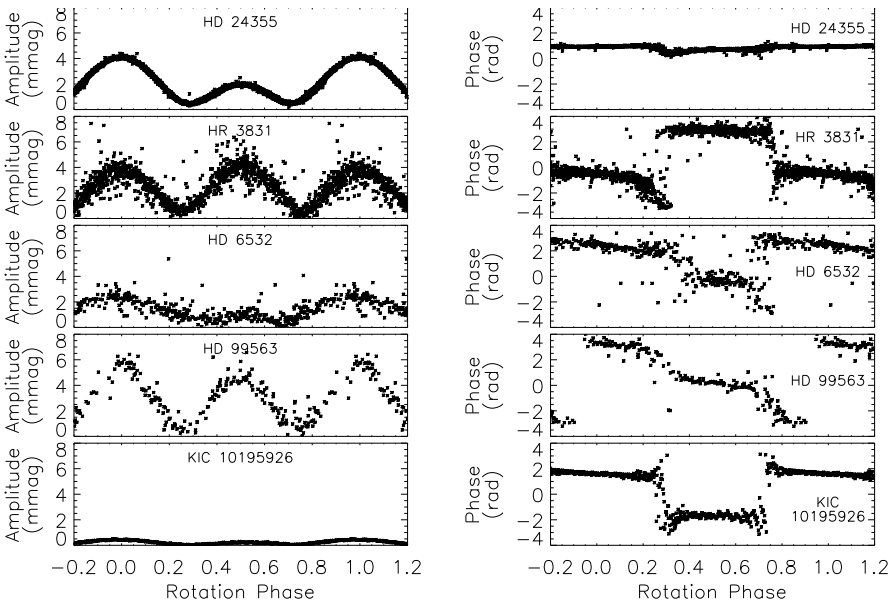

Figure 3. A comparison of non-distorted pulsations in roAp stars (bottom 4 panels), and the distorted mode in HD 24355. The amplidue modulation is as expected, but the lack of a π-rad phase change allows us to conclude that the mode in HD 24355 is distorted. Figure from Holdsworth et al. (2016).

2.1. WET observations of roAp stars

Although the Whole Earth Telescope was primarily designed for the observations of pulsating white dwarf stars (e.g. Kepler et al., 1995; Sullivan et al., 2008; Provencal et al., 2012), it is well suited for the study of pulsations in Ap stars. The need for continuos observations to reduce (or ideally remove) the effects of aliases in an amplitude spectrum is key to identifying real frequencies which are not perturbed by cross talk with the spectral window. The roAp stars can have a rich spectrum of closely spaced modes (cf. HR 1217; Kurtz et al., 2005) representing the large and small frequency separation, thus allowing for a full asteroseismic model of the star.

The most extensively studied (from the ground) roAp star is HD 1217. This star was the first roAp star targeted with the WET in 2000 after observation in 1986 showed this to be a promising star to perform asteroseismology on. The campaign lasted a total of 35 d, achieved a duty cycle of 36 % and provided the most precise ground-based measurements of the amplitudes in roAp stars, reaching a precision of 14 μmag (see Fig. 4 Kurtz et al., 2005). With such precise data, predictions by Cunha (2001) of a missing mode in the 1986 data were

proven to be true, allowing for a complete asteroseismic model of the star to be computed.

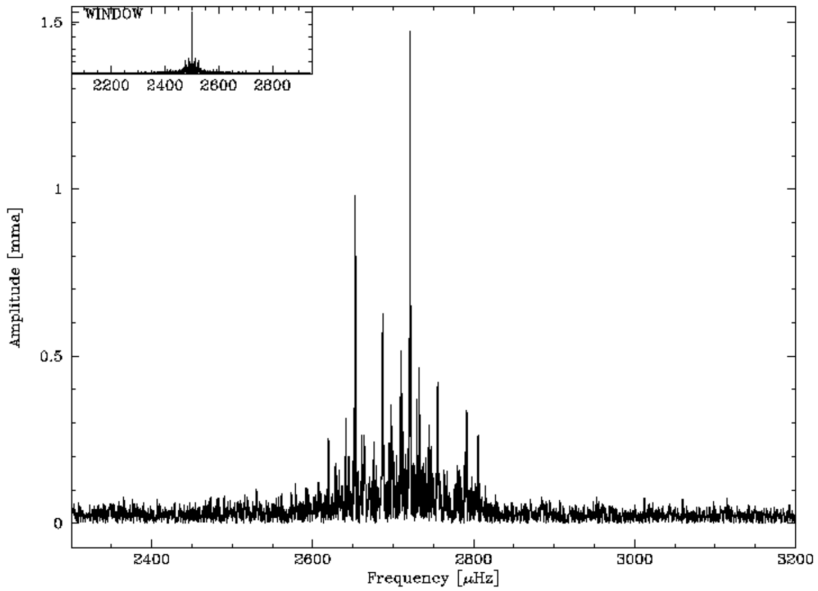

Figure 4. The amplitude spectrum of WET data for HR 1217. The high duty cycle (for ground-based observations) led to a suppression of aliases, and the data length provided high frequency precision. Most of the structure seen in the frequency range $2600 - 2800\,\mu$mag is real. The amplitude unit, milli-modulation amplitude, converts to milli-magnitude as 1 mma=1.086 mmag. Figure from the WET team.

More recently, the WET targeted the largest amplitude roAp star known: J1940 (Holdsworth et al., 2014, 2018a). Although only achieving a duty cycle of 21 %, the multi-site observations revealed that J1940 pulsates in a very distorted quadrupole mode. Through modelling the pulsational phase variations (after the method of Saio 2005), which are sensitive to mass and the polar magnetic field strength, it was shown that the pulsation frequency is much higher than the theoretical cut-off frequency i.e. the pulsation frequency cannot be recreated with the κ-mechanism alone.

Other multi-site campaigns of roAp stars have also unveiled stars which show a suppression of the pulsation phase. Holdsworth et al. (2018b) collected data from three observatory sites (Siding Springs, Australia; Sutherland, South Africa; Cerro Tololo Inter-American Observatory, Chile) to study J1640, while Holdsworth et al. (2018c) utilised the Las Cumbres Observatory's 0.4-m telescopes to observe J0855. Both projects aimed to obtain continuous observations

in the same way as the WET, but through independent means. These multi-site campaigns, coupled with results from the *Kepler* Space Telescope, have identified many roAp stars that pulsate with frequencies greater than their respective acoustic cut-off frequencies (Fig. 5). All of these stars show suppressed phase variations, with the modes being strongly distorted by the star's magnetic field.

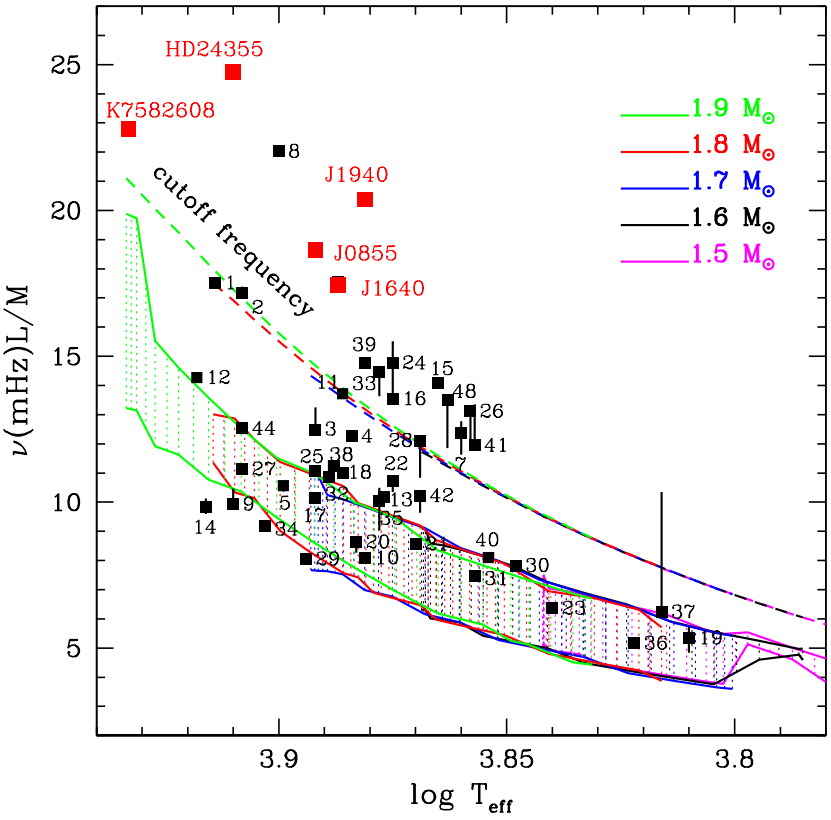

Figure 5. The $\log T_{\rm eff} - \nu L/M$ plane showing the positions of the roAp stars. The squares represent the principal pulsation frequency, with vertical bars showing the range of frequencies for multi-periodic stars. The hatched region represents where high-order p modes are excited by the κ-mechanism in the H-ionization zone in non–magnetic models. Acoustic cutoff frequencies are represented by the dashed lines. The stars shown in red are those which show suppressed phase variations. The numerical labels correspond to the stars in table A1 of Holdsworth et al. (2018b). Figure from Holdsworth et al. (2018c), after Saio (2014).

3. Observations of exoplanets

It is not just asteroseismology that benefits from continuous observations; the study of transiting exoplanets can make good use of uninterrupted data sets. A prime example of this is the TRAPPIST-1 planetary system (Gillon et al., 2017). The presence of three transiting planets were well established not long after discovery of the system, however the precise period of the (then) outer most planet was not known. A total of 10 telescopes were used to try and confirm the parameters of the system through near-continuous observations. However, it was not until the *Spitzer* space telescope observed the system, with complementary data from the ground, that the full extent of the planetary system was known. Uninterrupted data provides the opportunity to probe the full period range of planets without diurnal gaps.

A further point that should be mentioned is the power of multi-site spectroscopy. Although this is by far not a new concept, the Las Cumbres Observatory is installing 6 identical high-resolution spectrographs at a selection of their sites. With the use of identical instruments and telescopes, instrumental profiles become less of an issue so that the data require less processing to be analysed together. Since spectroscopy is also more sensitive to smaller planets (from the ground at least), continuous spectroscopic observations have the potential to provide many planetary systems with many terrestrial planets.

Acknowledgements. The author acknowledges financial support from the STFC via grant ST/M000877/1 and the National Research Foundation of South Africa. Thanks go to Judith Provencal for assistance in compiling the original talk.

References

Abt, H. A. & Morrell, N. I., The Relation between Rotational Velocities and Spectral Peculiarities among A-Type Stars. 1995, *Astrophys. J., Suppl.*, **99**, 135, DOI: 10.1086/192182

Balmforth, N. J., Cunha, M. S., Dolez, N., Gough, D. O., & Vauclair, S., On the excitation mechanism in roAp stars. 2001, *Mon. Not. R. Astron. Soc.*, **323**, 362, DOI: 10.1046/j.1365-8711.2001.04182.x

Bowman, D. M., Buysschaert, B., Neiner, C., et al., K2 space photometry reveals rotational modulation and stellar pulsations in chemically peculiar A and B stars. 2018, *Astron. Astrophys.*, **616**, A77, DOI: 10.1051/0004-6361/201833037

Cunha, M. S., The sixth frequency of roAp star HR 1217. 2001, *Mon. Not. R. Astron. Soc.*, **325**, 373, DOI: 10.1046/j.1365-8711.2001.04434.x

Cunha, M. S., Alentiev, D., Brandão, I. M., & Perraut, K., Testing excitation models of rapidly oscillating Ap stars with interferometry. 2013, *Mon. Not. R. Astron. Soc.*, **436**, 1639, DOI: 10.1093/mnras/stt1679

Gillon, M., Triaud, A. H. M. J., Demory, B.-O., et al., Seven temperate terrestrial planets around the nearby ultracool dwarf star TRAPPIST-1. 2017, *Nature*, **542**, 456, DOI: 10.1038/nature21360

Holdsworth, D. L., Kurtz, D. W., Saio, H., et al., Whole Earth Telescope discovery of a strongly distorted quadrupole pulsation in the largest amplitude rapidly oscillating Ap star. 2018a, *Mon. Not. R. Astron. Soc.*, **473**, 91, DOI: 10.1093/mnras/stx2401

Holdsworth, D. L., Kurtz, D. W., Smalley, B., et al., HD 24355 observed by the Kepler K2 mission: a rapidly oscillating Ap star pulsating in a distorted quadrupole mode. 2016, *Mon. Not. R. Astron. Soc.*, **462**, 876, DOI: 10.1093/mnras/stw1711

Holdsworth, D. L., Saio, H., Bowman, D. M., et al., Suppressed phase variations in a high amplitude rapidly oscillating Ap star pulsating in a distorted quadrupole mode. 2018b, *Mon. Not. R. Astron. Soc.*, **476**, 601, DOI: 10.1093/mnras/sty248

Holdsworth, D. L., Saio, H., Sefako, R. R., & Bowman, D. M., LCO observations of a super-critical distorted pulsation in the roAp star J0855 (TYC 2488-1241-1). 2018c, *Mon. Not. R. Astron. Soc.*, **480**, 2405, DOI: 10.1093/mnras/sty2039

Holdsworth, D. L., Smalley, B., Gillon, M., et al., High-frequency A-type pulsators discovered using SuperWASP. 2014, *Mon. Not. R. Astron. Soc.*, **439**, 2078, DOI: 10.1093/mnras/stu094

Joshi, S., Martinez, P., Chowdhury, S., et al., The Nainital-Cape Survey. IV. A search for pulsational variability in 108 chemically peculiar stars. 2016, *Astron. Astrophys.*, **590**, A116, DOI: 10.1051/0004-6361/201527242

Kepler, S. O., Giovannini, O., Wood, M. A., et al., Whole Earth Telescope Observations of the DAV White Dwarf G226-29. 1995, *Astrophys. J.*, **447**, 874, DOI: 10.1086/175924

Kurtz, D. W., 12.15 Minute Light Variations in Przybylski's Star, HD 101065. 1978, *Information Bulletin on Variable Stars*, **1436**

Kurtz, D. W., Rapidly oscillating AP stars. 1982, *Mon. Not. R. Astron. Soc.*, **200**, 807

Kurtz, D. W., Cameron, C., Cunha, M. S., et al., Pushing the ground-based limit: 14-μmag photometric precision with the definitive Whole Earth Telescope asteroseismic data set for the rapidly oscillating Ap star HR1217. 2005, *Mon. Not. R. Astron. Soc.*, **358**, 651, DOI: 10.1111/j.1365-2966.2005.08807.x

Mathys, G., Ap stars with resolved magnetically split lines: Magnetic field determinations from Stokes I and V spectra. 2017, *Astron. Astrophys.*, **601**, A14, DOI: 10.1051/0004-6361/201628429

Provencal, J. L., Montgomery, M. H., Kanaan, A., et al., Empirical Determination of Convection Parameters in White Dwarfs. I. Whole Earth Telescope Observations of EC14012-1446. 2012, *Astrophys. J.*, **751**, 91, DOI: 10.1088/0004-637X/751/2/91

Provencal, J. L., Shipman, H. L., Montgomery, M. H., & WET Team, An overview of Whole Earth Telescope. 2014, *Contributions of the Astronomical Observatory Skalnate Pleso*, **43**, 524

Ryabchikova, T., Nesvacil, N., Weiss, W. W., Kochukhov, O., & Stütz, C., The spectroscopic signature of roAp stars. 2004, *Astron. Astrophys.*, **423**, 705, DOI: 10.1051/0004-6361:20041012

Saio, H., A non-adiabatic analysis for axisymmetric pulsations of magnetic stars. 2005, *Mon. Not. R. Astron. Soc.*, **360**, 1022, DOI: 10.1111/j.1365-2966.2005.09091.x

Saio, H., Pulsation of magnetic stars. 2014, in IAU Symposium, Vol. **301**, *Precision Asteroseismology*, ed. J. A. Guzik, W. J. Chaplin, G. Handler, & A. Pigulski, 197–204

Smalley, B., Niemczura, E., Murphy, S. J., et al., KIC 4768731: a bright long-period roAp star in the Kepler field. 2015, *Mon. Not. R. Astron. Soc.*, **452**, 3334, DOI: 10.1093/mnras/stv1515

Stępień, K., Loss of angular momentum of magnetic Ap stars in the pre-main sequence phase. 2000, *Astron. Astrophys.*, **353**, 227

Stibbs, D. W. N., A study of the spectrum and magnetic variable star HD 125248. 1950, *Mon. Not. R. Astron. Soc.*, **110**, 395

Sullivan, D. J., The Whole Earth Telescope Collaboration. 2001, in Astronomical Society of the Pacific Conference Series, Vol. **226**, *12th European Workshop on White Dwarfs*, ed. J. L. Provencal, H. L. Shipman, J. MacDonald, & S. Goodchild, 417

Sullivan, D. J., Metcalfe, T. S., O'Donoghue, D., et al., Whole Earth Telescope observations of the hot helium atmosphere pulsating white dwarf EC20058-5234. 2008, *Mon. Not. R. Astron. Soc.*, **387**, 137, DOI: 10.1111/j.1365-2966.2008.13074.x

Contrib. Astron. Obs. Skalnaté Pleso **49**, 484 – 487, (2019)

Science with Global Astrophysical Telescope System

M. Polińska, K. Kamiński, W. Dimitrov, M.K. Kamińska and A. Marciniak

Astronomical Observatory Institute, Faculty of Physics, Adam Mickiewicz University, ul. Słoneczna 36, 60-286 Poznań, Poland, (E-mail: polinska@amu.edu.pl)

Received: November 27, 2018; Accepted: January 24, 2019

Abstract. We present the Global Astrophysical Telescope System project arranged by the Astronomical Observatory Institute of Adam Mickiewicz University in Poznań (Poland) and exemplary results obtained from it, including asteroids, eclipsing binary stars, and artificial satellites.

Key words: telescopes – spectroscopy – photometry – stars – asteroids

1. About GATS

The Global Astrophysical Telescope System (GATS[1]) operates as a global network of robotic telescopes and consists of two telescopes: PST1 (the Poznan Spectroscopic Telescope) (Baranowski et al., 2009) located near Poznań (Poland), and RBT/PST2 (the Roman Baranowski Telescope) in Winer Observatory in Arizona (USA). Both telescopes are equipped with fibre-fed echelle spectrographs, which are based on a modified MUSICOS design with a rotating carousel removed and only one fixed prism being used (Baudrand & Bohm, 1992) of resolution R∼35000 (PST1) and R∼40000 (RBT/PST2). PST1 consists of: a Binary 2 x 0.5 m Newtonian telescope, a low noise back-illuminated 2k x 2k Andor DZ 436 CCD camera and it is equipped with an equatorial, robotic mount capable to work in a remotely controlled mode. RBT/PST2 telescope is: 0.7 m f/6.6 Planewave CDK700 on an alt-az robotic direct-drive mount (Corrected Dall-Kirkham, dual Nasmyth focus), a spectroscopic CCD camera Andor iKon-L 936 back-illuminated, and a photometric CCD camera Andor iXon3 back-illuminated.

GATS main research topics are: eclipsing binary stars, asteroseismology of pulsating stars, stellar rotation and dynamical evolution in binary eclipsing stars, cataclysmic variables, photometric observations of Main Belt asteroids and Near Earth Objects, artificial satellites and space debris, and "targets of opportunity" (Gamma Ray Burst or Gaia alerts). Telescopes also participate in research programs of the BRITE consortium.

[1] www.astro.amu.edu.pl/GATS

1.1. Asteroids – example of (737) Arequipa

RBT/PST2 participates in a project of photometric asteroid studies to find their rotation periods, spins, and 3D shapes. As one of the nodes of the network consisting of 20 stations worldwide, it participates in round-the-globe campaigns to observe slowly rotating main belt asteroids (Marciniak et al., 2018). In summer months, when most asteroids are on the southern sky hemisphere, it helps to reach low-declination targets. Fig. 1.A shows a lightcurve of asteroid Arequipa, where the observations from RBT/PST2 helped to find the rotation period of 7.0259±0.0001 hours.

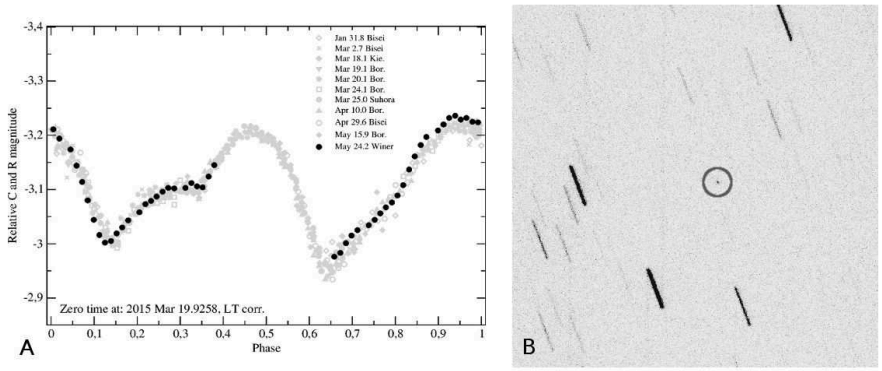

Figure 1. A. Composite lightcurve of (737) Arequipa observed in 2015 during 1 night with RBT/PST2. **B**. UKube-1 satellite tracking - RBT/PST2, exp. time 0.05 s, observed brightness ∼14 mag.

1.2. Eclipsing binary star - example of BD-00 2862 (component A)

Spectroscopic PST1 observations of the BD-00 2862 system show that it is a triple star, consisting of an eclipsing binary (component A), and a visual third object (component B) (Dimitrov et al., 2018). Spectra of BD-00 2862 (component A) are dominated by the lines of the main component, thus we treat them in analysis as single-lined spectra. We used twelve selected spectra with the best signal-to-noise ratio to create an averaged spectrum. To obtain atmospheric parameters (effective temperature, $T_{\rm eff}$ (from Balmer lines); surface gravity, $\log g$; metallicity [M/H]; and projected rotational velocity, $v \sin i$) the spectrum synthesis method implemented in the iSpec code was used (Blanco-Cuaresma et al., 2014). Fig. 2 shows the comparison of the average spectrum (Mg b I region) of BD-00 2862 (component A), and the calculated synthetic spectrum.

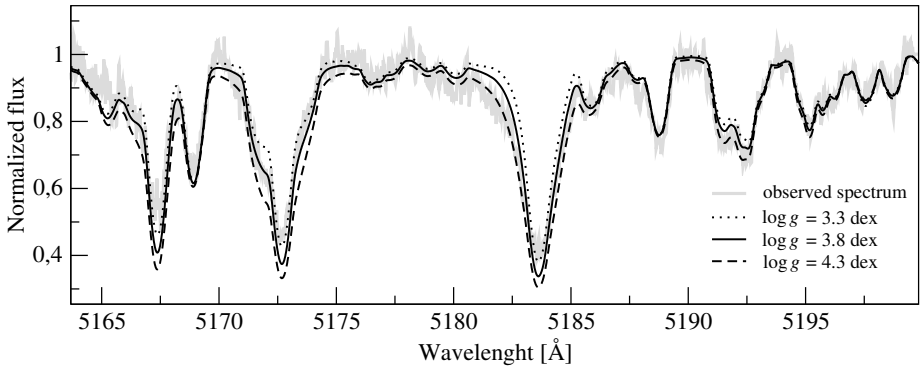

Figure 2. The combined spectrum (gray) with the fitted spectrum (black, different line style corresponds to various $\log g$ within the error limits) for Mg b I line regions for parameters: $T_{\rm eff} = 5600 \pm 400$ K, $\log g = 3.8 \pm 0.5$, [M/H]$= -0.30 \pm 0.20$, $v \sin i = 30 \pm 4\,{\rm km\,s^{-1}}$.

1.3. Satellites and space debris

Both GATS telescopes are capable of observing artificial Earth satellites. PST1 is mainly a survey telescope with its 1 × 1 deg field of view. RBT/PST2 is mainly a tracking (follow up) telescope. RBT/PST2 is equipped with a sensitive Andor EMCCD camera, and can detect all TLE (Two-Line Elements) catalog objects, even the smallest cubesats ($10 \times 10 \times 10\,{\rm cm}^3$) on low Earth orbits (LEO) (Kamiński et al., 2017). It can follow all satellites down to about 14.5 mag (with 0.05 sec exposure time) moving on the sky with proper motion up to 2° per sec (Fig. 1.B.). Both telescopes are equipped with our custom designed GPS based timing devices, allowing us to measure shutter opening and closing time with 1ms accuracy. We are involved in several ESA and European Space Surveillance and Tracking (EU SST) consortium projects. Based on gathered experience we are currently building an innovative cluster of 5 satellite surveillance and tracking telescopes - Poznań SST Telescope 3 (PST3). Its first light is expected in 2019.

Acknowledgements. This work has been supported by the Polish National Science Centre through grants no. 2014/13/B/ST9/00902 and 2014/13/D/ST9/01818.

References

Baranowski, R., Smolec, R., Dimitrov, W., et al., V440 Per: the longest–period overtone Cepheid. 2009, *Mon. Not. R. Astron. Soc.*, **369**, 2194, DOI: 10.1017/S1743921316000922

Baudrand, J. & Bohm, T., MUSICOS - A fiber-fed spectrograph for multi-site observations. 1992, *Astron. Astrophys.*, **259**, 711

Blanco-Cuaresma, S., Soubiran, C., Heiter, U., & Jofré, P., Determining stellar atmospheric parameters and chemical abundances of FGK stars with iSpec. 2014, *Astron. Astrophys.*, **569**, 14, DOI: 10.1051/0004-6361/201423945

Dimitrov, W., Żywucka, N., Polińska, M., Kamiński, K., & Kamińska, M. K., Spectroscopy of the Eclipsing Binary BD-00 2862. Possible Multiplicity. 2018, *Acta Astron.*, **68**, 269, DOI: 10.32023/0001-5237/68.3.6

Kamiński, K., Koshkin, L., Shakun, J., et al., Determination of orbital and spin parameters of LEO satellites by Polish and Ukrainian optical observatories. 2017, in *7th European Conference on Space Debris*, ed. T. Flohrer & F. Schmitz

Marciniak, A., Bartczak, P., Müller, T., et al., Photometric survey, modelling, and scaling of long-period and low-amplitude asteroids. 2018, *Astron. Astrophys.*, **610**, 33, DOI: 10.1051/0004-6361/201731479

PRÁCE ASTRONOMICKÉHO OBSERVATÓRIA
NA SKALNATOM PLESE
XLIX, číslo 2

Zostavovatelia:	RNDr. Ján Budaj, CSc.
	RNDr. Richard Komžík, CSc.
	RNDr. Theodor Pribulla, CSc.
	RNDr. Augustín Skopal, DrSc.
Vedecký redaktor:	RNDr. Augustín Skopal, DrSc.
Vydal:	Astronomický ústav SAV, Tatranská Lomnica
IČO vydavateľa:	00 166 529
Periodicita:	2-krát ročne
ISSN (on-line verzia):	1336-0337
CODEN:	CAOPF8
Rok vydania:	2019
Počet strán:	420

Contributions of the Astronomical Observatory Skalnaté Pleso are processed using
LaTeX 2ε CAOSP DocumentClass file 3.06 ver. 2017.